

Reprint Compendium

Bio-protocol Selections 2022

Neuroscience

Foreword

We are pleased to launch the 2022 *Bio-protocol* series of reprint collections, comprising some of the most used protocols published in 2021 in several research areas. This collection focuses on Neuroscience.

Established in 2011 by a group of Stanford scientists, Bio-protocol aims to improve research reproducibility and usability through the publication of high quality step-by-step peer-reviewed life science protocols. *Bio-protocol* invites contributions from authors who have published methods in brief, as part of other research articles, and who might want to provide more detailed versions to facilitate use by others.

A survey carried out in 2018 showed that, of more than 2300 users who had followed a protocol published in *Bio-protocol*, 91% (2166 users) were able to successfully reproduce the method they tried.

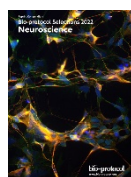
In this reprint collection, we have selected 24 of the most viewed, downloaded, and cited research protocols related to Neuroscience that were published in *Bio-protocol* in 2021.

Hopefully, you will find this collection intriguing and visit <http://www.bio-protocol.org> to check out the entire archive of protocols. Please feel free to email us (eb@bio-protocol.org) with feedback, and please consider contributing a protocol to Bio-protocol in the future.

The Bio-protocol Editorial Team

1. Optimized Immunostaining of Embryonic and Early Postnatal Mouse Brain Sections 1
Harb, K. *et al.* 【Original Research Article: *Elife*, e09531】
2. Establishing an Adult Mouse Brain Hippocampal Organotypic Slice Culture System that Allows for Tracing and Pharmacological Manipulation of *ex vivo* Neurogenesis 13
Mayerl, S. and Ffrench-Constant, C. 【Original Research Article: *Stem Cell Rep* 14(5), 845-860】
3. A Parkinson's Disease-relevant Mitochondrial and Neuronal Morphology High-throughput Screening Assay in LUHMES Cells 22
Leah *et al.* 【Original Research Article: *Neuroscience* 390, 46-59】
4. Relative Quantification of NaV1.1 Protein in Mouse Brains using a Meso Scale Discovery-Electrochemiluminescence (MSD-ECL) Method 38
Han *et al.* 【Original Research Article: *Sci Transl Med* 12(558), eaaz6100】
5. Generation of Human iPSC-derived Neural Progenitor Cells (NPCs) as Drug Discovery Model for Neurological and Mitochondrial Disorders 49
Zink *et al.* 【Original Research Article: *Cell Stem Cell* 20(5), 659-674.e9】
6. Generation of Mouse Primary Hypothalamic Neuronal Cultures for Circadian Bioluminescence Assays 63
Schmidt *et al.* 【Original Research Article: *Elife*, e55388】
7. Ligand and Carbohydrate Engagement (LACE) Assay and Fluorescence Quantification on Murine Neural Tissue 73
Clegg, J. M. and Pratt, T. 【Original Research Article: *J Neurosci* 39(8), 1386-1404】
8. Investigate Synaptic Vesicles Mobility in Neuronal Culture Axons by FRAP Imaging 81
Zhang *et al.* 【Original Research Article: *Elife*, e50401】
9. Single or Repeated Ablation of Mouse Olfactory Epithelium by Methimazole 91
Håglin *et al.* 【Original Research Article: *J Neurosci* 40(21), 4116-4129.】
10. Production of Phenotypically Uniform Human Cerebral Organoids from Pluripotent Stem Cells 102
Sivitilli *et al.* 【Original Research Article: *Life Sci Alliance* 3(5), e202000707】
11. Transcardiac Perfusion of the Mouse for Brain Tissue Dissection and Fixation 111
Wu *et al.* 【Original Research Article: *Cell Rep* 34(6), 108712】
12. Development of a Chemical Reproductive Aging Model in Female Rats 121
Pestana-Oliveira *et al.* 【Original Research Article: *eNeuro* 5(1), ENEURO.0247-17.2017】
13. *Ex vivo* Tissue Culture Protocols for Studying the Developing Neocortex 134
Namba *et al.* 【Original Research Article: *Elife*, e49808】
14. Electrophysiological Properties of Neurons: Current-Clamp Recordings in Mouse Brain Slices and Firing-Pattern Analysis 143
Nagaeva *et al.* 【Original Research Article: *Elife*, e59328】

15. A Method for Estimating the Potential Synaptic Connections Between Axons and Dendrites From 2D Neuronal Images 164
Tecuati et al. 【Original Research Article: J Neurosci 41(8), 1665-1683】
16. Isolation of Microglia and Analysis of Protein Expression by Flow Cytometry: Avoiding the Pitfall of Microglia Background Autofluorescence 182
Burns et al. 【Original Research Article: Elife, e57495】
17. Isolation of Nuclei from Mouse Dorsal Root Ganglia for Single-nucleus Genomics 197
Yang et al. 【Original Research Article: Neuron 108(1), 128-144.e9】
18. CRISPR-mediated Labeling of Cells in Chick Embryos Based on Selectively Expressed Genes 205
Yamagata, M. and Sanes, J. R. 【Original Research Article: Elife, e63907】
19. Cell-attached and Whole-cell Patch-clamp Recordings of Dopamine Neurons in the Substantia Nigra Pars Compacta of Mouse Brain Slices 226
Cattaneo et al. 【Original Research Article: Cell Death Dis 11(11), 963】
20. 3D-printed Recoverable Microdrive and Base Plate System for Rodent Electrophysiology .. 241
Vöröslakos et al. 【Original Research Article: Elife, e65859】
21. Cortical Laminar Recording of Multi-unit Response to Distal Forelimb Electrical Stimulation in Rats 268
Latchoumane et al. 【Original Research Article: Sci Adv 7(10), eabe0207】
22. Macroscopic Structural and Connectome Mapping of the Mouse Brain Using Diffusion Magnetic Resonance Imaging 280
Arefin et al. 【Original Research Article: Elife, e58301】
23. Pericyte Mapping in Cerebral Slices with the Far-red Fluorophore TO-PRO-3 293
Mai-Morente et al. 【Original Research Article: J Neurochem 157(4), 1377-1391.】
24. Visual-stimuli Four-arm Maze test to Assess Cognition and Vision in Mice 312
Vit et al. 【Original Research Article: Sci Rep 11(1), 1255】



On the Cover:

Image from protocol **“Generation of Human iPSC-derived Neural Progenitor Cells (NPCs) as Drug Discovery Model for Neurological and Mitochondrial Disorders”**

Optimized Immunostaining of Embryonic and Early Postnatal Mouse Brain Sections

Kawssar Harb^{1,2}, Michele Bertacchi¹ and Michèle Studer^{1,*}

¹Université Côte d'Azur, CNRS, Inserm, iBV, France

²Neuronal Translational Control Group, Center for Molecular Neurobiology (ZMNH), University Medical center Hamburg-Eppendorf (UKE), Falkenried 94, 20251, Hamburg, Germany

*For correspondence: michele.studer@unice.fr

Abstract

The mammalian neocortex, the outer layer of the cerebrum and most recently evolved brain region, is characterized by its unique areal and laminar organization. Distinct cortical layers and areas can be identified by the protein expression of graded transcription factors and molecular determinants that define the identity of different projection neurons. Thus, specific detection and visualization of protein expression is crucial for assessing the identity of neocortical neurons and, more broadly, for understanding early and late developmental mechanisms and function of this complex system. Several immunostaining/immunofluorescence methods exist to detect protein expression. Published protocols vary with regard to subtle details, which may impact the final outcome of the immunofluorescence. Here, we provide a detailed protocol, suitable for both thin cryostat sections and thick vibratome sections, which has successfully worked for a wide range of antibodies directed against key molecular players of neocortical development. Ranging from early technical steps of brains collection down to image analysis and statistics, we include every detail concerning sample inclusion and sectioning, slide storage and optimal antibody dilutions aimed at reducing non-specific background. Routinely used in the lab, our background-optimized immunostaining protocol allows efficient detection of area- and layer- specific molecular determinants of distinct neocortical projection neurons.

Keywords: Mouse brain, Neocortex, Immunofluorescence, Cryostat section, Vibratome section, Protein expression, Imaging

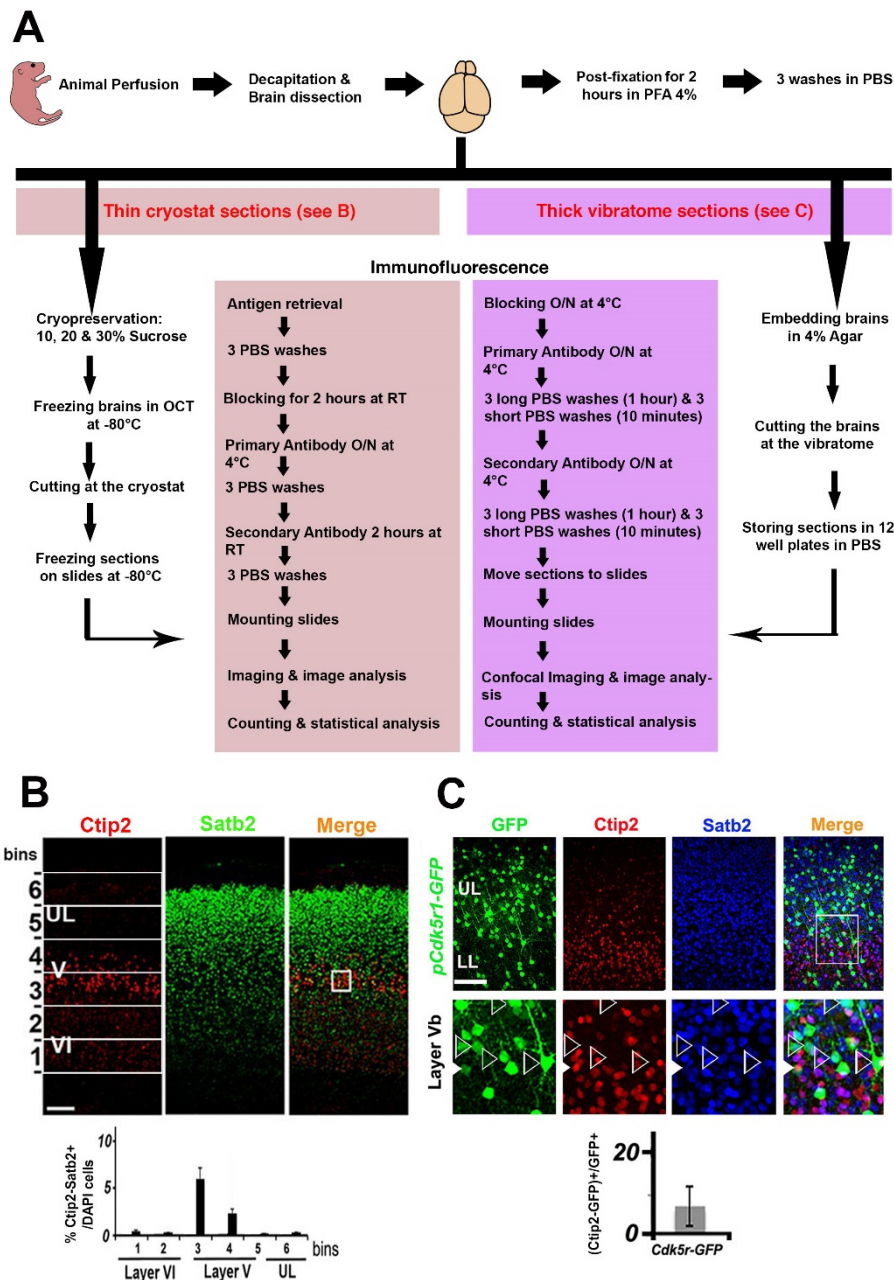
This protocol was validated in: eLife (2016), DOI: 10.7554/eLife.09531

Cite as: Harb, K. *et al.* (2021). Optimized Immunostaining of Embryonic and Early Postnatal Mouse Brain Sections¹. Bio-protocol 11(1): e3868. DOI: 10.21769/BioProtoc.3868.

 Copyright Harb et al.

This article is distributed under the terms of the [Creative Commons Attribution License](#) (CC BY 4.0).

Graphical Abstract:



Workflow chart for the optimized immunostaining protocol of mouse brain sections.

A. A flow chart for different steps of the optimized immunostaining protocol on both thin cryostat and thick vibratome sections. B. Example for immunostaining against Satb2 and Ctip2 on a thin coronal section (20 μ m) at the level of the somatosensory cortex. The first column to the left shows the binning system where 6 bins can be overlaid on the image. On the bottom, an example of counting analysis showing the percentage of marker-positive cells normalized to the total number of DAPI or Hoechst-positive cells. C. Example for immunostaining against Satb2 and Ctip2 on a GFP+ thick vibratome section (200 μ m). Images are taken at low magnification (10 \times , left) and high magnification (40 \times , right). The graph shows a counting of the percentage of Ctip2-positive neurons normalized to the total number of GFP-electroporated neurons on high-magnification images. Images on B and C are modified from Harb *et al.* (2016).

Background

The mammalian neocortex is characterized by its radial subdivision into six distinct neuronal layers. In addition, during embryonic development and with further refinement postnatally, the neocortex gets organized tangentially into distinct primary areas dedicated to the elaboration and analysis of both motor outputs and sensory inputs, a developmental process termed “arealization”. These areas within the neocortex are positioned along the antero-posterior and medio-lateral axes by graded expression of key nuclear transcription factors. The basic neocortical structure of the six layers adapts within each area, as layers are populated with specific neuronal populations, which are defined by the expression of key molecular determinants driving the area-specific acquisition of their identity, morphology and connectivity. Thus, detection of selected protein of interest in neocortical neurons is crucial for investigating the tangential and radial expression of these determinants, which in turn is critical for exploring developmental and functional mechanisms occurring in this complex structure. Widely used in biology labs to determine the tissue and cellular localization of a protein of interest, the immunohistochemistry (or immunofluorescence) is a technical procedure that assesses the presence of a specific protein or antigen by the use of a specific primary antibody, followed by a secondary antibody coupled with a fluorochrome, thus allowing indirect visualisation and examination under a microscope. Many immunostaining protocols are available in literature; however, even subtle changes in the whole procedure can affect the final outcome. Here, we present a protocol that worked in our hands for most of the antibodies aimed at detecting key determinants of neocortical development in thick vibratome or thin cryostat sections. We added exhaustive details regarding all steps, from animal sample collection until image analysis, which can help beginners in the field to easily use the protocol. Optimized for the detection of nuclear determinants in neocortical neurons of embryonic or early postnatal mouse neocortex, the protocol is easily adaptable to a wide variety of biological samples, such as other neural or non-neural tissues.

Materials and Reagents

For animal perfusion:

1. 12-well plates (Falcon, catalog number: 353043)
2. Needles, syringes
 - a. Butterfly needles:
Winged Infusion Set: 25 G 0.50 × 19mm + 30 cm tubing (Braun, catalog number: 4056370)
Winged Infusion Set: 21 G 0.80 × 19mm + 30 cm tubing (Braun, catalog number: 4056337)
 - b. Hypodermic needles:
18 G (Terumo Neolus, catalog number: NN-1838R)
21 G (Terumo Neolus, catalog number: NN-2138R)
25 G (Terumo Neolus, catalog number: NN-2516R)
30 G (BD Microlance 3, catalog number: 304000)
 - c. Syringes without needle:
20 mL (Terumo, catalog number: SS+20ES1)
50 mL (Terumo, catalog number: SS+50ES1)
 - d. Syringes with needle:
U-100 Insulin syringe, 0.5 mL 0.33 mm (29G) (Fisher Scientific, BD Medical, catalog number: 324892)
3. Ketamine
4. Xylazine
5. Paraformaldehyde (PFA) (Sigma-Aldrich, catalog number: P6148-1KG, Lot: MKCD5277)
6. Phosphate Buffer Saline (PBS) (Gibco, catalog number: 14190-094) or homemade PBS (Recipe below)
7. Sodium chloride (VWR, AnalaR Normapur, catalog number: 27810.295)
8. Potassium chloride (Merck Millipore, catalog number: 1.04936.1000)
9. Sodium phosphate dibasic heptahydrate (Sigma-Aldrich, catalog number: S9390-2.5KG)
10. Potassium dihydrogen phosphate (Merck Millipore, catalog number: 1.04873.1000)

11. 4% PFA (see Recipes)
12. 1× PBS (see Recipes)

Tissue sample fixation and washing:

1. 12-well plates (Falcon, catalog number: 353043)
2. Paraformaldehyde (PFA) (Sigma-Aldrich, catalog number: P6148-1KG, Lot #MKCD5277)
3. Phosphate Buffer Saline (PBS) (Gibco, catalog number: 14190-094) or homemade PBS (Recipe below)
4. Sodium Azide (Sigma-Aldrich, catalog number: S8032-100G, Lot #0001453190)
5. 4% PFA (see Recipes)
6. 1× PBS (see Recipes)

Embedding in agar for thick vibratome sections:

1. 12-well plates (Falcon, catalog number: 353043)
2. Select Agar ≥ 99.5% (GC) (Sigma-Aldrich, catalog number: S5054-250G, Lot #MKCB2702V)
3. Phosphate Buffer Saline (PBS) (Gibco, catalog number: 14190-094) or homemade PBS (Recipe below)
4. 4% Agar (see Recipes)

Cryopreservation and Freezing for thin cryostat sections:

1. 6 cm Petri dish
2. Optimal cutting medium (OCT) (Leica Tissue Freezing Medium, catalog number: 14020108926)
3. Dry ice
4. Sucrose (Sigma-Aldrich, catalog number: S9378-1KG, Lot #BCBS5325V)
5. Phosphate Buffer Saline (PBS) (Gibco, catalog number: 14190-094) or homemade PBS (Recipe below)
6. 1× PBS (see Recipes)
7. 10, 20 and 30% sucrose (see Recipes)

Vibratome sectioning (thick sections):

1. 12-well plates (Falcon, catalog number: 353043)
2. Blades (Gillette "Bleue Extra")
3. Phosphate Buffer Saline (PBS) (Gibco, catalog number: 14190-094) or homemade PBS (Recipe below)
4. Glue (Henkel, Loctite superglue-3)
5. 1× PBS (see Recipes)

Immunofluorescence on thick vibratome sections:

1. 12-well plates (Falcon, catalog number: 353043)
2. Slides (Thermo Scientific, Superfrost Plus: J1800AMNZ, Lot #0180)
3. Cover slips (Dia path, catalog number: 061061)
4. Nail polish
5. Phosphate Buffer Saline (PBS) (Gibco, catalog number: 14190-094) or homemade PBS (Recipe below)
6. Goat serum (GS) (Thermo Fisher scientific, Gibco, catalog number: 16210-064, Lot #16711329)
7. Newborn calf serum (NBCS) (Thermo Fisher scientific, Gibco, catalog number: 16010-167)
8. Bovine serum albumin (BSA) (Sigma-Aldrich, catalog number: A-4503 or A7906-50G, Lot #SLBX7550)
9. Triton (Sigma-Aldrich, catalog number: T8787-250ML, Lot #SLBV4122)
10. N-propyl Gallate (Sigma-Aldrich, catalog number: P3130-100G, Lot #SLBD6728V)
11. Glycerol (VWR Chemicals, catalog number: 24388.295, Batch: 14E050030)
12. Hoechst 33342, Trihydrochloride (Invitrogen, catalog number: H3570, Lot #1116437)
13. Primary antibodies, example:
 - a. Nr2f1/COUP-TFI (Abcam, catalog number: ab181137 or R&D, catalog number: H8132)
 - b. Ctip2 (Abcam, catalog number: ab18465)
 - c. Satb2 (Abcam, catalog number: ab51502)
14. Secondary antibodies, Example: Alexa Fluor 488, 555, 594 and 647 anti-mouse or anti-rabbit IgG conjugates

- (Thermo Fisher scientific)
15. Blocking Solution (see Recipes)
 16. Antibody Solution (see Recipes)
 17. Mounting medium (see Recipes)
 18. Antibody Solution for vibratome thick sections (see Recipes)

Cryostat sectioning (thin sections):

1. Slides (Thermo Scientific, Superfrost Plus: J1800AMNZ, Lot #0180)
2. Blades (Thermo Fisher scientific, Edge-Rite: 4280L)
3. Optimal cutting medium (OCT) (Leica Tissue Freezing Medium, 14020108926)

Immunofluorescence on thin cryostat sections:

1. Coverslips (Dia Path, catalog number: 061061)
2. Phosphate Buffer Saline (PBS) (Gibco, catalog number: 14190-094) or homemade PBS (Recipe below)
3. Distilled water
4. Trisodium Citrate Dihydrate (Sigma-Aldrich, catalog number: S1804-1KG, Lot #BCBF5684V)
5. Citric acid (Sigma-Aldrich, catalog number: C-0759, Lot #34H1314)
6. Goat serum (GS) (Thermo Fisher scientific, Gibco, catalog number: 16210-064, Lot #16711329)
7. New-born calf serum (NBCS) (Thermo Fisher scientific, Gibco, catalog number: 16010-167)
8. Triton (Sigma-Aldrich, catalog number: T8787-250ML, Lot #SLBV4122)
9. N-propyl Gallate (Sigma-Aldrich, catalog number: P3130-100G; Lot #SLBD6728V)
10. Glycerol (VWR Chemicals, catalog number: 24388.295; Batch 14E050030)
11. Hoechst 33342, Trihydrochloride (Invitrogen, catalog number: H3570; Lot #1116437)
12. Primary antibodies, example:
 - a. Nr2f1/COUP-TFI (Abcam, catalog number: ab181137 or R&D, catalog number: H8132)
 - b. Ctip2 (Abcam, catalog number: ab18465)
 - c. Satb2 (Abcam, catalog number: ab51502)
 - d. Sox5 (Abcam, catalog number: ab94396)
 - e. GFP (Thermo Fisher scientific, catalog number: A-11122; or: Abcam, catalog number: ab13970)
 - f. Ski (Santa Cruz, catalog number: sc-9140)
 - g. For other antibodies, see “Materials and Methods” in Harb *et al.* (2016).
13. Secondary antibodies, Example: Alexa Fluor 488, 555, 594 and 647 anti-mouse or anti-rabbit IgG conjugates (Thermo Fisher Scientific)
14. Unmasking Solution (see Recipes)
15. Blocking Solution (see Recipes)
16. Antibody Solution (see Recipes)

Equipment

1. Scissors, forceps, dissection and tissue handling tools
 - a. Sharp scissors (Holtex, model: IC12411)
 - b. Fine scissors (Fine Science Tool, catalog number: 14060-11)
 - c. 45° angled tip forceps (Fine Science Tool, model: Dumont #5, catalog number: 11251-35)
 - d. Straight tip forceps (Fine Science Tool, Dumont Mini Forceps – Style 5)
 - e. Double-ended micro spatula (Fine Science Tool, catalog number: 10091-12)
 - f. Perforated spoon (WPI, catalog number: 501997)
2. Microwave
3. Embedding moulds:
Peel-A-Way® embedding moulds (Sigma-Aldrich, catalog number: E6032-1CS)

- Peel-A-Way® Disposable Embedding Moulds (VWR Polysciences, catalog number: 18646A-1)
- 4. Brush
 - 5. Boxes for storage (Dutscher, catalog number: 037516)
 - 6. Glass (Leica, Insert Glass 70 mm, catalog number: 14047742497)
 - 7. Boxes for boiling (Tissue-Tek® Staining Dish, Sakura, catalog number: 4456)
 - 8. Vertical boxes for slides wash (Fisher Scientific, Fisherbrand 5-place slide mailer: HS15986)
 - 9. Shaker (Stuart 3D gyratory rocker, catalog number: SSL3)
 - 10. Horizontal Microscope slide boxes (Kartell Labware, #276 [98 mm × 83 mm], #277 [230 mm × 97 mm] and #278 [230 mm × 180 mm])
 - 11. pH meter (Fisher Scientific, model: accumet AE150)
 - 12. Cryostat (Leica, model: CM3050S)
 - 13. Vibratome (Leica, model: VT1000S)
 - 14. Microscope (Leica, model: DM6000B +CTR6000)
 - 15. Confocal microscope (Zeiss, model: LSM 710, 2012)
 - 16. Water bath (Fisher Scientific, catalog number: Polystat 24, +5L/8662F)

Software

- 1. Adobe Photoshop CS (CS5 Extended, Version 12.0 x32)
- 2. Microsoft Excel (2005 Version)
- 3. GraphPad Prism (Version 7.00)
- 4. Zen software for confocal images (Zen Black, Version 11 SP3 HF88.1.8.484)
- 5. Leica Microsystem CMS GmbH LASX (Version: 3.3.3.16958)

Procedure

A. Mouse Brain Collection and Fixation

- 1. Anesthetize the mouse with an intra-peritoneal injection of Ketamine/Xylazine mix (100 mg/kg Ketamine mixed with 10 mg/kg Xylazine in isotonic saline solution; contact local animal ethical committee for drug use and animal procedures). In our case, all mouse experiments were conducted in accordance with relevant national and international guidelines (European Union rules; 2010/63/UE), and have been approved by the local ethical committee in France (CIEPAL NCE/2014-209 and NCE/2019-548).
- 2. For postnatal/adult mice, perfuse them intracardially with 4% PFA; for embryonic stages, recover embryos on ice-cold PBS from the uterus of the anesthetized mother.
- 3. Decapitate adults/embryos and dissect the brains; for early stage embryos (embryonic age < 15.5 days), brain dissection is not mandatory, but highly recommended to reduce background signal on skin and other tissues surrounding the brain.
- 4. Keep brains in ice-cold PBS in 12-well plates during and after collection.
- 5. Post-fix brains for 2 h in 4% PFA at 4 °C (gentle agitation on shaker).
- 6. Wash the brains 3 times for 10 min each in PBS at 4 °C (on shaker).
- 7. Store brains at 4 °C until further treatment (few days); for long-term storage (few weeks), supplement PBS with 0.05% Sodium Azide.

B. Embedding in Agar for vibratome sectioning (thick sections: 50-200 µm)

- 1. Prepare a solution of 4% agar in PBS.
- 2. Boil in the microwave until homogenization.

3. Keep the 4% agar in a water bath at 50°C.
4. Add 4% agar to a 12-well plate.
5. Remove the brain from PBS with perforated spoon and dry it on a paper towel.
6. Quickly immerge the brain in agar and correctly position it with forceps before agar polymerization.
7. Store the brain at 4°C for short term or immediately proceed with sectioning.

C. Cutting vibratome thick sections

1. Trim the agar surrounding the brain and fix it on the vibratome with glue.
2. Add ice cold PBS to the vibratome and keep it cold by adding ice around the mould for cutting.
3. Cut 50-200 µm thick sections.
4. Use a brush to gently collect the sections from the vibratome before moving them to a 12-well plate; keep the plate on ice-cold PBS.
5. Create series of sections representing the whole cortex or brain by distributing similar sections on subsequent wells.
6. You can add up to 3-4 sections in each well.

D. Immunostaining on vibratome sections (50-200 µm)

1. Remove the PBS by carefully aspirating it with a pipette tip, without touching the sections (repeat for following passages).
2. Incubate the sections in Blocking solution (10% GS, 3% BSA, 0.3% Triton) over-night (O/N) at 4 °C by adding 1 mL for each well.
3. The following day add 500 µL of primary antibodies by diluting them to the appropriate concentration with the antibody solution (3% GS, 3% BSA, 0.3% Triton).
4. Incubate the sections with primary antibodies O/N at 4 °C.
5. The day after, wash the sections 3 times for 1 h each in PBS, followed by 3 short washes for 10 min each in PBS (all washes are performed at room temperature (RT), on shaker).
6. Prepare secondary antibodies by diluting them to 1/500 in the antibody solution (3% GS, 3% BSA, 0.3% Triton).
7. Incubate the sections with 500 µL of diluted secondary antibodies O/N at 4°C by shaking.
8. The following day wash the sections in PBS as described in Step D5.
9. Incubate the sections in 1 µg/mL Hoechst in PBS for 1 h.
10. Carefully move the sections using a brush from the wells to a slide covered with PBS.
11. Aspirate the PBS with a pipette tip and let the sections dry.
12. Add 3 drops of mounting solution (80% glycerol, 2% N-propyl gallate, 1 µg/mL Hoechst) to each slide.
13. Cover the slides with cover slips and seal the edges with nail polish.
14. Leave the nail polish to dry for 5 min at RT.
15. Store the slides until imaging at -20°C.

E. Cryopreservation and Freezing brains for thin sectioning at the cryostat (thin sections: 10-20 µm)

1. Prepare 10%, 20% and 30% sucrose in PBS.
2. Put the brains (dissected and post-fixed as detailed in Procedure A) in 10% sucrose, keep at 4°C with gentle shaking. Wait to equilibrate (usually 8-12 h) until they sink to the bottom of the wells.
3. Repeat Step E2 with sucrose 20% and then 30%. Increasing sucrose concentration in a gradual way is key for preserving optimal histology.
4. Remove all sucrose from the brains by shaking them with a Pasteur pipette in OCT in a 6 cm Petri dish.
5. Transfer the brains in OCT in Peel-A-Way® boxes.

6. Snap freeze them on dry ice.
7. Store them at -80°C until sectioning.

F. Cutting sections at the cryostat (10-20 µm)

1. Equilibrate the brains at -20°C for 30 min at the cryostat.
2. Cut 20 µm thin sections for postnatal brains and 12-16 µm for embryonic brains.
3. During cutting, collect series of sections on cryostat slides.
4. Let the slides dry O/N at RT.
5. Store them at -80°C until use.

G. Immunostaining on cryostat sections

1. Defreeze the sections for 1 h at RT.
2. Put the slides on a vertical slide box for boiling.
3. If your antibody needs unmasking, boil the slides for 15 s in an unmasking solution (0.1 M sodium citrate, pH 6).
4. Boil them a second time for 1 s with fresh unmasking solution (0.1 M sodium citrate, pH 6).
5. Cool the sections on ice for 10 min.
6. Move the slides to a vertical slide box for washing
7. Wash the sections 3 times in PBS for 10 min each at RT (on shaker).
8. Create a humidified chamber by adding water or PBS in a plastic box where the slides can lay horizontally.
9. Lay your slides horizontally and avoid the sections to dry by immediately adding the blocking solution (10% GS, 0.3% Triton in PBS).
10. Block the sections in blocking solution for 1 h at RT by adding 1 mL for each slide.
11. Prepare 200-300 µL of primary antibodies for each slide by diluting them to the appropriate concentration with the antibody solution (3% GS, 0.3% Triton in PBS).
12. Add 200-300 µL of the diluted primary antibodies to the slides and cover them with cover slips to homogeneously distribute the antibody.
13. Incubate the sections with primary antibodies (ON at 4°C).
14. The following day move the slides to the vertical slide box containing PBS.
15. Wash the sections 3 times for 10 min each in PBS at RT while shaking.
16. Prepare 200-300 µL of secondary antibodies per slide by diluting them to 1/300 in the antibody solution (3% GS, 0.3% Triton).
17. Lay the slides horizontally again in the humidified chamber.
18. Add 200-300 µL of the diluted secondary antibodies to the slides and cover them with cover slips to homogeneously distribute the antibody.
19. Incubate the sections for 2 h at RT with diluted secondary antibodies.
20. Move the slides to the vertical slide box containing PBS.
21. Wash the sections 3 times for 10 min each in PBS at RT while shaking.
22. Lay the slides horizontally after taking away extra PBS.
23. Add 3 drops of mounting solution (80% glycerol, 2% N-propyl gallate, 1 µg/mL Hoechst) to each slide.
24. Cover the slides with cover slips and seal the edges with nail polish.
25. Leave the nail polish dry for 5 min at RT.
26. Store the slides at -20°C until imaging.

H. Imaging

1. Take images of your area and layer of interest with the appropriate magnification
 - a. For thin sections:
Acquire plane images with a 10×/20× magnification using a fluorescent optical microscope.

- b. For thick sections: Acquire Z-stack images using a confocal microscope.
Acquire Z-stack images using a confocal microscope.
2. Use low (10x) and high magnification (40x) images of your layer of interest.

Data analysis

A. Data analysis for thin cryostat sections (coronal cutting plane)

1. Process the 1 plane images acquired with 10x/20x magnification using Adobe Photoshop.
2. For quantification of specific markers based on their layer position, use a binning system in Adobe Photoshop by overlaying a grid with 6-8 bins on the neocortical area of interest, from the marginal zone until the glial surface. Six bins are typically used for embryonic or postnatal day (P) 0 brains, while 8 bins can be used from P7.
3. Count the cells expressing the protein of interest using Photoshop counting tool or an automated counting software like ImageJ.
4. Normalize the number of marker-positive cells to the total number of cells (quantified by counting Hoechst⁺ nuclei) in each bin.
5. Count at least 3 sections per animal and use at least 3 animals of each genotype for reliable statistical analysis.
6. To avoid variability occurring between litters, the best option is to use littermate controls to compare the expression of specific genes/proteins of interest in different genetic backgrounds.
7. Use two-tailed Student's *t*-test on Microsoft Excel or on GraphPad Prism for statistical analysis of two independent data groups. For comparing multiple (> 2) groups, use analysis of variance (ANOVA) or other appropriate statistical tests.

B. Data analysis for thick vibratome sections

1. Process the Z-Stack images using the correspondent software of your confocal microscope (for example, Zen lite) and make a maximum intensity projection image.
2. Count the cells expressing the protein of interest and normalize them to the total number of cells or to another marker depending on the purpose.
3. Count at least 3 sections per animal and use at least 3 animals of each genotype for statistical analysis.
4. Use littermate controls to compare the expression of specific genes/proteins of interest in different genetic backgrounds (example: wild-type *versus* knock-out) or after specific treatments, depending on your scientific question.
5. Use two-tailed Student's *t*-test on Microsoft Excel or on GraphPad Prism for statistical analysis of two independent data groups. For comparing multiple (> 2) groups, use analysis of variance (ANOVA) or other appropriate statistical tests.

Notes

1. To minimize subjective bias, sample identity (*e.g.*, genotypes) can be randomized by associating an identification number to each sample before processing.
2. Fixed embryos/brains/sections with clearly damaged tissue must be excluded from any further analysis/processing.
3. Long O/N incubation with Blocking solution BEFORE addition of antibodies, together with long and repeated PBS washes, are crucial for background reduction and signal specificity, as they contribute to mask non-specific epitope sites and to remove excess antibodies, respectively.

4. *Troubleshooting 1:* Poor tissue fixation can result from perfusion with low-quality PFA. Avoid repeated thaw-freeze cycles by freezing PFA aliquots of appropriate volumes, and by using in one-two weeks after thawing.
5. *Troubleshooting 2:* Poor histology commonly results from inefficient tissue dehydration prior OCT embedding. Be sure to cryopreserve with long incubation in increasingly concentrated sucrose solutions (see Steps E1-E3).
6. *Troubleshooting 3:* In our experience, poor adhesion of cryostat tissue sections on glass slides can happen when using expired slides. Always check the expiring date of SuperFrost slides for optimal adhesion.
7. *Troubleshooting 4:* For correct background removal, be sure to use a normal serum from the same species as the one in which the secondary antibody was generated. The use of the incorrect serum can result in non-specific signal.
8. *Tips 1:* Many of the antibodies we used for studying cortical development detect nuclear transcription factors. The easiest way to check for the specificity of the staining, is to check for proper localization of the signal inside the cell nucleus.
9. *Tips 2:* When performing multiple co-staining, use secondary antibodies associated to fluorochromes that do not overlap on the light spectrum. This largely depends on your microscope settings; check technical specifications of your microscope lasers/filters. As an example, we experienced some signal overlap when using Alexa Fluor 594 (Rhodamine) together with Alexa Fluor 647 (Far red/Cy5) on our Leica Microscope; better results (no signal overlap) were obtained by replacing Alexa Fluor 594 with Alexa Fluor 555 (Texas Red).

Recipes

1. 4% PFA

To prepare 1 L of PFA 4%:

- a. Dissolve 40 g of Paraformaldehyde powder (Sigma-Aldrich) in 1x PBS to reach 1 L
- b. Heat while stirring under the chemical hood on a temperature of approximately 60°C
- c. When solution is transparent, let cool down then filter with Whatman paper to remove undissolved particles
- d. Freeze PFA aliquots in 50 ml tubes at -20°C

2. 1× PBS

- a. Add the following chemicals to 1 L of distilled water
8 g Sodium chloride
200 mg Potassium chloride
1.44 g Sodium phosphate dibasic heptahydrate
240 mg Potassium dihydrogen phosphate
- b. Adjust pH to 7.4 with HCl
- c. Autoclave it
- d. Store it at RT

3. Unmasking Solution

- a. Prepare 1 M Trisodium Citrate Dihydrate solution in distilled water (store at 4°C)
- b. Prepare 1 M citric acid solution in distilled water (store at 4°C)

To prepare 1 L of unmasking solution, add 85 mL of sodium citrate 1 M to 800 ml of distilled water.

- a. Measure pH while stirring
- b. Adjust to pH 6 using 1 M citric acid solution
- c. Bring the volume to 1 L with distilled water
- d. Filter your solution
- e. Store it at 4°C

4. Agar 4%

For each brain, you need to use approximately 5 mL of Agar 4% in a 12-well plate, to prepare 100 mL of Agar 4%:

- a. Dissolve 4 g of Select Agar ≥ 99.5% (GC) in 100 mL of PBS
- b. Boil in the microwave to obtain a clear Agar solution with no aggregates
- c. Incubate the agar solution in the water bath at 50°C until mounting all the brains

5. 10, 20 and 30% Sucrose

To prepare 50 mL of sucrose 10, 20 and 30%:

- a. Add respectively 5 g, 10 g and 15 g of sucrose and reach 50 mL with PBS 1×
- b. Vortex the solutions vigorously until fully dissolving the sucrose
- c. Store the solutions at 4°C; for long term storage, freeze them at -20°C

6. Blocking Solution for cryo-sections

50 mL for immunostaining on thin cryo-sections:

- a. Add 5 mL Goat serum or NBCS (in case one of your primary antibody is made in goat)
- b. Add 150 µL of Triton
- c. Reach 50 mL by adding PBS
- d. Vortex until fully homogenizing the solution
- e. Store it at 4°C (for few days)

7. Antibody Solution for thin cryo-sections

50 mL for immunostaining on thin cryo-sections:

- a. Add 3 mL Goat serum (or NBCS, in case one of your primary antibody is made in goat)
- b. Add 150 µL of Triton
- c. Reach 50 mL by adding PBS
- d. Vortex until fully homogenizing the solution
- e. Store it at 4°C (for few days)

8. Blocking Solution for vibratome sections

50 mL for immunostaining on vibratome thick sections:

- a. Add 5 mL Goat serum or NBCS (in case one of your primary antibodies is made in goat or sheep)
- b. Add 150 µL of Triton 100
- c. Add 1.5 g of BSA
- d. Reach 50 mL by adding PBS
- e. Vortex until fully homogenizing the solution
- f. Store it at 4°C (up to two weeks)

9. Antibody Solution for vibratome thick sections

50 mL for immunostaining on vibratome thick sections:

- a. Add 3 mL Goat serum or NBCS (in case one of your primary antibody is made in goat)
- b. Add 150 µL of Triton 100
- c. Add 1.5 g of BSA
- d. Reach 50 mL by adding PBS
- e. Vortex until fully homogenizing the solution
- f. Store it at 4°C (up to two weeks)

10. Mounting medium

For 50 mL

- a. Add 40 mL glycerol
- b. Add 1 g N-propyl gallate

- c. Reach 50 mL with distilled water
- d. Boil in the microwave until homogenizing the solution
- e. Add 5 µL of Hoechst 33342, Trihydrochloride
- f. Store at 4°C covered with aluminium foil to protect from light

Acknowledgments

This work was supported by the “Agence Nationale de la Recherche” under grant reference # ANR-13-BSV4-0011, by the “Fondation Recherche Médicale; Equipe FRM 2011” #DEQ20110421321 and by the “Fondation Jérôme Lejeune” under n° R13098AA to MS and by a postdoctoral fellowship from the city of Nice, France (“Aides Individuelles aux Jeunes Chercheurs”), to MB. KH was funded by a CNRS from Lebanon, AFM fellowship from France and an Alexander Von Humboldt fellowship from Germany. This protocol was elaborated on a previous work published in Harb *et al.* (2016).

Competing interests

The authors declare no competing interests.

Ethics

All animal procedures were conducted in strict accordance with relevant national and international guidelines and regulations (European Union rules; 2010/63/UE; and: Guide for the Care and Use of Laboratory Animals of the French Ministry of Research). All animal experiments were approved by the local ethical committee (CIEPAL registration numbers: NCE/2014-209 and NCE/2019-548). Standard approved housing conditions consisted in a 12 h light-dark cycle and housing with the recommended environmental enrichment (wooden cubes, cotton pad, igloo) with food and water *ad libidum*, three animals per cage max.

References

Harb, K., Magrinelli, E., Nicolas, C. S., Lukianets, N., Frangeul, L., Pietri, M., Sun, T., Sandoz, G., Grammont, F., Jabaudon, D., Studer, M. and Alfano, C. (2016). [Area-specific development of distinct projection neuron subclasses is regulated by postnatal epigenetic modifications](#). *Elife* 5: e09531.

Establishing an Adult Mouse Brain Hippocampal Organotypic Slice Culture System that Allows for Tracing and Pharmacological Manipulation of *ex vivo* Neurogenesis

Steffen Mayerl^{1,2,*} and Charles Ffrench-Constant¹

¹MRC Centre for Regenerative Medicine, University of Edinburgh, Edinburgh, United Kingdom

²University Hospital Essen, Department of Endocrinology, University of Duisburg-Essen, Essen, Germany

*For correspondence: steffen.mayerl@uk-essen.de

Abstract

The function of the hippocampus depends on the process of adult hippocampal neurogenesis which underpins the exceptional neural plasticity of this structure, and is also frequently affected in CNS pathologies. Thus, manipulation of this process represents an important therapeutic goal. To identify potential strategies, organotypic adult brain slices are emerging as a valuable tool. Over the recent years, this methodology has been refined and here we present a combined protocol that brings together these refinements to enable long-term culture of adult hippocampal slices. We employ a sectioning technique that retains essential afferent inputs onto the hippocampus as well as serum-free culture conditions, so allowing an extended culture period. To sustain the neurogenic potential in the slices, we utilize the gliogenesis-inhibitor Indomethacin. Using EdU retention analysis enables us to assess the effects of pharmacological intervention on neurogenesis. With these improvements, we have established an easy and reliable method to study the effects of small molecules/drugs on proliferation and neuron formation *ex vivo* which will facilitate future discovery driven drug screenings.

Keywords: Adult hippocampal neurogenesis, Organotypic adult slice culture, Drug screening, Indomethacin, Thyroid hormone, Mct8

This protocol was validated in: Stem Cell Rep (2020), DOI: 10.1016/j.stemcr.2020.03.014

Background

The hippocampus is a unique region of the brain with a high degree of plasticity as a result of the ongoing neurogenesis in the dentate gyrus throughout life. This process of adult hippocampal neurogenesis starts with the asymmetric division of neural stem cells (NSCs) in the subgranular zone (SGZ) that preserves the stem cell pool and generates progenitor cells poised for neuronal differentiation (Kempermann *et al.*, 2004; Anacker and Hen, 2017; Toda and Gage, 2018). These latter cells go through a well-defined sequence of distinct stages: NSC-generated transiently amplifying progenitor cells divide rapidly and give rise to neuroblasts. Neuroblasts are characterized by their expression of the immature neuronal marker Doublecortin (Dcx). They exit the cell cycle to differentiate into immature post-mitotic neurons that in addition to Dcx transiently express the Calcium-binding protein Calretinin as well as the neuronal marker NeuN. In the final step, these newly generated neurons migrate and integrate functionally into the existing neuronal network as mature granule cell neurons which cease to express Dcx and Calretinin, but maintain NeuN expression.

Adult hippocampal neurogenesis plays a fundamental role in physiological CNS functions such as memory consolidation and cognitive flexibility. Thus, not surprisingly, it is implicated in pathologies like Alzheimer's disease, depression, or schizophrenia (Winner and Winkler, 2015; Anacker and Hen, 2017; Moreno-Jimenez *et al.*, 2019; Park, 2019) and therefore represents an important target for pharmaceutical intervention. However, drug testing is currently often based on cell culture systems that lack the complex architecture and connectivity of the intact brain (Pena, 2010; Humpel, 2015). On the other hand, drug testing in the intact brains of hundreds of animals is not practicable. Organotypic brain slices thus constitute a potential intermediate step as they maintain higher brain cyto-architecture and, as multiple sections can be obtained from one brain, enable comparison of different time points and/or drug concentrations with greatly reduced inter-animal variability. To study the effects of these drugs on neurogenesis, however, a reliable and easy lineage tracing approach is required.

Previously, Kim and colleagues established a protocol to culture adult mouse organotypic hippocampal slices for an extended period of four weeks by employing a serum-free culture medium (Kim *et al.*, 2013). Moreover, they introduced a Hibernate-A based dissection medium as an alternative to more complicated media that required constant gassing with CO₂. However, they were unable to trace the fate of single cells, nor did their slices maintain the essential afferent connection to the entorhinal cortex. Kleine Borgmann and co-workers used a different sectioning approach to overcome the latter problem and employed retrovirus labelling to study lineage progression in the SGZ (Kleine Borgmann *et al.*, 2013). Here, we combined and refined these existing organotypic adult slice culture protocols. Moreover, we established EdU label tracing as a suitable read-out for neurogenesis. To circumvent the problem of a decreased neurogenic efficiency following a prolonged culture period, we utilized the Cyclooxygenase-inhibitor Indomethacin that has been shown before to reduce gliogenesis and exert protective effects on neurogenesis *in vivo* and *ex vivo* (Gerlach *et al.*, 2016; Hain *et al.*, 2018; Melo-Salas *et al.*, 2018). Finally, establishing proof of concept as to the value of this protocol we compared the effects of Silychristin, iopanoic acid, and BCH on neurogenesis. These drugs are small molecular inhibitors of the monocarboxylate transporter 8 (Mct8), deiodinase type 2 (Dio2), and L-type amino acid transporters 1/2 (Lat 1/2) respectively—components of central thyroid hormone signalling. While neither iopanoic acid nor BCH treatment altered *ex vivo* neurogenesis, the number of new neurons was significantly reduced in Silychristin-treated cultures (Mayerl *et al.*, 2020).

Taken together, these improvements enabled us to establish a method that allows for i) an extended culture period of adult brain slices for at least three weeks with good neurogenic efficiency, ii) easy lineage tracing using EdU that also provides a defined and controlled starting point, and iii) pharmacological manipulation of *ex vivo* hippocampal neurogenesis. We believe that our advanced methodology will be useful for future drug screening approaches to sustain or improve hippocampal neurogenesis in various pathological conditions or physiological alterations such as ageing.

Materials and Reagents

1. 10 cm Petri dish (Thermo Fisher Scientific, Corning, catalog number: BP94A01)
2. 6-well-plate (Corning, catalog number: 3516)
3. 12-well-plate (Corning, catalog number: 3513)
4. Tin foil
5. Microscope slides SuperFrost PlusTM (Thermo Fisher Scientific, catalog number: 10149870)
6. Coverslips (*e.g.*, 24 × 50 mm) (Thermo Scientific Menzel x1000 Coverslip 24 × 50 mm #1, catalog number: 15737592)
7. Peel-A-Way[®] 22 × 40 mm × 20 mm deep, rectangular embedding molds (Ted Pella, catalog number: 27114)
8. Millicell Cell Culture Insert, 30 mm, hydrophilic PTFE, 0.4 µm pore size (Merck, catalog number: PICMORG50), shelf storage
9. Mice (*e.g.*, C57/Bl6N)
10. EdU (5-ethynyl-2-deoxyuridine) (Thermo Fisher Scientific, InvitrogenTM, catalog number: A10044 (50 mg), stored in 500 µl aliquots at -20°C)
11. HibernateTM-A Medium (Thermo Fisher Scientific, GibcoTM, catalog number: A1247501), stored at 4°C for a maximum of 4 months
12. B-27TM supplement (50×) (Thermo Fisher Scientific, GibcoTM, catalog number: 17504001), aliquots stored at -20°C, after defrosting stored at 4 °C for a maximum of 1 month
13. Agarose, low melting point (Merck, Calbiochem, catalog number: 2070-100GM). 4% solution in PBS can be stored on shelf for up to 6 months and re-used 3-4×
14. NeurobasalTM-A Medium (Thermo Fisher Scientific, GibcoTM, catalog number: 10888022), stored at 4°C for a maximum of 4 months
15. Indomethacin (Merck, Sigma-Aldrich, catalog number: I7378-5G), stored at 4°C as stock solution of 100 mM in DMSO for a maximum of 4 months
16. Silychristin (Merck, Sigma-Aldrich, catalog number: 51681-10MG), stored at 4°C as a stock solution of 100 mM in DMSO for a maximum of 4 months
17. Iopanoic acid (Merck, Sigma-Aldrich, catalog number: I0330000), stored at 4°C as a stock solution of 100 mM in DMSO for a maximum of 4 months
18. BCH (R&D Systems, catalog number: 5027/50), stored at 4 °C as a stock solution of 100 mM in Neurobasal A for a maximum of 4 months
19. Formaldehyde 37% (Merck, Sigma-Aldrich, catalog number: 252549-500ML), stored in a ventilated fume hood
20. Click-iT[®] EdU Alexa Fluor[®] 647 Imaging Kit (Thermo Fisher Scientific, Molecular Probes, catalog number: C10340), components diluted and stored according to manufacturer's instructions
21. Rabbit-anti-Ki67 antibody (Abcam, catalog number: ab16667), aliquots stored at -20°C
22. Guinea pig-anti-Doublecortin (Dcx) antibody (Merck, Millipore, catalog number: ab2253), aliquots stored at -20°C
23. Mouse-anti-NeuN antibody (Merck, Millipore, catalog number: mab377), stored at 4°C
24. Fluoromount-G[®] (Southern Biotech, catalog number: 0100-01), stored at room temperature
25. Super glue
26. Triton X-100 (Merck, Sigma-Aldrich, catalog number: X100-1L), stored at room temperature
27. Glycine (Merck, Sigma-Aldrich, catalog number: G7126-1KG), stored at room temperature
28. 10× PBS (Thermo Fisher Scientific, Life Technologies, catalog number: 70011-036 500ml), stored at room temperature; dilute with distilled water
29. BSA (Merck, Sigma-Aldrich, catalog number: A7906-50G), stored at 4°C
30. Goat serum (Merck, Sigma-Aldrich, catalog number: G6767-100ML), stored at -20°C
31. Hoechst33258 (Thermo Fisher Scientific, Life Technologies, catalog number: 62249 5ML), stored at 4°C
32. L-Glutamine (Invitrogen, catalog number: 25030-024), aliquots stored at -20°C
33. Penicillin/Streptomycin (10,000 U/ml Pen; 10,000 µg/ml Strep; Invitrogen, catalog number: 15140-122), aliquots stored at -20°C
34. DMSO (Thermo Fisher Scientific, catalog number: D12345 3ML), stored at room temperature
35. 7 mL tubes (Sarstedt, Tube 7ml 47x20PC+Cap, catalog number: 71.9923.610), stored at room temperature

Cite as: Mayerl, S. and Ffrench-Constant, C. (2021). Establishing an Adult Mouse Brain Hippocampal Organotypic Slice Culture System that Allows for Tracing and Pharmacological Manipulation of ex vivo Neurogenesis. Bio-protocol 11(1): e3869. DOI: 10.21769/BioProtoc.3869.

15

36. Dissection buffer (see Recipes)
37. Serum-free slice culture medium (see Recipes)

Equipment

1. Pipettes
2. Brush
3. Spatula (Thermo Fisher Scientific, FisherbrandTM Nickel Chattaway Spatula, catalog number: 11583462)
4. Scalpel (disposable scalpel, Swann Morton No. 11, Medisave, catalog number: SKU0503)
5. Tissue culture hood
6. Water bath
7. Forceps (Fine Science Tools, Dumont #5 Forceps Standard Carbon, catalog number: 11251-10)
8. Scissors (Fine Science Tools, Fine Scissors, Sharp, catalog number: 14060-10)
9. Rocker
10. Confocal microscope (Leica SP8)
11. Vibratome (Leica VT1000 S)

Software

1. ImageJ (NIH, <https://imagej.nih.gov/ij/>)

Procedure

A. Preparation of slices

1. For EdU label tracing studies, inject a 6-8-week old C57/Bl6N mouse i.p. with 100 µL EdU (10 mg/mL). To increase number of labeled cells, we injected EdU twice: 4 h and 2 h before sacrifice.
2. Prepare 4% low melting agarose in 1x PBS and keep it in a water bath at 37°C until use.
3. Sacrifice the animal by exposing it to rising concentrations of CO₂.
4. Isolate brain rapidly and transfer it into 2 mL serum-free dissection buffer (Kim *et al.*, 2013) in a 7 mL tube on ice. Allow brain to equilibrate for at least 5 min.
5. Prepare for sectioning (Figure 1A): Transfer brain into a 10 cm Petri dish (Figure 1B), remove cerebellum and brainstem with a scalpel (Figure 1C) and cut along the midline of the brain (Figure 1D). According to the instructions provided in Kleine Borgmann *et al.* (2013) place hemispheres on the cut surface (Figure 1E) and remove a small part of the cerebral cortex cutting from dorsolateral to ventromedial at an angle of approximately 70° (Figures 1F, 1G). Flip the hemispheres onto these new cut surfaces and place them into an embedding mold on ice. Gently fill the mold with 4% low melting agarose and wait till it solidifies (Figure 1H). Trim the agarose block using a scalpel and glue it onto a vibratome tissue platform using super glue (Figure 1I). Hemispheres can be embedded, glued and cut separately or in parallel. We obtained the best results by cutting them in parallel oriented in a lateral-to-medial direction (*i.e.*, the lateral part facing the vibratome and being cut first).
6. Transfer platform into the vibratome tissue container filled with chilled dissection buffer. To keep the temperature low, cover the container with ice (if possible) or store it on ice if not in use.
7. Cut 300 µm thick sections using high frequency (level 7-8) and low speed (level 1-2).
8. Carefully transfer sections containing the hippocampus into a 10 cm Petri dish containing 4-5 mL dissection buffer on ice using a brush and spatula (Figure 1J). Note examples of a well cut section with preserved brain cyto-architecture (Figure 1K) and a badly sectioned slice (Figure 1L). We did not trim the

sections as we did not find any discernable difference in long term viability between trimming them so that they only contain the hippocampus and entorhinal cortex or culturing the entire sections.

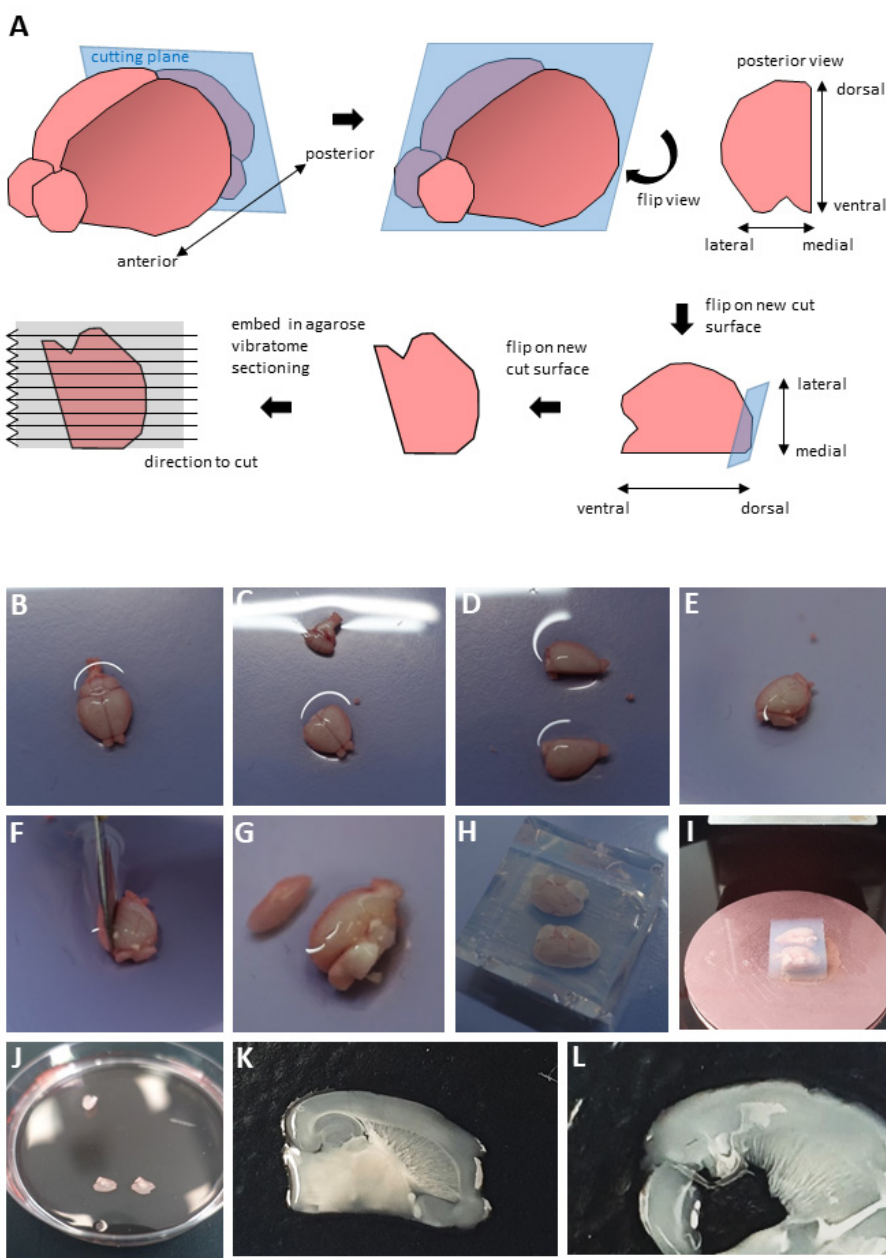


Figure 1. Dissection procedure.

(A) Schematic representation of brain sectioning. Panels B-L show photographs of the key steps, as follows. Place the brain in a Petri dish (B). Having cut away cerebellum and brainstem (C), bisect brain along the midline (D). Place hemispheres onto the new cut surfaces (E) and cut off a small part of the cerebral cortex in a dorsolateral to ventromedial direction at an angle of 70° (F). Flip onto the newest cut surface (G), embed in 4% low melting agarose (H), glue the block onto a tissue platform (I) and section hemispheres using a vibratome. Collect slices in a 10 cm Petri dish (J). Representative pictures of a well-cut slice suitable for culturing (K) and of a badly cut slice (L).

B. Slice culture

1. Before sacrificing the animal, place the required amount of Millicell inserts into 6-well-plate wells.
2. Prepare stock solutions. Dissolve Indomethacin in DMSO to obtain a 100 mM stock solution. Dissolve drugs in DMSO or medium.
3. Add 1 mL serum-free culture medium (Kim *et al.*, 2013) containing Indomethacin and inhibitor (or solvent control) per well. Work in a tissue culture hood. Equilibrate at 37°C and 5% CO₂ for one to two hours in a standard cell culture incubator.
4. Add a small drop of culture medium (approx. 50 µL) from the well onto the insert using a standard 200 µL pipette to facilitate transfer of the sections. Using a brush and spatula transfer the vibratome sections from chilled dissection medium onto the Millicell inserts so that they are at the air/liquid-interface. Culture 2-3 sections per insert at 37°C and 5% CO₂.
5. On the next day, remove the culture medium containing inhibitors or solvent control completely using a 1 mL pipette. Keep the insert in the well and carefully raise it on one side using a pipette tip or forceps to allow for the removal of residual medium. Replace immediately with 1 mL of fresh medium (containing inhibitors) carefully pipetted into the well so that the sections on the insert are once again at the air/liquid interface. Repeat every other day.

C. Fixation

1. Fix slices by removing the culture medium and adding 1 mL 3.7% formaldehyde in PBS into the well and an additional 1 mL carefully on top of the slices. Fix for 1 h at ambient temperature.
2. Wash slices 3 × 20 min in PBS.
3. Store the fixed slices in PBS at 4°C or proceed with immuno-histochemistry.

Note: Slices may detach from the membrane during fixation. This does not affect further steps.

D. Immuno-histochemistry

1. Use forceps, scissors or a scalpel to cut the Millicell insert membrane from the plastic ring.
2. For EdU detection, transfer all slices from the same animal and condition (on the membrane or free-floating) into a 12-well-plate well and permeabilize them in PBS containing 0.1% Triton X100/0.1 M glycine. Block slices for 2 h in PBS containing 3% BSA. Incubate slices with 300 µL Click-iT reaction cocktail prepared according to the manufacturer's instructions (Thermo Fisher Scientific Click-iT® EdU Alexa Fluor® 647 Imaging Kit, chapter EdU detection) at room temperature on a rocker for 3 h. For this and all subsequent steps protect the plate from light (*e.g.*, by covering it with tin foil).
3. Block slices in 10% normal goat serum in PBS containing 0.5% Triton X100 overnight at 4°C.
4. Prepare primary antibodies in blocking buffer (400 µL per well). Incubate slices at 4°C on a rocker for 48 h. In our experiments, we used rabbit-anti Ki67 (1:250) to visualize proliferating cells, mouse-anti-NeuN (1:300) as a marker for neurons, and guinea pig-anti Dcx (1:300) to label neuroblasts and immature neurons
5. Wash slices 3 × 1 h in PBS.
6. Incubate slices with secondary antibodies (1:500 in blocking buffer) on a rocker at 4°C over night.
7. Remove secondary antibodies, add 400 µL Hoechst33258 (in water; 5 µg/mL) per well and incubate for 30 min.
8. Wash slices 3 × 1 h in PBS.
9. Using forceps, transfer membranes (slices facing upwards) onto microscope slides or, in case of detached slices, use a brush and spatula.
10. Place the slices in the center of the slide. Add 200 µL Fluoromount-G onto the slices and gently apply a coverslip (*e.g.*, 24 × 50 mm). Be careful not to squeeze the slices as they are extremely thick. Dry at 4°C.

E. Imaging

Image slices using a confocal microscope. We employed a Leica SP8 confocal microscope and a 20x objective and imaged a 30-50 μm thick stack in the middle of the 300 μm thick slice.

Data analysis

For data analysis, use the freely available software ImageJ/Fiji. Enumerate marker positive cells (Ki67, Dcx, EdU, NeuN) in the SGZ in one picture every 10 μm from the z-stack taken and normalize these numbers to the length of the SGZ (measured using ImageJ's segmented line tool) for quantification (Figure 2). For nuclear markers (Ki67, EdU, NeuN), ascertain that there is a clear overlay with Hoechst33258 staining. Average results from all slices that were obtained from the same animal and cultured under the same condition. In our studies, we quantified EdU incorporation into different cell populations at different time points and then determined statistical significance by unpaired two-tailed Student's *t*-test using slices from 4-6 animals per time point and condition. Depending on the focus of the analysis, one-way or two-way ANOVA may be required, *e.g.*, for longitudinal analysis of the same parameter such as proliferative capacity. To view our results, see Mayerl *et al.* (2020).



Figure 2. Quantification of results.

Marker single or double positive cells along the SGZ were enumerated (arrows). Length of the SGZ was measured using ImageJ's segmented line tool (dotted line). Quotients of positive cell numbers over length were calculated. (scale bar = 100 μm)

Notes

1. Note that sacrificing the animal by overexposure to CO₂ can be accompanied by a reduction in brain tissue pH and increase in tissue stiffness (Holtzmann *et al.*, 2016). Whether this change in stiffness alters the quality of the sectioning process in comparison to standard methods of euthanasia such as cervical dislocation or decapitation has not been investigated and may be determined individually.
2. While extracting the brain from the skull be careful not to cut into the brain tissue. Smaller, superficial cuts do not compromise the procedure, but larger incisions will result in cutting problems and ultimately lead to fractured and unsuitable slices. If the latter happens, do not proceed. Likewise, when preparing brain hemispheres for sectioning, take care not to pierce the tissue while trying to hold it in place with forceps. Better to use a blunt spatula to fix the tissue for cutting with the scalpel. When removing a small part of the cortex at a 70° angle you should be able to perceive a small strip of white matter in the removed part (see Figure 1G). In a few cases, brain hemispheres may not be cut as desired and the slices may be damaged (for comparison see Figures 1K and 1L). Problems can include ripped, fractured sections, severing of the hippocampus-cortex

connection and visibly unequal thickness over the slice. The latter is common if agarose penetrates underneath a hemisphere while solidifying. As a result, brain tissue will not be glued to the vibratome tissue platform and is free to move if pressure from the blade is applied. If problems occur during cutting our experience is that trouble-shooting possibilities are very limited. We recommend repeating the procedure with another animal instead of using damaged slices.

3. One of the major points that needs considering is the thickness of the slices that—unlike neonatal slices—do not noticeably flatten over the culture period. Thus, the slices produce a pronounced background fluorescent intensity which will be a problem for some antibodies. In our hands, well-established, highly specific antibodies worked reliably, while other less specific antibodies did not give staining that could be used for quantifications or did not work at all. Moreover, we usually imaged on the day after mounting. Delayed imaging, however, may lead to the formation of air-filled gaps in the mounting medium that may dry out the sections. Thus, for longer storage before imaging sealing the coverslip *e.g.* with nail varnish constitutes a feasible option though we never further explored this possibility.
4. We never investigated whether the first block step (3% BSA in PBS) is sufficient and the second block step using 10% goat serum can be skipped. This likely depends on the performance of the antibodies employed.
5. Moreover, the protocol conditions are optimized for adult stem cells and neurons (hence using Hibernate A, Neurobasal A and Indomethacin) while they might be less efficient in keeping glia cells alive. Therefore, we do not recommend this protocol for the analysis of glia cells unless the culture conditions are further optimized.

Recipes

Following buffer recipes are based on Kim *et al.* (2013):

1. Dissection buffer (100 mL)

96 mL Hibernate A
2 mL B-27™ supplement (50x)
1 mL 200 mM L-Glutamine
1 mL Penicillin/Streptomycin

2. Serum-free slice culture medium (100 mL)

96 mL Neurobasal A
2 mL B-27TM supplement (50x)
1 mL 200 mM L-Glutamine
1 mL Penicillin/Streptomycin
80 µL 100 mM Indomethacin

Acknowledgments

This work was supported by a grant from the DFG to SM (MA7212/ 2-1), by a Wellcome Trust Senior Investigator award (104783/Z/14/Z) and funding from the BBSRC (BB/L00402X/1) to CffC. We thank SCRM animal facility staff (Luke McPhee, Chris Wilson, Lorraine McNeil, John Agnew, and Jamie Kelly) and SCRM imaging facility staff (Bertrand Vernay) for their excellent help. The protocol was first published in our original research paper “Hippocampal Neurogenesis Requires Cell-Autonomous Thyroid Hormone Signaling” in Stem Cell Reports (Mayerl *et al.*, 2020).

Competing interests

The authors declare that no conflict of interests exists.

Ethics

All studies were executed under Project Licence PPL 70/8748, valid from 6 Dec 2015 to 5 Dec 2020, in compliance with UK Home Office regulations and local guidelines by The University of Edinburgh.

References

- Anacker, C. and Hen, R. (2017). [Adult hippocampal neurogenesis and cognitive flexibility - linking memory and mood](#). *Nat Rev Neurosci* 18(6): 335-346.
- Gerlach, J., Donkels, C., Münzner, G. and Haas, C. A. (2016). [Persistent gliosis interferes with neurogenesis in organotypic hippocampal slice cultures](#). *Front Cell Neurosci* 10: 131.
- Hain, E. G., Sparenberg, M., Rasinska, J., Klein, C., Akyuz, L. and Steiner, B. (2018). [Indomethacin promotes survival of new neurons in the adult murine hippocampus accompanied by anti-inflammatory effects following MPTP-induced dopamine depletion](#). *J Neuroinflammation* 15(1): 162.
- Holtzmann, K., Gautier, H. O. B., Christ, A. F., Guck, J., Káradóttir, R. T., and Franze, K. (2016). [Brain tissue stiffness is a sensitive marker for acidosis](#). *J Neurosci Methods* 271: 50-54.
- Humpel, C. (2015). [Organotypic brain slice cultures: A review](#). *Neuroscience* 305: 86-98.
- Kempermann, G., Jessberger, S., Steiner, B. and Kronenberg, G. (2004). [Milestones of neuronal development in the adult hippocampus](#). *Trends Neurosci* 27(8): 447-452.
- Kim, H., Kim, E., Park, M., Lee, E. and Namkoong, K. (2013). [Organotypic hippocampal slice culture from the adult mouse brain: a versatile tool for translational neuropsychopharmacology](#). *Prog Neuropsychopharmacol Biol Psychiatry* 41: 36-43.
- Kleine Borgmann, F. B., Bracko, O. and Jessberger, S. (2013). [Imaging neurite development of adult-born granule cells](#). *Development* 140(13): 2823-2827.
- Mayerl, S., Heuer, H. and ffrench-Constant, C. (2020). [Hippocampal neurogenesis requires cell-autonomous thyroid hormone signaling](#). *Stem Cell Reports* 14(5): 845-860.
- Melo-Salas, M. S., Perez-Dominguez, M. and Zepeda, A. (2018). [Systemic inflammation Impairs proliferation of hippocampal type 2 intermediate precursor cells](#). *Cell Mol Neurobiol* 38(8): 1517-1528.
- Moreno-Jimenez, E. P., Flor-Garcia, M., Terreros-Roncal, J., Rabano, A., Cafini, F., Pallas-Bazarría, N., Avila, J. and Llorens-Martin, M. (2019). [Adult hippocampal neurogenesis is abundant in neurologically healthy subjects and drops sharply in patients with Alzheimer's disease](#). *Nat Med* 25(4): 554-560.
- Park, S. C. (2019). [Neurogenesis and antidepressant action](#). *Cell Tissue Res* 377(1): 95-106.
- Pena, F. (2010). [Organotypic cultures as tool to test long-term effects of chemicals on the nervous system](#). *Curr Med Chem* 17(10): 987-1001.
- Toda, T. and Gage, F. H. (2018). [Review: adult neurogenesis contributes to hippocampal plasticity](#). *Cell Tissue Res* 373(3): 693-709.
- Winner, B. and Winkler, J. (2015). [Adult neurogenesis in neurodegenerative diseases](#). *Cold Spring Harb Perspect Biol* 7(4): a021287.

A Parkinson's Disease-relevant Mitochondrial and Neuronal Morphology High-throughput Screening Assay in LUHMES Cells

Tom Leah, Irina Vazquez-Villaseñor, Laura Ferraiuolo, Stephen B Wharton and Heather Mortiboys*

Sheffield Institute for Translational Neuroscience, University of Sheffield, Sheffield, UK

*For correspondence: H.Mortiboys@sheffield.ac.uk

Abstract

Parkinson's disease is a devastating neurodegenerative disorder affecting 2-3% of the population over 65 years of age. There is currently no disease-modifying treatment. One of the predominant pathological features of Parkinson's disease is mitochondrial dysfunction, and much work has aimed to identify therapeutic compounds which can restore the disrupted mitochondrial physiology. However, modelling mitochondrial dysfunction in a disease-relevant model, suitable for screening large compound libraries for ameliorative effects, represents a considerable challenge. Primary patient derived cells, SHSY-5Y cells and *in vivo* models of Parkinson's disease have been utilized extensively to study the contribution of mitochondrial dysfunction in Parkinson's. Indeed many studies have utilized LUHMES cells to study Parkinson's disease, however LUHMES cells have not been used as a compound screening model for PD-associated mitochondrial dysfunction previously, despite possessing several advantages compared to other frequently used models, such as rapid differentiation and high uniformity (*e.g.*, in contrast to iPSC-derived neurons), and relevant physiology as human mesencephalic tissue capable of differentiating into dopaminergic-like neurons that highly express characteristic markers. After previously generating GFP⁺-LUHMES cells to model metabolic dysfunction, we report this protocol using GFP⁺-LUHMES cells for high-throughput compound screening in a restoration model of PD-associated mitochondrial dysfunction. This protocol describes the use of a robust and reproducible toxin-induced GFP⁺-LUHMES cell model for high throughput compound screening by assessing a range of mitochondrial and neuronal morphological parameters. We also provide detailed instructions for data and statistical analysis, including example calculations of Z'-score to assess statistical effect size across independent experiments.

Keywords: Parkinson's disease, Mitochondria, Compound screening, LUHMES

This protocol was validated in: Neuroscience (2018), DOI: 10.1016/j.neuroscience.2018.07.029

Background

Parkinson's disease (PD) is a neurodegenerative disorder characterised primarily by loss of dopaminergic neurons in the substantia nigra of the midbrain and the accumulation of α -synuclein in intra-neuronal inclusions. It is the second most common neurodegenerative disorder affecting 2-3% of the population over 65 years of age (Poewe *et al.*, 2017). Patients present with resting tremors, bradykinesia and muscle rigidity, along with non-motor symptoms which can include depression, anosmia and memory problems. There is currently no disease-modifying treatment that can prevent or slow the progression of PD, presenting an urgent need for an effective therapeutic (Armstrong and Okun, 2020).

Mitochondrial dysfunction is a key pathological hallmark of PD; many of the genetic loci associated with familial PD encode proteins that are involved in mitochondrial function or regulation (Hauser and Hastings, 2013). A variety of mitochondrial pathways are disturbed in PD pathology including ATP production, mitophagy, trafficking, biogenesis and calcium buffering (Park *et al.*, 2018). It is therefore unsurprising that mitochondrial dysfunction is a popular target for therapeutic discovery in PD, which aims to identify compounds capable of enhancing those mitochondrial pathways disturbed in the disease state back towards normal physiological levels. This presents the challenge of finding an effective method to model mitochondrial dysfunction *in vitro* whereby large compound libraries can be screened efficiently within a disease-relevant model.

We have previously reported the use of primary patient fibroblasts to screen for compounds which rescue mitochondrial phenotypes seen in those fibroblasts (Mortiboys *et al.*, 2013). Furthermore, recently a patient derived iPSC neuron model using a high-throughput, semi-automatic, imaging system was described to identify compounds which ameliorate mitochondrial clearance deficits (Yamaguchi *et al.*, 2020). Both of these systems utilize patient derived cells, one potential issue when using patient derived models is the amount of material required and uniformity of sample. An alternative approach is the use of Lund human mesencephalic (LUHMES) cells. LUHMES cells are a subclone of the MESC2.10 cell line, derived from human embryonic ventral mesencephalic tissue and immortalised by integration of a *v-myc* retroviral factor which is tetracycline regulatable (Lotharius *et al.*, 2002 and 2005). Briefly, LUHMES cells exist in a proliferative state until the addition of tetracycline, dibutyryl cyclic AMP (dCAMP) and glial cell derived neurotrophic factor (GDNF) which halts proliferation and induces uniform differentiation into a dopaminergic-like phenotype. As PD predominantly affects the dopaminergic neurons of the substantia nigra, the differentiated LUHMES cell phenotype is highly physiologically relevant as a model. Further characterisation has demonstrated that differentiated LUHMES cells resemble primary neuron cultures in many aspects: broad upregulation of neuronal markers, extensive neurite outgrowth and basic electrophysiological features (Scholz *et al.*, 2011). Unlike many other transformed neuronal cell lines, LUHMES cells in the differentiated state have *c-myc* switched off and no dysregulation of the cell cycle is seen. This is particularly important when considering cell cycle mechanisms involved in neuronal DNA repair and neurodegeneration modelling. LUHMES cells are candidates for use in high-throughput screening due to their ease of handling, uniformity and high purity following differentiation induction (> 99%) compared to the often capricious and phenotypically variable culturing of primary neurons (Scholz *et al.*, 2011). A comparative study also showed LUHMES cells express higher levels of neuronal markers (*TUBB3*, *ENO2*, *MAP2*) and have increased neurotoxicant sensitivity compared to two other commonly used neuronal models, SH-SY5Y neuroblastoma cells and human foetal neural stem cells (Tong *et al.*, 2017).

LUHMES cells have been used extensively in high-throughput screening for the identification of neurotoxicants (Stiegler *et al.*, 2011; Krug *et al.*, 2013), including one specific to mitochondrial toxicity (Delp *et al.*, 2019). However, we have only found one study to date that has exploited the high-throughput potential of LUHMES cells in PD therapeutic discovery. Höllerhage *et al.* used a previously developed alpha-synuclein LUHMES model to screen 1,600 FDA-approved drugs for protective effects by measuring cell viability after treatment (Höllerhage *et al.*, 2017). Previously, we reported the generation of GFP⁺-LUHMES and the use of them to model metabolic dysfunction in co-culture with astrocytes (Ratcliffe *et al.*, 2018).

Here we utilise the GFP⁺-LUHMES which we previously generated and validated as a useful model for metabolic dysfunction, to present a detailed and reproducible protocol for high-throughput screening of compounds in a toxin-induced differentiated LUHMES cell model relevant to PD. This protocol improves on previous studies by using high-content live cell imaging and analysis to assess mitochondrial parameters and neuronal morphology.

In the approach described here, differentiated LUHMES cells are treated with rotenone to model PD-associated mitochondrial dysfunction and neuronal loss in accordance with previous studies (Krug *et al.*, 2013; Dolga *et al.*, 2014). LUHMES cells are grown to full confluence before the addition of differentiation factors, and then replated into 384-well plates after two days. The cells remain in differentiation media for the full time course of the experiment. The plate is treated with rotenone on the fifth day, then treated with test compounds on the sixth day and live imaged on the seventh day (Figure 1). When designing a toxin induced model for screening, there are generally two paradigms. The first being a protection model, where the potential beneficial compound is added to the cells before the toxin. Secondly, and is the case in this protocol, is a restoration model; where the toxin is added first and then the potential beneficial compounds are added afterwards. This is testing the beneficial compounds to restore a defect already present as opposed to protecting from damage occurring. The advantage of this technique lies in the relative ease and speed in generating a uniform population of disease-relevant human dopaminergic neurons that can be used for large-scale compound screening. Furthermore, high-content live cell imaging and analysis allows the assessment of compound dose-response effects on a broad range of mitochondrial and neuronal morphological parameters.

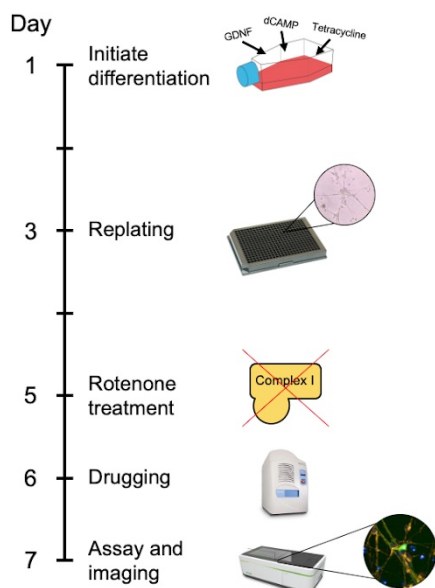


Figure 1. Timeline of the GFP-LUHMES drug screening protocol

Materials and Reagents

1. 384-well black plates (Greiner-Bio, catalog number: 781091)
2. 384-well LDV source plates (Labcyte, catalog number: LP-0200)
3. 384-well source plate seals (Fluidix, catalog number: 41-1011)
4. 5 mL serological pipettes (Fisher Scientific, catalog number: 13-676-10H)
5. 10 mL serological pipettes (Fisher Scientific, catalog number: 13-676-10J)
6. 25 mL serological pipettes (Fisher Scientific, catalog number: 13-678-11)
7. 10 µL pipette tips (Fisher Scientific, catalog number: 02-707-441)
8. 200 µL pipette tips (Fisher Scientific, catalog number: 02-707-422)
9. 1,000 µL pipette tips (Fisher Scientific, catalog number: 02-707-402)
10. 15 mL Falcon tubes (Greiner-Bio, catalog number: 188271)
11. 50 mL Falcon tubes (Greiner-Bio, catalog number: 227261)
12. T75 flasks (Greiner-Bio, catalog number: 658175)

13. Cryovials (Greiner-Bio, catalog number: 122261)
14. LUHMES cells (ATCC® CRL-2927™)
15. GFP-LUHMES cells (RRID: CVCL_B056, Ratcliffe *et al.*, 2018)
16. GFP-expressing lentiviral particles
17. Advanced DMEM/F-12 (Thermo Scientific, catalog number: 12634010)
18. Fibronectin (Sigma-Aldrich, catalog number: FC010)
19. Poly-L-Ornithine (Sigma-Aldrich, catalog number: P4957)
20. PBS Tablets (Thermo Scientific, catalog number: BR0014G)
21. Trypsin 10× (Lonza, catalog number: BE02-007E)
22. L-Glutamine (Lonza, catalog number: BE-17-605E)
23. N-2 Supplement (Gibco, catalog number: 11520536)
24. Pen-Strep (Lonza, catalog number: DE17-603E)
25. FGF-basic (Peprotec, catalog number: 100-18B)
26. dCAMP (Sigma-Aldrich, catalog number: D0627)
27. GDNF (Peprotech, catalog number: 450-10)
28. Tetracycline (Sigma-Aldrich, catalog number: T7660)
29. Hoechst (Sigma, catalog number: 94403)
30. TMRM (Invitrogen, catalog number: T668)
31. Sterile 1× PBS (see Recipes)
32. Sterile 1× Trypsin (see Recipes)
33. LUHMES Base Media (see Recipes)
 - Advanced DMEM/F-12
 - N-2 Supplement
 - Pen-Strep
 - L-Glutamine
34. LUHMES Proliferation Media (see Recipes)
 - LUHMES Base Media
 - FGF-basic
 - LUHMES Differentiation Media
 - Tetracycline
 - dCAMP
 - GDNF

Equipment

1. Mechanical pipette gun for serological pipettes
2. Mechanical pipettes (P20, P200, P1000)
3. Multichannel mechanical pipettes (P10, P200)
4. 4°C fridge
5. -20°C freezer
6. -80°C freezer
7. Sterile tissue culture hood
8. Autoclave
9. Centrifuge for tissue culture (MSE Harrier 15/80, catalog number: MSB080.CX1.5)
10. Centrifuge for source plates
11. CO₂ Incubator (Sanyo, model: MCO-19AIC)
12. Echo 550 Liquid Handler (Labcyte, catalog number: Echo 550)
13. MultiPod Controller (Roylan Developments, catalog number: SPOD0012)
14. StoragePod Enclosure (Roylan Developments, catalog number: SPOD0010)
15. Opera Phenix High-Content Screening System (PerkinElmer)

Software

1. Echo Liquid Handler Software (Labcyte)
2. Echo Plate Reformat (Labcyte)
3. Harmony High-Content Imaging and Analysis Software (PerkinElmer)
4. Columbus Image Data Storage and Analysis System (PerkinElmer)
5. Excel 2016 (Microsoft)
6. GraphPad Prism 8.2 (GraphPad)

Procedure

Generation of GFP-LUHMES cells

GFP-LUHMES cells are generated by the transduction of proliferative LUHMES cells with GFP-expressing lentiviral particles under the control of a PGK promoter (Ratcliffe *et al.*, 2018).

1. Seed proliferative LUHMES cells (p3-p5) at 1.5×10^6 per T75 flask.
2. Transduce with GFP-expressing lentiviral particles for 24 h. MOI of 8; for transduction, a 1:100 dilution was used. Transduction efficiency was previously assessed by FACS sorting to be 98.5%. GFP-expressing lentiviral particles were a kind gift from Eva Karyka and Mimoun Azzouz at the University of Sheffield.
3. After 24 h, maintain in LUHMES Proliferation Media for 72 h before beginning experiments.

Part I: GFP-LUHMES cell Maintenance Protocol

A. Defrost and seed GFP-LUHMES cells in a sterile culture hood

1. Prepare LUHMES Proliferation Media and sterile 1x PBS according to recipes below.
2. Prepare a Fibronectin Poly-L-Ornithine coated T75 flask.
 - a. Prepare 10 mL of Fibronectin Poly-L-Ornithine Coating Solution per T75 flask by adding 1 $\mu\text{g}/\text{mL}$ Fibronectin and 50 $\mu\text{g}/\text{mL}$ Poly-L-Ornithine to sterile distilled water.
 - b. Mix the Fibronectin Poly-L-Ornithine Coating Solution and transfer 10 mL to the T75 flask using a 10 mL serological pipette.
 - c. Incubate the flask with the Fibronectin Poly-L-Ornithine Coating Solution at 37 °C for at least 3 h or overnight.
 - d. Remove the Fibronectin Poly-L-Ornithine Coating Solution from the flask using a 10 mL serological pipette.
 - e. Wash the coated surface by transferring 5 mL of sterile 1x PBS to the flask using a 10 mL serological pipette and gently tilting the flask from side to side allowing the PBS to run across the whole surface. The PBS should be left in the flask until immediately before the cells are seeded in the flask to prevent the coating from drying out. The flasks can be prepared up to 1 hour before use.
3. Defrost and seed GFP-LUHMES cells into LUHMES Proliferation Media.
 - a. Remove prepared LUHMES Proliferation Media from the fridge and allow to warm to room temperature.
 - b. Take one frozen vial of GFP-LUHMES cells from freezer storage. Generally, we recommend to revive a vial of passage 1-10 so that revived cells can undergo numerous splits before retiring at passage 15.
 - c. Add 10 mL room temperature LUHMES Proliferation Media to a 15 mL Falcon using a 10 mL serological pipette.
 - d. Transfer ~500 μL of room temperature LUHMES Proliferation Media to the GFP-LUHMES cell vial using a P1000 mechanical pipette and slowly mix by aspirating and expelling the liquid in the tip repeatedly.
 - e. When the solution in the GFP-LUHMES cell vial is fully defrosted, transfer the solution to the room

- temperature LUHMES Proliferation Media in the 15 mL Falcon.
- f. Remove all 1x PBS from the coated T75 flask and add all of the cell solution from the 15 mL Falcon to the T75 flask using a 10 mL serological pipette.
 - g. Tilt the flask back and forward and then side to side 2-3 times to distribute the GFP-LUHMES cells evenly over the coated surface.
 - h. Incubate the flask in a 37 °C/5% CO₂ incubator.
4. On the following day, change the GFP-LUHMES cell media to remove any cells not fully attached.
 - a. Remove all media from the T75 flask using a 10 mL serological pipette.
 - b. Add 10 mL room temperature LUHMES Proliferation Media to the T75 flask using a 10 mL serological pipette.
 - c. Incubate the flask in a 37 °C/5% CO₂ incubator.

B. Split the GFP-LUHMES cells every 3-4 days or when confluence is 80-90% in a sterile culture hood

1. Prepare two Fibronectin Poly-L-Ornithine coated T75 flasks according to the procedure described above (Step A2).
2. Prepare LUHMES Proliferation Media and 1x Trypsin according to the recipes below. If pre-prepared, remove from the fridge and allow to warm to room temperature.
3. Split GFP-LUHMES cells into two flasks containing LUHMES Proliferation Media. One flask will be used for stock maintenance and one flask will be used for differentiation.
 - a. Remove all LUHMES Proliferation Media from GFP-LUHMES cell flask using a 10 mL serological pipette and transfer 5 mL into a 15 mL Falcon.
 - b. Add 5 mL room temperature 1x Trypsin to GFP-LUHMES cell flask using a 10 mL serological pipette.
 - c. Incubate GFP-LUHMES cell flask for 5 min in a 37 °C/5% CO₂ incubator.
 - d. Firmly smack the side of the GFP-LUHMES cell flask 2-3 times to dislodge cells into the solution. If successful, cell clouds should be visible in the solution.
 - e. Transfer all cell solution from GFP-LUHMES cell flask into the 15 mL Falcon containing 5 mL of used LUHMES Proliferation Media.
 - f. On the bench, centrifuge the 15 mL Falcon at 400 *x g* for 4 min.
 - g. Remove the supernatant using a 10 mL serological pipette and discard.
 - h. Resuspend the pelleted GFP-LUHMES cells in an appropriate amount of LUHMES Proliferation Media according to desired splitting ratio. We recommend a 1:15 splitting ratio of a fully confluent flask to be ready to split again in 3 days, although this may need to be adjusted slightly depending on cell behavior.
 - i. Remove all 1x PBS from the coated T75 flasks and add 10 mL LUHMES Proliferation Media per flask using a 10 mL serological pipette.
 - j. Add an appropriate amount of re-suspended GFP-LUHMES cell solution to the LUHMES Proliferation Media in both T75 flasks.

C. Change the Proliferation Media on the GFP-LUHMES cells every 2 days (following a split)

1. Remove a Falcon tube of LUHMES Proliferation Media from the fridge and allow to warm to room temperature.
2. Change the media on the GFP-LUHMES cells to fresh Proliferation Media.
 - a. Remove all LUHMES Proliferation Media from GFP-LUHMES cell flask using a 10 mL serological pipette and discard.
 - b. Add 10 mL of room temperature LUHMES Proliferation Media to the GFP-LUHMES cell flask using a 10 mL serological pipette.
 - c. Incubate the flask in a 37 °C/5% CO₂ incubator.

Part II: GFP-LUHMES cell Differentiation and Replating Protocol

A. Initiate differentiation of GFP-LUHMES cells (Day 1)

1. Wait 2-3 days following a split of the GFP-LUHMES cells to allow proliferation.
2. Prepare LUHMES Differentiation Media according to the recipe below. This must be made fresh before every use.
3. Change the Proliferation Media on the GFP-LUHMES cells to Differentiation Media.
 - a. Remove all LUHMES Proliferation Media from GFP-LUHMES cell flask using a 10 mL serological pipette and discard.
 - b. Add 10 mL of room temperature LUHMES Differentiation Media to the GFP-LUHMES cell flask using a 10 mL serological pipette.
 - c. Incubate the flask in a 37 °C/5% CO₂ incubator.

B. Replate differentiating GFP-LUHMES into a 384-well plate (catalog number: 781091) (Day 3)

1. Prepare a Fibronectin Poly-L-Ornithine coated 384-well plate.
 - a. Prepare 15 mL of Fibronectin Poly-L-Ornithine Coating Solution per 384-well plate by adding 1 µg/mL Fibronectin and 50 µg/mL Poly-L-Ornithine to sterile distilled water.
 - b. Mix the Fibronectin Poly-L-Ornithine Coating Solution and transfer 15 mL to a suitable reservoir for multichannel pipetting (for example but not limited to an upturned pipette box lid, clean and sterile).
 - c. Transfer 50 µL of the Fibronectin Poly-L-Ornithine Coating Solution to each well of the 384-well plate except for the two outermost columns and rows using a P200 multichannel mechanical pipette.
 - d. Transfer 40 µL of sterile 1x PBS to each of the empty outermost wells to act as a firewall using a P200 multichannel mechanical pipette.
 - e. Incubate the flask with the Fibronectin Poly-L-Ornithine Coating Solution at 37 °C for at least 3 h or overnight.
 - f. Remove the Fibronectin Poly-L-Ornithine Coating Solution from the 384-well plate using a P200 multichannel mechanical pipette.
 - g. Wash the coated surface by transferring 50 µL of sterile PBS to each coated well using a P200 multichannel mechanical pipette.
2. Prepare LUHMES Differentiation Media according to the recipe below.
3. Lift GFP-LUHMES cells and seed 10,000 cells/well into a coated 384-well plate.
 - a. Remove all LUHMES Differentiation Media from the differentiating GFP-LUHMES cell flask using a 10 mL serological pipette and transfer 5 mL into a 15 mL Falcon.
 - b. Add 5 mL room temperature 1x Trypsin to the differentiating GFP-LUHMES cell flask using a 10 mL serological pipette.
 - c. Incubate differentiating GFP-LUHMES cell flask for 5 min in a 37 °C/5% CO₂ incubator.
 - d. Firmly smack the side of the differentiating GFP-LUHMES cell flask 2-3 times to dislodge cells into the solution.
 - e. Transfer all cell solution from differentiating GFP-LUHMES cell flask into the 15 mL Falcon containing 5 mL of used LUHMES Differentiation Media.
 - f. On the bench, centrifuge the 15 mL Falcon at 400 x g for 4 min.
 - g. Remove the supernatant using a 10 mL serological pipette and discard.
 - h. Resuspend the pelleted GFP-LUHMES cells in 5 mL of LUHMES Differentiation Media, homogenising thoroughly by aspirating and expelling the GFP-LUHMES resuspension 10-15 times

- with a P1000 mechanical pipette.
- i. Prepare a Haemocytometer and transfer 10 µL of GFP-LUHMES resuspension onto the counting grid.
 - j. Count the number of GFP-LUHMES cells and calculate the cells/mL in the GFP-LUHMES resuspension.
 - k. Remove quantity of GFP-LUHMES resuspension containing 4×10^6 cells and transfer to a 15 mL Falcon. This will be the plating suspension.
 - l. Top up the plating suspension to a final volume of 12 mL with LUHMES Differentiation Media using a 10 mL serological pipette.
 - m. Remove the PBS from the coated wells on the first half of the 384-well plate using a P200 multichannel mechanical pipette.
 - n. Homogenise the plating suspension thoroughly by aspirating and expelling the solution 10-15 times with a 10 mL serological pipette.
 - o. Transfer half of the plating suspension (6 mL) into a suitable reservoir for multichannel pipetting.
 - p. Transfer 30 µL of plating suspension to each coated well of the 384-well plate.
 - q. Remove the PBS from the coated wells on the second half of the 384-well plate using a P200 multichannel mechanical pipette.
 - r. Re-homogenise the plating suspension in the 15 mL Falcon thoroughly by aspirating and expelling the solution 10-15 times with a 10 mL serological pipette.
 - s. Transfer the rest of the plating suspension to the reservoir and fill the remaining coated wells with 30 µL of plating suspension per well using a P200 multichannel mechanical pipette.
 - t. Move the plate back and forth, then side to side, several times to ensure the cells are evenly distributed across the well bottoms.
 - u. Incubate the 384-well plate in a 37 °C/5% CO₂ incubator.

Part III: GFP-LUHMES Drug Screening Protocol (timeline continued from Part II)

A. Treat differentiated GFP-LUHMES 384-well plate with rotenone (Day 5)

1. Prepare LUHMES Differentiation Media according to the recipe below.
2. Prepare rotenone-treated media and vehicle-treated media in a sterile culture hood.
 - a. To avoid cell disturbance, we avoid removing media and instead top up each well with 10 µL rotenone-treated media giving a final volume of 40 µL media per well. Therefore, rotenone-treated media must be prepared at four times the desired final concentration (4 µM).
 - b. Transfer 4 mL of LUHMES Differentiation Media to a 15 mL Falcon and label “Rotenone”. Transfer 4 mL of LUHMES Differentiation Media to another 15 mL Falcon and label “Vehicle”.
 - c. Prepare 10 mM rotenone in ethanol. Rotenone powder should be weighed in a fume hood.
 - d. Add 6.4 µL 10 mM rotenone to the media in the 15 mL Falcon labeled “Rotenone” using a P20 mechanical pipette. The final rotenone concentration in the well will be 4 µM.
 - e. Add an equal volume of ethanol (6.4 µL) to the 15 mL Falcon labeled “Vehicle” using a P20 mechanical pipette.
 - f. Mix both 15 mL Falcons by slowly inverting 3-4 times.
3. Transfer treated media to the differentiated GFP-LUHMES 384-well plate. We suggest a plate map as shown in Figure 2A (*i.e.*, “DMSO vehicle” wells are treated with vehicle-treated media, and all other wells treated with rotenone-treated media).
 - a. Transfer the contents of “Rotenone” media Falcon and “Vehicle” media Falcon into separate reservoirs for multichannel pipetting. Label the reservoirs accordingly.
 - b. Transfer 10 µL of rotenone-treated media to each well of the 384-well plate using a P10 multichannel mechanical pipette, ensuring the pipette tips are placed deep enough in the well to ensure ejected liquid mixes with the contents of the well. Leave some wells untreated for addition of vehicle-treated media to measure rotenone effect later. We suggest including vehicle-treating some wells in each DMSO only control column as explained in Step B3 below. Transfer 10 µL of vehicle-treated media

to each untreated well of the 384-well plate using a P10 multichannel mechanical pipette.

- Incubate the 384-well plate in a 37 °C/5% CO₂ incubator.

B. Prepare compounds in DMSO and write protocols for using the Echo 550 Liquid Handler and Opera Phenix High-Content Screening System

- Prepare compound library in 100% anhydrous DMSO on 384-well source plates (catalog number: LP-0200) with plate seal. Store in the StoragePod Enclosure and maintain a dry nitrogen atmosphere using the MultiPod Controller.
- Write a compound transfer protocol using the Echo Liquid Handler software. The source plate should be set to “384LDV-DMSO”, the destination plate to “Griener_384PS_781096” and custom mapping should be selected.
- Set the protocol to transfer an appropriate volume from each well of the source plate to the corresponding well on the destination plate to give the desired final drug concentration. We suggest splitting the destination plate into quarters and using the first column of each quarter for DMSO only treatment to act as a negative control (Figure 2). Parameter values for each compound-treated well in each quarter can then be normalised to the respective DMSO control well values in that quarter. For a full dose response curve, we recommend testing 8 concentrations for each compound at every half-log, *i.e.*, 3 nM, 10 nM, 30 nM, 100 nM, 300 nM, 1,000 nM, 3,000 nM, 10,000 nM. We also recommend including at least one positive control compound on each plate; we used a compound previously identified in house that showed beneficial effects on mitochondrial and morphological parameters.

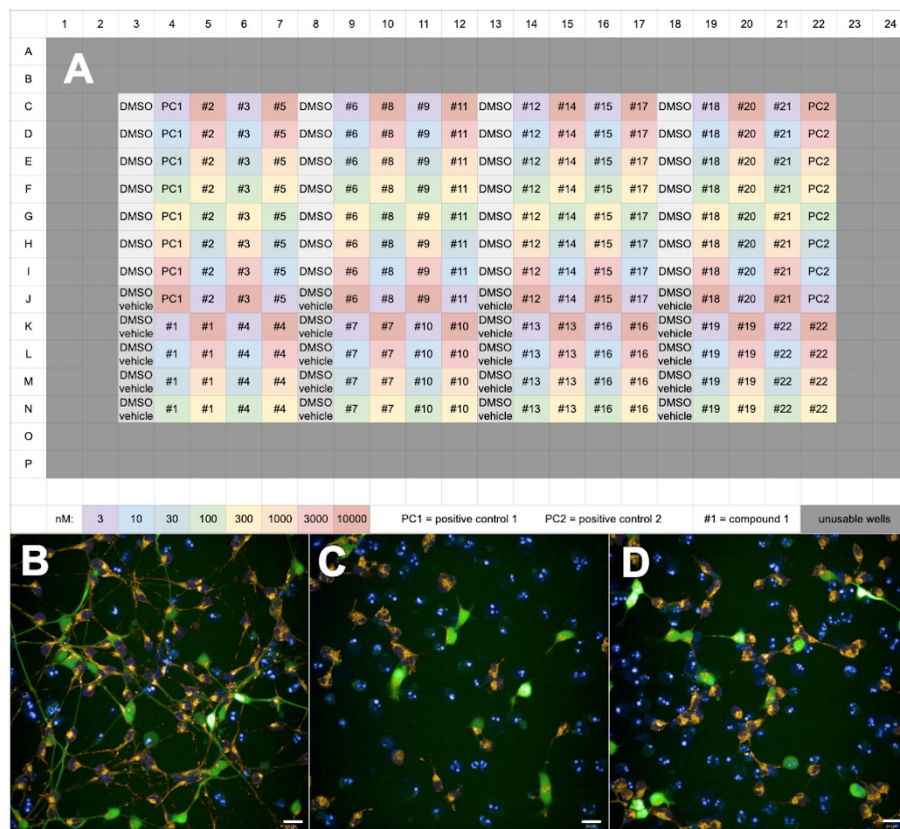


Figure 2. Plate map and example images following assaying of a GFP-LUHMES 384-well plate drug screen.

A. Plate map showing the suggested arrangement of control wells and test compound wells. All wells are treated with rotenone except for “DMSO vehicle” wells. The colours represent the concentration in nM

for each compound. B-D. Blue = DAPI, orange = TMRM, green = GFP, scale bars = 20 µm. Z stack maximum projection confocal images captured using the Opera Phenix High-Content Screening System from (B) a vehicle-treated DMSO control well, (C) a rotenone-treated DMSO control well and (D) a rotenone-treated positive control well (1,000 nM).

4. Write an imaging protocol (details below) for imaging the LUHMES cells on the Harmony High-Content Imaging and Analysis Software. Use the DAPI, Alexa 488 and Cy3 channels to capture the Hoechst signal, GFP signal and TMRM signal respectively. Use test images to ensure appropriate exposure time for each laser; this needs to be set by the user as it depends on the signal strength of laser power of each imaging system. Use a 40x water confocal objective, set the number of fields to 10 and set the number of stacks to 6. Select the wells to be imaged (note the outermost two columns and rows cannot be imaged by the Opera Phenix) and select the location of the fields in each well.

C. Treat differentiated GFP-LUHMES 384-well plate with compounds (Day 6)

1. Depressurise the StoragePod Enclosure using the Multipod Enclosure and remove the 384-well source plate.
2. Centrifuge the 384-well source plate at 2,500 $\times g$ for 2 min to remove any gas bubbles from the plate contents.
3. Calibrate and focus on the Echo 550 liquid handler before each independent plate shoot.
4. Survey the 384-well ldv source plate using the Echo 550 liquid handler. Ensure the volume in each well is high enough for transfer of the desired volume to the destination plate according to the compound transfer protocol. Note that the volume of each well in the 384-well source pate should not exceed 12 µL. Ensure that the water content of the contents of each well does not exceed 30% (this is inferred from the measurement of DMSO content which should not be lower than 70%; if this is the case then the contents of that well must be refreshed).
5. Remove the seal from the 384-well source plate and initiate the compound transfer protocol. Transfer the 384-well source plate and the destination plate into the machine when prompted.
6. When the protocol is complete, remove the destination plate and incubate immediately in a 37 °C/5% CO₂ incubator.
7. Replace the seal on the 384-well source plate and depressurise the StoragePod Enclosure using the Multipod Controller. Replace the 384-well source plate in the StoragePod Enclosure. Lock and repressurise the StoragePod Enclosure using the MultiPod Controller.

D. Assay and image the GFP-LUHMES 384-well plate (Day 7)

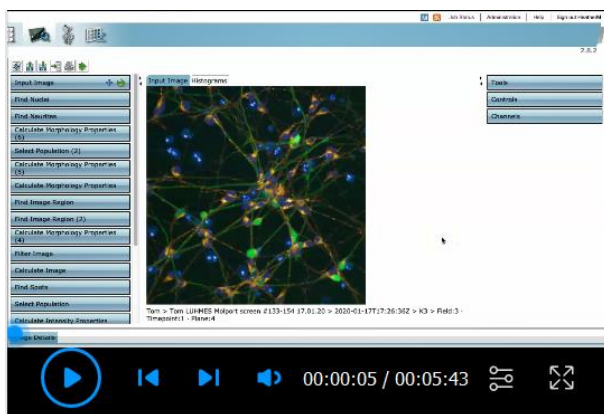
1. Prepare LUHMES Differentiation Media according to the recipe below.
2. Prepare the assay media.
 - a. Prepare 10 mM Hoechst in sterile distilled water.
 - b. Prepare 80 µM TMRM in DMSO.
 - c. Transfer 4 mL of LUHMES Differentiation media into a 15 mL Falcon.
 - d. Add 20 µL of x mM Hoechst solution to the 15 mL Falcon.
 - e. Add 20 µL of x mM TMRM solution to the 15 mL Falcon.
 - f. Mix the contents of the 15 mL Falcon (assay media) by slowly inverting the Falcon 4-5 times.
3. Incubate the GFP-LUHMES 384-well plate with assay media for 1 h.
 - a. Transfer the assay media to a suitable reservoir for multichannel pipetting.
 - b. Transfer 10 µL of assay media to each well of the 384-well plate using a P10 multichannel mechanical pipette, ensuring the pipette tips are placed deep enough in the well to ensure ejected liquid mixes with the contents of the well.
 - c. Incubate the GFP-LUHMES 384-well plate in a 37 °C/5% CO₂ incubator for 1 h.
4. Image the GFP-LUHMES 384-well plate using the Opera Phenix High-Content Screening System.

- a. Set the TCO (temperature and CO₂) settings on the Opera Phenix to 37 °C and 5% CO₂ and set both to “On”. Open the connected CO₂ gas cylinder when prompted. Allow the system to reach the desired temperature and gas level.
- b. Open the prepared imaging protocol.
- c. Load the GFP-LUHMES 384-well plate.
- d. Flush the water objective lens.
- e. Run a test and adjust the exposure time of each channel so that the intensity is significant over background levels. Adjust the height of the stacks if needed so that images are well focused across the height of the cell.
- f. Run the imaging protocol (Figure 2).

Data analysis

The images will be analysed in batch using the Columbus Image Data Storage and Analysis System. The GFP-signal will be used to assess neuronal morphology parameters and the TMRM-signal will be used to assess mitochondrial function and morphology.

A short video (Video 1) is available to show the analysis software and provide guidance to parts of the protocol, with detailed instructions below.



Video 1. Analysis set up using Columbus analysis software

1. Once the imaging protocol is completed, export the measurement file to a convenient location. Ensure “Measurements Inc. Associated Files” is selected and note the export path.
2. Import the exported files to the Columbus Image Data Storage and Analysis System.
3. Select the Image Analysis tab and open the imported file.
4. Write an analysis protocol using the following building blocks. Add a new building block by clicking the blue plus symbol.
 - a. Input Image. This is where the images are loaded into the analysis tool. Select “Maximum Projection” for Stack Processing and select “Basic” for Flatfield Correction. Uncheck the box next to Quick Tune.
 - b. Find Nuclei. This first Find Nuclei building block is used to aid the GFP-neurite detection in the following building blocks. The Hoechst signal will be used later to more accurately count the nuclei. Set the channel to “Alexa 488” (GFP) and use Method A. Label the Output Population as “Nuclei (GFP neurites)”.
 - c. Find Neurites. Set the Channel to “Alexa 488” (GFP) and ensure Population is set to “Nuclei (GFP neurites)” and Region to “Nucleus”. Two selections will be made, shown by the tabs above the image. The first is made via the positions of the nuclei selected above, and labeled “Nuclei (GFP neurites)” (Figure 3A). The second detects any neurite structures in the image, labeled “Neurite Segments”. Click the black

- downward-facing arrow and adjust the values for each detection parameter so that as many neurites are selected as possible. Do not be concerned about background detection in the “Neurite Segments” selection as this will be removed in the following building block. Label the Output Population as “Neurite Segments”.
- d. Select Population. We will now filter out background debris detected in the Find Neurites selection above. Set the Population to “Neurite Segments” and the Method to “Filter by Property”. Expand the drop down menu by clicking the black downward-facing arrow. Select “Segment Length”, “Neurite Segment Area” and “Neurite Segment Roundness” and adjust the values until most of the debris is removed from selection but the ‘real’ neurites remain selected. We used values of > 12.5 , > 0.7 , and > 0 respectively. Label the Output Population as “Neurite Segments Selected”.
 - e. Calculate Morphology Properties. Select Population “Neurite Segments Selected” and use Method “Standard”. Expand the drop down menu and check the box next to each parameter.
 - f. Calculate Morphology Properties (2). Select Population “Nuclei (GFP neurites)”, Region “Neurite Tree” and Method “Standard”. Expand the drop down menu and check the box next to each parameter.
 - g. Find Image Region. Select Channel “Cy3”, ROI Population to “None” and Method to “Common Threshold”. Expand the drop down menu and change the threshold to an appropriate level to select most of the signal without excessive background. Tick “Split into Objects”, expand the further drop down menu and change the minimum area to an appropriate value to remove background (we used $> 25 \mu\text{m}^2$). Leave “Fill Holes” unticked. Label the Output Population “Image Region (Cy3)”.
 - h. Find Image Region (2). Repeat as in (g.) but use Channel “Alexa 488” to select the GFP-neurite image region (Figure 3B). Label the Output Population “Image Region (GFP-neurites)”.
 - i. Filter Image. We will now segment the mitochondria. Set Channel “Cy3” and Method to “Texture SER”. Expand the drop down menu and set Filter to “SER Ridge”, Scale to 1 px and Normalization to “Unnormalized”. Label the Output Image as “SER Ridge”.
 - j. Calculate Image. This step amplifies the signal to improve segmentation. Set Method to “By Formula” and enter the Formula “A*1000”. Set Channel A to “SER Ridge” and label the Output Image as “Calculated Image”.
 - k. Find Spots. Set Channel “Calculate Image” and the ROI Population to “Image Region (GFP-neurites)”. This ensures only mitochondria within the GFP-neurite selection will be segmented. Set Method “D” and label the Output Population as “Mitochondria”.
 - l. Select Population. Set Population to “Mitochondria” and Method to “Filter by Property”. Choose the parameter “Spot Area [px²]”, select “ $>$ ” and enter a minimum value to remove any debris in the selection (we used 8 px^2) (Figure 3C). Label the Output Population as “Mitochondria Selected”.
 - m. Calculate Intensity Properties (2). Set Channel “Cy3”, Population “Image Region (GFP-neurites)” and Region “Image Region”. Set Method to “Standard” and expand the drop down menu to tick “Mean”. This will measure the TMRM signal intensity within the GFP-neurite selection.
 - n. Calculate Morphology Properties. Set Population “Mitochondria Selected” and Method “Standard”. Expand the drop down menu and tick “Area” and “Roundness”. This will measure the morphological properties of the segmented mitochondria. Label Output Properties as “Mitochondria Morphology”.
 - o. Calculate Texture Properties. Set Channel “Cy3”, Population “Mitochondria” and use Method “SER Features”. This will measure the texture properties of the segmented mitochondria. Label Output Properties as “Mitochondria Texture”.
 - p. Find Nuclei (2). Set Channel “DAPI” and use Method “C”. Expand the drop down menu and adjust the Common Threshold appropriately. Adjust the minimum area to remove background debris (we used $> 20 \mu\text{m}^2$) (Figure 3D). Label the Output Population “Nuclei (DAPI)”.
 - q. Define Results. Use Method “List of Outputs”. For each Population, expand the drop down menu and select the type of output you wish from each measured parameter. Alternatively, use “Apply to All” to select an output type for all measured parameters in that population. Click the green arrow at the top of the building block to apply changes and then save the protocol.
5. Select the Batch Analysis tab and select the data folder from the left-hand panel that you wish to analyse. Then, select the analysis protocol written above. Click the green arrow to start the analysis.
 6. When the analysis finishes, the results will be shown in the corresponding data folder in the left-hand panel. Select the Browse tab. Open the corresponding data folder by clicking the plus symbol next to it, and select the

“Result” file to open it. In the bottom-right-hand panel, the “Summary” tab will show the data from that analysis. Click the adjacent tab corresponding to the name of the “Result” file to see the raw data in full. Download the file using the blue “Download” link.

7. Open the downloaded file in Excel 2016. Organise the data so that parameter values for each compound at each concentration as well as control wells are ordered sequentially.
8. Input the data for each compound into GraphPad Prism 8.2 using a separate data table for each parameter. Ensure each compound is organised by column and each concentration by row. Include the data for positive control compounds.

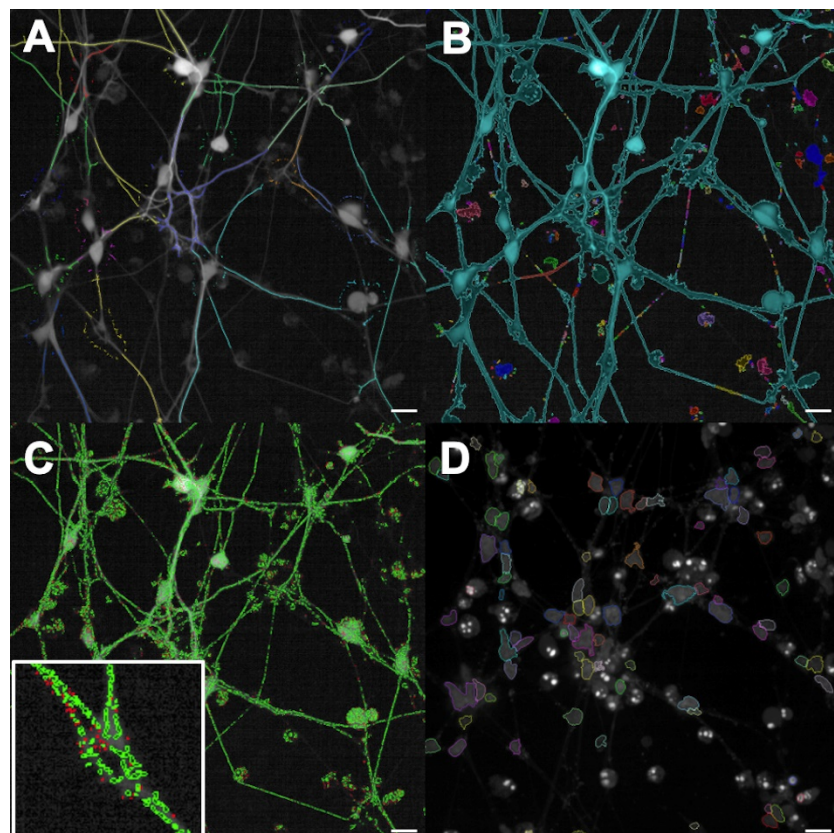


Figure 3. Analysis protocol selections using the Columbus Image Data Storage and Analysis System.

A. “Find Neurites” selection using the Alexa 488 channel, see step 4c of the Data analysis protocol. B. “Find Image Region” selection using the Alexa 488 channel, see step 4h. C. “Select Population” using the segmented Mitochondria channel, see step 4l. The indented image shows a close up of the individual selections. D. “Find Nuclei” selection using the DAPI channel, see step 4q. All scale bars = 20 μm .

Statistical analysis

The statistical analysis will depend on the experimental setup. However, some important plate effects should be controlled to ensure robustness and reproducibility of the assay.

1. Create another data table and plot the nuclei number (DAPI) across the whole plate. This should remain consistent to minimise plate drift effects.
2. Create another data table and plot the values for DMSO vehicle control wells against DMSO rotenone control wells for each parameter (Figure 4A). A significant difference should be seen for each parameter.
3. Calculate Z' and SW scores in order to ensure the robustness of the assay. The formulae are:

$$SW = \frac{(AVGmax - 3SDmax/\sqrt{n}) - (AVGmin + 3SDmin/\sqrt{n})}{SDmax/\sqrt{n}}$$

$$Z' = \frac{(AVGmax - 3SDmax/\sqrt{n}) - (AVGmin + 3SDmin/\sqrt{n})}{AVGmax - AVGmin}$$

In this protocol, ‘max’ would refer to values from DMSO vehicle control wells, and ‘min’ would refer to values from DMSO rotenone control wells. Example data for Z’ scores for various parameters in this assay are given in Figure 4B. In general, a Z’ score of above 0.5 and an SW score of above 2 are acceptable for use in phenotypic screening assays.

4. Typically, One-Way ANOVA with Dunnet’s *post-hoc* test would be performed to compare single concentration drug effects against vehicle treated wells. Alternatively, if a concentration response plate map is undertaken, a Nonlinear regression (curve fit) analysis on the data, using log(agonist) vs. response (three parameters) is typically used. All analysis is carried out in GraphPad Prism 8.2.

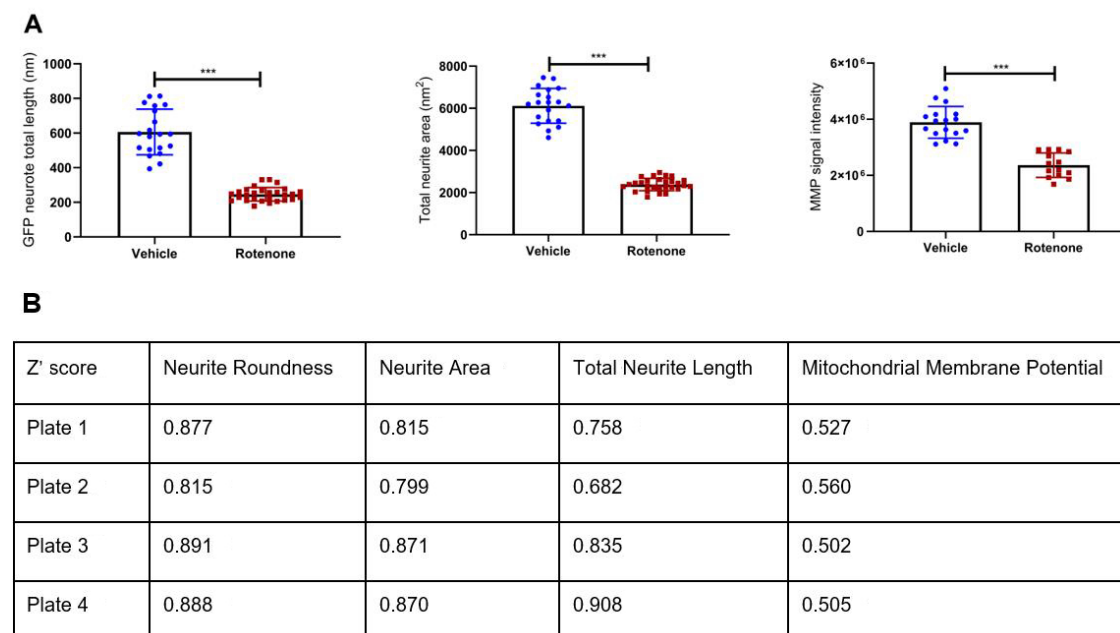


Figure 4. Example data showing rotenone effect, Z'-scores from GFP-LUHMES 384-well plate drug screening.

A. Rotenone effect for three example parameters is shown by comparing values for DMSO vehicle-treated wells against DMSO rotenone-treated wells. In both cases, the mean parameter value for rotenone-treated wells is significantly different to vehicle-treated wells (**P < 0.0001). B. Z'-scores for several parameters across four separate plates, each performed three weeks apart. The parameter ‘Neurite Roundness’ represents a measure of cell shape by comparing cell area to cell perimeter; a healthy neuron with extensive neurites would have a very low score approaching 0, compared to a spherical cell which should score up to 1.

Notes

1. GFP-LUHMES cells should be retired once they reach passage 15 and replaced with younger stocks.
2. When freezing GFP-LUHMES stocks, we recommend to split a fully confluent T75 flask, resuspend the pellet in 5 mL LUHMES Proliferation Media, add 10% DMSO and 20% FBS, then divide equally between 5 cryovials.
3. When counting GFP-LUHMES cells on the haemocytometer, only circular, bright spheres should be counted.
4. When transferring the differentiated GFP-LUHMES cells into the 384-well plate, act quickly and rehomogenise the cell suspension in the reservoir using the multichannel pipette between transfers. This is to

- ensure the number of cells plated per well is as consistent as possible across the plate.
5. The analysis software can output several additional parameters, including cell number and number of cells with neurites which can be useful parameters to assess cell viability, drift across plates and conditions as well as variability between assay days.

Recipes

1. Sterile 1x PBS

- a. Add 5 PBS tablets to 500 mL of distilled water in a flask suitable for autoclaving
- b. Mix until tablets dissolve and autoclave
- c. Store at room temperature

2. Sterile 1x Trypsin

- a. Add 500 mL of distilled water to a flask suitable for autoclaving
- b. Autoclave the flask and transfer to a sterile culture hood
- c. In the hood, add 45 mL of sterile distilled water to 5 mL of Trypsin 10x in a 50 mL Falcon
- d. Mix by inverting 2-3 times
- e. Store at 4 °C

3. LUHMES Base Media

Store at 4 °C
500 mL Advanced DMEM/F-12
5 mL N-2 Supplement
5 mL Pen-Strep
5 mL L-Glutamine

4. LUHMES Proliferation Media

Store for one week at 4 °C
50 mL LUHMES Base Media
40 ng/mL FGF-basic

5. LUHMES Differentiation Media

Prepare fresh for each use
20 mL LUHMES Base Media
1 µg/mL Tetracycline
1 mM dCAMP
2 ng/mL GDNF

Acknowledgments

This work was funded by a Parkinson's UK Senior Fellowship award to HM (F-1301) and a Parkinson's UK Virtual Biotech project grant to HM (I-1904). LF is supported by the Academy of Medical Sciences (SBF002\1142) and the Medical Research Council (MRC, grant 1812144). IV was supported by Consejo Nacional de Ciencia y Technologia (CONACyT), Mexico.

The generation of GFP-LUHMES cells was based on a previously established protocol from Ratcliffe *et al.*, 2018.

Competing interests

The authors declare no competing interests.

References

- Armstrong, M. J. and Okun, M. S. (2020). [Diagnosis and Treatment of Parkinson Disease: A Review](#). *JAMA* 323(6): 548-560.
- Delp, J., Funke, M., Rudolf, F., Cediel, A., Bennekou, S. H., van der Stel, W., Carta, G., Jennings, P., Toma, C., Gardner, I., van de Water, B., Forsby, A. and Leist, M. (2019). [Development of a neurotoxicity assay that is tuned to detect mitochondrial toxicants](#). *Arch Toxicol* 93(6): 1585-1608.
- Dolga, A. M., de Andrade, A., Meissner, L., Knaus, H. G., Höllerhage, M., Christophersen, P., Zischka, H., Plesnila, N., Hoglinger, G. U. and Culmsee, C. (2014). [Subcellular expression and neuroprotective effects of SK channels in human dopaminergic neurons](#). *Cell Death Dis* 5: e999.
- Hauser, D. N. and Hastings, T. G. (2013). [Mitochondrial dysfunction and oxidative stress in Parkinson's disease and monogenic parkinsonism](#). *Neurobiol Dis* 51: 35-42.
- Höllerhage, M., Moebius, C., Melms, J., Chiu, W.-H., Goebel, J. N., Chakroun, T., Koeglsperger, T., Oertel, W. H., Rösler, T. W., Bickle, M. and Höglinder, G. U. (2017). [Protective efficacy of phosphodiesterase-1 inhibition against alpha-synuclein toxicity revealed by compound screening in LUHMES cells](#). *Sci Rep* 7(1): 11469.
- Krug, A. K., Balmer, N. V., Matt, F., Schonenberger, F., Merhof, D. and Leist, M. (2013). [Evaluation of a human neurite growth assay as specific screen for developmental neurotoxicants](#). *Arch Toxicol* 87(12): 2215-2231.
- Lotharius, J., Barg, S., Wiekop, P., Lundberg, C., Raymon, H. K. and Brundin, P. (2002). [Effect of mutant alpha-synuclein on dopamine homeostasis in a new human mesencephalic cell line](#). *J Biol Chem* 277(41): 38884-38894.
- Lotharius, J., Falsig, J., van Beek, J., Payne, S., Dringen, R., Brundin, P. and Leist, M. (2005). [Progressive degeneration of human mesencephalic neuron-derived cells triggered by dopamine-dependent oxidative stress is dependent on the mixed-lineage kinase pathway](#). *J Neurosci* 25(27): 6329-6342.
- Park, J. S., Davis, R. L. and Sue, C. M. (2018). [Mitochondrial dysfunction in parkinson's disease: new mechanistic insights and therapeutic perspectives](#). *Curr Neurol Neurosci Rep* 18(5): 21.
- Mortiboys, H., Aasly, J. and Bandmann, O. (2013). [Ursodeoxycholic acid rescues mitochondrial function in common forms of familial Parkinson's disease](#). *Brain* 136(Pt 10): 3038-50.
- Yamaguchi, A., Ishikawa, K. I., Inoshita, T., Shiba-Fukushima, K., Saiki, S., Hatano, T., Mori, A., Oji, Y., Okuzumi, A., Li, Y., Funayama, M., Imai, Y., Hattori, N. and Akamatsu, W. (2020). [Identifying Therapeutic Agents for Amelioration of Mitochondrial Clearance Disorder in Neurons of Familial Parkinson Disease](#). *Stem Cell Reports* 14(6): 1060-1075.
- Poewe, W., Seppi, K., Tanner, C. M., Halliday, G. M., Brundin, P., Volkmann, J., Schrag, A. E. and Lang, A. E. (2017). [Parkinson disease](#). *Nat Rev Dis Primers* 3: 17013.
- Ratcliffe, L. E., Vázquez Villaseñor, I., Jennings, L., Heath, P. R., Mortiboys, H., Schwartzentruber, A., Karyka, E., Simpson, J. E., Ince, P. G., Garwood, C. J. and Wharton, S. B. (2018). [Loss of IGF1R in human astrocytes alters complex I activity and support for neurons](#). *Neuroscience* 390: 46-59.
- Scholz, D., Pöltl, D., Genewsky, A., Weng, M., Waldmann, T., Schildknecht, S. and Leist, M. (2011). [Rapid, complete and large-scale generation of post-mitotic neurons from the human LUHMES cell line](#). *J Neurochem* 119(5): 957-971.
- Stiegler, N. V., Krug, A. K., Matt, F. and Leist, M. (2011). [Assessment of chemical-induced impairment of human neurite outgrowth by multiparametric live cell imaging in high-density cultures](#). *Toxicol Sci* 121(1): 73-87.
- Tong, Z. B., Hogberg, H., Kuo, D., Sakamuru, S., Xia, M., Smirnova, L., Hartung, T. and Gerhold, D. (2017). [Characterization of three human cell line models for high-throughput neuronal cytotoxicity screening](#). *J Appl Toxicol* 37(2): 167-180.

Relative Quantification of NaV1.1 Protein in Mouse Brains using a Meso Scale Discovery-Electrochemiluminescence (MSD-ECL) Method

Zhou Han*, Anne Christiansen, Meena and Gene Liau

Stoke Therapeutics, Inc., Bedford, MA, USA

*For correspondence: zhan@stoketherapeutics.com

Abstract

Densitometric analysis is often used to quantify Nav1.1 protein on immunoblots, although the sensitivity and dilution linearity of the method are usually poor. Here we present a protocol for quantification of Nav1.1 in mouse brain tissues using a Meso Scale Discovery-Electrochemiluminescence (MSD-ECL) method. MSD-ECL is based on ELISA (enzyme-linked immunosorbent assay) and uses electrochemiluminescence to produce measurable signals. Two different antibodies are used in this assay to capture and detect Nav1.1 respectively in brain tissue lysate. The specificity of the antibodies is confirmed by *Scn1a* gene knock-out tissue. The calibration curve standards used in this assay were generated with mouse liver lysate spiked with mouse brain lysate, instead of using a recombinant protein. We showed that this method was qualified and used for quantification of Nav1.1 in mouse brain tissues with specificity, accuracy and precision.

Keywords: Nav1.1, *Scn1a*, Dravet syndrome, Quantification, Meso Scale Discovery, MSD, Electrochemiluminescence, ECL, Immunoassay, Mouse, Brain

This protocol was validated in: Sci Transl Med (2020), DOI: 10.1126/scitranslmed.aaz6100

Background

Nav1.1, also known as the alpha subunit of voltage gated sodium channel, type I, is a transmembrane protein encoded by the *Scn1a* gene (Meisler *et al.*, 2010). Decreased expression of functional Nav1.1 leads to Dravet syndrome (DS), a severe early-onset epileptic encephalopathy (Dravet *et al.*, 2005). Expression of Nav1.1 in biological samples has been used as a non-clinical pharmacological biomarker for DS and can be measured using densitometric analysis of immunoblots. Densitometry methods are often not as accurate and sensitive as standard immunoassays. In addition, some Nav1.1 antibodies may cross react with other voltage gated sodium channels (VGSCs), including Nav1.2, Nav1.3 and Nav1.8, due to homology of the protein sequences. We developed a specific and sensitive method to quantify Nav1.1 protein in mouse brain tissue using a Meso Scale Discovery-Electrochemiluminescence (MSD-ECL) method. MSD-ECL method is ELISA (enzyme-linked immunosorbent assay) based and uses electrochemiluminescence to produce measurable signals based on labeled antibody binding to the target (Kuhle *et al.*, 2016). Scheme of antibody binding in MSD-ECL assay described in this protocol is shown in Figure 1. The MSD-ECL method has advantages of low background and high sensitivity. The specificity of this assay was confirmed by using capture and detection antibodies that were validated using *Scn1a* knock-out (*Scn1a*^{-/-}) mouse brain tissue (Figure 2). Since Nav1.1 is a transmembrane protein, reproducible production of a high-quality reference standard in cells could be challenging. Therefore, in this method, reference standards composed of mouse liver lysate spiked with mouse brain lysate was utilized. Mouse liver lysate was selected as a diluent to maintain equivalent protein load in each standard since it did not show detectable levels of Nav1.1 protein expression (Figure 3). This “fit for purpose” MSD-ECL method was qualified and used for quantification of Nav1.1 in mouse brain tissues with specificity, accuracy and precision. This method is limited, however, to have a relative narrow dynamic range of detection: The upper limit of quantification (ULOQ) is set to 100% of the Nav1.1 expression in adult mouse brain. Further dilution of some sample lysate may be necessary if the Nav1.1 expression in those samples exceed the ULOQ in the initial run.

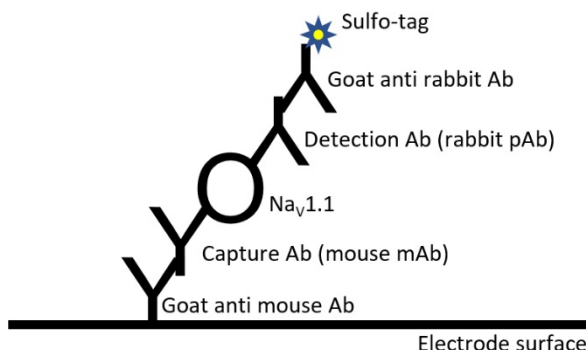


Figure 1. Scheme of antibody binding in MSD-ECL assay described in this protocol.

The electrode surface of each well is pre-coated with goat anti-mouse antibody (Ab). A mouse monoclonal antibody (mAb) is used as capture Ab for Nav1.1. A rabbit polyclonal antibody (pAb) is used as detection Ab. The capture and detection antibodies bind to different epitopes within Nav1.1. A Sulfo-tag labeled goat anti-rabbit Ab produces electrochemiluminescence signal.

Materials and Reagents

1. 2-mL Eppendorf microcentrifuge tubes, LoBind for protein (Fisher Scientific, catalog number: 13-698-795)
2. 1.5-mL Eppendorf microcentrifuge tubes, LoBind for protein (Fisher Scientific, catalog number: 13-698-794)
3. 0.2 µm nitrocellulose membrane (GE Healthcare Life Sciences, catalog number: 10600004)
4. MULTI-ARRAY 96 Small Spot GAM Plate (Meso Scale Discovery, catalog number: L45MA-2)
5. *Scn1a*^{tm1Kea} 129S6.*Scn1a*^{+/−} mice (The Jackson Laboratory, catalog number: 37107-Jax)

6. Liquid nitrogen
7. PageRuler Plus prestained protein ladder (Thermo Fisher Scientific, catalog number: 26620)
8. Halt protease inhibitor cocktail (100×) (Thermo Fisher Scientific, catalog number: 78429)
9. Capture antibody, mouse anti Nav1.1 monoclonal antibody (NeuroMab, catalog number: 75-023)
10. Detection antibody, rabbit anti Nav1.1 polyclonal antibody (Alomone, catalog number: ASC-001)
11. Anti-Rabbit antibody, Goat, Sulfo-Tag labeled (Meso Scale Discovery, catalog number: R32AB-1)
12. Anti-vinculin antibody (E1E9V), rabbit monoclonal antibody (Cell Signaling Technology, catalog number: 13901)
13. Phosphate-buffered saline (PBS), pH 7.4 (Thermo Fisher Scientific, catalog number: 10010023)
14. TGX acrylamide gradient gel (Bio-Rad, catalog number: 5671124)
15. ECL Prime blocking reagent (GE Healthcare Life Sciences, catalog number: RPN418V)
16. ECL Plus Western Blotting Substrate (Thermo Fisher Scientific, catalog number: 32132)
17. MSD Blocker B, 2 grams (Meso Scale Discovery, catalog number: R93BB-2)
18. MSD read buffer T (4×) (Meso Scale Discovery, catalog number: R92TC-2)
19. TBS, 10× (Bio-Rad, catalog number: 170-6435)
20. 10% Tween-20 (Bio-Rad, catalog number: 1610781)
21. TX-100 (Sigma-Aldrich, catalog number: T8787-100ML)
22. Nonidet P-40, IGEPAL CA-630 (Sigma-Aldrich, catalog number: 56741-250ML-F)
23. Sodium deoxycholate (Sigma-Aldrich, catalog number: D6750-25G)
24. 0.5 M EDTA pH 8.0 (Ambion, catalog number: AM9260G)
25. BCA protein assay kit (Pierce, catalog number: 23227)
26. MSD lysis buffer (see Recipes and Note 1)

Equipment

1. Meso Quickplex SQ 120 (Meso Scale Discovery, model: SQ120)
2. Microplate shaker (Corning, model: S2020-P4-COR)
3. Analytical balance (Mettler Toledo, model: AB54-S)
4. Cryo-cup grinder (Biospec, model: 206)
5. Teflon coated pestle and mortar tissue grinder Size A. Chamber volume 10 mL (Thomas Scientific, model: 3431D76)
6. Teflon coated pestle and mortar tissue grinder Size B. Chamber volume 30 mL (Thomas Scientific, model: 3431D88)
7. 5-speed drill press (Wen, catalog number: 4208)
8. Refrigerated Centrifuge (Eppendorf, model: 5430R)
9. Dry Blotting System (Thermo Fisher Scientific, model: iBlot 2)
10. Laser scanner (GE Healthcare Life Sciences, model: Typhoon FLA 9500)

Software

1. MSD Discovery Workbench 4.0 (Meso Scale Diagnostics, LLC., www.mesoscale.com)
2. GraphPad Prism 8.0 (GraphPad Software, www.graphpad.com)

Procedure

A. Preparation of tissue lysate

Cite as: Han, Z. et al. (2021). Relative Quantification of NaV1.1 Protein in Mouse Brains Using a Meso Scale Discovery-Electrochemiluminescence (MSD-ECL) Method. Bio-protocol 11(3): e3910. DOI: 10.21769/BioProtoc.3910.

1. Prepare mouse liver lysate as diluent for MSD calibration curve standards
 - a. Perfuse an adult mouse liver with PBS, pH 7.4 (see Note 2) through the portal vein until the color of liver turns yellow or white (Cabral *et al.*, 2018). Cut off the liver tissue and weigh on an analytical balance (Mettler Toledo).
 - b. Freeze the liver tissue in liquid nitrogen and pulverize it using a liquid nitrogen cooled mortar and pestle Cryo-cup grinder (Biospec).
 - c. Add ice-chilled MSD lysis buffer to the pulverized liver tissue in the amount of 2 mL of buffer per 100 mg of tissue. Homogenized the tissue with a motor-driven Teflon coated mortar and pestle tissue grinder, size B (Thomas Scientific) on ice, at a speed of 740 rpm for 30 strokes.
 - d. Transfer the homogenate to 2-mL Eppendorf tubes and centrifuge at 16,000 × *rcf*, 4 °C, for 15 min with a refrigerated centrifuge (Eppendorf).
 - e. Transfer the supernatant (liver lysate) to a new tube without disturbing the precipitation (containing nuclei and cellular debris) and avoid taking any fat or oil droplet floating on the surface of the lysate. Keep the supernatant on ice.
 - f. Measure the protein concentration of liver lysate following a protocol using the Bicinchoninic acid (BCA) method (Pierce, see Note 3). The protein concentration typically ranges from 5 to 7 mg/mL for liver lysate obtained from this process. Adjust protein concentration to 4 mg/mL with the MSD lysis buffer.
2. Prepare mouse brain lysate for MSD calibration curve standards and for test samples
Prepare brain lysate for standards using adult mouse brains, as Nav1.1 expression is developmentally regulated and stays at a high level in adulthood (Han *et al.*, 2020). Prepare brain lysate in similar way as liver lysate, except that brain tissue is not pulverized in liquid nitrogen before homogenization, and 1.5-mL of MSD lysis buffer is added to every 100 mg of brain tissue. Smaller sized Teflon coated mortar and pestle tissue grinder, size A (Thomas Scientific) could be used for homogenization of test samples. The protein concentration typically ranges from 5 to 7 mg/mL for brain lysate obtained from this process. At the end of preparation, adjust the concentration of brain lysate to 4 mg/mL with MSD lysis buffer.

B. Qualification and characterization of MSD-ECL assay

1. Validate the specificity of antibodies with *Scn1a*^{-/-} mouse brain tissue (see Note 4).
 - a. Prepare brain lysate from *Scn1a*^{-/-} mice and wild type (WT) littermates. We bred the *Scn1a*^{tm1Kea} 129S6.*Scn1a*^{+/-} mice (The Jackson Laboratory) to create *Scn1a*^{-/-} mice. Alternatively, Nav1.1 null tissue could be obtained from CRISPR engineered *Scn1a* knock-out cell culture.
 - b. Perform SDS-PAGE (sodium dodecyl sulfate polyacrylamide gel electrophoresis) with 50 µg of brain lysate on each lane of a precast TGX acrylamide gradient gel (Bio-Rad). Run SDS-PAGE at 120 V for ~90 min.
 - c. Transfer total protein to a 0.2 µm nitrocellulose membrane (GE Healthcare Life Sciences) with a dry blotting system (Thermo Fisher Scientific). Use the following transfer program for protein transfer: step 1: 20 V for 1 min; step 2: 23 V for 4 min; step 3: 25 V for 5 min.
 - d. Perform immunoblotting with the test antibodies. Block the membrane with 2% ECL Prime blocking reagent (GE Healthcare Life Sciences) for 30 min. Use Tris-buffered saline containing 0.1% Tween-20 (TBS-T) to prepare the blocking buffer. Use the blocking buffer as diluent for primary and secondary antibodies incubation. Wash the nitrocellulose membrane with TBS-T between antibody incubation. Develop immunoblotting signals with the ECL Plus Western Blotting Substrate (Thermo Fisher Scientific) and capture the immunoblot images with a laser scanner (GE Healthcare Life Sciences). Antibodies specific to Nav1.1 should detect a protein band at about 223 kDa with WT mouse brain lysate but not with *Scn1a*^{-/-} mouse brain lysate. An example of Nav1.1 specific antibody validation is given in Figure 2.
2. Evaluation of mouse liver lysate as diluent for MSD calibration curve standards
Perform SDS-PAGE with 50 µg of mouse liver lysate or brain lysate on each lane. Transfer total protein to a 0.2 µm nitrocellulose membrane and perform immunoblotting with a validated Nav1.1 antibody.

Antibodies specific to Nav1.1 should detect a protein band about 223 kDa with brain lysate but not with the diluent (liver lysate in this case). Results confirming mouse liver lysate as a suitable diluent for brain lysate are shown in Figure 3.

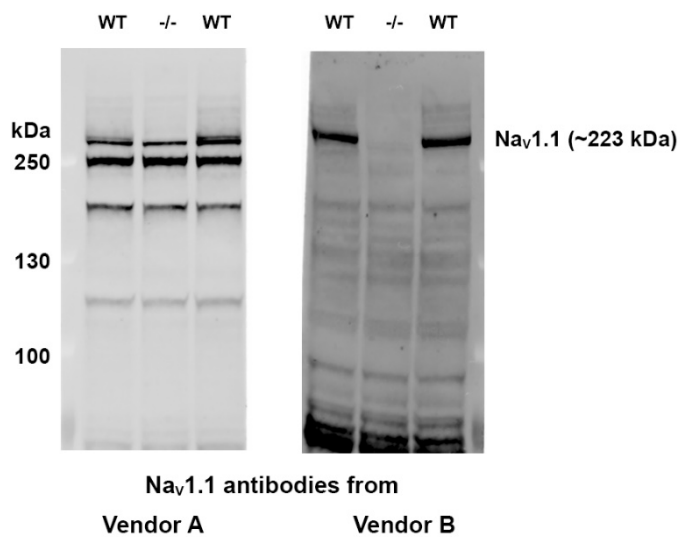


Figure 2. Examples of Nav1.1 antibody validation. Immunoblotting was performed with brain lysate from a *Scn1a*^{-/-} mouse (mid lane) and two wild type (WT) littermates (flanking lanes).

The Nav1.1 antibody from vendor A (left panel) is not specific and may cross react with other VGSCs homologs. The Nav1.1 antibody from vendor B (right panel) is specific since Nav1.1 protein band is not seen in the lane of *Scn1a*^{-/-} brain lysate. Therefore, Nav1.1 antibody from Vendor B is found to be suitable for MSD-ECL assay development. (Protein ladder: PageRuler Plus)

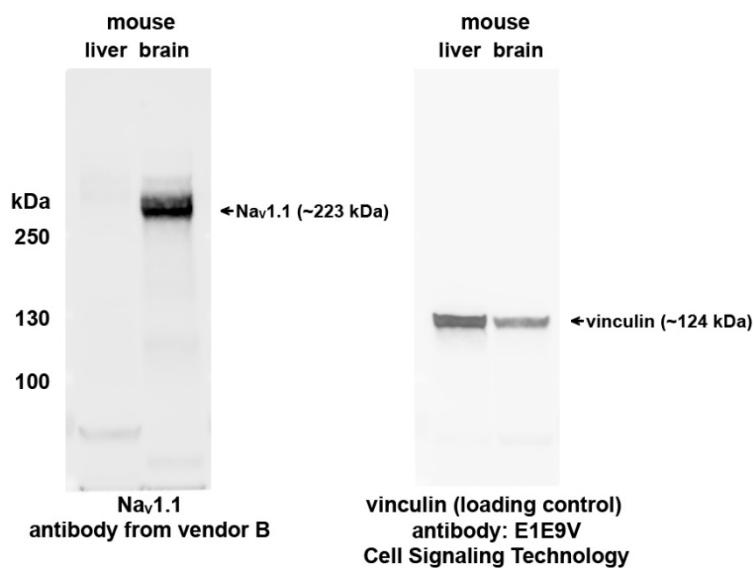


Figure 3. Evaluation of mouse liver lysate as diluent for brain lysate.

Immunoblotting was performed with mouse liver lysate and brain lysate with a validated Nav1.1 antibody (from vendor B, the same antibody as in Figure 2). Vinculin immunoblotting was shown for loading control. (Protein ladder: PageRuler Plus)

3. Preparation of MSD calibration curve standards

Prepare MSD calibration curve standards by mixing WT mouse brain lysate (4 mg/mL) and WT mouse liver lysate (4 mg/mL) at various ratios (Table 1). Store MSD calibration curve standards in small aliquots at -80 °C to avoid multiple freeze-thaw cycles (see Note 5).

Table 1. Preparation of calibration curve standards (STDs)

STD name	% Nav1.1 expression (normalized to adult WT mouse brain)	Brain (mL)	lysate	Liver (mL)	lysate
STD 1	0	0		3	
STD 2	5	0.15		2.85	
STD 3	10	0.3		2.7	
STD 4	20	0.6		2.4	
STD 5	30	0.9		2.1	
STD 6	40	1.2		1.8	
STD 7	50	1.5		1.5	
STD 8	60	1.8		1.2	
STD 9	70	2.1		0.9	
STD 10	80	2.4		0.6	
STD 11	90	2.7		0.3	
STD 12	100	3		0	

4. Characterization and acceptance criteria for the MSD-ECL assay

a. Accuracy and precision

- i. Perform MSD-ECL assay with standards and quality controls (QCs) in duplicate wells. We typically prepare high concentration quality control (HQC) at 70-75% level and medium concentration quality control (MQC) at 45-55% level of the largest non-zero calibrator (STD12 in this case). We prepare low concentration quality control (LQC) approximately 3 times the smallest non-zero calibrator (STD2 in this case). Prepare the QCs using mouse liver lysate as diluent (see Note 5).
- ii. As a measure of assay accuracy (A), the mean back-calculated concentrations for all standards should be $\pm 15\%$ of their nominal values. 75% of the non-zero standards should meet the above criteria. The mean back-calculated concentrations for QCs should be $\pm 20\%$ of their nominal values.
- iii. As a measure of assay precision (P), the % CV between duplicates should be $\leq 20\%$.

b. Lower limit of quantification (LLOQ) and upper limit of quantification (ULOQ)

- i. LLOQ is defined by the smallest non-zero calibrator with MSD signal at least 3 times greater than the blank (STD1) or greater than blank plus 10 times the standard deviation (SD) of the blank. LLOQ should meet the accuracy and precision criteria.
- ii. ULOQ is defined by the largest non-zero calibrator (STD12 in this case) that meets the accuracy and precision criteria.

c. Specificity

Perform MSD-ECL assay with brain lysate from *Scn1a^{-/-}* mouse following steps in Procedure C. The MSD signal from *Scn1a^{-/-}* brain lysate should be below the lower limit of quantification (BLQ).

d. Dilution linearity

The three QC samples (HQC, MQC and LQC) serve the purpose of evaluating the dilution linearity of the assay. If more stringent test is desired, MSD-ECL assay could be performed with 4 or more levels of dilution for the QC samples. The mean back-calculated concentrations for QCs should be $\pm 20\%$ of their nominal values.

Establishment of dilution linearity helps to extend the dynamic range of the standard curve beyond 100% of Nav1.1 expression in WT mouse brain. Test samples for which anticipated Nav1.1 expression is higher than WT mouse brain tissues or showing levels above ULOQ can be diluted using the established dilution factors.

e. Storage stability

Store standards and QCs at -80 °C and perform MSD-ECL assay in 1 week, 1 month and 3 months (or longer as appropriate for the study). The mean back-calculated concentrations for all standards and QCs should be \pm 15% and \pm 20% of their nominal values respectively, while both passing the precision criteria.

C. Performing MSD-ECL assay

1. Block the MSD GAM (goat anti-mouse antibody) plates with 5% MSD blocker B (see Note 6) in Tris-Buffered Saline, 0.1% Tween-20 (TBS-T), 100 μ L/well. Seal the plates and shake on a microplate shaker (Corning) for 1 h, at room temperature, speed 700 rpm.
2. Tap blocker B out of the plates over a stack of paper towels. Coat the wells with capture antibody (NeuroMab, 0.95 mg/mL, dilute to 1:200 in 5% Block B/TBS-T), 25 μ L/well. Seal the plates and shake for 4 h at room temperature, speed 700 rpm.
3. Tap the capture antibody out of plates over paper towels. Wash the wells with TBS-T (150 μ L/well) for 3 times while shaking the plates, at room temperature, speed 700 rpm. Five minutes for each wash.
4. Add 25 μ L of MSD calibration curve standard (4 mg/mL) or test sample lysate (4 mg/mL) to individual wells. Include high, medium and low concentration quality controls (HQC, MQC and LQC, respectively) on the same plate. Run each standard and test sample as duplicate. An example of MSD plate layout is given in Figure 4. Seal the plates, shake overnight, at 4 °C, speed 700 rpm.
5. Tap the content out of plates over paper towels. Wash the wells with TBS-T (150 μ L/well), for 3 times while shaking the plates, at room temperature, speed 700 rpm. Five minutes for each wash.
6. Add 25 μ L of detection antibody (Alomone, 0.6 mg/mL, dilute to 1:250 in 5% Block B/TBS-T) to each well. Seal the plates and shake for 2 h, at room temperature, speed 700 rpm.
7. Tap the detection antibody out of plates over paper towels. Wash the wells with TBS-T (150 μ L/well), for 3 times while shaking the plates, at room temperature, speed 700 rpm. Five minutes for each wash.
8. Add 25 μ L of Sulfo-tagged anti-rabbit Ab (MSD, 0.5 mg/mL, dilute to 1:250) to each well. Seal the plates and shake for 1 h at room temperature, speed 700 rpm.
9. Tap the content out of plates over paper towels. Wash the wells with TBS-T (150 μ L/well), for 3 times while shaking the plates, at room temperature, speed 700 rpm. Five minutes for each wash.
10. Add 150 μ L of 1 \times MSD Read Buffer T (diluted in dH₂O) to each well. Make sure bubbles are not created when dispensing the read buffer. Read the plates immediately on a Meso Quickplex SQ 120 machine with the MSD Discovery Workbench 4.0 software (Meso Scale Diagnostics, LLC).

STD1	STD2	STD3	STD4	STD5	STD6	STD7	STD8	STD9	STD10	STD11	STD12
STD1	STD2	STD3	STD4	STD5	STD6	STD7	STD8	STD9	STD10	STD11	STD12
SPL1	SPL2	SPL3	SPL4	SPL5	SPL6	SPL7	SPL8	SPL9	SPL10	SPL11	SPL12
SPL1	SPL2	SPL3	SPL4	SPL5	SPL6	SPL7	SPL8	SPL9	SPL10	SPL11	SPL12
SPL13	SPL14	SPL15	SPL16	SPL17	SPL18	SPL19	SPL20	SPL21	SPL22	SPL23	SPL24
SPL13	SPL14	SPL15	SPL16	SPL17	SPL18	SPL19	SPL20	SPL21	SPL22	SPL23	SPL24
SPL25	SPL26	SPL27	SPL28	SPL29	SPL30	SPL31	SPL32	SPL33	HQC	MQC	LQC
SPL25	SPL26	SPL27	SPL28	SPL20	SPL30	SPL31	SPL32	SPL33	HQC	MQC	LQC

Figure 4. Example of plate layout for a 96-well MSD-ECL assay.

Each standard (STD) and test sample (SPL) was run as duplicate. High, medium and low concentration quality controls (HQC, MQC and LQC, respectively) are included in the plate. One can also run one standard curve and one set of QCs before the test samples and the second set of standard curve and QCs at the end of the test samples.

Data analysis

- Import the signals of MSD calibration curve standards and test samples to the GraphPad Prism 8 software (GraphPad Software). Check if the standards and test samples meet the accuracy and precision criteria. See an example of an MSD-ECL data set in Table 2.

Table 2. Example of MSD calibration curve generation and evaluation of Nav1.1 expression in representative test samples

STD name	% Nav1.1 expression (nominal)	MSD signal			% Nav1.1 expression (interpolated)		Recovery (%)	
		repeat 1	repeat 2	%CV	2nd order polynomial	4PL	2nd order polynomial	4PL
STD1	0	1303	1235	3.8	BLQ	BLQ	N/A	N/A
STD2	5	4572	4963	5.8	4.7	4.8	94.8	96.0
STD3	10	8410	9243	6.7	10.4	11.4	104.1	113.7
STD4	20	16505	17320	3.4	20.7	21.8	103.7	108.9
STD5	30	25789	25059	2.0	30.6	31.2	101.9	104.0
STD6	40	33821	33094	1.5	39.1	39.3	97.8	98.3
STD7	50	41928	47594	9.0	50.2	49.9	100.3	99.9
STD8	60	57065	54643	3.1	60.2	59.7	100.3	99.5
STD9	70	65153	62717	2.7	67.0	66.5	95.7	95.0
STD10	80	89640	77442	10.3	82.4	82.1	103.1	102.7
STD11	90	98015	92896	3.8	91.1	91.2	101.3	101.3
STD12	100	108910	104363	3.0	98.9	99.4	98.9	99.4
SPL1	N/A	15697	15143	2.5	18.9	20.0	N/A	N/A
SPL2	N/A	13630	14060	2.2	17.0	18.1	N/A	N/A
SPL3	N/A	13786	13443	1.8	16.7	17.8	N/A	N/A
SPL4	N/A	12903	12511	2.2	15.5	16.6	N/A	N/A
SPL5	N/A	13425	16106	12.8	18.1	19.2	N/A	N/A
SPL6	N/A	15493	14147	6.4	18.2	19.3	N/A	N/A
SPL7	N/A	15021	16930	8.4	19.6	20.7	N/A	N/A
SPL8	N/A	15070	15661	2.7	18.9	19.9	N/A	N/A
SPL9	N/A	27183	30487	8.1	34.3	34.7	N/A	N/A
SPL10	N/A	32746	29349	7.7	36.6	36.9	N/A	N/A
SPL11	N/A	30121	29539	1.4	35.3	35.7	N/A	N/A
SPL12	N/A	36951	34568	4.7	41.4	41.6	N/A	N/A
SPL13	N/A	33546	36913	6.8	40.9	41.0	N/A	N/A
SPL14	N/A	29073	31291	5.2	35.7	36.1	N/A	N/A
SPL15	N/A	31355	26931	10.7	34.6	35.0	N/A	N/A
SPL16	N/A	30716	34868	9.0	38.4	38.7	N/A	N/A
HQC	70	70022	70597	0.6	72.2	71.7	103.1	102.4
MQC	50	40367	43335	5.0	47.4	47.3	94.8	94.6
LQC	20	15445	15775	1.5	19.2	20.2	96.0	101.0

BLQ: Below the limit of quantification

4PL: Four parameter logistic

N/A: Not applicable

Fit standards to a non-linear regression curve (2nd order polynomial or four-parameter logistic). See an example of MSD standard curve fitting in Figure 5.

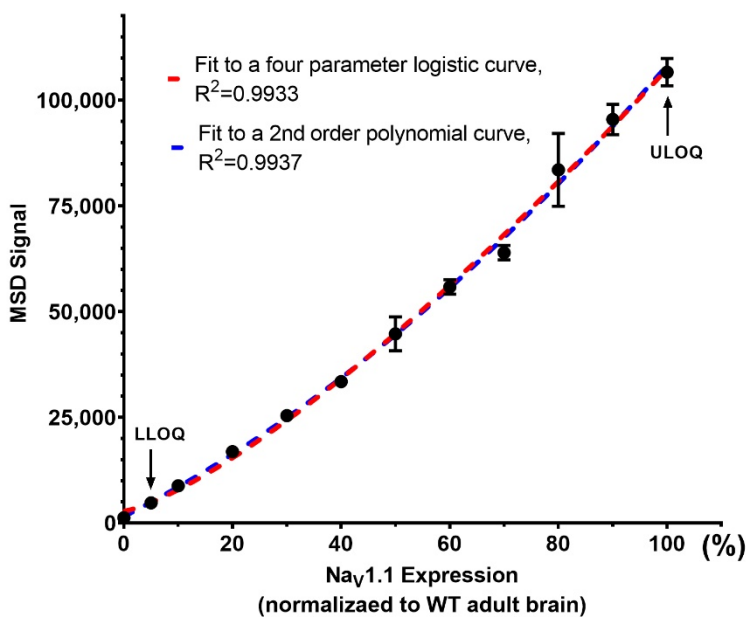


Figure 5. Example of MSD standard curve fitting.

The MSD signals from calibration curve standards (Table 2) were fit to a four-parameter logistic curve (in red) or a 2nd order polynomial curve (in blue). STD12 defines the upper limit of quantification (ULOQ). STD2 defines the lower limit of quantification (LLOQ).

2. Interpolate Nav1.1 concentration in each test sample against the standard curve. Any sample with MSD signal above the ULOQ should be diluted with mouse liver lysate and rerun with a new MSD-ECL assay.
3. Use proper statistic test to compare Nav1.1 expression between different groups. Most used tests are Student's *t*-test, Mann Whitney Wilcoxon test and two-way ANOVA. See an example of MSD-ECL data presentation and statistical analysis in Figure 6.

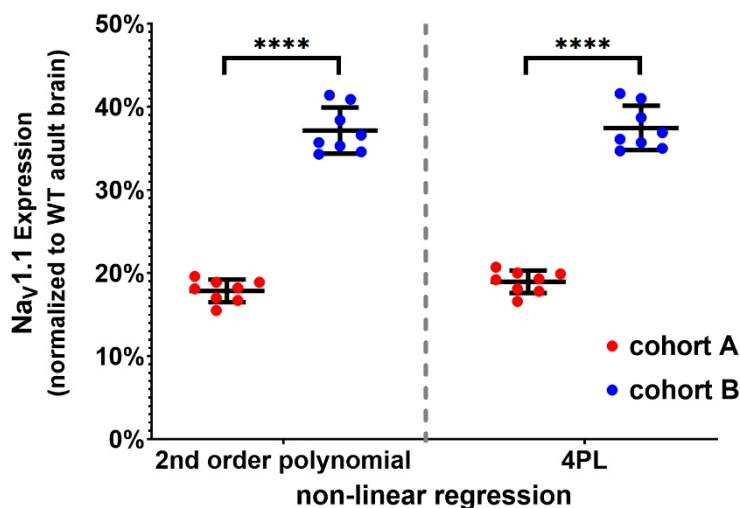


Figure 6. Example of MSD-ECL data presentation and statistical analysis.

Interpolated results of Nav1.1 expression (mean \pm SD and individual values, also reported in Table 2) in brain tissues from two cohorts of pre-weaning mice (A and B) were plotted and mean values were compared with unpaired two-tailed Student's *t*-test (****, $P < 0.0001$). Interpolation using 2nd order polynomial (left) and four-parameter logistic (4PL) standard curves (right) yielded similar results.

Notes

1. Protease inhibitors are not included in the MSD lysis buffer used in this protocol. It was reported that dimethylsulfoxide (DMSO), a solvent used for many proteinase inhibitors, can change the properties of proteins in solution, leading to protein denaturation, aggregation, or degradation. DMSO can also change the apparent binding properties of the proteins (Chan *et al.*, 2017). To avoid possible adverse effect of DMSO on this assay, which requires the integrity of the target protein and its binding to antibodies, we explored protocol without proteinase inhibitors and compared it to a similar protocol with protease inhibitors (Thermo Fisher Scientific, Halt Protease Inhibitor Cocktail). We did not find any difference between the two protocols in terms of assay results and storage stability as long as all the standards, QCs and test samples were processed on ice or at 4 °C, and stored at -80 °C in small aliquots.
2. Perfusion of mouse liver with PBS prior to tissue lysis greatly reduces background for liver lysate.
3. Prepare the standards for BCA assay with the MSD lysis buffer.
4. We strongly recommend validating any new lot of polyclonal antibody used in the MSD-ECL assay, since they may come from different immunized animals and the specificity of antibody may be different.
5. Store calibration curve standards, QCs and test sample lysates in small aliquots at -80 °C to avoid multiple freeze-thaw cycles (although establishment of freeze-thaw stability is recommended).
6. Blocker A (R93BA-4) for MSD-ECL assay is based on bovine serum albumin (BSA) and causes high background in our hands. Blocker B (R93BB-2) for MSD-ECL is based on milk proteins and results in low background in MSD-ECL assay.

Recipes

1. MSD lysis buffer

Components	Amount	Final Concentration
10× TBS, pH 7.4	5 mL	1×
10% TX-100	5 mL	1%
10% Nonidet P-40	2.5 mL	0.5%
Na deoxycholate	125 mg	0.25%
0.5 M EDTA	100 μ L	1 mM
Bring up the volume to 50 mL with dH ₂ O		

Acknowledgments

This protocol was originally used in the research paper “Antisense oligonucleotides increase *Scn1a* expression and reduce seizures and SUDEP incidence in a mouse model of Dravet syndrome” (Han *et al.*, 2020).

Competing interests

ZH, AC, M and GL are employees of Stoke Therapeutics, Inc. ZH is one of the inventors on patent/patent application (PCT/US2018/48031; WO/2019/040923) submitted by Stoke Therapeutics, Inc. that covers use of therapeutic agents to promote exclusion of the NMD exon from the NMD exon mRNA encoding Nav1.1.

Ethics

Procedures involving mice were performed under protocols approved by the Institutional Animal Care and Use Committee (IACUC) of Stoke Therapeutics, Inc. Approval ID: STK2019-03-CNS. Validity period: 04/11/2019 to 04/11/2022. All *in vivo* experiment procedures were in accordance with the NIH Guide for the Care and Use of Laboratory Animals. No human subject was involved in this study.

References

- Meisler, M. H., O'Brien, J. E. and Sharkey, L. M. (2010). [Sodium channel gene family: epilepsy mutations, gene interactions and modifier effects](#). *J Physiol* 588(Pt 11): 1841-1848.
- Dravet, C., Bureau, M., Oguni, H., Fukuyama, Y. and Cokar, O. (2005) [Severe myoclonic epilepsy in infancy: Dravet syndrome](#). *Adv Neurol* 95: 71-102.
- Kuhle, J., Barro, C., Andreasson, U., Derfuss, T., Lindberg, R., Sandelius, Å., Liman, V., Norgren, N., Blennow, K. and Zetterberg, H. (2016). [Comparison of three analytical platforms for quantification of the neurofilament light chain in blood samples: ELISA, electrochemiluminescence immunoassay and Simoa](#). *Clin Chem Lab Med* 54(10): 1655-1661.
- Cabral, F., Miller, C. M., Kudrna, K. M., Hass, B. E., Daubendiek, J. G., Kellar, B. M., and Harris, E. N. (2018). [Purification of Hepatocytes and Sinusoidal Endothelial Cells from Mouse Liver Perfusion. Journal of visualized experiments](#). *J Vis Exp* (132): 56993.
- Chan, D. S., Kavanagh, M. E., McLean, K. J., Munro, A. W., Matak-Vinković, D., Coyne, A. G. and Abell, C. (2017). [Effect of DMSO on Protein Structure and Interactions Assessed by Collision-Induced Dissociation and Unfolding](#). *Anal Chem* 89(18): 9976-9983.
- Han, Z., Chen, C., Christiansen, A., Ji, S., Lin, Q., Anumonwo, C., Liu, C., Leiser, S. C., Meena, Aznarez, I., Liau, G. and Isom, L. L. (2020). [Antisense oligonucleotides increase Scn1a expression and reduce seizures and SUDEP incidence in a mouse model of Dravet syndrome](#). *Sci Transl Med* 12(558): eaaz6100.

Generation of Human iPSC-derived Neural Progenitor Cells (NPCs) as Drug Discovery Model for Neurological and Mitochondrial Disorders

Annika Zink^{1,2}, Paweł Lisowski^{1,2,3} and Alessandro Prigione^{1,2,*}

¹Department of General Pediatrics, Neonatology, and Pediatric Cardiology, Heinrich Heine University, Duesseldorf, Germany

²Max Delbrück Center for Molecular Medicine (MDC), Berlin, Germany

³Institute of Genetics and Animal Biotechnology, Polish Academy of Sciences, Magdalanka, Warsaw, Poland

*For correspondence: alessandro.prigione@hhu.de

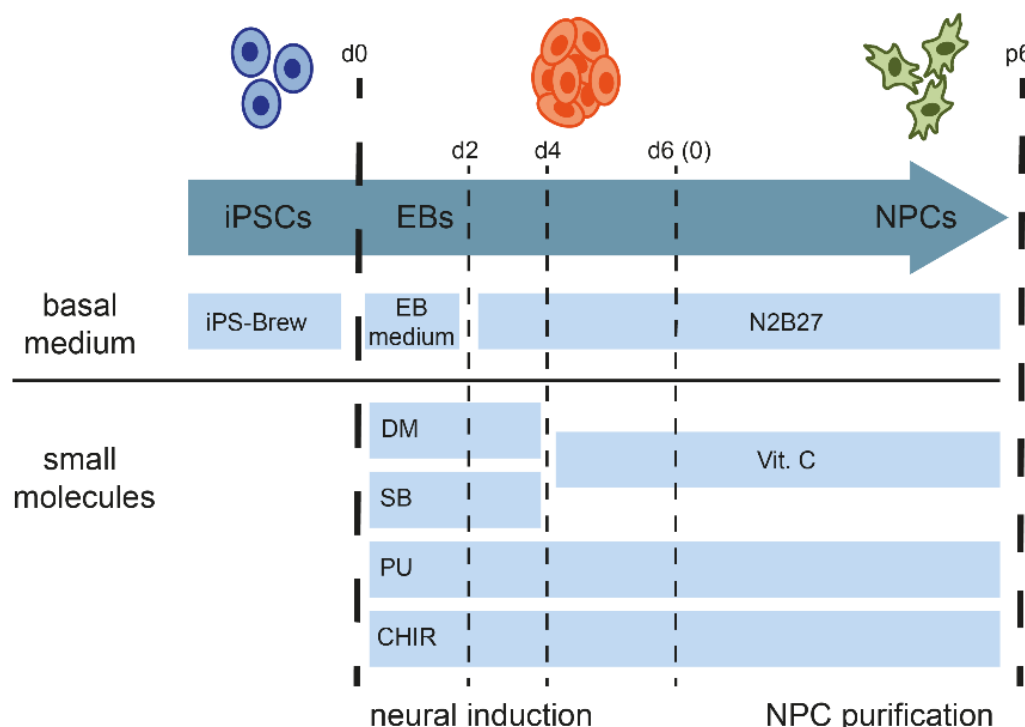
Abstract

The high attrition rate in drug development processes calls for additional human-based model systems. However, in the context of brain disorders, sampling live neuronal cells for compound testing is not applicable. The use of human induced pluripotent stem cells (iPSCs) has revolutionized the field of neuronal disease modeling and drug discovery. Thanks to the development of iPSC-based neuronal differentiation protocols, including tridimensional cerebral organoids, it is now possible to molecularly dissect human neuronal development and human brain disease pathogenesis in a dish. These approaches may allow dissecting patient-specific treatment efficacy in a disease-relevant cellular context. For drug discovery approaches, however, a highly reproducible and cost-effective cell model is desirable. Here, we describe a step-by-step process for generating robust and expandable neural progenitor cells (NPCs) from human iPSCs. NPCs generated with this protocol are homogeneous and highly proliferative. These features make NPCs suitable for the development of high-throughput compound screenings for drug discovery. Human iPSC-derived NPCs show a metabolism dependent on mitochondrial activity and can therefore be used also to investigate neurological disorders in which mitochondrial function is affected. The protocol covers all steps necessary for the preparation, culture, and characterization of human iPSC-derived NPCs.

Keywords: Human iPSCs, Neural progenitor cells, Drug discovery, Stem cell differentiation, Neuronal disease modeling, Mitochondrial disorders

This protocol was validated in: Cell Stem Cell (2017), DOI: 10.1016/j.stem.2016.12.013

Graphical abstract:



Schematic of the protocol for the generation of human iPSC-derived NPCs

Background

In recent years, the downsides of target-centered drug discovery have become evident, in particular for programs addressing neurological diseases (Paul *et al.*, 2010). The challenges of target-based drug discovery led to the revival of phenotypic drug discovery. Phenotypic screenings require the identification of a disease-specific trait (phenotype) that can be modulated within the physiological environment of a cell or organism (Khurana *et al.*, 2015). This approach has the advantage of identifying compounds that show an effect within complex biological environments. At the same time, phenotypic drug discovery requires the presence of a robust disease-relevant phenotype that can be efficiently modulated using a reliable high-throughput detection method. Current drug discovery pipelines strongly rely on cancer-derived immortalized cell lines that lack the functional properties of brain cells. Moreover, immortalized cell lines are mostly glycolytic and less sensitive to mitochondrial impairment than neuronal cells (Bénit *et al.*, 2016). Therefore, immortalized cells are not an effective drug discovery model for neurological diseases and diseases in which mitochondrial oxidative phosphorylation (OXPHOS) is dysfunctional, such as mitochondrial disorders and neurodegeneration (Cunnane *et al.*, 2020).

An important breakthrough in the field of neuronal disease modeling and drug discovery is represented by cellular reprogramming technologies. Cellular reprogramming allows the conversion of the identity of a given cell, thereby enabling the generation of brain cells from patient-specific somatic cells. Cellular conversion can be accomplished through the derivation of induced pluripotent stem cells (iPSCs) (Takahashi *et al.*, 2007) or through the process of direct conversion, which can reprogram skin cells directly into post-mitotic induced neurons (iNs) (Vierbuchen *et al.*, 2010). iPSCs can also be used to derive three-dimensional (3D) cerebral organoids that may recapitulate the organization of the developing human brain (Lancaster *et al.*, 2013).

In order to perform meaningful phenotypic screens, it is necessary to use disease-relevant cellular models. Among reprogramming-derived cell types, patient-specific neural progenitor cells (NPCs) appear particularly well suited

for phenotypic drug discovery of neurological diseases, given their homogeneous features, cost-effective culture conditions, and mild proliferative state. Indeed, iPSC-derived NPCs have been successfully employed for drug discovery in the context of neurological and neuropsychiatric disorders (Lorenz *et al.*, 2017; Readhead *et al.*, 2018; Walter *et al.*, 2019).

During the process of neurogenesis, which is characterized by a metabolic shift from glycolysis to OXPHOS (Zheng *et al.*, 2016), NPCs represent the first cell type to depend on mitochondrial respiration (Beckervordersandforth, 2017; Lorenz and Prigione, 2017). Since NPCs show sensitivity to conditions that impair OXPHOS, they can be used as an effective cell model to carry out high-throughput screenings for neurological and mitochondrial diseases. Accordingly, iPSC-derived NPCs from patients affected by mitochondrial diseases exhibited meaningful phenotypes that could be harnessed to perform phenotypic compound screenings (Lorenz *et al.*, 2017). Altogether, iPSC-derived NPCs might be instrumental for identifying novel treatments in the context of neurological and mitochondrial diseases that are hard to model using conventional drug discovery systems (Inak *et al.*, 2017).

Here, we describe in detail the generation and maintenance of human iPSC-derived NPCs. Different protocols can be used to obtain these cells. Some protocols give rise to NPC populations with limited proliferative features (Elkabetz *et al.*, 2008), while others may depend on the addition of human LIF, which makes culturing the cells very cost-intensive (Li *et al.*, 2011). However, most useful approaches rely solely on small molecule to produce highly proliferative NPC populations (Reinhardt *et al.*, 2013). A key characteristic of these NPCs is their capability of robust and homogenous expansion. At the same time, NPCs should be able to efficiently differentiate into neuronal and glial cell types (Reinhardt *et al.*, 2013; Lorenz *et al.*, 2017).

Our approach is based on the protocol of Reinhardt *et al.* (2013) and was published in Lorenz *et al.* (2017) for drug discovery applications in the context of neurological mitochondrial diseases. The protocol allows the generation of NPCs that maintain their characteristics under chemically defined conditions over several passages and can be readily differentiated into the desired brain cell types. The protocol is highly reproducible and leads to homogenous cell populations. It is similarly effective starting from human embryonic stem cells, healthy control iPSCs, and patient-specific iPSCs (Lorenz *et al.*, 2017).

To initiate neural induction, bone morphogenic protein (BMP) inhibitor dorsomorphin (DM), and transforming growth factor β (TGF β)-signaling inhibitor SB43152 (SB) are supplemented to the basic NPC media (BM1). Purmorphamine (PU) and CHIR99021 (CHIR) are added to stimulate the sonic hedgehog (SHH) signaling pathway, inhibit glycogen synthase kinase-3 (GSK3), and activate canonical WNT signaling (Chambers *et al.*, 2009; Kim *et al.*, 2010). After the first days in the induction medium, embryoid bodies (EBs) form neuroepithelial structures (**Figure 1A**). After 6 days, the EBs are gently dissociated and seeded on Matrigel-coated plates for purification. Neural progenitor morphology becomes homogenous after 4-6 passages post neural induction (**Figure 1A**). NPCs should express typical NPC markers such as NESTIN, PAX6, SOX1, SOX2, and DACH1. Spontaneous differentiation of cells expressing the pan-neuronal marker TUJ1 is always present (**Figure 1C-1D**). Conversely, pluripotency markers like OCT4, NANOG, DNMT3B, and DPPA4 should be downregulated compared to the parental iPSC lines. NPCs retain their multipotent identity over multiple passages (> 30) as well as after freezing and thawing without changes in cell morphology.

The following step-by-step protocol allows the experimenter to obtain human iPSC-derived NPCs with a high degree of homogeneity within 4-8 weeks, and to culture and characterize the cells for subsequent use in disease modeling or drug discovery applications.

Materials and Reagents

The following list provides examples of the materials and equipment that we routinely use in our laboratory. Nevertheless, reagents and equipment with similar specifications will work as well.

1. Cellstar cell culture multiwell plates (6-24 well) (Greiner Bio-One, catalog numbers: 657 160 [6-well]; 665 180 [12-well]; 662 160 [24-well])
2. Corning 60 mm Ultra-low attachment culture dish (Corning, catalog number: 3261)
3. Cell spatula (TPP, catalog number: 99010)
4. Serological pipettes (Greiner Bio-One, catalog numbers: 760180 [2 mL]; 606180 [5 mL]; 607180 [10 mL];

- 760107 [25 mL]; 768160 [50 mL]
5. BemisTM Curwood ParafilmTM M Laboratory Film (Fisher Scientific, product code HS234526C, catalog number: 10018130)
 6. Greiner centrifuge tubes (50 mL and 15 mL) (Sigma-Aldrich, manufacturer: Greiner; catalog number for 15 mL: T1818, for 50 mL: T2318)
 7. Liquid nitrogen
 8. Corning[®] Matrigel[®] Growth Factor Reduced (GFR) Basement Membrane Matrix, Phenolred-free, LDEV-free (Corning, CAS number: 356231, format: 10 mL, store at -20 °C and follow instructions from supplier for preparation)
 9. CHIR 99021 (Caymen Chemical, CAS number: 252917-06-9, catalog number: 13122; product format: 2.5 mg/ml in DMSO; storage at -20 °C as 6 mM stock; stability: ≥ 2 years)
 10. SB431542 in solution (MACS Miltenyi, CAS number: 130-106-543, catalog number: 130-106-543; product format: 10 mM in DMSO; storage at -20 °C as 10 mM stock, protected from light; stability: 6 months)
 11. Dorsomorphin (StemCell; CAS number: 866405-64-3, catalog number: 72102; product format 10 mg solid; storage at -20 °C as 5 mM stock in DMSO (heat applied) or ethanol; stability: 12 months)
 12. Purmorphamlin (MACS Miltenyi, CAS number: 483367-10-8; catalog number: 130-104-465 product format: 5 mg solid; storage at -20 °C as 10mM stock in DMSO, protected from light)
 13. (+)-Sodium L-ascorbate (Vitamin C) (Merck, Sigma-Aldrich, catalog number: A4034; product format solid powder; store as 200 μM stock in water at -20 °C)
 14. N-2 Supplement (100×) (Thermo Fisher Scientific, Gibco, catalog number: 17502-048; product format: 5 mL liquid; store at -20 °C, protected from light; stability: 18 months)
 15. B27 without Vitamin A (50×) (Thermo Fisher Scientific, Gibco, catalog number: 12587010; product format: 10 mL liquid; store at -20 °C protected from light)
 16. Neurobasal[®] Medium (Thermo Fisher Scientific, Gibco, catalog number: 21103049; product format: 500 mL liquid; store at 2-8 °C, protected from light; shelf life: 12 months)
 17. DMEM/F12, HEPES (Thermo Fisher Scientific, Gibco, catalog number: 31330038; product format: 500 mL liquid; store at 2-8 °C, protected from light; shelf life: 12 months)
 18. KnockOut DMEM (Thermo Fisher Scientific, Gibco, catalog number: 10829018; product format: 500 mL liquid; store at 2-8 °C protected from light)
 19. KnockOut Serum replacement (Thermo Fisher Scientific, Gibco, catalog number: 10828010; product format: 500 mL liquid; store at -20 °C protected from light)
 20. StemMACS[™] iPS-Brew XF, human (MACS Miltenyi Biotec, catalog number: 130-104-368)
 21. mTeSR[™]1 (STEMCELL Technologies, catalog number for 500 mL kit: 85850)
 22. Penicillin-Streptomycin (P/S; 10,000 U/ml Penicillin, 10,000 μg/ml Streptomycin) (Thermo Fisher Scientific, Gibco, catalog number 15140122; product format: 100 mL liquid; store at -20 °C; shelf life: 12 months)
 23. L-Glutamine (200 mM) (Thermo Fisher Scientific, Gibco, Catalog number: 25030081; product format: 100 mL liquid; store at -20 °C, protected from light; shelf life: 24 months)
 24. Non-essential amino acids (NEAA, 100×) (Thermo Fisher Scientific, Gibco, catalog number: 11140035, product format: 100 mL, store at 2-8 °C; shelf life: 12 months)
 25. Sodium pyruvate (100 mM) (Thermo Fisher Scientific, Gibco, catalog number: 11360070; product format: 100 mL; store at 2-8 °C protected from light; shelf life: 12 months)
 26. MycoZap Plus-CL (Lonza, catalog number VZA-2012; product format: 20 mL liquid; store at -20 °C, protected from light)
 27. StemPro[™] Accutase[™] Cell Dissociation Reagent (Thermo Fisher Scientific, Gibco/StemPro, catalog number: A1110501; product format: 100 mL liquid, store at -20 °C, protected from light)
 28. DPBS (without calcium and magnesium) (Thermo Fisher Scientific, Gibco, catalog number: 14190250; product format: 500 mL liquid; store at 15-30 °C; shelf life: 36 months)
 29. ROCK inhibitor (RI), Y-27632, dihydrochloride (Enzo, CAS number: 129830-38-2; catalog number: ALX-270-333-M005; product format 5 mg powder; store at -20 °C; soluble in DMSO as 25 mg/ml; stability: stock solution stable for 1 month at -20 °C)
 30. UltraPure[™] 0.5 M EDTA (Invitrogen, catalog number: 15575020)

31. Bambanker (NIPPON Genetics, catalog number: BB03)
32. ShandonTM Immu-MountTM (Thermo ScientificTM, catalog number: 77-86-1; reference number 9990402; product formal: 20 mL)
33. Anti-Nestin Antibody, clone 10C2 (Millipore, catalog number: MAB5326; Brand family: Chemicon[®])
34. Anti-Pax-6 Antibody (Covance, catalog number: 901301)
35. SOX2 antibody (R&D Systems, catalog number: AF2018)
36. DACH1 antibody (ProteinTech, catalog number: 10914-1-AP)
37. Anti-β-Tubulin III (TUJ-1) (Sigma-Aldrich, catalog number: T8578)
38. MAP2 (Synaptic system, catalog number: 188004)
39. Hoechst 33342 (Hoechst) (InvitrogenTM, catalog number: H3570)
40. 16% Paraformaldehyde Aqueous Solution (PFA) (Electron Microscopy Sciences; catalog number: 50-980-487)
41. Tween-20 (Sigma-Aldrich, catalog number: P9416)
42. TritonTM-X100 (Sigma-Aldrich, catalog number: T8532)
43. Alexa FluorTM 488 donkey anti-rabbit IgG (H+L) secondary antibody (Thermo Fisher Scientific, catalog number: A-21206)
44. Alexa FluorTM 647 donkey anti-mouse IgG (H+L) secondary antibody (Thermo Fisher Scientific, catalog number: A-31571)
45. Donkey anti-goat Cy 3 (Sigma-Aldrich, catalog number: AP180C)
46. Donkey anti-guinea pig Cy 3 (Sigma-Aldrich, catalog number: AP193C)
47. SYBRTM Green PCR Master Mix (Thermo Fisher Scientific, catalog number: 4309155)
48. M-MLV Reverse Transcriptase (Invitrogen, catalog number: 28025013)
49. RNeasy Mini Kit (50) (Qiagen, catalog number: 74104)
50. Rnase-Free Dnase Set (50) (Qiagen, catalog number: 79254)
51. Oligo(dT) 12-18 Primer (Invitrogen, catalog number: 18418012)
52. dNTP-Mix (10 mM) (Invitrogen, catalog number: 18427088)
53. MicroAmpTM Optical 348-well-reaction plate with barcode (Thermo Fisher Scientific, catalog number: 4343814)
54. Basic medium 1 (BM1) (see Recipes, Table 1)
55. BM2 (sm-) medium (see Recipes, Table 1)
56. M1 medium (see Recipes, Table 2)
57. M2 medium (see Recipes, Table 2)
58. M3 (sm+) medium (see Recipes, Table 2)

Equipment

1. Centrifuge (Eppendorf, model: 5810R)
2. Water bath (Thermo Fisher Scientific, FisherbrandTM IsotempTM Digital-Control Water Baths: Model 220)
3. CO₂ incubator for cell culture (Thermo Fisher Scientific, model: Heraeus BBD 6220)
4. Hypoxia incubator for iPSC culture (Binder GmbH, model: Binder BCB 160)
5. qPCR machine (Thermo Fisher Scientific, model: ViiA 7)
6. Confocal Microscope system (Zeiss, model: Axio Imager Z1)
7. Freezing container (Nalgene, model: Mr. Frosty; Corning CoolCellTM)
8. -80°C Freezer (New Brunswick, model: Innova 4725)
9. Laminar flow hood (BDK, Luft und Reinraumtechnik GMBH)
10. Sterile scissor (for example: Surgical scissors, sharp, Sigma-Aldrich, catalog number: Z265977)
11. Shaker (Rocky, LTF Labortechnik)

Procedure

In general:

1. Work under sterile conditions, *e.g.*, under a laminar flow hood.
2. Disinfect reagents and consumables before transferring under the hood.
3. All media should be prepared fresh and used within one week.
4. Do not thaw N-2 Supplement and B-27 Supplement in the water bath. Instead thaw them at room temperature (RT, 20–22 °C) for 2–4 h or in the fridge (4 °C) over night.
5. All media should be pre-warmed before applying to the cells. Do not keep the media at 37 °C for long periods but rather pre-warm at RT.
6. Culture the NPCs and iPSCs in a controlled environment with 37 °C and 5% CO₂.
 - a. Optional: If possible, culture the iPSCs under hypoxic conditions (37 °C, 5% CO₂, 5% O₂), which more closely mimics *in vivo* conditions.
 - b. We culture iPSCs under feeder-free conditions in either StemMACS™ iPS-Brew XF, or mTeSR™1 on Matrigel-coated 6-well plates.
 - c. We passage iPSCs using 0.5 mM EDTA/PBS in ratios ranging from 1:4–1:12. To increase cell survival, we recommend adding ROCK inhibitor (RI) after each splitting in a concentration of 10 µM.

A. Step-by-step protocol for NPC generation

Day 0 (Monday): Harvesting of the iPSCs and transfer on Corning Ultra-Low Attachment 60mm/15mm dishes.

1. Prepare the basic medium 1 (**BM1**) (Table 1).
2. Prepare **M1** medium (Table 2).
3. Choose one to two wells of iPSCs (~80% confluent).
4. Remove the media and rinse the wells twice with DPBS to remove dead cells and debris.
5. Detach cells from the plate using Accutase (1 mg/ml). Add 0.5–1 mL/well and incubate for 2–5 min at 37 °C, check visually in between.
6. Continue when colonies are mainly detaching from the plate.
7. Add 4–10 mL PBS or medium to reduce Accutase activity.
8. Optional: Mechanically detach cells using a cell spatula if cells are not completely detached by Accutase activity.
9. Transfer the cell suspension to a 15 mL Falcon tube (pool both wells), let the cells settle to the bottom (10–15 min) in water bath.
10. Optional: Centrifuge at 120 × g for 5 min (potentially more damaging but faster and results in a more solid pellet).
11. Remove as much medium as possible from the sedimented cells by pipetting (for example with a 5 mL serological pipette). Make sure not to disperse or suck up the cells.
12. Add 5 mL of M1 to the cells, transfer the cells to a non-treated Corning Ultra-Low Attachment 60 mm/15 mm dish (1:1; or X number of wells in case of high confluence).
13. Incubate at 37 °C, 5% CO₂ for 2 days.
14. Incubation with M1 will form embryoid bodies (EBs) floating in the media. If they attach at day 1 to the bottom of the Corning Ultra-Low attachment 60 mm/15 mm dish, detach them by gently pipetting using a 1 mL pipette (cut off the tip with sterile scissors!). Make sure not to shred the floating EBs. Alternatively, use a cell spatula. Keep the media in the well and gently scrape throughout the well using a cell spatula to detach EBs.

Day 2 (Wednesday): 50% media exchange to **M2**

1. Prepare **BM2 (sm-)** medium (Table 1).
2. Prepare **M2** medium (Table 2).

3. Cut off the tip of a 1 mL pipet tip using a sterile scissor.
4. Transfer EBs to a 15 mL Falcon tube using a 1 mL pipette tip (cut off the tip!).
5. Optional: If some EBs attached, detach EBs using a cell spatula.
6. Let EBs settle for 15 min in the water bath at 37 °C.
7. Remove 50% of **M1** and add 50% of **M2** instead.
Optional: Remove all M1 and add 100% M2 (but potentially more damaging for the cells).
8. Transfer the EBs back to the same Corning Ultra-Low Attachment 60 mm/15 mm dish using a 1 mL pipette tip (cut off the tip using a sterile scissor!).

Day 3 (Thursday): 100% media exchange to **M2**

1. Prepare **M2** medium (Table 2).
2. Cut off the tip of a 1 mL pipet tip using a sterile scissor.
3. Transfer EBs to a 15 mL Falcon tube using a 1 mL pipette tip (cut off the tip!).
4. Optional: If necessary, detach EBs using a cell spatula as described before.
5. Let EBs settle for 15 min in the water bath at 37 °C.
6. Exchange the medium completely to 100% of **M2** medium (5-6 mL final volume).
7. Transfer EBs back to the same Corning Ultra-Low Attachment 60 mm/15 mm dish using a 1 mL pipette tip (cut off the tip using a sterile scissor!).

Day 4 (Friday): 100% media exchange to **M3 (sm+)** and preparation of Matrigel-coated plates

1. Prepare **M3 (sm+)** medium (Table 2).
2. Cut off the tip of a 1 mL pipet tip using a sterile scissor.
3. Transfer EBs to a 15 mL Falcon tube using a 1 mL pipette tip (cut off the tip!).
4. Optional: If necessary, detach EBs using a cell spatula as described before.
5. Let EBs settle for 15 min in the water bath at 37 °C.
6. Exchange the media completely to 100% of **M3 (sm+)** medium (5-6 mL final volume).
7. Transfer EBs back to the same Corning Ultra-Low Attachment 60 mm/15 mm dish using a 1 mL pipette tip (cut off the tip using a sterile scissor!).
8. Coat a 6-well plate with Matrigel (procedure described separately) as preparation for day 7.

Day 7 (Monday): Transfer the cells to Matrigel-coated plates

1. Prepare **M3 (sm+)** medium (Table 2).
2. Transfer EBs from the Corning Ultra-Low Attachment 60 mm/15 mm dish to a 15 mL Falcon tube. Use a 1 mL tip (cut off the tip!).
If necessary, detach neural tube-like formations using a cell spatula as described for EBs.
3. Let EBs settle down in the water bath at 37 °C (10-15 min).
4. Remove old media.
5. Add new **sm+** medium.
6. Shred the cell formations by pipetting 5-10 times using a normal 1 mL tip.
7. Transfer the whole suspension to the Matrigel-coated 6-well plate, distribute equally to 2-X wells depending on the amount of EBs.
8. Fill up to 2 mL **sm+** each 6-well.
9. Add ROCK inhibitor (RI) (10 µM final concentration).

Note: To increase cell survival, we recommend adding RI to the cells for the first 1-2 splittings. Afterwards, RI is not needed!

10. Check the next day, NPC-like cells should be already visible (see Figure 1A–right image, and Figure 1E).
11. Try to keep the cells in the first well for 1 week.
12. If necessary, split the cells as described in the maintenance protocol.

Note: NPCs should appear homogenous after 4-5 passages, expressing NESTIN, PAX6, and SOX2. NPCs usually also express the immature pan-neuronal marker TUJ1. Spontaneous differentiation can occur, and some cells can express the neuronal marker MAP2. Cells do not necessarily need to be cultured in 6-well plates.

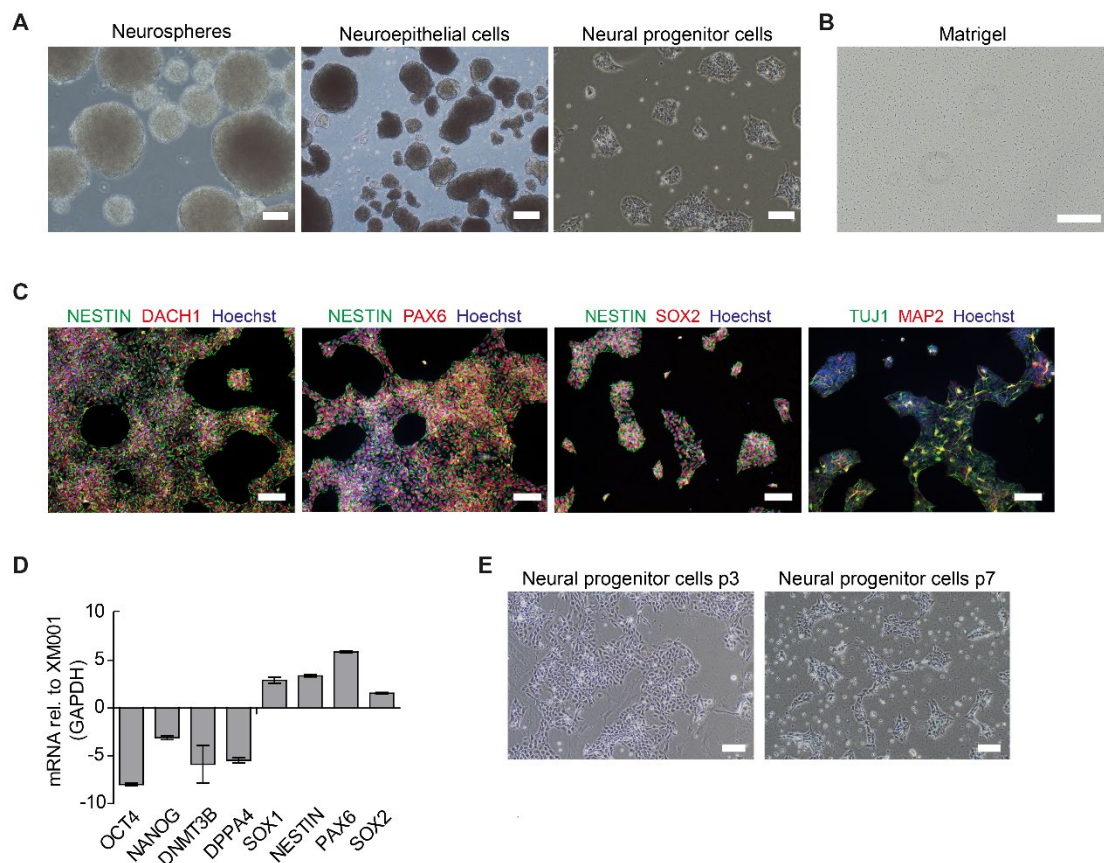


Figure 1. Generation and characterization of human iPSC-derived NPCs.

A. Representative images of neurospheres, neuroepithelial cells, and neural progenitor cells (NPCs). B. Image of a matrigel coated well. Scale bar: 200 μ m. C. Immunocytochemistry of NPCs obtained from the control iPSC line XM001 (Wang *et al.*, 2018) stained for the neural progenitor markers NESTIN, DACH1, PAX6, and SOX2. Spontaneous differentiation of cells expressing TUJ1 or MAP2 can be present. Scale bar: 100 μ m. D. Quantitative real-time reverse transcription PCR (qRT-PCR) of neural progenitor markers SOX1, NESTIN, PAX6, and SOX2, and of pluripotency-associated markers OCT4, NANOG, DNMT3B, and DPPA4. Transcription levels in NPCs were normalized using GAPDH housekeeper gene (mean=SD +/-; n=3 technical replicates) and reported in relation to the transcription level of the respective control iPSC line XM001. E. Representative images of neural progenitor cells (NPCs) from passage 3 (p3) and passage 7 (p7) demonstrating the change in morphology towards homogenous NPC cultures. Scale bar: 100 μ m.

B. Matrikel preparation

1. Thaw frozen Matrikel (stored at -20 °C) OVERNIGHT (ON) **on ice at +4 °C**.
2. Check protein concentration (stock concentration) of Matrikel as provided in Lot datasheet.

3. Calculation: Add a specific volume (=x) of cold KnockOut-DMEM to the 10 mL thawed Matrigel in the vial to dilute it to 5 mg/ml final concentration. The stock concentration of your vial (=y) should be written on the lot datasheet. Calculate the needed volume using the formula: $x = y * 2-10 \text{ mL}$.
4. Perform next steps under the hood and on ice!
5. Prepare a pre-chilled 50 mL Falcon tube with specific volume of cold KnockOut-DMEM.
6. Prepare pre-chilled 15 mL Falcon tubes on ice labeled with 1 M.
7. Transfer Matrigel quickly to KnockOut-DMEM and mix carefully.
8. Aliquot 1 mL of the diluted Matrigel in each pre-chilled 15 mL Falcon tube.
9. Store Aliquots immediately at -20 °C.
10. Final concentration in 6/12-well-plates: 200 µg/ml.

C. Coating plates with Matrigel

1. Transfer 30 mL **cold** KnockOut-DMEM into a 50 mL Falcon tube.
2. Dilute 1 mL aliquot 1:30 in cold KnockOut-DMEM.
3. Resuspend the 1 mL Matrigel aliquot (15 mL Falcon tube, -20 °C) with 5 mL of the 30 mL **cold** KnockOut-DMEM in the 15 mL Falcon tube until pellet is resolved! (It may take a while).
4. 1 mL Matrigel aliquot resuspended in 30 mL cold KnockOut-DMEM as described in C2 is enough for 4 plates.
 - a. 6-well: 1.25 mL.
 - b. 12-well: 500 µL.
 - c. 24-well: 300 µL.
5. Add Matrigel-medium to the wells (see point 4).
6. Polymerization:
 - a. Store at 4 °C in the fridge, ON (preferentially!).
 - b. 2 h at 37 °C is possible.
7. Check polymerization in phase contrast before use! The evenly distributed formation of an extracellular matrix should be visible (Figure 1B). Coated plates can be stored for 1-2 weeks (4 °C). For storage seal the plates with Parafilm.
8. Before use, pre-warm the plate either at RT or 37 °C.

D. Maintenance of NPC cultures

1. Media needs to be changed every 2nd day.
2. Media should be pre-warmed before applying to the cells. Do not keep media at 37 °C for long periods but rather pre-warm at RT.
3. Typically, cells were split using Accutase in ratios of 1:3 up to 1:10 every 4-5 days depending on the cell density.

E. Splitting NPCs

1. Aspirate growth media.
2. Add 500 µl Accutase and incubate for 2-5 min at RT or 37 °C if cells do not detach easily.
3. Dilute Accutase activity by addition of 2 mL **sm-** (without any supplementation) or PBS.
4. Gently detach the cells by pipetting.
5. Transfer the cells to a 15 mL Falcon tube and centrifuge at 200 × g for 3 min at RT.
6. In the meantime, prepare Matrigel-coated plates for plating the cells.
 - a. Aspirate Matrigel-mix.
 - b. Add 1 mL **sm+** and store in the incubator until further use.
 - c. Fill blank wells with 2 mL DPBS.

Note: Matrigel coating should not dry out.

7. Aspirate the supernatant.
8. Resuspend the pellet in **sm+** medium.
9. Distribute cells to Matrigel-coated 6-well plates.
10. Fill up with media to 2 mL **sm+**.

Note: To increase cell survival, we recommend adding RI (10 µM) to the cells for the first 1-2 splittings. Afterwards, RI is not needed!

F. Freezing NPCs

1. Detach NPCs according to the splitting procedure.
2. Resuspend NPCs in 0.5 mL of **sm+**. Add freezing medium (**2× sm+ freeze:sm+**, 1:1).
Note: 10 mL of 2× sm+ freeze is prepared by mixing 2 mL of sm+, 6 mL of KnockOut-SR, and 2 mL of DMSO.
3. Alternatively, use commercial freezing media according to manufacturer's protocol.

Note: For example, Bambanker (Nippon Genetics, catalog number: BB03).

4. Transfer the resuspended NPCs into a cryovial and place the vials at -80 °C in a cryo-freezing container.

Note: Use a freezing container such as Mr. Frosty™ (Nalgene) to freeze the cells, which allows slow freezing at a rate of -1 °C per minute.

5. Store NPCs at -80 °C or in a liquid nitrogen tank for long term storage (1-3 years).

G. Thawing NPCs

1. Quickly but gently thaw the cryovial containing NPCs in a 37 °C pre-warmed water bath.
2. Transfer NPCs into a 15 mL Falcon tube set with 1 mL of **sm+** and up to 10 mL of pre-warmed PBS.
3. Centrifuged the cells at 200 × g for 3 min.
4. Remove the supernatant and resuspend NPCs in **sm+** medium.
5. Seed NPCs on previously prepared Matrigel-coated plates 1:1 (see Coating plates with Matrigel).

Note: Add 10 µM RI after thawing to support cell survival.

H. Characterization of NPCs by immunofluorescence

1. After 4-6 passages, seed NPCs on Matrigel-coated 24-well plates containing 12 mm coverslips. When reaching approximately 80% of confluence, rinse NPCs with PBS, and fix the cells with a 4% paraformaldehyde (PFA)/PBS solution for 15 min at RT.
2. Remove the PFA and rinse NPCs with PBS calcium/magnesium free (PBS -/-) 3 times for 5 min.
3. Add blocking solution to the cells for 1 h at RT.

Note: Blocking solution is prepared with 10% donkey serum and 1% Triton X-100 in PBS -/- with 0.1% Tween-20.

4. Incubate the cells with specific primary antibodies overnight at 4 °C on an orbital shaker (60-80 rpm).

Note: Dilute primary antibody in blocking solution. Following antibodies are commonly used in our laboratory: NESTIN (Millipore, 1:200), PAX6 (Covance, 1:200), SOX2 (Santa Cruz, 1:100), DACH1 (ProteinTech, 1:100), TUJ-1 (Sigma-Aldrich, 1:1,000), MAP2 (Synaptic system, 1:1,000).

5. Rinse the cells with PBS -/-, 3 times for 5 min.
6. Incubate the cells with a specific secondary antibody and Hoechst staining (1:2500) for nucleus visualization for at least 1 h at RT.

Note: Dilute secondary antibodies 1:300 using blocking solution. Following secondary antibodies are commonly used in our laboratory: Alexa FluorTM 488 donkey anti-rabbit IgG (H+L) (Thermo Fisher Scientific), Alexa FluorTM 647 donkey anti-mouse IgG (H+L) (Thermo Fisher Scientific), donkey anti-goat Cy 3 (Sigma-Aldrich) and donkey anti-guinea pig Cy 3 (Sigma-Aldrich).

7. Rinse the cells with PBS -/-, 3 times for 5 min.
8. Invert coverslips and mount them to a glass slide using mounting medium (IMMU-MOUNTTM or similar). After the mounting medium is dry the samples can be analyzed by confocal imaging.

I. Characterization of NPCs by quantitative real-time reverse transcription PCR (qRT-PCR)

1. Prepare SYBR Green PCR Master Mix according to the manufacturer's description.
2. Pipette the PCR master mix and the cDNA samples into the 384-Well Optical Reaction Plates (Applied Biosystems).

Note: RNA was extracted from cell pellets using the RNeasy Mini Kit (50) from Qiagen according to the manufacturers protocol. cDNA was generated using the Moloney Murine Leukemia Virus (M-MLV) Reverse Transcriptase kit from Thermo Fisher Scientific according to the manufacturers protocol. For each target gene, cDNA samples and negative controls should be measured in biological triplicates.

3. Set the PCR cycle conditions as follows: 1 cycle 50 °C 2 min, 1 cycle 95 °C 10 min, 40 cycles 95 °C 15 s → 60 °C 30 s → 72 °C 30 s, 1 cycle 72 °C 10 min.
4. Primers used were:

For OCT4

F: GTGGAGGAAGCTGACAACAA and R: ATTCTCCAGGTTGCCTCTCA

For NANOG

F: CCTGTGATTGTGGCCTG and R: GACAGTCTCCGTGAGGCAT

For SOX2

F: GTATCAGGAGTTGTCAAGGCAGAG and R: TCCTAGTCTAAAGAGGCAGCAAAC

For DNMT3B

F: GCTCACAGGGCCCGATACTT and R: GCAGTCCTGCAGCTCGAGTTA

For DPP4

F: TGTTGTCAGGTGGTGTGG and R: CCAGGCTTGACCAGCATGAA

For VIM

F: GGAGCTGCAGGAGCTGAATG and R: GACTTGCCTGGCCCTTGAG

For NESTIN

F: TTCCCTCAGCTTCAGGAC and R: GAGCAAAGATCCAAGACGC

For PAX6

F: GAATTCTGCAGACCCATGC and R TCTCGTAATACCTGCCAG

For SOX1

F: TTGGCATCTAGGTCTGGCTCA and R: CGGGCGCACTAACTCAGCTT

For SOX2

F: GTATCAGGAGTTGTCAAGGCAGAG and R: TCCTAGTCTAAAGAGGCAGCAAAC

For GAPDH

F: CTGGTAAAGTGGATATTGTTGCCAT and R: TGGAATCATATTGGAACATGTAAACC

Data analysis

Fluorescent images were visualized using the Zeiss Axio Imager Z1 confocal microscope in combination with AxioVision V4.6.3.0 software. Images were merged either directly during image acquisition using AxioVision V4.6.3.0 software, or afterwards using Adobe Photoshop CS6 (Adobe, California, USA).

Gene expression analysis was performed by qRT-PCR using SYBR Green PCR Master Mix and the ViiA™ 7 Real-Time PCR System (Applied Biosystems, California, USA). Relative transcript levels of each gene were calculated based on the $2^{-\Delta\Delta CT}$ method. Data were normalized to the housekeeping gene *GAPDH* and presented as mean LOG2 ratios in relation to control iPSCs.

Recipes

Media formulation (Table 1 and Table 2):

1. All media should be prepared fresh and used within one week.
2. Do not thaw N-2 Supplement and B-27 Supplement in the water bath. Instead thaw them at RT for 2-4 h or in the fridge (4 °C) over night.
3. All media should be pre-warmed before applying to the cells. Do not keep media at 37 °C for long periods but rather pre-warm them at RT.

Table 1. Basic media formulation

Medium	Components	Volume	Stock conc.	Final conc.
Basic Medium 1 (BM1)	KnockOut-DMEM	40 mL	1×	1×
	KnockOut-SR	10 mL	5×	1×
	Pen/Strep	500 µL	10 mg/ml; 10.000 U/ml	0.1 mg/ml; 100 U/ml
	Glutamine	500 µL	200 mM	2 mM
	NEAA	500 µL	100×	1×
	Pyruvate	500 µL	100 mM	1 mM
Basic Medium sm- (base for sm+)	MycoZap	100 µL	500×	1×
	DMEM/F12	240 mL	1×	0.5×
	Neurobasal	240 mL	1×	0.5×
	N-2 Supplement	2.5 mL	100×	0.5×
	B-27 Supplement	5 mL	50×	0.5×
	without vitamin A			
	Pen/Strep	5 mL	10 mg/ml; 10.000 U/ml	0.1 mg/ml; 100 U/ml
	Glutamine	5 mL	200 mM	2 mM
	MycoZap	1 mL	500×	1×

Table 2. Culture media formulation

Medium	Components	Volume	Stock conc.	Final conc.
Medium 1 (M1); day 0-day 2	BM1	10 mL	1×	1×
	CHIR	5 µL	6 mM	3 µM
	SB	10 µL	10 mM	10 µM
	Dorsomorphin	2 µL	5 mM	1 µM
	Purmorphamine	7.69 µL	0.65 mM	500 nM
	sm-	10 mL	1×	1×

Medium 2 (M2); day 2-day 4	CHIR SB Dorsomorphin Purmorphamine	5 µL 10 µL 2 µL 7.69 µL	6 mM 10 mM 5 mM 0.65mM	3 µM 10 µM 1 µM 500 nM
M3/sm+ (maintenance of NPCs)	sm ⁺ CHIR Purmorphamine Vitamin C	10 mL 5 µL 7.69 µL 7.5 µL	1× 6 mM 0.65 mM 200 mM	1× 3 µM 500 nM 150 µM

Acknowledgments

We acknowledge support from the Deutsche Forschungsgemeinschaft (DFG) (PR1527/5-1 to A.P.), Spark-Berlin Institute of Health (BIH Validation Funds to A.P.), National Science Center, Poland (No. 2016/22/M/NZ2/00548; No. 2017/27/B/NZ1/02401 to P.L), the United Mitochondrial Disease Foundation (UMDF to A.P.), and the German Federal Ministry of Education and Research (BMBF) (AZ.031A318 & 031L0211 to A.P.). The original research paper was: Lorenz *et al.*(2017).

Competing interests

The authors declare no competing financial and non-financial competing interests.

Ethics

The study was approved by the ethic committee of the Medical Faculty of Heinrich Heine University (study number 2019/681).

References

- Beckervordersandforth, R. (2017). [Mitochondrial Metabolism-Mediated Regulation of Adult Neurogenesis](#). *Brain Plast* 3(1): 73-87.
- Bénit, P., Schiff, M., Cberman-Thibault, H., Corral-Debrinski, M. and Rustin, P. (2016). [Drug development for mitochondrial disease: recent progress, current challenges, and future prospects](#). *Expert Opin Orphan Drugs* 4: 83-92.
- Chambers, S. M., Fasano, C. A., Papapetrou, E. P., Tomishima, M., Sadelain, M. and Studer, L. (2009). [Highly efficient neural conversion of human ES and iPS cells by dual inhibition of SMAD signaling](#). *Nat Biotechnol* 27(3): 275-280.
- Cunnane, S. C., Trushina, E., Morland, C., Prigione, A., Casadesus, G., Andrews, Z. B., Beal, M. F., Bergersen, L. H., Brinton, R. D., de la Monte, S., Eckert, A., Harvey, J., Jeggo, R., Jhamandas, J. H., Kann, O., la Cour, C. M., Martin, W. F., Mithieux, G., Moreira, P. I., Murphy, M. P., Nave, K. A., Nuriel, T., Oliet, S. H. R., Saudou, F., Mattson, M. P., Swerdlow, R. H. and Millan, M. J. (2020). [Brain energy rescue: an emerging therapeutic concept for neurodegenerative disorders of ageing](#). *Nat Rev Drug Discov* 19(9): 609-633.
- Elkabetz, Y., Panagiotakos, G., Al Shamy, G., Socci, N. D., Tabar, V. and Studer, L. (2008). [Human ES cell-derived neural rosettes reveal a functionally distinct early neural stem cell stage](#). *Genes Dev* 22(2): 152-165.
- Inak, G., Lorenz, C., Lisowski, P., Zink, A., Mlody, B. and Prigione, A. (2017). [Concise Review: Induced Pluripotent Stem Cell-Based Drug Discovery for Mitochondrial Disease](#). *Stem Cells* 35(7): 1655-1662.

- Khurana, V., Tardiff, D. F., Chung, C. Y. and Lindquist, S. (2015). [Toward stem cell-based phenotypic screens for neurodegenerative diseases](#). *Nat Rev Neurol* 11(6): 339-350.
- Kim, D. S., Lee, J. S., Leem, J. W., Huh, Y. J., Kim, J. Y., Kim, H. S., Park, I. H., Daley, G. Q., Hwang, D. Y. and Kim, D. W. (2010). [Robust enhancement of neural differentiation from human ES and iPS cells regardless of their innate difference in differentiation propensity](#). *Stem Cell Rev Rep* 6(2): 270-281.
- Lancaster, M. A., Renner, M., Martin, C. A., Wenzel, D., Bicknell, L. S., Hurles, M. E., Homfray, T., Penninger, J. M., Jackson, A. P. and Knoblich, J. A. (2013). [Cerebral organoids model human brain development and microcephaly](#). *Nature* 501(7467): 373-379.
- Li, W., Sun, W., Zhang, Y., Wei, W., Ambasudhan, R., Xia, P., Talantova, M., Lin, T., Kim, J., Wang, X., Kim, W. R., Lipton, S. A., Zhang, K. and Ding, S. (2011). [Rapid induction and long-term self-renewal of primitive neural precursors from human embryonic stem cells by small molecule inhibitors](#). *Proc Natl Acad Sci U S A* 108(20): 8299-8304.
- Lorenz, C., Lesimple, P., Bukowiecki, R., Zink, A., Inak, G., Mlody, B., Singh, M., Semtner, M., Mah, N., Aure, K., Leong, M., Zabiegalo, O., Lyras, E. M., Pfiffer, V., Fauler, B., Eichhorst, J., Wiesner, B., Huebner, N., Priller, J., Mielke, T., Meierhofer, D., Izsvak, Z., Meier, J. C., Bouillaud, F., Adjaye, J., Schuelke, M., Wanker, E. E., Lombes, A. and Prigione, A. (2017). [Human iPSC-Derived Neural Progenitors Are an Effective Drug Discovery Model for Neurological mtDNA Disorders](#). *Cell Stem Cell* 20(5): 659-674 e659.
- Lorenz, C. and Prigione, A. (2017). [Mitochondrial metabolism in early neural fate and its relevance for neuronal disease modeling](#). *Curr Opin Cell Biol* 49: 71-76.
- Paul, S. M., Mytelka, D. S., Dunwiddie, C. T., Persinger, C. C., Munos, B. H., Lindborg, S. R. and Schacht, A. L. (2010). [How to improve R&D productivity: the pharmaceutical industry's grand challenge](#). *Nat Rev Drug Discov* 9: 203-214.
- Readhead, B., Hartley, B. J., Eastwood, B. J., Collier, D. A., Evans, D., Farias, R., He, C., Hoffman, G., Sklar, P., Dudley, J. T., Schadt, E. E., Savic, R. and Brennand, K. J. (2018). [Expression-based drug screening of neural progenitor cells from individuals with schizophrenia](#). *Nat Commun* 9(1): 4412.
- Reinhardt, P., Glatza, M., Hemmer, K., Tsutsyura, Y., Thiel, C. S., Hoing, S., Moritz, S., Parga, J. A., Wagner, L., Bruder, J. M., Wu, G., Schmid, B., Ropke, A., Klingauf, J., Schwamborn, J. C., Gasser, T., Scholer, H. R. and Sterneckert, J. (2013). [Derivation and expansion using only small molecules of human neural progenitors for neurodegenerative disease modeling](#). *PLoS One* 8(3): e59252.
- Takahashi, K., Tanabe, K., Ohnuki, M., Narita, M., Ichisaka, T., Tomoda, K. and Yamanaka, S. (2007). [Induction of pluripotent stem cells from adult human fibroblasts by defined factors](#). *Cell* 131(5): 861-872.
- Vierbuchen, T., Ostermeier, A., Pang, Z. P., Kokubu, Y., Sudhof, T. C. and Wernig, M. (2010). [Direct conversion of fibroblasts to functional neurons by defined factors](#). *Nature* 463(7284): 1035-1041.
- Walter, J., Bolognin, S., Antony, P. M. A., Nickels, S. L., Poovathingal, S. K., Salamanca, L., Magni, S., Perfeito, R., Hoel, F., Qing, X., Jarazo, J., Arias-Fuenzalida, J., Ignac, T., Monzel, A. S., Gonzalez-Cano, L., Pereira de Almeida, L., Skupin, A., Tronstad, K. J., Schwamborn, J. C. (2019). [Neural Stem Cells of Parkinson's Disease Patients Exhibit Aberrant Mitochondrial Morphology and Functionality](#). *Stem Cell Reports* 12(5): 878-889.
- Wang, X., Sterr, M., Burtscher, I., Chen, S., Hieronimus, A., Machicao, F., Staiger, H., Haring, H. U., Lederer, G., Meitinger, T., Cernilgar, F. M., Schotta, G., Irmler, M., Beckers, J., Hrabe de Angelis, M., Ray, M., Wright, C. V. E., Bakhti, M. and Lickert, H. (2018). [Genome-wide analysis of PDX1 target genes in human pancreatic progenitors](#). *Mol Metab* 9: 57-68.
- Zheng, X., Boyer, L., Jin, M., Mertens, J., Kim, Y., Ma, L., Ma, L., Hamm, M., Gage, F. H. and Hunter, T. (2016). [Metabolic reprogramming during neuronal differentiation from aerobic glycolysis to neuronal oxidative phosphorylation](#). *Elife* 5: e13374.

Generation of Mouse Primary Hypothalamic Neuronal Cultures for Circadian Bioluminescence Assays

Cosima X. Schmidt¹, Anthony H. Tsang^{1,§} and Henrik Oster^{1,*}

¹Institute of Neurobiology, Center of Brain, Behavior and Metabolism, University of Lübeck, Lübeck, Germany

[§]Current address: Wellcome Trust-MRC Institute of Metabolic Science, University of Cambridge, Cambridge, United Kingdom

*For correspondence: henrik.oster@uni-luebeck.de

Abstract

An endogenous circadian clock system enables organisms to adapt to time-of-day dependent environmental changes. In consequence, most physiological processes exhibit daily rhythms of, e.g., energy metabolism, immune function, sleep, or hormone production. Hypothalamic circadian clocks have been identified to play a particular role in coordinating many of these processes. Primary neuronal cultures are widely used as a physiologically relevant model to study molecular events within neurons. However, as circadian rhythms include dynamic molecular changes over longer timescales that vary between individual cells, longitudinal measurement methods are essential to investigate the regulation of circadian clocks of hypothalamic neurons. Here we provide a protocol for generating primary hypothalamic neuronal cultures expressing a circadian luciferase reporter. Such reporter cells can be used to longitudinally monitor cellular circadian rhythms at high temporal resolution by performing bioluminescence measurements.

Keywords: Primary hypothalamic neurons, Circadian clocks, Luciferase reporter, *Bmal1*, Circadian rhythms

This protocol was validated in: *Elife* (2020), DOI: 10.7554/eLife.55388

Background

To adapt to recurring time-of-day dependent changes in their environment, many organisms have developed an endogenous circadian clock system that regulates 24-h rhythms of behavioral and physiological processes (Sharma, 2003). In mammals, a master circadian pacemaker resides in the hypothalamic suprachiasmatic nucleus (SCN). It coordinates cellular clock regulation throughout the body with external time. Daily patterns of sleep, appetite, and metabolism are regulated by cellular circadian clocks residing in hypothalamic neurons (Cedernaes *et al.*, 2019).

In mammalian cells, circadian clocks consist of interlocked transcriptional-translational feedback loops (TTFLs). In the core TTFL, the transcription factors circadian locomotor output cycles kaput (CLOCK) and brain and muscle aryl hydrocarbon receptor nuclear translocator-like protein 1 (BMAL1 or ARNTL) activate the expression of their own repressors, period (PER1-3) and cryptochrome (CRY1/2), which leads to circadian oscillations of gene expression and abundance of protein products (Ko and Takahashi, 2006).

Methods to directly quantify mRNA and protein levels, such as quantitative PCR or Western blotting, require repetitive sampling from different individuals or preparations at different time points, which is labor-intensive, and, in case of short time intervals or low amounts of cellular material, highly impractical (Yu and Hardin, 2007). To overcome these problems, circadian reporters, where the expression of the firefly luciferase enzyme is under the control of a clock gene promoter (*e.g.*, *Bmal1* or *Per2*), have been developed (Brown *et al.*, 2005; Ramanathan *et al.*, 2012; Fang *et al.*, 2017). They allow real-time tracking of cellular circadian rhythms by performing bioluminescence measurements and therefore are widely used to study circadian clock function (Ramanathan *et al.*, 2012).

Immortalized cell lines are valuable tools for molecular biological research, as they are readily available and can be expanded without limitations (Pan *et al.*, 2009). In recent years, they have become established *in-vitro* models for the investigation of hypothalamic clocks (Fick *et al.*, 2010 and 2011; Tsang *et al.*, 2020). However, since immortalized cell lines are genetically and phenotypically different from their tissue origins, data obtained from such systems has to be interpreted critically and a verification with a more physiologically relevant model system is advised (Pan *et al.*, 2009).

Primary neuronal cultures are obtained directly from the animal's central nervous system and maintain many physiological and biochemical characteristics of their tissue origin (Gordon *et al.*, 2013; Verma *et al.*, 2020). Therefore, they are useful model systems to address physiological relevance. Here we provide a protocol for the generation of primary hypothalamic neuron cultures stably transduced with a circadian *Bmal1*-luciferase reporter. Creation of these reporter cells allows observation and quantitative description of hypothalamic neuronal circadian rhythms in real-time, avoiding labor-intensive and material-consuming biochemical experiments. These cells can further be used to investigate clock resetting effects of various factors such as hormones or metabolites.

Materials and Reagents

1. 96-well plate (Corning, catalog number: 3610)
2. BD Falcon cell strainer, 70 µm (BD Biosciences, catalog number: 352350)
3. 100-mm culture dish
4. 35-mm dish
5. 15-mL Falcon tube
6. 10-mL serological pipette
7. Fire-polished glass pipette
- 2-8-month-old male and female C57BL/6J mice
8. *Bmal1*-luciferase lentivirus (Brown *et al.*, 2005)
9. Poly-D-lysine hydrobromide (Millipore Sigma, catalog number: P6407)
10. Laminin (BD Biosciences, catalog number: 354232)
11. Hank's balanced salt solution, HBSS (PAA, catalog number: H15-008)
12. Earle's balanced salt solution, EBSS, with Phenol Red (Thermo Fisher Scientific, Gibco, catalog number: 24010043)

13. Papain, suspension (Worthington Biochemical Corporation, catalog number: LS003126)
14. Deoxyribonuclease I, DNaseI (Worthington Biochemical Corporation, catalog number: LS002058)
15. Neurobasal medium, minus phenol red (Thermo Fisher Scientific, Gibco, catalog number: 12348017)
16. B-27 supplement (Thermo Fisher Scientific, Gibco, catalog number: 17504044)
17. GlutaMAX supplement (Thermo Fisher Scientific, Gibco, catalog number: 35050061)
18. Ovomocoid (Worthington Biochemical Corporation, catalog number: LS003085)
19. Bovine serum albumin (MilliporeSigma, catalog number: A7030)
20. L-cysteine (MilliporeSigma, catalog number: C7352)
21. Fetal bovine serum, FBS (Thermo Fisher Scientific, Gibco, catalog number: 10500-064)
22. Trypan blue solution (MilliporeSigma, catalog number: T8154)
23. Cytosine β-D-arabinofuranoside, AraC (Millipore Sigma, catalog number: C1768)
24. Pasteur pipettes (Th. Geyer, catalog number: 7691061)
25. 2-Mercaptoethanol (Millipore Sigma catalog number: M3148)
26. Adhesive clear PCR seal (Biozym, catalog number: 600208)
27. D-luciferin sodium salt (Applichem, catalog number: A1006)
28. Polybrene, Hexadimethrine bromide (Millipore Sigma, catalog number: H9268)

Equipment

1. Sterile laminar flow hood (Thermo Fisher Scientific, model: MSC-Advantage, catalog number: 51025411)
2. Multimode microplate reader (Berthold Technologies, model: Tristar LB941)
3. Fluorescence microscope (Nikon, model: Eclipse Ts2R)
4. LED unit (Nikon, model: C-LEDFL470)
5. Fluorescence filter cube (Nikon, model: C-LED470, Excitation: 470/40 nm, Dichroic: 500 nm, Emission: 535/55 nm)
6. 10× objective (Nikon, model: CFI Achromat ADL-10×, NA: 0.4)
7. 20× objective (Nikon, model: CFI Achromat LWD ADL-20×, NA: 0.4)
8. Hemocytometer (Laboroptik, model: Neubauer)
9. Water bath (GFL, model: 1002)
10. Dissecting microscope (Leica, model: MZ6)
11. Dissection scissors (Fine Science Tools, catalog number: 91402-14)
12. Dissection forceps (Fine Science Tools, catalog number: 11000-12)
13. No.11 scalpel (Feather, catalog number: 200210011)
14. No.5 sharp forceps (Fine Science Tools, catalog number: 11252-20)
15. 2 × curved forceps (Fine Science Tools, catalog number: 11274-20)
16. Student Fine Scissors (Fine Science Tools, catalog number: 91460-11)

Software

1. MicroWin 2000 (Labsis, <https://labsis.de>)

Procedure

A. Schedule matings

1. To generate E15-16 embryos, schedule the mating day of the adult mice 15-16 d before dissection. We use 2-8-month-old adult C57BL/6J mice for mating.

2. On the next morning, confirm successful mating by vaginal plug check as described previously (Behringer *et al.*, 2016).
3. Confirm pregnancy by palpitation or visually before dissection.

B. Reagent preparation

Note: Avoid repeated freeze-thaw cycles for labile reagents.

1. Prepare poly-D-lysine (PDL) stock solution (500 µg/mL). Divide into 5-mL aliquots and store at -20°C.
2. Prepare laminin stock solution (0.1 µg/µL) in PBS. Divide into 250-µL aliquots and store at -20°C.
3. Prepare ovo/albumin inhibition solution, containing 6 mg ovomucoid and 6 mg bovine serum albumin in 6 mL EBSS. Store at 4°C until use.
4. Prepare DNaseI solution, with 1,000 U DNase I in 500 µL EBSS and store at -20°C.
5. Prepare plating medium (Neurobasal + 2% (v/v) B27 + 2 mM Glutamax + 10% (v/v) FBS + 1× penicillin/streptomycin) and store at 4°C until use. Equilibrate at 37 °C before adding it to the culture.
6. Prepare feeding medium (same as plating medium, but without FBS) and store at 4°C until use. Equilibrate at 37 °C before adding it to the culture.
7. Prepare digestion solution (100 U Papain, 5 mL EBSS, 1.1 mM EDTA (11 µL 0.5 M EDTA), 5.5 mM cysteine (3.3 mg), 0.067 mM 2-Mercaptoethanol (2.34 µL 1% (v/v)/14.3 M pure liquid) and 250 µL DNaseI solution), sterile filtrate with a 0.2-µm filter. Activate at 37°C for 20-30 min before use.
8. Prepare resuspension medium (2.7 mL EBSS, 300 µL ovo/albumin inhibition solution, 150 µL DNaseI solution).

C. PDL and laminin double coating

1. One day before dissection coat 96-well plates with PDL and laminin.
2. Dilute PDL stock solution with PBS to working concentration 50 µg/mL. Mix 0.5 mL PDL stock solution (500 µg/mL) with 4.5 mL PBS to prepare 5 mL diluted PDL solution (50 µg/mL).
3. Filter with 0.2-µm filter before use.
4. Coat the culture surface of a 96-well plate with 7.5 µg/cm² PDL. Cover the wells of a 96-well plate with 48 µL diluted PDL solution (50 µg/mL).
5. Incubate overnight at room temperature (or at least for 2 h at 37°C).
6. Wash 3 times with 100 µL sterile H₂O.
7. Allow to dry completely under a sterile cell culture hood.
8. Thaw laminin stock solution slowly at 2-8°C.
9. Dilute laminin stock solution with PBS to a working concentration of 6.4 µg/mL. Mix 320 µL laminin stock solution (0.1 µg/µL) with 4.68 mL PBS to prepare 5 mL diluted laminin solution (6.4 µg/mL).
10. Cover the PDL-coated wells with 50 µL diluted laminin solution (6.4 µg/mL). The final coating concentration will be around 1 µg/cm².
11. Incubate for 2 h at 37°C.
12. Wash 3 times with sterile 100 µL PBS, add 100 µL plating medium and store at 37°C and 5 % CO₂ in the incubator.

D. Dissection

Note: A swiftly executed preparation procedure is crucial for cell viability. Consider practicing the procedure several times before preparing experimental samples. Before starting the dissection, ensure that required materials are in place and that all equipment is disinfected.

1. Use embryonic day 15 to 16 (E15-16) old embryos from a pregnant mother (C57BL/6J mothers usually have 8-10 pups).

2. Work under a laminar flow hood and always apply aseptic techniques to reduce the risk of contamination with bacteria, fungi, and mycoplasma.
3. Sacrifice mother by cervical dislocation, open the abdominal cavity with dissection scissors and forceps. The embryos are located at the posterior part of the abdominal cavity.
4. Carefully remove the uterus horns with two curved forceps with gentle opposite pulling motions and transfer them into a 100-mm culture dish filled with ice-cold HBSS.
5. Extract embryos with dissection scissors and curved forceps and transfer them into a new 100-mm culture dish with ice-cold HBSS.
6. Decapitate the embryos with dissection scissors.
7. Hold the head in position by piercing No. 5 sharp forceps into orbital cavities and by pushing the rostral part of the brain down. Simultaneously use curved forceps to remove the outer skin and skull, by peeling them gently off from caudal to rostral. Start with the left hemisphere and then repeat that step with the right hemisphere. Carefully remove the brain with curved forceps and deposit it into a 35-mm Petri dish with ice-cold HBSS. Repeat Steps D5 to D7 for the other embryos.

Note: Avoid applying pressure onto the tissue while extracting the brains, to maintain brain integrity. Furthermore, take care that the brains are always covered with medium, do not let them dry out.

8. Under a dissecting microscope, isolate the hypothalami with forceps and scalpel (see Figure 1 for details). Collect them in a 35-mm dish with ice-cold HBSS and keep on ice. Use a cut 1,000- μ L pipette tip or a dropper with a wide opening to transfer the dissected tissue.

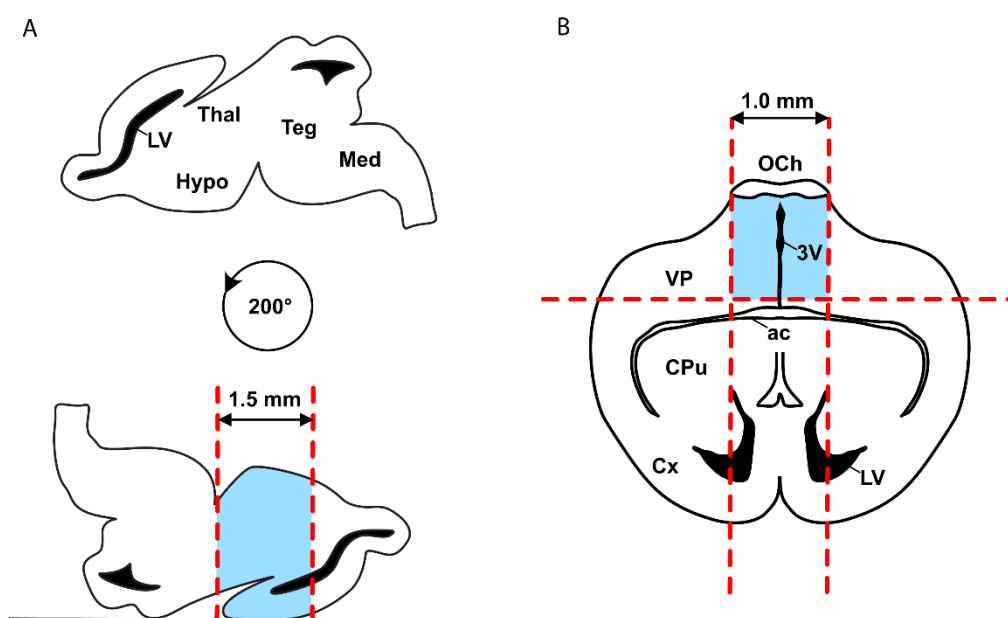


Figure 1. Steps for hypothalamus dissection from intact E16 brains.

A. Turn the brain over so that the ventral part is facing upwards. Remove the caudal part of the brain by making a coronal cut at the posterior border of the mammillary bodies. Make a second coronal cut ~1.5 mm anterior from the first to remove the rostral part of the brain. B. Rotate the remaining brain to get a coronal orientation and make sure that the rostral part is facing upwards. Dissect the hypothalamic tissue block: make two lateral cuts ~0.5 mm each from the midline and one additional cut ventral to the anterior commissure (ac). Red dashed lines indicate the cutting positions. The dissected area is highlighted in blue. Further abbreviations: LV – lateral ventricle, Thal – thalamus, Hypo – hypothalamus, Teg – tegmentum, Med – medulla oblongata, VP – ventral pallidum, OCh – optic chiasm, 3V – 3rd ventricle, Cx – cortex, CPu – caudate putamen.

E. Dissociation and plating

1. Transfer dissected hypothalami into a 15-mL Falcon tube, remove remaining HBSS and add 5 mL digestion solution.
2. Digest the tissue pieces for 30-60 min at 37°C while stirring gently every 4-5 min.

Note: A longer digestion period may increase cell yield, but it will also decrease viability. The incubation time must be determined empirically. Start with 30 min, determine yield and viability as described in Step E13. Increase incubation time if necessary.

3. Triturate 13 times with a 10-mL serological pipette.
4. Carefully and slowly triturate 13 times with a fire-polished glass pipette. Avoid creating bubbles during trituration.
5. Wait 2 min for remaining undissociated tissue to settle and transfer supernatant into a new 15-mL Falcon tube.
6. Centrifuge at 300 × g for 5 min.
7. Remove the clear supernatant and resuspend the cell pellet with 3 mL resuspension medium.
8. Gently triturate 7 times with a fire-polished glass pipette.
9. Remove remaining tissue clumps by using a 70 µm cell strainer.
10. Carefully and slowly transfer the cell suspension to 5 mL ovo/albumin inhibition solution in a 15-mL Falcon tube and centrifuge at 70 × g for 5 min to prepare a discontinuous density gradient.
11. Remove supernatant.
12. Add 2-3 mL plating medium and resuspend 7 times with a fire-polished glass pipette.
13. Quantify the number of viable cells by trypan blue exclusion assay (e.g., with a Neubauer chamber).
14. Seed 3.25×10^5 viable cells/cm² in plating medium into a 96-well plate double coated with PDL and laminin.

F. Feeding and lentiviral transduction with *Bmal1*-luciferase reporter

1. On the next day, transduce the cells with *Bmal1*-luciferase lentivirus (Brown *et al.*, 2005). Details for lentiviral particle production are described in Tsang *et al.* (2020).

Note: It is recommended to use a GFP-expressing control virus to determine transduction efficiency.

2. Thaw lentiviral aliquots at room temperature immediately before use. Avoid keeping them for prolonged times at ambient temperature and avoid unnecessary freeze-thaw cycles.
3. Prepare several lentiviral dilutions (e.g., 0, 1:5, 1:50, 1:250) in feeding medium containing 16 µg/mL polybrene.

Note: It is recommended testing at least three different concentrations to determine the optimal transduction conditions. We transduced the cells with ~1 × 10⁸ infection units (IFUs) per 1 mL in the presence of 8 µg/mL polybrene.

4. Replace half of the volume of the plating medium by half of the volume of lentiviral particle-containing feeding medium.
5. 24 h later, refresh half of the volume of the old medium with fresh feeding medium containing 5 µM AraC.
6. Feed the cells every 3 d with feeding medium, as above, but without AraC.

Note: It is recommended to perform quality control experiments to ensure that the prepared culture is free from microbial contamination (e.g., bacteria, fungi, or mycoplasma). Mycoplasma contamination can be tested by using PCR-based detection kits (LookOut Mycoplasma PCR Detection Kit, MilliporeSigma). Although cell identification and integrity tests are commonly performed in cell culture, they are not

necessary for these primary cultures, since isolated cells are directly used for the experiment and not maintained for longtime.

G. Synchronization and bioluminescence measurements

1. On day 9 *in vitro* (DIV9), synchronize the cells for 2 h with 100 nM dexamethasone. Therefore, pipette 25 μ L pre-warmed feeding medium containing 900 nM dexamethasone into the wells containing 200 μ L medium and incubate for 2 h at 37°C and 5% CO₂.
2. During incubation prepare the feeding medium containing 0.5 mM D-luciferin and place it into a water bath at 37°C.

Note: D-luciferin is light sensitive. Protect from light.

3. After incubation aspirate medium and change to pre-warmed feeding medium with 0.5 mM D-luciferin.
4. Seal the plate with transparent adhesive foil, place it into the microplate reader and start the measurement.
5. Perform the luminescence measurement without filter at 34°C with an integration time of 1 min per well.
6. Normalize all bioluminescence traces by subtracting the 24-h running average and analyze circadian parameters as described previously (Landgraf *et al.*, 2015).

Note: Synaptic formation starts to be evident at DIV7 (Figure 2). Neurons are considered to be mature at DIV14 (Biffi *et al.*, 2013; Kos *et al.*, 2016). We use DIV9 neurons for standard circadian luciferase experiments. Bmal1-luciferase reporter rhythms are stable for a week without further medium refreshing during the recording.

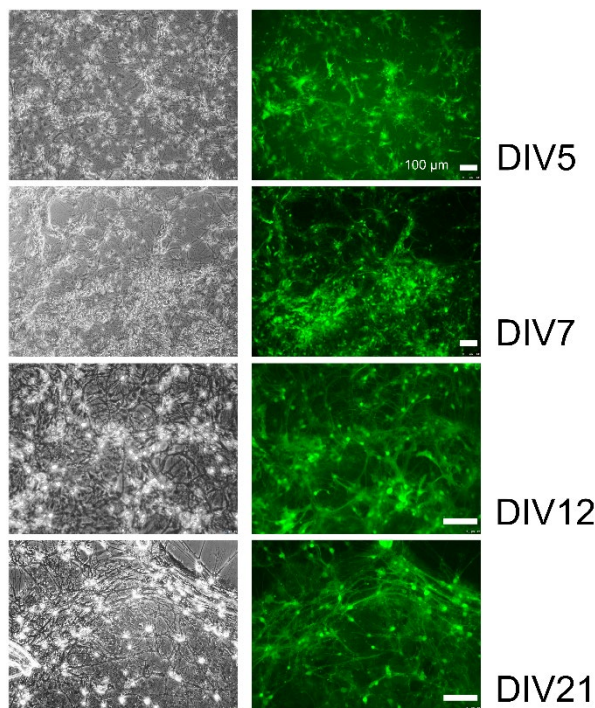


Figure 2. Synaptic connectivity increases with days *in vitro*.

Representative bright-field (left) and fluorescence (right) images of primary hypothalamic neurons transduced with a GFP-expressing lentivirus. 10 \times and 20 \times magnification.

Data analysis

The Mikrowin2000 software allows real-time monitoring of bioluminescence signals. *Bmall*-luciferase rhythms are plotted and displayed. During the measurement, wells of interest can be selected and examined. Mikrowin2000 continuously saves the experiment as a *.dat file, which can be opened by the software once the measurement procedure has been completed. To analyze the data, export the raw data to Excel. Calculate the 24-h running average and subtract that from baseline readings for normalization (Figure 3). We use GraphPad Prism for plotting, sine wave fitting, rhythm parameter determination and statistical analyses. Statistical assessment of rhythmicity is done with JTK_cycle or CircaCompare (Hughes *et al.*, 2010; Parsons *et al.*, 2020).

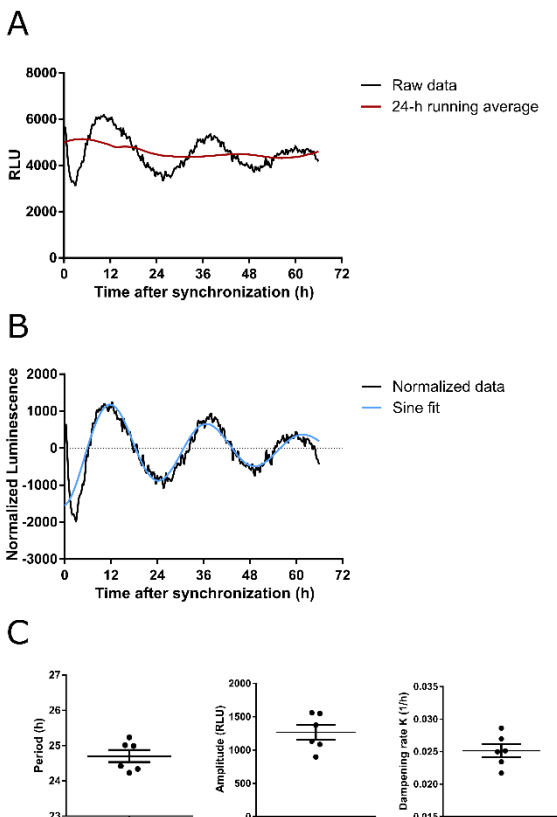


Figure 3. Bioluminescence measurements of synchronized primary hypothalamic neurons expressing *Bmall*-luciferase.

Bioluminescence traces are normalized by subtracting their 24-h running average. Circadian parameters, such as amplitude, period (wavelength), and dampening rate (K) are determined by fitting a damped sine wave function ($Y = \text{Amplitude} \cdot \exp(-K \cdot X) \cdot \sin((2\pi/Wavelength) \cdot X + \text{Phase shift})$). A. Representative raw data (black) and the calculated 24-h running average (red). B. Representative normalized data (black) and damped sine wave fit (blue). C. Quantification of period, amplitude and dampening rate. Data are presented as mean ± SEM (n = 6).

Acknowledgments

This study was supported by funds of the German Research Foundation (DFG; OS353-7/1, OS353-10/1 and GRK-1957). The protocol was used for Tsang *et al.* (2020).

Competing interests

The authors report no conflict of interest.

Ethics

Animal experiments reported in this protocol have been approved by the ethics commission of the Ministry of Energy Change, Agriculture, Environment and Digitalization (MELUR) of the State of Schleswig-Holstein (Az 4_2019-10-01_Oster; 2019-2021).

References

- Biffi, E., Regalia, G., Menegon, A., Ferrigno, G. and Pedrocchi, A. (2013). [The Influence of Neuronal Density and Maturation on Network Activity of Hippocampal Cell Cultures: A Methodological Study](#). *PLOS ONE* 8(12): e83899.
- Behringer, R., Gertsenstein, M., Nagy K.V. and Nagy A. (2016). [Selecting Female Mice in Estrus and Checking Plugs](#). *Cold Spring Harb Protoc*. 2016(8). doi: 10.1101/pdb.prot092387.
- Brown, S. A., Fleury-Olela, F., Nagoshi, E., Hauser, C., Juge, C., Meier, C. A., Chicheportiche, R., Dayer, J.-M., Albrecht, U. and Schibler, U. (2005). [The Period Length of Fibroblast Circadian Gene Expression Varies Widely among Human Individuals](#). *PLOS Biol* 3(10): e338.
- Cedernaes, J., Huang, W., Ramsey, K. M., Waldeck, N., Cheng, L., Marcheva, B., Omura, C., Kobayashi, Y., Peek, C. B. and Levine, D. C., et al. (2019). [Transcriptional Basis for Rhythmic Control of Hunger and Metabolism within the AgRP Neuron](#). *Cell Metab* 29(5): 1078-1091.e5.
- Fang, M., Kang, H.-G., Park, Y., Estrella, B. and Zarbl, H. (2017). [In Vitro Bioluminescence Assay to Characterize Circadian Rhythm in Mammary Epithelial Cells](#). *J Vis Exp* 127: e55832.
- Fick, L. J., Fick, G. H. and Belsham, D. D. (2010). [Rhythmic clock and neuropeptide gene expression in hypothalamic mHypoE-44 neurons](#). *Mol Cell Endocrinol* 323(2): 298-306.
- Fick, L. J., Fick, G. H. and Belsham, D. D. (2011). [Palmitate alters the rhythmic expression of molecular clock genes and orexigenic neuropeptide Y mRNA levels within immortalized, hypothalamic neurons](#). *Biochem Biophys Res Commun* 413(3): 414-419.
- Gordon, J., Amini, S. and White, M. K. (2013). [General overview of neuronal cell culture](#). *Methods Mol Biol* 1078: 1-8.
- Hughes, M. E., Hogenesch, J. B. and Kornacker, K. (2010). [JTK_CYCLE: An efficient non-parametric algorithm for detecting rhythmic components in genome-scale datasets](#). *J Biol Rhythms* 25(5): 372-380.
- Ko, C. H. and Takahashi, J. S. (2006). [Molecular components of the mammalian circadian clock](#). *Human Molecular Genetics* 15(suppl_2): R271-R277.
- Kos, A., Wanke, K. A., Gioio, A., Martens, G. J., Kaplan, B. B. And Aschrafi, A. (2016). [Monitoring mRNA Translation in Neuronal Processes Using Fluorescent Non-Canonical Amino Acid Tagging](#). *J Histochem Cytochem* 64(5):323-333.
- Landgraf, D., Tsang, A. H., Leliavski, A., Koch, C. E., Barclay, J. L., Drucker, D. J. and Oster, H. (2015). [Oxyntomodulin regulates resetting of the liver circadian clock by food](#). *eLife* 4: e06253.
- Pan, C., Kumar, C., Bohl, S., Klingmueller, U. and Mann, M. (2009). [Comparative proteomic phenotyping of cell lines and primary cells to assess preservation of cell type specific functions](#). *Mol Cell Proteomics* 8(3): 443-450.
- Parsons, R., Parsons, R., Garner, N., Oster, H. and Rawashdeh, O. (2020). [CircaCompare: A method to estimate and statistically support differences in mesor, amplitude and phase, between circadian rhythms](#). *Bioinformatics* 36(4): 1208-1212.
- Ramanathan, C., Khan, S. K., Kathale, N. D., Xu, H. and Liu, A. C. (2012). [Monitoring Cell-autonomous Circadian Clock Rhythms of Gene Expression Using Luciferase Bioluminescence Reporters](#). *J Vis Exp* 67: e4234.

- Sharma, V. K. (2003). [Adaptive Significance of Circadian Clocks](#). *Chronobiol Int* 20(6): 901-919.
- Tsang, A. H., Koch, C. E., Kiehn, J.-T., Schmidt, C. X. and Oster, H. (2020). [An adipokine feedback regulating diurnal food intake rhythms in mice](#). *eLife* 9: e55388.
- Verma, A., Verma, M. and Singh, A. (2020). [Animal tissue culture principles and applications](#). *Animal Biotechnology* 269-293.
- Yu, W. and Hardin, P. E. (2007). [Use of firefly luciferase activity assays to monitor circadian molecular rhythms *in vivo* and *in vitro*](#). *Methods Mol Biol* 362: 465-480.

Ligand and Carbohydrate Engagement (LACE) Assay and Fluorescence Quantification on Murine Neural Tissue

James M. Clegg and Thomas Pratt*

Simons Initiative for the Developing Brain & Centre for Discovery Brain Sciences, University of Edinburgh, Edinburgh, UK

*For correspondence: t.pratt@ed.ac.uk

Abstract

The interaction between cell surface heparan sulphate and diffusible ligands such as FGFs is of vital importance for downstream signaling, however, there are few techniques that can be used to investigate this binding event. The ligand and carbohydrate engagement (LACE) assay is a powerful tool which can be used to probe the molecular interaction between heparan sulphate and diffusible ligands and can detect changes in binding that may occur following genetic or pharmacological intervention. In this protocol we describe an FGF17:FGFR1 LACE assay performed on embryonic mouse brain tissue. We also describe the method we have used to quantify changes in fluorescent LACE signal in response to altered HS sulphation.

Keywords: Ligand, Carbohydrate, LACE, Heparan Sulphate, HSPG, FGF, FGFR

This protocol was validated in: J Neurosci (2019), DOI: 10.1523/JNEUROSCI.1747-17.2018

Background

Heparan sulphate (HS) is an extracellular matrix and cell surface glycosaminoglycan molecule that is extensively modified by sulphation. HS interacts with a wide range of developmentally important signaling molecules including FGFs, Wnts, BMPs and Slits. During FGF signalling, for example, HS acts as a co-receptor, facilitating the binding of the FGF ligand to the cell surface FGFR receptor. The formation of this FGF:FGFR:HS complex is required for FGF signaling to occur (Allen *et al.*, 2001). Differential sulphation of HS has been shown to affect the binding of FGF ligands to their FGFR cell surface receptors. In our recent paper we used a ligand and carbohydrate engagement (LACE) assay to probe the interaction between HS and FGF proteins (Clegg *et al.*, 2019). This method involves the addition of recombinant FGF and FGFR protein to form the FGF:FGFR:HS complex on tissue sections. The recombinant FGFR can then be labelled using a fluorescently conjugated antibody allowing the visualization of the binding event (Allen *et al.*, 2001; Allen and Rapraeger., 2003).

The LACE assay allows us to observe any change in FGF:FGFR:HS binding caused by altered HS sulphation. For example, in our recent study we were able to show reduced FGF17:FGFR1 binding in embryos lacking 2-O HS sulphation (Clegg *et al.*, 2019). Using image analysis software, we were also able to quantify the change in fluorescent LACE signal, and in this protocol we will detail our robust quantification procedure. In our experiments we have used the LACE assay to analyze the binding of FGF17 and FGF8 to FGFR1 and FGFR3, however, this technique could be adapted to probe the binding properties and HS interaction of a wide range of different ligand and receptor pairs.

Materials and Reagents

Materials

1. 7 mL bijou tubes (Greiner, catalog number: 189170)
2. Pipette tips (Greiner, catalog number: 739288)
3. 1.5 mL microcentrifuge tubes (Greiner, catalog number: 616201)
4. Peel-A-Way® Embedding Molds (Square-S22, Polysciences)
5. Sterilin™ Standard 90 mm Petri Dishes (Thermo Fisher, catalog number: 101R20)

Animals

Mice used in our original study were maintained on a CBA background. Mice used for timed matings were aged between 6 and 24 weeks.

Reagents

1. Sucrose (Thermo Fisher, catalog number: S25590)
2. 1× PBS (Thermo Fisher, catalog number: 14190094)
3. Tris-HCl (Thermo Fisher, catalog number: 10812846001)
4. CaCl₂ (Thermo Fisher, catalog number: 10657662)
5. Ethanol (Thermo Fisher, catalog number: AC615090010)
6. Bovine serum albumin (Merck, catalog number: A1933)
7. Paraformaldehyde (Merck, catalog number: 158127)
8. OCT embedding matrix (Cellpath, catalog number: KMA-0100-00A)
9. Sodium borohydride (Merck, catalog number: 452882)
10. Glycine (Merck, catalog number: G8898)
11. Bovine serum albumin (Merck, catalog number: 05470)

12. Heparinase I and III blend (Millipore Sigma, catalog number: H3917)
13. Recombinant Human FGFR1 beta (IIIc) Fc Chimera Protein (R&D Systems, catalog number: 661-FR-050)
14. Recombinant Human/Mouse FGF-8b Protein (R&D Systems, catalog number: 423-F8)
15. Recombinant Mouse FGF-17 Protein (R&D Systems, catalog number: 7400-FG)
16. Anti-Human IgG (Fc specific)-Cy3 antibody (Merck, catalog number: C2571)
17. DAPI (Thermo Fisher, catalog number: D1306)
18. Vectashield Hardset (Vector Labs, catalog number: H-1400)
19. Heparinase Buffer (see Recipes)

Equipment

1. Pipettes
2. Dissecting microscope (Euromex, catalog number: DZ1100)
3. Cryostat (Leica, catalog number: CM3050 S)
4. Incubator (37°C)
5. Forceps, size 5 (Fine Science Tools, catalog number: 11251-20)
6. Microscissors, 5 mm cutting edge (Fine Science Tools, catalog number: 15003-08)
7. Scissors, 9 cm (Fine Science Tools, catalog number: 14060-09)
8. Super-frost Plus slides (Thermo Fisher, catalog number: J1800AMNZ)
9. Coplin jar (Millipore Sigma, catalog number: S6016)
10. Analog Rocking Platform Shaker (VWR, catalog number: 10127-872)
11. Hydrophobic barrier pen (VectorLabs, catalog number: H-4000)
12. Humidified chamber/slides staining tray (Heathrow Scientific, catalog number: HS15951A)
13. Epifluorescence or confocal microscope with image capture software (e.g., Leica AF6000 epifluorescence microscope)

Software

1. ImageJ/FIJI, version 1.53 (<https://imagej.net/Fiji>)

Procedure

Summary: This protocol is divided into two sections. In part A we describe the LACE assay beginning with the dissection of the embryonic brain, the embedding of the tissue and cryo-sectioning. We then detail the LACE assay itself including the incubation of recombinant ligand and receptor proteins with the tissue sections followed by the detection of bound receptor protein using a fluorescent conjugated antibody. In part B we describe the imaging of reacted tissue sections and the quantification of fluorescent LACE signal using FIJI software.

A. LACE Assay

1. Cull pregnant female mouse at desired embryonic stage. Using scissors, open the abdomen and remove the uterus which should be clearly visible.

Note: In our testing we have successfully performed the LACE assay using mouse brain tissue aged between E11.5 and E18.5. Other groups have successfully used embryonic heart, lung and liver tissue in addition to CHO cell lines (Allen and Rapraeger, 2003).

2. Place the uterus in a dish of chilled PBS. Using forceps open the uterus, carefully remove the embryos and transfer to a fresh dish of PBS.
3. Cut the head from the body of the embryo using scissors and transfer to fresh, chilled PBS. Use forceps to peel away the skin from the head to expose the skull, cut down the midline of the skull using microscissors and peel back the skull to expose the brain. Carefully detach the brain from the base of the head and remove using forceps (Figures 1A-1D).

Note: Take a tissue sample for genotyping if required.

4. Fix the brains in 4% paraformaldehyde (PFA) in PBS in 7 mL bijou tubes, overnight at 4°C, with shaking (20 rpm).

Note: 7 mL PFA is sufficient for embryonic brains. Postnatal brains up to P3 should be fixed in 20 mL tubes, older brains should be fixed by trans-cardial perfusion.

5. Wash brains briefly with 1× PBS and cryoprotect tissue using 30% sucrose in PBS at 4°C overnight, or until the tissue has sunk.

Note: PFA and PBS can be poured off without needing to change containers.

6. Transfer the brain to an embedding mold and cover the tissue in 50% OCT embedding matrix; 50% Sucrose/PBS. Position the tissue at the desired orientation and freeze on dry ice (Figures 1E, 1F).
7. Section tissue using a cryostat at a thickness of 10 µm and collect sections on Superfrost Plus slides. (Figures 1G-1I).

Note: Sections can be stored at -20 °C until needed.

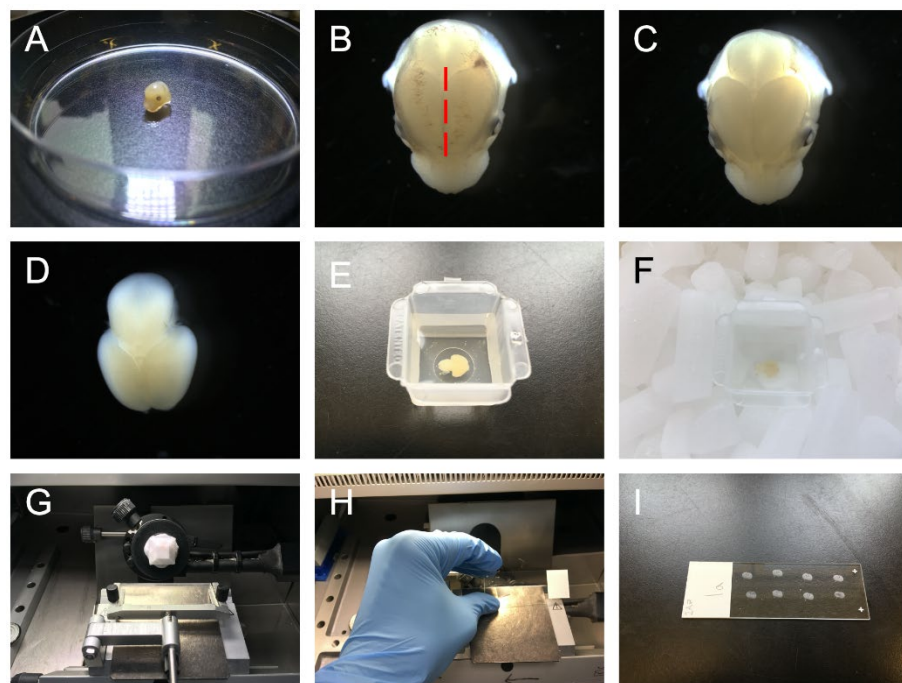


Figure 1. Images of the dissection, embedding and sectioning of embryonic mouse brain tissue.

A. The head of the embryo is detached from the body. B. An incision is made along the midline of the skull (dashed red line). C. The skull is peeled away to reveal the brain. D. The brain is detached from the head.

- E. The brain is placed in an embedding mold and submerged in OCT/sucrose solution. F. Brain tissue is then frozen on dry ice. G-I. Frozen tissue can then be sectioned using a cryostat and sections mounted on superfrost slides.
8. Select slides to be used for the LACE assay, remember to include slides for the heparinase digest and no-ligand controls.
 9. Place slides in 95% ethanol at room temperature for 5 min.
 10. Post fix the sections by placing slides in 4% PFA in PBS at room temperature for 10 min, with shaking
 11. Wash sections in 1× PBS at room temperature with shaking, 2 × 5 min.

Note: All wash steps should be performed at room temperature, placing the slides in a coplin jar, covering with 1× PBS and shaking at 50 rpm.

12. Incubate sections with 0.05% Sodium borohydride solution in a coplin jar for 5 min at room temperature.

Note: Bubbles of hydrogen gas should form on the tissue sections during incubation, if bubbles do not form make up fresh Sodium borohydride solution and repeat.

13. Replace with fresh 0.05% Sodium borohydride and incubate sections for a further 10 min.
14. Wash sections in 1× PBS, 2 × 5 min.
15. Incubate sections in 0.1 M Glycine in 1× PBS at 4°C overnight with shaking.

Note: Sodium borohydride/glycine treatment reduces aldehyde fixation-induced autofluorescence, reducing background fluorescence and therefore allowing easier detection of LACE signal.

16. Wash sections in 1× PBS, 2 × 5 min.
17. Dilute heparinase in heparinase buffer (0.5 mU/ml working concentration).
18. Select slides for heparinase digest control and ligand negative control, draw around sections using a hydrophobic barrier pen.

Note: Heparinase digest and ligand negative controls are included to ensure that observed LACE signal is the result of HS:ligand:receptor complex formation. If signal is detected after heparinase digestion (i.e., removing HS) or in the ligand negative control this indicates that the receptor is binding to the tissue directly without complex formation.

19. Apply heparinase solution to the selected slides, leave untreated slides in 1× PBS.
20. Place slides in a sealable humidified chamber and incubate at 37°C for 2 h.
21. Replace with fresh heparinase solution and incubate at 37°C for a further 2 h.
22. Wash treated slides in ddH₂O, 1 × 5 min.
23. Wash all slides in 1× PBS, 1 × 5 min.
24. Block sections using a blocking solution of 1% bovine serum albumin in 1× TBS for 1 h.
25. FGFR1/FGF treatment, at 4°C overnight.
 - a. In our experiments we have used FGFR1 and FGFR3 at a concentration of 9 μM and 100 nM respectively. FGF8 and FGF17 were used at a concentration of 30 nM and 3 μM respectively.
 - b. Recombinant FGFR and FGF is diluted in 1% bovine serum albumin in 1× TBS.
 - c. 100 μl FGFR/FGF solution is applied to each slide.
 - d. Slides should be placed in a humidified chamber for overnight incubation.

Notes:

- a. The recombinant Fc chimeric fusion proteins used in this protocol are proteins (in our case FGFR1/3) to which the Fc domain of IgG has been genetically linked. This Fc tag allows for easy detection of

the protein of interest using antibodies. Fc fusion proteins are commercially available for a wide range of different receptors including FGFRs, VEGFRs, Robos, Neuropilins and DCC.

- b. FGFR/FGF concentrations used here were obtained from the literature which originally described these binding assays (Friedl et al., 2001; Allen and Rapraeger, 2003). In our testing we have always maintained a roughly 3:1 receptor/ligand ratio for the FGFR/FGF combinations we have used. To perform this assay using other receptor/ligand pairs, users would need to titrate these concentrations however we would recommend starting with the concentrations used here and maintaining the 3:1 receptor/ligand ratio.
26. Wash sections in 1× TBS, 4 × 5 min.
 27. Apply fluorescent conjugated secondary antibody (anti-human IgG, Fc-specific Cy3) diluted 1 in 200 in blocking solution.
 28. Wash sections in 1× TBS, 4 × 5 min.
 29. Counterstain with DAPI diluted at 1 in 1,000 in 1× PBS for 5 min.

Note: DAPI stock solution is at a concentration of 1 mg/ml.

30. Wash all slides in 1× PBS, 1 × 5 min
31. Coverslip slides using Vectashield Hardset and leave to dry at room temperature for 1 h.
32. Once dried, slides can be imaged using epifluorescence or confocal microscopy.

B. LACE Quantification

1. Image slides using epifluorescence or confocal microscopy.

Note: All images acquired for quantification must be imaged at constant exposure time and gain using the same objective lens. Care should also be taken to make sure no pixels within the images are overexposed.

2. LACE signal should be apparent in those tissue sections treated with both ligand and Fc-tagged receptor which have not undergone heparinase digestion (Figures 2A, 2E). Control sections in which the ligand was omitted should be blank (Figures 2D, 2H). Sections which have undergone heparinase digestion should see LACE signal reduced compared to undigested sections (Figures 2C, 2G), this indicates that binding of the ligand/receptor pair is HS dependent.

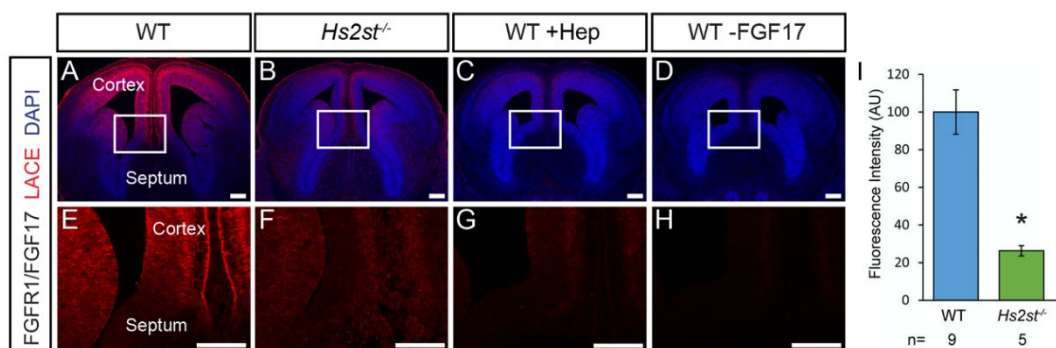


Figure 2. FGFR1/FGF17 LACE assay on E14.5 mouse brain tissue.

A, E. LACE signal (red) is visible in the cortex of WT embryos. B, F. LACE signal is greatly reduced in *Hs2st^{-/-}* embryos. C, G. LACE signal is greatly reduced in WT tissue after heparinase digestion. D, H. LACE signal is completely abolished when FGF17 ligand is omitted from the binding step. I. Quantification of LACE signal in the WT and *Hs2st^{-/-}* cortex shown in E and F. LACE signal is significantly

reduced in *Hs2st^{-/-}* cortex compared to WT (*t*-test, $P = 0.014$). E, F, G, H. are higher magnification images of the boxed regions in A, B, C, D respectively. Scale bars = 200 μm .

- LACE images should be opened in ImageJ (or FIJI) software (Figure 3A).

Note: Images should not be modified in any way between acquisition and quantification.

- Click ‘Analyze’ on the menu bar and select ‘Set Measurements’, in the resulting pop-up window ensure that ‘Mean grey value’ is checked (Figure 3B).

Note: Any other desired measurements can be selected in this window.

- Open the ligand-negative control in ImageJ software and using either the rectangle, oval or polygon tool, draw a shape around the region to be quantified, the shape used should be of a known size that can be kept consistent throughout the quantification (Figure 3C).
- Click ‘Analyze’ and select ‘Measure’, the resulting pop-up window will give the mean greyscale value of the quantified region under ‘Mean’ (Figure 3D). Repeat this process on at least 2 other ligand-negative control tissue sections and calculate a mean greyscale value. This can then be used as the background fluorescence value for sections within the same LACE experiment.

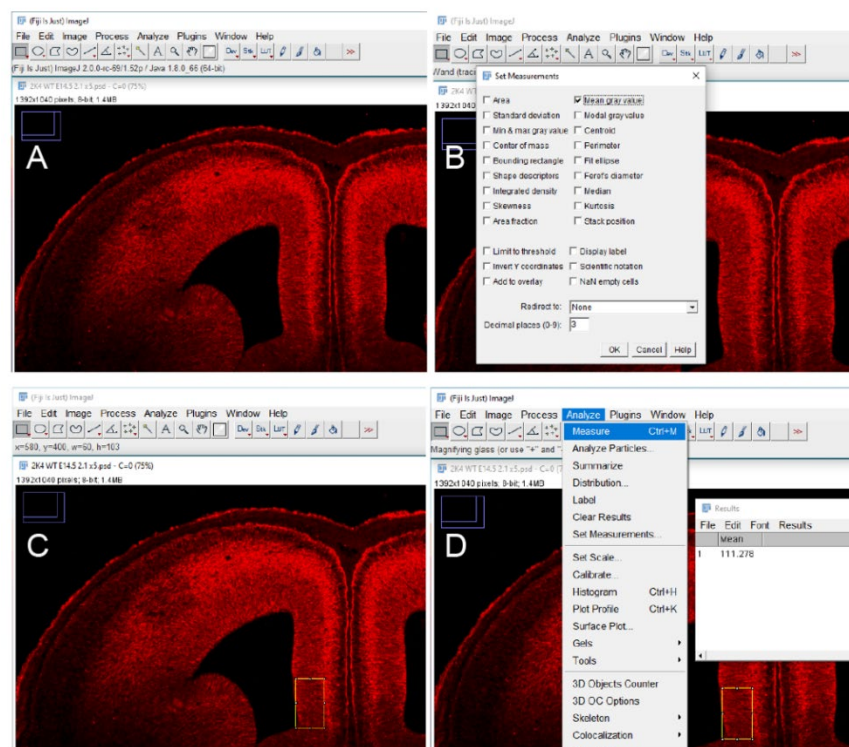


Figure 3. LACE Fluorescence Quantification using FIJI software.

A. Open image file in Fiji software. B. Ensure ‘Mean grey value’ is checked in ‘Set Measurements’ window. C. Draw a shape of consistent size at the region to be quantified. D. Click ‘Measure’ and record mean greyscale value.

- Open experimental image in ImageJ and draw the chosen shape around the region to be quantified as in Step B5. Ensure that the shape is the same size and in the same anatomical position within the tissue section.
- Click ‘Analyze’ and select ‘Measure’ as in Step B6 and record the mean greyscale value. Perform

- background fluorescence subtraction by subtracting the background fluorescence value from the greyscale value recorded for the section.
9. Repeat Step B8 using at least 2 more tissue sections and calculate a mean greyscale value for that individual animal.
 10. Repeat Steps B8 and B9 for tissue sections from all other animals included in the experiment.

Recipes

1. Heparinase Buffer

20 mM Tris-HCl
4 mM CaCl₂
0.1 mg/mL BSA

Acknowledgments

This work was supported by funding from the Wellcome Trust, the Biotechnology and Biological Sciences Research Council (BB/M00693X/1) and The Simons Initiative for the Developing Brain (SFARI - 529085).

Competing interests

The authors declare no competing financial interests.

Ethics

All mice were bred in-house according to Home Office UK legislation and licenses approved by the University of Edinburgh Ethical Review Committees and Home Office. Animal husbandry was in accordance with UK Animals (Scientific Procedures) Act of 1986 regulations. All work was carried out under Home Office project license number, P1351480E.

References

- Allen, B. L. and Rapraeger, A. C. (2003). [Spatial and temporal expression of heparan sulfate in mouse development regulates FGF and FGF receptor assembly](#). *J Cell Biol* 163(3): 637-648.
- Allen, B. L., Fillia, M. S. and Rapraeger, A. C. (2001). [Role of heparan sulfate as a tissue-specific regulator of FGF-4 and FGF receptor recognition](#). *J Cell Biol* 155(5): 845-858.
- Clegg, J. M., Parkin, H. M., Mason, J. O. and Pratt, T. (2019). [Heparan sulfate sulfation by Hs2st restricts astroglial precursor somal translocation in developing mouse forebrain by a Non-cell-autonomous mechanism](#). *J Neurosci* 39(8): 1386-1404.
- Friedl, A., Fillia, M. and Rapraeger, A. C. (2001). [Tissue-specific binding by FGF and FGF receptors to endogenous heparan sulfates](#). *Methods Mol Biol* 171: 535-546.

Investigate Synaptic Vesicles Mobility in Neuronal Culture Axons by FRAP Imaging

Xiao Min Zhang^{1,*}, Fabrice P. Cordelieres² and Etienne Herzog^{3,*}

¹Department of Pathophysiology, Guangdong Provincial Key Laboratory of Brain Function and Disease, Zhongshan School of Medicine, Sun Yat-sen University, Guangzhou, China

²University Bordeaux, CNRS, INSERM, Bordeaux Imaging Center, BIC, UMS, Bordeaux, France

³University Bordeaux, CNRS, Interdisciplinary Institute for Neuroscience, IINS, UMR, Bordeaux, France

*For correspondence: zhangxm225@mail.sysu.edu.cn; etienne.herzog@u-bordeaux.fr

Abstract

Synaptic vesicles (SVs) are clustered in the presynaptic terminals and consistently trafficking along axons. Based on their release features, SVs are classified into different “pools”. Imaging of SVs that are traveling among multiple presynaptic terminals has helped define a new pool named “SV super-pool”. Here we describe a Fluorescent Recovery After Photobleaching (FRAP) approach to elucidate the relationship between SVs from the super-pool with SV clusters at presynaptic terminals. This method is powerful to investigate SV mobility regulation mechanisms.

Keywords: Synaptic vesicle, Membrane trafficking, Live-cell imaging, FRAP, Axonal transport, Synapse

This protocol was validated in: eLife (2021), DOI: 10.1038/s41598-021-9915

Background

Synaptic vesicles (SVs) are key organelles involved in neurotransmission through the storage and release of neurotransmitters. SVs are mostly identified in a cluster adjacent to the active zone of the presynaptic terminals.

SVs have a homogeneous appearance with a diameter of 40-50 nm under electron microscopy (EM) (Landis *et al.*, 1988; Korogod *et al.*, 2015). While, to our knowledge, there is no significant biochemical distinction between SVs. Under different stimulation paradigms, they show different release properties. Thus, SVs were classified into different functional pools: the reserve pool, the recycling pool and the readily releasable pool (Figure 1) (Denker and Rozzoli, 2010). The detailed synapse structure, SV localization, SV release mechanisms were intensively studied with EM. SVs were found linked to one or two neighboring vesicles by filaments, and synapsins were thought to be part of the connector and maintain the SVs in the reserve pool (Siksou *et al.*, 2007). The dissection of molecular steps for SVs docking and fusion was also revealed by ultrastructure study (Imig *et al.*, 2014). The fusion of SV with the plasma membrane exposes the acidic lumen (pH around 5.0) to the neutral extracellular medium (pH of 7.4) (Südhof, 1995). Therefore, SVs recycling and related molecular mechanisms were also intensively studied by labeling SVs with pH sensors (Sankaranarayanan *et al.*, 2000; Soykan *et al.*, 2017).

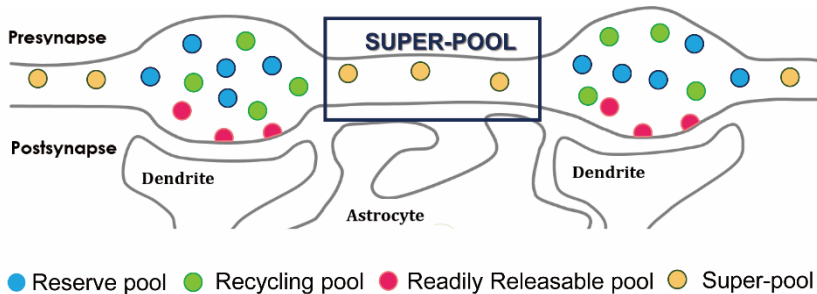


Figure 1. Synaptic vesicle pools.

The classical model of synaptic vesicle (SV) pools are the reserve pool, the recycling pool, and the readily releasable pool. A newly defined “super-pool” comprises SVs that share among *en-passant* presynaptic boutons along the axon.

For many years, it was thought that SVs recycle inside a single presynaptic terminal without major exchange with neighboring *en-passant* boutons of the same axon, while terminals may function with significant autonomy from the distant cell soma. In the past decade, SVs were observed trafficking and sharing between multiple *en-passant* presynaptic boutons along the axon. This axonal SV population was designated as “super-pool” (Figure 1) (Denker and Rozzoli, 2010). This super-pool was observed through both *in vitro* and *in vivo* paradigms (Staras *et al.*, 2010; Herzog *et al.*, 2011; Zhang *et al.*, 2019). Yet, how SVs in super-pool contribute to the neurotransmission remains largely unknown. We could recently show that, changes in the super-pool size impact spontaneous release frequency (Zhang *et al.*, 2019).

FRAP is normally used for determining the kinetics of cell membrane diffusion or protein binding (Axelrod *et al.*, 1976; Qin *et al.*, 2008), while the kinetics of SV mobility is unlike these cases. However, as described above, a certain number of SVs are clustered in each presynaptic bouton and consistently refresh with SVs in super-pool. FRAP allows to measure diffusion of SVs between the presynaptic bouton and the axon. Here, we detail a protocol for FRAP imaging that is able to elucidate the exchange of SVs between the super-pool and presynaptic SV clusters. SVs are labeled with a synaptic vesicle protein tagged with a fluorescent protein, such as VGLUT1^{venus} or Synaptobrevin 2^{EGFP} (Figures 2A-2D). This FRAP method can be applied to both *in vitro* and *in vivo* systems. In this paper, we will describe the detailed protocol applied to dissociated hippocampal neuronal culture. This FRAP imaging method will be useful for further explorations of SV mobility related mechanisms.

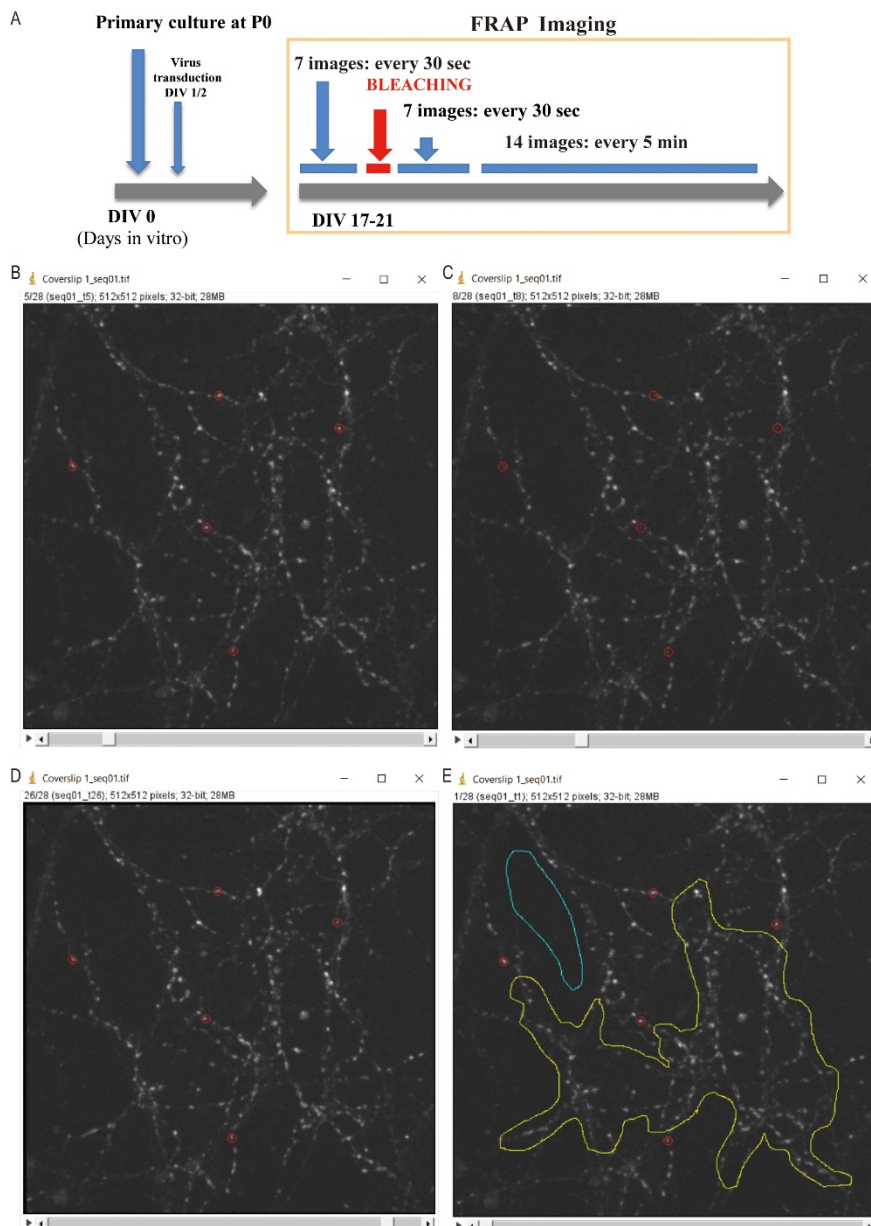


Figure 2. FRAP sequences acquisition and analysis.

In neurons, SVs are labeled by fluorescent protein Venus/EGFP. A presynaptic bouton contains a cluster of SVs, this is shown as a bright individual bouton. A. The experiment work flow. The virus transduction is performed on DIV 1/2 of the culture, and the FRAP imaging is acquired from DIV 17 to 21. Detailed FRAP imaging procedure is showed in the yellow box. B. Randomly select a field of culture for imaging. In the field, select 5 boutons (labeled as red circles) that are distant from each other as ROIs for bleaching. C. The frame acquired just after photobleaching. The fluorescent intensity of 5 selected boutons is significantly decreased due to the photobleaching. D. A frame acquired 1 h after photobleaching, the ROIs fluorescent intensity is gradually recovered. E. Analyze the FRAP sequence with FRAP Analysis Macro. Following menus on the pop-up windows, select the regions of bleached boutons (red circles), the cells in the field for photobleaching correction (yellow region), and the background area for background subtraction (blue region).

Materials and Reagents

1. Round cover glass, #1 thickness, 18 mm (Warner Instruments, catalog number: 64-0384)
2. 35 mm Glass bottom dish with 10 mm micro-well (Cellvis, catalog number: D35-10-1-N)
3. 15 mL Conical centrifuge tubes (Falcon™, catalog number: 14-959-53A)
4. 200 µL pipette tips (QuickRack, catalog number: NC9640144)
5. C57/BL6J mice (The Jackson Laboratory, catalog number: 000664)
6. Leibovitz's L-15 medium (Gibco, catalog number: 11415064), store at 4°C
7. 0.05% trypsin-EDTA (Gibco, catalog number: 25300054), store at -20°C
8. Dulbecco's Modified Eagle's Medium (DMEM) (Gibco, catalog number: 61965026), store at 4°C
9. Fetal bovine serum (Eurobio, catalog number: CVFSVF001), store at -20°C
10. Penicillin-streptomycin (Gibco, catalog number: 15140122), store at -20°C
11. Poly-L-lysine (Sigma, catalog number: P2636), store at -20°C
12. Neurobasal A medium (Gibco, catalog number: 12349105), store at 4°C
13. B27 supplement (Gibco, catalog number: 17504044), store at -20°C
14. Glutamax (Gibco, catalog number: 35050038), store at -20°C
15. MycoZap plus-PR (Lonza, catalog number: VZA2021), store at -20°C
16. HEPES buffer (Stemcell, catalog number: 07200), store at 4°C
17. BrainPhys™ without phenol red medium (Stemcell, catalog number: 05791), store at 4°C
18. F(syn)W-RBN::VGLUT1-venus (PMID: 23581566, available upon request to Dr. Etienne Herzog), store at -80°C
19. F(syn)W-RBN::Synaptobrevin2-EGFP (PMID: 23581566, available upon request to Dr. Etienne Herzog), store at -80°C
20. Complete DMEM medium (see Recipes)
21. Complete Neurobasal A medium (see Recipes)
22. Complete BrainPhys medium (see Recipes)

Equipment

1. Leica DMI 6000 microscope (Leica Microsystems, Wetzlar, Germany)
2. Spinning disk confocal head Yokogawa CSU-X1(Yokogawa Electric Corporation, Tokyo, Japan)
3. EM-CCD QuantEM camera (Photometrics, Tucson, USA)
4. iLAS FRAP scanner system (Roper Scientific, Evry, France)
5. Piezo nanofocusing scanner P721.LLQ (Physik Instrumente, Karlsruhe, Germany)
6. Thermal incubator (Life Imaging Services, Switzerland)

Software

1. MetaMorph microscopy automation and image analysis software (Molecular Devices, Sunnyvale, USA, <https://www.moleculardevices.com/products/cellular-imaging-systems/acquisition-and-analysis-software/metamorph-microscopy>)
2. ImageJ (NIH, USA, <https://imagej.nih.gov/ij>)
3. FRAP Analysis Macro (Fabrice P. Cordelieres, https://github.com/fabricecordelieres/IJ-Macro_FRAP-MM)

Procedure

A. Prepare dissociated hippocampal neuronal culture for live imaging

1. Coat the glass coverslips or glass bottom dishes with 0.1 mg/mL poly-L-lysine overnight, and rinse with ddH₂O 3 times before using.
2. Dissect hippocampi from P0 (Post-natal day 0) C57/BL6 mice in ice-cold Leibovitz's L-15 medium.
3. Collected all hippocampi in a 15 mL Falcon tube filled with ice-cold Leibovitz's L-15 medium.
4. Remove Leibovitz's L-15 medium. Incubate tissues in 5 mL of 0.05% trypsin-EDTA solution at 37°C for 15 min. Trypsin will digest extracellular proteins to facilitate cell dissociation.
5. Remove 0.05% trypsin-EDTA solution, and replace with complete DMEM medium to stop the reaction.
6. Then remove the DMEM medium, and wash the tissue with 5 mL complete Neurobasal A medium.
7. Add 1 mL complete Neurobasal A medium in the tube. Dissociate cells mechanically by pipetting up and down with a 200 μL tip for 10-15 strokes.
8. Incubate the cell suspension for 3 min to allow the sedimentation of large tissue debris. Take the 800 μL upper suspension and avoid sampling of tissue clusters.
9. Measure cell density and plate cells to pre-coated poly-L-lysine glass coverslips/glass bottom dishes at a density of 20,000 cells/cm².

Note: Cells are grown in 2 mL complete Neurobasal A medium in the well of 12-well plate, or 3 mL medium in a 35 mm glass bottom dish.

10. Cells are grown in complete Neurobasal A medium for 5 days *in-vitro* (DIV).
11. From DIV 5-6, replace half conditioned medium (1 mL for each well of 12-well plate, and 1.5 mL for 35 mm glass bottom dishes) with complete BrainPhys medium every 2-3 days.

B. Viral transduction of reporter gene

On DIV 1 or 2, transduce cells with the lentivirus vector allowing for the expression of a fluorescent reporter of synaptic vesicles. We use F(syn)W-RBN::Synaptobrevin2-EGFP or F(syn)W-RBN::VGLUT1-venus. For each vector batch, Western-blot and fluorescent imaging are performed to adjust the dilution to limit protein overexpression to 2-fold of wild-type levels.

The lenti vector dilution and protein expression are measured by Western-blot and fluorescent imaging:

1. Cells are grown in 6 cm dishes that are pre-coated with poly-L-lysine with the same cell density as described above.
2. On DIV 1 or 2, lentivirus (titer range in ~×10⁸ TU/mL) is diluted to 1/100 with Neurobasal A medium. Add 20/40/80 μL diluted virus to each dish of the culture for transduction. Return the culture to the incubator.
3. On DIV17, the cells are scraped and collected from the dishes. The targeted protein expression level in each sample is measured by Western-blot. VGLUT1-venus or Synaptobrevin2-EGFP has ~27 kDa higher molecular weight, thus can be easily distinguished from the corresponding endogenous wildtype protein. The increased virus transduction normally will result a linearized increase of protein expression.
4. Compare the expression of VGLUT1-venus/Synaptobrevin2-EGFP with the wildtype VGLUT1/Synaptobrevin2. Calculate the right dilution of virus which results less than 2-fold of protein overexpression. Normally, the fluorescent intensity of the presynaptic boutons is bright enough and is suitable for FRAP imaging with this protein expression level.
5. Based on the cell amount, proportionally add the right dilution of virus to the 12-well plates or 35 mm glass bottom dishes culture on DIV 1 or 2 that are prepared for FRAP imaging (Figure 2A).

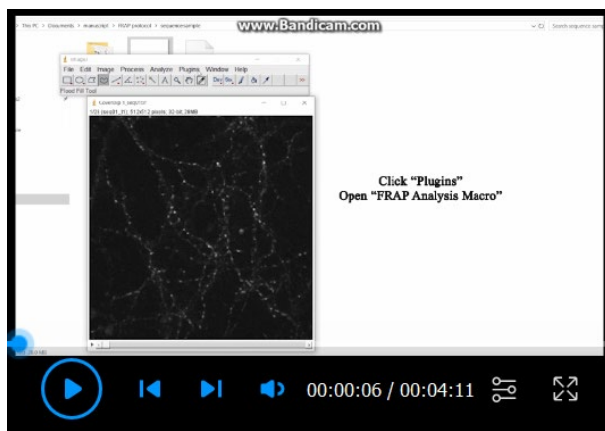
C. FRAP Imaging

Note: FRAP imaging is performed with a spinning disk confocal microscope that is controlled by MetaMorph microscopy automation software. Take DIV 17-21 cell culture for imaging, normally neurons are mature and synaptic networks are well established at this time point. Incubate the cultures in conditioned culture medium (cells are grown in) containing HEPES (40 mM) and at physiological temperature (37°C) during the imaging procedure.

1. Use MetaMorph to control the entire FRAP procedure.
2. RandomLy select one field of the cell culture for imaging with a 63 \times /1.4 numerical aperture oil-immersion objective (Figure 2B).
3. Select up to 5 fluorescent boutons that are distant from each other as Regions of Interest (ROIs) for bleaching (Figure 2B). Selecting too many boutons that are closely related on the same axon would affect the measurement. Before bleaching, monitor the boutons fluorescence every 30 s for 3 min (Figure 2A). Image as a Z-stack of 4.8 μ m thickness with 0.8 μ m step interval. ROIs should be at the midplane of the stack. Stack imaging allows for a more robust measurement of bouton intensity and to buffer fluctuations due to small Z-directed movements.
4. Apply three passes of 491 nm laser (40 mW) to bleach the Syb2^{EGFP} labeling boutons; two laser passes of 491 nm laser (30 mW) and the 405 nm laser (10 mW) to bleach the VGLUT1^{venus} labeling boutons (Figure 2B). After bleaching, the fluorescence of ROIs should remain around 40%-60% of the initial fluorescence intensity (Figure 2C). VENUS and EYFP related dyes require a stimulation at 405 nm to prevent fluorescence recovery from a reversible dark state of the fluorescent proteins (McAnaney *et al.*, 2005; Herzog *et al.*, 2011).
5. Monitor the fluorescence recovery after bleaching every 30 s during the first 3 min and then every 5 min during the next 70 min (Figure 2A).

Data analysis

1. Open the stack sequence with ImageJ and perform a sum Z projection that will generate a 32 bits/pixel sequences (Video 1).



Video 1. An example of image processing with ImageJ FRAP analysis Macro

2. Use Image J FRAP Analysis Macro under “plugin” (https://github.com/fabricecordelieres/IJ-Macro_FRAP_MM) to automate image analysis (Video 1).
 - a. The macro commands apply x-y realignment to each individual stack.

- b. Then extract the integrated fluorescence intensity of bleached boutons, the cells in the field for photobleaching correction, and the background area for background subtraction (Figure 2E).
- c. The Macro will output all the raw data and processed data in a table named “Results” (Figure 3A) and a plot named “Values” that shows all ROIs’ intensity value V_x (x stands for time point) as a function of time (Figure 3B).
3. The boutons intensity slightly varies in each frame before bleaching. Take the average value before bleaching ($V_{pre-ave}$) as prebleaching reference. Normalize boutons intensity at different time point V_x in the sequence as:

$$\hat{V}_x = \frac{V_x}{V_{pre-ave}}$$

4. Filter out rejected ROIs from the final quantification which may correspond to the following cases:
 - a. The bouton (ROI) fluorescence \hat{V}_b (b stands for the frame right after bleaching) are over-bleached or less-bleached, which means $\hat{V}_b < 20\%$ or $> 70\%$ (Figure 3B, the bouton with black curve). Indeed, \hat{V}_b below 20% the risk of photodamage to the sample is high, and above 70% the recovery will not be measured accurately.
 - b. Because axonal exchange is not entirely linear and continuous, some boutons may receive or loose massive fluorescent clusters during the fluorescence recovery time (Figure 3B, the bouton with green curve). This was extensively described in our former paper (Herzog *et al.*, 2011).
5. Calculate the percentage of recovered fluorescence of each bouton. Normalize the boutons average intensity before bleaching as 1, right after bleaching as 0. The total bleached fluorescence is $I - \hat{V}_b$, the recovered fluorescence at different time point is $\hat{R}_x = \hat{V}_x - \hat{V}_b$.

$$\hat{R}_x = \frac{\hat{V}_x - \hat{V}_b}{I - \hat{V}_b}$$

The recovered fluorescent value \hat{R}_x stands for the SVs exchange between presynaptic cluster and super-pool.

6. Summarize the normalized bouton fluorescence data in your favorite software for statistics and plotting (Figure 3C). Fit the average of all normalized FRAP traces with a double exponential function (Figure 3D).

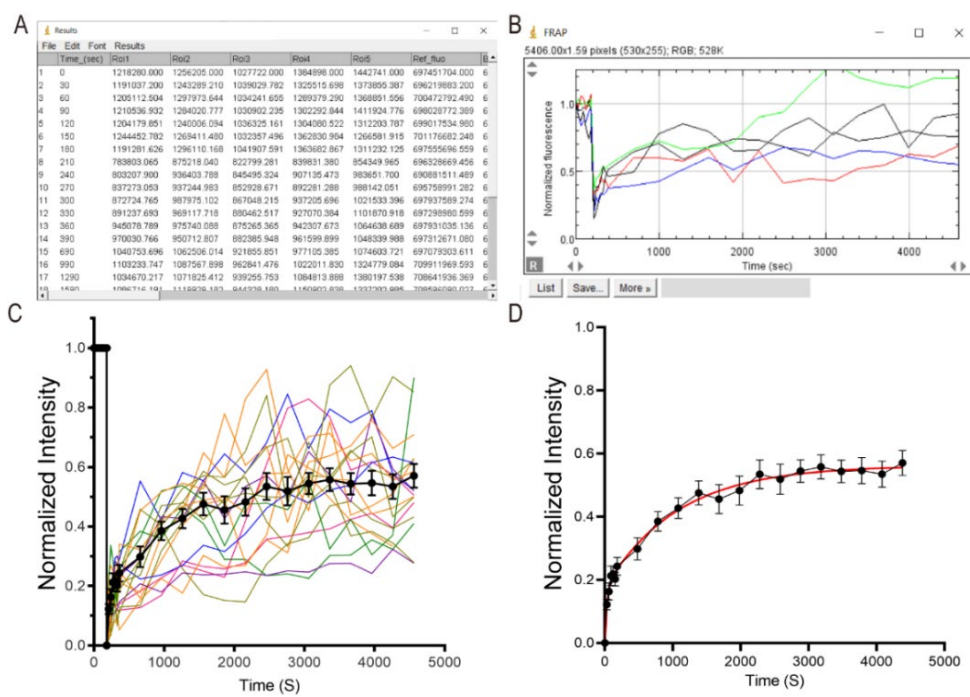


Figure 3. FRAP Data analysis.

A. When FRAP Analysis Macro analysis is done, a results file with the ROIs' raw data and normalized data is generated. B. And a plot presenting the corrected normalized values as a function of time for all ROIs is generated. C. An example figure showed the summary of normalized FRAP traces. One colorful trace stands for an individual bouton fluorescence variation in the FRAP experiment. The black dots stand for the mean value of all the ROIs at different time points. D. A double exponential trace is fitted to the average FRAP curve.

Notes

1. Use serum-free medium for mixed glial-neuronal culture. Because it is important to keep the cell morphology stable during the whole acquisition. Neurons grown on a layer of astrocytes will not be suitable for imaging, because of movements during the imaging procedure. Mixed culture containing few glia cells or banker culture are suitable for this long-time FRAP imaging.
2. Select a field with nice neuronal network but with at least one empty region (no fluorescent material) for imaging. The dark region is essential to be taken as a background reference for later imaging analysis.
3. Apply certain amount of 405 nm laser for Venus/EYFP fluorescence bleaching. As previously reported, YFP has a photochemical reversible dark state representing roughly 20% of YFP/VENUS molecules. This dark pool of fluorescent proteins is emptied by photoactivation at 405 nm (McAnaney *et al.*, 2005; Herzog *et al.*, 2011). Thus, accompanying bleaching with UV light significantly reduces the unwanted recovery.
4. Set the right laser power for the bouton fluorescence bleaching. The bleach will result a ~50% fluorescence reduction. To avoid the bleaching variance caused by a single laser pass, repeat a mild laser pass for 2-3 times to the selected boutons is recommended. The appropriate laser power needs to be tested based on your own culture before experiments.

Recipes

1. Complete DMEM medium

Cite as: Zhang, X. M. et al. (2021). Investigate Synaptic Vesicles Mobility in Neuronal Culture Axons by FRAP Imaging. Bio-protocol 11(6): e3962. DOI: 10.21769/BioProtoc.3962.

450 mL DMEM medium
50 mL FBS
and 5 mL Penicillin-streptomycin
store at 4°C

2. Complete Neurobasal A medium

50 mL Neurobasal A medium
1 mL B27 supplement
125 µL Glutamax
And 100 µL Mycozap plus-PR
Store at 4°C

3. Complete BrainPhys medium

50 mL BrainPhys medium
1 mL B27 supplement
125 µL Glutamax
And 100 µL Mycozap plus-PR
Store at 4°C

Acknowledgments

We thank Bordeaux Imaging Center for their excellent technical support and equipment for the experiments. This work is supported by the Erasmus Mundus ENC program and the LabEx BRAIN extension grant (ANR-10-LABX-43 BRAIN), Agence Nationale de la Recherche (ANR-12-JSV4-0005-01 VGLUT-IQ; ANR-10-LABX-43 BRAIN; ANR-10-IDEX-03-02 PEPS SV-PIT) and Fondation pour la Recherche Médicale (ING20150532192). This protocol introduced here was detailed from past studies (Herzog *et al.*, 2011; Zhang *et al.*, 2019).

Competing interests

The authors declare no financial or non-financial competing interests related to this work.

Ethics

The experimental design and all procedures were performed in accordance with the European guide for the care and use of laboratory animals and approved by the ethics committee of Bordeaux University (CE50) under the APAFIS n°1692.

References

- Axelrod, D., Koppel, D. E., Schlessinger, J., Elson, E. and Webb, W. W. (1976). [Mobility measurement by analysis of fluorescence photobleaching recovery kinetics](#). *Biophys J* 16(9): 1055-1069.
- Denker, A. and Rizzoli, S. O. (2010). [Synaptic vesicle pools: an update](#). *Front Synaptic Neurosci* 2: 135.
- Herzog, E., Nadirny, F., Silm, K., Biesemann, C., Helling, I., Bersot, T., Steffens, H., Schwartzmann, R., Nagerl, U. V., El Mestikawy, S., Rhee, J., Kirchhoff, F. and Brose, N. (2011). [In vivo imaging of intersynaptic vesicle exchange using VGLUT1 Venus knock-in mice](#). *J Neurosci* 31(43): 15544-15559.

- Imig, C., Min, S. W., Krinner, S., Arancillo, M., Rosenmund, C., Sudhof, T. C., Rhee, J., Brose, N. and Cooper, B. H. (2014). [The morphological and molecular nature of synaptic vesicle priming at presynaptic active zones](#). *Neuron* 84(2): 416-431.
- Korogod, N., Petersen, C. C. and Knott, G. W. (2015). [Ultrastructural analysis of adult mouse neocortex comparing aldehyde perfusion with cryo fixation](#). *Elife* 4: e05793.
- Landis, D. M., Hall, A. K., Weinstein, L. A. and Reese, T. S. (1988). [The organization of cytoplasm at the presynaptic active zone of a central nervous system synapse](#). *Neuron* 1(3): 201-209.
- McAnaney, T. B., Zeng, W., Doe, C. F., Bhanji, N., Wakelin, S., Pearson, D. S., Abbyad, P., Shi, X., Boxer, S. G. and Bagshaw, C. R. (2005). [Protonation, photobleaching, and photoactivation of yellow fluorescent protein \(YFP 10C\): a unifying mechanism](#). *Biochemistry* 44(14): 5510-5524.
- Qin, K., Sethi, P. R. and Lambert, N. A. (2008). [Abundance and stability of complexes containing inactive G protein-coupled receptors and G proteins](#). *FASEB J* 22(8): 2920-2927.
- Sankaranarayanan, S., De Angelis, D., Rothman, J. E. and Ryan, T. A. (2000). [The use of pHluorins for optical measurements of presynaptic activity](#). *Biophys J* 79(4): 2199-2208.
- Siksou, L., Rostaing, P., Lechaire, J. P., Boudier, T., Ohtsuka, T., Fejtova, A., Kao, H. T., Greengard, P., Gundelfinger, E. D., Triller, A. and Marty, S. (2007). [Three-dimensional architecture of presynaptic terminal cytomatrix](#). *J Neurosci* 27(26): 6868-6877.
- Soykan, T., Kaempf, N., Sakaba, T., Vollweiter, D., Goerdeler, F., Puchkov, D., Kononenko, N. L. and Haucke, V. (2017). [Synaptic Vesicle Endocytosis Occurs on Multiple Timescales and Is Mediated by Formin-Dependent Actin Assembly](#). *Neuron* 93(4): 854-866 e854.
- Staras, K., Branco, T., Burden, J. J., Pozo, K., Darcy, K., Marra, V., Ratnayaka, A. and Goda, Y. (2010). [A vesicle superpool spans multiple presynaptic terminals in hippocampal neurons](#). *Neuron* 66(1): 37-44.
- Südhof, T. C. (1995). [The synaptic vesicle cycle: a cascade of protein-protein interactions](#). *Nature* 375(6533): 645-653.
- Zhang, X. M., Francois, U., Silm, K., Angelo, M. F., Fernandez-Busch, M. V., Maged, M., Martin, C., Bernard, V., Cordelieres, F. P., Deshors, M., Pons, S., Maskos, U., Bemelmans, A. P., Wojcik, S. M., El Mestikawy, S., Humeau, Y. and Herzog, E. (2019). [A proline-rich motif on VGLUT1 reduces synaptic vesicle super-pool and spontaneous release frequency](#). *Elife* 8: e50401.

Single or Repeated Ablation of Mouse Olfactory Epithelium by Methimazole

Sofia Håglin^{*,§}, Staffan Bohm and Anna Berghard

Department of Molecular Biology, Umeå University, Umeå, Sweden; [§]Current address: Department of Integrative Medical Biology, Umeå University, Umeå, Sweden

*For correspondence: sofia.haglin@umu.se

Abstract

Odor-detecting olfactory sensory neurons residing in the nasal olfactory epithelium (OE) are the only neurons in direct contact with the external environment. As a result, these neurons are subjected to chemical, physical, and infectious insults, which may be the underlying reason why neurogenesis occurs in the OE of adult mammals. This feature makes the OE a useful model for studying neurogenesis and neuronal differentiation, with the possibility for systemic as well as local administration of various compounds and infectious agents that may interfere with these cellular processes. Several different chemical compounds have been shown to cause toxic injury to the OE, which can be used for OE ablation. We, and others, have found that the systemic administration of the hyperthyroid drug, methimazole, reliably causes olfactotoxicity as a side effect. Here, we outline an OE lesioning protocol for single or repeated ablation by methimazole. A single methimazole administration can be used to study neuroepithelial regeneration and stem cell activation, while repeated ablation and regeneration of OE enable the study of tissue stem cell exhaustion and generation of tissue metaplasia.

Keywords: Olfactory epithelium, Methimazole, Lesion, Regeneration, Tissue stem cell, Metaplasia

This protocol was validated in: J Neurosci (2020), DOI: 10.1523/JNEUROSCI.2468-19.2020

Background

New neurons are generated throughout life in the OE of mammals including humans (Hahn *et al.*, 2005) and mice (Graziadei *et al.*, 1979b; Kondo *et al.*, 2010). Continuous cell generation is primarily achieved by globose progenitor cells (Jang *et al.*, 2014). Progenitor cells also have the potential to reconstitute all OE cell types after injury, with horizontal basal cells having the greatest tissue stem cell potential (Leung *et al.*, 2007; Schnittke *et al.*, 2015; Gadye *et al.*, 2017).

There exist different methods to specifically injure the OE in laboratory rodents, which in turn allows the study of the regenerative process including stem cell activation, neurogenesis, and neuronal differentiation. Methods include removal of the olfactory bulb (OB) (Schwob *et al.*, 1992), olfactory nerve axotomy (Graziadei *et al.*, 1979a; Suzuki and Takeda, 1991), intranasal administration of zinc sulphate (Matulionis, 1975), inhalation of methyl bromide gas (Hurtt *et al.*, 1988), and intraperitoneal (i.p.) injection of olfactotoxic chemicals such as methimazole, colchicine, and dichlobenil (Genter *et al.*, 1995; Suzuki *et al.*, 1998; Bergman and Brittebo, 1999). All these methods induce the destruction of one or several OE cell types followed by detachment of the OE and subsequent regeneration. The mechanism of action differs depending on the method; thus, there are important differences regarding which cell types are affected and how. Noteworthy, viruses such as SARS-CoV-2 can also specifically damage OE cells (Zhang *et al.*, 2020).

Methimazole (1-methyl-2-mercaptoimidazole, also called thiamazole) is used to treat hyperthyroidism (Astwood *et al.*, 1945) and is known to cause a loss of the sense of smell (olfaction) as a side effect of treatment (Cooper, 1999). The OE is a pseudostratified epithelium in which all mature cells and horizontal basal cells are in contact with the basal lamina. In response to i.p. methimazole, several cell types in the OE, such as Bowman's gland cells, sustentacular cells, and olfactory sensory neurons, display swollen organelles within four hours, which is followed by detachment of cells from the basal lamina (Bergström *et al.*, 2003). After methimazole injury, the OE completely regenerates in approximately one month, and the first olfactory sensory neurons begin to make synaptic contacts with the OB at approximately 1-2 weeks (Suzukawa *et al.*, 2011). Methimazole has been shown to affect young and aged mice differently, on postnatal day 10 compared with 18 months old (Suzukawa *et al.*, 2011).

In rats, i.p. methimazole doses from 25 mg/kg to 300 mg/kg have been evaluated for OE toxicity (Genter *et al.*, 1995). We conducted a pilot study to elucidate the lowest dose suitable for reproducible OE ablation in mice (Håglin *et al.*, 2020). Single injection of either 75 mg/kg or 100 mg/kg resulted in detachment of the entire OE, whereas 50 mg/kg caused incomplete lesioning since there were residual patches of OE cells that appeared relatively unaffected. These results are in accordance with those of previous studies showing that lower doses of i.p. methimazole are insufficient to obtain complete OE lesions in mice (Brittebo, 1995) or rats (Genter *et al.*, 1995). Since 75 mg/kg and 100 mg/kg yielded similar results, we used the lower dose for further studies.

In our hands, methimazole more reliably causes OE ablation than does dichlobenil, and in practice, methimazole is easier to use than zinc sulphate or methyl bromide gas. Our protocol is the first to describe repeated OE ablation–regeneration cycles. By repeating the injury up to three times, we found a gradual decrease in the regenerative potential of the OE, which is accompanied by the progressive accumulation of two different types of metaplasia (Håglin *et al.*, 2020). Thus, repeated ablation–regeneration cycles of the mouse OE following methimazole treatment may be used, for example, to study: i) the exhaustion of the regenerative capacity of neurogenic tissue stem cells, which may mimic aging; ii) the robustness of the re-establishment of a tissue niche when subjected to repeated injury; iii) the plasticity of target neurons in the OB when challenged to re-establish synapses several times over; iv) the role of OE barrier function in protecting against a nasal route of infection as well as uptake of chemical substances to the brain; and v) the roles of different normal and disease variants of genes in these processes since there are many genetically modified mice available for study.

Materials and Reagents

1. 50 mL plastic, conical-base centrifuge tubes with screw cap (Sarstedt, catalog number: 62.547.254)
2. 2 mL sterile plastic microcentrifuge tubes with snap cap (Eppendorf 022363433, Fisher Scientific, catalog number: 05-402-11)
3. Micropipettes with appropriate tips
4. 0.5-1 mL insulin syringe (for example Beckton-Dickinson, catalog number: 329651) with 27G × 13 mm needle (BD, catalog number: 300635) or 0.5 mL syringe with attached 29G × 13 mm needle (BD, catalog number: 323001)
5. 100 mL and 250 mL glass bottles (VWR, catalog numbers: 10754-814 and 10754-816)
6. Permanent marker (please use one that withstands ethanol and freezing, such as the black Science-Marker VWR, catalog number: 76276-060)
7. Peel-A-way® embedding molds (Sigma-Aldrich, catalog number: E6032-1CS)
8. Superfrost Plus microscope slides (Thermo Fisher Scientific, catalog number: 12727307)
9. Cover slips no. 1 1/2 (Sigma-Aldrich, catalog number: CLS2980224-1000EA)
10. Boxes for microscope slides (VWR, catalog number: 82024-584)
11. Mice of the strain, genotype, age, and sex that you wish to analyze. See Procedure A for the protocol for C57BL/6 mice (Taconic, Denmark)
12. Methimazole (Sigma-Aldrich, catalog number: M8506), keep the container closed in a dry and well-ventilated area. Store at 4°C
13. Sterile physiological saline 9 mg/mL (*e.g.*, Estericlean, catalog number: 7053249369080)
14. Paraformaldehyde (VWR, catalog number: 28794.295). Store the powder at 4°C
15. Sucrose (VWR, catalog number: 27480.294)
16. 10× phosphate-buffered saline (PBS), pH 7.4 (*e.g.*, PanReac Applichem, catalog number: A0965,9010). Dissolve and store at room temperature
17. 5 M NaOH (VWR, catalog number: 31625.293)
18. OCT cryomount embedding medium (Sakura FineTek, catalog number: 45830)
19. Dry ice
20. Glycerol (VWR, catalog number: BDH1172-1LP)
21. Hoechst 33258 (Sigma-Aldrich, catalog number: ab228550). Prepare a 1000× stock solution of 0.5% (weight/volume) in water. Store the aliquots at -20°C
22. Primary antibodies used to identify cell types in Figures 1 and 3 are:
 - a. Anti-cytokeratin 5 for horizontal basal cells (rabbit; dilution 1:300, BioLegend, catalog number: 905501)
 - b. Anti-IgGFc-binding protein (FcγBP) for respiratory secretory cells (rabbit, dilution 1:200, Novus Biologicals, catalog number: NBP1-90462)
 - c. Anti-antigen Ki-67 (Ki-67) for cells in the cell cycle (rabbit, 1:500, Merck, catalog number: AB9076)
 - d. Anti-olfactory marker protein (OMP) for mature olfactory sensory neurons (goat; dilution 1:1,000, Wako Chemicals, catalog number: 544-10001)
 - e. Anti-retinaldehyde dehydrogenase type 1/2 (RALDH1/2) for supporting and respiratory cells (mouse; dilution 1:1,000, Santa Cruz Biotechnology, catalog number: SC-166362)
 - f. Anti-stathmin-1 (STMN1) for immature olfactory sensory neurons (rabbit; dilution 1:500, Abcam, catalog number: ab24445)

Equipment

1. Dissection instruments
 - a. Scissors around 15 cm (Fine Science Tools, catalog number: 14001-14) and 10 cm (Fine Science Tools, catalog number: 14370-22) for the removal of fur and cutting through bone, respectively (expensive scissors will be destroyed)
 - b. A smaller pair of fine scissors for trimming soft tissue (preferably blunt tip, Fine Science Tools, catalog

- number: 14108-09)
- c. A few forceps, such as the fine pointed ones that are used to remove the teeth (Fine Science Tools, catalog number: 11231-30), blunt ones (Fine Science Tools, catalog number: 11000-12), and ones with teeth (Fine Science Tools, catalog number: 11028-15). Use blunt plastic forceps to check for decalcification (Fine Science Tools, catalog number: 11700-03)
 - 2. RDO Rapid Decalcifier (ApexEngineering directly www.rdodecal.com/contact/ or ESBE Scientific, catalog number: APE-RDOL4L)
 - 3. Precision laboratory scale and analytical balance (for chemicals)
 - 4. Precision laboratory scale (for mice)
 - 5. Rocking platform or orbital shaker
 - 6. Magnetic stirrer
 - 7. Microwave oven
 - 8. Cryostat with a knife for hard tissue
 - 9. Inverted fluorescence microscope with camera and $\times 4$, $\times 10$, $\times 20$ and $\times 40$ objectives. A filter for fluorescence in blue (Hoechst 33258 is excited by light at 350 nm and emits at around 455 nm) is required at the least
 - 10. -80°C freezer
 - 11. Optional: Vacuum chamber or vacuum oven

Procedure

A. Pilot experiment to determine the methimazole dose required (recommended)

- 1. We strongly recommend determining the specific methimazole dose required before setting up a larger experimental study in order to ascertain that reproducible ablation of the OE can be achieved in mice of the age and specific strain you wish to study. Note that it is unknown whether methimazole is toxic to the OE in mice younger than 10 days old (Suzukawa *et al.*, 2011). It is known that several enzymes in the OE are important for the metabolism of methimazole; therefore mouse strain differences will account for differences in the required dose (Xie *et al.*, 2011). In the planning stage, decide which methamizole doses you wish to evaluate. We evaluated 50 mg/kg, 75 mg/kg, and 100 mg/kg for adult 2-5 month-old male and female C57BL/6 mice weighing 40-60 g (Håglund *et al.*, 2020). Note that RTECS (Registry of Toxic Effects of Chemical Substances) lists the i.p. LD₅₀ as 500 mg/kg for mice. It is recommended that at least 3 animals are analyzed per dose.
- 2. Prepare methimazole under aseptic conditions in sterile physiological saline on the same day as the injections. Methimazole powder will dissolve completely without visible precipitate. For example, if an injection of 75 mg/kg is planned, prepare 75 mg methimazole powder in 2 mL sterile physiological saline. Inject 2 $\mu\text{l/g}$ or dilute further in physiological saline if you are more comfortable with injecting a larger volume. The maximum volume for i.p. injection in mice is 10 mL/kg (Morton *et al.*, 2001).
- 3. Be sure that you can identify each mouse, the dose the mouse received, and the tissue sample taken from that mouse, throughout the experiment. Weigh each mouse to determine the individual dose and make notes for each mouse.
- 4. When performing i.p. injections, it is imperative to be aware of the relatively frequent rate of unsuccessful injections due to problems with technique (Steward *et al.*, 1968). Useful instruction videos are available (Machholz *et al.*, 2012; Newcastle University, 2021). Practicing i.p. injections on recently euthanized mice with food coloring diluted in saline, followed by immediate examination of the color distribution in the peritoneal cavity can serve to reassure the performance of correct technique (Figure 1A).
- 5. Monitor the mice closely immediately following and the day after methimazole injections since a successful i.p. injection of methimazole normally results in some discomfort, which can be observed as sneezing and rubbing of the nose. Importantly, the mouse is not supposed to experience deterioration in its general condition.
- 6. Sacrifice the mice 2 days after i.p. injection and evaluate the effect of ablation by analyzing sections of

tissue (see protocol C for histological analysis). The earliest effects of methimazole occur after 4 h (Brittebo, 1995; Bergström *et al.*, 2003), and the OE is not completely regenerated until one month post-treatment with methimazole (Suzukawa *et al.*, 2011).

- Evaluate the degree of ablation in the different regions (called zones) of the OE and at several levels along the anterior–posterior axis of the nasal cavity (Figures 1C, D). Successful injection of an effective dose of methimazole results in the detachment of all cells, except for a monolayer of normally very flat horizontal basal cells lining the basal lamina. Varying amounts of detached tissue can often be observed in the nasal cavity 2 days after methimazole administration (Figure 1B).

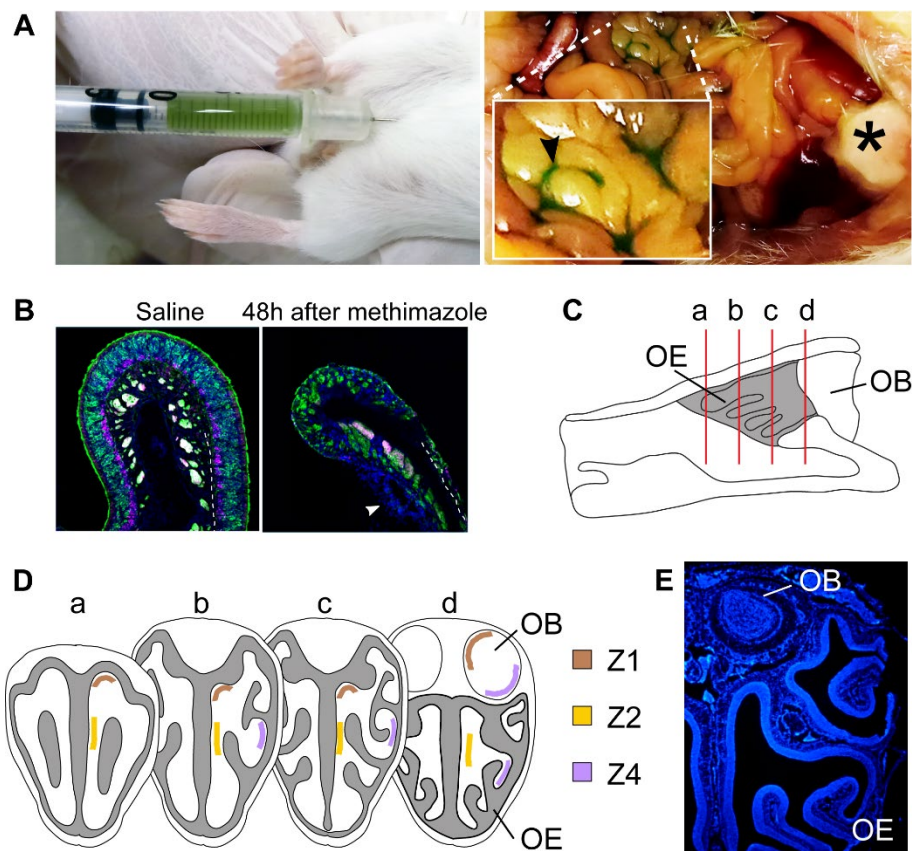


Figure 1. Example of methimazole ablation of the OE and a guide for analyzing different anatomical levels.

A. Example of i.p. injection of a euthanized mouse with green food coloring. Open the abdomen immediately after injection since correct injection results in the rapid dilution and distribution of the color throughout the entire abdominal cavity. Note some green color outside of the intestines (arrowhead in insert). Incorrect injection into an abdominal organ is usually visible. Asterisk (*) indicates the sternum. B. Immunofluorescence analysis of a part of the OE in control (saline) mice and 48 h after a single dose of methimazole shows OE ablation after treatment. The dashed line shows the location of the basal lamina. Analysis using antibodies against marker proteins for immature (STMN1 in magenta) and mature (OMP in green) neurons shows that these cells are ablated simultaneously with all OE cells, except for horizontal basal progenitor cells (see Figure 3 for a close-up example). Note that detached cell debris (arrow) can be present in considerable amounts or absent from an individual OE section 48 h after methimazole treatment. C. Schematic illustration of the front part of a mouse head cut sagittally at the midline; a-d represent the approximate anatomical levels suggested for analysis of the OE throughout the anterior–posterior axis. D. Illustrations of the appearance of tissue sections taken from levels a-d in C. The OE is divided into several regions often termed zones. These zones have different characteristics; therefore, it is wise to assess the

effect of methimazole at representative points in the OE and also in the corresponding region of the synaptic area for olfactory sensory neurons in the OB. Colored lines for zones 1 (Z1, brown), 2 (Z2, yellow), and 4 (Z4, purple) mark the representative locations. E. A micrograph of a section taken from level d, with the nuclei stained with Hoechst.

B. Methimazole injections for single or repeated ablation–regeneration cycles (main protocol)

1. Firstly, make an experimental plan and decide which stage of regeneration is to be analyzed (proliferative phase, neuronal differentiation phase, or synaptogenesis). This will determine how long after ablation mice will be sacrificed. Analyze proliferation at 2-6 days, different phases of neuronal differentiation at 3-21 days, and synaptogenesis at 7-21 days (from the first synaptic contacts to virtually complete regeneration) after methimazole treatment. Next, consider whether you wish to study the OE after a single methimazole ablation, repeated injury, or both. The mature OE cells likely produce enzymes that metabolize methimazole into cytotoxic products. We waited 21 days between methimazole-induced ablations to allow for the regeneration of mature OE cells. Plan to include control mice in your experiment, which receive saline i.p. injection. You may also consider injecting bromodeoxyuridine to check for cells in S-phase at a specific time point after methimazole treatment (if so, see references An and Kang, 2013; Håglin *et al.*, 2020).
2. Administer the first dose of methimazole as outlined in protocol A. Note that this protocol for repeated ablation–regeneration cycles was established for C57BL/6 mice that typically weigh 40-60 g and receive a 75 mg/kg i.p. dose of methimazole. If you have optimized the dose according to protocol A for the particular mouse line that you plan to analyze, use that dose instead.
3. Optional: For a single ablation cycle, sacrifice the mice at the decided time point and prepare the tissue (protocol C).
4. For analysis of the tissue after repeated methimazole-induced ablation, wait 21 days.
5. Administer the second injection of methimazole at 75 mg/kg i.p. (or your optimized dose).
6. Optional: For two ablation cycles, sacrifice the mice at the decided time point and prepare the tissue (protocol C).
7. Wait 21 days post-injection.
8. Administer the third injection of methimazole at 75 mg/kg i.p. (or your optimized dose). We evaluated up to three ablation–regeneration cycles, after which the OE was quite severely affected by large regions of metaplasia.
9. For three ablation cycles, sacrifice the mice at the decided time point and prepare the tissue (protocol C).

C. Tissue preparation, fixation, and histological analysis (support protocol)

1. This is a generic protocol for generating OE tissue sections for quick analysis when optimizing the dose required for complete ablation of the OE, as addressed by protocol A. This generic protocol is also useful for analysis of the OE and OB using many different antibodies. However, you may need to tailor the protocol or use another protocol, depending on the analyses you plan to perform on the tissue since certain antibodies recognize antigen epitopes that are not accessible after paraformaldehyde fixation of tissue. Moreover, for superior standard histological examination after staining, with hematoxylin–eosin for example, it is recommended that you embed tissue in paraffin before sectioning.
2. Prepare 4% (weight/volume) paraformaldehyde in PBS (4% PFA) on the same day. Note that PFA is assigned hazard statements H350 (may cause cancer) and H317 (may cause allergic skin reaction); therefore, take precautions by wearing gloves and protective goggles. Work in a fume hood when handling the powder and solutions. For 100 mL: Weigh 4 g PFA and transfer to a glass bottle containing a magnet and place on a magnetic stirrer. Warm 90 mL distilled water in a microwave oven to almost boiling, and pour the hot water into the glass bottle while stirring. Add 5-10 µL 5 M NaOH to facilitate dissolution of the PFA. Once dissolved, add 10 mL 10× PBS. Plan for at least 40 mL 4% PFA per mouse.

Also, prepare the same volume of 1× PBS and 20% sucrose in 1× PBS. These solutions should be cold

when used (*e.g.*, keep on ice).

3. Plan to sacrifice and collect tissue from an experimental mouse and its control in parallel to avoid possible experimental confounding factors. For each mouse, label one 50-mL tube with the animal's unique identification number (or equivalent) and place on ice.
4. Sacrifice mice in accordance with local regulations. One suggestion is cervical dislocation followed by immediate exsanguination. Be sure to receive training how to perform this procedure correctly.
5. Quickly dissect the OE and OB as shown in Figure 2. Tissues should not have time to dry. If you plan on analyzing markers with very rapid expression dynamics, such as protein phosphorylation, you may need to use a protocol for the fixation of tissues via heart perfusion. Note however, that as the OE is superficial in the nasal cavity, the fixation liquid reaches the cells in the OE quite fast once the tissue is submerged in 4% PFA, and particularly if the nasal cavity is cut open.
6. Allow fixation of the OE tissue for at least 3 h at 4°C in 4% PFA (note that overnight fixation is needed for analysis using some antibodies). Use approximately 40 mL 4% PFA per tube. Very gentle agitation of the sample using a rocking platform is recommended.
7. Pour off the 4% PFA and rinse the tissue and tube with 1× PBS. Remove the excess PBS from the tube using a small piece of paper towel.
8. For mice younger than 2 weeks old, this step is optional. Tissue from mice older than 2.5-3 weeks needs to be decalcified to obtain intact tissue sections since OE tissue contains calcified bone in the nasal cavity turbinates. Cover the tissue with the RDO decalcifying solution until the bone in the tissue softens. Use blunt plastic (not metal) forceps from now on to monitor as the bone softens. The bone should be compliant to light pressure, and decalcification takes 30-60 min depending on the age of the mouse. Treat experimental and control tissue in parallel for the same length of time.

*Note: RDO decalcification significantly decreases the *in situ* hybridization signal. If *in situ* hybridization analysis is to be employed, consider 4% PFA fixation overnight at 4°C followed by decalcification with 0.215-0.5 M EDTA in 1× PBS at 4°C instead (at least 1-2 nights, check bone softness with forceps) (Ryan et al., 1991; Ishii et al., 2004).*

9. Pour off the RDO and rinse the tissue and tube with 1× PBS. Remove the excess PBS from the tube with a small piece of paper towel.
10. Cryoprotect the tissue by incubating overnight to 24 h in 20% (weight/volume) sucrose in 1× PBS at 4°C. Very gentle agitation is recommended. Use 40 mL per sample.
11. Residual sucrose on the surface of the tissue may result in difficulty in retrieving the tissue sections since they may separate from the cryomount embedding medium. Pour off the sucrose and quickly remove the excess by rinsing the tissue and tube with a small volume of 1× PBS; this will avoid the formation of a sucrose film around the tissue once frozen. Remove the excess PBS from the tissue with a small piece of paper towel but do not allow the tissue to dry.
12. Place the tissue in a labeled cryomold with the nose oriented upward. Indicate the orientation of the nose on the mold to allow you to later mount the cryoembedded tissue in the right orientation in the cryostat. Fill the mold with cryomount embedding medium so that it completely covers the tissue.
13. Optional: Orient the nose upwards and place the mold under a vacuum of up to 500 mbar for 10-20 min at room temperature. If there is air trapped in the nasal cavities, this will slowly surface (note bubbles). Removing air makes tissue sectioning less difficult.
14. Place the mold on dry ice and use forceps or pipette tips to hold the tissue in the right orientation while it freezes. Leave to freeze completely and move the mold directly to -80°C for storage.
15. Coronal OE tissue sections are commonly used for analysis. Plan how you should arrange the sections on microscope slides and analyze different levels along the anterior-posterior axis of the nasal cavity (Figure 1D). Cut 10-12 µm thick sections, at a relatively cold temperature, *e.g.*, around -20°C. Start sectioning from the nose end of the tissue. Collect a section approximately every 10-20 sections to assess whether you are reaching the region of OE and/or OB and when to collect sections more frequently for your specific experiment.

Note: It is harder to collect intact sections from the nasal cavity than from soft tissue since the nasal region has a combination of tissues possessing very different hardness and elasticity. If it is very difficult to obtain intact sections, consider decalcifying for longer than 30 min.

16. Store slides of tissue sections at -20°C or -80°C until use.
17. Thaw slides at room temperature and let dry for about 15 min.
18. Perform a quick evaluation of the degree of ablation stain, *e.g.*, using fluorescent nuclear stain Hoechst at a concentration of 0.0005% (weight/volume) for 3-5 min, followed by tap water for 3-5 min. Mount with glycerol or the mounting media of choice and cover slip.

Examine the tissue sections under a fluorescence microscope with a filter for emission in blue (Figure 1E).

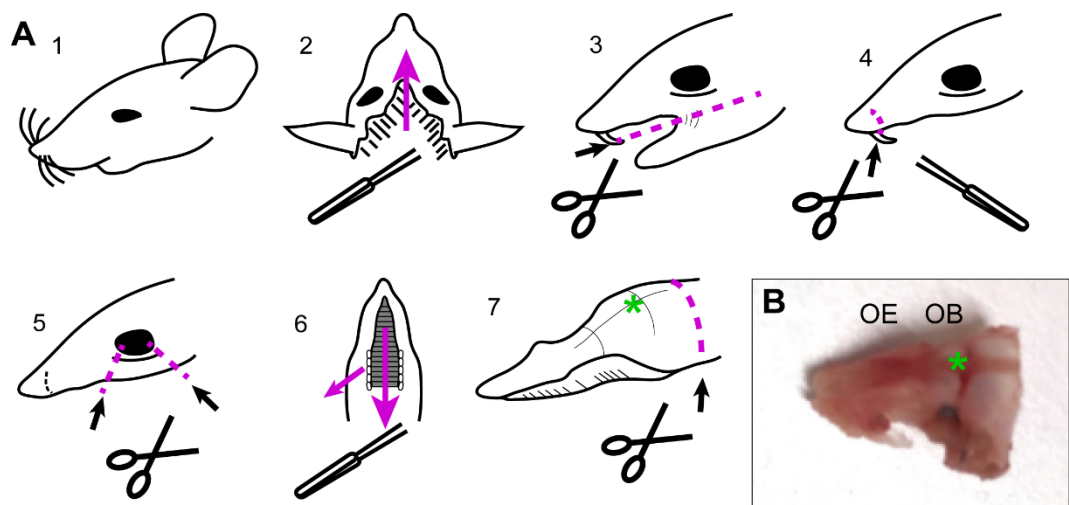


Figure 2. Dissection of nasal and OB tissue.

A. Schematic illustration of the dissection procedure. Be light-handed and do not squeeze with the hand holding the tissue, while dissecting with the other hand. Be quick (practice dissection before performing the planned experiment). 1 = Head; 2 = Peel off the skin using blunt dissection (*i.e.*, fingers) and forceps; 3 = Cut off the lower jaw; 4 = Carefully cut open the bone around the front teeth; and remove teeth by careful detachment using repeated gentle sideways movements with forceps; 5 = Cut off the Os zygomaticum bone and remove the eyes and any soft tissue still on the facial bones; 6 = Peel off the soft palate (in grey) with forceps. Remove teeth by holding them and bending carefully outward using forceps; 7 = Cut off the skull so that it can stand with “nose pointing upwards” in the cryoembedding mold. Be sure that you know where the OB is so that you do not cut it away if you plan to analyze the OB (if not, it can be removed). B. Image of dissected nasal tissue. Marks where the OE is within the nasal cavity and the position of the olfactory bulbs in the OB. A green asterisk (*) marks the corresponding region in the schematic illustration in A7 and B.

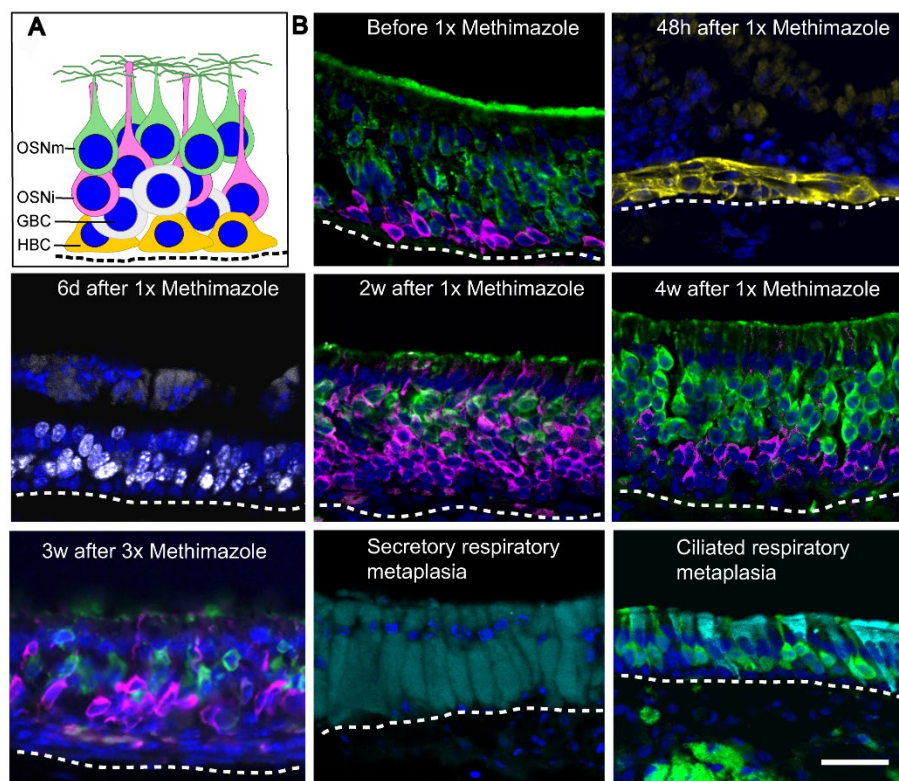


Figure 3. Example of cell types in the OE after one methimazole treatment or repeated OE ablation–regeneration cycles.

A. Schematic representation of the neural lineage in the OE (sustentacular, microvillar, and Bowmann's gland cells are not illustrated). Mature olfactory sensory neurons (OSNm, positive for OMP, in green), immature olfactory sensory neurons (OSNi, positive for STMN1, in magenta), globose basal progenitor cells (GBC, positive for Ki-67, in white), and horizontal basal progenitor cells (HBC, positive for cytokeratin 5, in yellow). B. Immunofluorescence analysis of the normal OE before methimazole treatment (mature neurons in green, immature neurons in magenta). 48 h after methimazole treatment, only activated horizontal basal cells that have acquired a rounded morphology remain (yellow). 6 days post-treatment with methimazole, the most prominent cell type is the dividing globose progenitor (white). The difference in the appearance of the OE between 2 and 4 weeks after a single dose of methimazole is that more immature neurons (magenta) have differentiated into mature neurons (green) by 4 weeks. Repeated ablations by methimazole treatment every 21 days results in the OE no longer regenerating efficiently. Moreover, after repeated ablations, there is a gradual increase in secretory (positive for FcγBP, in green) and ciliated respiratory metaplastic patches (positive for RALDH1/2, in green) in the OE (Håglin *et al.*, 2020). The dashed line marks the location of the basal lamina. All sections were stained with the nuclear stain Hoechst, which is in blue. Scale bar, 25 μ m.

Acknowledgments

This work was supported by the Swedish Brain Foundation (project no. FO20180195) and the Technical-natural science faculty at Umeå University. The protocol is adapted from Håglin *et al.* (2020).

Competing interests

The authors declare no competing financial interests.

Ethics

The experiments leading to the development of the protocol were approved by the Local Ethics Committee for Animal Research at the Court of Appeal for the upper northern area of Norrland, Umeå, Sweden (ID A15-2015 for period 4/24/2015 to 4/24/2020).

References

- An, N. and Kang, Y. (2013). [In vivo BrdU Incorporation Assay for Murine Hematopoietic Stem Cells](#). *Bio-protocol* 3(21): e960.
- Astwood, E. B., Bissell, A. and Hughes, A. M. (1945). [Further studies on the chemical nature of compounds which inhibit the function of the thyroid gland](#). *Endocrinology* 37(6): 456-481.
- Bergman, U. and Brittebo, E. B. (1999). [Methimazole toxicity in rodents: covalent binding in the olfactory mucosa and detection of glial fibrillary acidic protein in the olfactory bulb](#). *Toxicol Appl Pharmacol* 155(2): 190-200.
- Bergström, U., Giovanetti, A., Piras, E. and Brittebo, E. B. (2003). [Methimazole-induced damage in the olfactory mucosa: effects on ultrastructure and glutathione levels](#). *Toxicol Pathol* 31(4): 379-387.
- Brittebo, E. B. (1995). [Metabolism-dependent toxicity of methimazole in the olfactory nasal mucosa](#). *Pharmacol Toxicol* 76(1): 76-79.
- Cooper, D. (1999). [The side effects of antithyroid drugs](#). *Endocrinologist* 9(6): 457-467.
- Gadye, L., Das, D., Sanchez, M. A., Street, K., Baudhuin, A., Wagner, A., Cole, M. B., Choi, Y. G., Yosef, N., Purdom, E., Dudoit, S., Risso, D., Ngai, J. and Fletcher, R. B. (2017). [Injury Activates Transient Olfactory Stem Cell States with Diverse Lineage Capacities](#). *Cell Stem Cell* 21(6): 775-790 e779.
- Genter, M. B., Deamer, N. J., Blake, B. L., Wesley, D. S. and Levi, P. E. (1995). [Olfactory toxicity of methimazole: dose-response and structure-activity studies and characterization of flavin-containing monooxygenase activity in the Long-Evans rat olfactory mucosa](#). *Toxicol Pathol* 23(4): 477-486.
- Graziadei, G. A. and Graziadei, P. P. (1979a). [Neurogenesis and neuron regeneration in the olfactory system of mammals. II. Degeneration and reconstitution of the olfactory sensory neurons after axotomy](#). *J Neurocytol* 8(2): 197-213.
- Graziadei, P. P. and Graziadei, G. A. (1979b). [Neurogenesis and neuron regeneration in the olfactory system of mammals. I. Morphological aspects of differentiation and structural organization of the olfactory sensory neurons](#). *J Neurocytol* 8(1): 1-18.
- Håglin, S., Berghard, A. and Bohm, S. (2020). [Increased retinoic acid catabolism in olfactory sensory neurons activates dormant tissue-specific stem cells and accelerates age-related metaplasia](#). *J Neurosci* 40(21): 4116-4129.
- Hahn, C. G., Han, L. Y., Rawson, N. E., Mirza, N., Borgmann-Winter, K., Lenox, R. H. and Arnold, S. E. (2005). [In vivo and in vitro neurogenesis in human olfactory epithelium](#). *J Comp Neurol* 483(2): 154-163.
- Hurt, M. E., Thomas, D. A., Working, P. K., Monticello, T. M. and Morgan, K. T. (1988). [Degeneration and regeneration of the olfactory epithelium following inhalation exposure to methyl bromide: pathology, cell kinetics, and olfactory function](#). *Toxicol Appl Pharmacol* 94(2): 311-328.
- Ishii, T., Omura, M. and Mombaerts, P. (2004). [Protocols for two- and three-color fluorescent RNA in situ hybridization of the main and accessory olfactory epithelia in mouse](#). *J Neurocytol* 33(6): 657-669.
- Jang, W., Chen, X., Flis, D., Harris, M. and Schwob, J. E. (2014). [Label-retaining, quiescent globose basal cells are found in the olfactory epithelium](#). *J Comp Neurol* 522(4): 731-749.
- Kondo, K., Suzukawa, K., Sakamoto, T., Watanabe, K., Kanaya, K., Ushio, M., Yamaguchi, T., Nibu, K., Kaga, K. and Yamasoba, T. (2010). [Age-related changes in cell dynamics of the postnatal mouse olfactory](#)

- [neuroepithelium: cell proliferation, neuronal differentiation, and cell death.](#) *J Comp Neurol* 518(11): 1962-1975.
- Leung, C. T., Coulombe, P. A. and Reed, R. R. (2007). [Contribution of olfactory neural stem cells to tissue maintenance and regeneration.](#) *Nat Neurosci* 10(6): 720-726.
- Machholz, E., Mulder, G., Ruiz, C., Corning, B. F. and Pritchett-Corning, K. R. (2012). [Manual restraint and common compound administration routes in mice and rats.](#) *J Vis Exp* (67): 2771.
- Matulionis, D. H. (1975). [Ultrastructural study of mouse olfactory epithelium following destruction by ZnSO₄ and its subsequent regeneration.](#) *Am J Anat* 142(1): 67-89.
- Morton, D. B., Jennings, M., Buckwell, A., Ewbank, R., Godfrey, C., Holgate, B., Inglis, I., James, R., Page, C., Sharman, I., Verschoyle, R., Westall, L., Wilson, A. B. and Joint Working Group on, R. (2001). [Refining procedures for the administration of substances. Report of the BVAWF/FRAME/RSPCA/UFAW Joint Working Group on Refinement.](#) British Veterinary Association Animal Welfare Foundation/Fund for the Replacement of Animals in Medical Experiments/Royal Society for the Prevention of Cruelty to Animals/Universities Federation for Animal Welfare. *Lab Anim* 35(1): 1-41.
- Newcastle University (2021). [Intraperitoneal injection in the mouse.](#) Available at: <http://www.procedureswithcare.org.uk/intraperitoneal-injection-in-the-mouse/> (Accessed: 6 January 2021).
- Ryan, A. F., Watts, A. G. and Simmons, D. M. (1991). [Preservation of mRNA during *in situ* hybridization in the cochlea.](#) *Hear Res* 56(1-2): 148-152.
- Schnittke, N., Herrick, D. B., Lin, B., Peterson, J., Coleman, J. H., Packard, A. I., Jang, W. and Schwob, J. E. (2015). [Transcription factor p63 controls the reserve status but not the stemness of horizontal basal cells in the olfactory epithelium.](#) *Proc Natl Acad Sci U S A* 112(36): E5068-5077.
- Schwob, J. E., Szumowski, K. E. and Stasky, A. A. (1992). [Olfactory sensory neurons are trophically dependent on the olfactory bulb for their prolonged survival.](#) *J Neurosci* 12(10): 3896-3919.
- Steward, J. P., Ornellas, E. P., Beernink, K. D. and Northway, W. H. (1968). [Errors in the technique of intraperitoneal injection of mice.](#) *Appl Microbiol* 16(9): 1418-1419.
- Suzukawa, K., Kondo, K., Kanaya, K., Sakamoto, T., Watanabe, K., Ushio, M., Kaga, K. and Yamasoba, T. (2011). [Age-related changes of the regeneration mode in the mouse peripheral olfactory system following olfactotoxic drug methimazole-induced damage.](#) *J Comp Neurol* 519(11): 2154-2174.
- Suzuki, Y., Takeda, M., Obara, N. and Suzuki, N. (1998). [Colchicine-induced cell death and proliferation in the olfactory epithelium and vomeronasal organ of the mouse.](#) *Anat Embryol (Berl)* 198(1): 43-51.
- Suzuki, Y. and Takeda, M. (1991). [Basal cells in the mouse olfactory epithelium after axotomy: immunohistochemical and electron-microscopic studies.](#) *Cell Tissue Res* 266(2): 239-245.
- Xie, F., Zhou, X., Genter, M. B., Behr, M., Gu, J. and Ding, X. (2011). [The tissue-specific toxicity of methimazole in the mouse olfactory mucosa is partly mediated through target-tissue metabolic activation by CYP2A5.](#) *Drug Metab Dispos* 39(6): 947-951.
- Zhang, A. J., Lee, A. C., Chu, H., Chan, J. F., Fan, Z., Li, C., Liu, F., Chen, Y., Yuan, S., Poon, V. K., Chan, C. C., Cai, J. P., Wu, K. L., Sridhar, S., Chan, Y. S. and Yuen, K. Y. (2020). [SARS-CoV-2 infects and damages the mature and immature olfactory sensory neurons of hamsters.](#) *Clin Infect Dis.* doi: 10.1093/cid/ciaa995.

Production of Phenotypically Uniform Human Cerebral Organoids from Pluripotent Stem Cells

Adam Sivitilli^{1, #}, Parisa Ghiasi^{1, #} and Liliana Attisano^{1, *}

¹Department of Biochemistry, Donnelly Centre, University of Toronto, Toronto, ON, Canada

*For correspondence: liliana.attisano@utoronto.ca.

#Contributed equally to this work

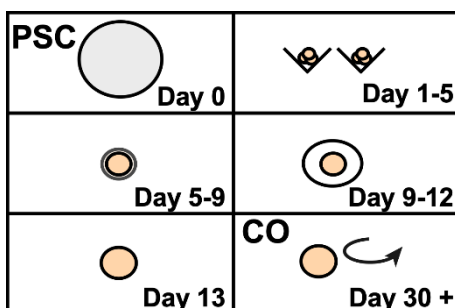
Abstract

Recent advances in stem cell technology have allowed researchers to generate 3D cerebral organoids (COs) from human pluripotent stem cells (hPSCs). Indeed, COs have provided an unprecedented opportunity to model the developing human brain in a 3D context, and in turn, are suitable for addressing complex neurological questions by leveraging advancements in genetic engineering, high resolution microscopy, and tissue transcriptomics. However, the use of this model is limited by substantial variations in the overall morphology and cellular composition of organoids derived from the same pluripotent cell line. To address these limitations, we established a robust, high-efficiency protocol for the production of consistent COs by optimizing the initial phase of embryoid body (EB) formation and neural induction. Using this protocol, COs can be reproducibly generated with a uniform size, shape, and cellular composition across multiple batches. Furthermore, organoids that developed over extended periods of time (3–6 months) showed the establishment of relatively mature features, including electrophysiologically active neurons, and the emergence of oligodendrocyte progenitors. Thus, this platform provides a robust experimental model that can be used to study human brain development and associated disorders.

Keywords: Stem cells, Organoids, Cerebral organoids, Brain organoids, 3D culture, Neural development, Neuroscience

This protocol was validated in: Life Sci Alliance (2020), DOI: 10.26508/lsa.202000707

Graphical Abstract:



Overview of cerebral organoid development from pluripotent stem cells.

Background

Recent advancements in the *in vitro* development of 3D cerebral organoids (COs) derived from human pluripotent stem cells (hPSCs) have provided an unprecedented opportunity to model the developing human brain and relevant complex diseases in an experimentally tractable system. Indeed, this approach has allowed researchers to study early brain development and the consequences of alterations associated with various human neurological disorders, such as Alzheimer's, blindness, Autism Spectrum Disorder (ASD), and Zika virus infection (Lancaster and Knoblich, 2014b; Quadrato *et al.*, 2016; Di and Kriegstein, 2017; Huch *et al.*, 2017; Amin and Pașca, 2018; Rossi *et al.*, 2018; Chen *et al.*, 2019). In addition, several groups have applied COs to study and establish preclinical models of human brain cancers such as glioblastoma multiforme (Drost and Clevers, 2018; Linkous *et al.*, 2018). In recent years, numerous protocols have emerged to facilitate the development of region specific-COs by controlling the underlying cell signaling pathways with exogenous growth factors and small molecule inhibitors to guide cell fate changes as the organoid matures (Lancaster *et al.*, 2013; Mariani *et al.*, 2015; Jo *et al.*, 2016; Qian *et al.*, 2016; Birey *et al.*, 2017; Quadrato *et al.*, 2017; Watanabe *et al.*, 2017; Pollen *et al.*, 2019; Velasco *et al.*, 2019; Yoon *et al.*, 2019). However, due to the fact that human whole-brain organoids are largely produced by intrinsic self-patterning and do not rely on controllable exogenous factors, stochastic differentiation often leads to cellular diversity, which is amplified with extended culture. Unfortunately, the considerable variability between individual organoids obtained using whole-brain differentiation platforms can therefore limit the utility of these COs for studying disease mechanisms or the development of potential therapeutics. Here, we describe our robust protocol for efficiently and reproducibly generating mature, uniform human COs (Figure 1). By optimizing an established protocol for the creation of self-patterned whole-brain organoids (Lancaster and Knoblich, 2014a; Lancaster *et al.*, 2013), we successfully generated phenotypically uniform forebrain organoids with reproducible cell-type compositions.

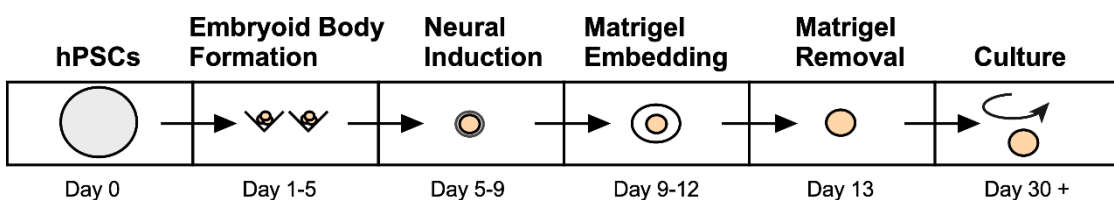


Figure 1. Overview of the developed method to generate human COs from pluripotent stem cells

Materials and Reagents

1. 96-well V-bottomed non-binding plates (Greiner Bio-One, catalog number: 651970)

Cite as: Sivitilli, A., et al. (2021). Production of Phenotypically Uniform Human Cerebral Organoids from Pluripotent Stem Cells. Bio-protocol 11(8): e3985. DOI: 10.21769/BioProtoc.3985.

2. 24-well clear flat-bottomed ultra-low attachment plates (Corning, catalog number: 3473)
3. 4-well cell culture plates (ASI, catalog number: TP9004)
4. 50 mL and 15 mL conical centrifuge tubes (Corning, Falcon, catalog numbers: 352096, 352070)
5. Low-retention microcentrifuge tubes (1.5 mL and 0.6 mL, Thermo Fisher Scientific, catalog numbers: 3451 and 3446)
6. 50 ml sterile disposable reagent reservoirs (Corning, catalog number: 4870)
7. DMEM/F-12, HEPES (Thermo Fisher Scientific, Gibco, catalog number: 11330032, store at 4°C)
8. KnockOut™ Serum Replacement – Multi-Species (Thermo Fisher Scientific, Gibco, catalog number: A3181502, store at -20°C)
9. MEM Non-Essential Amino Acid Solution (100×) (Thermo Fisher Scientific, Gibco, catalog number: 11140050, store at 4°C)
10. 2-Mercaptoethanol (1,000×) (Thermo Fisher Scientific, Gibco, catalog number: 21985023, store at 4°C)
11. Animal-Free Recombinant Human FGF-basic (Peprotech, catalog number: AF-100-18B, store at -80°C)
12. TrypLE™ Express Enzyme (1×) (Thermo Fisher Scientific, Gibco, catalog number: 12604013, stored at room temperature [22°C] in the dark)
13. Neural Basal Medium (Thermo Fisher Scientific, Gibco, catalog number: 21103049, store at 4°C)
14. Y27632 ROCK Inhibitor (Cedarlane, catalog number: S1049-10MG, store at -80°C)
15. GlutaMAX™ Supplement (Thermo Fisher Scientific, Gibco, catalog number: 35050-061, store at 4°C)
16. Heparin sodium salt (Sigma-Aldrich, catalog number: H4784, store at -20°C)
17. Insulin solution human (Sigma-Aldrich, catalog number: I9278, store at 4°C)
18. N-2 Supplement (100×) (Thermo Fisher Scientific, Gibco, catalog number: 17502001, aliquots of 500 µL, store at -20°C)
19. B-27™ Supplement (50×), minus vitamin A (Thermo Fisher Scientific, Gibco, catalog number: 12587010, aliquots of 500 µL, store at -20°C)
20. B-27™ Supplement (50×), serum-free (Thermo Fisher Scientific, Gibco, catalog number: 17504044, aliquots of 500 µL, store at -20°C)
21. Matrigel® Growth Factor Reduced (GFR) Basement Membrane Matrix (Corning, catalog number: 356231, aliquots of 500 µL, store at -20°C)
22. D-PBS^{-/-}, 1×, without calcium and magnesium (Wisent Bioproducts, catalog number: 311-425-CL, store at 4°C)
23. Embryoid Body Media (EB Media) (see Recipes)
24. Neural Induction Media (see Recipes)
25. Cerebral Organoid Differentiation Media without Vitamin A (CDM-A) (see Recipes)
26. Cerebral Organoid Differentiation Media with Vitamin A (CDM+A) (see Recipes)

Equipment

1. Nalgene™ Square PETG media bottles (250 ml) (Gibco, Thermo Fisher Scientific, catalog number: 2019-0250)
2. Pipettes (5 ml, 10 ml, 25 ml, 50 ml), micro-pipettes (10 µL, 20 µL, 200 µL, 1,000 µL)
3. Multi-channel pipette (Eppendorf, model: Research plus 12 channel pipette, catalog number: ES-12-300)
4. Water bath
5. Centrifuge
6. Phase contrast microscope
7. Hemocytometer
8. 37°C, 5% CO₂ cell culture incubator
9. Orbital shaker that can be installed inside the incubator (such as Thermo Fisher, catalog number: 88881101)
10. Blade and scalpel

Procedure

A. Embryoid Body Production: Singularizing and Plating Human Embryonic Stem Cells (hESCs)

1. Prepare EB Media without growth factors and prewarm to 37°C using a water bath. EB Media (without growth factors) can be stored for up to 1 week at 4°C, and once warmed, the stock should be used or discarded.
2. Wash hESCs, which have reached 70–80% confluence, twice with 3 volumes of D-PBS^{-/-}.

Note: This protocol was established using hESCs cultured in mouse embryoinic fibroblast (MEF) conditioned media supplemented with bFGF to a final concentration of 4 ng/ml (Sivitilli et al., 2020).

3. Add 1 ml TrypLE and incubate for 5 min at room temperature (22°C).
4. Gently pipette up and down to dissociate colonies to a single-cell suspension.
5. Neutralize TrypLE with 4 volumes (*i.e.*, 4 mL) EB media and add the resulting suspension to a 15-mL Falcon tube.
6. Use a hemocytometer to count the cells. Avoid using an automated cell counter, which can result in inaccurate cell numbers because hESCs are prone to clumping.
7. Centrifuge cells at 150 × g for 5 min at room temperature (22°C).
8. During centrifugation, prepare EB Media by supplementing with 4 ng/mL bFGF and 50 μM Y-27632 (ROCK inhibitor). For this, use 15 mL EB media with 1.5 μL bFGF (from a 40 ng/μL stock) and 7.5 μL Y-27635 (from a 100 mM stock).
9. Resuspend single hESCs to a final concentration of 80,000 cells/mL in the freshly prepared EB Media supplemented with bFGF and Y-27632.
10. Transfer the resuspended cells to a sterile disposable reagent reservoir and add 150 μL cell suspension (12,000 cells) to each well of a 96-well V-bottomed non-binding plate using a multi-channel pipette.
11. Place the plate at 37°C in a CO₂ incubator for 2 days.

B. Embryoid Body Production: Feeding

1. Prepare EB Media fresh daily and prewarm to 37°C using a water bath.
2. On day 2, feed the EBs with EB media supplemented with 2 ng/mL bFGF. To reach the required concentration, mix 15 mL EB media with 0.75 μL bFGF (40 ng/μL).
3. Remove 135 μL media from each well of the incubated 96-well plate using the multi-channel pipette.
4. Transfer the EB media (supplemented with 2 ng/mL bFGF) into a sterile disposable reagent reservoir and add 150 μL EB media using the multi-channel pipette.
5. Return the plate to the CO₂ incubator for a further 2 days.

Note: Due to evaporation, wells toward the peripheral edge of the 96-well plate may have a slightly lower volume. This is normal and EBs should still form correctly.

C. Embryoid Body Production: Assessment Checkpoint

On day 5, measure the EB size using a brightfield microscope to determine whether the EBs are ready for neural induction (Figure 2). If the size of the EBs is 350–600 μm, proceed to Procedure D (Neural Induction); if the size is below 350 μm, then repeat Procedure B; if the size is above 600 μm, we do not recommend continuing with the protocol. Restart the protocol and double check cell counting in Procedure A to ensure accuracy when seeding EBs and start another batch.

D. Neural Induction: Transfer to Neural Induction

1. Prepare Neural Induction Media fresh for each differentiation and prewarm an aliquot to 37°C using a water bath. Neural Induction Media can be stored for 1 week at 4°C. Once warmed, Neural Induction Media should not be reused.
2. Choose EBs that meet the size and visual criteria (Figure 2).
3. Cut 2–3 mm off the extremity of a 200-μL filtered pipette tip using a razor blade to make a wider opening.
4. Prepare a 24-well ultra-low attachment plate by adding 500 μL prewarmed Neural Induction Media to each well.
5. Using a dissecting scope and a cut 200 μL pipette tip, pick up the EB and transfer to a 24-well ultra-low attachment plate. Set the pipette to 20 μL, place the end at the bottom of the well and pipette up the EB. A maximum of 2 EBs per well can be added; additional EBs increase the likelihood of further aggregation.
6. Place the plate in a CO₂ incubator for 2 days.

E. Neural Induction: Feeding

1. Prewarm Neural Induction Media to 37°C using a water bath.
2. Feed the EBs by adding an additional 500 μL Neural Induction Media to each well.
3. Return the plate to a CO₂ incubator for a further 2 days.

F. Neural Induction: Assessment Checkpoint

1. Use a brightfield microscope to examine the neuralized EBs for optical clearing in the outer 100 μm of the EB (Figure 3). The outer ring structure should be prominent and marked by a stark change in opacity as compared with the central region of the EB. This is a critical checkpoint; EBs that do not have the correct organization of the neuroepithelial ring will not form organoids.

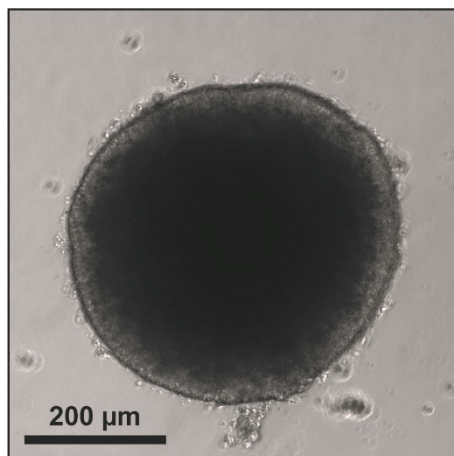


Figure 2. Representative EB derived from H9 hESCs on Day 5

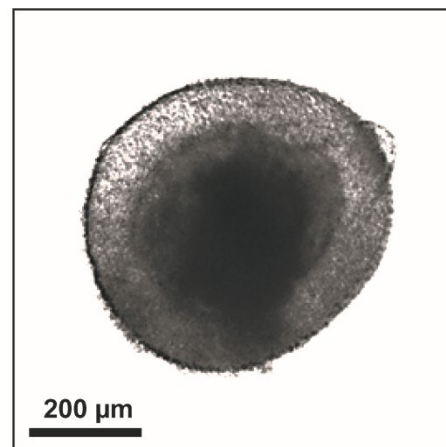


Figure 3. Neuroectoderm formation in an EB derived from H9 hESCs at Day 9

G. Neuroepithelial Expansion: Transfer to Solid Phase Matrigel Scaffold

1. Thaw Growth Factor Reduced Matrigel on ice for 2 h. Once thawed, Matrigel can be used for up to 6 h but must be kept on ice. Matrigel cannot be refrozen once thawed.
2. Prepare CO Differentiation Media without Vitamin A (CDM-A) fresh for each differentiation and prewarm an aliquot to 37°C using a water bath. CDM-A can be stored for 2 weeks at 4°C. Once warmed, CDM-A should not be reused.

3. Prepare a box of wide-bore tips by cutting 3–4 mm off the extremity of a 200 µL filtered pipette tip using a razor blade to make a wider opening. Pick up the EBs one by one using a 200 µL cut tip and transfer to the center of each well of the 4-well plate (1 EB per well).
4. Using an uncut 200 µL tip, draw 25 µL to aspirate the remaining Neural Induction Media from each well. It is critical to remove all media from the EB in the 4-well plate; failure to do so will prevent the Matrigel from attaching to the plate surface and prevent removal of the Matrigel in Procedure J.
5. Cover the neuralized EB with a drop of cold Matrigel (30 µL) using an uncut 200 µL tip.
6. Position the EB in the center of the Matrigel droplet using a 10 µL tip. Ensure that the EB is not resting on the bottom of the plate.
7. Once a plate has been filled (4 EBs), transfer the full plate to a CO₂ incubator for 10 min at 37°C to polymerize the Matrigel.
8. After 10 min, carefully add 500 µL prewarmed CDM-A and return to a CO₂ incubator for a further 2 days.

Note: Be consistent with the amount of media collected when transferring the EB. We recommend collecting EBs with 25 µL media to create a droplet in the 4-well plates.

H. Neuroepithelial Expansion: Feeding

1. Prewarm an aliquot of CDM-A to 37°C using a water bath.
2. Carefully aspirate all media and add 500 µL CDM-A to each well of the 4-well plate.
3. Return the plate to the incubator for a further 2 days.

I. Neuroepithelial Expansion: Assessment of Checkpoint

1. Use a brightfield microscope to examine the COs for ring structures in the peripheral regions of the organoid (Figure 4). COs should be approximately 500–700 µm in diameter and have multiple ring structures throughout; this is a critical checkpoint, those without ring structures will not form organoids.

J. Transfer to Spinning Culture: Extraction from Solid Phase Matrigel

1. Prepare CO Differentiation Media (CDM) fresh and prewarm an aliquot to 37°C using a water bath. CDM can be stored for 2 weeks at 4°C. Once warmed, CDM should not be reused.
2. Prepare wide-bore pipette tips by cutting 4–5 mm off the extremity of 200 µL pipette tips to make a wider opening.
3. Prepare a 6-well plate with 3 mL prewarmed CDM per well.
4. Using a dissection microscope, carefully cut around the COs implanted in the Matrigel droplet; the goal here is to remove as much Matrigel as possible without damaging the CO. Excess Matrigel remaining on the CO at this stage will result in formation of cyst-like structures in the spinning culture.
5. Use a cut 200 µL tip to transfer the COs to the 6-well plate containing CDM; a maximum of 4 hCOs per well is acceptable.
6. Once all the COs have been transferred, place the 6-well plate on an orbital shaker (ThermoFisher Cat: 88881101) in a 37°C incubator at a speed of 80–90 rpm (rpm may vary if a different orbital shaker model is used).

K. Transfer to Spinning Culture: Feeding in Spinning Culture

1. Prewarm CDM using a 37°C water bath.
2. Pause the orbital shaker and collect the plate containing the COs.
3. Carefully aspirate 2/3 of the total media volume from each well; be mindful not to aspirate the COs with the media since they are in suspension.
4. Add 3 mL prewarmed CDM to each well.
5. Return the plate to the orbital shaker in the incubator and initialize (Figure 5).

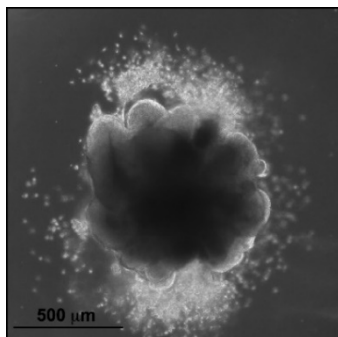


Figure 4. Representative hCOs derived from H9 hESCs on day 13 prior to Matrigel extraction

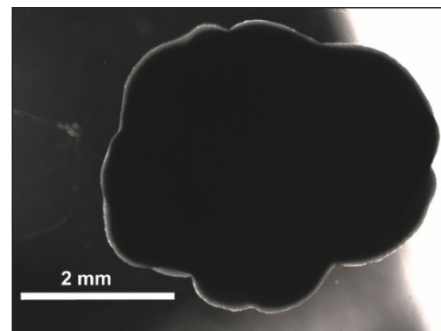


Figure 5. Representative hCO in a spinning culture derived from H9 hESCs at 12 weeks

Recipes

1. Embryoid Body Media (EB Media) (Table 1)

Table 1. EB Media Composition. A list of components, stock and final concentrations (Con.), and volumes for working stocks are indicated.

Components	Stock Con.	Final Con.	/50 mL medium
DMEM/F12			39.5 mL
KOSR			10 mL
MEM:NEAA	100×	1×	500 μL
2-mercaptoethanol	100×	1×	50 μL

2. Neural Induction Media (prepared fresh every week) (Table 2)

Table 2. Composition of Neural Induction Media (prepared fresh every week). Once warmed, Neural Induction Media should not be reused. A list of components, stock and final concentrations (Con.), and volumes for working stocks are indicated.

Components	Stock Con.	Final Con.	/50 mL medium
DMEM/F12			48.5 ml
GlutaMax	100×	1×	500 μL
MEM:NEAA	100×	1×	500 μL
N2	100×	1×	500 μL
Heparin	10 mg/ml	0.001 mg/ml	5 μL

3. Cerebral Organoid Differentiation Media without Vitamin A (CDM-A) (Table 3)

Table 3. Composition of Cerebral Organoid Differentiation Media without Vitamin A. A list of components, stock and final concentrations (Con.), and volumes for working stocks are indicated.

Components	Stock Con.	Final Con.	/50 mL medium
DMEM/F12			24 mL
Neural Basal Media			24 mL

MEM:NEAA	100×	0.5×	250 µL
GlutaMax	100×	1×	500 µL
B27-Vit A	50×	0.5×	500 µL
N2	100×	0.5×	250 µL
2-mercaptoethanol	1,000×	1×	50 µL
Insulin	9.5–11.5 mg/ml	2–3 µg/ml	12.5 µL

4. Cerebral Organoid Differentiation Media with Vitamin A (CDM+A) (Table 4)

Table 4. Composition of Cerebral Organoid Differentiation Media with Vitamin A. A list of components, stock and final concentrations (Con.), and volumes for working stocks are indicated.

Components	Stock Con.	Final Con.	/100 mL medium
DMEM/F12			48 mL
Neural Basal Media			48 mL
MEM:NEAA	100×	0.5×	500 µL
GlutaMax	100×	1×	1 mL
B27 (with Vit A)	50×	0.5×	1 mL
N2	100×	0.5×	500 µL
2-mercaptoethanol	1,000×	1×	100 µL
Insulin	9.5–11.5 mg/mL	2–3 µg/mL	25 µL

Acknowledgments

This work was supported by funds from the Canada First Research Excellence Fund/Medicine by Design, the Krembil Foundation, and the Canadian Institute for Health Research (CIHR) Foundation grant FDN148455 to L.A. This protocol is adapted from the method published in Sivitilli *et al.*, (2020). We thank Javier J. Hernandez and the staff of the Applied Organoid Core (ApOC) at the University of Toronto for advice.

Competing interests

The authors declare that they have no conflicts of interest.

References

- Amin, N. D. and Pașca, S. P. (2018). [Building models of brain disorders with three-dimensional organoids](#). *Neuron* 100(2): 389–405.
- Birey, F., Andersen, J., Makinson, C. D., Islam, S., Wei, W., Huber, N., Fan, H. C., Metzler, K. R. C., Panagiotakos, G. and Thom, N. (2017). [Assembly of functionally integrated human forebrain spheroids](#). *Nature* 545(7652): 54–59.
- Chen, H. I., Song, H. and Ming, G. I. (2019). [Applications of human brain organoids to clinical problems](#). *Dev Dyn* 248(1): 53–64.
- Di, L. E. and Kriegstein, A. R. (2017). [The use of brain organoids to investigate neural development and disease](#). *Nat Rev Neurosci* 18(10): 573.
- Drost, J. and Clevers, H. (2018). [Organoids in Cancer Research](#). *Nat Rev Cancer* 18(7): 407–418.
- Huch, M., Knoblich, J. A., Lutolf, M. P. and Martinez-Arias, A. (2017). [The hope and the hype of organoid research](#). *Development* 144(6): 938–941.

- Jo, J., Xiao, Y., Sun, A. X., Cukuroglu, E., Tran, H.-D., Göke, J., Tan, Z. Y., Saw, T. Y., Tan, C. and Lokman, H. (2016). [Midbrain-like organoids from human pluripotent stem cells contain functional dopaminergic and neuromelanin-producing neurons](#). *Cell Stem Cell* 19(2): 248-257.
- Lancaster, M. A. and Knoblich, J. A. (2014a). [Generation of cerebral organoids from human pluripotent stem cells](#). *Nat Protoc* 9(10): 2329-2340.
- Lancaster, M. A. and Knoblich, J. A. (2014b). [Organogenesis in a dish: modeling development and disease using organoid technologies](#). *Science* 345(6194).
- Lancaster, M. A., Renner, M., Martin, C.-A., Wenzel, D., Bicknell, L. S., Hurles, M. E., Homfray, T., Penninger, J. M., Jackson, A. P. and Knoblich, J. A. (2013). [Cerebral organoids model human brain development and microcephaly](#). *Nature* 501(7467): 373-379.
- Linkous, A., Balamatsias, D., Snuderl, M., Edwards, L., Miyaguchi, K., Milner, T., Reich, B., Cohen-Gould, L., Storaska, A., Nakayama, Y., Schenkein, E., Singhania, R., Cirigliano, S., Magdeldin, T., Lin, Y., Nanjangud, G., Chadalavada, K., Pisapia, D., Liston, C., Fine, H. A. (2019). [Modeling Patient-Derived Glioblastoma with Cerebral Organoids](#). *Cell Rep* 26(12): 3203-3211.
- Mariani, J., Coppola, G., Zhang, P., Abyzov, A., Provini, L., Tomasini, L., Amenduni, M., Szekely, A., Palejev, D. and Wilson, M. (2015). [FOXP1-dependent dysregulation of GABA/glutamate neuron differentiation in autism spectrum disorders](#). *Cell* 162(2): 375-390.
- Pollen, A. A., Bhaduri, A., Andrews, M. G., Nowakowski, T. J., Meyerson, O. S., Mostajo-Radji, M. A., Di, L. E., Alvarado, B., Bedolli, M. and Dougherty, M. L. (2019). [Establishing cerebral organoids as models of human-specific brain evolution](#). *Cell* 176(4): 743-756.e717.
- Qian, X., Nguyen, H. N., Song, M. M., Hadiono, C., Ogden, S. C., Hammack, C., Yao, B., Hamersky, G. R., Jacob, F. and Zhong, C. (2016). [Brain-region-specific organoids using mini-bioreactors for modeling ZIKV exposure](#). *Cell* 165(5): 1238-1254.
- Quadrato, G., Brown, J. and Arlotta, P. (2016). [The promises and challenges of human brain organoids as models of neuropsychiatric disease](#). *Nat Med* 22(11): 1220-1228.
- Quadrato, G., Nguyen, T., Macosko, E. Z., Sherwood, J. L., Yang, S. M., Berger, D. R., Maria, N., Scholvin, J., Goldman, M. and Kinney, J. P. (2017). [Cell diversity and network dynamics in photosensitive human brain organoids](#). *Nature* 545(7652): 48-53.
- Rossi, G., Manfrin, A. and Lutolf, M. P. (2018). [Progress and potential in organoid research](#). *Nat Rev Genet* 19(11): 671-687.
- Sivitilli, A. A., Gosio, J. T., Ghoshal, B., Evstratova, A., Trcka, D., Ghiasi, P., Hernandez, J. J., Beaulieu, J. M., Wrana, J. L. and Attisano, L. (2020). [Robust production of uniform human cerebral organoids from pluripotent stem cells](#). *Life Sci Alliance* 3(5).
- Velasco, S., Kedaigle, A. J., Simmons, S. K., Nash, A., Rocha, M., Quadrato, G., Paulsen, B., Nguyen, L., Adiconis, X. and Regev, A. (2019). [Individual brain organoids reproducibly form cell diversity of the human cerebral cortex](#). *Nature* 570(7762): 523-527.
- Watanabe, M., Butth, J. E., Vishlaghi, N., de la Torre-Ubieta, L., Taxidis, J., Khakh, B. S., Coppola, G., Pearson, C. A., Yamauchi, K. and Gong, D. (2017). [Self-organized cerebral organoids with human-specific features predict effective drugs to combat Zika virus infection](#). *Cell Rep* 21(2): 517-532.
- Yoon, S. J., Elahi, L. S., Paşa, A. M., Marton, R. M., Gordon, A., Revah, O., Miura, Y., Walczak, E. M., Holdgate, G. M. and Fan, H. C. (2019). [Reliability of human cortical organoid generation](#). *Nat Methods* 16(1): 75-78.

Transcardiac Perfusion of the Mouse for Brain Tissue Dissection and Fixation

Jinyun Wu[#], Yuqi Cai[#], Xiaoyang Wu, Yue Ying, Yilin Tai and Miao He^{*}

Institutes of Brain Sciences, Fudan University, Shanghai 200032, China

*For correspondence: hem@fudan.edu.cn

[#]Contributed equally to this work

Abstract

Transcardiac perfusion with saline followed by 4% paraformaldehyde (PFA) is widely used to clear blood and preserve brain for immunostaining or *in situ* hybridization. PFA breaks into formaldehyde in solution, which cross-link protein and DNA molecules to preserve tissue and cell structure. Here we provide a step by step guide for performing this procedure in mouse.

Keywords: Mouse, Transcardiac perfusion, Aorta, Paraformaldehyde, Brain

This protocol was validated in: Cell Rep (2021), DOI: 10.1016/j.celrep.2021.108712

Materials and Reagents

1. Protective gear (gloves, goggles, masks, lab coat)
2. Deionized water
3. Sodium pentobarbital (Sigma, catalog number: P-010)
4. 1.5% sodium pentobarbital (in saline)
5. NaCl (Sigma-Aldrich, catalog number: S7653)
6. Saline (0.9% sodium chloride)
7. NaH₂PO₄·2H₂O (Sigma-Aldrich, catalog number: 71645)
8. Na₂HPO₄·12H₂O (Sigma-Aldrich, catalog number: 71663)
9. Paraformaldehyde (PFA) (Sigma-Aldrich, catalog number: P6148)
10. NaOH (Sigma-Aldrich, catalog number: S8045)
11. Hydrochloric acid (HCl) (Sigma, catalog number: H1758)
12. Heparin (Sigma, catalog number: H3149)
13. Sodium azide (Sigma, catalog number: S2002)
14. 4% paraformaldehyde (PFA, in 0.1 M Phosphate Buffer, pH 7.0-7.4) (see Recipes)

Equipment

1. Chemical fume hood
2. Dissecting forceps (RWD, catalog number: F12018-13) (Figure 1)
3. Ophthalmic forceps (RWD, catalog number: F12006-10) (Figure 1)
4. Hemostatic forceps (RWD, catalog number: F21002-12) (Figure 1)
5. Tissue scissors (RWD, catalog number: S13052-12) (Figure 1)
6. Fine scissors (RWD, catalog number: S12005-10) (Figure 1)
7. Vascular clamp (RWD, catalog number: R33001-48) (Figure 1)
8. Micro spatula (Thermo Fisher, catalog number: 21-101-10) (Figure 1)
9. 1 mL and 20 mL syringe (Figure 1)
10. 25- or 27-gauge infusion needle (Figure 1)
11. (Optional) Peristaltic pump (LONGERPUMP, catalog number: BT100-2J)
12. 2.5 L and 5 L beakers
13. Thermometer (measuring range:100 °C, division value:1 °C)
14. Measuring cylinder
15. Analytical balance (SARTORIUS, catalog number: BSA124S)
16. Benchtop vacuum
17. 0.22 µm PVDF filter set (Nalgene, catalog number: 291-4520)
18. 50 mL conical tube (Thermo Fisher, catalog number: 339652)
19. Fume hood
20. Microwave
21. Magnetic stirrer with heating device (SCILOGEX, catalog number: MS7-H550-Pro)



Figure 1. Surgical instruments

Procedure

A. Preoperative preparation

1. Measure and record the body weight to the nearest gram.
2. Pick the mouse up by its tail, place it on top of a cage rack, and gently pull its tail with one hand while allowing it to grab the iron wire firmly to stabilize it at a steady position.
3. Press the mouse down around the neck with one hand and hold it by the scruff of the neck. Hold as much skin as possible to have a secure grip so that the mouse cannot move during injection.
4. Administer 1.5% sodium pentobarbital at a dose of 0.06 mL per 10 g body weight through intraperitoneal injection at the lower left or right quadra of the abdomen (Hou *et al.*, 2021) (Figure 2).

Note: To avoid injuring the internal organ, do not advance the needle too much. Hold the mouse at a head-down position may also help.



Figure 2. Intraperitoneal injection

5. Place the mouse back to its cage. Wait ~5 min. Assess if the mouse has reached a surgical plane of anesthesia by loss of response to tail or toe pinches (Reference 4).

Note: For neonatal mouse younger than 6 days of age, anesthesia can be achieved through hypothermia (Behringer et al., 2013). Place mouse pup in a conical tube or wrap it with latex glove (cut off the thumb of the glove for this purpose) and bury it up to the neck in crushed ice for 10-15 min to obtain a surgical plane of anesthesia. Analgesia state lasts ~10 min, thereby do not leave the pup on surgical station for too long. Perform the surgery as soon as possible.

6. (From this step on, please operate in fume hood.) Place the mouse on its back. Firmly tape or pin its four paws to a Styrofoam or wood surgical station so that nothing moves during the perfusion procedure.

Note: If the heart stops beating due to excessive anesthesia, perfusion should be started immediately, preferentially with saline containing 20 units/ml heparin to avoid clotting of blood.

7. Trim the tip of a 25- or 27-gauge infusion needle to make it slightly blunt (Figure 3) to reduce the risk of puncturing the aorta wall in the following steps (Reference 1). Polish the edges with sandpaper if necessary.

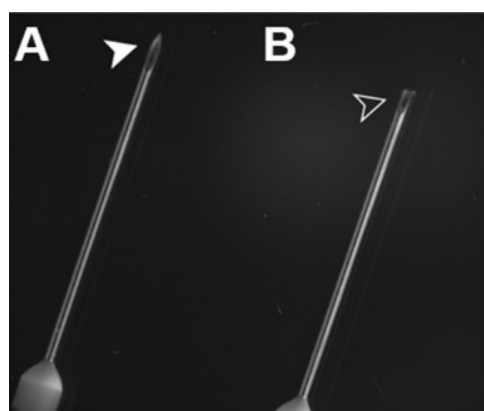


Figure 3. Needle trimming.

A. Untrimmed needle. B. Trimmed needle.

8. Connect the transfusion needle to a 20 mL syringe filled with saline. Flush the tubing and needle with saline to expel any air.

9. Fill another 20 mL syringe with 4% PFA solution.

B. Transcardiac perfusion with saline

1. Grip the skin on the chest with ophthalmic forceps and make an incision using tissue scissors to expose the xiphoid (a piece of arrowhead-shaped white bone).
2. Grip the xiphoid with ophthalmic forceps and make lateral incisions beneath the ribcage using tissue scissors to expose the diaphragm and liver.
3. Carefully make incisions in the diaphragm along the entire length of the rib cage using fine scissors.
4. Make two cuts through both sides of the rib cage up to the collarbone using tissue scissors. Reflect the sternum up over the head of the mouse with hemostat (or pint it to the surgical station, or cut it off) to fully expose the heart and lung (Figure 4).

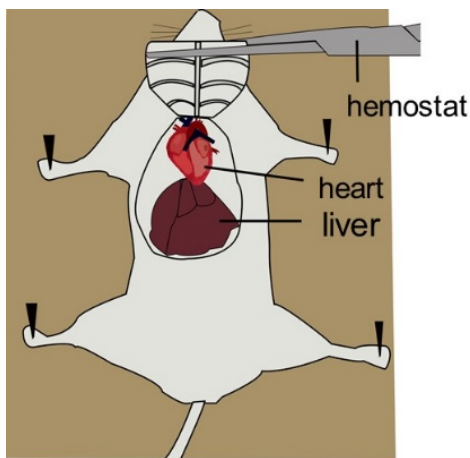


Figure 4. Thoracotomy

5. Carefully tear off pericardial sac and any other tissues covering the heart using dissecting forceps to provide a clear view of the heart and vessels.
6. Secure the heart with dissecting forceps at a steady position. Insert the trimmed needle from the tip of the left ventricle at an angle approximately parallel to the midline of the heart (Figure 5A). As the needle tip is blunt, enough pressure needs to be applied to get through the ventricle wall. However, do not push too hard and mind the angle to make sure the needle does not advance into the left atrium or right ventricle. With experience, one will clearly feel the resistance before penetration and the loss of it afterwards. The heart should be beating and one may observe backflow of blood into the needle before perfusion starts.
7. Steadily advance the needle until it enters the ascending aorta. The tip of the needle is visible through the aorta wall (Figure 5B-5D). No resistance should be encountered if the needle moves in the right direction. Secure the needle in the aorta with vascular clamp or hemostatic forceps at appropriate position (arrowhead in Figure 5C).

Notes:

- a. *If the needle cannot be successfully inserted into the aorta, leave it in the left ventricle (~5 mm in for adult mouse, shorter for younger mouse; adjust wisely depending on the size of the heart) (Figure 5B), but it has to be secured with pins or tape to avoid slipping out of the heart during perfusion (Video 1). For neonatal pups, the aorta may be too narrow to fit the needle tip and too delicate to clamp, in which case leaving needle tip in the ventricle is preferred.*
- b. *If the needle advanced too much into right ventricle or even pierce through the heart, withdraw and re-insert the needle promptly. If the wound is not too bad, it may not affect perfusion.*

8. Make a small incision on the right atrium using fine scissors. Dark venous blood should flow out immediately. Start the saline perfusion at once at a constant speed of ~1 mL/5 s by manually pushing the syringe or using a peristaltic pump. As saline flushes out the blood, the liver gradually turns pale (Figures 5E-F).

Notes:

- a. If the needle tip is in the left ventricle instead of aorta, slower perfusion speed is preferred.
 - b. If the needle tip goes into right ventricle, one may observe signs of failed perfusion including inflation of lung (Figure 6), liquid dripping out of nose or mouth and incomplete decolor of liver.
- Optional: Instead of manual injection, peristaltic pump can be used to better control the perfusion speed.

9. Stop perfusion when the fluid flowing out is clear of blood. For adult mice, it takes ~20 mL saline.

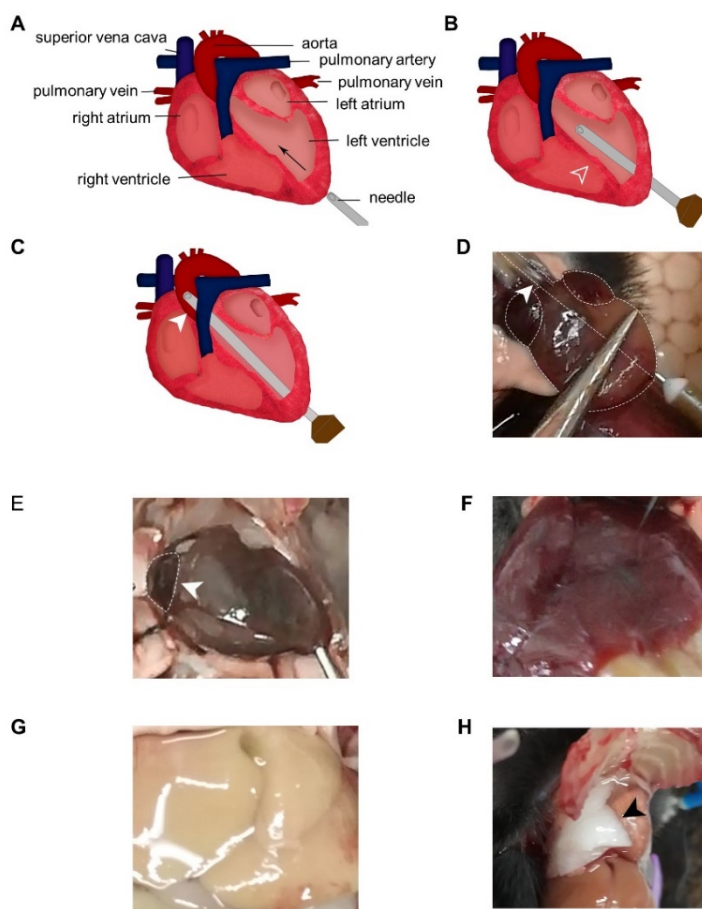


Figure 5. Needle insertion.

A. Position and direction of needle insertion. B. The needle tip can be left in the left ventricle halfway through the heart. Mind the trajectory so that the needle does not pierce through the septum (open arrowhead) into the right ventricles. C. Advance the needle into the aorta and clamp it at appropriate position (closed arrowhead). D. The needle tip is visible through the aortic wall (closed arrowhead). E. Make a small incision in the right atrium (closed arrowhead). F. The liver is filled with blood and appears red before perfusion. G. The liver loses blood and becomes pale after perfusion. H. Improper perfusion leads to accumulation of liquid in the lung and pulmonary edema (black arrowhead).



Video 1. Transcardiac Perfusion of the Mouse.

C. Transcardiac perfusion with 4% PFA (Video 1)

1. Switch from saline to 4% PFA. Make sure no bubble gets into the perfusion system during the switch (Gage *et al.*, 2012).
2. Steadily perfuse 4% PFA at a constant speed of ~1 mL/5 s. As PFA goes into circulation, one can observe signs including body twitching, tail flicking and head moving.
3. Perfuse ~15-20 mL 4% PFA for adult mouse. The whole mouse body should be very stiff and the liver may turns slightly pale brownish (a little bit darker color than it was before 4% PFA perfusion).
4. Remove the needle and unpin the mouse from the surgical station.

D. Brain dissection (Video 1)

1. Decapitate the mouse with tissue dissecting scissors (Figure 6, horizontal line). Remove the skin by first making an incision along the midline from the neck to the nose (Figure 6, vertical line) and then reflect the two flaps of skin rostrally and laterally to expose the skull (Figure 6B).
2. Hold the head tightly with one hand. Trim off bones at the caudal end with dissecting scissors (Figure 6B, dashed line). Clear off any residual muscle on the skull with forceps or scissors. If the 4% PFA was done properly, the brain will shrink a little bit and there will be some space between the brain and the bones forming the foramen magnum.
3. Slide one blade of the fine scissors into the foramen magnum (underneath the brain) with the sharp side facing the bone on one side. Make a lateral cut. Repeat the cut on the contralateral side. Carefully remove the skull covering the cerebellum with ophthalmic forceps.
4. At the rostral end of the mid-sagittal suture, insert the tip of one blade of the fine scissors between the foramen magnum and the brain with the sharp side facing the bone. Rapidly slide and cut the cranium along the mid-sagittal suture. Carefully remove the skull with forceps to expose the brain. An additional cut may be necessary to expose the olfactory bulb (Figure 6C).

Note: Be careful not to damage the brain during the operation. Peel off any meninges attaching to the skull before removing the bone chips; otherwise it may slice the soft brain tissue.

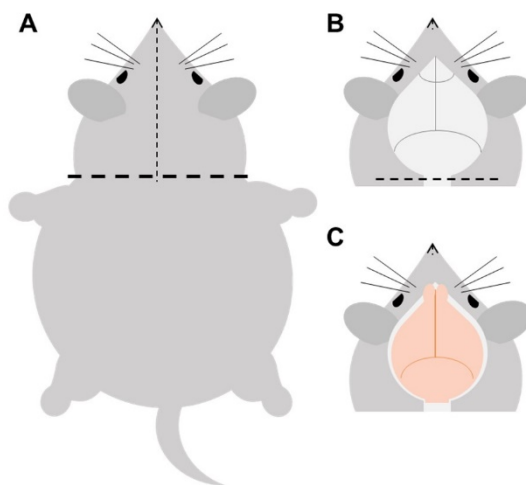


Figure 6. Brain dissection.

A. Cut the head off, cut the fur from the neck towards the tip of the nose (the dotted line), and expose the skull. B-C. Cut off the skull below the brainstem along the dotted line, and then remove the skull covering the cerebellum and cerebrum in turn to expose the brain tissue.

5. Using a micro spatula (or other flat and blunt tool) to sever the nerve bundle on the ventral surface of the brain and scoop the brain out.

Notes:

- Compared to freshly dissected brain (Figure 7A, very soft and full of blood), successfully perfused and fixed brain will shrink a little bit, become harder and appear slightly pale brownish (Figure 7C). Unsuccessful perfusion may leave blood in the brain (Figure 7B) and make it appear pinkish. Post-fix the brain in 4% PFA overnight at 4°C.*
- Postfix will further shrink, harden and darken the brain (Figure 7D).*

6. Transfer the brain into PBS containing 0.01% sodium azide for long term storage at 4°C. Alternatively, transfer the brain into 30% sucrose solution, wait until it sinks to the bottom, and store at minus 20–80°C (Hou *et al.*, 2021).

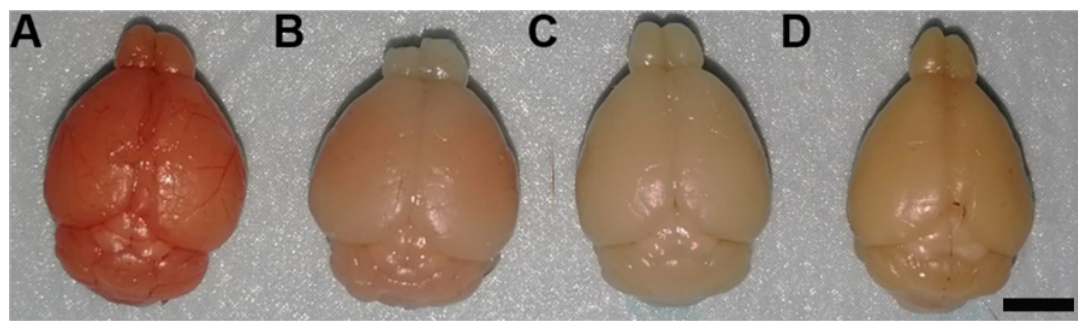


Figure 7. Representative images of brains dissected out under different conditions.

- A. Freshly dissected brain is full of blood and very soft. B. Unsuccessfully perfused brain retains some blood. C. Successfully perfused and fixed brain before post-fixation. D. Brain after post-fixation. Scale bar: 4 mm.

Notes

Table 1. Troubleshooting

Problem observed	Possible cause	Solution
Fluid flows out from a position other than the right atrium.	Needle piercing through the heart or aorta	Withdraw the needle and re-insert it at the right angle and depth
Expanded lung; fluid flows out from the mouth and nose	Needle goes into the right ventricle	Withdraw the needle and re-insert it at the right angle and depth
Blood in the brain after perfusion; liver does not turn pale	Ineffective perfusion of saline due to cardiac arrest before operation Blood clotting Air bubble in the perfusion system	Be careful not to overdose the mouse when administering anesthesia Practice to avoid unnecessary delay during the operation procedure Perfuse with saline containing 20 units/ml heparin Avoid air bubble in the perfusion system
Brain is pale but soft after perfusion	Ineffective perfusion of fixative due to air bubble in the perfusion system, or misplaced needle Low-quality 4% PFA (contains undissolved particles or expired)	Be careful not to introduce air bubble in the perfusion system when changing from saline to PFA; Adjust the position of the needle Filter PFA with 0.22 μm PVDF; use freshly prepared PFA or properly stored PFA (for more details, please refer to the appendix)

Recipes

1. 4% paraformaldehyde (Table 2)

Precaution! Wear protective gear including goggles, mask, gloves and lab coat in the whole process.

- a. Wash the measuring cylinder and beaker with deionized water.
- b. Weigh 12.481 g $\text{NaH}_2\text{PO}_4 \cdot 2\text{H}_2\text{O}$ and 114.605 g $\text{Na}_2\text{HPO}_4 \cdot 12\text{H}_2\text{O}$ with an analytical balance.
- c. Dissolve the salts in 2 L deionized water in a 2.5 L beaker with magnetic stirrer until the solution became clear.
- d. Heat up the phosphate buffer to ~60°C using microwave or heater.
- e. Weigh 160 g PFA powder with analytical balance. Carefully add the PFA powder into the bottom of a 5 L beaker placed on a magnetic stirrer with heating device in a chemical fume hood.
- f. Slowly pour the preheated phosphate buffer into the beaker with PFA while stirring. Adjust the heat setting to keep the buffer at a temperature between 50 and 60°C. Stir the solution until PFA is fully dissolved which may take several hours. Use a thermometer to monitor the temperature throughout the whole process.

Note: 5 mol/L(N) NaOH solution can be added dropwise to raise the pH and help dissolving PFA, but equimolar HCl should be added to bring back the pH. Prepare 5 N NaOH solution: Weigh 2 g NaOH in a 50ml conical tube and add 10 mL deionized water. Gently shake the tube to fully dissolve NaOH. Do not close the cap or shake the tube too vigorously to avoid explosion of the tube or splashing of the solution due to sudden accumulation of large amount of heat during this process.

- g. Add deionized water to bring up the volume to 4 L.
- h. Connect the 0.22 µm PVDF bottle top filter set with a benchtop vacuum and a collecting bottle to filter the PFA solution.
- i. For long term storage, aliquot the filtered solution into 50 mL centrifuge tube and store at -20°C. Melt at 4°C or room temperature and mix well before use.

Note: Aliquot no more than 45 mL per tube as the volume will expand when the liquid freezes.

Table 2. Recipe of 4% PFA

Chemical	Molecular weight	Working concentration	1 L (g)	2 L (g)	4 L (g)	5 L(g)
NaH ₂ PO ₄ ·2H ₂ O	156.01	0.02 N	3.1202	6.2404	12.4808	15.601
Na ₂ HPO ₄ ·12H ₂ O	358.14	0.08 N	28.651	57.302	114.605	143.256
Paraformaldehyde	30.03	4%	40	80	160	200

Acknowledgments

The present protocol is modified from the original version of our article (*Hou et al., 2021*). This work is supported by funds from Shanghai Municipal Science and Technology Major Project (No.2018SHZDZX01) and ZJLab.

Competing interests

The authors declare no conflict of interest or competing interest.

Ethics

Experimental protocols and the use of animals were approved by the Institutional Animal Care and Use Committee at Fudan University and conducted in accordance with institutional guidelines of Institutes of Brain Science (IOBS), Fudan University, China.

Reference

- Adult Mouse Transcardiac Perfusion. https://www.mbl.edu/bie/files/2015/01/mouse_transcard_perf11.pdf.
- Behringer, R., Gertsenstein, M., Nagy, K. and Nagy, A. (2013). Manipulating the mouse embryo: a laboratory manual. 4th edition. Cold Spring Harbor Laboratory Press.
- Gage, G. J., Kipke, D. R. and Shain, W. (2012). Whole animal perfusion fixation for rodents. *J Vis Exp* 65(65).
- Hou, Y., Qi, Z., Hongzhi, L., Jinyun, W., Shi, Y., Yanqing, Q., Mengmeng, S., Zhenggang, Y., Jiangteng, L., Zhuhao, W., Ling, G. and Miao, H. (2021). Topographical organization of mammillary neurogenesis and efferent projections in the mouse brain. *Cell Rep* 34(6).
- Standard Operating Procedures (Transcardiac Perfusion). https://www.mcgill.ca/research/files/research/305-transcardiac_perfusion - jan 2018_1.pdf.

Development of a Chemical Reproductive Aging Model in Female Rats

Nayara Pestana-Oliveira^{1,2,*}, Ruither O. G. Carolino⁵, Bruna Kalil-Cutti³, Cristiane M. Leite⁴, Litamara C. Dalpoeto⁵, Bruna Balbino De Paula⁶, Jonh P. Collister¹ and Janete Anselmo-Franci⁵

¹Department of Veterinary and Biomedical Sciences, College of Veterinary Medicine, University of Minnesota, Saint Paul, MN, USA

²Department of Physiology, School of Medicine of Ribeirão Preto, University of São Paulo, Ribeirão Preto, São Paulo, Brazil

³Department of Physiology, Institute of Biomedical Science, Federal University of Alfenas, Alfenas, MG, Brazil

⁴University of Northern Paraná (UNOPAR), Londrina, PR, Brazil

⁵Department of Basic and Oral Science, School of Dentistry of Ribeirão Preto, University of São Paulo, Ribeirão Preto, São Paulo, Brazil

⁶Department of Psychology, School of Philosophy, Science and Letter of Ribeirão Preto, University of São Paulo, Ribeirão Preto, SP, Brazil

*For correspondence: pesta016@umn.edu

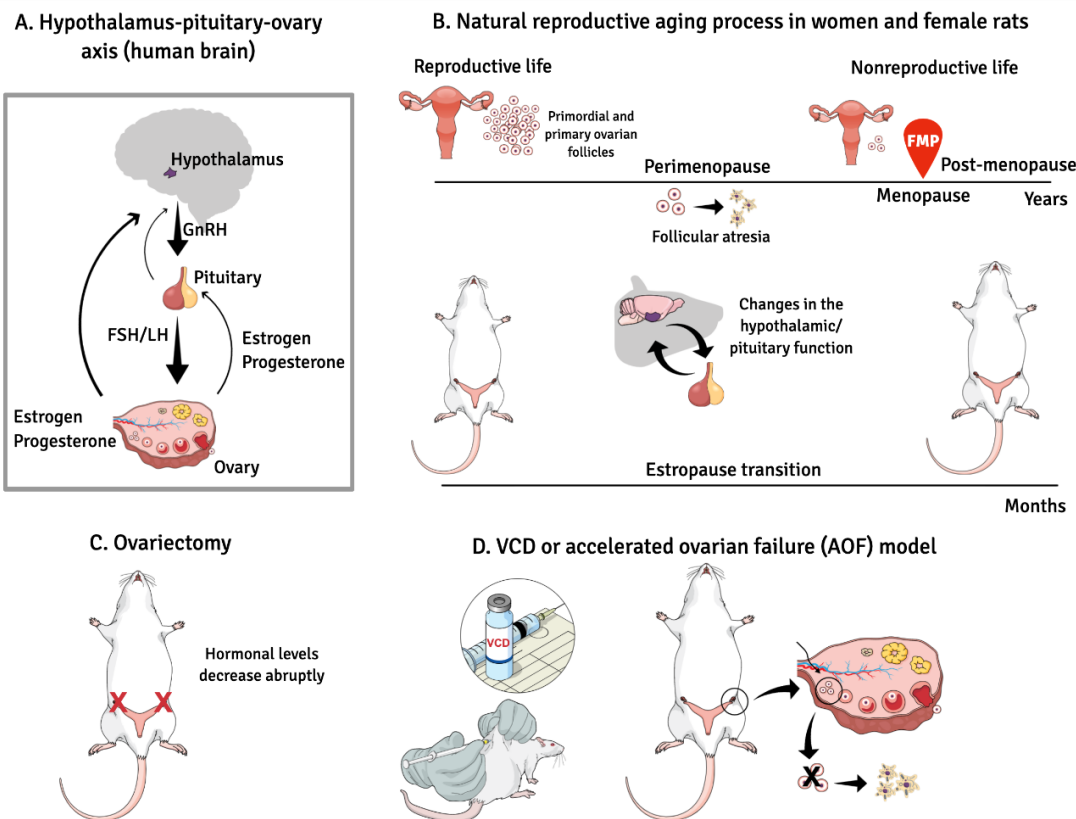
Abstract

Women are born with an abundant but finite pool of ovarian follicles, which naturally and progressively decreased during their reproductive years until menstrual periods stop permanently (menopause). Perimenopause represents the transition from reproductive to non-reproductive life. It is usually characterized by neuroendocrine, metabolic and behavioral changes, which result from a follicular depletion and reduced number of ovarian follicles. During this period, around 45-50 years old, women are more likely to express mood disorders, anxiety, irritability and vasomotor symptoms. The current animal models of reproductive aging do not successfully replicate human perimenopause and the gradual changes that occur in this phase. While the traditional rat model of menopause involves ovariectomy or surgical menopause consisting of the rapid and definitive removal of the ovaries resulting in a complete loss of all ovarian hormones, natural or transitional menopause is achieved by the selective loss of ovarian follicles (perimenopause period). However, the natural aging rodent (around 18-24 months) model fails to reach very low estrogen concentrations and overlaps the processes of somatic and reproductive aging. The chronic exposure of young rodents to 4-vinylcyclohexene diepoxide (VCD) is a well-established experimental model for perimenopause and menopause studies. VCD induces loss of ovarian small follicles (primary and primordial) in mice and rats by accelerating the natural process of atresia (apoptosis). The VCD, ovary-intact or accelerated ovarian failure (AOF) model is the experimental model that most closely matches natural human progression to menopause mimicking both hormonal and behavioral changes typically manifested by women in perimenopause.

Keywords: Perimenopause, Chemical reproductive aging, 4-vinylcyclohexene diepoxide (VCD), Accelerated ovarian failure (AOF), Follicular depletion

This protocol was validated in: eNeuro (2018), DOI: 10.1523/ENEURO.0247-17.2017

Graphical Abstract:



The female reproductive system is regulated by a series of neuroendocrine events controlled by central and peripheral components.

(A). The mechanisms involved in this control are extremely complex and have not yet been fully clarified. In female mammals whose ovulation (the most important event in a reproductive cycle) occurs spontaneously, reproductive success is achieved through the precise functional and temporal integration of the hypothalamus-pituitary-ovary (HPO) axis. (B). In women, loss of fertility appears to be primarily associated with exhaustion of ovarian follicles, and this process occurs progressively until complete follicular exhaustion marked by the final menstrual period (FMP). (C). While in female rodents, reproductive aging seems to begin as a neuroendocrine process, in which changes in hypothalamic/pituitary function appear independently of follicular atresia. The traditional rat model of menopause, ovariectomy or surgical menopause consists of the rapid and definitive removal of the ovaries resulting in a complete loss of all ovarian hormones. (D). The chronic exposure (15-30 days) to the chemical compound 4-vinylcyclohexene diepoxide (VCD) in young rodents accelerates gradual failure of ovarian function by progressive depletion of primordial and primary follicles, but retains residual ovarian tissue before brain alterations that occurs in women in perimenopause. Low doses of VCD cause the selective destruction of the small preantral follicles of the ovary without affecting other peripheral tissues.

Background

Perimenopause, the transition period from reproductive to non-reproductive life, is defined as the period immediately before menopause. This period is marked by the onset of endocrine and biological changes, as well as clinical symptoms suggestive of the approach of menopause and can extend up to twelve months after the final menstruation, with an average duration of five years (WHO, 1996; Soules *et al.*, 2001; Bacon, 2017; Wang *et al.*, 2019). In addition

to menopause or definitive cessation of menstrual cycling, perimenopause is a uniquely human process, but it can be mimicked by experimental models, especially in rodents. According to Prior and Hitchcock, perimenopause, previously seen as a period of hypoestrogenism, can be characterized by three main hormonal changes in women whose menstrual cycle remains regular: 1) normal or erratically high concentrations of estradiol; 2) decline in plasma progesterone concentrations and 3) changes at all levels of the reproductive axis (Prior and Hitchcock, 2011). During perimenopause a high percentage of women manifest typical symptoms of this period, which include: vasomotor changes, variations in menstrual cycle duration, sleep disorders, worsening cognitive functions, behavioral and mood changes (irritability, nervousness, anxiety and depression), in addition to metabolic and physiological changes (Mitchell and Woods, 1996; Brinton *et al.*, 2015; Chalouhi, 2017). Considering the brain changes during this period, Brinton *et al.* (2015) defined perimenopause as a “state of neurological transition”.

The process of reproductive senescence in mammal species is complex and poorly understood, especially in humans (Brinton *et al.*, 2009; Brinton, 2010). Consequently, animal models of menopause and perimenopause function as windows into the complex mechanisms involved in reproductive biology senescence at different levels (systemic, cellular, molecular, and genomic), which are not possible to perform in humans (Brinton, 2012). Nonetheless, current animal models of menopause do not successfully replicate human perimenopause and the gradual changes that occur in this phase. While the traditional rat model of menopause, ovariectomy or surgical menopause that consist of the rapid and definitive removal of the ovaries resulting in a complete loss of all ovarian hormones, natural or transitional menopause is achieved by the selective loss of ovarian follicle (perimenopause period). However, natural aging models fail to reach very low estrogen concentrations and overlapping changes related to somatic aging and those of reproductive aging (Kermath and Gore, 2012; Frye *et al.*, 2012; Kirshner *et al.*, 2020). Additionally, these models do not reproduce what occurs in women, since the primary causes of reproductive aging between species diverge significantly. In women, loss of fertility appears to be primarily associated with exhaustion of ovarian follicles (Faddy *et al.*, 1992; Rubin, 2000), while in female rodents, reproductive aging seems to begin as a neuroendocrine process, with the changes in hypothalamic/pituitary function appearing independently of the follicular atresia (Gore *et al.*, 2000).

A well-established experimental model in the literature for studying perimenopause and menopause is exposure of rodents to the chemical 4-vinylcyclohexene diepoxide (VCD), which leads a gradual failure of ovarian function by progressive depletion of primordial and primary follicles, but retains residual ovarian tissue similar to women in perimenopause (Springer *et al.*, 1996; Kao *et al.*, 1999; Hoyer *et al.*, 2001). Importantly, the VCD model or model of Accelerated Ovarian Failure (AOF, Brooks *et al.*, 2016) mimic both hormonal (Reis *et al.*, 2014; Pestana-Oliveira *et al.*, 2018; Carolino *et al.*, 2019) and behavioral changes such as anxiety (Reis *et al.*, 2014), impaired memory (Koebele *et al.*, 2016), depression (Kalil *et al.*, 2020) and aggressiveness (Dalpogeto *et al.*, 2016; Scafuto *et al.*, 2017) typically manifested by women in perimenopause. Low doses of VCD specifically cause selective destruction of ovarian small pre-antral follicles without affecting other peripheral tissues. Furthermore this occupational chemical doesn't cross the blood-brain barrier (Lukefahr *et al.*, 2012).

Therefore, the VCD-induced follicular depletion model, followed by ovarian failure has been widely used in experimental research on perimenopause and menopause (Reis *et al.*, 2014; Liu *et al.*, 2015; Brooks *et al.*, 2016; Koebele *et al.*, 2016; Pestana-Oliveira *et al.*, 2018; Wang *et al.*, 2019; Carolino *et al.*, 2019; Kirshner *et al.*, 2020) and is the experimental model that most closely matches the natural human progression to menopause, since the majority of women enter menopause through a gradual and irreversible process of reduction in ovarian function, while retaining the residual tissue of the ovary (Brooks *et al.*, 2016). Thus, considering that it is a critical number of ovarian follicles and not the woman's age that determines the onset of menopause (Faddy *et al.*, 1992), VCD-induced perimenopause is a translational model that presents analogy, predictability and homology, and allows plausible inferences to be made about the dynamics of follicular loss and its effects on the neurochemistry of women in perimenopause and menopause, periods in which affective disorders, vasomotor alterations and several other symptoms compromise the quality of life of middle-aged women.

Recently (2015-2017) the AOF model was applied to the streets and subways of large North American cities such as Chicago, New York, San Francisco, and Los Angeles with the aim of reducing the population of rats that has infested those cities (<https://www.chicagomag.com/Chicago-Magazine/March-2015/birth-control-for-rats/>).

Materials and Reagents

1. Polyethylene tubing (Thermo Scientific™ Immuno Tubes and Stoppers, catalog number: 12-565-150), stored at room temperature (RT)
2. Plastic funnel
3. Pipet tips (Eppendorf®, catalog numbers: 1300 RN [1-100 µL, yellow]; 1400 [101-1,000 µL, blue]), stored at room temperature
4. Glass slides for immunofluorescence (dimensions: size 25.4 × 76.2 mm; thickness: 1.0 × 1.2 mm), twelve transparent circles (Perfecta, catalog number: 214-6), stored at RT
5. Flexible, translucent silicone elastomer tubing (Silastic, Dow Corning™, 7.8 mm × 12.7 mm × 2.38, catalog number: 11-189-13B), stored at RT
6. Syringe (1 ml Tuberculin Syringe Regular Tip) (Monoject™, catalog number: 8881501400), stored at RT
7. Sterile Gloves (Synthetical Surgical Gloves Powder-Free, Confiderm® SPT), stored at RT
8. Gauze sponges (Non-woven Gauze Sponges, 2 in. × 2 in. [5.08 cm × 5.08 cm]) (AVANT GAUZE®, catalog number: 25223), stored at RT
9. Needles (Standard Hypodermic Needles, Monoject™, catalog numbers: 8881250255 [23G], 8881250149 [21G]), stored at RT
10. Females Wistar rats (age 28 days) from the animal facilities of the University of São Paulo, campus Ribeirão Preto, Brazil
11. 4-vinylcyclohexene diepoxide (VCD [C₈H₁₂O₂] Sigma-Aldrich, catalog number: 94956-250ML), stored at RT
12. 17-β-estradiol (Sigma-Aldrich, catalog number: E8875-1G), stored at RT
13. Corn oil (Liza-900ML), stored at RT
14. Ketamine HCl Injection, USP (Ketaset®, 100 mg/kg; NDC: 0856-2013-1), RT
15. Xylazine (Schering-Plough, Coopers of Brazil, Cotia, São Paulo, 14 mg/kg), RT
16. Small Veterinary Pentabiotic® (Zoetis, 1.7 g/3 mL, catalog number: 232092), RT
17. Banamine Solution Injectable (Schering-Plough Animal Health, 2.5 mg/kg; catalog number: 12080097), stored at room temperature Sodium Chloride (NaCl) 0.9% (Samtec Biotechnology, 10 mL), RT
18. 5% Povidone-iodine antiseptic microbicide for animal use (Betadine® Solution, catalog number: 12265), stored at RT
19. 70% Isopropyl Alcohol (473 mL) (Medline Industries, catalog number: 53329-800-06), stored at RT
20. ELISA estradiol kit (DRG® Instruments GmbH DRG, EIA 2693), storage: 2°C-8°C
21. Progesterone double antibody RIA kit (P4) (MP Biomedicals, catalog number: SKU 07-170105 CF), storage: 2°C-8°C
22. Standard Rat Chow (23.2% Protein Rodent Diet, LabDiet®, catalog number: 5012), stored at RT
23. Heparin 50 units/mL (Heparin Sodium Injection USP, 50 units USP per mL) (B. Braun Medical Inc., catalog number: 0264-9577-10), stored at RT
24. 4-vinylcyclohexene diepoxide dilution (VCD) (see Recipes)

Equipment

1. Standard cages (Bonther, 40 × 33 × 17 cm)
2. Guillotine (Bonther, model: Inox 420)
3. Surgical scissors
4. Forceps
5. Needle holder
6. Microscope (Zeiss Axioskop 2 Plus Ergonomic Trinocular, catalog number: 452342)
7. Centrifuge (Eppendorf, model: 5425, catalog number: 5405000042; 24 × 1.5/2.0 mL Capacity, up to 21,330 × g (15,060 rpm), includes FA-24x2 rotor with aerosol-tight QuickLock lid, keypad control, 120 V)
8. Magnetic Stirrer Magnetic Stirrer with Heating (Thermo Scientific, catalog number: N2400-3010)
9. Shaker/Vortexer with racks (BenchMixer XLQ, catalog number: BV 1010-TST)

10. Detector Gamma Counter (Wizard2™, PerkinElmer®, catalog number: 2470-0020)
11. Absorbance Reader 800 TS (BioTek)
12. Pipette single channel (Eppendorf™ Research [0.5-10 µL, EP: 3123000020 yellow; 20-200 µL, EP: 312300055 yellow; 100-1,000 µL, EP: 312300063 blue]
13. Electronic Pipette Multichannel (Eppendorf™ Research, 100 µL, SKU #184287407894)

Software

1. GraphPad Prism 7 software (GraphPad Software, La Jolla, CA)
2. Adobe Photoshop (Adobe Photoshop Lightroom, version 5.3; Adobe Systems, Inc.)
3. Mind the graph (www.mindthegraph.com)
4. Microsoft Excel

Procedure

Although many women in perimenopause have normal or erratically high estradiol plasma concentrations (Santoro *et al.*, 1996), estrogenic therapy is very common in clinical practice. Interestingly, improvement was observed regarding the typical symptoms of this transition period (Schmidt *et al.*, 2000). The study that inspired this protocol (Pestana-Oliveira *et al.*, 2018) had as one of its objectives to understand the possible effects of estradiol in the model of accelerated ovarian failure (Figure 1).

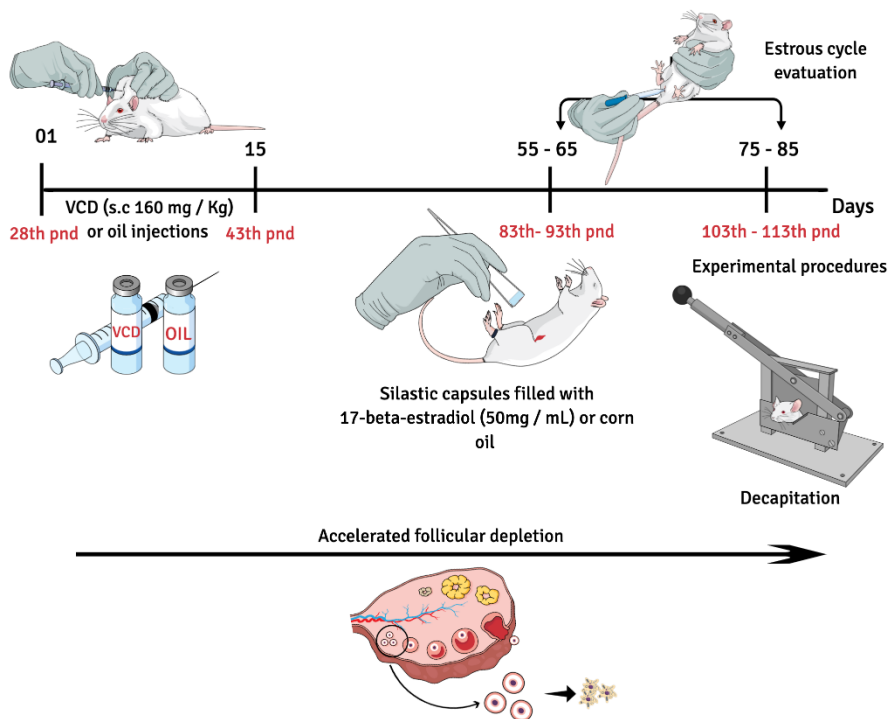


Figure 1. Schematic diagram showing the timeline of the experimental protocol.

Female Wistar rats (28 post-natal days) must be daily injected with VCD (160 mg/Kg) or corn oil (O; 1.25 mL/kg of body weight) for 15 days. Approximately 55 days after the first VCD or O injection, insert implant pellets of 17 β -estradiol or O s.c in the dorso-lateral region (Groups O + O; VCD + O; VCD + E). 21 days after oil or estradiol pellets implantation rats must be decapitated in the morning of diestrus.

A. VCD or corn oil injections (Figure 2)

1. Weigh and identify the female rats (28th post-natal day) individually and calculate the volume of VCD or corn oil that each will receive. It is important that this procedure is performed every two days. Then prepare and arrange the environment to give the injections. Cover the table or bench with paper and fill the syringes with the volume of VCD or oil previously calculated.
2. Take one animal and apply the subcutaneous injection on the back near to the neck region. Repeat the same procedure for all animals. Perform the applications slowly as the oil is viscous and the syringe may burst from the needle with pressure. In the case of animals that will receive injections containing VCD, avoid wasting liquid after the injection.
3. After finishing all the injections, return the animals to the specific animal facility. Repeat the entire procedure for 15 consecutive days. To avoid cutaneous and subcutaneous injuries we strongly suggest that injections be applied to different parts of the animal's body.

Note: The contact of the skin and mucous membranes with the VCD should be avoided as much as possible, especially if it is handled by female individuals. Therefore, the use of individual safety equipment such as gloves, masks and glasses is strongly recommended.

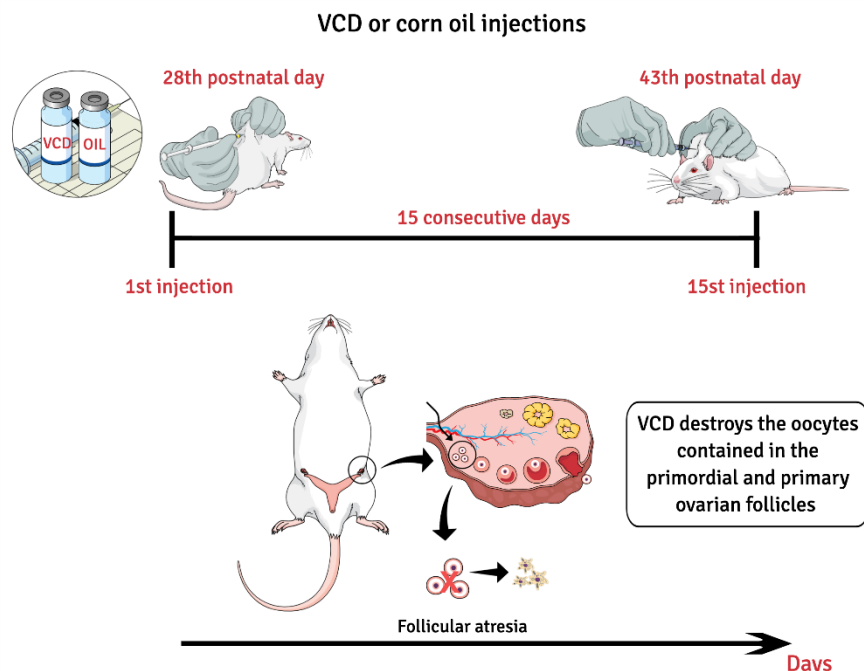


Figure 2. Schematic diagram showing the preparation of the accelerated ovarian failure model and control groups

B. Estrogen therapy

Silastic capsules preparation (Figure 3)

1. Extend the silastic tubing on a table or bench, with the aid of a ruler, divide it into 15 mm long pieces. Then cut the pieces. Insert the tip of one end of the silastic into a drop of silicone glue, press the opposite end so that the glue enters into tube. With the aid of hemostatic scissors, clamp the end filled with glue. Repeat this procedure with the remaining pieces of silastic. Place the tubes on a flat surface for 24 h so that the glue can dry and thus seal the tube end (Figure 3-1).

2. Use a pipette and a plastic tip (0.5-10 μ L) to fill the silastic capsules with 8 μ L of 17- β -estradiol (50 mg/mL, previously diluted in corn oil). The estradiol suspension must be placed on a magnetic stirrer to ensure homogeneity throughout the process of filling the pellets. In addition, on the previous day it is important to subject the solution to ultrasound for 3 h followed by overnight stirring. When ready, it should appear as a homogeneous milky solution. At rest, the suspension settles, and it is possible to observe two phases: the upper one (vehicle) represented by the oil is transparent while the lower one is whitish. The oil pellets must be filled with 8 μ L of corn oil. The sealing process of the open end of the capsules is the same as described above except that it requires greater care considering that the capsules are filled with liquid. After complete sealing, it is important to trim the ends using small scissors (Figure 3-2).

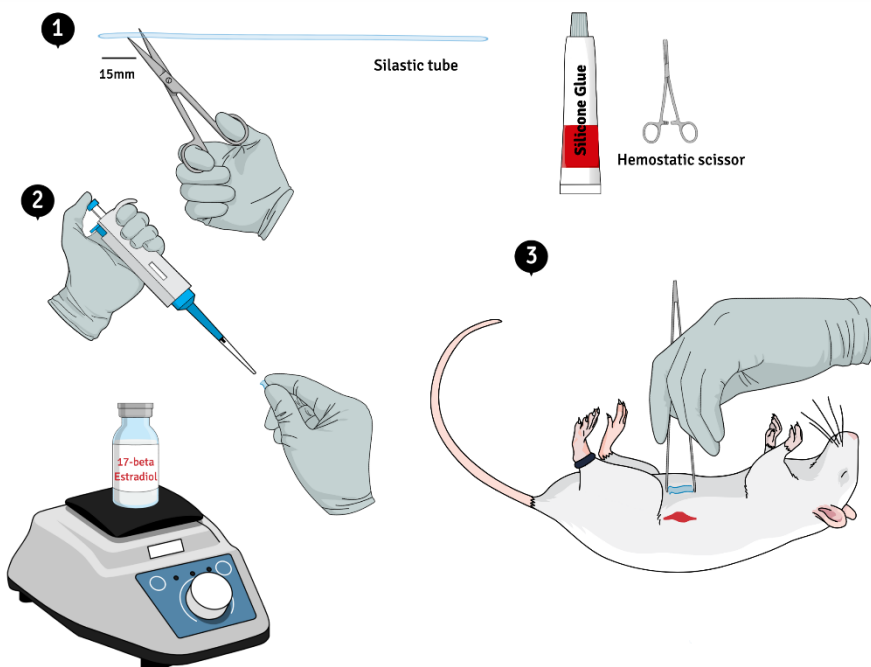


Figure 3. Schematic diagram showing the silastic capsules preparation and surgery implantation

Pellets implantation surgery

All Instruments and materials used for surgery must be previously sterilized. We recommend steam sterilization (autoclaving). Furthermore, female rats should be weighed for the doses of anesthetics and medications be given according to individual body weight.

3. The animals must be anesthetized with ketamine (55 mg/kg, IP) and xylazine (10 mg/kg, IP) and perform aseptic procedures as follows: shave the rats, scrub the surgical site with antiseptic solution (Betadine).

Note: In this protocol we use injectable anesthesia. However, is possible to use other approach such as inhaled anesthetics.

4. With the aid of a small scissors, make a discreet incision (0.5 cm) and insert the tip of the scissors to separate the tissue, a subcutaneous pocket is formed to store the pellet. This surgery is minimally invasive and quick. After surgery, the animals must receive prophylactic antibiotics (Pentabiotico 0.2 mL/rat, i.m.) and anti-inflammatory treatment (Banamine, 2.5 mg/kg, s.c).

C. Vaginal smears collection and estrous cycle evaluation (Figure 4)

The estrous cycle of female rats lasts an average of 4 to 5 days and has 4 distinct phases: proestrus, estrus, metestrus (or diestrus I) and diestrus (or diestrus II), which can be easily identified by the cell types observed in the vaginal smear (Marcondes *et al.*, 2002).

Vaginal smear collection and estrous cycle evaluation

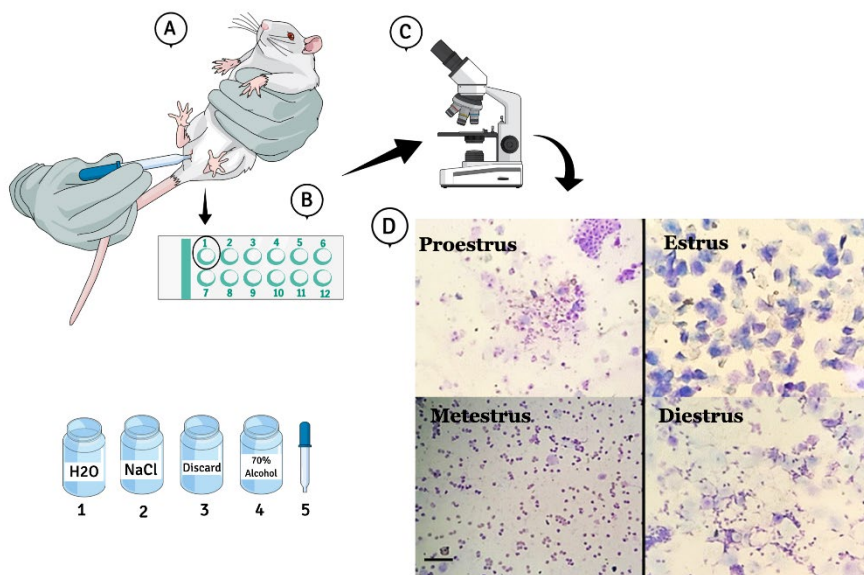


Figure 4. Schematic diagram showing the vaginal smear collection and estrous cycle evaluation.

Photomicrography (10 \times) kindly provided by Thalita de Oliveira Gonçalves and Guilherme de Souza Gagliano.

1. With one hand, hold the animal firmly so that the vagina is visible. With the other hand, gently insert the tip of a plastic pipette previously filled with 0.9% NaCl (approx. 10 μ L) into the vagina of the rat, it is not necessary to deepen the pipette. Press the rubber on the surface of the pipette to push the NaCl, repeat this process twice as if washing (Figure 4A-1).
2. Remove the vaginal fluid and deposit a drop on a glass slide (Figure 4B). Discard the excess of the collected smear in the specific container (Figure 4-3). The pipette must be sanitized between one animal and another, filling it with water (Figure 4-1) and discarding it in container 3. Repeat the wash 3 times, then fill the pipette with 70% alcohol (Figure 4-4) and discard, the pipette will dry immediately and be ready to be reused in another animal. One drop from each rat must to be placed sequentially on the slide (Figure 4B).
3. After collecting the vaginal smear from all rats, the glass slide is ready to be observed under an optical or light microscope without the need for a lens condenser. 10 \times and 40 \times objective lenses are suitable for observing fresh material (Figure 4C).
4. When observing the slide under the microscope, it will be possible to recognize 3 distinct cell types: 1) the round and nucleated ones that resemble bunches of grape or fried eggs are non-cornified squamous epithelial cells typically observed during the proestrus; 2) irregular cells, in the shape of a dry leaf or corn flakes, are the cornified epithelial cells, characteristic of estrus; 3) small round cells are the leukocytes present in the diestrus (Figure 4D). Animals in metestrus will present a variety of these cells. It is important to emphasize that the proportion between them should be used to determine the estrous cycle phases (Marcondes *et al.*, 2002).

*Note: The collection of the vaginal smear and evaluation of the estrous cycle must be carried out in the early morning, between 7:30 and 9:30 am to prevent the cells present in the vaginal fluid from moving from one phase to the next. Since until close to 90 days after the onset of VCD treatment the proportion of rats that cycle regularly (about 20%) is the same in control rats and those treated with VCD (Carolina *et al.*, 2019). Only*

control and VCD treated rats cycling regularly be used in the experiments performed before 90 days after starting VCD injections.

D. Euthanasia and blood samples collection

Between 75 and 85 days after the start of the VCD/oil injections, the animals should be euthanized in the morning, by decapitation or anesthetic overdose (ketamine [110 mg/kg, IP] and xylazine [20 mg/kg, IP]).

1. Before starting the decapitation, make sure the guillotine is sharp enough. Quickly and firmly hold the animal and position the head at the height of the trunk between the guillotine blades, once positioned, lower the lever.
2. With the aid of a plastic funnel previously heparinized and identified attached to the polyethylene tube, position the animal's body downwards, facilitating the exit of the blood. Shake the tube gently, facilitating the mixing of blood and heparin to prevent clotting. Store the tube containing blood in a refrigerated environment (2°C-8°C).
3. Remove the brain quickly and gently from the skull and freeze it immediately either on dry ice or liquid nitrogen. Store the brain at -70°C.
4. Centrifuge the blood samples in a refrigerated centrifuge at 1,200 × g for 20 min at 4°C. Separate the plasma and store at -70°C until the assay.

Note: The decapitation must be done the most humane way possible, guaranteeing the animal's well-being as well as the safety of the experimenter. Avoid noise, odors and crowding in the experimental room. The environment should be well lit with circulating air. We recommend using exhaust fans to help dispel specific odors such as blood. We recommend that the guillotine, the sink and the counter be cleaned with water and 70% alcohol to avoid the odor of blood between becapitations.

Data analysis

All comparisons were performed using one-way ANOVA followed by Newman-Keuls *post hoc* test. Data are presented as the mean ± SEM. Significance was accepted at $P > 0.05$. All statistical analyses and graphs were performed using GraphPad Prism 7 software.

Notes

An important question regarding the accelerated ovarian failure model is: how to assess whether the VCD injections were effective in promoting the depletion of primordial and primary follicles?

We suggest performing at least 1 of the three positive control tests:

1. **Ovarian histology.** This procedure is highly effective, since significant qualitative and quantitative changes are expected in ovarian follicles (Reis *et al.*, 2014). The disadvantage of this method is the time to obtain the results. Depending on the demand of each laboratory, between the collection of samples and obtaining the slides ready for microscopy, it will require at least 1 week.

After euthanasia (decapitation or perfusion), remove the ovaries, separate them from the connective tissue and fat and fix them in 10% formaldehyde for 24 h. Perform the histological processing that includes the dehydration processes (subject the material successively in increasing concentrations of alcohol to 70%, 90%, 100%), clearing with xylol, assembling the paraffin blocks and obtaining sections with a microtome of 8 µm thickness. To assemble the slides, we recommend semi-serial sections and stained with hematoxylin and eosin (HE). With the aid of an optical microscope, count and classify the ovarian follicles. The Leica Biosystems website provides the detailed guidance on procedures (Overview of the steps in tissue processing for paraffin sections; <https://www.leicabiosystems.com/knowledge-pathway/an-introduction-to-specimen-processing/>).

2. **Measurement of estradiol and progesterone plasma concentrations.** Most perimenopause women have a

typical hormonal profile, with reduction in progesterone plasma concentrations while estradiol concentrations are normal or erratically high (Santoro *et al.*, 1996; Prior and Hitchcock, 2011). The same pattern was observed in rats submitted to chronic VCD injections (Reis *et al.*, 2014; Pestana-Oliveira *et al.*, 2018; Carolino *et al.*, 2019). Therefore, we consider this an effective way to assess whether perimenopause was induced in female rats.

Immediately after the decapitation collect the blood samples and centrifuge at $1,200 \times g$ for 20 min at 4°C . The plasma must then be separated and be stored at -70°C until the assay. All samples must be measured in the same assay to avoid intraassay variation.

Progesterone assay: To measure progesterone plasma concentrations we recommend specific radioimmunoassay (RIA) kits for humans provided by MP Biomedicals. Polyethylene tubes must be numbered with a permanent pen in ascending order. For a more accurate assay we recommend that samples be measured in duplicate or triplicate. However, before the test it is necessary to perform a dilution test in order to identify the volume of plasma needed so that the value obtained from the samples plasma concentrations is in accordance with the kit standard curve. The MP Biomedicals website provides the step-by-step instructions on how to perform the assay.

Estradiol assay: To measure estradiol plasma concentrations we recommend specific kit for an enzyme-linked immunosorbent assay provided by DRG.

3. **Measurement of anti-Mullerian plasma concentrations.** It is well established in the literature that the anti-Mullerian hormone concentrations (AMH) have a direct correlation with the number of ovarian follicles, being thus considered a marker of ovarian follicular reserve whose levels decrease with increasing age, and therefore practically undetectable after menopause (Cui *et al.*, 2015). Also, the AOF model in both monkeys and mice has demonstrated a linear correlation between reduced levels of AMH and reduced number of developing follicles (Sahambi *et al.*, 2008). In a recently published study using the AOF model in female rats, Dr. Anselmo-Franci's laboratory (Carolino *et al.*, 2019) demonstrated that in fact plasma AMH concentrations can be considered a good index of ovarian follicular reserve as well as effectiveness of VCD injections in follicular depletion. To measure AMH plasma concentrations, use a specific enzyme-linked immunosorbent assay kit for mice and rat provided by Ansh Labs (Webster, TX, USA).

Recipes

1. 4-vinylcyclohexene diepoxide dilution (VCD, Figure 5)

The chemical compound VCD is obtained through epoxidation catalyzed by cytochrome P450 from 4-vinylcyclohexene (HCV), an occupational ovarian toxin produced from the dimerization of 1,3-butadiene during the manufacture of synthetic rubber, flame retardants, insecticides and plasticizers (Mayer *et al.*, 2002). The occupational chemical 4-vinylcyclohexene diepoxide (VCD) has been shown to cause selective destruction of ovarian small pre-antral (primordial and primary) follicles in rats and mice by accelerating the natural, apoptotic process of atresia (Kappeler and Hoyer, 2012).

To obtain the dose of 160mg/Kg (1.25 $\mu\text{L}/\text{g}$ body weight) dilute the VCD reagent in corn oil at a concentration of 12%, in other words, if you want to prepare 100 ml of stock solution, measure 12 ml of VCD in a graduated cylinder and make up to 100 ml with corn oil. With the aid of a magnetic stirrer, homogenize the solution. The ultrasound is not necessary to improve the dilution.

Notes:

- a. *The amount of solution can be prepared according to the demand of each laboratory. On average every 6 months it is possible to prepare 1 L of stock solution that should be stored at RT and kept in an amber bottle or wrapped in aluminum foil to avoid exposure to light. We recommend distributing the stock solution in smaller bottles that will be used routinely.*
- b. *In all processes involving the handling of the chemical compound VCD, the use of personal protective equipment is essential. In addition, dilution of the VCD must be performed under ventilation and properly cleaned with 70%*

alcohol. Avoid skin contact and inhalation.

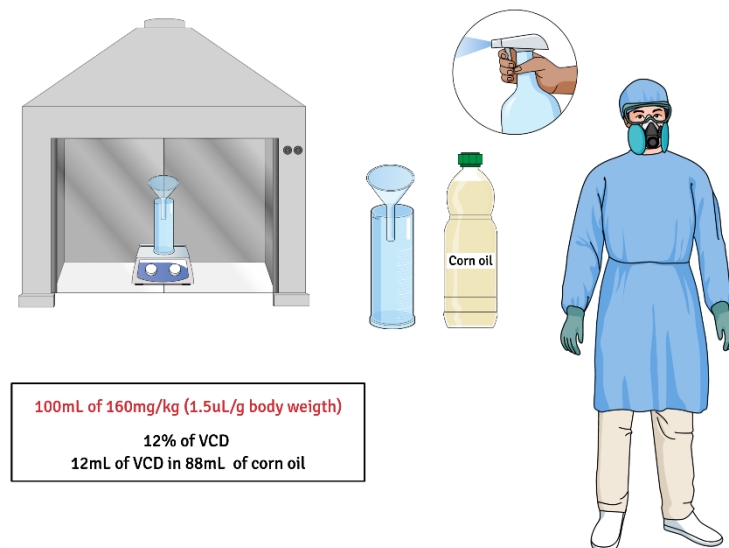


Figure 5. Schematic diagram showing the 4-vinylcyclohexene diepoxide (VCD) dilution

Acknowledgments

The original study that supported this paper, “Effects of Estrogen Therapy on the Serotonergic System in an Animal Model of Perimenopause Induced by 4-Vinylcyclohexen Diepoxide (VCD)” was funded by Brazilian National Council for Scientific and Technological Development (CNPq, Portuguese: Conselho Nacional de Desenvolvimento Científico e Tecnológico) and São Paulo Research Foundation (FAPESP, Portuguese: Fundação de Amparo à Pesquisa do Estado de São Paulo). This study was developed in the Laboratory of Neuroendocrinology of Female Reproduction under the guidance of Dr. Janete A Anselmo-Franci, Department of Basic and Oral Science, School of Dentistry of Ribeirão Preto, University of São Paulo, Ribeirão Preto, São Paulo, Brazil.

Competing interests

The authors declare that they have no conflict of interest.

Ethics

All procedures were approved by the Committee for Animal Care and Use (2013.1.1412.58.7), University of São Paulo.

References

- Bacon, J. L. (2017). [The Menopausal Transition](#). *Obstet Gynecol Clin N Am* 44(2): 285-296.
Brinton, R. D., Gore, A. C., Schmidt, P. J. and Morrison, J. H. (2009). [Hormones, Brain and Behavior \(2nd edition\)](#). In: Pfaff, D. W. *et al.* (Eds.). Elsevier 2199-2222.

- Brinton, R. D. (2010). In: [Brockelhurst's Textbook of Geriatric Medicine and Gerontology](#). Fillit, H., Rockwood, K. and Young, J. (Eds.). Saunders 163-171.
- Brinton, R. D. (2012). [Minireview: translational animal models of human menopause: challenges and emerging opportunities](#). *Endocrinology* 153(8): 3571-3578.
- Brinton, R. D., Yao, J., Yin, F., Mack, W. J. and Cadenas, E. (2015). [Perimenopause as a neurological transition state](#). *Nat Rev Endocrinol* 11(7): 393-405.
- Brooks, H. L., Pollow, D. P. and Hoyer, P. B. (2016). [The VCD Mouse Model of Menopause and Perimenopause for the Study of Sex Differences in Cardiovascular Disease and the Metabolic Syndrome](#). *Physiology (Bethesda)* 31(4): 250-7.
- Carolina, R. O. G., Barros, P. T., Kalil, B. and Anselmo-Franci, J. (2019). [Endocrine profile of the VCD-induced perimenopausal model rat](#). *PLoS One* 14(12): e0226874.
- Chalouhi, S. (2017). [Menopause: A complex and controversial journey](#). *Post Reprod Health* 23(3): 128-131.
- Cui, L., Qin, Y., Gao, X., Lu, J., Geng, L., Ding, L., Qu, Z., Zhang, X. and Chen, Z. J. (2016). [Antimullerian hormone: correlation with age and androgenic and metabolic factors in women from birth to postmenopause](#). *Fertil Steril* 105(2): 481-485 e481.
- Dalpogeto, L. C., Pestana, de Oliveira Nayara, Anselmo-Franci, J. A. (2016). [Evaluation of aggressive behavior in an animal model of perimenopause](#). *Annual Meeting Society of Neuroscience*, Washington, DC, USA.
- Faddy, M. J., Gosden, R. G., Gougeon, A., Richardson, S. J. and Nelson, J. F. (1992). [Accelerated disappearance of ovarian follicles in mid-life: implications for forecasting menopause](#). *Hum Reprod* 7(10): 1342-1346.
- Frye, J. B., Lukefahr, A. L., Wright, L. E., Marion, S. L., Hoyer, P. B. and Funk, J. L. (2012). [Modeling perimenopause in Sprague-Dawley rats by chemical manipulation of the transition to ovarian failure](#). *Comp Med* 62(3): 193-202.
- Gore, A. C., Oung, T., Yung, S., Flagg, R. A. and Woller, M. J. (2000). [Neuroendocrine mechanisms for reproductive senescence in the female rat: gonadotropin-releasing hormone neurons](#). *Endocrine* 13(3): 315-323.
- Hoyer P. B., Devine P. J., Hu, X., Thompson, K. E., Sipes, I. G. (2001). [Ovarian toxicity of 4-vinylcyclohexene diepoxide: a mechanistic model](#). *Toxicol Pathol* 29(1): 91-9.
<https://www.chicagomag.com/Chicago-Magazine/March-2015/birth-control-for-rats/>.
- <https://www.leicabiosystems.com/knowledge-pathway/an-introduction-to-specimen-processing/>
- Kalil, B., Pestana-Oliveira, N., Santos, I. R., Carolina, R. O. G. and Anselmo-Franci, J. A. (2020). [Effect of Estradiol Therapy on Depressive like Behavior in an Ovarian Intact Rat Model of Perimenopause](#). *J Endocrine Society* MON-017. <https://doi.org/10.1210/jendso/bvaa046.1298>.
- Kao, S. W., Sipes, I. G. and Hoyer, P. B. (1999). [Early effects of ovotoxicity induced by 4-vinylcyclohexene diepoxide in rats and mice](#). *Reprod Toxicol* 13(1): 67-75.
- Kappeler, C. J. and Hoyer, P. B. (2012). [4-vinylcyclohexene diepoxide: a model chemical for ovotoxicity](#). *Syst Biol Reprod Med* 58(1): 57-62.
- Kermath, B. A. and Gore, A. C. (2012). [Neuroendocrine control of the transition to reproductive senescence: lessons learned from the female rodent model](#). *Neuroendocrinology* 96(1): 1-12.
- Kirshner, Z. Z., Yao, J. K., Li, J., Long, T., Nelson, D. and Gibbs, R. B. (2020). [Impact of estrogen receptor agonists and model of menopause on enzymes involved in brain metabolism, acetyl-CoA production and cholinergic function](#). *Life Sci* 256: 117975.
- Koebele, S. V. and Bimonte-Nelson, H. A. (2016). [Modeling menopause: The utility of rodents in translational behavioral endocrinology research](#). *Maturitas* 87: 5-17.
- Liu, W., Wang, L. Y., Xing, X. X. and Fan, G. W. (2015). [Conditions and possible mechanisms of VCD-induced ovarian failure](#). *Altern Lab Anim* 43(6): 385-392.
- Lukefahr, A. L., Frye, J. B., Wright, L. E., Marion, S. L., Hoyer, P. B. and Funk, J. L. (2012). [Decreased bone mineral density in rats rendered follicle-deplete by an ovotoxic chemical correlates with changes in follicle-stimulating hormone and inhibin A](#). *Calcif Tissue Int* 90(3): 239-249.
- Marcondes, F. K., Bianchi, F. J. and Tanno, A. P. (2002). [Determination of the estrous cycle phases of rats: some helpful considerations](#). *Braz J Biol* 62(4A): 609-614.
- Mayer, L. P., Pearsall, N. A., Christian, P. J., Devine, P. J., Payne, C. M., McCuskey, M. K., Marion, S. L., Sipes, I. G. and Hoyer, P. B. (2002). [Long-term effects of ovarian follicular depletion in rats by 4-vinylcyclohexene diepoxide](#). *Reprod Toxicol* 16(6): 775-781.

- Mitchell, E. S. and Woods, N. F. (1996). [Symptom experiences of midlife women: observations from the Seattle Midlife Women's Health Study](#). *Maturitas* 25(1): 1-10.
- Pestana-Oliveira, N., Kalil, B., Leite, C. M., Carolino, R. O. G., Debarba, L. K., Elias, L. L. K., Antunes-Rodrigues, J. and Anselmo-Franci, J. A. (2018). [Effects of Estrogen Therapy on the Serotonergic System in an Animal Model of Perimenopause Induced by 4-Vinylcyclohexen Diepoxide \(VCD\)](#). *eNeuro* 5(1): ENEURO.0247-17.2017. doi: 10.1523/ENEURO.0247-17.2017.
- Prior, J. C. and Hitchock, C. L. (2011). [The endocrinology of perimenopause: need for a paradigm shift](#). *Front Biosci (Schol Ed)* 3: 474-486.
- Reis, F. M., Pestana-Oliveira, N., Leite, C. M., Lima, F. B., Brandao, M. L., Graeff, F. G., Del-Ben, C. M. and Anselmo-Franci, J. A. (2014). [Hormonal changes and increased anxiety-like behavior in a perimenopause-animal model induced by 4-vinylcyclohexene diepoxide \(VCD\) in female rats](#). *Psychoneuroendocrinology* 49: 130-140.
- Rubin, B. S. (2000). [Hypothalamic alterations and reproductive aging in female rats: evidence of altered luteinizing hormone-releasing hormone neuronal function](#). *Biol Reprod* 63(4): 968-976.
- Sahambi, S. K., Visser, J. A., Themmen, A. P., Mayer, L. P. and Devine, P. J. (2008). [Correlation of serum anti-Mullerian hormone with accelerated follicle loss following 4-vinylcyclohexene diepoxide-induced follicle loss in mice](#). *Reprod Toxicol* 26(2): 116-122.
- Santoro, N., Brown, J. R., Adel, T. and Skurnick, J. H. (1996). [Characterization of reproductive hormonal dynamics in the perimenopause](#). *J Clin Endocrinol Metab* 81(4): 1495-1501.
- Scafuto, M., Pestana-Oliveira, N., Almeida, R. M., Carolino, R. O., Anselmo-Franci, J. A. (2017). [Effects of Hormonal Therapy on Aggressive Behavior and Central Nervous System in an Animal Model of Perimenopause](#). Annual Meeting Society of Neuroscience, DC, USA.
- Schmidt, P. J., Nieman, L., Danaceau, M. A., Tobin, M.B., Roca, C. A., Murphy J. H., Rubinow, D. R. (2000) [Estrogen replacement in perimenopause-related depression: a preliminary report](#). *Am J Obstet Gynecol* 183:414-420.
- Soules, M. R., Sherman, S., Parrott, E., Rebar, R., Santoro, N., Utian, W. and Woods, N. (2001). [Executive summary: Stages of Reproductive Aging Workshop \(STRAW\)](#). *Fertil Steril* 76(5): 874-878.
- Springer, L. N., Flaws, J. A., Sipes, I. G. and Hoyer, P. B. (1996). [Follicular mechanisms associated with 4-vinylcyclohexene diepoxide-induced ovotoxicity in rats](#). *Reprod Toxicol* 10(2): 137-143.
- Wang, Y., Liu, Y., Xiong, J., Di, T., Yuan, Z., Wu, J. and Chen, L. (2019). [Reduced serotonin impairs long-term depression in basolateral amygdala complex and causes anxiety-like behaviors in a mouse model of perimenopause](#). *Exp Neurol* 321: 113030.
- WHO Scientific Group. (1996). [Research on the menopause in the 1990s](#). Geneva: World Health Organization: 1-79.

Ex vivo Tissue Culture Protocols for Studying the Developing Neocortex

Takashi Namba^{1,2,*}, Christiane Haffner¹ and Wieland B. Huttner^{1,*}

¹Max Planck Institute of Molecular Cell Biology and Genetics, 01307 Dresden, Germany

²Neuroscience Center, HiLIFE - Helsinki Institute of Life Science, University of Helsinki, FI-00014 Helsinki, Finland

*For correspondence: takashi.namba@helsinki.fi; huttner@mpi-cbg.de

Abstract

The size of the neocortex and its morphology are highly divergent across mammalian species. Several approaches have been utilized for the analysis of neocortical development and comparison among different species. In the present protocol (Note: This protocol requires basic knowledge of brain anatomy), we describe three *ex vivo* neocortical slice/tissue culture methods: (i) organotypic slice culture (mouse, ferret, human); (ii) hemisphere rotation culture (mouse, ferret); and (iii) free-floating tissue culture (mouse, ferret, human). Each of these three culture methods offers distinct features with regard to the analyses to be performed and can be combined with genetic manipulation by electroporation and treatment with specific inhibitors. These three culture methods are therefore powerful techniques to examine the function of genes involved in neocortical development.

Keywords: Human, Mouse, Ferret, Neocortex, Development, Evolution, Neural stem/Progenitor cells

This protocol was validated in: eLife (2020) DOI: 10.7554/eLife.49808

Background

Several slice/tissue culture methods have been reported for studying brain development ex vivo (Noctor *et al.*, 2001; Miyata *et al.*, 2002; Tabata and Nakajima, 2003; Namba *et al.*, 2007 and 2019; Schenk *et al.*, 2009; Betizeau *et al.*, 2013; Lim *et al.*, 2018; Long *et al.*, 2018; Nakagawa *et al.*, 2019; Güven *et al.*, 2020). In combination with *in/ex utero* and *ex vivo* genetic manipulation techniques [e.g., electroporation (Tabata and Nakajima, 2003; Namba *et al.*, 2014), virus transfection (Noctor *et al.*, 2001), and microinjection (Taverna *et al.*, 2012)], the slice/tissue culture methods allow the investigation of cell behavior by time-lapse imaging (Miyata *et al.*, 2001; Noctor *et al.*, 2001; Tabata and Nakajima, 2003; Namba *et al.*, 2011 and 2014; Taverna *et al.*, 2012; Betizeau *et al.*, 2013; Lim *et al.*, 2018; Long *et al.*, 2018; Nakagawa *et al.*, 2019), signaling pathways by studying the effects of pharmacological reagents (Schenk *et al.*, 2009; Long *et al.*, 2018; Kalebic *et al.*, 2019; Namba *et al.*, 2020), and brain tissue development by immunohistochemistry (Schenk *et al.*, 2009; Long *et al.*, 2018; Güven *et al.*, 2020; Namba *et al.*, 2020) (Figure 1). In the present protocol, we describe three different methods to study developing neocortical tissue: (i) organotypic slice culture (Taverna *et al.*, 2012); (ii) hemisphere rotation (HERO) culture (Schenk *et al.*, 2009); and (iii) free-floating tissue (FFT) culture (Long *et al.*, 2018).

Organotypic slice culture has been widely used over the past few decades (Noctor *et al.*, 2001; Miyata *et al.*, 2002; Tabata and Nakajima, 2003; Namba *et al.*, 2007; Taverna *et al.*, 2012) and readily allows time-lapse imaging of labeled cells (Miyata *et al.*, 2001; Noctor *et al.*, 2001; Tabata and Nakajima, 2003; Namba *et al.*, 2011 and 2019; Taverna *et al.*, 2012; Mora-Bermudez *et al.*, 2014; Long *et al.*, 2018; Nakagawa *et al.*, 2019); however, the tissue can become damaged by slicing. The other two methods may overcome this potential problem. HERO culture was originally described by Schenk and colleagues (Schenk *et al.*, 2009) and has been used for the pharmacological treatment of neocortical tissue (Schenk *et al.*, 2009; Namba *et al.*, 2020). FFT culture has recently been developed and used in our group (Long *et al.*, 2018) to study human neocortical development following pharmacological and genetic manipulation (Long *et al.*, 2018; Kalebic *et al.*, 2019; Kostic *et al.*, 2019; Namba *et al.*, 2020).

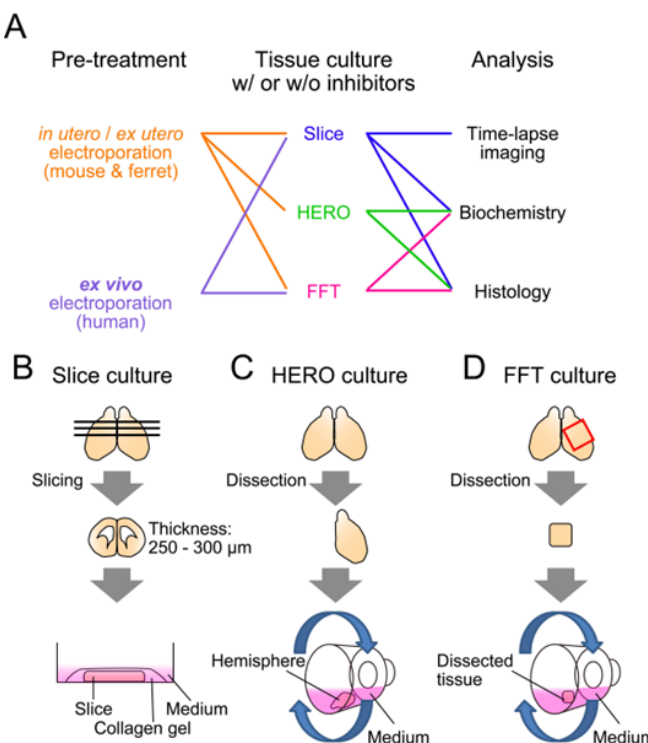


Figure 1. Overview of *ex vivo* slice/tissue culture protocols and their applications.

- A. Summary of the three methods.
- B. Slice culture method.
- C. Hemisphere rotation (HERO) culture method.
- D. Free-floating tissue (FFT) culture method.

The optimal method for a given experiment depends on the species of the sample, the specific application, and the degree of tissue architecture preservation that is required. The cultured slice/hemisphere/tissue can be subjected to histological and biochemical analyses (Long *et al.*, 2018; Kalebic *et al.*, 2019; Kostic *et al.*, 2019; Güven *et al.*, 2020; Namba *et al.*, 2020). Due to the limitation of sample availability, FFT and organotypic slice culture can lend themselves to the analysis of human neocortical development following manipulation of gene function (Long *et al.*, 2018; Kalebic *et al.*, 2019; Kostic *et al.*, 2019; Namba *et al.*, 2020). Time-lapse imaging (Taverna *et al.*, 2012; Mora-Bermudez *et al.*, 2014; Long *et al.*, 2018) is generally performed in organotypic slice culture. If an experiment requires maintenance of intact tissue architecture, HERO and FFT cultures are the methods of choice.

Materials and Reagents

A. Animals and human samples

1. Ferret embryos (E33-E36)
2. Human neocortical tissue [11 post-conception week (PCW)-14 PCW]
3. Mouse embryos [embryonic day (E) 13.5-E15.5]

B. Common materials and reagents

1. Pasteur pipet (*e.g.*, SARSTEDT, catalog number 86.1171.001)
2. Fine-tip Pasteur pipet (*e.g.*, SARSTEDT, catalog number 86.1175.001)
3. 3.5-cm dishes (for time-lapse imaging, use glass-bottomed dishes, *e.g.*, Thermo Fisher Scientific, Nunc, catalog number: 150680)
4. 6-cm Petri dishes (Greiner, catalog number: 628102)
5. 100× N2 supplement (Thermo Fisher Scientific, Invitrogen, catalog number: 17502048)
6. 100× Penicillin-Streptomycin (Merck, Gibco, catalog number: 15140122)
7. 10 mM HEPES-NaOH (pH 7.3)
8. 50× B27 supplement (Thermo Fisher Scientific, Invitrogen, catalog number: 17504044)
9. Knockout Serum Replacement (KOSR, Thermo Fisher Scientific, Gibco, catalog number: 10828028)
10. 200 mM L-glutamine (Thermo Fisher Scientific, Gibco, catalog number: 25030081)
11. Neurobasal medium (Thermo Fisher Scientific, Gibco, catalog number: 21103049)
12. PBS (made in-house)
13. Rat serum (Charles River Laboratories Japan, catalog number: P00052)

C. Organotypic slice culture

1. DMEM-F12 (Merck, catalog number: D8900-10X1L)
2. Low-melting agarose (Merck, catalog number: A2790)
3. Sodium bicarbonate (NaHCO_3) (Merck, catalog number: 1063290500)
4. Type IA collagen (Nitta Gelatin, Cellmatrix, catalog number: 631-00651)
5. Tyrode's salt (Merck, catalog number: T2145)
6. Tyrode's solution (see Recipes)
7. 3% (w/v) low-melting agarose (see Recipes)
8. Slice culture medium for mouse and ferret tissue (SCM, see Recipes)
9. Slice culture medium for human tissue (SCM-KOSR, see Recipes)
10. Collagen gel mixture (see Recipes)

11. Reconstitution buffer (see Recipes)
12. 5× DMEM-F12 solution (see Recipes)

Equipment

1. Cell culture hood/biological safety cabinet for human samples
2. Cell culture incubator
3. Dissection microscope (*e.g.*, Olympus, catalog number: SZX10)
4. Dissection scissors (FST, catalog number: 15000-10)
5. Heating plate (VWR, catalog number: 75838-286)
6. Gas mixture (5% CO₂ + 40% O₂ + 55% N₂ or 5% CO₂ + 60% O₂ + 35% N₂)
7. Scalpels (Surgical Disposable Scalpel, Braun, catalog number: 5518032)
8. Spoon (for HERO culture, FST, catalog number: 10370-19)
9. Spoon (for human tissue samples, chemical spoon)
10. Vibratome (*e.g.*, Leica, catalog number: VT1000S)
11. Water bath
12. Whole-embryo culture bottles (Nakayama, catalog number: 010-032-11)
13. Whole-embryo culture system (Nakayama, catalog number: 10-0310)

Procedure

Part I: Organotypic slice culture

Please see Figure 2 for images of the selected procedures.

A. Dissection and slicing

1. Warm 2 × 50 mL Tyrode's solution, SCM (see below) to 37°C.
2. Melt 3% low-melting agarose in PBS and keep at 37°C.
3. Dissect mouse or ferret embryos in Tyrode's solution (3 embryos per experiment).
4. Move the heads to warm Tyrode's solution (37°C) and dissect the brains one by one in a 6-cm Petri dish.
5. Dissect the telencephala and store on a heating plate in Tyrode's solution.

Note: For human tissues, start from this step.

6. Remove the meninges after incubating the telencephala in Tyrode's solution.
7. Embed the telencephala in low-melting agarose (takes about 30 min).
8. Cut the telencephala in PBS with a vibratome into 250-300-μm slices.
9. Dissect the neocortical region of interest using a scalpel, if necessary.

B. Collagen gel embedding and culture

1. Prepare the collagen gel mixture (see below) on ice under a hood.
2. Transfer the slices, pre-rinsed in collagen, to a dish containing collagen (on ice) using a Pasteur pipet and ensure that the slices are fully immersed in the collagen gel mixture by gently pipetting up and down.
3. Transfer the slices and collagen gel mixture (200-300 μL) to a clean dish.
4. Place the slices in the desired position.
5. Remove the excess collagen using a fine-tip Pasteur pipet (<200 μL).

6. Polymerize the collagen gel on a heating plate at 37°C for 5 min.
7. Transfer the dishes to a cell culture incubator and incubate the slices for 30-40 min.
8. Add 2 ml SCM (for mouse and ferret) or SCM-KOSR (for human) and continue slice culture for the desired time.

Note: Start inhibitor treatment at this step.

9. Keep the slices in the cell culture incubator at 37°C in an atmosphere of 5% CO₂ + 40% O₂ + 55% N₂ for up to two days.

Part II: Hemisphere rotation (HERO) culture

A. Dissection

1. Dissect the mouse or ferret brain from the head and place into a 6-cm Petri dish containing PBS at room temperature.
2. Remove the meninges in PBS.

Note: You do not need to completely remove the meninges. If you are interested in the lateral neocortex, you can keep the meninges in the medial part.

3. Remove the medulla and cerebellum.

B. Culture

1. Warm the SCM to 37°C.
2. Add 1.5 mL SCM to a whole-embryo culture bottle.
3. Transfer the hemisphere(s) to the whole-embryo culture bottle (1-3 hemispheres per bottle) using a spoon.

Note: Start inhibitor treatment at this step.

4. Place the hemispheres in the whole-embryo culture incubator at 37°C, in an atmosphere of 5% CO₂ + 40% O₂ + 55% N₂ for mouse tissue and 5% CO₂ + 60% O₂ + 35% N₂ for ferret tissue, with continuous rotation at 6 rpm for up to two days.

Part III: Free-floating tissue (FFT) culture

A. Dissection and culture of mouse and ferret neocortex

1. Dissect the brain from the head and place in a 6-cm Petri dish containing PBS at room temperature.
2. Remove the meninges in PBS.
3. Dissect the neocortical region of interest using a scalpel and dissection scissors. The size of the tissue is approximately 20-50 mm².
4. Warm the SCM to 37°C.
5. Add 1.5 mL SCM to a whole-embryo culture bottle.

Note: Start inhibitor treatment at this step.

6. Transfer the tissue to the whole-embryo culture bottle (1-2 tissue pieces per bottle) using a spoon.
7. Place the tissue in the whole-embryo culture incubator at 37°C, in an atmosphere of 5% CO₂ + 40% O₂ + 55% N₂ for mouse tissue and 5% CO₂ + 60% O₂ + 35% N₂ for ferret tissue, with continuous rotation at

6 rpm for up to three days.

B. Dissection, pre-incubation, and culture of human neocortex

1. Remove the meninges in PBS.
2. Dissect the neocortical region of interest using a scalpel and dissection scissors. The size of the tissue is approximately 20-50 mm².
3. Warm the SCM to 37°C.
4. Add 1.5 ml SCM-KOSR to a whole-embryo culture bottle.
5. Transfer the tissue to the whole-embryo culture bottle (1-2 tissue pieces per bottle) using a spoon.
6. Pre-incubate the tissues in the whole-embryo culture incubator at 37°C in an atmosphere of 5% CO₂ + 60% O₂ + 35% N₂ with continuous rotation at 6 rpm for 3-5 h.
7. Remove the SCM-KOSR and add 1.5 ml fresh SCM-KOSR to the bottle.

Notes: Start inhibitor treatment at this step.

8. Place the tissues in the whole-embryo culture incubator at 37°C in an atmosphere of 5% CO₂ + 60% O₂ + 35% N₂ with continuous rotation at 6 rpm for up to three days.

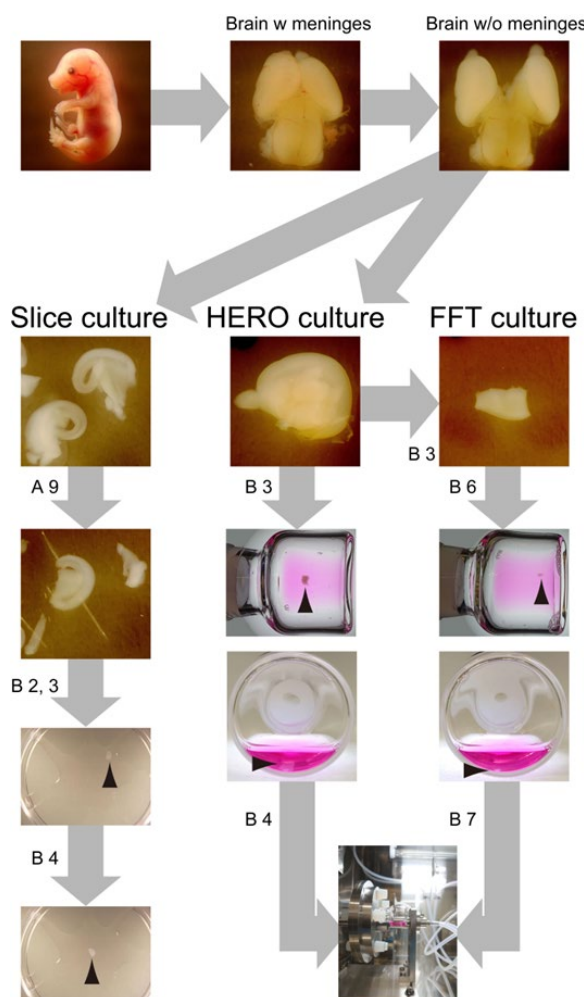


Figure 2. Images illustrating key steps of the *ex vivo* slice/tissue culture protocols.

Representative images of the slice, hemisphere rotation (HERO), and free-floating tissue (FFT) culture methods. The combination of letters and numbers corresponds to the steps of each protocol. Arrowheads indicate the neocortical slices/tissues/hemispheres.

Recipes

1. Lysis buffer (Ingredients/1,000 mL)

- a. Dissolve Tyrode's salt and sodium bicarbonate (NaHCO_3 , 1 g for 1 L) in sterile water
 - b. Add 13 mL 1 M HEPES-NaOH (pH 7.3) for 1 L
- Sterile-filter the solution

2. 3% (w/v) low-melting agarose

- Low-melting agarose (3 g)
Sterile PBS (100 mL)

3. Slice culture medium for mouse and ferret (SCM) tissue, 100 mL

- Neurobasal medium (84 mL)
Rat serum (10%, vol/vol) (10 mL)
200 mM L-glutamine (1 mL)
100× Pen-strep (1 mL)
100× N2 supplement (1 mL)
50× B27 supplement (2 mL)
1 M HEPES-NaOH (pH 7.3) (1 mL)
Store aliquots at -20°C

4. Slice culture medium for human tissue (SCM-KOSR), 100 mL

- Neurobasal medium (84 mL)
KOSR (10%, vol/vol) (10 mL)
200 mM L-glutamine (1 mL)
100× Pen-strep (1 mL)
100× N2 supplement (1 mL)
50× B27 supplement (2 mL)
1 M HEPES-NaOH (pH 7.3) (1 mL)
Store aliquots at -20°C

5. Collagen gel mixture, 2.5 mL

- Type IA collagen (1.25 mL)
Distilled water (0.5 mL)
5× DMEM-F12 solution (0.5 mL)
Reconstitution buffer (0.25 mL)

6. Reconstitution buffer (100 mL)

- NaHCO_3 (262 mM, 2.2 g in 100 mL)
1 M NaOH (5 mL for 100 mL)
1 M HEPES-NaOH (pH 7.3) (20 mL for 100 mL)
Add distilled water to 100 mL
Sterile-filter the solution and store at 4°C in air-tight tubes

7. 5× DMEM-F12 solution (200 mL)

Add 1 bottle DMEM-F12 to 200 mL distilled water

Acknowledgments

This protocol was adapted from Long *et al.* (2018), Güven *et al.* (2020), and Namba *et al.* (2020).

We are grateful to P. Wimberger for providing human fetal samples, and to the Services and Facilities of the Max Planck Institute of Molecular Cell Biology and Genetics for the outstanding support provided, notably J. Helppi and his Biomedical Services (BMS) team. We would like to thank all members of the Huttner group for helpful discussions. We appreciate support from the Laboratory Animal Center of the University of Helsinki. We thank V. Gkini for her technical assistance. We also thank D. Gerrelli, S. Lisgo, and their teams at the HDBR for the invaluable support from this resource. W.B.H. was supported by grants from the DFG (SFB 655, A2), ERC (250197), and ERA-NET NEURON (MicroKin).

Competing interests

The authors declare no competing interests.

Ethics

All animal experiments (mice and ferrets) were performed in accordance with the German Animal Welfare legislation (“Tierschutzgesetz”). All procedures regarding the animal experiments were approved by the Governmental IACUC (“Landesdirektion Sachsen”) and overseen by the Institutional Animal Welfare Officer(s). The mouse embryo shown in Figure 2 was collected with approval from the University of Helsinki.

Fetal human brain tissue (PCW 10-14) was obtained from the Klinik und Poliklinik für Frauenheilkunde und Geburtshilfe, Universitätsklinikum Carl Gustav Carus of the Technische Universität Dresden, with approval from the local University Hospital Ethical Review Committees and informed written maternal consent, and from the Human Development Biology Resource (HDBR), with the human fetal material being provided by the Joint MRC/Wellcome Trust (MR/R006237/1) Human Developmental Biology Resource (<http://www.hdbr.org>).

References

- Betizeau, M., Cortay, V., Patti, D., Pfister, S., Gautier, E., Bellemain-Menard, A., Afanassieff, M., Huissoud, C., Douglas, R. J., Kennedy, H. and Dehay, C. (2013). [Precursor diversity and complexity of lineage relationships in the outer subventricular zone of the primate](#). *Neuron* 80(2): 442-457.
- Güven, A., Kalebic, N., Long, K. R., Florio, M., Vaid, S., Brandl, H., Stenzel, D. and Huttner, W. B. (2020). [Extracellular matrix-inducing Sox9 promotes both basal progenitor proliferation and gliogenesis in developing neocortex](#). *Elife* 9: e49808.
- Kalebic, N., Gilardi, C., Stepien, B., Wilsch-Brauninger, M., Long, K. R., Namba, T., Florio, M., Langen, B., Lombardot, B., Shevchenko, A., Kilimann, M. W., Kawasaki, H., Wimberger, P. and Huttner, W. B. (2019). [Neocortical Expansion Due to Increased Proliferation of Basal Progenitors Is Linked to Changes in Their Morphology](#). *Cell Stem Cell* 24(4): 535-550 e539.
- Kostic, M., Paridaen, J. T. M. L., Long, K. R., Kalebic, N., Langen, B., Grubling, N., Wimberger, P., Kawasaki, H., Namba, T. and Huttner, W. B. (2019). [YAP activity is necessary and sufficient for basal progenitor abundance and proliferation in the developing neocortex](#). *Cell Rep* 27(4):1103-1118.

- Lim, L., Pakan, J. M. P., Selten, M. M., Marques-Smith, A., Llorca, A., Bae, S. E., Rochefort, N. L. and Marin, O. (2018). [Optimization of interneuron function by direct coupling of cell migration and axonal targeting](#). *Nat Neurosci* 21(7): 920-931.
- Long, K. R., Newland, B., Florio, M., Kalebic, N., Langen, B., Kolterer, A., Wimberger, P. and Huttner, W. B. (2018). [Extracellular Matrix Components HAPLN1, Lumican, and Collagen I Cause Hyaluronic Acid-Dependent Folding of the Developing Human Neocortex](#). *Neuron* 99(4): 702-719 e706.
- Miyata, T., Kawaguchi, A., Okano, H. and Ogawa, M. (2001). [Asymmetric inheritance of radial glial fibers by cortical neurons](#). *Neuron* 31(5): 727-741.
- Miyata, T., Kawaguchi, A., Saito, K., Kuramochi, H. and Ogawa, M. (2002). [Visualization of cell cycling by an improvement in slice culture methods](#). *J Neurosci Res* 69(6): 861-868.
- Mora-Bermudez, F., Matsuzaki, F. and Huttner, W. B. (2014). [Specific polar subpopulations of astral microtubules control spindle orientation and symmetric neural stem cell division](#). *Elife* 3: e02875.
- Nakagawa, N., Plestant, C., Yabuno-Nakagawa, K., Li, J., Lee, J., Huang, C. W., Lee, A., Krupa, O., Adhikari, A., Thompson, S., Rhynes, T., Arevalo, V., Stein, J. L., Molnar, Z., Badache, A. and Anton, E. S. (2019). [Memol-Mediated Tiling of Radial Glial Cells Facilitates Cerebral Cortical Development](#). *Neuron* 103(5): 836-852 e835.
- Namba, T., Shinohara, H. and Seki, T. (2019). [Non-radial tortuous migration with cell polarity alterations of newly generated granule neurons in the neonatal rat dentate gyrus](#). *Brain Struct Funct* 224(9): 3247-3262.
- Namba, T., Mochizuki, H., Onodera, M., Namiki, H. and Seki, T. (2007). [Postnatal neurogenesis in hippocampal slice cultures: early in vitro labeling of neural precursor cells leads to efficient neuronal production](#). *J Neurosci Res* 85(8): 1704-1712.
- Namba, T., Mochizuki, H., Suzuki, R., Onodera, M., Yamaguchi, M., Namiki, H., Shioda, S. and Seki, T. (2011). [Time-lapse imaging reveals symmetric neurogenic cell division of GFAP-expressing progenitors for expansion of postnatal dentate granule neurons](#). *PLoS One* 6(9): e25303.
- Namba, T., Doczi, J., Pinson, A., Xing, L., Kalebic, N., Wilsch-Brauninger, M., Long, K. R., Vaid, S., Lauer, J., Bogdanova, A., Borgonovo, B., Shevchenko, A., Keller, P., Drechsel, D., Kurzchalia, T., Wimberger, P., Chinopoulos, C. and Huttner, W. B. (2020). [Human-Specific ARHGAP11B Acts in Mitochondria to Expand Neocortical Progenitors by Glutaminolysis](#). *Neuron* 105(5): 867-881 e869.
- Namba, T., Kibe, Y., Funahashi, Y., Nakamura, S., Takano, T., Ueno, T., Shimada, A., Kozawa, S., Okamoto, M., Shimoda, Y., Oda, K., Wada, Y., Masuda, T., Sakakibara, A., Igarashi, M., Miyata, T., Faivre-Sarrailh, C., Takeuchi, K. and Kaibuchi, K. (2014). [Pioneering axons regulate neuronal polarization in the developing cerebral cortex](#). *Neuron* 81(4): 814-829.
- Noctor, S. C., Flint, A. C., Weissman, T. A., Dammerman, R. S. and Kriegstein, A. R. (2001). [Neurons derived from radial glial cells establish radial units in neocortex](#). *Nature* 409(6821): 714-720.
- Schenk, J., Wilsch-Bräuninger, M., Calegari, F. and Huttner, W. B. (2009). [Myosin II is required for interkinetic nuclear migration of neural progenitors](#). *Proc Natl Acad Sci U S A* 106(38): 16487-16492.
- Tabata, H. and Nakajima, K. (2003). [Multipolar migration: the third mode of radial neuronal migration in the developing cerebral cortex](#). *J Neurosci* 23(31): 9996-10001.
- Taverna, E., Haffner, C., Peppercok, R. and Huttner, W. B. (2011). [A new approach to manipulate the fate of single neural stem cells in tissue](#). *Nat Neurosci* 15(2): 329-337.

Electrophysiological Properties of Neurons: Current-Clamp Recordings in Mouse Brain Slices and Firing-Pattern Analysis

Elina Nagaeva^{1,*}, Ivan Zubarev² and Esa R. Korpi¹

¹Department of Pharmacology, Faculty of Medicine, FI-00014 University of Helsinki, Helsinki, Finland; ²Department of Neuroscience and Biomedical Engineering, Aalto University, 11000 Espoo, Finland

*For correspondence: elina.nagaeva@helsinki.fi

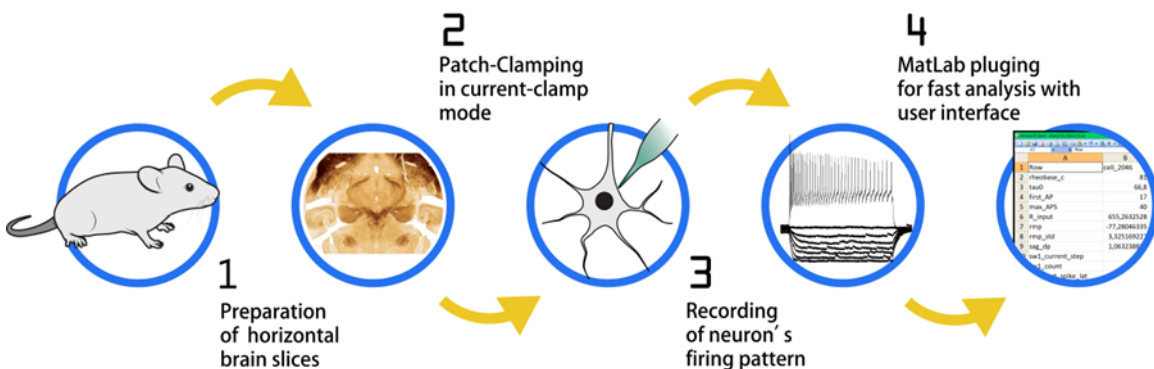
Abstract

Characterization of an electrically active cell, such as a neuron, demands measurement of its electrical properties. Due to differences in gene activation, location, innervation patterns, and functions, the millions of neurons in the mammalian brain are tremendously diverse in their membrane characteristics and abilities to generate action potentials. These features can be measured with a patch-clamp technique in whole-cell current-clamp configuration followed by detailed post-hoc analysis of firing patterns. This analysis can be time-consuming, and different laboratories have their own methods to perform it, either manually or with custom-written scripts. Here, we describe in detail a protocol for firing-pattern registration in neurons of the ventral tegmental area (VTA) as an example and introduce a software for its fast and convenient analysis. With the help of this article, other research groups can easily apply this method and generate unified types of data that are comparable between brain regions and various studies.

Keywords: Patch-clamp, Current-clamp, Action potential, Single-cell electrophysiology, Acute brain slices, Ventral tegmental area, Automated firing pattern analysis

This protocol was validated in: eLife (2020) DOI: 10.7554/eLife.59328

Graphical Abstract:



Workflow of the Protocol

Background

The main feature of a neuron is its ability to engage in fast chemo-electrical communication with other cells. The unique neuronal membrane constitution with a high density of ion channels and other specific proteins allows the generation of an action potential within milliseconds after receiving an adequate input. Therefore, characterization of any neuron would be incomplete without description of the electrical properties of its membrane. For this purpose, we can use a convenient “patch-clamp” technique (Neher and Sakmann, 1976), which resulted from centuries of evolution in electrophysiological methods (Verkhratsky and Parpura, 2014). A big advantage of this method is the possibility to combine it with other modern single-cell approaches and collect all necessary data for defining a neuron’s type. Filling of the cell with intracellular dyes through the patch pipette (Marx *et al.*, 2012) and collecting the cell’s aspirate after electrophysiological registration (Sucher and Deitcher, 1995; Fuzik *et al.*, 2016) allow the simultaneous reconstruction of 3D morphology and analysis of mRNA content and firing pattern of the same cell. There are several types of patch-clamp configurations, but we focus here on the whole-cell current-clamp modification, which allows registering changes in the membrane voltage while controlling the electrical current flow; in other words, it allows registering action potentials (AP) in response to specific current injections.

The whole-cell current-clamp configuration of the patch-clamp technique is a well-established method that has been used for decades in the characterization of intrinsic membrane properties of electrically active cells (Neher and Sakmann, 1976; Andrew, 1986; Sanchez-Aguilera *et al.*, 2020). Although most of the researchers are interested in a similar set of parameters and use similar protocols, the experimental details and final data are variable and, therefore, hard to compare (see <https://neuroelectro.org/article/index>). While preparing to describe somatostatin-expressing neurons in the mouse ventral tegmental area (VTA) for our recent article (Nagaeva *et al.*, 2020), we tried to collect a maximal set of membrane properties for firing pattern analysis based on previous publications (Halabisky, 2006; Ma *et al.*, 2006; Wierenga *et al.*, 2010). The list of these properties can be found in [Nagaeva *et al.*, 2020, Appendix Table 1](#). Similarly, we made a current-stimulation protocol that allowed registering all these properties in one short run. Additionally, we developed a MatLab plugin for fast and convenient extraction of all these parameters.

Our protocol article aims to provide a clear workflow for firing pattern analysis and includes all steps from the preparation of acute brain slices to the final data extraction. It can be applied for electrophysiological studies of previously unknown neurons or as part of the currently popular patch-seq approach (Cadwell *et al.*, 2016; Gouwens *et al.*, 2020). For newly described neurons, the extracted data can be further used for neuron subtyping according to their electrical membrane properties. To do so, one just needs to upload the resulting tables to a clustering algorithm previously published by our group (see further Nagaeva *et al.*, 2020; <https://github.com/elifesciences-publications/clustering-for-nagaeva-et-al.-sst-vta>). This protocol will simplify the firing pattern registration and analysis in future studies.

Materials and Reagents

A. Preparation of acute brain slices

1. Beakers: 1 L, 2 × 250 mL (VWR, catalog numbers: 213-1128, 213-1124)
2. Petri dish 60 × 18 mm (VWR, catalog number: 734-2815p)
3. Tubes for carbogen delivery into solution (Ismatec, catalog number: MF0028)
4. Paint brush (VWR, catalog number: 470020-430)
5. Pasteur pipette with a wide neck (you can simply cut off the tip) (Sarstedt, catalog number: NC9891525)
6. Super glue (Loctite, catalog number: 230992)
7. Filter paper (Whatman, WHA1001110)
8. A box full of crushed ice
9. Medical spatula with smooth ends 150 × 40 × 6 mm (Bochem, VWR catalog number: 231-0601)
10. Carbogen (95% O₂ + 5% CO₂)
11. Floating net for brain slices
A nice one can be 3D-printed from here <https://3dprint.nih.gov/discover/3dpx-001623>.
12. Reagents for Artificial Cerebrospinal Fluid (ACSF) and Cutting solution:
 - a. NaCl (Fisher BioReagents, catalog number: BP358)
 - b. KCl (Amresco, catalog number: 0395)
 - c. MgCl₂·6H₂O (Fisher BioReagents, catalog number: BP214)
 - d. NaH₂PO₄·H₂O (Merck, catalog number: 1.0634)
 - e. NaHCO₃ (Sigma-Aldrich, catalog number: 31437)
 - f. D-(+)-Glucose (Alfa Aesar, catalog number: A16828)
 - g. Sucrose (Fisher Scientific, catalog number: 10634932)
 - h. CaCl₂ (Amresco, catalog number: 0556)

B. Electrophysiology

1. Beakers: 250 and 25 mL (VWR, catalog numbers: 213-1128, 213-1120)
2. 1-mL micropipette (Thermo Scientific, Finnpipette F2)
3. 1.5-mL Eppendorf tubes for intracellular solution (Eppendorf, catalog number: 0030120086)
4. Glass capillaries with filament (World Precision Instruments, catalog number: TW150F-4)
5. Paint brush (VWR, catalog number: 470020-430)
6. Silver/platinum wire or special net for slice holding in the microscopy chamber (see Figure 9)
7. 1 mL syringe (Terumo, catalog number: SS+01T1)
8. Syringe PVDF Durapore filter (Merck Millipore, catalog number: SLGV013SL)
9. Plastic tubing ID 010 × OD 030 (Tygon, catalog number: AAD04091)
10. Reagents for Intracellular solution (IS):
 - a. K-gluconate (Sigma-Aldrich, catalog number: P1847)
 - b. HEPES (Alfa Aesar, catalog number: A14777)
 - c. EGTA (Sigma-Aldrich, catalog number: E4378)
 - d. Na₂-ATP (Sigma-Aldrich, catalog number: A6419)
 - e. Na-GTP (Sigma-Aldrich, catalog number: G8877)
 - f. Na₂-phosphocreatine (Sigma-Aldrich, catalog number: P7936)
 - g. KOH (Sigma-Aldrich, catalog number: 221473)
11. ASCF solution (see Recipes)
12. Cutting solution (see Recipes)
13. Intracellular solution (see Recipes)

Equipment

1. Volumetric flask 1 L (Brand, VWR catalog number: 612-5082)
2. Big scissors (Fiskars, catalog number: 1005151)
3. Small scissors (Bochem, VWR catalog number: 233-2121)
4. Small tweezers 105 mm (Usbeck, VWR catalog number: 232-0094)
5. Scalpel (Swann-morton, VWR catalog number: swan0565)
6. Teaspoon
7. Razor blade for the vibratome (World Precision Instruments, catalog number: 752-1-SS)
8. The same can be used for the brain dissection in Step A2b of the Procedure section.
9. Laboratory scale (0.001-100 g; Mettler PJ360 DeltaRange)
10. pH-meter (Metrohm, 827 pHlab)
11. Magnetic stirrer (Merck, IKA big-squid)
12. Laboratory water bath (Grant Instruments, Bath JB Aqua 12 Plus)
13. Vibratome (Thermo Scientific, Microm HM650V)
14. Osmometer (Advanced Instruments Inc., Model 3320)
15. Micropipette puller (Sutter Instruments, Model P-1000)
16. Epifluorescent microscope (Olympus, BX51WI)
17. Fluorescent light source – 100 W mercury arc lamp with a power supply (Olympus, U-RFL-T)
18. CCD camera (Sony, XC-E150)
19. Heat controller (Warner Electric, TC-324B single channel)
20. Laboratory vacuum pump (KNF, N 811 KTP)
21. Amplifier (Molecular Devices, Axon Instruments, Multiclamp 700B)
22. Digidata (Molecular Devices, Axon Instruments, Model 1322a)
23. Micromanipulators (Sensapex, μ Mp-3)

Software

1. pClamp 8.2 (or later) package (Molecular Devices, <https://www.moleculardevices.com/products/axon-patch-clamp-system/acquisition-and-analysis-software/pclamp-software-suite#Resources>)
2. Software for your microscopy camera
3. MATLAB R2018b (Mathworks, <https://se.mathworks.com/products/matlab.html>)
4. Microsoft Excel 2016 (Microsoft, <https://www.microsoft.com/en-ww/microsoft-365/excel>)

Procedure

A. Preparation of acute brain slices

*Note: Here, we prepare horizontal slices of the mouse midbrain, aiming to patch *dtTomato*-positive fluorescent cells from the VTA. The reader can prepare slices from any other brain area using the same reagents and procedure.*

1. Prepare Artificial Cerebrospinal Fluid (ACSF) and Cutting solutions (see Recipes) if you use juvenile mice younger than P30. Store solutions not longer than 3-4 days at 4°C.

Note: If you are using older animals, see Ting et al. (2018).

- a. Put all powders except CaCl₂ in 1-L beaker and mix with 800 ml MilliQ water using a magnetic

- stirrer. Add CaCl_2 after all other powders are fully dissolved.
- b. Pour the solution into 1-L volumetric flask and adjust the volume. Adjust pH to 7.3-7.4 by bubbling with carbogen.
 2. Prepare your working space for brain dissection.
 - a. Place “dry” instruments in a convenient order to reach them fast: big scissors, small scissors, small tweezers, scalpel, bent piece of filter paper, and waterproof superglue (Figure 1).



Figure 1. Set of “dry” instruments

- b. Put the instruments – teaspoon, razor blade, medical spatula with narrow, smooth ends, and 60-mm Petri dish covered by filter paper – and approximately 250 mL of cutting solution on ice (Figure 2).

Note: The ACSF solution should be chilled to 0°C beforehand and have floating pieces of ice. Aerate the solution with carbogen for 5 min before and during surgery (Figure 2).

Tip: Sharp and convenient instruments ensure the success of any surgical operation. All instruments should be cleaned with MilliQ water after use.



Figure 2. Set of “cold” instruments

- c. Put a 250-mL beaker with constantly aerated 200 mL of ACSF solution and a floating net in a water bath at 33°C (Figure 3).



Figure 3. Beaker filled with ACSF solution and a floating net for incubation of brain slices at 33°C

- d. Prepare vibratome: insert the blade and tune the program. It is convenient to have a small paint brush, small tweezers, and a Pasteur pipette with a wide neck near the vibratome (Figure 4).

Note: We have used a vibratome program with the following parameters: feed=225 μm , frequency=88 Hz, amplitude=0.9 mm, and velocity=0.9 mm/s.



Figure 4. Set of instruments for brain slicing

We recommend having all necessary equipment and instruments at hand range as you would need to move between them quickly. When everything is ready, it is time to start the brain dissection.

3. Brain dissection (approx. 1 min).

Notes:

- a. As the brain cells are very sensitive to hypoxia, and the metabolism is faster in warm environment, it is essential to transfer the brain from a live animal to cold cutting solution as rapidly as possible. We recommend using a stopwatch in the beginning, aiming to finish the whole procedure within 60-80 s.
- b. **Important note:** Consult your local animal welfare authorities for information on the appropriate anesthesia type to use before animal decapitation.
- c. For brain research purposes, authorities sometimes allow fast physical euthanasia of neonatal/juvenile mice with the method of decapitation, but it should be only performed by well-trained personnel.
 - a. Decapitate the mouse with big scissors in one move.
 - b. Cut the skin from the neck to between the eyes with small scissors.
 - c. Cut the skull from the back to the bregma along the midline with the same small scissors. Be careful not to touch the brain surface with the scissors.
 - d. Open the skull half by half with small tweezers from the midline to the side.

Note: It is very important to choose appropriate tweezers and use them carefully, especially if your target is the cerebral cortex.

- e. Use the scalpel to cut out unnecessary parts of the brain within the skull. We cut out half of the cerebellum and frontal pole, as shown in Figure 5.

Note: From here on, all cutting procedures aim at getting midbrain horizontal slices and should be revised for obtaining other brain regions of interest.

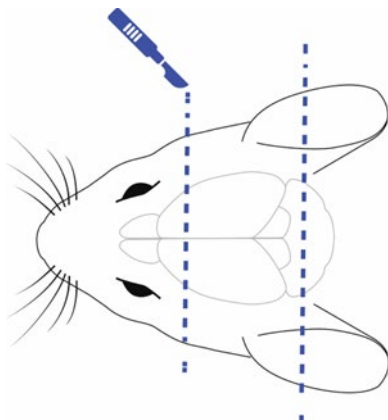


Figure 5. Schematic representation of mouse head with the brain inside.

Dashed lines illustrate scalpel cuts.

Note: Here, we switch to “cold” instruments and environment to slow down the metabolism.

- f. Take out the brain from the skull with the help of a medical spatula and immediately transfer it into the cold aerated cutting solution. Leave it there for 1 min while preparing the cold vibratome platform for supergluing the brain.
4. Brain slicing (max 5-10 min).

Note: Background knowledge on the use of the vibratome is required to perform brain slicing.

- a. Take out the brain from the cutting solution with a teaspoon and put it onto the Petri dish with the cortex facing down (that is, “on the cortex”). Then, you can cut out all unnecessary parts with a cold razor blade if you did not do so already before taking the brain out from the skull (see above).
- b. Put a small drop of superglue onto the vibratome platform and immediately transfer the brain onto it with the help of the bent piece of filter paper. Do not change brain orientation (ventral part is up) and glue it so that the cerebellum is facing the vibratome blade.
- c. Place the platform into the buffer tray and fill up the tray with the cold aerated cutting solution (Step A3f).
- d. With the help of small tweezers, carefully take off the filter paper, which still is stuck to the brain.

Note: If you would like to extend the time of slicing, you can aerate the cutting solution also in the buffer tray.

- e. When the brain is placed as shown in Figure 6, it is ready for making horizontal midbrain slices. Carefully cut away unnecessary upper slices with 225- μm steps until the brain and cerebellum are fully connected. At this level [corresponds to -4.72 from Bregma (Franklin and Paxinos, 2008)], you will also see a distinctive “circle” in the center of the slice (see Figure 7). The next slice is the first midbrain slice that contains the VTA.

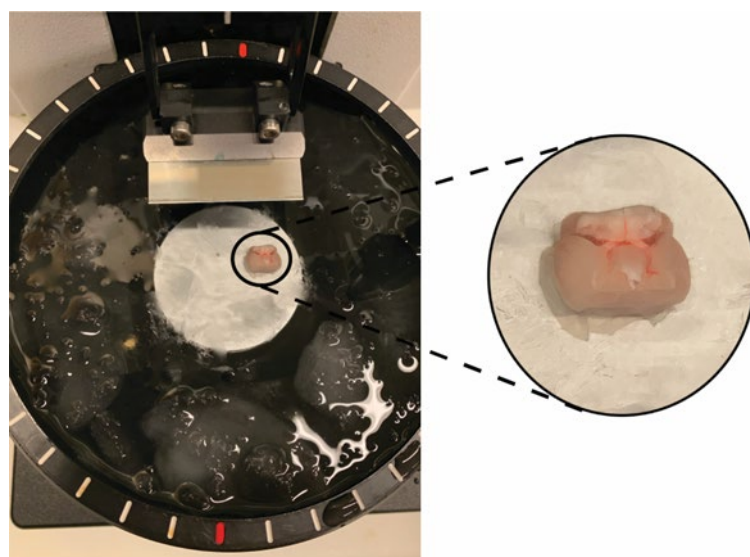


Figure 6. Orientation of the brain inside the vibratome tray.

The ventral part up and cerebellum is facing the blade. The right part of Figure 6 shows a close-up of the brain inside the tray.

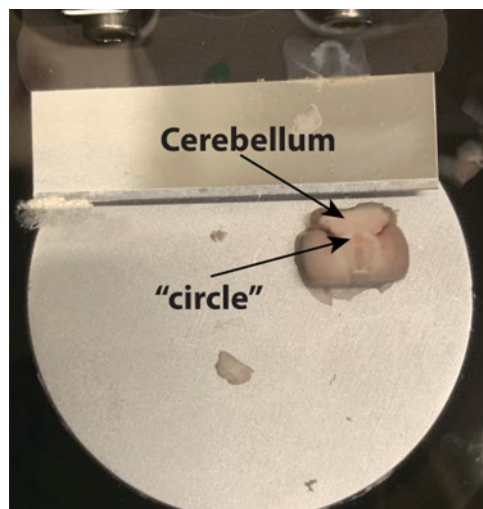


Figure 7. The correct level to start cutting horizontal VTA-containing slices (approximately at -4.72 from Bregma)

- f. It is possible to get two or three 225- μm -thick horizontal slices from the mouse VTA, which correspond to Bregma levels of about -4.72 mm, -4.56 mm, and -4.28 mm.
- g. Transfer the resulting slices into 33°C ACSF solution with the help of a Pasteur-pipette immediately after cutting each slice.
- h. Incubate the slices at 33°C for 60 min; then, keep the beaker with slices at room temperature. The slices are viable for at least 4 h. We start electrophysiology right after 60 min of incubation at 33°C.

Note: It is critical that during incubation the slices are continuously aerated but do not float around because of the bubbles.

B. Electrophysiology

Note: Previous theoretical knowledge on electrophysiology and technical training in cell patching are required to perform further protocol steps.

1. Prepare K-gluconate-based Intracellular solution (IS).
 - a. Mix all reagents with 15 mL of MilliQ water in a 20-mL beaker.
 - b. Put the beaker on ice before adding ATP, GTP, and phosphocreatine.

Note: From here on, try to keep the solutions cold all the time, as ATP and GTP are sensitive to temperature.

- c. While mixing with a magnetic stirrer, measure the pH and adjust to 7.2 with KOH.
- d. Measure osmolarity and adjust it to 285 mOsm by adding MilliQ water milliliter by milliliter.
- e. Aliquot the IS solution in 1.5-mL Eppendorfs and store at -20°C for a maximum 2-3 months.

Note: Thaw an Eppendorf tube containing IS every time just prior to the experiment and remember to keep it cold during the experiment (on ice or in the fridge at 4°C).

2. Prepare 3-5 MΩ glass electrodes from borosilicate capillaries according to puller manufacturer's instructions. We recommend preparing electrodes with a 4-step program. Figure 8 depicts our program for the Sutter P-1000 puller as an example. Note that parameters might be different depending on the capillaries' RAMP test result (melting point temperature) and puller type.

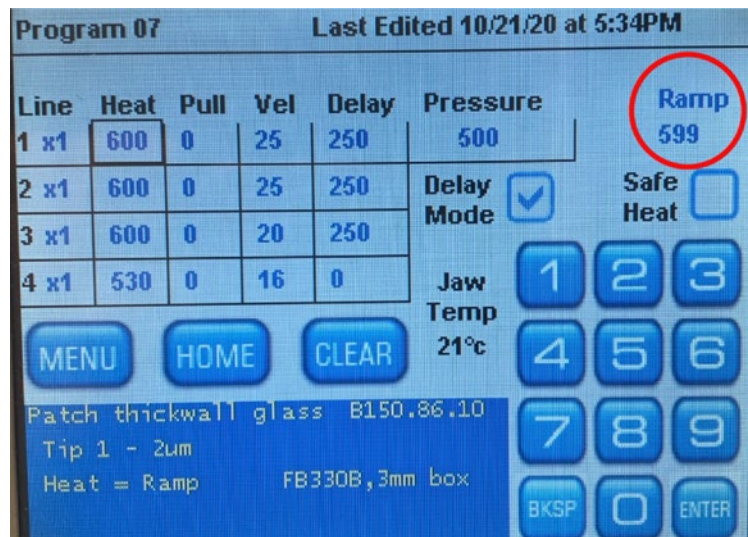


Figure 8. Example of the Sutter P-1000 puller program for suitable glass electrode preparation. Please note the RAMP.

3. Prepare your electrophysiological setup for patching.
 - a. Switch on the computer, fluorescent lamp, bright-field lamp, camera, solution heat controller, vacuum pump, amplifier, digidata, and manipulators.
 - b. Prepare a 250-mL beaker with a constantly aerated ACSF solution. Tune the perfusion speed to 1-3 mL/min for a 1-mL recording chamber. Tune the heat controller to keep the solution at 33°C.
4. Patching.
 - a. Transfer a slice from the incubation beaker into the recording chamber with a wide-neck Pasteur pipette.

- b. Place the brain slice in the middle of the chamber with the cerebellum in its lower part, as shown in Figure 9. Press the slice down with a silver wire or special net slice holder.

Note: The brain slice should be at the bottom of the recording chamber and remain stationary during the solution flow.

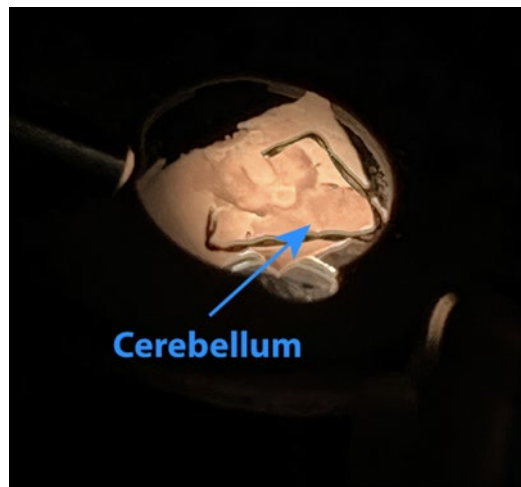


Figure 9. Orientation of the brain slice within the recording chamber with the cerebellum toward the researcher.

A silver wire holds the slice at the bottom of the chamber.

- c. Fill up the glass electrode with cold IS solution and attach it to the headstage.

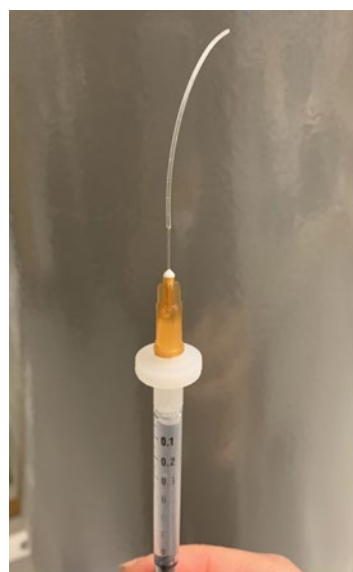


Figure 10. Example of the custom-made syringe for filling the intracellular solution

Tip: You can make a very convenient syringe for IS filling (Figure 10) by using a 1 ml syringe, a Merck Millex Durapore filter, and a piece of flexible plastic tubing ID 010 × OD 030.

- d. Make positive pressure in the patch pipette by blowing into the tube and close it with a valve (Figure 11).

Tip: To check whether the pressure is good enough, you can open the valve near your ear. If the pressure is good, you should hear a hollow flop.

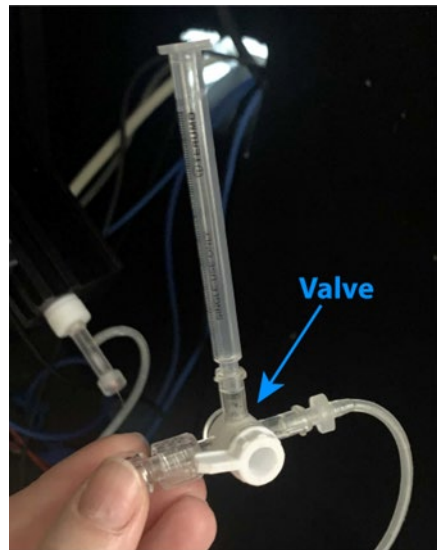


Figure 11. The tube and valve set is connected to the headstage for making positive/negative pressure inside the glass electrode

- e. Put the electrode down into the solution and check the resistance of the pipette in the Seal Test window (Figure 12). It should be 3-5 M Ω . Reset the pipette offset to 0 mV.

Note: From here to step (v), the amplifier is in Voltage Clamp (VC) mode. While searching for a cell, the voltage is not clamped.

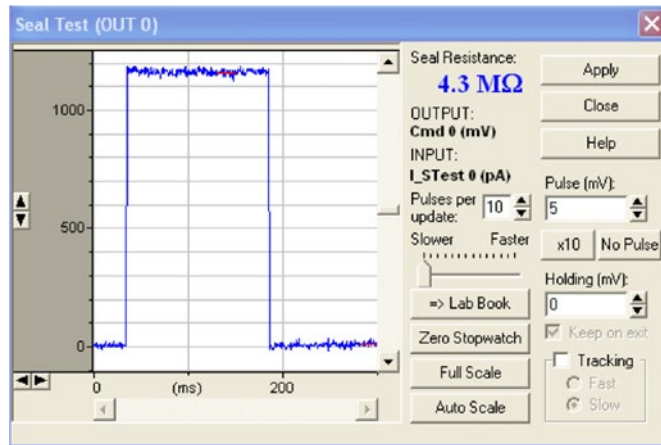


Figure 12. Seal test window showing the pipette resistance of 4.3 M Ω

- f. Locate the pipette over the region of interest under small magnification, e.g., 5 \times . To patch cells in the VTA, locate the pipette over the region shown in Figure 13.

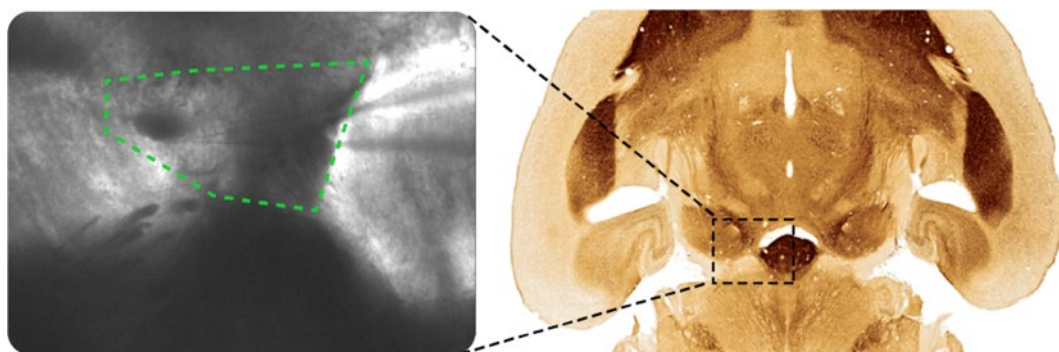


Figure 13. VTA region (marked with green dashed line on the left) under a microscope 5 \times magnification

Note: For convenience, the right image shows the same midbrain region marked with a dark dashed line within the horizontal brain slice at -4.72 cm from the bregma (Franklin and Paxinos, 2008).

- g. Go down with the pipette at 4/5 manipulator speed until the pipette is slightly above the slice focus.
- h. Switch to a higher magnification (e.g., 40 \times) and find the pipette.
- i. Switch to camera view.
- j. Slow down manipulator speed to 2-3/5 and slowly go down towards the slice surface, first with the objective and then with the pipette.
- k. Stop the pipette right above the slice surface.

Tip: At this level, you can already evaluate the condition of the slice. If there are many bubbled cells on the surface, it might be difficult to find a healthy cell in the slice.

- l. Dim the light and switch to fluorescence. Search a healthy neuron with the objective. Do not move the objective too far; otherwise, it will be difficult to find your pipette again.

Note: An unhealthy neuron is usually round, has clear visible nuclei, and an unclear or, sometimes, very contrasting contour.

- m. After finding a suitable neuron, remember its location. You can put some sign on the screen or mark it otherwise (Figure 14).

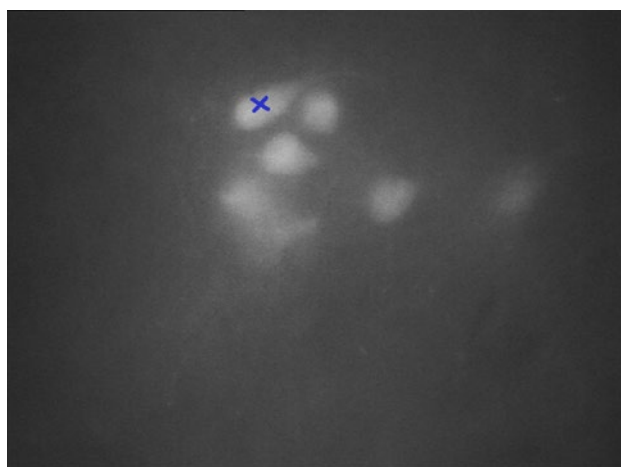


Figure 14. Neurons expressing a fluorescent marker protein under the microscope at 40 \times magnification.

The blue cross indicates a neuron suitable for patching.

- n. Go up with the objective and find the pipette. Move it to the neuron's location above the slice.
- o. Blow into the tube to make sure there is a positive pressure inside the pipette. Reset the pipette offset to 0 mV once more. Pipette resistance must be stable all the time you go down towards the neuron.
- p. Go down to the cell at the slowest manipulator speed. Follow the pipette resistance.
- q. When the resistance rises by 0.1-0.2 M Ω (you might also see a small black dot on the cell, which corresponds to the pipette shadow), release the pipette pressure by opening the valve. Simultaneously, make a slight negative pressure in the pipette by sucking or with the help of a syringe.
- r. At this point, resistance rises to G Ω values (named gigaseal) (Figure 15), which is the first indication of a successful patch.

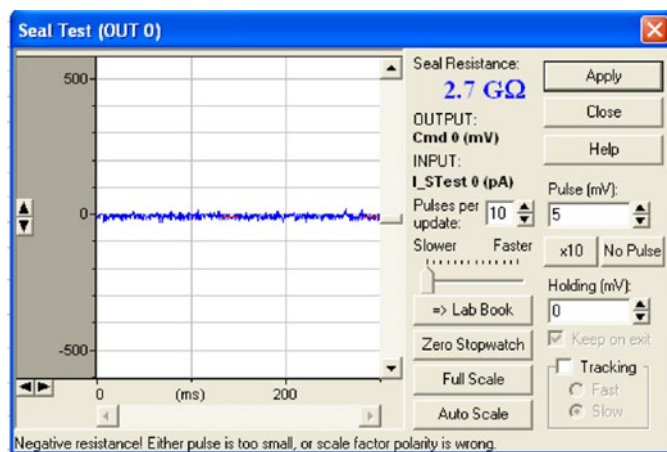


Figure 15. Seal test window showing the gigaseal configuration (Seal Resistance = 2.7 G Ω)

- s. Clamp the holding potential at -70 mV; compensate fast and slow capacitances by clicking c-fast and c-slow buttons to get rid of transient currents. Hold the cell at gigaseal for 1-2 min to make the contact more stable.
- t. Break the membrane by making a strong but short suction to establish a whole-cell configuration.

Note: At this point, the electrode and neuron become one electrical unit. This allows registration of the currents flowing through the neuronal channels and/or changes in the whole-cell membrane voltage.

- u. Immediately after the breakage, switch to the Membrane Test window and read the cell parameters (Figure 16).

*Notes: It is good to know the cell's capacitance (**Cm** in pF), access resistance (**Ra** in M Ω), and holding current (**Hold** in pA).*

- i. ***Cm** may vary depending on the cell size and usually is the 10-100 pF range. You can use this parameter for further characterization of the neuron along with other parameters extracted from the firing pattern analysis.*
- ii. ***Ra** shows the quality of the contact between the glass electrode and cell membrane; it should not exceed 20 M Ω . If it does, just try to suck a bit one more time and re-break the membrane.*

- iii. **Hold** shows the applied current that is required to hold the cell at a certain voltage (-70 mV in our case); this value should be between 0 and -50 pA.
- v. Switch to the I=0 mode and read the neuron's Resting Membrane Potential (RMP) in the MultiClamp software window V (mV).

Note: Please, make a note of the liquid junction potential (LJP), which appears between two liquids with different ionic compositions. For extracellular ACSF and IS solutions used here, LJP is +12 mV. Usually, we do not correct it during recordings but always mention it in the Method section.

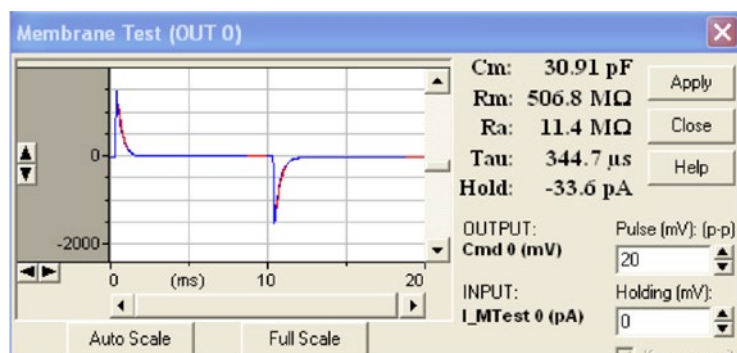


Figure 16. Membrane Test window showing a successful whole-cell configuration in voltage-clamp mode and several cell parameters

- w. Switch to the Current Clamp (IC) mode and run the current-steps protocol provided below (Figure 17).

Notes:

- We do not recommend injecting any current in the current-clamp mode unless you are sure of the normal RMP for a certain cell type.
- The episodic stimulation protocol lasts 2 s. It includes an 800-ms current step ranging from -60 to 680 pA in 10-pA increments and a 1.2-s recovery pause to allow the cell to get back to its normal RMP. This pause might be longer, depending on cell type and stimulation intensity.
- If you want to define AP threshold and rheobase current more precisely, you can additionally run a similar protocol from 0 to 30-50 pA in 1-pA increments.

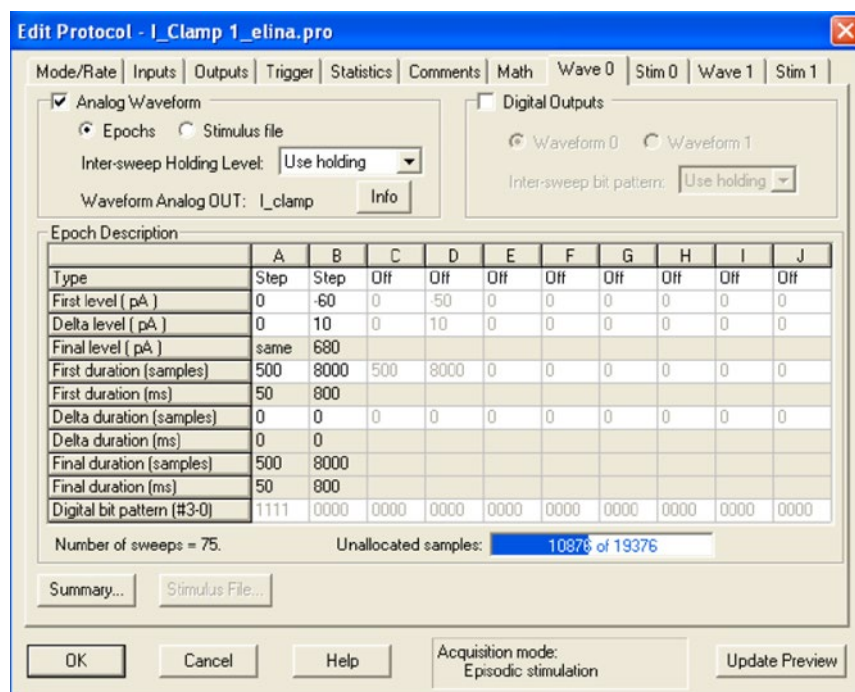


Figure 17. Recommended protocol for current-steps: 800-ms current steps from -60 pA to +680 pA in 10-pA increments

Data analysis

The features from raw *.abf traces are extracted in a semi-automatic way using FFFPA (fast-forward firing pattern analysis), an open-source plugin for MATLAB. FFFPA provides a flexible method to detect the most common parameters of APs (including peaks, thresholds, and AHPs) (Figure 18) and compute the most frequently analyzed features automatically, allowing to process of large batches of files quickly and accurately. Results of the automatic detection are visualized and can be inspected and adjusted manually if needed. Detailed definitions of the extracted features are summarized in [Nagaeva et al., 2020, Appendix Table 1](#).

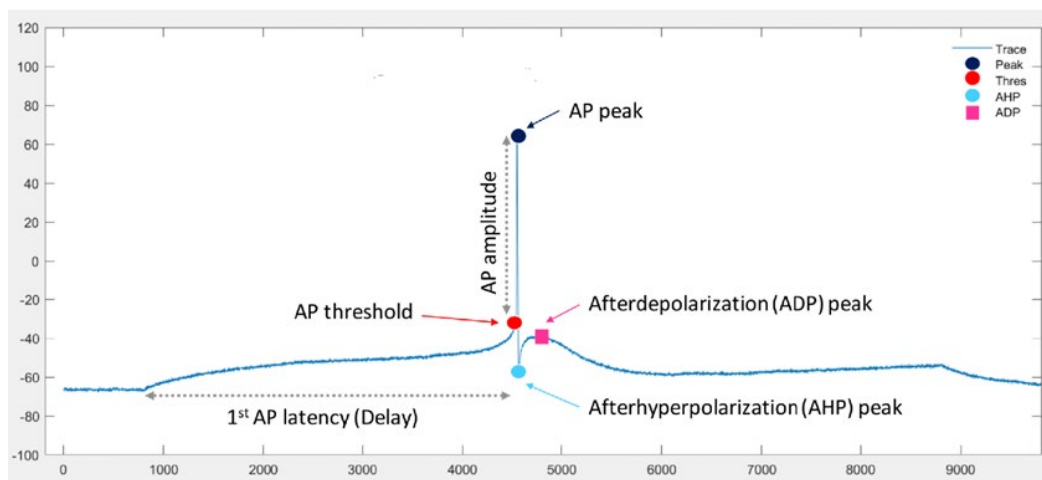


Figure 18. Basic parameters of action potential (AP), which are detected automatically by the FFFPA plugin.

For definition of the parameters, see [Nagaeva et al., 2020, Appendix Table 1](#).

Installation

1. Installation requires MATLAB 2018a or a newer version with Signal Processing and Curve Fitting toolboxes.
2. Download the FFFPA plugin from <https://github.com/zubara/fffpa> and unzip it to a local directory.
3. Double-click on the ‘fffpa.mlappinstall’ file from MATLAB file explorer.
4. Click “Install” in the opened dialog window.
5. Once installed, open the app from the MATLAB Apps toolbar. The graphical user interface for data import will appear (Figure 19).

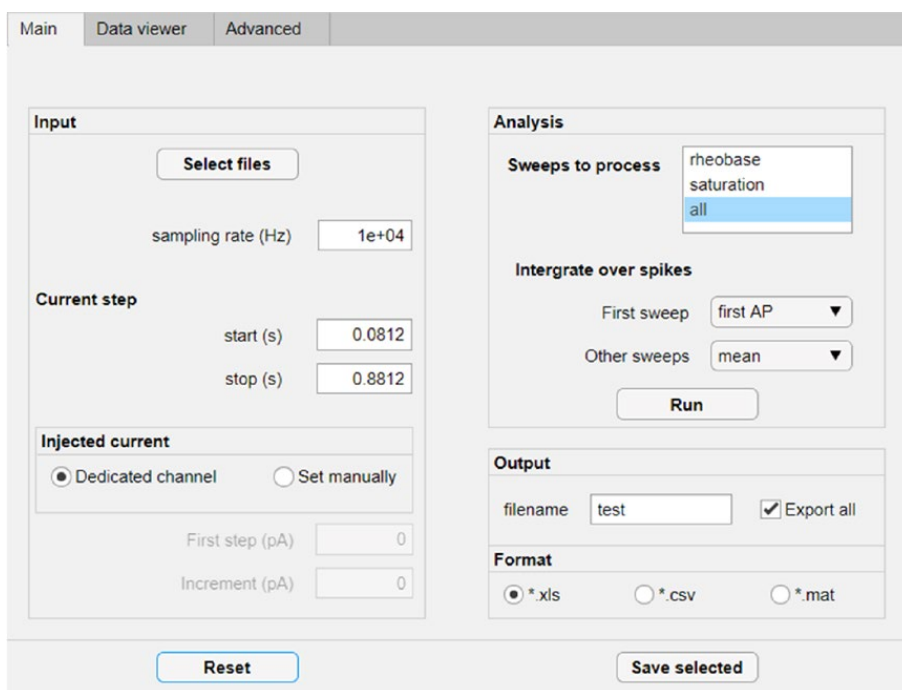


Figure 19. FFFPA graphical user interface for data import

Data import

1. Click “Select files” and choose one or several ‘.abf’ files to process.
2. Specify the sampling frequency in Hz and the time of the onset and the offset of the injected current step in seconds.
3. Choose the sweeps that you wish to analyze. FFFPA can detect, for example, the rheobase current step defined as the first sweep where APs occurred, or the saturation current step defined as the sweep with the maximum number of APs.
4. Specify the summary statistics for the analyzed APs. If multiple sweeps are analyzed, these options can differ between the first and other sweeps.
5. Specify the filename and the desired output format.

Event detection and feature extraction

1. (Optional) Go to the ‘Advanced’ tab (Figure 20) to specify the features that you wish to extract from the traces. Detailed definitions of the extracted features are summarized in [Nagaeva et al., 2020, Appendix Table 1](#).

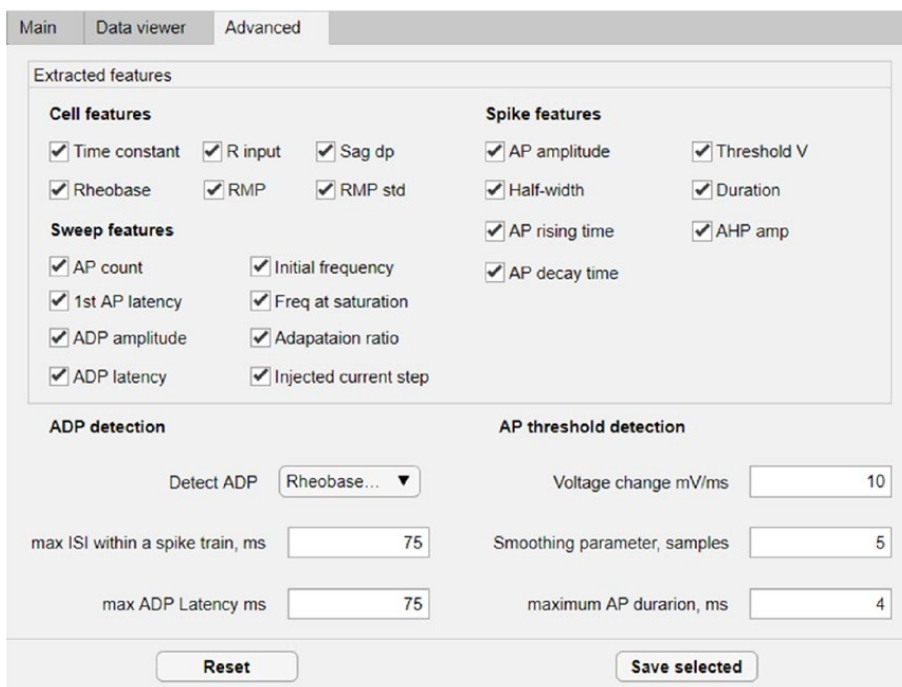


Figure 20. FFFPA feature selection and advanced options tab

- Click the ‘Run’ button on the ‘Main’ tab (Figure 19).

Inspection and manual correction of detection results

- To inspect the results of automatic feature detection, go to the ‘Data viewer’ tab (Figure 21). This tab opens automatically after clicking ‘Run’ once the data is processed.
- The plot area displays the raw trace and the detected events AP peaks (blue circles), activation thresholds (red), afterhyperpolarization (AHP, cyan), and afterdepolarization (ADP, not shown). Please note that, by default, the ADP is only detected after the first AP or train of APs at rheobase.
- Use the ‘Next’ button to go through all sweeps of all analyzed cells consecutively or use the ‘cell ID’ and ‘sweep #’ fields to navigate to the specific sweep of the specific cell manually.
- If needed, the Data viewer allows you to correct the detection results. To do this, first click ‘Edit,’ then click the element that you want to adjust and specify its new position by clicking on the trace. To correct another point, click “Z” to activate the editing option again. After all corrections have been made, press ‘X’ to save the results.
- You can also discard the current cell from the output by unchecking the ‘Save to output’ box.
- Once satisfied with the results, click ‘Save selected.’ This step will compute features based on the (adjusted) detections and save the output file to disk. The summary file can be found in the same directory as the input data.

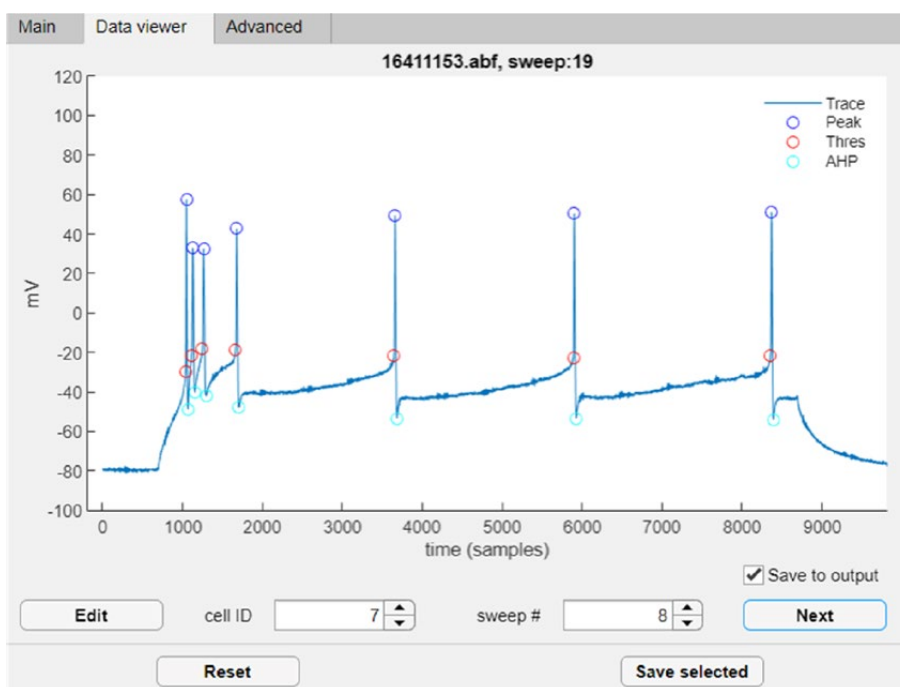


Figure 21. FFFPA Data viewer tab

Notes

You can watch a short tutorial for the FFFPA plugin here: <https://vimeo.com/497798349>.

Recipes

Note: All recipes should be made in MilliQ water.

1. Artificial Cerebral Spinal Fluid (ACSF) solution (Table 1)

Table 1. Artificial Cerebral Spinal Fluid (ACSF) solution recipe

ACSF solution	Concentration in mM	g/L
NaCl	126	7.36
KCl	1.6	0.12
MgCl ₂ ·6H ₂ O	1.2	0.243
NaH ₂ PO ₄ ·H ₂ O	1.2	0.166
NaHCO ₃	18	1.5
D-Glucose	11	1.98
CaCl ₂	2.5	0.37
Carbogen needed for pH adjustment	final pH 7.3-7.4	Final osmolarity: 300-310 mOsm

2. Sucrose-based cutting solution (Table 2)

Table 2. Sucrose-based cutting solution recipe

Cutting solution	Concentration in mM	g/L
NaCl	60	3.506
KCl	2	0.148
MgCl ₂ ·6H ₂ O	8	1.626
NaH ₂ PO ₄ ·H ₂ O	1.2	0.172
NaHCO ₃	30	2.52
D-Glucose	10	1.802
Sucrose	140	47.922
CaCl ₂	0.3	0.044
Carbogen needed for pH adjustment		Final osmolarity: 300-310 mOsm

3. Potassium gluconate-based intracellular solution (Table 3)

Table 3. Potassium gluconate-based intracellular solution recipe

Intracellular solution	Concentration in mM	g/20 mL
K-gluconate	130	0.609
NaCl	6	0.007
HEPES	10	0.047
EGTA	0.5	0.004
Na ₂ -ATP	4	0.044
Na-GTP	0.35	0.004
Na ₂ -phosphocreatine	8	0.041
KOH for pH adjustment	final pH 7.2-7.3	Final osmolarity: 280-290 mOsm

Acknowledgments

This work was supported by grants from the Academy of Finland (1317399), The Finnish National Agency for Education EDUFI, and the Sigrid Juselius Foundation.

The protocol described here was adapted from a previous publication: Nagaeva, E., Zubarev, I., Bengtsson Gonzales, C., Forss, M., Nikouei, K., de Miguel, E., Elsila, L., Linden, A. M., Hjerling-Leffler, J., Augustine, G. J. and Korpi, E. R. (2020). [Heterogeneous somatostatin-expressing neuron population in mouse ventral tegmental area](#). *Elife* 9: e59328. doi: 10.7554 (Nagaeva *et al.*, 2020).

Competing interests

The authors declare no competing interests.

Ethics

Animal procedures described in the current protocol were authorized by the National Animal Experiment Board in Finland (Eläinkoelautakunta, ELLA; Permit Number: ESAVI/1172/04.10.07/2018).

References

- Andrew, R. D. (1986). [Intrinsic membrane properties of magnocellular neurosecretory neurons recorded *in vitro*. Fed Proc](#) 45(9): 2306-2311.
- Cadwell, C. R., Palasantza, A., Jiang, X., Berens, P., Deng, Q., Yilmaz, M., Reimer, J., Shen, S., Bethge, M., Tolias, K. F., Sandberg, R. and Tolias, A. S. (2016). [Electrophysiological, transcriptomic and morphologic profiling of single neurons using Patch-seq. Nat Biotechnol](#) 34(2): 199-203.
- Franklin, K.B.J. and Paxinos, G. (2008). The Mouse Brain in Stereotaxic Coordinates, 3rd Ed. Elsevier, Amsterdam.
- Fuzik, J., Zeisel, A., Mate, Z., Calvignoni, D., Yanagawa, Y., Szabo, G., Linnarsson, S. and Harkany, T. (2016). [Integration of electrophysiological recordings with single-cell RNA-seq data identifies neuronal subtypes. Nat Biotechnol](#) 34(2): 175-183.
- Gouwens, N. W., Sorensen, S. A., Baftizadeh, F., Budzillo, A., Lee, B. R., Jarsky, T., Alfiler, L., Baker, K., Barkan, E., Berry, K., Bertagnolli, D., Bickley, K., Bomben, J., Braun, T., Brouner, K., et al. (2020). [Integrated Morphoelectric and Transcriptomic Classification of Cortical GABAergic Cells. Cell](#) 183(4): 935-953 e919.
- Halabisky, B., Shen, F., Huguenard, J. R. and Prince, D. A. (2006). [Electrophysiological classification of somatostatin-positive interneurons in mouse sensorimotor cortex. J Neurophysiol](#) 96(2): 834-845.
- Ma, Y., Hu, H., Berrebi, A. S., Mathers, P. H. and Agmon, A. (2006). [Distinct subtypes of somatostatin-containing neocortical interneurons revealed in transgenic mice. J Neurosci](#) 26(19): 5069-5082.
- Marx, M., Gunter, R. H., Hucko, W., Radnikow, G. and Feldmeyer, D. (2012). [Improved biocytin labeling and neuronal 3D reconstruction. Nat Protoc](#) 7(2): 394-407.
- Nagaeva, E., Zubarev, I., Bengtsson Gonzales, C., Forss, M., Nikouei, K., de Miguel, E., Elsila, L., Linden, A. M., Hjerling-Leffler, J., Augustine, G. J. and Korpi, E. R. (2020). [Heterogeneous somatostatin-expressing neuron population in mouse ventral tegmental area. Elife](#) 9: e59328.
- Neher, E. and Sakmann, B. (1976). [Single-channel currents recorded from membrane of denervated frog muscle fibres. Nature](#) 260(5554): 799-802.
- Sanchez-Aguilera, A., Monedero, G., Colino, A. and Vicente-Torres, M. A. (2020). [Development of Action Potential Waveform in Hippocampal CA1 Pyramidal Neurons. Neuroscience](#) 442: 151-167.
- Sucher, N. J. and Deitcher, D. L. (1995). [PCR and patch-clamp analysis of single neurons. Neuron](#) 14(6): 1095-1100.
- Ting, J. T., Lee, B. R., Chong, P., Soler-Llavina, G., Cobbs, C., Koch, C., Zeng, H. and Lein, E. (2018). [Preparation of Acute Brain Slices Using an Optimized N-Methyl-D-glucamine Protective Recovery Method. J Vis Exp](#)(132).
- Verkhratsky, A. and Parpura, V. (2014). [History of electrophysiology and the patch clamp. Methods Mol Biol](#) 1183: 1-19.
- Wierenga, C. J., Mullner, F. E., Rinke, I., Keck, T., Stein, V. and Bonhoeffer, T. (2010). [Molecular and electrophysiological characterization of GFP-expressing CA1 interneurons in GAD65-GFP mice. PLoS One](#) 5(12): e15915.

A Method for Estimating the Potential Synaptic Connections Between Axons and Dendrites From 2D Neuronal Images

Carolina Tecuati[#], Dick W. Wheeler[#] and Giorgio A. Ascoli^{*}

Center for Neural Informatics, Structures, & Plasticity, Krasnow Institute for Advanced Study; and Bioengineering Department, Volgenau School of Engineering, George Mason University, Fairfax, VA 22030-4444, USA

*For correspondence: ascoli@gmu.edu

[#]Contributed equally to this work

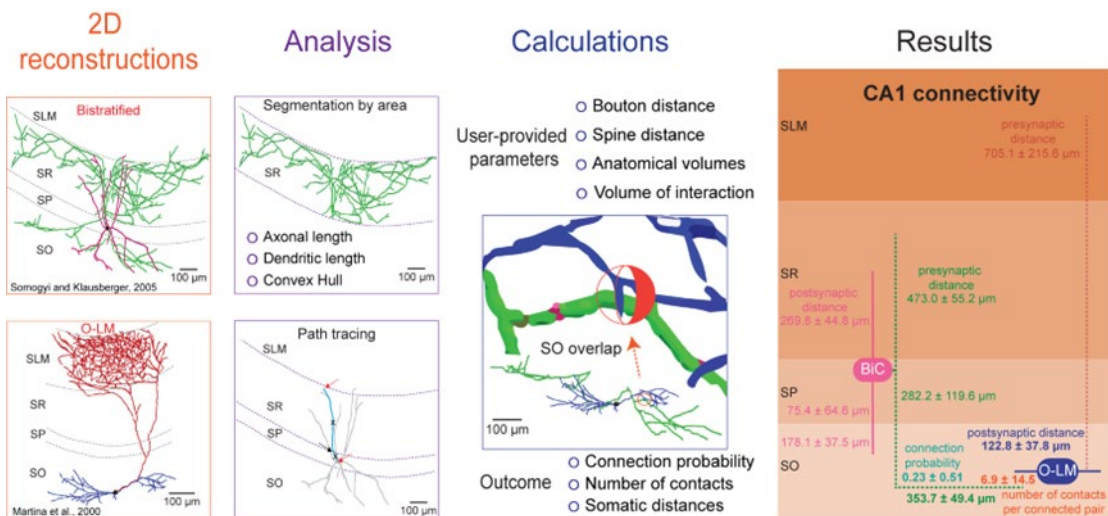
Abstract

Computational neuroscience aims to model, reproduce, and predict network dynamics for different neuronal ensembles by distilling knowledge derived from electrophysiological and morphological evidence. However, analyses and simulations often remain critically limited by the sparsity of direct experimental constraints on essential parameters, such as electron microscopy and electrophysiology pair/multiple recording evidence of connectivity statistics. Notably, available data are particularly scarce regarding quantitative information on synaptic connections among identified neuronal types. Here, we present a user-friendly data-driven pipeline to estimate connection probabilities, number of contacts per connected pair, and distances from the pre- and postsynaptic somas along the axonal and dendritic paths from commonly available two-dimensional tracings and other broadly accessible measurements. The described procedure does not require any computational background and is accessible to all neuroscientists. This protocol therefore fills the important gap from neuronal morphology to circuit organization and can be applied to many different neural systems, brain regions, animal species, and data sources.

Keywords: Synaptic connectivity, Neuronal network, Connection probabilities, Contacts, Convex hull, Propagation error, Axonal-dendritic overlap

This protocol was validated in: J Neurosci (2021) DOI: 10.1523/JNEUROSCI.1193-20.2020

Graphical Abstract:



The processing protocol from 2D reconstructions to quantitated synaptic connections

Background

Synaptic connectivity is a key determinant of the interaction between neurons, and its quantitation is pivotal to understanding the organization of brain circuits and the relationship with network function (Ascoli and Atkeson, 2005). Current knowledge of synaptic probability relies on empirical evidence, which is limited by the number of simultaneously recorded neurons (*e.g.*, by pair recording, octopatch, multielectrode array) and affected by experimental conditions (*in vitro* vs. *in vivo*, slice orientation and thickness, distance between cells, *etc.*). Connections in a particular brain region are often probed by evoked responses upon stimulation of the afferent fiber tracts; however, such tests do not allow the identification of the specific neuronal types involved (Moradi and Ascoli, 2020). Alternatively, synaptic connectivity can be calculated computationally by embedding three-dimensionally (3D) reconstructed neuronal morphologies into 3D brain atlases and counting the possible locations of axonal-dendritic overlap (Ropireddy and Ascoli, 2011). Nevertheless, this approach requires a large amount of labor-intensive data, is limited by the precision of the 3D registration, and has so far proven impractical to scale up.

Despite its importance, connectivity information remains incomplete for most animal species and neural systems (Rees *et al.*, 2017). This protocol describes a simple process for the extraction of important quantitative synaptic parameters – namely the connection probability, number of contacts per connected pair, and distance from the pre- and postsynaptic somas along the neurite paths – from commonly available two-dimensional images of axonal and dendritic morphology. To the best of our knowledge, there are no alternative solutions available to obtain the same results. Initially, this approach was used to estimate hippocampal connectivity and demonstrated high correlation of the resulting estimates with sparsely available data (Tecuati *et al.*, 2021).

The overall workflow of the presented pipeline consists of seven main logical components: (i) quantitation of parcel-specific axonal and dendritic lengths; (ii) determination of parcel-specific axonal and dendritic path distances; (iii) measurement of parcel-specific axonal and dendritic convex hull volume; (iv) calculation of the average number of synapses per neuronal pair in each parcel; (v) calculation of the number of contacts per connected pair; (vi) calculation of the connection probability per neuronal pair; and (vii) calculation of the confidence intervals on these values by propagation of error analysis. All steps can be carried out on a basic desktop or laptop computer using readily available software (Figure 1).

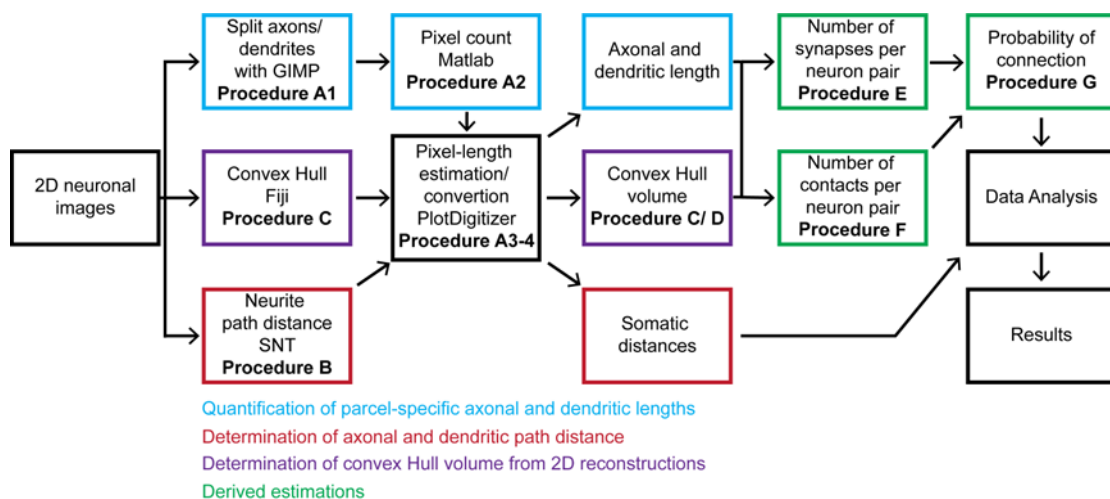


Figure 1. Flow chart of the described pipeline.

The procedure starts from 2D neuronal images that are processed to quantitate axonal and dendritic lengths, path distances from the soma by parcel, and convex hull volumes. From these quantitations, we calculate the number of synapses and contacts per neuronal pair and subsequently estimate the probabilities of connection from multiple neuronal pairs. The generated information is analyzed and presented as the mean and standard deviation

Equipment

1. Standard personal computer

The described analysis was performed using a Bionic G32 144Hz All In One PC [i7-8700] with Windows 10. The recommended minimal configuration is AMD Ryzen 5 2600X Six-Core Processor 3.60 GHz, 16 GB RAM, 64-bit operating system.

Software

1. GNU Image Manipulation Program, free access (GIMP 2.8; gimp.org/downloads/).
2. Custom-made MATLAB algorithm, free access (github.com/Hippocampome-Org/QuantifyNeurites)
3. Plot Digitizer, free access (plotdigitizer.sourceforge.net)
4. Fiji: Shape Analysis plugin, free access (Wagner and Lipinski, 2013; imagej.net/Shape_Filter)
5. Fiji: Simple Neurite Tracer plugin, free access (Longair *et al.*, 2011; imagej.net/Simple_Neurite_Tracer:_Basic_Instructions)
6. Fiji: 3D Convex Hull, free access (imagej.nih.gov/ij/plugins/3d-convex-hull)
7. MATLAB: commercial license; 30-day free trial available (mathworks.com/products/get-matlab.html)

Image Dataset and Additional Requirements

8. Required are figures containing drawings of neuronal morphology, such as dendritic and axonal arbors (Recipe 1). If both axons and dendrites originate from the same neuron, they need to be drawn in distinct colors. If the arbors invade multiple anatomical parcels, the figure must demarcate the parcel boundaries when parcel-specific data are required. **IMPORTANT: All figures need to contain a calibration bar.** The examples used in this protocol are accessible at hippocampome.org/php/data/Bio-protocol_sample_files.zip.
9. Required are estimations of the volumes of anatomical parcels in which the neurons of interest are contained

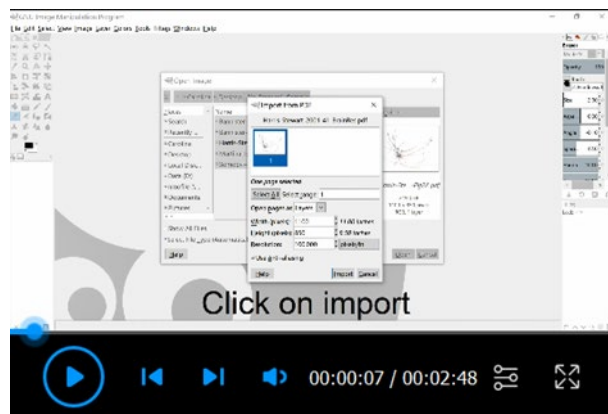
(Recipe 2). The examples used in this protocol are listed in Table 1 and accessible at bbp.epfl.ch/nexus/cell-atlas.

10. Required are estimations of the average distance between presynaptic elements (boutons) along the axons and of the average distance between postsynaptic elements (spines or shaft densities) along the dendrites for the species and neural system of interest (Recipe 3). The examples used in this protocol are accessible at hippocampome.org/php/data/Bio-protocol_sample_files.zip.

Procedure

A. Quantitation of parcel-specific axonal and dendritic lengths

1. Generate the necessary PNG files with GIMP. From the original unmodified neuronal reconstruction (Recipe 1), manually segregate the axons and dendrites within each anatomical parcel. If parcel-specific information is not required, simply separate the axons from the dendrites to estimate the corresponding axonal and dendritic length (Video 1).



Video 1. 2D image manipulation.

GIMP is used to selectively erase axons or dendrites from the various parcels to isolate them for later analysis.

2. Load a PDF into GIMP (e.g., File: Open “Harris-Stewart-2001-41-BrainRes-Fig2A.pdf”) (Figure 2A).
3. Use GIMP to erase the extraneous parts of the figure (Figure 2B).
4. Select the eraser tool from the *Toolbox* window.
5. Select Hardness 100 from the *Brushes* window.
6. Set the brush size to the desired size (e.g., 25) in the Tool Options windows (Figure 2B, red box).
7. Hold down the left button of the mouse to erase parts of the figure.
8. Save the XCF version of the erased figure that includes both kinds of neurites in all layers (e.g., File: Save As... “SCA_all_allColors_both”). **IMPORTANT:** The structure of the name should be preserved for the pixel count.
9. Export the PNG version from the XCF version of the figure to the same folder (e.g., File: Export As... “SCA_all_allColors_both.png”). The PNG is selected as the file format of choice because its default background is transparent. This reduces any potential errors from accidentally counting pixels included in the background.
10. Use GIMP to erase the axons from the figure based on the color code (axons are shown in red in Figure 2B) by repeating steps b i-iv (Figure 2C, Video 1).
11. Save the XCF version of the figure with the dendrites in the layer of interest to the same folder (e.g., File: Save As... “SCA_SO_allColors_Ds.xcf”).

12. Export the PNG version from the XCF version of the figure to the same folder (e.g., *File: Export As...* “SCA_SO_allColors_Ds.png”).
13. Use GIMP to erase the dendrites from the figure based on the color code (dendrites are shown in black in Figure 2B) by repeating steps b i-iv (Figure 2D, Video 1).
14. Save the XCF version of the figure with the axons in the layer of interest to the same folder (e.g., *File: Save As...* “SCA_SO_allColors_Ax.xcf”).
15. Export the PNG version from the xcf version of the figure to the same folder (e.g., *File: Export As...* “SCA_SO_allColors_As.png”).
16. Save the axonal and dendritic domains in distinct files for every layer and subregion to the same folder (Figure 2E and 2F).

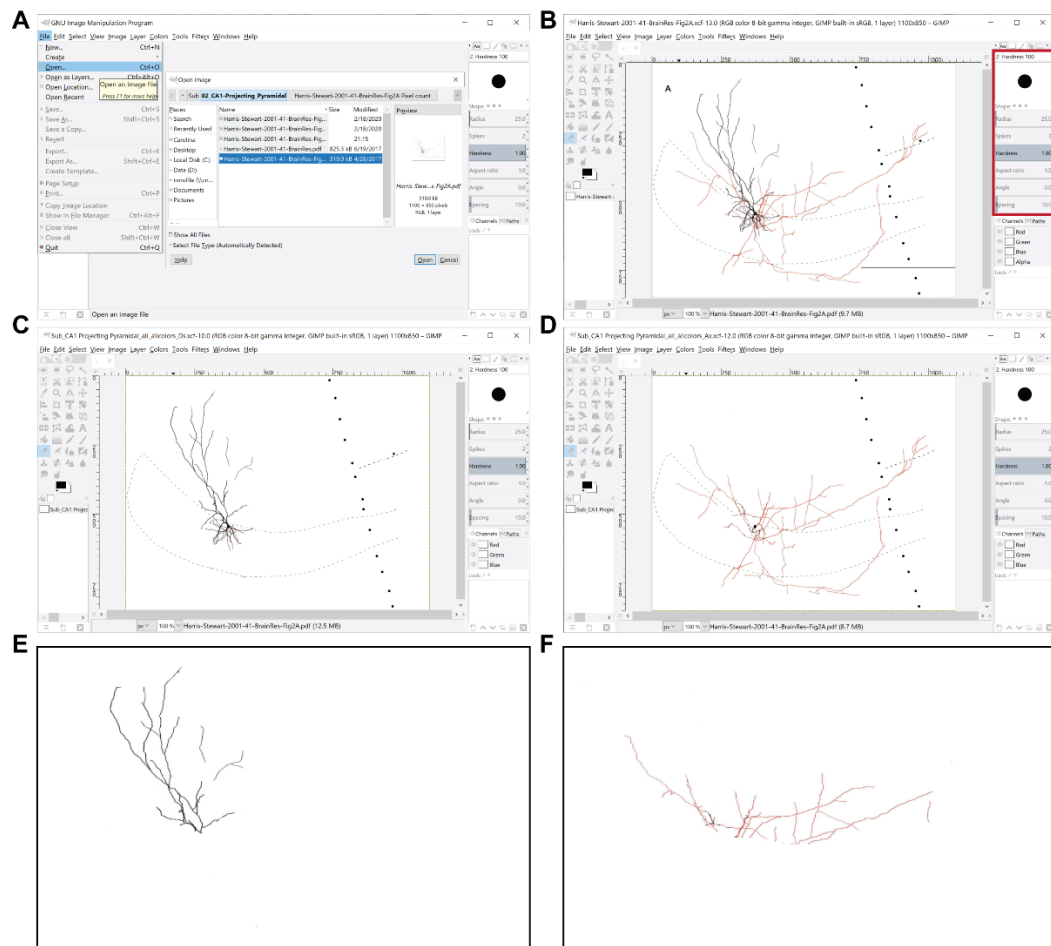


Figure 2. Preprocessing of images for the quantitation of axonal and dendritic lengths.

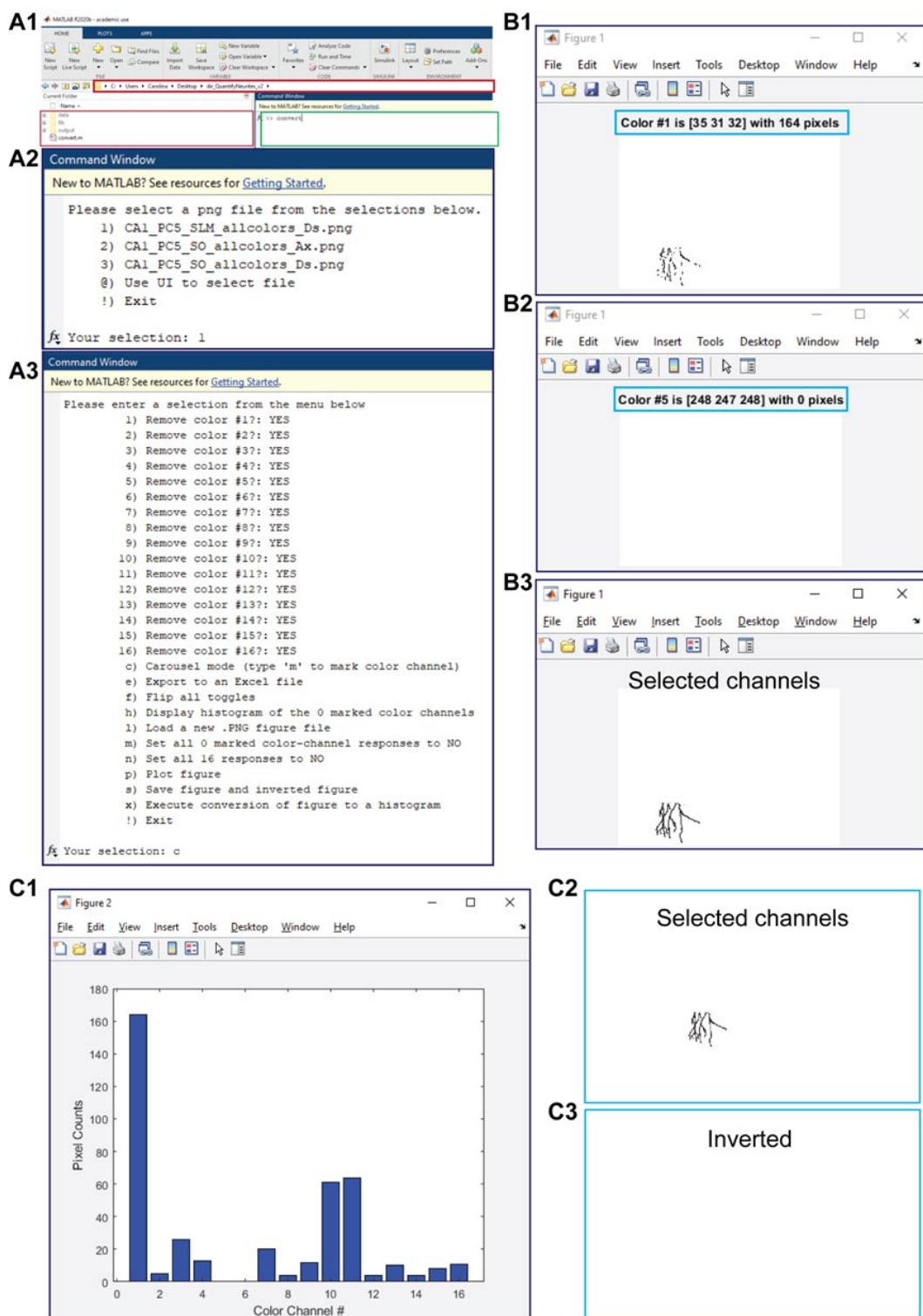
A. The GIMP File menu is used to open an image file to be processed. **B.** Representative image is in preparation for processing (Harris *et al.*, 2001), where the red box delimits the toolbox location and the circle represents the eraser tool. **C, D.** Shown are processed images containing only dendrites (**C**) or axons (**D**) in all the layers of the region of interest (in this example, the subiculum), which were obtained from the original image shown in (**B**). **E, F.** Shown are representative images displaying only dendrites (**E**) or axons (**F**) in the parcel of interest (in this case, the stratum moleculare of the subiculum), which were obtained from the original image shown in (**B**).

17. Pixel counting using a custom-made MATLAB algorithm (Figure 3; Video 2).

**Video 2. Pixel count from 2D images.**

A custom-made MATLAB program is used to count all pixels included in the 16 color channels of an image.

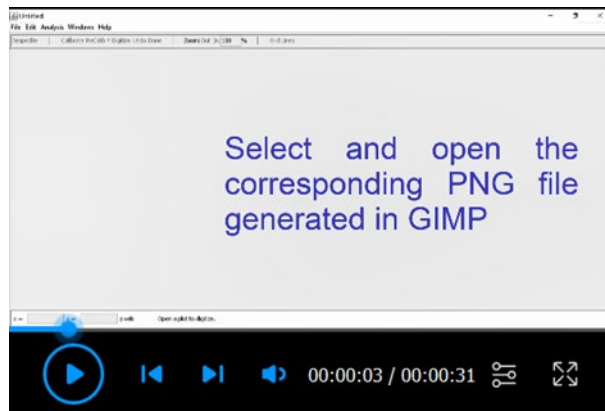
18. Place the separated images in the data folder.
19. Open MATLAB, making sure that the current working folder is open (e.g., “dir_QuantifyNeurites_v2”) (Figure 3A1, red boxes).
20. Run the command *convert* (Figure 3A1, green box).
21. From the displayed menu, select the image to be worked on by typing the number and pressing enter (Figure 3A2).
22. After the image is open, select the carousel mode to identify the color channels that contain pixels (Figure 3A3).
23. Press *m* to choose the color channels that contain pixels (the number of pixels is displayed in brackets) (Figure 3B1).
24. If the channel does not contain any pixels, just press the space bar to move to the next channel (Figure 3B2).
25. Optional step: plot the image with the selected color channels to verify that the selected channels contain all of the pixels by typing *p* and pressing *enter* (Figure 3B3).
26. A histogram with the total pixel count is displayed (Figure 3C1). The command window displays the selected channels and number of pixels.
27. Optional step: save the images that contain the selected (Figure 3C2) and unselected (Figure 3C3) channels by typing *s* and pressing *enter*. The images are automatically saved to the output folder.
28. Select a new image from the data folder by typing *l* and pressing *enter*.
29. End the process by typing */* and pressing *enter*.

**Figure 3. Pixel counting.**

A1. Shown is a MATLAB window with the open working folder “dir_QuantifyNeurites_v2” in a red box and the command window to run the command “convert” in a green box. **A2.** The displayed menu that appears after running the command “convert” to select the image to process. **A3.** The displayed menu options that appear in order to analyze the selected figure. **B.** Shown is a representative carousel mode, where the color number and the number of pixels present (**B1**) or absent (**B2**) are delimited within the

blue boxes and where a final plot figure contains only the channels selected during the full run of the carousel mode. **C.** Presented are a histogram of the selected channels and the number of pixels per channel (**C1**) and the generated PNG files for the selected (**C2**) and unselected (**C3**) channels.

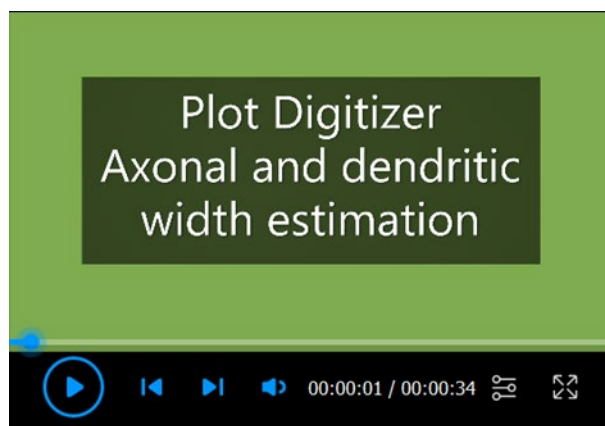
30. Pixel length estimation using Plot Digitizer (Video 3).



Video 3. Measuring a calibration bar in pixels.

Plot Digitizer is used to measure the length in pixels of a neuronal reconstruction's calibration bar. The X coordinates of the two ends of the calibration bar are recorded, and their difference is the final measurement in pixels.

31. Open the original reconstruction with Plot Digitizer.
32. Place the cursor over the start of the calibration bar and take note of the number.
33. Do the same at the other end of the calibration bar.
34. The difference between the numbers represents the length of calibration bar in pixels.
35. Conversion from pixel number to length.
36. Determine the mean neurite width by randomly selecting three locations for every neuron image, parcel, and neurite domain, measuring the branch width in pixels at each location, and averaging the three values (Video 4).



Video 4. Neurite width estimation.

Plot Digitizer is used to estimate the widths of axons and dendrites in each layer containing portions of a neuronal reconstruction. Three examples are measured for each layer to obtain an average estimate of the neurite width per layer.

37. Calculate the pixel length in physical units, which is simply the nominal calibration scale-bar value (in μm) divided by the measured bar length in pixels.
38. Obtain the parcel-specific neurite length by multiplying the pixel count for that neurite in the given parcel by the physical pixel length and dividing the result by the average branch width in pixels.
39. Correct for the artifactual flattening of three-dimensional arbors into two-dimensional images by combining the parcel-specific length, l_p , with the reported section thickness, t_s , using Pythagoras' formula:

$$L_p^c = \sqrt{l_p^2 + t_s^2} \quad (1)$$

where L_p^c represents the final corrected length.

B. Determination of the axonal and dendritic path distances (Figure 4, Video 5)



Video 5. Measuring somatic distance.

Fiji with the Simple Neurite Tracer plugin is used to measure the length in pixels from the soma to the end of the selected axon or dendrite. Three examples are measured for each type of neurite to determine the average.

1. Open the original file with Fiji: *File – Open – File source* (Figure 4A).
2. Convert the image to binary: *Process – Binary – Make Binary* (Figure 4B).
3. Open the plugin “Simple Neurite Tracer:” *Plugins – Neuroanatomy – SNT* (Figure 4C).
4. Open the image in the SNT command window: *File – Choose tracing image – From* (Figure 4D).
5. Trace the distance along the dendrite/axon by clicking on the soma and at the end of the segment. If the tracing does not correspond with the structure, increase the accuracy by clicking multiple times along the segment: press *y*, and continue tracing along the path (Figure 4E).
6. Once the tracing is complete, move on to the next one by accepting the trace. Press *F* to finish the tracing.
7. The values are estimated in pixels (Path manager window, if values are not visible: *tag – Morphometry – Length*), so convert them to length using the pixel/length factor (Section 3, Figure 4E).
8. When all traces are done, save them for future reference. *File – Export as – swc or traces*.

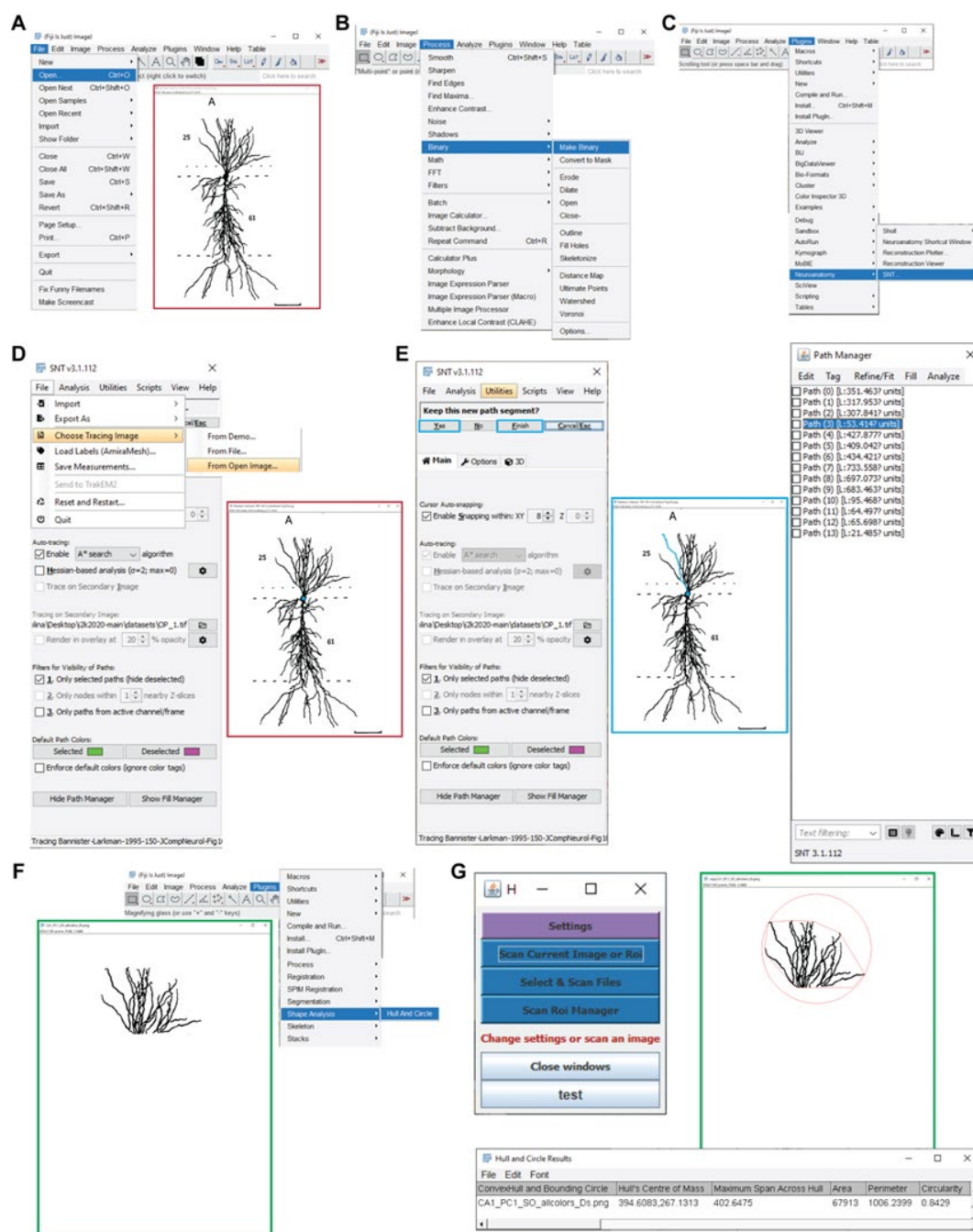


Figure 4. Determining the somatic distances and convex hull volumes.

A. Shown are the Fiji menu steps to open an image for path tracing (e.g., a CA1 pyramidal neuron; Bannister and Larkman, 1995). B. Displayed are the menu steps to convert the image into a binary image. C. Presented are the menu steps to run the Simple Neurite Tracer plugin. D. Shown are the Simple Neurite Tracer steps to load the open image for tracing. E. Presented is a representative Simple Neurite Tracer console that shows one path in blue (middle), with the options to finish the path and continue tracing on the console (left), and the path manager, with all the traces that correspond to the different parcels of the original image (right). F. Shown are the menu steps to run the *Hull And Circle* plugin for the dendrites located in the parcel of interest (e.g., CA1 stratum oriens; green box) for the convex hull measurement. G. The *Hull And Circle* toolbox (left) is used to scan the current image, where the image with the delimited area is shown in green and the bottom panel shows the emerging results window.

C. Determining the convex hull volume from 2D reconstructions (Figures 4F and 4G, Video 6)

1. Open the generated segmented images that only contain axons or dendrites (PNG file) with *Fiji: File – Open – File* source.
2. Convert the image to binary: *Process – Binary – Make Binary*.
3. Open the plugin: *Plugins – Shape Analysis – Hull And Circle* (Figure 4F).
4. From the new window, select the option *Scan current Image or Roi* (Figure 4G).
5. A new window containing the results is generated (Hull and Circle Results, Figure 4G).
6. Save the results: *File – Save as*.
7. An image with the calculated hull volume is displayed. This image cannot be saved, but it provides information about how the resulting convex hull area was calculated (Figure 4G).
8. Convert the area measurements from pixel units to μm^2 and multiply the resulting values by the reported slice thickness, assuming that the reconstruction is located in the middle of the slice.



Video 6. Convex hull estimation.

Fiji with the Hull and Circle plugin is used to measure the convex hull area in pixels from the region of interest in 2D neuronal reconstructions.

D. Determining the convex hull volume from 3D reconstructions

1. Directly estimate the real volume using the 3D Convex Hull plugin.

E. Calculating the average number of synapses per neuronal pair.

1. Calculate the average number of synapses per pair of presynaptic and postsynaptic neurons, N_s , from their parcel-specific axonal and dendritic lengths, by separately estimating the number, N_{sx} , of axonal-dendritic overlaps in each parcel x (Tecuatl *et al.*, 2021). For any x , the value N_{sx} can be derived as the product of three factors:
 2. The probability that presynaptic and postsynaptic elements occur within a given interaction distance, r , is the ratio between the volume of the interaction sphere, within which the two elements are found, and the volume of the entire parcel, V_x (Recipe 2).
 3. The number of presynaptic elements (axonal boutons) in a given anatomical parcel is specified by the presynaptic axonal length in parcel x , L_{ax} , divided by the average distance between consecutive presynaptic boutons, b_d (Recipe 3; example files are accessible at hippocampome.org/php/data/Bio-protocol_sample_files.zip).
 4. The number of postsynaptic elements (dendritic spines or shafts) in the same parcel is given by the postsynaptic dendritic length in x , L_{dx} , divided by the distance between postsynaptic elements, s_d .

- To calculate the average number of synapses per pair of presynaptic and postsynaptic neurons in a specific parcel, use the following formula:

$$N_{sx} = \frac{4\pi r^3}{3V_x} * \frac{L_{ax}}{bd} * \frac{L_{dx}}{sd} \quad (2)$$

- The total count of synapses per directed neuron pair, N_s , is just the sum of the number per parcel, N_{sx} , over all parcels.

F. Calculate the number of contacts per connected pair.

- Assume that a given pair of neurons forms at least a single synaptic contact, and calculate the expected number of additional contacts for that pair as:

$$N_{cx} = \frac{4\pi r^3}{3V_o} * \frac{L_{ax}}{bd} * \frac{L_{dx}}{sd} \quad (3)$$

where the volumetric ratio between the sphere defined by the radius of interaction r and V_o represents the chance of an encounter for any given pair of axonal boutons and dendritic spines or shafts, and Lax/bd and Ldx/sd correspond, respectively, to the number of axonal boutons and dendritic spines or shafts in parcel x.

- Determine the volume of the intersection, V_o , by:

$$V_o = \frac{1}{4}(V_{dx} + V_{ax}) \quad (4)$$

where V_{dx} and V_{ax} are the dendritic and axonal convex hull volumes in parcel x.

- Calculate the overall number of contacts per connected pair as the sum of the contacts in each parcel augmented by one, reflecting the initial assumption that the neuronal pair is connected:

$$N_c = 1 + \sum_x N_{cx} \quad (5)$$

where the symbol Σ_x represents the sum over all parcels.

G. Calculate the connection probabilities

- Compute the connection probability for a pair of neuronal types in parcel x by dividing the average number of synapses per neuronal pair by the number of contacts per connected pair in the same parcel:

$$p_x = \frac{N_x}{N_{cx}} = \frac{V_o}{V_x} \quad (6)$$

- Determine the overall probability of connection for a pair of presynaptic and postsynaptic neurons in any parcel by the sum of inclusive events:

$$p = 1 - \prod_x (1 - p_x) \quad (7)$$

where the symbol \prod_x represents the product over all parcels.

Table 1. List of all representative files

File name	Type	Description	Use
Neurite Quantitation.xlsx	XLSX	Spreadsheet to collect the data from the pixel count, pixel length estimation, convex hull area, and neurite path distance	Data collection of pixel count to estimate axonal/dendritic length and somatic distance
Bouton distance.docx	DOCX	List of reported ultrastructural measurements for axonal bouton distance in the hippocampal formation	Estimation of the number of synapses and contacts per neuronal pair
Dendritic spine distance.docx	DOCX	List of reported ultrastructural measurements for dendritic spine distance in the hippocampal formation	Estimation of the number of synapses and contacts per neuronal pair
Harris-Stewart-2001-41-BrainRes-Fig2A/Harris-Stewart-2001-41-BrainRes-Fig2A.pdf	PDF	Original file that contains the neuronal reconstruction from a Subiculum CA1 Projecting Pyramidal cell	Image manipulation with GIMP
Harris-Stewart-2001-41-BrainRes-Fig2A/Harris-Stewart-2001-41-BrainRes-Fig2A.xcf	XCF	File generated with GIMP for manipulation	Exported file without modifications
Harris-Stewart-2001-41-BrainRes-Fig2A/Harris-Stewart-2001-41-BrainRes-Fig2A.png	PNG	Exported PNG file without modifications from the XCF version	1. Scale bar conversion with Plot Digitizer 2. Somatic distance estimation with SNT
Harris-Stewart-2001-41-BrainRes-Fig2A/Sub_CA1 projecting Pyramidal_all_allcolors_both.xcf	XCF	File saved with GIMP for manipulation that includes brain region, cell type, and parcel information	Segregation of axons and dendrites with GIMP
Harris-Stewart-2001-41-BrainRes-Fig2A/Sub_CA1 projecting Pyramidal_all_allcolors_Ds.xcf	XCF	File that contains only dendrites in all the parcels	Segregation of dendrites based on parcel borders with GIMP
Harris-Stewart-2001-41-BrainRes-Fig2A/Sub_CA1 projecting Pyramidal_all_allcolors_Ds.png	PNG	Exported PNG file with only dendrites from the XCF version	Dendritic somatic distance estimation with SNT, if you cannot discern axons and dendrites from Harris-Stewart-2001-41-BrainRes-Fig2A.png file
Harris-Stewart-2001-41-BrainRes-Fig2A/Sub_CA1 projecting Pyramidal_SM_allcolors_Ds.xcf	XCF	File that contains only dendrites in SUB:SM	Saved file with dendrites in Sub:SM for future edits if needed
Harris-Stewart-2001-41-BrainRes-Fig2A/Sub_CA1 projecting Pyramidal_SM_allcolors_Ds.png	PNG	Exported PNG file with only dendrites in Sub:SM	1. Pixel count with MATLAB 2. Convex hull area estimation with Fiji: Hull And Circle

Harris-Stewart-2001-41-BrainRes-Fig2A/Sub_CA1 projecting Pyramidal_SP_allcolors_Ds.xcf	XCF	File that contains only dendrites in Sub:SP	Saved file with dendrites in Sub:SP for future edits if needed
Harris-Stewart-2001-41-BrainRes-Fig2A/Sub_CA1 projecting Pyramidal_SP_allcolors_Ds.png	PNG	Exported PNG file with only dendrites in Sub:SP	1. Pixel count with MATLAB 2. Convex hull area estimation with Fiji: Hull And Circle
Harris-Stewart-2001-41-BrainRes-Fig2A/Sub_CA1 projecting Pyramidal_all_allcolors_Ax.xcf	XCF	File that contains only axons in all the parcels	Segregation of axons based on parcel borders with GIMP
Harris-Stewart-2001-41-BrainRes-Fig2A/Sub_CA1 projecting Pyramidal_all_allcolors_Ax.png	PNG	Exported PNG file with only axons from the XCF version	Axonal somatic distance estimation with SNT, if you cannot discern axons and dendrites from Harris-Stewart-2001-41-BrainRes-Fig2A.png file
Harris-Stewart-2001-41-BrainRes-Fig2A/Sub_CA1 projecting Pyramidal_SM_allcolors_Ax.xcf	XCF	File that contains only axons in Sub:SM	Saved file with axons in Sub:SM for future edits if needed
Harris-Stewart-2001-41-BrainRes-Fig2A/Sub_CA1 projecting Pyramidal_SM_allcolors_Ax.png	PNG	Exported PNG file with only axons in Sub:SM	1. Pixel count with MATLAB 2. Convex hull area estimation with Fiji: Hull And Circle
Harris-Stewart-2001-41-BrainRes-Fig2A/Sub_CA1 projecting Pyramidal_SP_allcolors_Ax.xcf	XCF	File that contains only axons in Sub:SP	Saved file with axons in Sub:SP for future edits if needed
Harris-Stewart-2001-41-BrainRes-Fig2A/Sub_CA1 projecting Pyramidal_SP_allcolors_Ax.png	PNG	Exported PNG file with only axons in Sub:SP	1. Pixel count with MATLAB 2. Convex hull area estimation with Fiji: Hull And Circle
Harris-Stewart-2001-41-BrainRes-Fig2A/Sub_CA1 projecting Pyramidal_PL_allcolors_Ax.xcf	XCF	File that contains only axons in Sub:PL	Saved file with axons in Sub:PL for future edits if needed
Harris-Stewart-2001-41-BrainRes-Fig2A/Sub_CA1 projecting Pyramidal_PL_allcolors_Ax.png	PNG	Exported PNG file with only axons in Sub:PL	1. Pixel count with MATLAB 2. Convex hull area estimation with Fiji: Hull And Circle
Harris-Stewart-2001-41-BrainRes-Fig2A/Sub_CA1 projecting Pyramidal_CA1_SLM_allcolors_Ax.xcf	XCF	File that contains only axons in CA1:SLM	Saved file with axons in CA1:SLM for future edits if needed
Harris-Stewart-2001-41-BrainRes-Fig2A/Sub_CA1 projecting Pyramidal_CA1_SLM_allcolors_Ax.png	PNG	Exported PNG file with only axons in CA1:SLM	1. Pixel count with MATLAB 2. Convex hull area estimation with Fiji: Hull And Circle

Harris-Stewart-2001-41-BrainRes-Fig2A/Sub_CA1 projecting Pyramidal_CA1 SR_allcolors_Ax.xcf	XCF	File that contains only axons in CA1:SR	Saved file with axons in CA1:SR for future edits if needed
Harris-Stewart-2001-41-BrainRes-Fig2A/Sub_CA1 projecting Pyramidal_CA1 SR_allcolors_Ax.png	PNG	Exported PNG file with only axons in CA1:SR	1. Pixel count with MATLAB 2. Convex hull area estimation with Fiji: Hull And Circle
Bannister-Larkman-1995-150-JCompNeurol-Fig10A/Bannister-Larkman-1995-150-JCompNeurol-Fig10A.pdf	PDF	Original file that contains the neuronal reconstruction from a CA1 Pyramidal cell	Image manipulation with GIMP
Bannister-Larkman-1995-150-JCompNeurol-Fig10A/Bannister-Larkman-1995-150-JCompNeurol-Fig10A.png	PNG	Exported PNG file without modifications from the XCF version	Somatic distance estimation with SNT
Bannister-Larkman-1995-150-JCompNeurol-Fig10A/Bannister-Larkman-1995-150-JCompNeurol-Fig10A.traces	TRACES	File that includes the tracings and measurements associated with the neuronal reconstruction	Saved tracings for reference and review if needed
Bannister-Larkman-1995-150-JCompNeurol-Fig10A/Hull And Circle Results.csv	CSV	File with measurements for the convex hull area associated with the neuronal reconstruction	Saved measurements for reference and review if needed
Martina-Jonas-2000-295-Science-Fig1C.pdf	PDF	Original file that contains the neuronal reconstruction from a CA1 O-LM interneuron	Image manipulation with GIMP
Somogyi-Klausberger-2005-9-JPhysiol-Fig3A.pdf	PDF	Original file that contains the neuronal reconstruction from a CA1 Bistratified interneuron	Image manipulation with GIMP

Data analysis

1. Calculate the standard deviation for the average number of synapses per neuronal pair using the mean and standard deviation from all measurements for the presynaptic axonal and postsynaptic dendritic lengths.
2. Compute the number of synapses for a given parcel x utilizing Equation (2) for N_{sx} .
3. Consider r , V_x , b_d , and s_d to be constants.
4. Calculate the standard deviation of N_{sx} by propagating the standard deviations of L_{ax} and L_{dx} using the formulas for products and constants,

$$\Delta(L_{ax} * L_{dx}) = |L_{ax} * L_{dx}| \sqrt{\left(\frac{\Delta L_{ax}}{L_{ax}}\right)^2 + \left(\frac{\Delta L_{dx}}{L_{dx}}\right)^2} \quad (8)$$

$$\Delta N_{sx} = \left| \frac{4\pi r^3}{3V_x} * \frac{L_{ax}}{b_d} * \frac{L_{dx}}{s_d} \right| \sqrt{\left(\frac{\Delta L_{ax}}{L_{ax}}\right)^2 + \left(\frac{\Delta L_{dx}}{L_{dx}}\right)^2} = |N_{sx}| \sqrt{\left(\frac{\Delta L_{ax}}{L_{ax}}\right)^2 + \left(\frac{\Delta L_{dx}}{L_{dx}}\right)^2} \quad (9)$$

5. Determine the total number of synapses by summing across all parcels, and compute the associated standard deviation using the formula for sums,

$$\Delta N_s = \sqrt{\sum_x (\Delta N_{sx})^2} \quad (10)$$

6. Calculate the standard deviation for the number of contacts per connected pair using the mean and standard deviation from all measurements for the presynaptic axonal and postsynaptic dendritic lengths and for the convex hull volumes for the presynaptic axons and the postsynaptic dendrites.
7. Compute the number of contacts for a given parcel x utilizing Equation (3) for N_{cx} . Determine the standard deviation for the average volume of intersection using the formulas for sums and constants,

$$\Delta(V_{ax} + V_{dx}) = \sqrt{(\Delta V_{ax})^2 + (\Delta V_{dx})^2} \quad (11)$$

$$\Delta \bar{V}_o = \left| \frac{1}{4} \right| \sqrt{(\Delta V_{ax})^2 + (\Delta V_{dx})^2} \quad (12)$$

8. Calculate the standard deviation for the number of contacts for a given parcel x utilizing the formulas for products, quotients, and constants,

$$\Delta \left(\frac{L_{ax} * L_{dx}}{\bar{V}_o} \right) = \left| \frac{L_{ax} * L_{dx}}{\bar{V}_o} \right| \sqrt{\left(\frac{\Delta \bar{V}_o}{\bar{V}_o} \right)^2 + \left(\frac{\Delta L_{ax}}{L_{ax}} \right)^2 + \left(\frac{\Delta L_{dx}}{L_{dx}} \right)^2} \quad (13)$$

$$\Delta N_{cx} = \left| \frac{4\pi r^3}{3\bar{V}_o} * \frac{L_{ax}}{b_d} * \frac{L_{dx}}{s_d} \right| \sqrt{\left(\frac{\Delta \bar{V}_o}{\bar{V}_o} \right)^2 + \left(\frac{\Delta L_{ax}}{L_{ax}} \right)^2 + \left(\frac{\Delta L_{dx}}{L_{dx}} \right)^2} = |N_{cx}| \sqrt{\left(\frac{\Delta \bar{V}_o}{\bar{V}_o} \right)^2 + \left(\frac{\Delta L_{ax}}{L_{ax}} \right)^2 + \left(\frac{\Delta L_{dx}}{L_{dx}} \right)^2} \quad (14)$$

9. Determine the total number of contacts using Equation (5), and compute the associated standard deviation using the formula for sums,

$$\Delta N_c = \sqrt{\sum_x (\Delta N_{cx})^2} \quad (15)$$

10. Calculate the standard deviation for the connection probabilities for a pair of neuronal types in parcel x from Equation (6).
11. Compute the standard deviation for the connection probability using the formula for constants,

$$\Delta p_x = \left| \frac{1}{V_x} \right| \Delta \bar{V}_o \quad (16)$$

12. Determine the total connection probability from Equation (7), and calculate the associated standard deviation using the formulas for differences and products,

$$\Delta(1 - p_x) = \Delta p_x \quad (17)$$

$$\Delta(\prod_x (1 - p_x)) = |\prod_x (1 - p_x)| \sqrt{\sum_x \left(\frac{\Delta(1-p_x)}{(1-p_x)} \right)^2} = |\prod_x (1 - p_x)| \sqrt{\sum_x \left(\frac{\Delta p_x}{(1-p_x)} \right)^2} \quad (18)$$

$$\Delta p = |\prod_x (1 - p_x)| \sqrt{\sum_x \left(\frac{\Delta p_x}{(1-p_x)} \right)^2} \quad (19)$$

Notes

The accuracy of this procedure is limited by the incompleteness of axonal reconstructions and variability in neurite diameter.

This protocol can be used only for dendritic targeting connections: perisomatic connections cannot be estimated with this approach (but see Brown *et al.*, 2012 for those cases).

The computation of standard deviation in the above Data Analysis are performed manually for each pair of neuronal types. The time required to carry out this operation by applying the provided formulas is negligible relative to the time required to trace the neurons from microscopic images.

Recipes

A. Neuronal reconstructions

Include representative two-dimensional neuronal tracings for each neuronal type from peer-reviewed publications based on the following inclusion criteria:

1. Reconstructions should be representative of the neuronal type. At least one axonal reconstruction per presynaptic neuron type and one dendritic reconstruction per postsynaptic type must be included.
2. Images should contain a calibration scale bar and clear demarcations of relevant layers and subregional boundaries. The latter is optional and only required for parcel-specific estimates.
3. For tracings including both axons and dendrites, the two neurite types must be unambiguously discernable. Likewise, in tracings including multiple neurons, each neurite type must be unambiguously ascribable to a single neuron.
4. Species (*e.g.*, rat vs. mouse) and developmental stage (*e.g.*, young vs. adult) should be consistent for all the neuronal types.

Thousands of neuronal reconstructions are also available through open access databases such as MouseLight (ml-neuronbrowser.janelia.org) for mouse, Mapzebrain (fishatlas.neuro.mpg.de/neurons) for zebrafish, FlyCircuit for drosophila (flycircuit.tw), Insect Brain Database for insects (insectbraindb.org), and NeuroMorpho.Org for over 60 different species (Akram *et al.*, 2018).

B. Volume estimations

We use the anatomical volumes for the mouse brain reported from the Blue Brain Cell Atlas (bbp.epfl.ch/nexus/cell-atlas). Other sources are suitable for different species, such as rat (scalablebrainatlas.incf.org/rat/PLCJB14), drosophila (v2.virtualflybrain.org), and zebrafish (fishatlas.neuro.mpg.de). Independent studies that report parcel-specific volume estimations can also be considered (*e.g.*, Ropireddy *et al.*, 2012). NOTE: differences in brain sizes have been reported between males and females as well as among strains (Wang *et al.*, 2020).

C. Ultrastructural parameters

Dendritic spine or shaft postsynaptic density distance and axonal inter-bouton distance can have huge variability among species, brain regions, and neuronal types. For greater accuracy, collect specific values from the literature for the synapses of interest (see *e.g.*, the files at hippocampome.org/php/data/Bio-protocol_sample_files.zip for the examples used in this protocol description).

Acknowledgments

This work was supported in part by NIH grants R01NS39600 and U01MH114829. Carolina Tecuatl thanks the Consejo Nacional de Ciencia y Tecnología, México for providing fellowship 253060, allowing this project to start during her PhD training. This methodology was used in Tecuatl *et al.* (2021) “Comprehensive estimates of potential synaptic connections in local circuits of the rodent hippocampal formation by axonal-dendritic overlap.”

Competing interests

The authors declare no competing financial interests.

Ethics

All original data analyzed using this protocol were published previously in accordance with the authors' respective ethics committees.

References

- Akram, M. A., Nanda, S., Maraver, P., Armananzas, R. and Ascoli, G. A. (2018). [An open repository for single-cell reconstructions of the brain forest](#). *Sci Data* 5: 180006.
- Ascoli, G. A. and Atkeson, J. C. (2005). [Incorporating anatomically realistic cellular-level connectivity in neural network models of the rat hippocampus](#). *Biosystems* 79(1-3): 173-181.
- Bannister, N. J. and Larkman, A. U. (1995). [Dendritic morphology of CA1 pyramidal neurones from the rat hippocampus: I. Branching patterns](#). *J Comp Neurol* 360(1): 150-160.
- Brown, K. M., Sugihara, I., Shinoda, Y. and Ascoli, G. A. (2012). [Digital morphometry of rat cerebellar climbing fibers reveals distinct branch and bouton types](#). *J Neurosci* 32(42): 14670-14684.
- Harris, E., Witter, M. P., Weinstein, G. and Stewart, M. (2001). [Intrinsic connectivity of the rat subiculum: I. Dendritic morphology and patterns of axonal arborization by pyramidal neurons](#). *J Comp Neurol* 435(4): 490-505.
- Moradi, K, Ascoli, GA. [A comprehensive knowledge base of synaptic electrophysiology in the rodent hippocampal formation](#). *Hippocampus*. 2020; 30: 314– 331.
- Longair, M. H., Baker, D. A. and Armstrong, J. D. (2011). [Simple Neurite Tracer: open source software for reconstruction, visualization and analysis of neuronal processes](#). *Bioinformatics* 27(17): 2453-2454.
- Rees, C. L., Moradi, K. and Ascoli, G. A. (2017). [Weighing the Evidence in Peters' Rule: Does Neuronal Morphology Predict Connectivity?](#) *Trends Neurosci* 40(2): 63-71.
- Ropireddy, D. and Ascoli, G. A. (2011). [Potential Synaptic Connectivity of Different Neurons onto Pyramidal Cells in a 3D Reconstruction of the Rat Hippocampus](#). *Front Neuroinform* 5: 5.
- Ropireddy, D., Bachus, S. E. and Ascoli, G. A. (2012). [Non-homogeneous stereological properties of the rat hippocampus from high-resolution 3D serial reconstruction of thin histological sections](#). *Neuroscience* 205: 91-111.
- Tecuatl, C., Wheeler, D. W., Sutton, N. and Ascoli, G. A. (2021). [Comprehensive estimates of potential synaptic connections in local circuits of the rodent hippocampal formation by axonal-dendritic overlap](#). *J Neurosci* 41(8): 1665-1683.
- Wagner, T. and Lipinski, H. (2013). [IJBlob: An ImageJ Library for Connected Component Analysis and Shape Analysis](#). *J Open Res Softw* 1(1): e6.
- Wang, N., Anderson, R. J., Ashbrook, D. G., Gopalakrishnan, V., Park, Y., Priebe, C. E., Qi, Y., Laoprasert, R., Vogelstein, J. T., Williams, R. W. and Johnson, G. A. (2020). [Variability and heritability of mouse brain structure: Microscopic MRI atlases and connectomes for diverse strains](#). *Neuroimage* 222: 117274.

Isolation of Microglia and Analysis of Protein Expression by Flow Cytometry: Avoiding the Pitfall of Microglia Background Autofluorescence

Jeremy C. Burns^{1,2}, Richard M. Ransohoff³, Michaël Mingueneau^{1,*}

¹Multiple Sclerosis and Neurorepair Research Unit, Biogen, Cambridge, USA

²Pharmacology and Experimental Therapeutics, Boston University School of Medicine, Boston, USA

³Third Rock Ventures, Boston, USA

*For correspondence: michael.mingueneau@biogen.com

Abstract

Microglia are a unique type of tissue-resident innate immune cell found within the brain, spinal cord, and retina. In the healthy nervous system, their main functions are to defend the tissue against infectious microbes, support neuronal networks through synapse remodeling, and clear extracellular debris and dying cells through phagocytosis. Many existing microglia isolation protocols require the use of enzymatic tissue digestion or magnetic bead-based isolation steps, which increase both the time and cost of these procedures and introduce variability to the experiment. Here, we report a protocol to generate single-cell suspensions from freshly harvested murine brains or spinal cords, which efficiently dissociates tissue and removes myelin debris through simple mechanical dissociation and density centrifugation and can be applied to rat and non-human primate tissues. We further describe the importance of including empty channels in downstream flow cytometry analyses of microglia single-cell suspensions to accurately assess the expression of protein targets in this highly autofluorescent cell type. This methodology ensures that observed fluorescence signals are not incorrectly attributed to the protein target of interest by appropriately taking into account the unique autofluorescence of this cell type, a phenomenon already present in young animals and that increases with aging to levels that are comparable to those observed with antibodies against highly abundant antigens.

Keywords: Microglia isolation, Flow cytometry, Neuroimmunology, Autofluorescence, Neuroscience

This protocol was validated in: eLife (2020), DOI: 10.7554/eLife.57495

Background

Microglia are a type of tissue-resident macrophages residing in the central nervous system (CNS) and account for 10% to 15% of all cells within the CNS. While displaying some canonical macrophage activities, such as the phagocytosis of debris and apoptotic bodies, microglia are also endowed with functions specific to the CNS microenvironment, such as synaptic remodeling, neuronal support, and oligodendrogenesis (Ransohoff and Khoury, 2016; Clayton *et al.*, 2017; Li and Barres, 2018). This wide array of functions implies the existence of a diverse set of microglia phenotypes, states, and subsets well suited to characterization by single-cell analytical approaches. Fluorescence-based flow cytometry, a technique routinely used in immunological studies, allows for high-throughput, multiparametric analysis of single cells in suspension, isolated from blood or from dissociated tissues. However, the dissociation of CNS tissues generates a large amount of debris, principally myelin fragments, which must be removed before flow cytometry analysis. Commonly cited isolation techniques dissociate CNS tissue through enzymatic digestion and utilize magnetic bead-based strategies to remove myelin or isolate microglia. However, commonly used proteases in enzymatic tissue digestion, such as collagenase and trypsin, can lead to the unintended cleavage of surface antigens on microglia (Autengruber *et al.*, 2012) and promote cellular transcriptional changes during the 37°C incubations required for enzymatic activity (O'Flanagan *et al.*, 2019, Mattei *et al.*, 2020). In addition, magnetic bead isolation is costly, limits study throughput, and, in our hands, does not improve the yield or viability compared to this protocol, which in young (~3 month) mice yields approximately 2.5×10^5 microglia for analysis by flow cytometry. In this study, we describe the preparation of CNS single-cell suspensions for flow cytometry by utilizing a simple mechanical tissue dissociation procedure followed by myelin removal via density centrifugation. Cost-efficient and easy to perform, all steps of this protocol are carried out on ice or at 4°C, limiting cellular changes that would otherwise occur during isolation at higher temperatures.

By utilizing two surface markers (CD45 and CD11b), this protocol yields a population of microglia with uniformly high expression of core the homeostatic markers CX3CR1, P2RY12, and TMEM119 (Burns *et al.*, 2020, Figure 1D) and has also been successfully employed to isolate microglia in multiple states, both homeostatic and activated (Burns *et al.*, 2020, Figure 6—figure supplement 1A), from mice as old as 24 months of age. Although this workflow is optimized for cell analysis by flow cytometry, we highly recommend utilizing an alternative 2-phase Percoll protocol (described in Burns *et al.*, 2020) for fluorescence-activated cell sorting (FACS), as sorting instruments are more sensitive to the amount of debris remaining post-isolation, which can negatively impact FACS purity and yield.

While flow cytometry has become a routine method used in the analysis of immune cells, the analysis of microglia (minimally defined as CD45^{dim}, CD11b⁺) presents a particular challenge, as they exhibit a uniquely intense level of autofluorescence compared to other cell types, including CNS-resident macrophages (CD45^{bright}, CD11b⁺), which do not emit any detectable autofluorescence. In addition, the distribution of the autofluorescence signal in microglia is bimodal and biologically dynamic, with about two-thirds of the microglia showing a high autofluorescence signal (autofluorescence-positive) and the remaining third showing no or very low levels of autofluorescence (autofluorescence-negative) (Burns *et al.*, 2020). Interestingly, both autofluorescence subsets are differentially impacted by aging and genetic perturbations, which adds further complexity to their analysis (Burns *et al.*, 2020). In this protocol, we provide key considerations and analytical strategies to avoid the issues associated with microglia autofluorescence.

Materials and Reagents

1. 25G × ¾" butterfly needle (EXELINT, catalog number: 26768)
2. 20 mL luer-lock syringe (BD, catalog number: 302830)
3. 7 mL dounce homogenizer (Wheaton, catalog number: 57542)
4. 15 mL polypropylene conical tubes (ThermoFisher, catalog number: 339651)
5. 96 well v-bottom assay plates (Corning, catalog number: 3897)
6. 96 well 40 µm mesh filter plates (MilliporeSigma, catalog number: MANMN4010)
7. Cluster tubes (Corning, catalog number: 4411)

8. 10 cm plastic Petri dishes (Fisher Scientific, catalog number: FB0875713)
9. Ultracomp eBeads Plus Compensation Beads (ThermoFisher, catalog number: 01-333-42)
10. Fetal bovine serum (FBS) (ThermoFisher, catalog number: 26140079)
11. 10% FBS/HBSS
12. Flow staining buffer (ThermoFisher, catalog number: 00-4222-26)
13. DAPI (ThermoFisher, catalog number: 62248)
14. Percoll (GE Healthcare, catalog number: 17-0891-01)
15. 10× Hanks Balanced Salt Solution (ThermoFisher, catalog number: 14185052)
16. 1 M HEPES (ThermoFisher, catalog number: 15630080)
17. 1× HBSS (ThermoFisher, catalog number: 14175095)
18. 0.5 M EDTA (ThermoFisher, catalog number: 15575020)
19. TruStain FcX (Biolegend, catalog number: 101320)
20. Anti-CD45 BV785 (Biolegend, catalog number: 103149)
21. Anti-CD11b BV510 (Biolegend, catalog number: 101263)
22. 33% Isotonic Percoll (see Recipes)
23. 1× Hanks Balanced Salt Solution (HBSS) with 25mM HEPES (see Recipes)
24. Phosphate buffered solution (PBS) with 3mM EDTA (see Recipes)
25. Fc receptor blocking solution (see Recipes)
26. 2× Microglia Antibody Panel (see Recipes)

Equipment

1. Disposable scalpels (Fisher Scientific, catalog: 3120032) or common single-edge razor blades
2. 13 mm extra fine Bonn scissors (Fine Science Tools, catalog number: 14084-08)
3. Iris forceps (Fine Science Tools, catalog number: 11370-31)
4. 7 ml glass homogenizer (Wheaton, catalog number: 57542)
5. Refrigerated tabletop centrifuge (ThermoFisher Sorvall Legend XTR, Rotor TX-1000)
6. 5-laser LSR Fortessa X-20 (Becton Dickinson)
7. Vacuum line for aspirating

Procedure

A. Isolation of microglia

1. Keep all solutions ice-cold through the procedure.
2. Immediately following CO₂ euthanasia, open the chest cavity to expose the heart. Insert the 25G butterfly needle into the left ventricle, make a small incision in the right atrium, and slowly perfuse the mouse with 20 mL of PBS with 3 mM EDTA.
3. Cut and peel back the skin to expose the skull. Using scissors, cut the spine at the base of the skull. Starting from the brain stem, cut rostrally along the sagittal suture. Peel the two halves of the skull away to the side. Using tweezers, scoop out the brain and transfer into a 15 mL conical tube containing 5 mL of cold HBSS with 25 mM HEPES and keep on ice.
4. Transfer the brain to a fresh Petri dish on ice and mince the tissue with a scalpel or razor blade into pieces approximately 1 mm in size.
5. Transfer the minced tissue into the 7 ml dounce homogenizer and add 5 mL of HBSS with 25 mM HEPES.
6. The 7 mL dounce homogenizer is supplied with two pestles of slightly different sizes and labeled by the manufacturer. Using the pestle marked “loose,” gently disrupt the tissue, on ice, for approximately 10 strokes. Repeat with the pestle marked “tight” for another 10 strokes.
7. Pour the single-cell suspension into a fresh 15 mL conical tube. Rinse the homogenizer with 5 mL of

- HBSS with 25 mM HEPES and transfer to the same 15 mL conical tube.
8. Centrifuge the single-cell suspension at $600 \times g$ for 5 min at 4°C.
 9. Aspirate the supernatant and gently resuspend the cell pellet in 1 mL of 100% FBS.
 10. Add 9 mL of 33% isotonic Percoll solution and mix.
 11. Gently add 1 mL of 10% FBS/HBSS over the cell suspension.
 12. Centrifuge the cell suspension at $800 \times g$ for 15 min at 4°C with full acceleration and no brake.
 13. Carefully aspirate the resulting myelin layer located at the interface and down to the cell pellet.

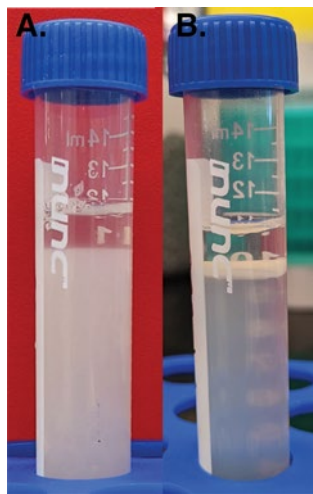


Figure 1. Percoll isolation of microglia.

A 30% Percoll cell-suspension overlaid with 1 mL 10% FBS/HBSS solution, A. before centrifugation and B. after centrifugation.

14. Resuspend the cell pellet in 1 mL of HBSS with 25 mM HEPES.
15. Add 9 mL of HBSS with 25 mM HEPES and centrifuge the single-cell suspension at $600 \times g$ for 5 min at 4°C with full acceleration and brake on.
16. Aspirate the cell pellet in a final volume of 1 mL of HBSS with 25 mM HEPES. Cells are now ready for antibody staining for flow cytometry.

B. Fluorochrome-conjugated antibody staining for flow cytometry analysis of cell surface markers on microglia

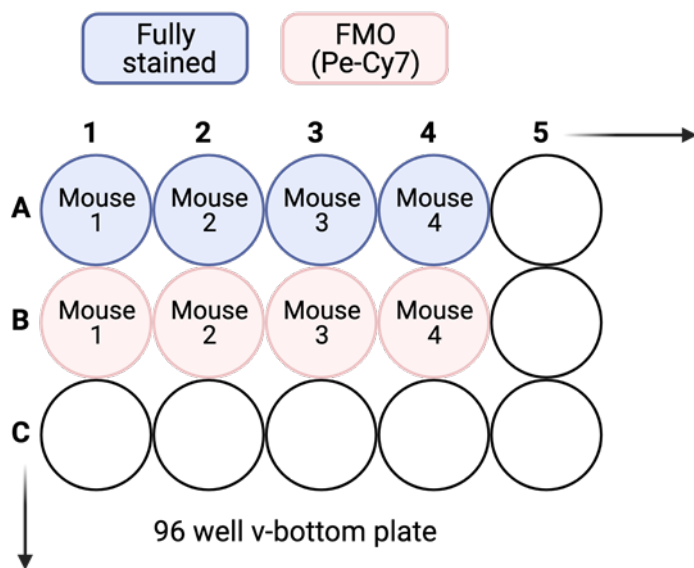


Figure 2. Example plate layout for anti-CD11c PE-Cy7 stained microglia and accompanying FMO controls

1. Transfer 150 μ L (approximately 1/7) of the single-cell suspension (approximately 300,000 live cells) from Step A16 to a well of a 96 well v-bottom plate. Repeat for any additional samples. Make sure to include wells for fluorescence-minus-one (FMO) controls for antigens of interest. For example, if the staining panel includes anti-CD11c PE-Cy7, include a well where cells are stained with all other antibodies EXCEPT for anti-CD11c PE-Cy7. This will account for background fluorescence in that specific channel for each sample.
2. Centrifuge the plate at 300 $\times g$ for 3 min at 4°C.
3. In one swift motion, decant the plate by flicking into a sink. Do not dab the plate dry. Do not flick the plate twice.
4. Resuspend the cells in the plate with 25 μ L of diluted FcBlock solution. Incubate at 4°C for 10 min.
5. Add 25 μ L of the 2 \times Microglia Antibody Panel to each well and mix well by pipetting. Incubate at 4°C for 30 min.
6. Add 150 μ L of Flow Staining Buffer to each well. Centrifuge the plate at 300 $\times g$ for 3 min at 4°C.
7. In one swift motion, decant the plate by flicking into a sink. Do not dab the plate dry. Do not flick the plate twice.
8. Resuspend the cells in 200 μ L of Flow Staining Buffer. Centrifuge the plate at 300 $\times g$ for 3 min at 4°C.
9. In one swift motion, decant the plate by flicking into a sink. Do not dab the plate dry. Do not flick the plate twice.
10. Repeat Steps B8 and B9.
11. Resuspend the cells in 200 μ L of Flow Staining Buffer containing 0.1 μ g/mL DAPI.
12. Transfer the samples to a 40 μ m mesh filter plate and centrifuge for 1 min at 100 $\times g$ to bring the samples to the lower chamber.
13. Transfer the samples to cluster tubes and keep on ice, protected from light. Promptly proceed with Section C: single-color compensation controls.

C. Preparation of single-color compensation controls

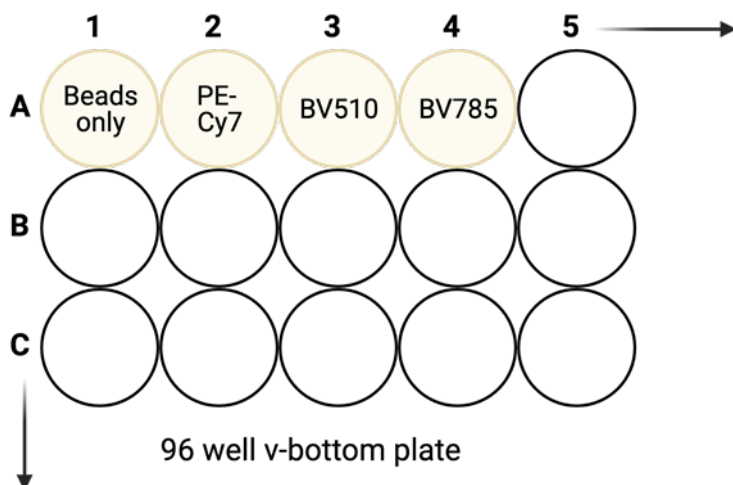


Figure 3. Sample plate layout for compensation control beads

1. For the number of fluorochromes used, add one drop of compensation beads to the same number of wells on a separate 96 well v-bottom plate. Include one extra well of beads for an unstained compensation control. Refer to Figure 3 for a sample layout.
2. Add 150 μ L of Flow Staining Buffer to each well.
3. Add 1 μ L of a single fluorochrome-conjugated antibody to a single well. Repeat for the remaining fluorochromes and wells. Do not add any antibody to the well containing the unstained compensation control. Incubate 15 min at room temperature, protected from light.
4. Centrifuge the plate at 300 $\times g$ for 3 min at 4°C.
5. In one swift motion, decant the plate by flicking into a sink. Do not dab the plate dry. Do not flick the plate twice.
6. Resuspend the beads in 200 μ L of flow staining buffer and transfer them to cluster tubes. Acquire promptly on the flow cytometer along with stained samples from Section B.

D. Sample acquisition on a 5-laser LSR Fortessa X-20

1. In Diva, create your experiment and select the detection channels corresponding to the fluorochrome panel used to stain your samples in Section B. For microglia, it is highly recommended to include an additional unoccupied detection channel (*e.g.*, 488 nm laser, 710/50 nm bandpass) to record background autofluorescence.
2. Create compensation controls for your experiment in Diva and acquire each individual single-color control, including the unstained beads, from Section C.
3. Calculate the compensation matrix and then run the samples of interest from Section B.

Data analysis

1. Identification of microglia from a CNS single-cell suspension

After sample acquisition, data analysis is performed in FlowJo V10. If a compensation matrix was not generated on the flow cytometer during sample acquisition, complete the compensation wizard in FlowJo before continuing. By utilizing the hierarchical gating strategy illustrated in Figure 4, singlets are gated first, followed by live cells (DAPI); lastly, microglia are identified by their relatively low CD45 expression and high CD11b expression.

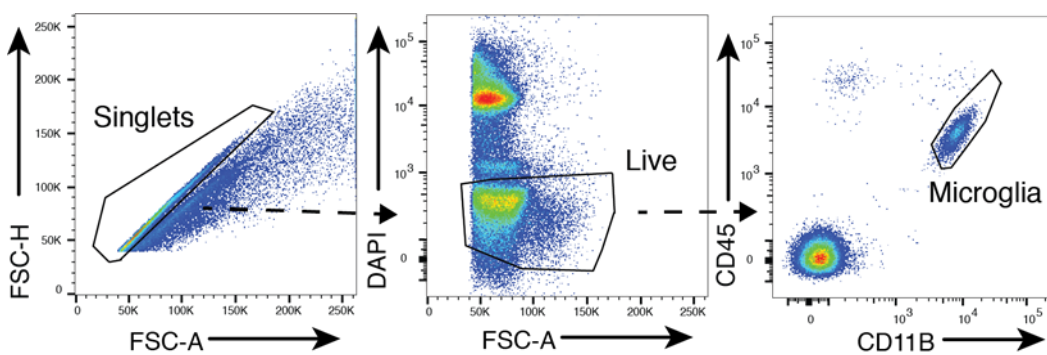


Figure 4. Hierarchical gating strategy to identify microglia from a CNS single-cell suspension. FSC, forward scatter. Reproduced from Burns *et al.*, 2020.

2. Analysis of protein target expression in microglia

Microglia subsets were recently identified based on their high or low/negligible levels of autofluorescence (Burns *et al.*, 2020). Because of the unusually high intensity, broad spectral properties, and bimodality of the autofluorescence signal in the microglia population (Figure 5), flow cytometry analysis of microglia poses specific challenges as experimental observations can be very easily confounded by background autofluorescence. Experiments should include “fluorescence-minus-one” controls (FMO) for antigen-fluorochrome combinations of interest to avoid this issue. In addition, when working with microglia, it is critical to include one or multiple unoccupied cytometer channels (*i.e.*, with no fluorescent antibody/dyes in those channels) during sample acquisition, preferably a channel equivalent to PerCP-Cy5.5 (488 nm blue laser line, 710/50 nm bandpass filter), which is one of the most sensitive channels for microglia autofluorescence (Figure 5).

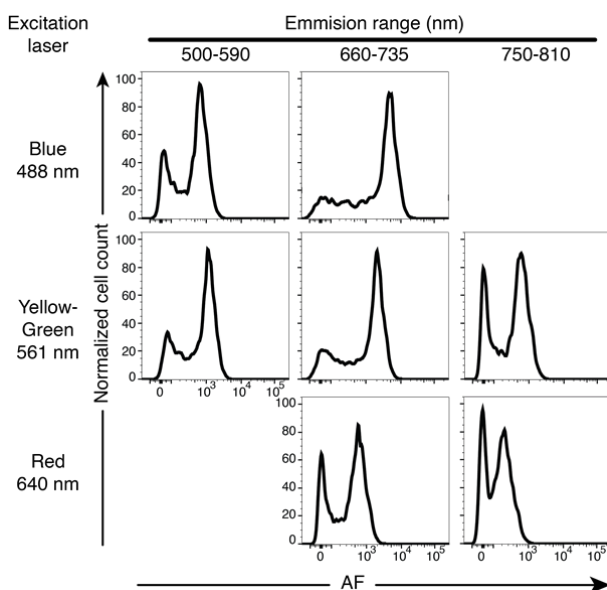


Figure 5. Representative flow cytometry histograms of autofluorescence intensity of the entire microglia population, in a single sample, from multiple combinations of excitation lasers and emission filters. AF, autofluorescence. Reproduced from Burns *et al.* (2020).

To illustrate these challenges, we present two examples where analysis of target protein expression in microglia can be easily confounded by autofluorescence if proper controls are not included to consider the

fraction of the fluorescence signal that is attributable to autofluorescence rather than the target protein marker of interest.

In this first example, we selected the surface antigen CD11c, which is an integrin transcriptionally expressed at relatively high levels on a small subset of microglia during development, injury, disease, and aging. In Figure 6A, CD45^{dim}CD11b⁺ microglia stained with anti-CD11c PE-Cy7 showed a clear bimodal distribution of signal in the PE-Cy7 channel, indicative at face value of positive CD11c staining in 57% of the microglia population. However, the histogram from the FMO control sample revealed a similar, bimodal pattern of fluorescence intensity with 44% of microglia gated as positive, reflective of the cellular autofluorescence in this cytometer channel (Figure 6A). When overlaid with the histogram from the CD11c PE-Cy7 stained sample, it was not possible to delineate an adequate gate to identify CD11c⁺ microglia given the bimodality of the autofluorescence signal in microglia and the existence of two subsets of microglia, one with high levels of autofluorescence and one with no or very low levels of autofluorescence (Figure 6B). Instead, visualizing the data in an XY dot plot format using an empty cytometer channel to measure autofluorescence (Blue laser, 710/50 nm) on one axis against the cytometer channel for the target antigen of interest on the other axis (CD11c PE-Cy7 in this example) allowed us to distinguish CD11c⁺ microglia previously confounded by the autofluorescence signal and use distinct thresholds for CD11c positivity for the autofluorescent negative and positive microglia populations (Figure 6C). Using this strategy, CD11c was found to be only expressed in 15% of the overall microglial population (Figure 6C). This result is markedly different from the one that mistakenly identified 57% of microglia as CD11c⁺ while ignoring the autofluorescence signal (Figure 6A). In imaging studies of young, healthy CD11c-YFP reporter mice, YFP⁺ cells were present as a minor population in the adult brain (Sato-Hashimoto *et al.*, 2019), and in a recent review (Benmamar-Badel *et al.*, 2020), it was estimated that approximately 2% of microglia are CD11c⁺ in these animals. Therefore, analyzing microglial CD11c expression by flow cytometry without taking AF into account could lead to misleading conclusions.

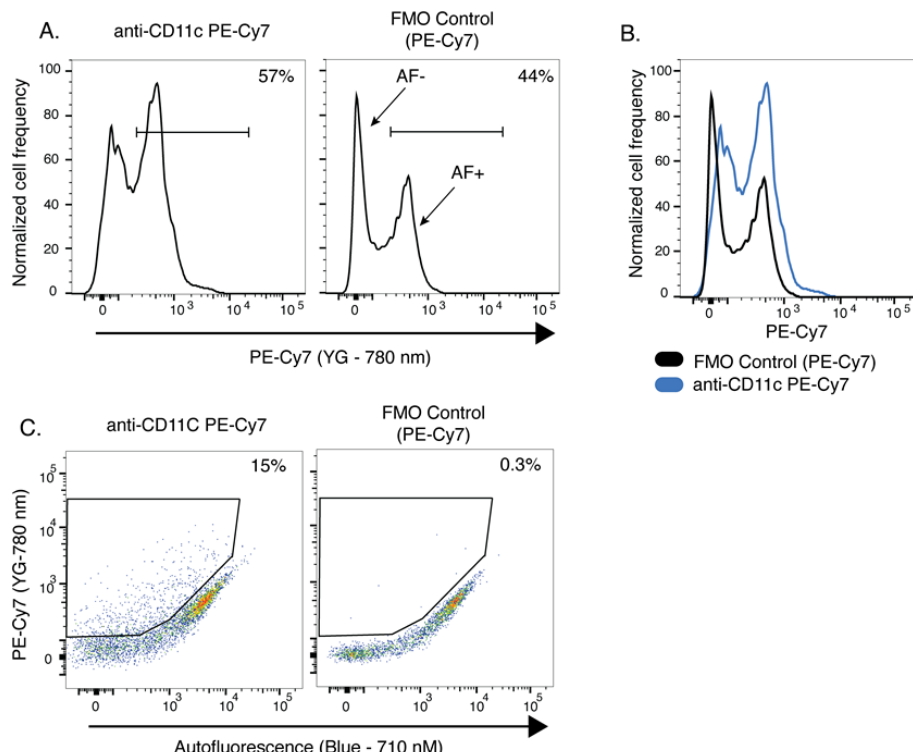


Figure 6. Analysis of microglia from 5-month-old mice by flow cytometry.

A. Histograms of fluorescence signal from FMO control and CD11c-stained microglia samples in the PE-Cy7 channel (Yellow-green laser, 780/60 nm). B. Overlay of the two previous histograms. C. Pseudocolor dot plots of signal in the PE-Cy7 fluorescence channel versus an unoccupied fluorescence

channel (Blue laser, 710/50 nm). AF⁺, autofluorescence-positive; AF⁻, autofluorescence-negative; FMO, fluorescence-minus-one; Blue, 488 nm laser; YG, 561 nm yellow-green laser.

As a second example, we analyzed the impact of microglia autofluorescence on the detection of proteins expressed in the entire microglia population (as opposed to a subset) with modest to high levels of expression at the single-cell level. For this, we specifically chose the receptor family for the Fc region of IgG immunoglobulins: CD16, CD32, and CD64. Fc-receptors comprise a large family of transmembrane proteins expressed at the plasma membrane of immune cells that bind the Fc region of antibodies and activate downstream signaling cascades. Microglia are known to express the gamma family of activating Fc receptors, which includes CD16/32 and CD64 (Pellerin *et al.*, 2021). *Fcer1g*-deficient mice lack the common signaling FCER1G chain required for surface expression of all activating Fc receptors. When stained with FITC conjugated anti-CD16/32 antibody and without considering microglia autofluorescence, wild-type microglia showed a clear positive staining with a bi-modal distribution (Figure 7A). However, microglia from *Fcer1g*^{-/-} mice retained a large fraction of this signal with a wider bimodal distribution, indicating that a significant fraction of the signal detected was not attributable to CD16/32 expression but to autofluorescence (Figure 7A). Accordingly, when the analytical strategy described in the prior example was used, and anti-CD16/32 stained samples were displayed on dot plots featuring CD16/32 expression on the y-axis against an empty channel on the x-axis, a large fraction of the signal associated with CD16/32 expression in Figure 7A became clearly attributable to the microglia autofluorescence signal in the *Fcer1g*^{KO} mice (Figure 7B). Inclusion and overlay of each sample's accompanying FMO control revealed the accurate expression levels of CD16/32 and the expected lack of CD16/32 staining in microglia from *Fcer1g*^{KO} mice (Figure 7B). Gating autofluorescence-positive (AF⁺) and autofluorescence-negative (AF⁻) microglia subsets (Burns *et al.*, 2020) using the autofluorescence channel further allowed the analysis of CD16/32 expression levels on these AF microglia subsets (Figure 7C).

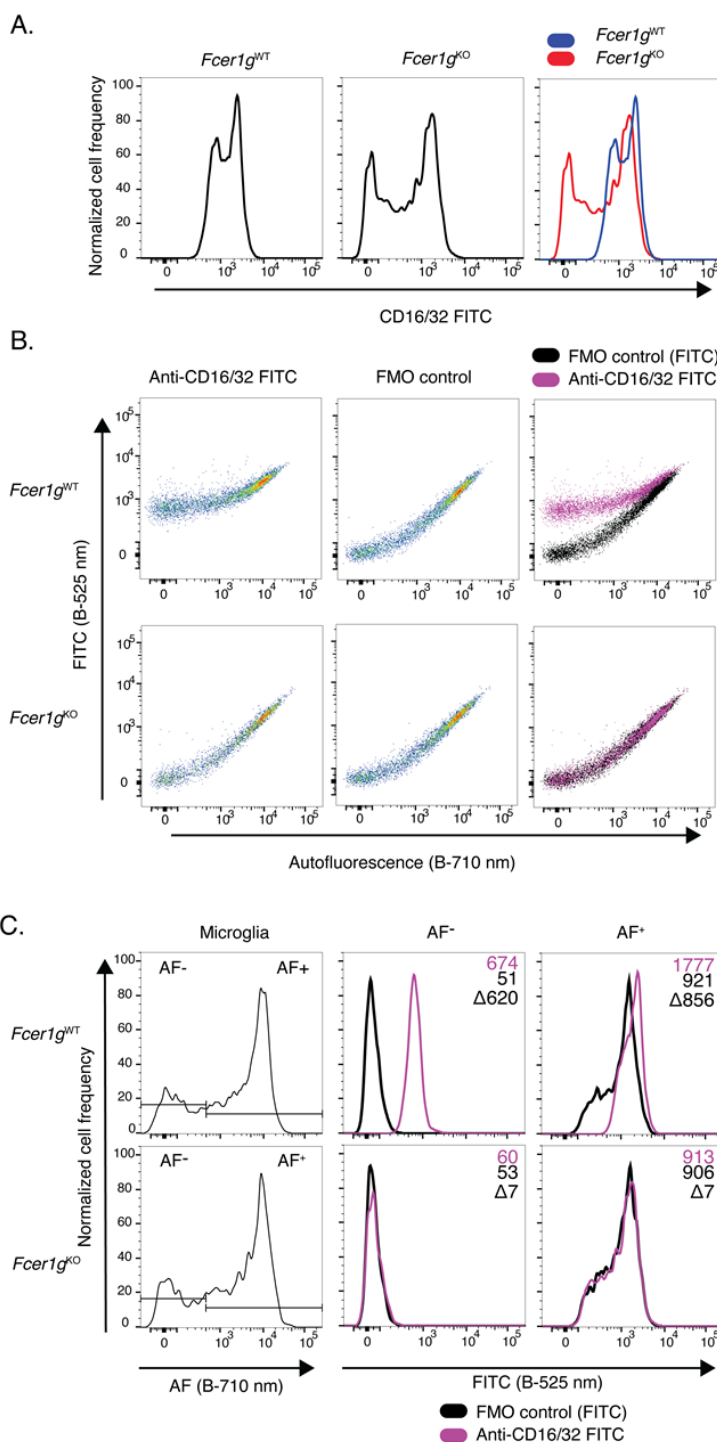


Figure 7. Analysis of Fc-receptor (CD16/32) surface expression levels in 6-month-old *Fcer1g* wild-type and knockout microglia.

A. Individual and overlaid histograms of CD16/32 surface levels on microglia isolated from wild-type and *Fcer1g*^{KO} animals. B. Individual and superimposed pseudocolor dot-plots of fluorescence signal detected in PerCP-Cy5.5 (B-710/50 nm, x-axis) and FITC (B-525/30 nm, y-axis) channels from anti-CD16/32 FITC stained and FMO control microglia isolated from wild-type or *Fcer1g*^{KO} mice. C. Gating of microglia AF subsets by AF intensity in the B-710/50 nm channel. Histograms of FITC signal intensity in autofluorescence⁺ (AF⁺) and autofluorescence⁻ (AF⁻) gated microglia subsets. Inset labels indicate geometric mean fluorescence intensity in the FITC channel for indicated population and the calculated

difference between anti-CD16/32 FITC stained and FMO control. AF, autofluorescence; FMO, Fluorescence minus one; B, 488 nm blue laser.

In contrast to the modest levels of expression of CD16/32, microglia express high levels of CD64, which exceed the autofluorescence intensity level seen in microglia. As a result, the detection of this highly expressed antigen is much less subject to autofluorescence confounding issues. This is highlighted by the bright, unimodal CD64 signal observed on wild-type microglia, which clearly surpasses the signal observed in *Fcer1g^{KO}* microglia (Figure 8A). This is confirmed by displaying the data in a pseudocolor dot plot, as the signal observed in anti-CD64 stained samples exceeds that of background autofluorescence (Figure 8B). Gating AF+ and AF- microglia subsets using the autofluorescence channel further allowed the analysis of CD64 expression levels on these AF microglia subsets (Figure 8C). These results highlight that autofluorescence represents a major confounding factor for the detection of protein expression in microglia using fluorescence-based methods, such as flow cytometry, and that care should be taken to account for autofluorescence using empty cytometer channels to achieve accurate detection and quantification of protein expression in this cell type.

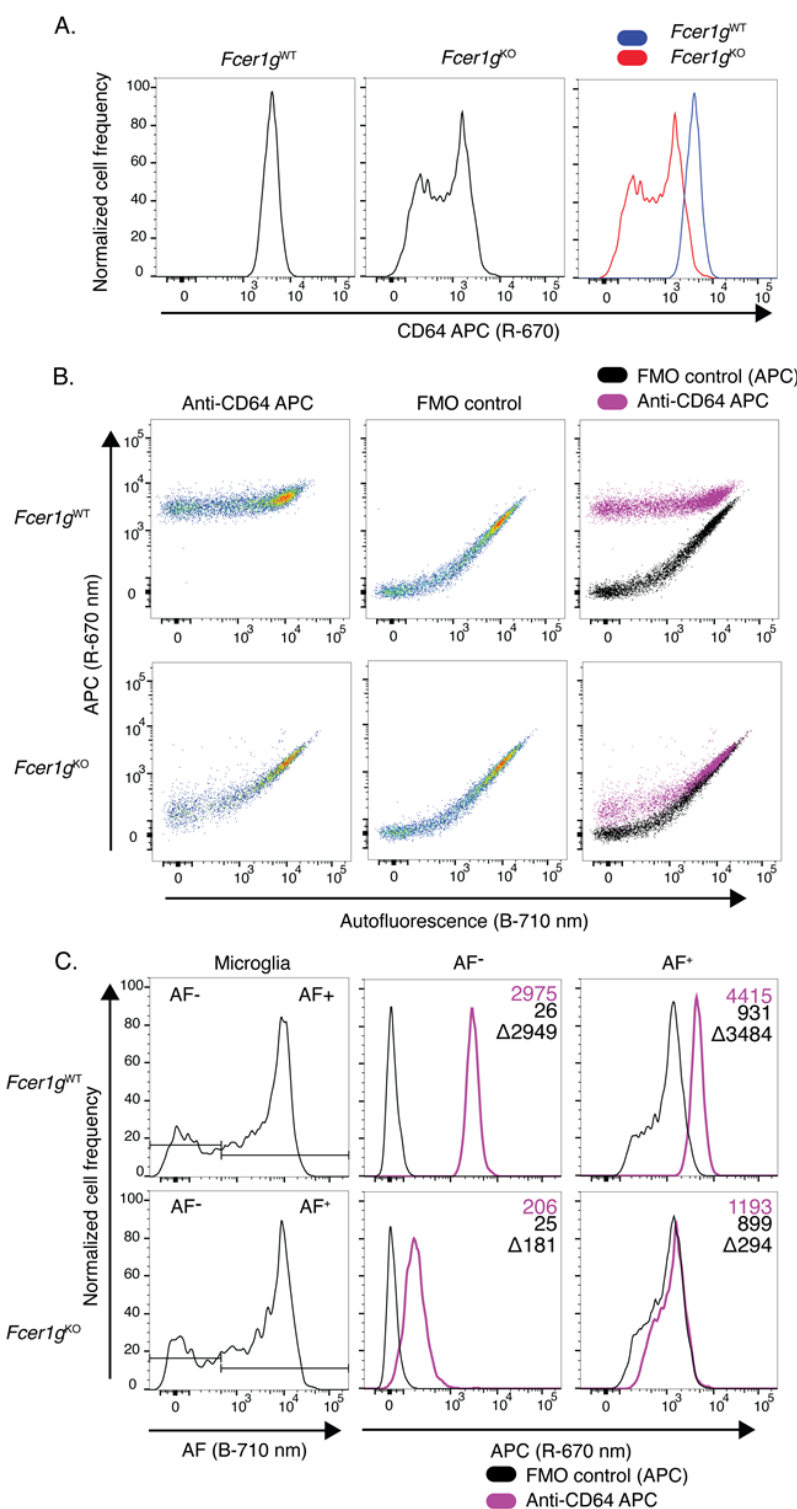


Figure 8. Analysis of Fc receptor (CD64) surface expression levels in 6-month-old *Fcer1g* wild-type and knockout microglia.

A. Individual and overlaid histograms of CD64 surface levels on microglia isolated from wild-type and *Fcer1g*^{KO} animals. B. Individual and superimposed pseudocolor dot-plots of fluorescence signal detected in PerCP-Cy5.5 (B-710/50 nm, x-axis) and APC (R-670/30 nm, y-axis) channels from anti-CD64 APC stained and FMO control microglia isolated from wild-type or *Fcer1g*^{KO} mice. C. Gating of microglia AF subsets by

AF intensity in the B-710/50 nm channel. Histograms of APC signal intensity in AF⁺ and AF⁻ gated microglia subsets. Inset labels indicate geometric fluorescence intensity in the APC channel for indicated population and the calculated difference between anti-CD64 APC stained and FMO control. AF, autofluorescence; FMO, Fluorescence minus one; B, 488 nm blue laser; R, 640 nm red laser.

Notes

1. During the wash steps of the flow cytometry staining procedure, flicking the plate twice or dabbing it dry after flicking may dislodge the cell pellet and increase cell loss.
2. Although microglia AF is detectable in all flow cytometer excitation/emission combinations we have tested, we have found that fluorescence detection channels for red-laser (640 nm) excited fluorochromes exhibit relatively lower levels of AF signal, which may minimize the confounding effects of cell autofluorescence on protein marker detection. In contrast, we found that blue-laser (488 nm) fluorescence detection channels were the more sensitive to detect microglia autofluorescence, and PerCP-Cy5.5 (710/50 nm bandpass) provided the highest resolution between AF microglia subsets.
3. If the microglial expression of an antigen of interest is expected to be low, it is advisable to test with brighter fluorochromes (*e.g.*, AlexaFluor 647); however, relative fluorochrome intensity will vary depending on the cytometer instrument ultimately used.
4. When generating single-color compensation controls, microglia should not be used, as the brightness level and bimodal nature of autofluorescence will result in an aberrant compensation matrix. Ideally, compensation beads should be used, but if unavailable, a surrogate non-autofluorescent cell population, such as splenocytes, may be used instead.
5. On the cytometer, PMT voltage levels should not be decreased to artificially minimize microglial autofluorescence, as this will also decrease the signal from antigens of interest.
6. Although we do not explicitly cover the methods to probe intracellular antigens, such as LAMP1 and Ki-67, we have successfully used the eBioscience FoxP3 Transcription Factor (ThermoFisher, catalog number: 00-5523-00) staining kit, per manufacturer protocol. However, because this strong fixation/permeabilization protocol alters the detection of several key markers to identify microglia, we recommend using the nuclear antigen PU.1 to accurately identify microglia within these fixed and permeabilized single-cell suspensions.
7. For murine samples, additional antibodies against microglia-specific cell surface markers have been successfully used (Burns *et al.*, 2020, Figure 1), including anti-P2RY12 (Biolegend, catalog number: 848004), anti-TMEM119 (AbCam, catalog number: 225494), and anti-CX3CR1 (Biolegend, catalog number: 149023).
8. Although this protocol has been applied primarily to mouse brain tissue, we have successfully used it for mouse spinal cord and brain tissue from rats and cynomolgus monkeys. When isolating CNS microglia from species other than mice, the tissue weight being processed should be kept under < 450 mg.
9. Aging critically impacts levels of autofluorescence observed in microglia. Although autofluorescence can be detected with a bimodal distribution in microglia as early as postnatal day 30, autofluorescence levels dramatically increase with aging and become more and more confounding when mice get into mature adulthood and older (Burns *et al.*, 2020).

Recipes

1. 33% isotonic Percoll

9 mL of Percoll
10× Hanks Balanced Salt Solution
20 mL of 1× HBSS with 25 mM HEPES

2. HBSS with 25 mM HEPES

12.5 mL 1 M HEPES

487.5 mL 1× HBSS

3. PBS with 3 mM EDTA

6 mL 0.5 M EDTA

494 mL 1× HBSS

4. Fc receptor blocking solution (for 10 samples)

245 µL Flow Staining buffer

5 µL TruStain FcX

5. 2× microglia antibody panel (for 10 samples)

2.5 µL of 0.2 mg/mL anti-CD45 BV785

2.5 µL of 0.2 mg/mL anti-CD11b BV510

245 µL Flow Staining buffer

6. DAPI working solution

1 µL of 1 mg/mL DAPI solution

10 mL of Flow Staining buffer

Acknowledgments

We thank the authors of Burns *et al.* (2020), from which this protocol was originally derived from.

Competing interests

JCB and MM are full-time employees of Biogen and Biogen shareholders. RMR is a full-time employee of Third Rock Ventures. No authors were provided compensation or free products by any vendors utilized in this protocol.

Ethics

This study was performed in accordance with the National Institutes of Health Guide for the Care and Use of Laboratory Animals. Research animals at Biogen were housed in an AAALAC accredited facility and handled according to an approved institutional animal care and use committee (IACUC) protocol (#756).

References

- Autengruber, A., Gereke, M., Hansen, G., Hennig, C. and Bruder, D. (2012). [Impact of enzymatic tissue disintegration on the level of surface molecule expression and immune cell function](#). *Eur J Microbiol Immunol (Bp)* 2(2): 112-120.
- Benmamar-Badel, A., Owens, T. and Wlodarczyk, A. (2020). [Protective Microglial Subset in Development, Aging, and Disease: Lessons From Transcriptomic Studies](#). *Front Immunol* 11: 430.
- Burns, J. C., Cotleur, B., Walther, D. M., Bajrami, B., Rubino, S. J., Wei, R., Franchimont, N., Cotman, S. L., Ransohoff, R. M. and Mingueneau, M. (2020). [Differential accumulation of storage bodies with aging defines discrete subsets of microglia in the healthy brain](#). *Elife* 9: e57495.

- Clayton, K. A., Van Enoo, A. A. and Ikezu, T. (2017). [Alzheimer's Disease: The Role of Microglia in Brain Homeostasis and Proteopathy](#). *Front Neurosci* 11: 680.
- Li, Q. and Barres, B. A. (2018). [Microglia and macrophages in brain homeostasis and disease](#). *Nat Rev Immunol* 18(4): 225-242.
- Mattei, D., Ivanov, A., van Oostrum, M., Pantelyushin, S., Richetto, J., Mueller, F., Beffinger, M., Schellhammer, L., Vom Berg, J., Wollscheid, B., Beule, D., Paolicelli, R. C. and Meyer, U. (2020). [Enzymatic Dissociation Induces Transcriptional and Proteotype Bias in Brain Cell Populations](#). *Int J Mol Sci* 21(21).
- O'Flanagan, C. H., Campbell, K. R., Zhang, A. W., Kabeer, F., Lim, J. L. P., Biele, J., Eirew, P., Lai, D., McPherson, A., Kong, E., Bates, C., Borkowski, K., Wiens, M., Hewitson, B., Hopkins, J., Pham, J., Ceglia, N., Moore, R., Mungall, A. J., McAlpine, J. N., Team, C. I. G. C., Shah, S. P. and Aparicio, S. (2019). [Dissociation of solid tumor tissues with cold active protease for single-cell RNA-seq minimizes conserved collagenase-associated stress responses](#). *Genome Biol* 20(1): 210.
- Pellerin, K., Rubino, S. J., Burns, J. C., Smith, B. A., McCarl, C. A., Zhu, J., Jandreski, L., Cullen, P., Carlile, T. M., Li, A., Rebollar, J. V., Sybulski, J., Reynolds, T. L., Zhang, B., Basile, R., Tang, H., Harp, C. P., Pellerin, A., Silbereis, J., Franchimont, N., Cahir-McFarland, E., Ransohoff, R. M., Cameron, T. O. and Mingueneau, M. (2021). [MOG autoantibodies trigger a tightly-controlled FcR and BTK-driven microglia proliferative response](#). *Brain*. doi: 10.1093/brain/awab231.
- Ransohoff, R. M. and El Khoury, J. J. (2016). [Microglia in health and disease](#). *Cold Spring Harb. Perspect. Biol* 8(1): a020560.
- Sato-Hashimoto, M., Nozu, T., Toriba, R., Horikoshi, A., Akaike, M., Kawamoto, K., Hirose, A., Hayashi, Y., Nagai, H., Shimizu, W., Saiki, A., Ishikawa, T., Elhanbly, R., Kotani, T., Murata, Y., Saito, Y., Naruse, M., Shibusaki, K., Oldenborg, P. A., Jung, S., Matozaki, T., Fukazawa, Y. and Ohnishi, H. (2019). [Microglial SIRPalpha regulates the emergence of CD11c\(+\) microglia and demyelination damage in white matter](#). *Elife* 8: e42025.

Isolation of Nuclei from Mouse Dorsal Root Ganglia for Single-nucleus Genomics

Lite Yang¹, Ivan Tochitsky², Clifford J. Woolf² and William Renthal^{1,*}

¹Department of Neurology, Brigham and Women's Hospital and Harvard Medical School, Boston, USA

²F.M. Kirby Neurobiology Center, Boston Children's Hospital, Boston, USA

*For correspondence: wrenthal@bwh.harvard.edu

Abstract

Primary somatosensory neurons, whose cell bodies reside in the dorsal root ganglion (DRG) and trigeminal ganglion, are specialized to transmit sensory information from the periphery to the central nervous system. Our molecular understanding of peripheral sensory neurons has been limited by both their heterogeneity and low abundance compared with non-neuronal cell types in sensory ganglia. We describe a protocol to isolate nuclei from mouse DRGs using iodixanol density gradient centrifugation, which enriches for neuronal nuclei while still sampling non-neuronal cells such as satellite glia and Schwann cells. This protocol is compatible with a range of downstream applications such as single-nucleus transcriptional and epigenomic assays.

Keywords: Dorsal root ganglion, Sensory neurons, Single-nucleus RNA-seq, Single-nucleus ATAC-seq, Gene regulation, Epigenomics

This protocol was validated in: Neuron (2020), DOI: 10.1016/j.neuron.2020.07.026.

Background

Gene expression is dynamically regulated in dorsal root ganglion (DRG) cells after peripheral nerve injury, a process important for axonal regeneration and the neuronal hyperexcitability that contributes to neuropathic pain. Previous studies have analyzed gene expression and chromatin structure from bulk DRG tissues (Perkins *et al.*, 2014; Chandran *et al.*, 2016), but their interpretation is complicated by the cellular heterogeneity of the DRG.

Single-cell/single-nucleus genomics has become an important tool for studying molecular features within distinct peripheral sensory neuronal subtypes (Usoskin *et al.*, 2015; Nguyen *et al.*, 2017 and 2019; Zeisel *et al.*, 2018; Sharma *et al.*, 2020). While single-cell transcriptional profiling from sensory ganglia appears to provide greater transcriptional diversity than single-nucleus transcriptional profiling, a key advantage of analyzing nuclei is that it can be applied to both fresh and archived frozen specimens. This offers flexibility in sample preparation and greater access to human samples. Nuclei isolation is also associated with induction of immediate early genes contrary to whole-cell isolation because it is faster, avoids cytoplasmic signaling cascades, and is conducted entirely at 4°C. These features make single-nucleus analyses particularly attractive for studying changes that occur rapidly after a stimulus.

Here, we describe a density gradient centrifugation protocol for purifying nuclei from frozen mouse DRG samples, which is compatible with droplet-based single-nucleus genomic analyses (Renthal *et al.*, 2020). This protocol, which is based on previous protocols for extracting mouse and human CNS nuclei (Mo *et al.*, 2015; Renthal *et al.*, 2018), yields a greater fraction of neuronal nuclei (40-50% neurons as measured by single-nucleus RNA sequencing) as compared with commonly used non-gradient dissociation methods (5-10% neurons) (Habib *et al.*, 2017; Avraham *et al.*, 2020; Slyper *et al.*, 2020), while still sampling a broad range of non-neuronal DRG cell types.

Materials and Reagents

1. 1.5-mL centrifuge tubes (Eppendorf, catalog number: 022431021)
2. 5-mL centrifuge tubes (Eppendorf, catalog number: 0030108310)
3. 50-mL conical centrifuge tubes (Falcon, catalog number: 352098)
4. Cell strainers, 40-µm (BD Falcon, catalog number: 352340)
5. Ultracentrifuge tubes (Beckman Coulter, catalog number: 344059)
6. Laboratory film (Parafilm, catalog number: PM-996)
7. Freshly dissected or freshly frozen mouse DRG tissue
8. RNase inhibitor (Promega, catalog number: N2611)
9. 60% Iodixanol solution (Sigma, catalog number: D1556)
10. IGEPAL CA-630 (Sigma, catalog number: I8896)
11. Nuclease-free water (Invitrogen, catalog number: 4387936)
12. 35% Bovine Serum Albumin solution (BSA; Sigma, catalog number: A7979-50ML)
13. Sucrose (Millipore, catalog number: 573113)
14. KCl (Thermo Fisher Scientific, catalog number: AM9640G)
15. MgCl₂ (Thermo Fisher Scientific, catalog number: AM9530G)
16. Tricine (Sigma, catalog number: T0377)
17. KOH (Sigma, catalog number: 221465)
18. Actinomycin (Sigma Aldrich, catalog number: A9415)
19. PBS (Thermo Fisher Scientific, catalog number: 10010023)
20. Trypan Blue (Fisher Scientific, catalog number: 15-250-061)
21. (Optional) Nuclei buffer (10× genomics, catalog number: PN-2000207)
22. Stock buffer HB (see Recipes)
23. Diluent buffer (see Recipes)

Equipment

1. Ultracentrifuge (Beckman Coulter, model: Optima L-90K)
2. Ultracentrifuge swinging-bucket rotor (Beckman Coulter, model: SW 41 Ti)
3. Centrifuge with swinging-bucket rotors (Thermo Scientific, model: 75004261)
4. 7-mL Dounce homogenizer (Thermo Fisher Scientific, model: 06435A)
5. Tissue-Tearor (Biospec Products Inc., model: 985370-04)
6. Hemocytometer (Hausser Scientific, 1492)

Procedure

A. Preparation

1. Prepare fresh DRGs from experimental animals (Lin *et al.*, 2018). Alternatively, DRG samples can be prepared in advance and stored at -80°C.
2. Prepare the fresh buffers listed below and maintain them at 4°C (buffer volumes shown below are for one DRG sample).

Note: It is important to vortex any solutions containing iodixanol well every time before use.

- a. 7.5 mL Working Solution (50% iodixanol): 6.25 mL 60% iodixanol solution + 1.25 mL Diluent.
 - b. 1.25 mL 30% iodixanol: 750 µL Working Solution + 500 µL Stock Buffer HB + 1.5 µL 35% BSA + 2 µL RNase inhibitor.
 - c. 1.25 mL 40% iodixanol: 1 mL Working Solution + 250 µL Stock Buffer HB + 1.5 µL 35% BSA + 2 µL RNase inhibitor.
 - d. 5 mL Working Buffer HB: 5 mL Stock Buffer HB + 6 µL 35% BSA + 7.5 µL RNase inhibitor.
 - e. 400 µL 5% IGEPAL CA-630: 20 µL IGEPAL CA-630 + 380 µL Working Buffer HB.
3. Pre-cool centrifuge, ultracentrifuge, and rotor to 4°C. All centrifugations should be done at 4°C.

Note: Using swing-bucket rotors is recommended to improve the final nuclei recovery.

4. Prepare one ultracentrifuge tube for each DRG sample. In each tube, prepare the density gradient solution by layering 1 mL 40% iodixanol at the bottom and then slowly adding 1 mL 30% iodixanol on top of it, without disturbing the interface. Pre-cool tubes on ice.

Note: While preparing the density gradient solution, pipette just above the 40% layer against the wall, allowing it to form two distinct layers. Try again if you do not see two distinct layers after sitting for 1 min. Before placing the tube on ice, pre-indent the ice with another tube to avoid disrupting the density gradient layers.

B. Lysis

1. Transfer each DRG sample to a 5-mL centrifuge tube. Prepare one DRG sample at a time.
2. Add 4 mL Working Buffer HB to the 7-mL Dounce homogenizer and pre-cool the homogenizer on ice.
3. Add 1 mL ice-cold Working Buffer HB to the DRG sample and place the tube on ice for 15-30 s until the DRGs sink.
4. Homogenize the DRG sample with a Tissue-Tearor using the low setting (< level four out of seven levels for Tissue-Tearor 985370-04) for about 5 s. Visually inspect the sample and confirm that the tissue is homogenized.

5. Transfer the homogenate to the pre-cooled 7-mL Dounce homogenizer.
6. Further homogenize the tissue by douncing with a tight pestle for 10-12 strokes.
7. Add 320 μ L 5% IGEPAL CA-630 and dounce with a tight pestle for five additional strokes. Dounce slowly to avoid bubbles.
8. Filter the homogenate through a 40- μ m cell strainer into a 50-mL conical tube.
9. Add 5 mL recently vortexed Working Solution to the lysed sample to reach a final volume of 10 mL. Gently pipette up and down to mix the solution.

Note: The iodixanol concentration in the lysed sample is 25%.

10. Place the 50-mL conical tube containing 10 mL lysed sample on ice. Repeat Steps B1-B9 for each additional DRG sample.

Note: Lysed samples can be placed on ice for as long as 30 min before proceeding to Procedure C. It is important to remove undissociated myelin and fully clean the Tissue-Tearor and 7-mL Dounce homogenizer by rinsing with Stock Buffer HB several times between samples.

C. Gradient formation and centrifugation

1. Using a 1-mL pipette tip, slowly pipette each of the lysed samples onto the 30% iodixanol layer of the density gradient solution prepared in Step A3.
2. Balance the weight of the samples with nuclease-free water prior to centrifugation. Seal the top of each ultracentrifuge tube with parafilm.
3. Ultracentrifuge samples at 10,000 \times g (equivalent to 7,600 rpm with SW 41 Ti rotor) for 18 min at 4°C.
4. After ultracentrifugation, white particles that contain the desired nuclei may be visible at the interface between 30% and 40% iodixanol if there is sufficient starting material (Figure 1).
5. Discard ~10 mL of the top layer to facilitate access to the interface between 30% and 40% iodixanol.
6. Place a 1-mL pipette tip at the interface between the 30% and 40% iodixanol layers. While moving the pipette tip around the layer, slowly aspirate 400 μ L nuclei sample just above the 40% iodixanol layer and transfer it to a new 1.5-mL centrifuge.

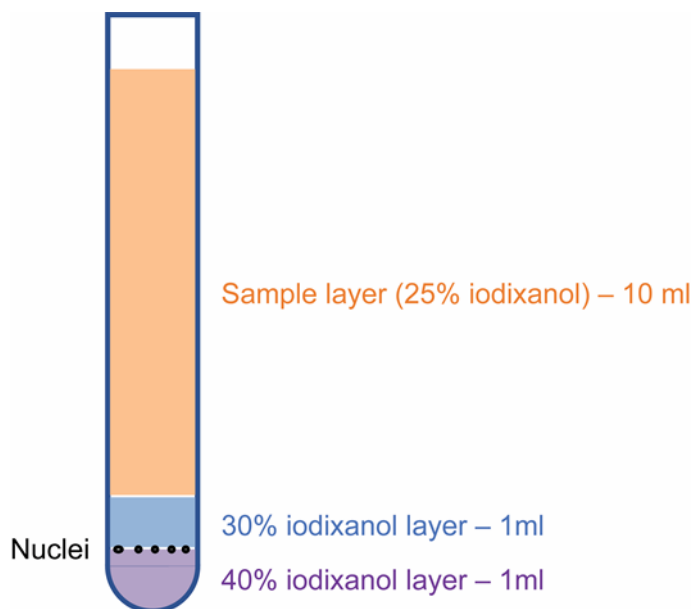


Figure 1. Illustration of iodixanol layers and nuclei positions after ultracentrifugation

D. Dilution and resuspension

Note: This step may vary based on the downstream analyses. Here, we demonstrate the sample preparation for inDrops single-cell RNA sequencing (Zilioniset et al., 2017) and 10× Genomics assays such as the Single Cell Gene Expression Assay and Single Cell Assay for Transposase-accessible Chromatin (ATAC). As an optional step, fluorescence-activated cell sorting can be used to further remove cellular debris and/or purify genetically labeled cell populations

1. inDrops
 - a. Take 10 μ L nuclei sample, stain it with Trypan Blue, and count nuclei using a hemocytometer (Figure 2).
 - b. Dilute nuclei with 30% iodixanol to 80,000 nuclei/mL.
 - c. Proceed to inDrops.

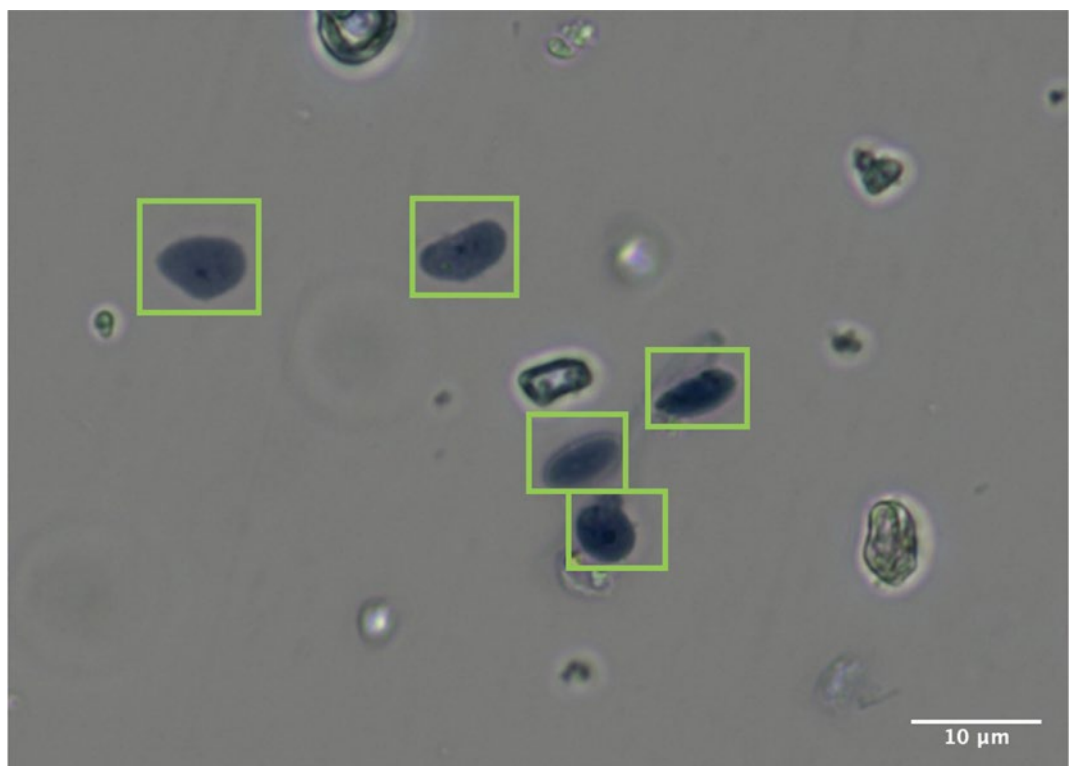


Figure 2. DRG nuclei sample stained with 0.2% Trypan Blue.

Image was taken at 60 \times magnification. The particles highlighted with green rectangles are intact nuclei.

Note: Some DRG nuclei have elongated shapes in this preparation.

2. 10 \times Genomics Single Cell assays
 - a. Single Cell Gene Expression
 - i. To dilute the iodixanol, add 4 mL PBS with 0.05% BSA to the nuclei sample. Gently pipette up and down to mix the solution.
 - ii. Centrifuge at 500 \times g for 5 min. Remove supernatant.
 - iii. Centrifuge at 500 \times g for 2 min. Remove excess supernatant.
 - iv. Resuspend the pellet in 45.5 μ L PBS with 0.05% BSA.
 - v. Take 2 μ L sample, stain it with Trypan Blue, and count nuclei using a hemocytometer (Figure 2).

- vi. Calculate the input volume of nuclei sample based on the Cell Suspension Volume Calculator Table in the 10 \times Genomics Single Cell Gene Expression User Guide.
 - vii. Proceed with the 10 \times Genomics Single Cell Gene Expression Protocol.
- b. Single Cell ATAC
- i. Take 10 μ L sample and visualize the nuclear membrane at 60 \times magnification to ensure no blebbing (Figure 3).

Note: Samples with blebbing nuclei are not recommended for use.

- ii. To dilute the iodixanol, add 4 mL PBS with 0.05% BSA to the nuclei sample. Gently pipette up and down to mix the solution.
- iii. Centrifuge at 500 \times g for 5 min. Remove supernatant.
- iv. Centrifuge at 500 \times g for 2 min. Remove excess supernatant.
- v. Resuspend the pellet in 7 μ L 1 \times nuclei buffer.
- vi. Take 2 μ L sample, stain it with Trypan Blue, and count nuclei using a hemocytometer (Figure 2).
- vii. Dilute the sample to the desired loading concentration based on the Nuclei Concentration Guidelines in the 10 \times Genomics Single Cell ATAC User Guide.
- viii. Proceed with the 10 \times Genomics Single Cell ATAC Protocol.

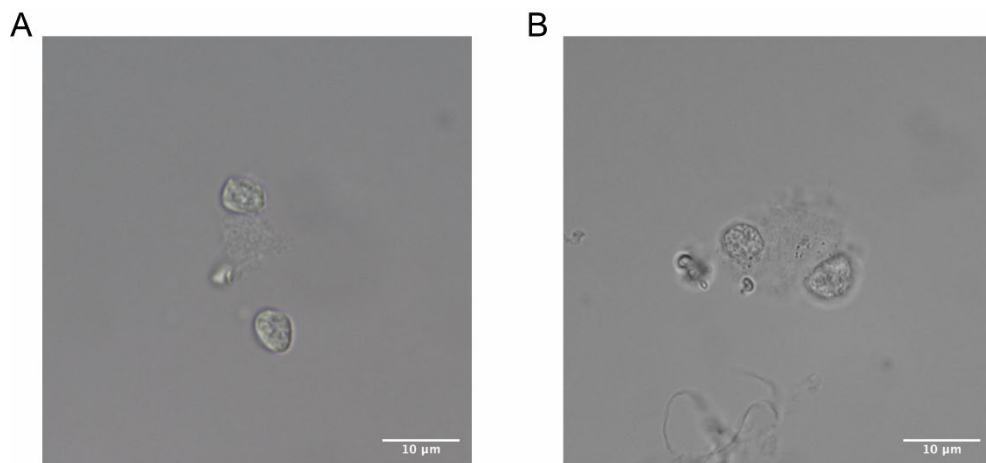


Figure 3. Representative images of mouse DRG nuclei at 60 \times magnification.

(A). High-quality intact nuclei show well-resolved edges. (B). Low-quality nuclei show evidence of blebbing.

Recipes

1. Stock buffer HB

0.25 M sucrose
25 mM KCl
5 mM MgCl₂
20 mM Tricine-KOH, pH 7.8
5 mg/mL actinomycin
Sterilize using a 0.2- μ m filter and store at 4°C for up to 1 month

2. Diluent buffer

150 mM KCl
30 mM MgCl₂
120 mM Tricine-KOH, pH 7.8
Sterilize using a 0.2-μm filter and store at 4°C for up to 1 month

Acknowledgments

W.R. is supported by the National Institute of Neurological Disorders and Stroke (NINDS) K08NS101064, the Burroughs Wellcome Fund, and the Migraine Research Foundation. C.J.W. is supported by NINDS R35NS105076-01, the DARPA Panacea program (HR0011-19-2-0022), and Adelson Medical Research Foundation.

Competing interests

L.Y. and W.R. have no competing interests. I.T. is an employee at Regeneron. C.J.W. is a founder of Nocion Therapeutics and QurAlis.

References

- Chandran, V., Coppola, G., Nawabi, H., Omura, T., Versano, R., Huebner, E. A., Zhang, A., Costigan, M., Yekkirala, A., Barrett, L., Blesch, A., Michaelevski, I., Davis-Turak, J., Gao, F., Langfelder, P., Horvath, S., He, Z., Benowitz, L., Fainzilber, M., Tuszyński, M., Woolf, C.J. and Geschwind, D. H. (2016). [A Systems-Level Analysis of the Peripheral Nerve Intrinsic Axonal Growth Program](#). *Neuron* 89: 956-970.
- Perkins, J. R., Antunes-Martins, A., Calvo, M., Grist, J., Rust, W., Schmid, R., Hildebrandt, T., Kohl, M., Orengo, C., McMahon, S. B. and Bennett, D. L. (2014). [A comparison of RNA-seq and exon arrays for whole genome transcription profiling of the L5 spinal nerve transection model of neuropathic pain in the rat](#). *Mol Pain* 10: 7.
- Usoskin, D., Furlan, A., Islam, S., Abdo, H., Lönnérberg, P., Lou, D., Hjerling-Leffler, J., Haeggström, J., Kharchenko, O., Kharchenko, P. V., Linnarsson, S. and Ernfors, P. (2015). [Unbiased classification of sensory neuron types by large-scale single-cell RNA sequencing](#). *Nat Neurosci* 18: 145-153.
- Zeisel, A., Hochgerner, H., Lönnérberg, P., Johnsson, A., Memic, F., van der Zwan, J., Häring, M., Braun, E., Borm, L. E., La Manno, G., Codeluppi, S., Furlan, A., Lee, K., Skene, N., Harris, K. D., Hjerling-Leffler, J., Arenas, E., Ernfors, P., Marklund, U. and Linnarsson, S. (2018). [Molecular Architecture of the Mouse Nervous System](#). *Cell* 174: 999-1014.e22.
- Sharma, N., Flaherty, K., Lezgiyeva, K., Wagner, D. E., Klein, A.M. and Ginty, D. D. (2020). [The emergence of transcriptional identity in somatosensory neurons](#). *Nature* 577: 392-398.
- Nguyen, M. Q., Le Pichon, C. E. and Ryba, N. (2019). [Stereotyped transcriptomic transformation of somatosensory neurons in response to injury](#). *Elife* 8: e49679.
- Nguyen, M. Q., Wu, Y., Bonilla, L. S., von Buchholtz, L. J. and Ryba, N. J. P. (2017). [Diversity amongst trigeminal neurons revealed by high throughput single cell sequencing](#). *PLoS One* 12: e0185543.
- Renthal, W., Tochitsky, I., Yang, L., Cheng, Y. C., Li, E., Kawaguchi, R., Geschwind, D. H. and Woolf, C. J. (2020). [Transcriptional Reprogramming of Distinct Peripheral Sensory Neuron Subtypes after Axonal Injury](#). *Neuron* 108: 128-144.e9.
- Renthal, W., Boxer, L. D., Hrvatin, S., Li, E., Silberfeld, A., Nagy, M. A., Griffith, E. C., Vierbuchen, T. and Greenberg, M. E. (2018). [Characterization of human mosaic Rett syndrome brain tissue by single-nucleus RNA sequencing](#). *Nat Neurosci* 21: 1670-1679.
- Mo, A., Mukamel, E. A., Davis, F. P., Luo, C., Henry, G. L., Picard, S., Urich, M. A., Nery, J.R., Sejnowski, T. J., Lister, R., Eddy, S. R., Ecker, J. R. and Nathans, J. (2015). [Epigenomic Signatures of Neuronal Diversity in the Mammalian Brain](#). *Neuron* 86: 1369-1384.

- Slyper, M. Porter, C. B. M., Ashenberg, O., Waldman, J., Drokhlyansky, E., Wakiro, I. and Smillie, C. *et al.* (2020). [A single-cell and single-nucleus RNA-Seq toolbox for fresh and frozen human tumors](#). *Nat Med* 26: 792-802.
- Habib, N., Avraham-David, I., Basu, A., Burks, T., Shekhar, K., Hofree, M., Choudhury, S. R., Aguet, F., Gelfand, E., Ardlie, K., Weitz, D. A., Rozenblatt-Rosen, O., Zhang, F. and Regev, A. (2017). [Massively parallel single-nucleus RNA-seq with DroNc-seq](#). *Nat Methods* 14: 955-958.
- Avraham, O., Deng, P. Y., Jones, S., Kuruvilla, R., Semenkovich, C. F., Klyachko, V. A. and Cavalli, V. (2020). [Satellite glial cells promote regenerative growth in sensory neurons](#). *Nat Commun* 11: 4891.
- Lin, Y. T. and Chen, J. C. (2018). [Dorsal Root Ganglia Isolation and Primary Culture to Study Neurotransmitter Release](#). *J Vis Exp* 140: e57569.
- Zilioniset, R. Nainys, J., Veres, A., Savova, V., Zemmour, D., Klein, A.M. and Mazutis, L. (2017). [Single-cell barcoding and sequencing using droplet microfluidics](#). *Nat Protoc* 12: 44-73.

CRISPR-mediated Labeling of Cells in Chick Embryos Based on Selectively Expressed Genes

Masahito Yamagata and Joshua R. Sanes*

Center for Brain Science and Department of Molecular and Cellular Biology, Harvard University, Cambridge MA, 02138, USA

*For correspondence: sanesj@mcb.harvard.edu

Abstract

The abilities to mark and manipulate specific cell types are essential for an increasing number of functional, structural, molecular, and developmental analyses in model organisms. In a few species, this can be accomplished by germline transgenesis; in other species, other methods are needed to selectively label somatic cells based on the genes that they express. Here, we describe a method for CRISPR-based somatic integration of reporters or Cre recombinase into specific genes in the chick genome, followed by visualization of cells in the retina and midbrain. Loci are chosen based on an RNA-seq-based cell atlas. Reporters can be soluble to visualize the morphology of individual cells or appended to the encoded protein to assess subcellular localization. We call the method eCHIKIN for electroporation- and CRISPR-mediated Homology-instructed Knock-IN.

Keywords: Chick embryo, Cre, CRISPR, GFP, Homologous recombination, Electroporation

This protocol was validated in: *eLife*. (2021). DOI:10.7554/eLife.63907

Background

Many functional, structural, molecular, and developmental analyses in model organisms now rely on the abilities to mark and manipulate specific cell types. In a limited number of species – *Mus musculus* (mice), *Danio rerio* (zebrafish), *C. elegans* (worms), and *Drosophila melanogaster* (flies) – this can be accomplished by germline transgenesis. For example, transgenic animals can be generated in which regulatory elements from a gene selectively expressed by a cell type of interest drive the expression of a reporter.

Alternatively, the transgene can encode an effector such as Cre recombinase, which enables selective expression of a second transgene provided either in the germline or to somatic cells via a viral or other vector (Luo *et al.*, 2018).

For other model organisms in which germline transgenesis is currently infeasible or limited, few methods are available for the selective labeling of somatic cells. One option is to incorporate cell type-specific promoters into viral vectors, but to date, this approach has generally resulted in labeling groups of related cell types (discussed in Domenger and Grimm, 2019; Juttner *et al.*, 2019). Genome editing using CRISPR (clustered regularly interspaced short palindromic repeats) (Jinek *et al.*, 2012; Cong *et al.*, 2013; reviewed in Pickar-Oliver and Gersbach, 2019; Nishizono *et al.*, 2020) provides an alternative approach. The CRISPR-associated endonuclease Cas9 is delivered to specific sites in the genome by a single guide RNA (sgRNAs) to generate double-strand breaks. The breaks can be repaired by non-homologous end-joining (NHEJ) or homology-directed repair (HDR) (Sander and Joung, 2014; Yeh *et al.*, 2019). If cDNAs encoding reporters are flanked by the sequences flanking the cut site, HDR can be harnessed to insert them into the genome at defined sites. Because homologous recombination activity is largely confined to mitotically active cells, methods involving HDR are generally applied to dividing cells (Heidenreich and Zhang, 2016).

The HDR method has primarily been used to generate germline “knock-ins” (Hsu *et al.*, 2014; Nishizono *et al.*, 2020) but can also be used to label somatic cells. By transducing dividing cells in the mouse brain with CRISPR-Cas9-based HDR tools using in utero electroporation, Mikuni *et al.* (2016) developed a method called SLENDR (single-cell labeling of endogenous proteins by CRISPR-Cas9-mediated homology-directed repair). This method introduces a plasmid encoding an sgRNA and Cas9, along with a single-stranded DNA (ssDNA) encoding a protein tag embedded between sequences that flank the sgRNA recognition site; this results in the HDR-mediated introduction of the tag at the desired genomic location. Related methods have been reported by Uemura *et al.* (2016), Nishiyama *et al.* (2017), and Matsuda and Oinuma (2019); Suzuki *et al.* (2016) devised a method in which homology-independent target integration by NHEJ allows tagging in post-mitotic cells.

Here, we modified these methods for use in chick (*Gallus gallus*) embryos. Chicks have been used for embryological studies for over a century and remain a well-used model (Stern, 2005). However, while germline transgenesis has been demonstrated in chicks, it remains a difficult and rarely used method (Lee *et al.*, 2017). Moreover, even though the method is likely to improve, few laboratories are equipped with the facilities for the avian husbandry that would be needed to generate or maintain transgenic lines.

Our own studies on the development of the chick retinotectal system have used viral and electroporation methods for gene transfer into chick embryos (e.g., Gray *et al.*, 1988; Galileo *et al.*, 1992; Leber *et al.*, 1996; Yamagata *et al.*, 2002; Yamagata and Sanes, 2008a). However, none of these enabled reliable labeling of specific cell types because neither cell type-specific promoters nor inventories of selectively expressed genes were available. Recently, we addressed the second of these problems by generating a cell atlas of the chick retina using high-throughput single-cell RNA-seq, which provided a set of genes selectively expressed by each of its ≥ 136 cell types (Yamagata *et al.*, 2021). We therefore attempted to use the CRISPR-based methods described above to insert reporters or tags into some of these genes.

The efficiency of those methods was, unfortunately, unworkably low, leading us to optimize the method in ways detailed here. Innovations include those described next. (A) Whereas previous methods for editing somatic cells introduced Cas9 via a cDNA, sufficient Cas9 protein production may occur too late for efficient editing. For this reason, CRISPR-dependent methods for germline HDR have introduced Cas9 mRNA (Yang *et al.*, 2013; Takahashi *et al.*, 2015), avoiding the need for transcription or translation of the Cas9 protein (Aida *et al.*, 2015; Chen *et al.*, 2016; Troder *et al.*, 2018; Gurumurthy *et al.*, 2019). We adopted this approach using the Cas9 protein to generate a Cas9-ribonucleoprotein complex. (B) In *Streptococcus pyogenes*, Cas9-based CRISPR uses an RNA that targets a genomic locus (crRNA; 35–36 nt in length) and a sequence that recruits Cas9 (tracrRNA; 67 nt). For most gene editing applications, these are fused to form an sgrRNA of 99–100 nt. We used separate crRNA and tracrRNA because

they are cheaper to purchase and likely to act more efficiently. (C) Because the brain vesicles of chick embryos are far larger than zygotes, far more ssDNA is required. To produce sufficient quantities, we used asymmetric PCR (Marimuthu *et al.*, 2012). (D) We added reagents to enhance HDR – carrier DNA and a DNA ligase IV inhibitor (Hu *et al.*, 2018). We call the method eCHIKIN (electroporation- and CRISPR-mediated Homology-instructed Knock-IN).

Figure 1 summarizes the key steps of eCHIKIN. The method begins with the design and preparation of CRISPR HDR reagents (Steps 1-3), which must be finished prior to *in ovo* electroporation. On the day of electroporation, a reagent cocktail including the CRISPR-Cas9 ribonucleoprotein (RNP) complex is prepared (Steps 4-6) and used for injection and electroporation (Steps 7 and 8). At later stages, tissues are dissected, fixed, and analyzed histologically (Step 9).

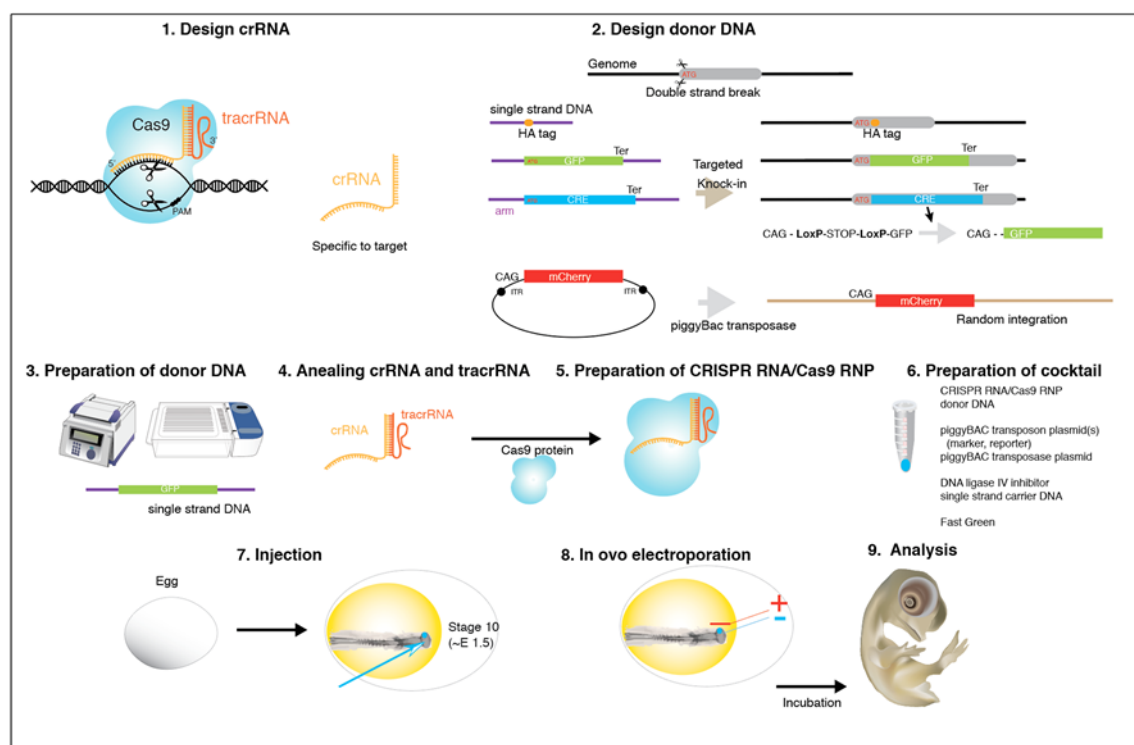


Figure 1. Overview of the eCHIKIN workflow. The main steps are the design and preparation of RNA and DNA reagents (Steps 1-3), preparation of the CRISPR-Cas9 cocktail (Steps 4-6), *in ovo* injection and electroporation (Steps 7 and 8), and immunohistochemical analysis (Step 9). Some panels are from <https://togotv.dbcls.jp/en/>.

Materials and Reagents

1. 1.5-mL microcentrifuge tubes (DNase, RNase-free low adhesion microcentrifuge tubes) (USA Scientific, catalog number: 1415-2600)
2. Fertilized chicken eggs: Specific-pathogen-free chicken (SPF) eggs from Charles River Laboratories (Wilmington, MA, USA)
Upon receipt, eggs should be stored at 16°C and used within 1 week. Embryonic development resumes when the eggs are placed into a humidified incubator at 38°C. Embryos can be staged according to the system of Hamburger and Hamilton (1951).

Note: The temperature of the eggs is sometimes poorly controlled during shipping, which decreases their viability, and does so differentially during summer and winter.

3. Alt-R® CRISPR-Cas9 crRNA, 2 nmol, designed as detailed below (Integrated DNA Technologies (IDT))
4. Alt-R® CRISPR-Cas9 tracrRNA, 20 nmol (IDT, catalog number: 1072533)
5. Alt-R® S.p. Cas9 Nuclease V3, 100 µg (IDT, catalog number: 1081058)
6. Alt-R® Cas9 Electroporation Enhancer, 2 nmol (IDT, catalog number: 1075915)
7. Alt-R® HDR Enhancer, 100 µL (IDT, catalog number: 1081072)
8. 10× Reaction Buffer (with Cas9 nuclease from GenScript, catalog number: Z03386) (200 mM HEPES, 1 M NaCl, 50 mM MgCl₂, 1 mM EDTA, pH 6.5 at 25°C)
9. Nuclease-free water (tubes with Alt-R® CRISPR-Cas9 RNAs from IDT)
10. Hanks' Balanced Salt Solution (HBSS, without calcium, magnesium, or phenol red, Thermo-Fisher Scientific, catalog number: 14175095)
11. DNA oligo 100 nmol scale, designed as discussed in the protocol (IDT)
12. Q5 DNA polymerase (NEB, catalog number: M0491)
13. Deoxynucleotide (dNTP) Solution Mix (NEB, catalog number: N0447S)
14. Exonuclease I (*E. coli*) (NEB, catalog number: M0293S)
15. EconoTaq PLUS GREEN 2× Master Mix (Lucigen, catalog number: 30033-1)
16. QIAquick Gel Extraction Kit (Qiagen, catalog number: 28704)
17. 2-Propanol BioReagent, for molecular biology, ≥99.5% (Sigma-Aldrich, catalog number: 19516)
18. Isoamyl alcohol, ≥98%, FG (Sigma-Aldrich, catalog number: W205702)
19. Ethanol Anhydrous 200 Proof (Koptec, catalog number: V1016)
20. pXL-BacII-CAG-Venus (plasmid containing piggyBac inverted terminal repeat (ITR) sequences flanking CAG and Venus) (Yamagata and Sanes, 2012)
21. pXL-BacII-CAG-mCherry (plasmid containing piggyBac ITRs flanking CAG and mCherry)
22. pXL-BacII-CAG-loxP-STOP-loxP-Venus (plasmid containing piggyBac ITRs flanking CAG, a loxP-STOP-loxP cassette and Venus)
23. pCAG-mPBorf (plasmid containing piggyBac transposase, codon-optimized)
24. tPT2A-Venus-pCR21 (plasmid containing tPT2A-Venus sequence) (This plasmid will be available from Addgene, plasmid 170521)
25. pCAG-Cre:GFP (Addgene, 13776)
26. Rabbit anti-GFP (Millipore, catalog number: AB3080P)
27. P-RAN-GFP1 Supernatant (Yamagata and Sanes, 2018a; Addgene plasmid, 106408)
28. TSA Plus Fluorescein Evaluation kit (PerkinElmer, NEL741E001KIT)
Standard lab reagents for molecular biology (e.g., 70% ethanol, agarose for gel electrophoresis)
29. Agarose (Agarose RA (Amresco); VWR Life Science, catalog number: 97064-258)
30. Buffer for agarose electrophoresis: 10× Tris-Acetate-EDTA (TAE) (Mediatech, catalog number: SC45001-074)
31. Kanamycin sulfate (Sigma-Aldrich, catalog number: K1377) (see Recipe 1 below for HBSS-kanamycin)
32. Fast Green FCF, Dye content ≥85% (Sigma-Aldrich, catalog number: F7252) (see Recipe 2 below for stock solution)
33. Chloroform, contains 100-200 ppm amylenes as a stabilizer, ≥99.5% (Sigma-Aldrich, catalog number: C2432) (see Recipe 3 below for Chloroform-isoamyl alcohol (25:1))
34. Phenol, BioUltra, for molecular biology, ≥99.5% (GC) (Sigma-Aldrich, catalog number: 77608) (see Recipe 4 below for Phenol-Chloroform (1:1))
35. Plasmids (#20, #21, #22) are available from Addgene (Addgene plasmids 170518, 170519, 170520), but current restrictions prevent Addgene from distributing plasmids encoding piggyBac transposase (<https://www.addgene.org/terms/1118/>). Phenol-chloroform treatment is required for all the plasmids for injection (see Recipe 5 below).

Equipment

1. Egg incubator
Many incubators are available commercially; we use a 1550 HATCHER (GQF MFG, Savannah, GA). The incubator should be kept humidified AND set to 38°C. Cartons in which eggs are delivered can be used as holders for incubation and electroporation.
2. ECM 830 square wave electroporation system (BTX; Holliston, MA)
3. Tungsten wire (0.1-mm diameter)
4. Glass capillaries, 3-inch length, 1-mm diameter (World Precision Instruments, 1B100F-3)
5. Genetrodes, 3-mm L-Shape (GOLD TIP) 45-0116
Accessories for holding and connecting electrodes to the electroporator are available from several vendors, including BTX and NEPAGENE.
6. Scotch transparent tape 2592 (25.4-mm width)

Warning: Chemical adhesives in some tapes from other vendors are toxic to embryos. Suspect tape if the survival rate is low.

7. 18 ½ G needles
8. 10-ml syringes
9. Sharp-edged curved surgical scissors (~4 inches)
10. #5 Forceps
11. Mastercycler Pro Thermal Cycler (Eppendorf, 950040015)
12. Strips of eight tubes, 0.2-ml (Corning PCR-0208-A and PCR-02CP-A)
13. Dissection stereoscope (for electroporation)
Carl Zeiss Stemi 2000 (444036-9000) equipped with 10×/23 eye pieces (magnification range: 6.5-50×). The viewing magnification should be adjusted as desired
14. Fluorescence stereozoom microscope (Olympus, SZX12 equipped with the cubes for observing GFP/fluorescein and mCherry/rhodamine fluorescence
15. Spectrophotometer (ThermoFisher, model: NanoDrop 2000) to measure OD₂₆₀

Procedure

A. Preparation of critical reagents

1. CRISPR-RNA (crRNA) (IDT)
Guidelines for designing crRNA are described in Note 1.
2. ssDNA donor
Guidelines for designing the ssDNA donor are described in Note 2.
 - a. Generate a double-stranded DNA template bearing homology arms.
Create a double-stranded DNA template (for an example, see Figures 2A and 2B) using two 90-bases ssDNA primers (for an example, see Figure 2C) and a GFP template (for example, pXL-BacII-CAG-Venus). We use a high-fidelity PCR enzyme (Q5 DNA polymerase), perform a 100-μl reaction in a thermocycler, run agarose gels, and purify the appropriately sized major PCR product (Left arm + GFP + right arm: ~850 bp; Figure 2C) using the QIAquick Gel Extraction Kit.

This PCR uses standard methods and equipment. A typical reaction is for 25 cycles (2 min, 95°C; 25 cycles of 94°C, 30 s/60°C, 30 s/72°C, 1 min + 1 s extension at 72°C/cycle; 72°C, 7 min; 4°C). If a clean single PCR band is not obtained, try using buffers optimized for GC-rich templates and/or adding DMSO.

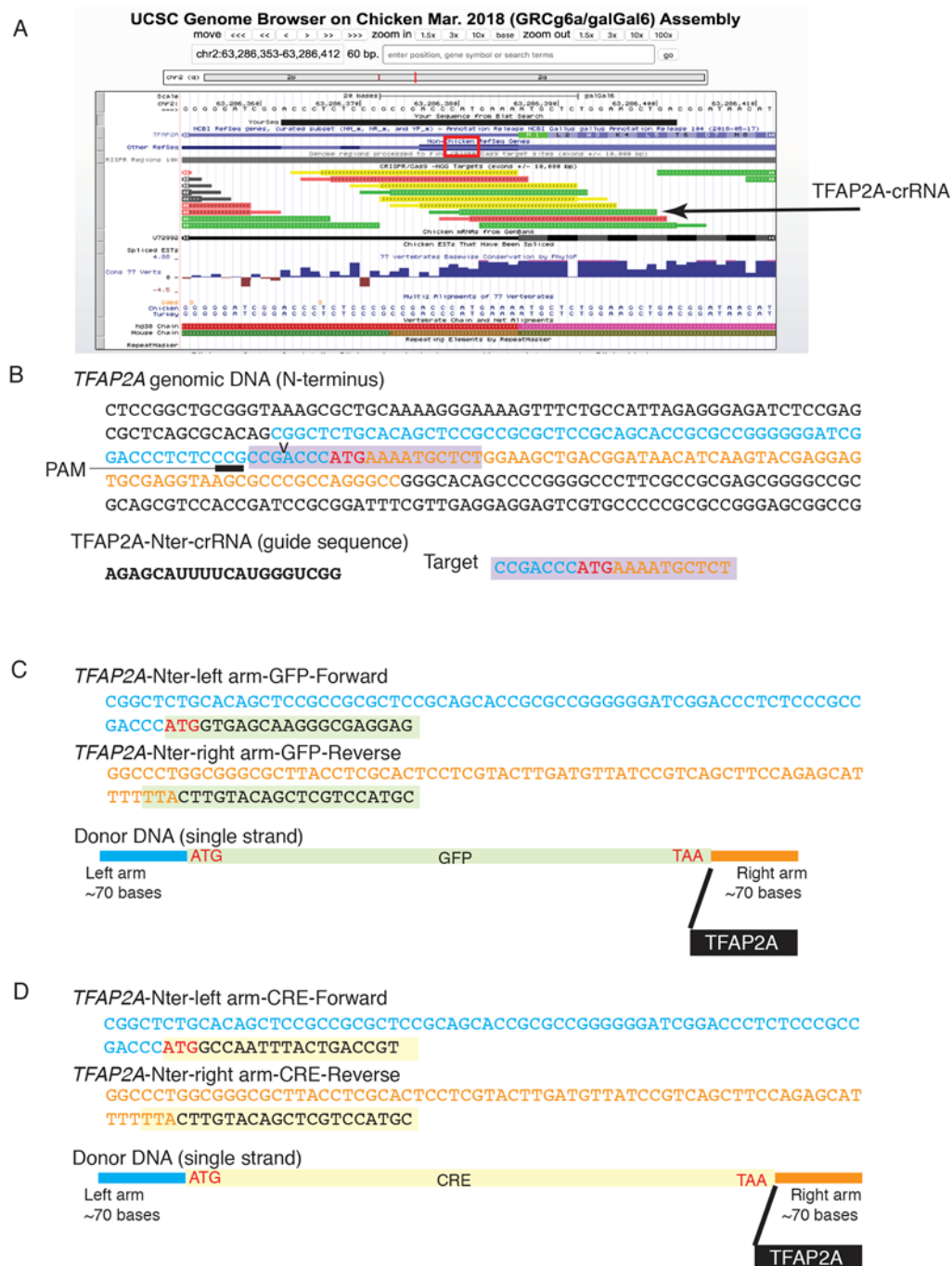


Figure 2. Designing crRNA and the ssDNA donor: *TFAP2A* is given as an example.

(A) The *TFAP2A* gene in the UCSC Genome Browser. (B) Genomic sequence of *TFAP2A* in the targeted region and *TFAP2A*-crRNA as shown in A. (C) 90 nucleotide primer sequences that anneal to the 5' (ATG) and 3' ends of GFP and the structure of the single-strand donor DNA used for inserting GFP into the *TFAP2A* locus. (D) Primers and single-strand donor DNA for inserting CRE into the *TFAP2A* locus. See Table 1 for sequences.

Table 1. Primer sequences (see Figure 2 and Figure 8)

TFAP2A-Nter-left arm-GFP-Forward	CGGCTCTGCACAGCTCCGCCGCGCTCCGCAGCACCGCGCCGGG GGGATCGGACCCTCTCCGCCGACCCATGGTGAGCAAGGGCGA GGAG
TFAP2A-Nter-right arm-GFP-Reverse	GGCCCTGGCGGGCGCTTACCTCGACTCCTCGTACTTGATGTTA TCCGTCAGCTCCAGAGCATTTTACTTGTACAGCTCGTCCAT GC
TFAP2A-Nter-left arm-CRE-Forward	CGGCTCTGCACAGCTCCGCCGCGCTCCGCAGCACCGCGCCGGG GGGATCGGACCCTCTCCGCCGACCCATGGCCAATTACTGAC CGT
TFAP2A-Nter-right arm-CRE-Reverse	GGCCCTGGCGGGCGCTTACCTCGACTCCTCGTACTTGATGTTA TCCGTCAGCTCCAGAGCATTTTACTTGTACAGCTCGTCCAT GC
TFAP2A-Cter-left arm-GFP-Forward	AGCAACAACCCCAACAGCCACACAGACAACAGCACCAAAAGC AGCGACAAAGAGGGAGAACGACCGAAAGATGGTGAGCAAGGG CGAGGAG
TFAP2A-Cter-right arm-GFP-Reverse	GGGAGGGAGGGAGATGAATGGACTGATGGGCTGCGAGGGGGGG AAGGGAGAGGAGTGGGGGGGAATCCTCACTTGTACAGCTCGT CCATGC
TFAP2A-Cter-left arm-tPT2A-GFP-F	AGCAACAACCCCAACAGCCACACAGACAACAGCACCAAAAGC AGCGACAAAGAGGGAGAACGACCGAAAGGGCAGCGGCCAC AAACTTC
TFAP2A-Cter-right arm-GFP-Reverse	GGGAGGGAGGGAGATGAATGGACTGATGGGCTGCGAGGGGGGG AAGGGAGAGGAGTGGGGGGGAATCCTCACTTGTACAGCTCGT CCATGC

b. Optimize PCR for ssDNA generation

Before carrying out a large-scale preparation of ssDNA by asymmetric PCR, it is helpful to optimize the reaction on a small scale. We use a robust and low-price PCR enzyme mixture for this purpose. First, using the double-stranded DNA template prepared above, we set up two reactions containing different molar ratios of primers: Reaction #1, 1 forward:100 reverse; Reaction #2, 100 forward:1 reverse.

Reaction #1 and Reaction #2 (2 tubes)

50 µL EconoTaq PLUS GREEN 2× Master

47 µL dH₂O

1 µL ~0.01 µg/µL template from Step A2a

1 µL 0.01 mM primer: (Reaction #1) Forward or (Reaction #2) Reverse

1 µL 1 mM primer: (Reaction #1) Reverse or (Reaction #2) Forward

Note: that typical PCR uses 0.1 mM primer stocks. Split into two PCR wells (50 µL each)

94°C, 2 min

40 cycles of 94°C, 30 s/60°C, 30 s/72°C, 1 min + 1 s extension at 72°C/cycle

72°C, 7 min

4°C

Run 1% (w/v) agarose gels (with ethidium bromide). Note that ssDNA is less effectively stained with ethidium bromide than is double-stranded DNA.

A typical result is shown in Figure 3A. In this case (*TFAP2A*), Reaction #1 gave one intense band (~850 bp) and several faint bands, including one that co-migrated with a ~500 bp double-strand DNA marker. Reaction #2 gave two clean bands: the slow-migrating band (asterisk) corresponds to double-stranded DNA (~850 bp) based on its predicted size. However, electrophoretic migration of ssDNA is often anomalous in regular non-denaturation electrophoresis buffers, making it difficult to be sure which band corresponds to ssDNA species. It is therefore useful to incubate a portion of the PCR product (2 μ L) with *E. coli* exonuclease I, which specifically digests linear ssDNA. As shown in Figure 3B, some bands from the digest, including part of the diffuse band at ~500 bp, were resistant to *E. coli* exonuclease I digestion, suggesting that some double-strand DNAs were present at ~500 bp. By contrast, in Reaction #2, the corresponding band was less diffuse and was completely digested by *E. coli* exonuclease I, indicating that it contained only ssDNA (arrow). Therefore, we used the conditions of Reaction 2 for large-scale preparation.

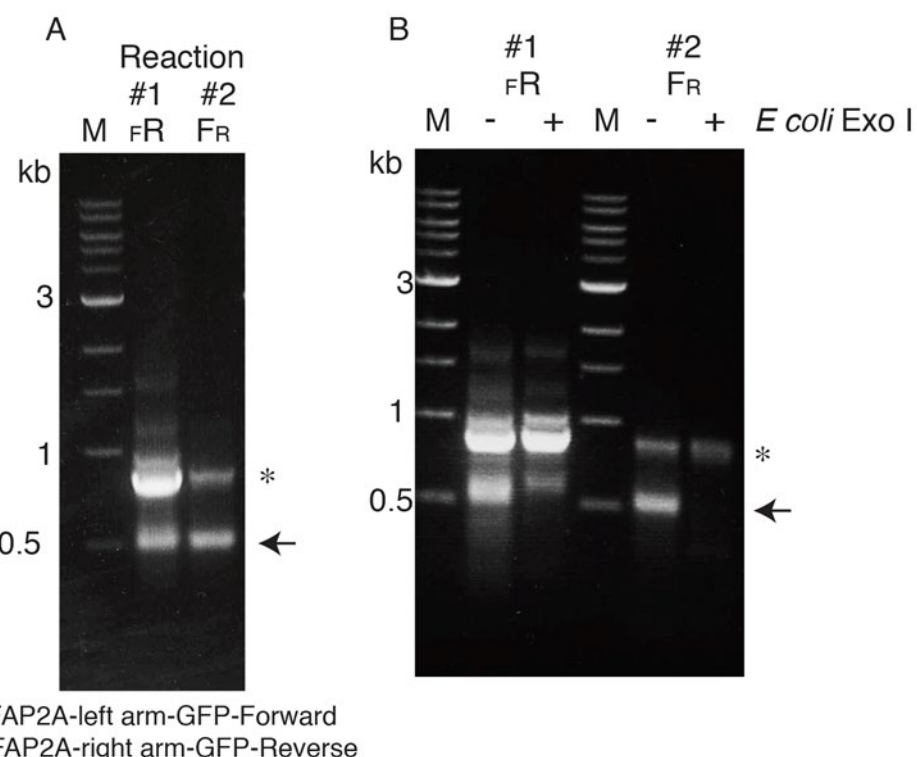


Figure 3. Assessing the quality of ssDNA.

(A) Products generated by asymmetric PCR (molar ratio of primers (forward/reverse): 1/100 in Reaction #1; 100/1 in Reaction #2). (B) PCR products were digested with *E. coli* Exonuclease I (*E. coli* Exo I), which specifically digests single-strand DNA (arrow). An additional band (asterisk) corresponds to double-strand DNA. See text for details.

- c. Large-scale preparation of the ssDNA donor
Scale-up the reaction optimized in b and then purify the ssDNA donor.

500 μ L EconoTaq PLUS GREEN 2 \times Master
470 μ L dH₂O
10 μ L ~0.01 μ g/ μ L template from Step A2a
10 μ L 0.01 mM Reverse primer
10 μ L 1 mM Forward primer

Split into 20 PCR wells (50 μ L each)
94°C, 2 min
40 cycles of 94°C, 30 s/60°C, 30 s/72°C, 1 min +1 s extension
72°C, 7 min
4°C

Run a large agarose gel and purify ssDNA using a QIAquick Gel Extraction Kit.

It is important to use thin wells so that the bands are clearly separated. Typically, we use an 11-cm wide \times 13-cm long \times ~7-mm thick gel. After solubilizing the agarose in the QG solution (QIAquick Gel Extraction Kit), add 20% volume 2-propanol, and load onto 4 mini spin-columns. Elute each tube with 100 μ L EB (QIAquick Gel Extraction Kit) and 50 μ L EB, successively. Add 1:10 volume 5 M NaCl, extract twice with phenol-chloroform, then twice with chloroform, and finally ethanol-precipitate by adding 2.5 volumes -20°C ethanol. Rinse the pellets three times with 70% ethanol at -20°C. Spin down, completely remove the residual ethanol, dry, and resuspend in RNase-free water (total 20 μ L).

Estimate the DNA concentration using a conventional or NanoDrop™ (Thermo Fisher) spectrophotometer. Note that OD₂₆₀ of ssDNA is lower due to hyperchromicity (40 μ g/mL for OD₂₆₀ as opposed to 50 μ g/mL for double-stranded DNA). Adjust the concentration to 1 μ g/ μ L, freeze, and store at -20°C until use.

B. Equipment setup

Figure 4 shows a stereomicroscope setup for injection and electroporation (Figure 4A and 4B).

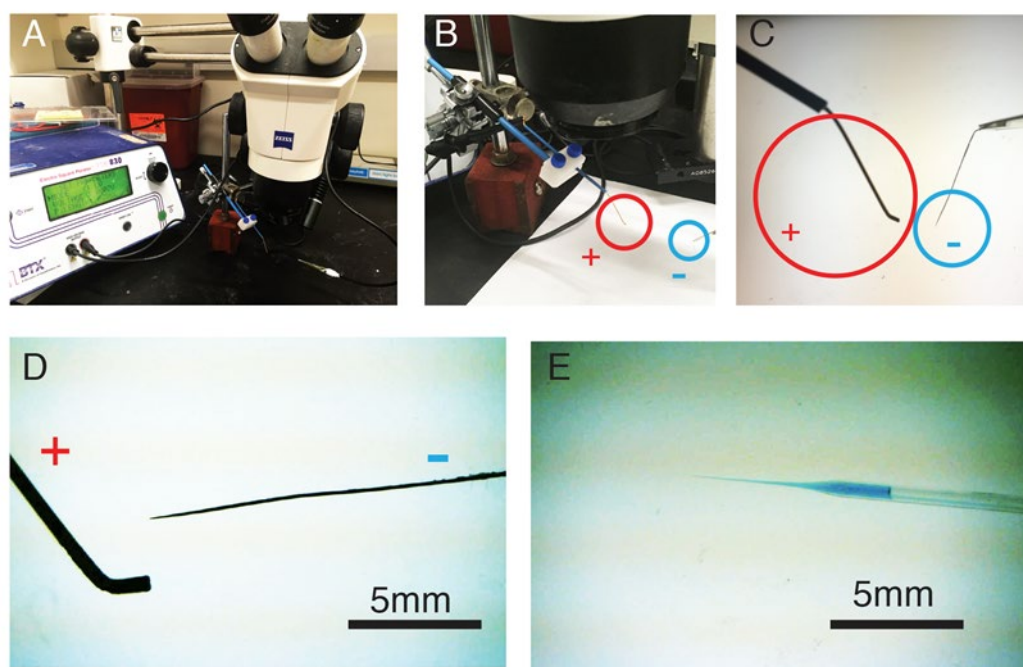


Figure 4. Equipment and instruments required for eCHIKIN.

A. Setup of the electroporator, dissection microscope, and electrode holder. B-D. Cathode (+) and tungsten anode (-). E. Glass capillary loaded with eCHIKIN cocktail plus Fast Green.

1. Tungsten needle

Cut a 0.1-mm tungsten wire to an appropriate length (~2 cm) and sharpen the tip. We sharpen it electrically (Brady, 1965) (see Figure 4C and 4D).

2. Glass capillaries for injection

Make glass capillaries for injection. We use home-made micropipettes that are finely drawn from glass capillaries (World Precision Instruments, 1B100F-3 (3-inch, 1-mm) using a puller. Break off the last few mm of the tip to allow facile injection while maintaining sharpness (Figure 4E).

C. Incubation of eggs

At appropriate times prior to injection and electroporation (see below), place the eggs in the incubator. Eggs need to be incubated on their side (horizontally; Figure 5A). Mark the top of each egg since the embryo will float on top of the yolk. Incubate more eggs than you plan to inject because some are likely to be infertile or have embryos poorly placed for injection.

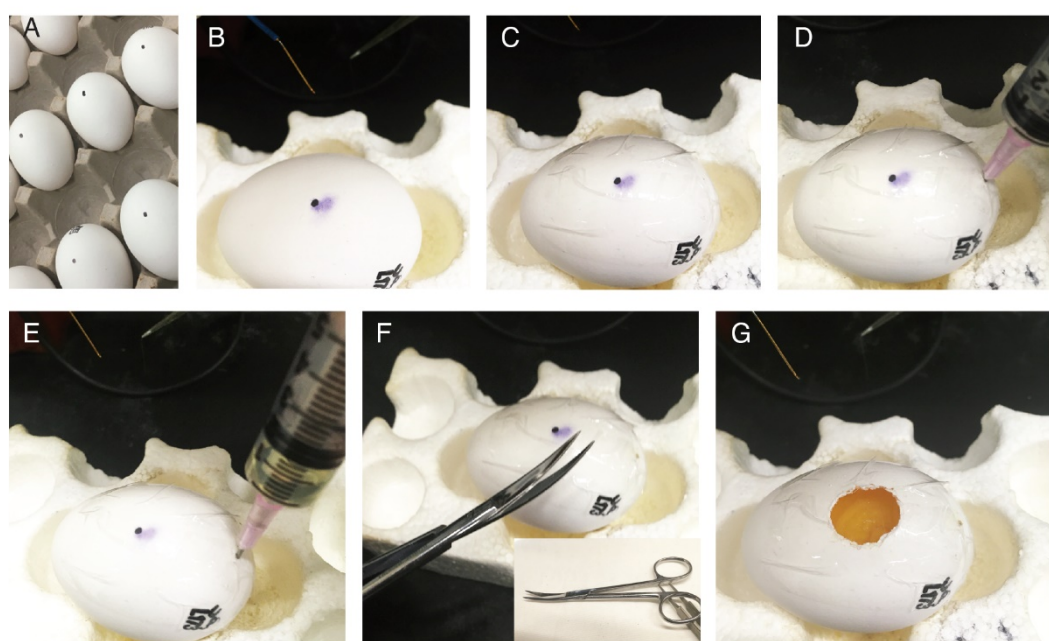


Figure 5. Preparation of chick embryos for injection and electroporation. A. Eggs incubated on their side. B-E. Placing plastic tape on the top of an egg and removing egg albumin from the round side of the egg. F, G. Using surgical scissors with curved blades, a small window (~5-mm diameter) is made on top of the egg by cutting through the tape and shell together.

D. Injection and *in ovo* electroporaton

1. Preparation of injection cocktail

On the day of *in ovo* electroporation, prepare the cocktail for injection. All plasticware and reagents must be RNase-free.

a. crRNA:transcrRNA/Cas9 RNP (Solution “R”)

To reconstitute the guide RNA duplex, the target-specific crRNA (35-36 nt) and tracrRNA (67 nt) are combined, heat-denatured, and annealed by slowly chilling to room temperature. In a 1.5-mL tube, add these reagents in this order:

2.5 μ L dH₂O
0.5 μ L 10 \times Reaction Buffer
1 μ L crRNA (2 nmol/20 μ L dH₂O; concentration, 100 μ M)
1 μ L tracrRNA (2 nmol/20 μ L dH₂O; concentration, 100 μ M)

Spin briefly and incubate for 5 min at 95°C in a heat block.
Leave at room temperature so that cooling is slow, maximizing annealing.
Leave for 5 min, briefly spin, and incubate for 30 min at room temperature.

Add 0.8 μ L 10 mg/mL Cas9 protein (*Streptococcus pyogenes* Cas9 Nuclease V3), mix, spin briefly, and incubate for 60 min at room temperature. This solution is Solution “R.”

b. Denaturation of the ssDNA donor

The ssDNA donor should be prepared in advance and stored at -20°C until use. Thaw the frozen aliquot, heat at 95°C for 5 min, and rapidly cool on ice. This denaturation can be carried out simultaneously with the annealing of crRNA:tracrRNA/Cas9 RNP described in the previous step. However, in contrast to slow annealing of the crRNA:tracrRNA, this tube needs to be cooled quickly by placing on ice immediately. Spin the tube briefly before use.

c. Dilution buffer with HDR enhancer (Solution “D”)

In an RNase-free 1.5-mL tube, add these reagents in this order:

21.5 μ L dH₂O
2.5 μ L 10 \times Reaction Buffer
1 μ L Alt-R® HDR Enhancer (available as a solution suspended in DMSO). Mix well and spin briefly.

d. piggyBac plasmid mixture (Solution “P”)

For GFP reporter eCHIKIN, mix in a 1.5-mL tube:

45 μ L 1 μ g/ μ L pXL-BacII CAG-mCherry
5 μ L 1 μ g/ μ L pCAG-mPB

For Cre reporter eCHIKIN, mix in a 1.5-mL tube:

22.5 μ L 1 μ g/ μ L pXL-BacII CAG-mCherry
22.5 μ L 1 μ g/ μ L pXL-BacII CAG-loxP-STOP-loxP-Venus
5 μ L 1 μ g/ μ L pCAG-mPB

Note that these plasmid DNAs must be RNase-free (see Recipe 5 and Note 3).

e. Final injection cocktail

To a tube of Solution “R” (total 5.8 μ L), add these reagents in this order (see Note 4):

11 μ L Solution “D”
3 μ L 1 μ g/ μ L ssDNA donor (denatured at 95°C in advance)
3 μ L Alt-R® Cas9 Electroporation Enhancer (2 nmol/50 μ L; concentration, 40 μ M)
3 μ L Solution “P”
2 μ L 0.1%(w/v) Fast Green

Mix well and place this solution on ice. Use within 5-6 h.

2. Preparation of eggs and embryos

- a. Embryos reach stage 9-10 in ~40 h at 38°C. Thus, if eggs are placed in the incubator at 8 pm (Day 0), they should be ready to electroporate at noon on Day 2. However, embryos should be staged according to Hamburger and Hamilton (1951) because the developmental rate is sensitive to small changes in temperature and also varies among eggs. To slow development when planning to inject

- many embryos, eggs can be removed from the incubator and maintained at room temperature for up to 5-6 h without compromising viability.
- b. Spray eggs with 70% ethanol and allow to dry. Always keep the previously marked top side of the egg facing upward (Figure 5B).
 - c. Apply a piece of transparent tape to the top of each egg (Figure 5C).
 - d. Insert an 18 ½ G needle on a 10-ml syringe into the rounded side of each egg (Figure 5D); this side contains the air sac.
 - e. Remove 1-2 mL egg albumin depending on the size of the eggs (Figure 5E). Some researchers omit this step to obtain better survival.
 - f. Make a small window (~5-mm diameter) on top of the egg by cutting through the tape and shell using surgical scissors with curved blades (Figure 5F and 5G).
3. Injection and *in ovo* electroporation
 - a. If necessary, gently rock the egg so that the embryo sits on top of the yolk. Make the window larger if needed (Figure 6A). In some cases, the translucent membrane beneath the shell needs to be carefully removed using #5 forceps.

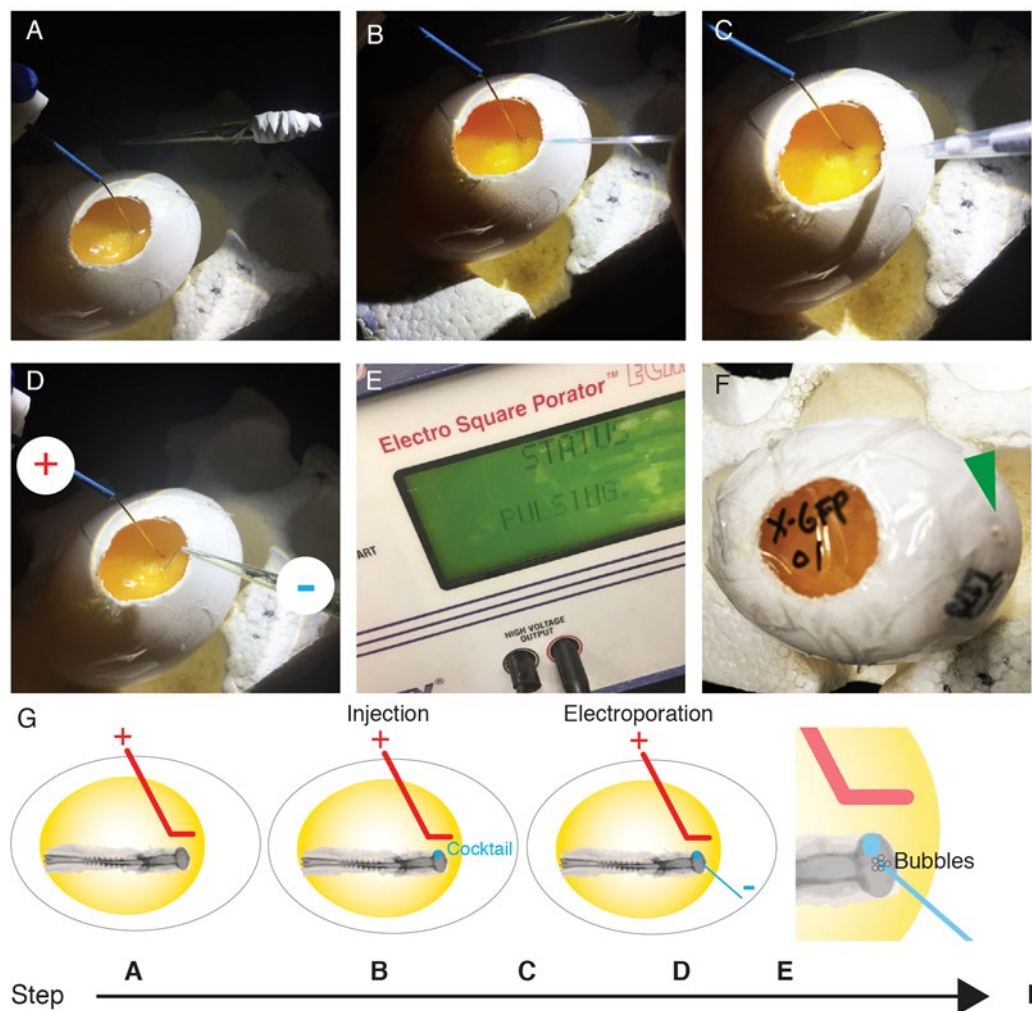


Figure 6. Key steps of injection and *in ovo* electroporation.

(A) Locate the embryo and expand the window. (B) Place the cathode as in G and inject the reagent cocktail (blue) into the embryo. (C) Wet the cathode and embryo with Hanks' + kanamycin. (D-E) Insert the anode as in G and electroporate. After successful electroporation, small bubbles appear at the anode. (F) Seal the egg

with plastic tape. It is important to seal the small hole (green) that was made for removing albumin. (G) Summary.

- b. Place the egg under the dissection microscope. For beginners, it may be challenging to see enough detail in the embryos for accurate injection. One aid is to inject a few μL black India ink beneath the embryo. Images in Hamburger and Hamilton (1951) are useful for orientation.
- c. Place the L-shaped cathode parallel to the embryo (Figure 6A and 6G).
- d. Load the CRISPR cocktail into a micropipette (Figure 4E) and inject $\sim 0.1\text{-}0.2 \mu\text{L}$ using a mouth pipette or microinjector (*e.g.*, FemtoJet, Eppendorf). To transduce the retina, inject to one side of the optic vesicle of stage 9–10 embryos (Figure 6B and 6G). To transduce the optic tectum, injection should be targeted to the midbrain vesicle at stage 11–12.
- e. Wet both the cathode and embryo with 20 μL HBSS + kanamycin using a pipette tip (Figure 6C).
- f. Insert the fine tungsten anode of the electroporator into the head of the embryo (Figure 6D and 6G).
- g. Deliver square wave pulses (Figure 6E and 6G). For optic vesicles, we use 6 pulses (7 V/25 ms) at 1-s intervals. A sign of successful electroporation is the appearance of numerous tiny bubbles at the anode.
- h. Close the window with transparent tape (Figure 6F). It is important to also seal the small hole (green arrowhead in Figure 6F) that was made to remove the albumin.
- i. Place the eggs back in the 38°C incubator.

This technique (Steps D2 and D3) relies heavily on the performer's skill and requires considerable practice. Experts can inject one embryo every few minutes or ~ 120 embryos in a 4-h session.

E. Histological analysis

Chick embryos hatch at E21; however, mortality increases greatly from E17. This is a common consequence of manipulations that introduce a window in the eggshell; it is not specific to eCHIKIN. Thus, it is best to retrieve tissue by E16, if possible. Both the retina and optic tectum are fairly mature by that age.

Although other methods can be used, the main analytical method is immunohistology. Embryos are retrieved, and the appropriate regions (retina or tectum in the cases described here) are dissected. The tissues are fixed with 4% (w/v) paraformaldehyde/PBS for 15 h, sunk in 15% (w/v) and 30% (w/v) sucrose/PBS successively, embedded in Tissue Freezing Medium (Triangle Biomedical Sciences), frozen at -80°C, and sectioned at 20 μm in a cryostat. Sections are then double-stained with anti-GFP and antibodies against cell class- or type-specific markers. Commercially available rabbit polyclonal anti-GFP, mouse monoclonal anti-GFP, and anti-GFP nanobody-reporter conjugates (RANbodies; Yamagata and Sanes, 2018a) can be used. However, commercially available chicken anti-GFP IgY antibodies display high background in chick tissues and should be avoided. Detailed immunohistochemical methods have been described in previous publications (Yamagata and Sanes, 2018b and 2019; Yamagata *et al.*, 2021).

A problem that we encountered was finding cells marked by eCHIKIN, both because they were rare and because in some cases expression levels were low. To circumvent this limitation, we co-electroporated a second reporter (usually a red fluorescent protein) expressed from a strong, ubiquitous (CAG) promoter. To guarantee maintained expression through multiple cell divisions, we ensured stable genomic integration using a piggyBac transposon/transposase system. In most cases, fluorescence from the CAG-driven fluorescent protein was readily detectable in tissue using a dissection microscope equipped with fluorescence. Regions identified in this way could then be dissected, sectioned, and immunostained.

A potential confounding factor is that HDR could lead to integration into, and thus inactivation of, both copies of a targeted allele, resulting in alterations in the target cell. We did not encounter this problem: labeled cells that we were able to visualize by alternative methods (*e.g.*, immunohistochemistry) were not detectably abnormal. Nonetheless, we cannot dismiss it and therefore tested two methods to circumvent it. In one, we maintain the function of endogenous protein by targeting the C-terminus to generate a fusion protein. For example, we appended GFP to the C-terminus of the TFAP2A coding region (Figure 7E, Figure 8A, and 8B). This method reveals the subcellular distribution of the tagged protein. In the case shown, the TFAP2A protein is a nuclear transcription factor, so the fusion protein is localized in the nucleus (Figure 7F). Subcellular

localization can be either advantageous or disadvantageous depending on the purpose of the experiment. As a second approach, when cell filling is desired, we use the self-cleavable 2A peptide to generate the inserted proteins and, separately, GFP (Figure 7E). We use a tandem fusion of two 2A sequences (tPT2A) comprising P2A (2A from porcine teschovirus-1) and T2A (2A from thosea asigna virus) (Liu *et al.*, 2017) to separate TFAP2A from GFP. In this case, GFP remained soluble and filled the cytoplasm (Figures 7G and 8C).

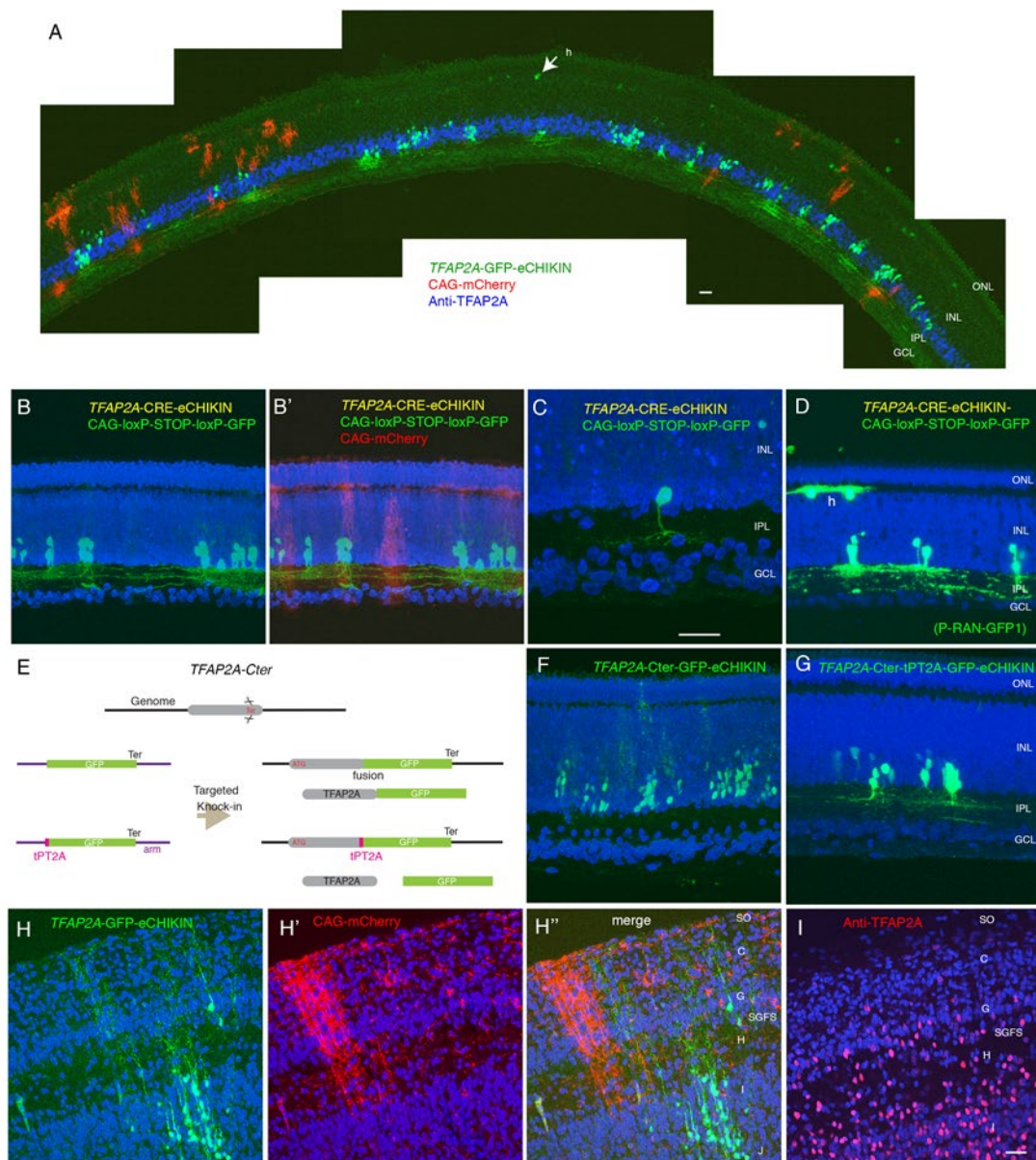


Figure 7. eCHIKIN for TFAP2A.

(A) Section of an E14 retina transduced with TFAP2A-eCHIKIN-GFP (green) and CAG-mCherry (red). Endogenous TFAP2A protein was stained with an anti-TFAP2A antibody (blue). TFAP2A marks most amacrine cells in the retina and is also weakly expressed by horizontal cells (arrow). (B, C) Sections of an E14 retina transduced with TFAP2A-eCHIKIN-CRE, CAG-loxP-STOP-loxP-GFP (green), and CAG-mCherry (red, shown only in B'). Nuclei were counterstained with NeuroTrace 635 (blue). (D) Similar to C but stained with a RANbody to GFP (P-RAN-GFP1). Note that this method (Yamagata and Sanes, 2018a) results in

efficient labeling of horizontal cells (H). (E) Schematic of TFAP2A-Cter-eCHIKIN-GFP and TFAP2A-Cter-tPT2A-GFP-eCHIKIN. (F) Section of an E12 retina transduced with TFAP2A-Cter-eCHIKIN-GFP. Since GFP is fused to the C-terminus of the TFAP2A protein, GFP is localized to the nucleus. Weak staining in the upper INL is bleed-through from the mCherry channel. (G) Section of an E12 retina transduced with TFAP2A-Cter-tPT2A-GFP-eCHIKIN. GFP is rendered soluble in this method, resulting in the cytoplasm being filled with GFP. (H) Section of an E12 optic tectum transduced with TFAP2A-eCHIKIN-GFP (green) and CAG-mCherry (red). (I) Section of an E12 optic tectum stained with an anti-TFAP2A antibody; positive cells are in several laminae of the stratum griseum fibrosum superficiale (SGFS). Laminar distribution matches that of transduced cells in H. ONL, outer nuclear layer, containing photoreceptors. INL, inner nuclear layer, containing interneurons (horizontal, bipolar, and amacrine cells). IPL, inner plexiform layer, containing processes of retinal neurons. GCL, ganglion cell layer, containing retinal ganglion cells and some amacrine cells. Bar in I, 10 μ m for B and F-I; Bars in A and C are 10 μ m.

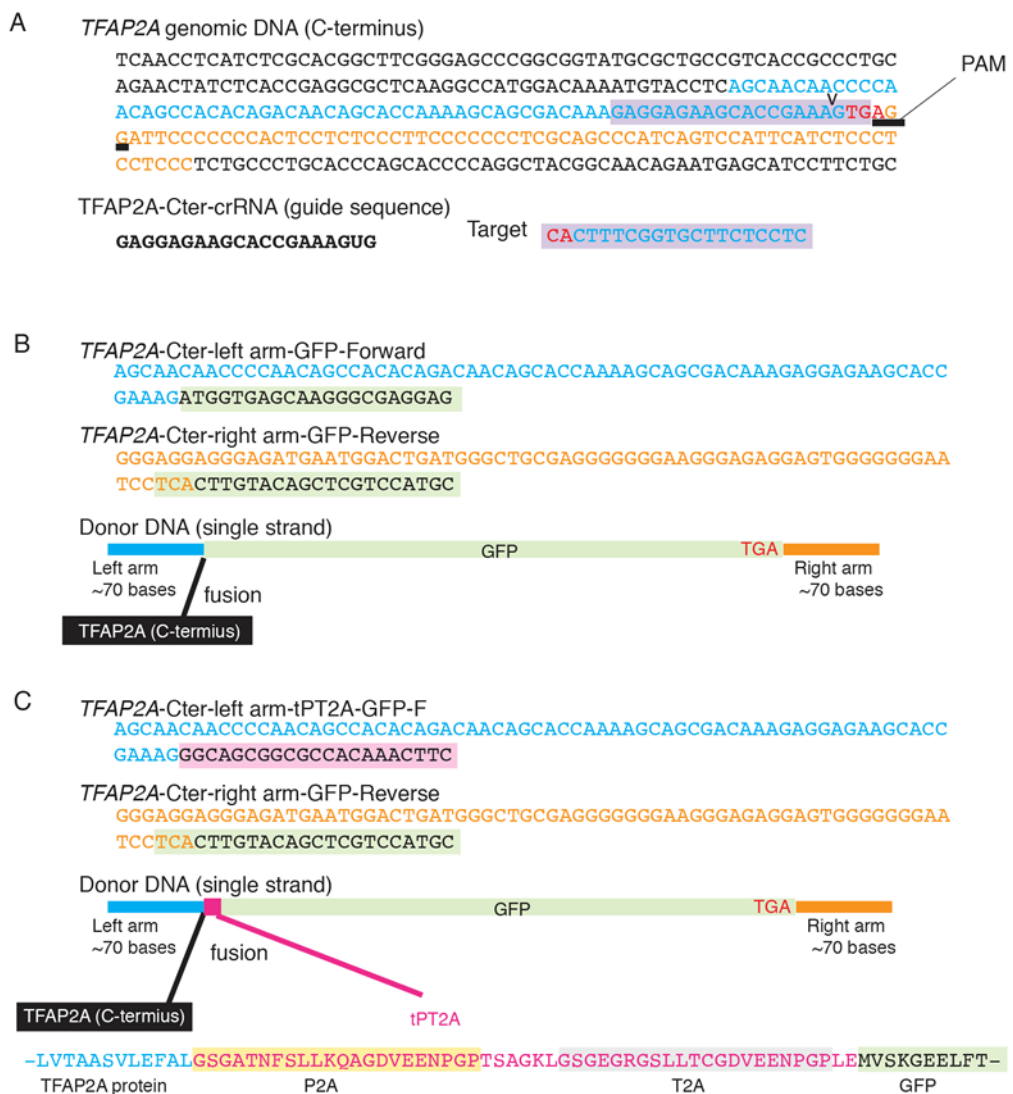


Figure 8. eCHIKIN for TFAP2A: Fusion protein and tPT2A.

(A) Genomic sequence of TFAP2A flanking its C-terminus. TGA (red) is a termination codon. The target sequence (opposite strand) of TFAP2A-Cter-crRNA is shown below. (B) To generate a donor DNA template

with 70 bases arms, two 90-nt primers were used. One primer (TFAP2A-Cter-left arm-GFP-Forward) links to the 5'end of the GFP sequence (ATG), the other primer (TFAP2A-Cter-right arm-GFP-Reverse) links to the 3' end of GFP. (C) To insert the tPT2A self-cleavable peptide sequence between TFAP2A and GFP, the donor DNA template was generated with two primers using a tPT2A-GFP plasmid as a template. See Table 1 for sequences.

EXAMPLES

Figure 7 shows examples of *TFAP2A*-expressing chick cells labeled using the eCHIKIN method. *TFAP2A* encodes a transcription factor expressed strongly by amacrine cells and weakly by horizontal cells in the inner nuclear layer of the retina. Figure 7A, from a retina transfection with a *TFAP2A*/GFP knock-in construct, shows that integration events were in some cases quite frequent. It is apparent that eCHIKIN-labeled cells are all present in the inner nuclear layer, where amacrine cells are localized, whereas CAG-mCherry labeled cells are distributed among all retinal layers. The number of cells per layer is likely influenced by the number of divisions between the integration of the piggyBac transposon plasmid and later analysis; this varies among cell classes and types. In this image, there are more eCHIKIN-GFP-labeled cells than mCherry-labeled cells, but this is atypical. Figure 7B-D shows sections from retinas labeled by co-electroporation of *TFAP2A*-cre and a cre-dependent reporter. Cells in Figure 7B and 7C were labeled with anti-GFP, while cells in Figure 7D were labeled with an anti-GFP RANbody (P-RAN-GFP1; Yamagata and Sanes, 2018a). The RANbody provides more intense labeling than conventional indirect immunofluorescence (Yamagata and Sanes, 2018a). Figure 7F and 7G, described above, shows cells labeled with *TFAP2A*-Cter-eCHIKIN-GFP and *TFAP2A*-Cter-tPT2A-GFP-eCHIKIN, respectively.

Application of eCHIKIN to 15 other genes, expressed by all retinal neuronal classes – photoreceptors, horizontal cells, bipolar cells, amacrine cells, and retinal ganglion cells – is illustrated in Yamagata *et al.* (2021). In our hands, eCHIKIN successfully labels ~90% of genes, although the efficiency of labeling is quite variable. In this fast-moving field, new methods can be added to the eCHIKIN protocol to enhance efficiency (Yeh *et al.*, 2019; Broeders *et al.*, 2020).

We also applied eCHIKIN to the optic tectum. Figure 7H shows labeling of cells with *TFAP2A*-GFP in the same laminar distribution as those labeled with anti-*TFAP2A* (Figure 7I). This result provides encouragement that eCHIKIN could be applied to multiple tissues in chick embryos and possibly to other birds. From our experience to date, we believe that the main key to the success of the technique is to achieve robust electroporation and choose appropriate CRISPR reagents; thus, the protocol may need to be modified for other tissues or species.

Notes

1. CRISPR-RNA

This protocol uses the CRISPR/Cas9 system from *Streptococcus pyogenes* because it is the most commonly used. Moreover, target-specific RNAs and Cas9 protein are readily procured from commercial vendors.

Genome editing performance of a crRNA is highly dependent on its sequence and secondary structure, as well as the chromatin status of the targeted locus (Doench *et al.*, 2014; Xu *et al.*, 2015). Here, we illustrate the selection process using the design of the *TFAP2A*-GFP vector (Figure 2 and Figure 8) as an example. One constraint of the CRISPR/Cas9 system is that a protospacer adjacent motif (PAM) must be incorporated into the design of the CRISPR; for *Streptococcus pyogenes* Cas9, the PAM is the trinucleotide NGG. The targeted CRISPR/Cas9 endonuclease generates blunt ends three nucleotides upstream of NGG. The target sequence needs to be designed such that the intended insertion is close to this double-strand break, preferably within <10 bp. First, sequences are retrieved from the most recent genome assembly (currently *Gallus gallus* GRCg6a). It may be helpful to confirm the reported sequence because some genes are still incompletely annotated. Ensembl (<https://ensembl.org>) offers a function, “Export data,” which allows easy retrieval of sequences flanking the searched sequence. The target sequence is then selected based on a panel of specificity and efficiency scores using publicly available tools (e.g., CRISPR 10K Super-track in the UCSC genome

server <https://genome.ucsc.edu>) (Figure 2A). Multiple recent methods are available; however, describing them is beyond the scope of this protocol [see Hanna and Doench (2020) for a comprehensive review]. Targets should not be in repetitive elements spread throughout the genome, but it is not necessary to rigorously rule out potential off-target crRNA cutting sites because HDR greatly enhances the specificity of integration at the targeted locus.

2. Design and preparation of the donor DNA for HDR

For HDR, single-stranded DNA (ssDNA) is widely used as a donor. To achieve HDR in high efficiency, ssDNA typically contains flanking sequences around 50-80 bases on each side homologous to the nuclease cleavage site (Chen *et al.*, 2011; Yang *et al.*, 2013; Richardson *et al.*, 2016; Quadros *et al.*, 2017). For eCHIKIN, we use 70 base homology arms because commercial synthesis of 90 bases DNA is available and affordable (see below). It is also possible to use double-strand circular plasmid DNA or double-strand linear DNA as HDR donors. However, they require much longer homology arms (200 bp-2 kbp or longer), which can be prepared by molecular cloning (e.g., Baker *et al.*, 2017). In addition, linearized double-strand DNAs often integrate randomly into the genome rather than specifically at CRISPR-mediated breaks, possibly leading to non-specific patterns of expression.

Short ssDNA can be obtained as single-strand oligonucleotides (e.g., up to 200 nt; IDT's Ultramer) that can incorporate short epitope tags with some flanking sequences (e.g., 27 nt for a HA tag) as well as both left and right arms (2 × 70 nt). Chemical synthesis can be used for longer ssDNA, sufficient to encode homology arms plus reporters (e.g., GFP [\sim 700 nt] or Cre [\sim 1,000 nt]); however, these methods are costly due to the large amount of ssDNA needed. Instead, we generate a template using two 90-bp DNA oligonucleotides (70 bases of the left and right arms, and 20 bases complementary to the 5' and 3' ends of the reporter cDNA, respectively) (Figure 1, Figure 2D-F). To prepare a large amount of long ssDNA using this template, we use asymmetric PCR, in which one primer is added at a 100-fold greater concentration. The amplified ssDNA can be purified by agarose gel electrophoresis, treated with phenol-chloroform and then chloroform, ethanol-precipitated, and stored at -20°C.

Although other methods have been used to prepare long ssDNA (e.g., a combination of T7 RNA polymerase/Reverse transcriptase/RNase H, or lambda exonuclease digestion of PCR products produced with one phosphorylated primer), our experience is that the asymmetric PCR protocol is more consistent, robust, and inexpensive.

It was demonstrated that an ssDNA donor complementary to the nontarget strand is slightly better for HDR than an ssDNA donor complementary to the target strand (Richardson *et al.*, 2016). Thus, the sequence corresponding to the target would be the first choice for ssDNA, although the opposite ssDNA is also effective in our hands. We choose either ssDNA based on the ease of purification from agarose gels.

3. piggyBac reporters

To monitor the success of electroporation, we add a piggyBac transposon plasmid equipped with CAG (CMV, beta-actin promoter/enhancer/globin leader)-driven mCherry together with a CAG-driven piggyBac transposase (Yamagata and Sanes, 2012). This transposon system is used to label the electroporated area stably by integration with the aid of the transposase. Randomly integrated mCherry is used to distinguish GFP, which is integrated specifically at the target locus. When Cre is used for HDR, we also use piggyBac to introduce the Cre-dependent GFP reporter (loxP-STOP-loxP-GFP).

4. HD enhancers

Two additional reagents are added to enhance HD and electroporation. A DNA ligase IV inhibitor (Alt-R® HDR Enhancer, an SCR7-related proprietary product from IDT) inhibits NHEJ, thereby leading to HDR. SCR7 has been used in several studies to improve HDR (Maruyama *et al.*, 2015; Hu *et al.*, 2018); although, this approach has not yet become common practice (Yeh *et al.*, 2019). For chick embryos, this reagent appears to be non-toxic. We also use the Alt-R® Cas9 Electroporation Enhancer from IDT; this is a mixture of purified carrier DNA fragments that improve the delivery of CRISPR/Cas9 RNP by electroporation. We found that inclusion of Alt-R® HDR Enhancer and Alt-R Cas9 Electroporation Enhancer in the injection cocktail improves the efficiency of eCHIKIN.

Recipes

1. HBSS with kanamycin

Add 50 µg kanamycin sulfate per mL HBSS

Keep at 4°C

2. 0.1% (w/v) Fast Green FCF

Dissolve 100 mg Fast Green FCF in 1 mL RNase-free water

Filter slowly through a 0.45-µm filter

Keep at 4°C

3. Chloroform-isoamyl alcohol (25:1)

25 chloroform:1 isoamyl alcohol

Keep at room temperature.

4. Phenol-chloroform (1:1)

1 phenol:1 chloroform-isoamyl alcohol.

Phenol needs to be saturated with 10 mM Tris-HCl, 1 mM EDTA, pH 8.0. Keep at 4°C.

5. Plasmids

All plasmids need to be RNase-free. After purification using kits (e.g., Qiagen), plasmids should be treated as follows:

- a. Add 1:10 volume of 5 M NaCl and the same volume of phenol-chloroform (1:1) and vortex for 30 s.
- b. Spin for 5 min at the maximum speed of a mini centrifuge (e.g., 16,100 × g) at room temperature. Recover the aqueous phase.
- c. Repeat the phenol-chloroform treatment.
- d. Add chloroform-isoamyl alcohol (25:1), vortex, spin, and recover the aqueous phase.
- e. Repeat the chloroform-isoamyl alcohol treatment.
- f. Add 2.5 volumes of ethanol to precipitate the plasmid DNA.
- g. Pellet and rinse three times with 70% ethanol (prechilled at -20°C).
- h. Dry and resuspend in RNase-free water to make a 1 µg/µl stock solution.

Keep at 4°C for use within a month or dispense into aliquots and freeze at -20°C for long-term storage.

Acknowledgments

This work was supported by grants R01EY022073 and R37NS029169 from the NIH. The method described here was used in a recent publication:

Yamagata, M., Yan, W., Sanes, J. R. (2021). A cell atlas of the chick retina based on single-cell transcriptomics. eLife 10: e63907. doi: 10.7554/eLife.63907.

Competing interests

The authors report no competing interests

Ethics

Animals were used in accordance with NIH guidelines and protocols approved by the Institutional Animal Use and Care Committee at Harvard University.

References

- Aida, T., Chiyo, K., Usami, T., Ishikubo, H., Imahashi, R., Wada, Y., Tanaka, K.F., Sakuma, T., Yamamoto, T., and Tanaka, K. (2015). [Cloning-free CRISPR/Cas system facilitates functional cassette knock-in in mice](#). *Genome Biol* 16: 87.
- Baker, O., Tsurkan, S., Fu, J., Klink, B., Rump, A., Obst, M., Kranz, A., Schrock, E., Anastassiadis, K. and Stewart, A. F. (2017). [The contribution of homology arms to nuclease-assisted genome engineering](#). *Nucleic Acids Res* 45(13): 8105-8115.
- Brady, J. (1965). [A simple technique for making very fine, durable dissecting needles by sharpening tungsten wire electrolytically](#). *Bull World Health Organ* 32(1): 143-144.
- Broeders, M., Herrero-Hernandez, P., Ernst, M. P. T., van der Ploeg, A. T. and Pijnappel, W. (2020). [Sharpening the Molecular Scissors: Advances in Gene-Editing Technology](#). *iScience* 23(1): 100789.
- Chen, F., Pruett-Miller, S. M., Huang, Y., Gjoka, M., Duda, K., Taunton, J., Collingwood, T. N., Frodin, M. and Davis, G. D. (2011). [High-frequency genome editing using ssDNA oligonucleotides with zinc-finger nucleases](#). *Nat Methods* 8(9): 753-755.
- Chen, S., Lee, B., Lee, A. Y., Modzelewski, A. J. and He, L. (2016). [Highly Efficient Mouse Genome Editing by CRISPR Ribonucleoprotein Electroporation of Zygotes](#). *J Biol Chem* 291(28): 14457-14467.
- Cong, L., Ran, F. A., Cox, D., Lin, S., Barretto, R., Habib, N., Hsu, P. D., Wu, X., Jiang, W., Marraffini, L. A. and Zhang, F. (2013). [Multiplex genome engineering using CRISPR/Cas systems](#). *Science* 339(6121): 819-823.
- Doench, J. G., Hartenian, E., Graham, D. B., Tothova, Z., Hegde, M., Smith, I., Sullender, M., Ebert, B. L., Xavier, R. J. and Root, D. E. (2014). [Rational design of highly active sgRNAs for CRISPR-Cas9-mediated gene inactivation](#). *Nat Biotechnol* 32(12): 1262-1267.
- Domenger, C. and Grimm, D. (2019). [Next-generation AAV vectors-do not judge a virus \(only\) by its cover](#). *Hum Mol Genet* 28(R1): R3-R14.
- Galileo, D. S., Majors, J., Horwitz, A. F. and Sanes, J. R. (1992). [Retrovirally introduced antisense integrin RNA inhibits neuroblast migration in vivo](#). *Neuron* 9(6): 1117-1131.
- Gray, G. E., Glover, J. C., Majors, J. and Sanes, J. R. (1988). [Radial arrangement of clonally related cells in the chicken optic tectum: lineage analysis with a recombinant retrovirus](#). *Proc Natl Acad Sci U S A* 85(19): 7356-7360.
- Gurumurthy, C. B., Sato, M., Nakamura, A., Inui, M., Kawano, N., Islam, M. A., Ogiwara, S., Takabayashi, S., Matsuyama, M., Nakagawa, S., Miura, H. and Ohtsuka, M. (2019). [Creation of CRISPR-based germline-genome-engineered mice without ex vivo handling of zygotes by i-GONAD](#). *Nat Protoc* 14(8): 2452-2482.
- Hamburger, V. and Hamilton, H. L. (1951). [A series of normal stages in the development of the chick embryo](#). *J Morphol* 88(1): 49-92.
- Hanna, R. E. and Doench, J. G. (2020). [Design and analysis of CRISPR-Cas experiments](#). *Nat Biotechnol* 38(7): 813-823.
- Heidenreich, M. and Zhang, F. (2016). [Applications of CRISPR-Cas systems in neuroscience](#). *Nat Rev Neurosci* 17(1): 36-44.
- Hu, Z., Shi, Z., Guo, X., Jiang, B., Wang, G., Luo, D., Chen, Y. and Zhu, Y. S. (2018). [Ligase IV inhibitor SCR7 enhances gene editing directed by CRISPR-Cas9 and ssODN in human cancer cells](#). *Cell Biosci* 8: 12.
- Hsu, P. D., Lander, E. S., and Zhang, F. (2014). [Development and applications of CRISPR-Cas9 for genome engineering](#). *Cell* 157: 1262-1278.
- Jinek, M., Chylinski, K., Fonfara, I., Hauer, M., Doudna, J. A. and Charpentier, E. (2012). [A programmable dual-RNA-guided DNA endonuclease in adaptive bacterial immunity](#). *Science* 337(6096): 816-821.

- Juttner, J., Szabo, A., Gross-Scherf, B., Morikawa, R. K., Rompani, S. B., Hantz, P., Szikra, T., Esposti, F., Cowan, C. S., Bharioke, A., Patino-Alvarez, C. P., Keles, O., Kusnyerik, A., Azoulay, T., Hartl, D., Krebs, A. R., Schubeler, D., Hajdu, R. I., Lukats, A., Nemeth, J., Nagy, Z. Z., Wu, K. C., Wu, R. H., Xiang, L., Fang, X. L., Jin, Z. B., Goldblum, D., Hasler, P. W., Scholl, H. P. N., Krol, J. and Roska, B. (2019). [Targeting neuronal and glial cell types with synthetic promoter AAVs in mice, non-human primates and humans](#). *Nat Neurosci* 22(8): 1345-1356.
- Leber, S. M., Yamagata, M. and Sanes, J. R. (1996). [Gene transfer using replication-defective retroviral and adenoviral vectors](#). *Methods Cell Biol* 51: 161-183.
- Lee, H. J., Kim, Y. M., Ono, T. and Han, J. Y. (2017). [Genome Modification Technologies and Their Applications in Avian Species](#). *Int J Mol Sci* 18(11).
- Liu, Z., Chen, O., Wall, J. B. J., Zheng, M., Zhou, Y., Wang, L., Vaseghi, H. R., Qian, L. and Liu, J. (2017). [Systematic comparison of 2A peptides for cloning multi-genes in a polycistronic vector](#). *Sci Rep* 7(1): 2193.
- Luo, L., Callaway, E. M. and Svoboda, K. (2018). [Genetic Dissection of Neural Circuits: A Decade of Progress](#). *Neuron* 98(4): 865.
- Marimuthu, C., Tang, T. H., Tominaga, J., Tan, S. C. and Gopinath, S. C. (2012). [Single-stranded DNA \(ssDNA\) production in DNA aptamer generation](#). *Analyst* 137(6): 1307-1315.
- Maruyama, T., Dougan, S. K., Truttmann, M. C., Bilate, A. M., Ingram, J. R. and Ploegh, H. L. (2015). [Increasing the efficiency of precise genome editing with CRISPR-Cas9 by inhibition of nonhomologous end joining](#). *Nat Biotechnol* 33(5): 538-542.
- Matsuda, T. and Oinuma, I. (2019). [Optimized CRISPR/Cas9-mediated in vivo genome engineering applicable to monitoring dynamics of endogenous proteins in the mouse neural tissues](#). *Sci Rep* 9(1): 11309.
- Mikuni, T., Nishiyama, J., Sun, Y., Kamasawa, N. and Yasuda, R. (2016). [High-Throughput, High-Resolution Mapping of Protein Localization in Mammalian Brain by In Vivo Genome Editing](#). *Cell* 165(7): 1803-1817.
- Nishiyama, J., Mikuni, T. and Yasuda, R. (2017). [Virus-Mediated Genome Editing via Homology-Directed Repair in Mitotic and Postmitotic Cells in Mammalian Brain](#). *Neuron* 96(4): 755-768 e755.
- Nishizono, H., Yasuda, R., and Laviv, T. (2020). [Methodologies and Challenges for CRISPR/Cas9 Mediated Genome Editing of the Mammalian Brain](#). *Front Genome Ed* 2: 602970.
- Pickar-Oliver, A. and Gersbach, C. A. (2019). [The next generation of CRISPR-Cas technologies and applications](#). *Nat Rev Mol Cell Biol* 20(8): 490-507.
- Quadros, R. M., Miura, H., Harms, D. W., Akatsuka, H., Sato, T., Aida, T., Redder, R., Richardson, G. P., Inagaki, Y., Sakai, D., Buckley, S. M., Seshacharyulu, P., Batra, S. K., Behlke, M. A., Zeiner, S. A., Jacobi, A. M., Izu, Y., Thoreson, W. B., Urness, L. D., Mansour, S. L., Ohtsuka, M. and Gurumurthy, C. B. (2017). [Easi-CRISPR: a robust method for one-step generation of mice carrying conditional and insertion alleles using long ssDNA donors and CRISPR ribonucleoproteins](#). *Genome Biol* 18(1): 92.
- Richardson, C. D., Ray, G. J., DeWitt, M. A., Curie, G. L. and Corn, J. E. (2016). [Enhancing homology-directed genome editing by catalytically active and inactive CRISPR-Cas9 using asymmetric donor DNA](#). *Nat Biotechnol* 34(3): 339-344.
- Sander, J. D. and Joung, J. K. (2014). [CRISPR-Cas systems for editing, regulating and targeting genomes](#). *Nat Biotechnol* 32(4): 347-355.
- Stern, C. D. (2005). [The chick: a great model system becomes even greater](#). *Dev Cell* 8(1): 9-17.
- Suzuki, K., Tsunekawa, Y., Hernandez-Benitez, R., Wu, J., Zhu, J., Kim, E. J., Hatanaka, F., Yamamoto, M., Araoka, T., Li, Z., Kurita, M., Hishida, T., Li, M., Aizawa, E., Guo, S., Chen, S., Goebel, A., Soligalla, R. D., Qu, J., Jiang, T., Fu, X., Jafari, M., Esteban, C. R., Berggren, W. T., Lajara, J., Nunez-Delicado, E., Guillen, P., Campistol, J. M., Matsuzaki, F., Liu, G. H., Magistretti, P., Zhang, K., Callaway, E. M., Zhang, K. and Belmonte, J. C. (2016). [In vivo genome editing via CRISPR/Cas9 mediated homology-independent targeted integration](#). *Nature* 540(7631): 144-149.
- Takahashi, G., Gurumurthy, C. B., Wada, K., Miura, H., Sato, M. and Ohtsuka, M. (2015). [GONAD: Genome-editing via Oviductal Nucleic Acids Delivery system: a novel microinjection independent genome engineering method in mice](#). *Sci Rep* 5: 11406.
- Troder, S. E., Ebert, L. K., Butt, L., Assenmacher, S., Schermer, B. and Zenvik, B. (2018). [An optimized electroporation approach for efficient CRISPR/Cas9 genome editing in murine zygotes](#). *PLoS One* 13(5): e0196891.

- Uemura, T., Mori, T., Kurihara, T., Kawase, S., Koike, R., Satoga, M., Cao, X., Li, X., Yanagawa, T., Sakurai, T., Shindo, T. and Tabuchi, K. (2016). [Fluorescent protein tagging of endogenous protein in brain neurons using CRISPR/Cas9-mediated knock-in and in utero electroporation techniques](#). *Sci Rep* 6: 35861.
- Xu, H., Xiao, T., Chen, C. H., Li, W., Meyer, C. A., Wu, Q., Wu, D., Cong, L., Zhang, F., Liu, J. S., Brown, M. and Liu, X. S. (2015). [Sequence determinants of improved CRISPR sgRNA design](#). *Genome Res* 25(8): 1147-1157.
- Yamagata, M. and Sanes, J. R. (2008). [Dscam and Sidekick proteins direct lamina-specific synaptic connections in vertebrate retina](#). *Nature* 451(7177): 465-469.
- Yamagata, M., Weiner, J. A. and Sanes, J. R. (2002). [Sidekicks: synaptic adhesion molecules that promote lamina-specific connectivity in the retina](#). *Cell* 110(5): 649-660.
- Yamagata, M. and Sanes, J. R. (2012). [Expanding the Ig superfamily code for laminar specificity in retina: expression and role of contactins](#). *J Neurosci* 32(41): 14402-14414.
- Yamagata, M. and Sanes, J. R. (2018a). [Reporter-nanobody fusions \(RANbodies\) as versatile, small, sensitive immunohistochemical reagents](#). *Proc Natl Acad Sci U S A* 115(9): 2126-2131.
- Yamagata, M. and Sanes, J. R. (2018b). [Expression and Roles of the Immunoglobulin Superfamily Recognition Molecule Sidekick1 in Mouse Retina](#). *Front Mol Neurosci* 11: 485.
- Yamagata, M., Yan, W. and Sanes, J. R. (2021). [A cell atlas of the chick retina based on single cell transcriptomics](#). *Elife* 10: e63907.
- Yang, H., Wang, H., Shivalila, C. S., Cheng, A. W., Shi, L. and Jaenisch, R. (2013). [One-step generation of mice carrying reporter and conditional alleles by CRISPR/Cas-mediated genome engineering](#). *Cell* 154(6): 1370-1379.
- Yeh, C. D., Richardson, C. D. and Corn, J. E. (2019). [Advances in genome editing through control of DNA repair pathways](#). *Nat Cell Biol* 21(12): 1468-1478.

Cell-attached and Whole-cell Patch-clamp Recordings of Dopamine Neurons in the Substantia Nigra Pars Compacta of Mouse Brain Slices

Stefano Cattaneo^{1,2}, Maria Regoni^{1,2}, Jenny Sassone^{1,2} and Stefano Taverna^{2,*}

¹Vita-Salute San Raffaele University, Milan, Italy

²Division of Neuroscience, San Raffaele Scientific Institute, Milan, Italy

*For correspondence: taverna.stefano@hsr.it

Abstract

The Substantia Nigra pars compacta (SNC) is a midbrain dopaminergic nucleus that plays a key role in modulating motor and cognitive functions. It is crucially involved in several disorders, particularly Parkinson's disease, which is characterized by a progressive loss of SNC dopaminergic cells. Electrophysiological studies on SNC neurons are of paramount importance to understand the role of dopaminergic transmission in health and disease. Here, we provide an extensive protocol to prepare SNC-containing mouse brain slices and record the electrical activity of dopaminergic cells. We describe all the necessary steps, including mouse transcardiac perfusion, brain extraction, slice cutting, and patch-clamp recordings.

Keywords: Acute brain slices, Transcardiac perfusion, Substantia Nigra, Dopaminergic neurons, Electrophysiology, Patch clamp, Mouse

This protocol was validated in: Cell Death Dis (2020), DOI: 10.1038/s41419-020-03172-8.

Background

The Substantia Nigra pars compacta (SNc) is a midbrain nucleus that provides a strong dopaminergic input to various areas of the brain, including the basal ganglia (BG) (Gerfen and Bolam, 2010). Dopaminergic axons originate from tyrosine hydroxylase (TH)-expressing neurons of the SNc. The neuromodulator dopamine (DA) released by synaptic terminals of these projections provides a vital contribution to the regulation of BG microcircuitry, which is crucially involved in modulating motor and reward functions (Zhai *et al.*, 2019).

Parkinson's disease (PD) is the second most common neurodegenerative disorder after Alzheimer's disease. Dopaminergic neurons degenerate in PD, leading to a depletion of dopamine in the striatal circuitry and causing a detrimental imbalance between direct and indirect output pathways (Gerfen and Surmeier, 2011). This ultimately results in devastating symptoms such as persistent tremors, bradykinesia, rigidity, and often neuropsychiatric alterations (Surmeier *et al.*, 2017). Thus, advancing our knowledge of dopaminergic neuronal functions in normal and pathological conditions is a task of great importance and a major goal for many neuroscience laboratories.

Although primary cultures are an interesting system to investigate the cellular physiology of dopaminergic neurons, a relatively low yield of about 5% in tyrosine hydroxylase (TH, a cytochemical marker of DA cells)-expressing neurons may represent a challenge for electrophysiological experiments (Choi *et al.*, 2013). Moreover, it has been reported that cultured dopaminergic neurons lose their autonomous acemaking activity (Masuko *et al.*, 1992), which is crucial for the sustained release of dopamine and plays a fundamental role in both physiological and pathological conditions. On the other hand, ex vivo brain slices represent a reliable and reproducible preparation preserving specific features of dopaminergic neurons, including their autonomous pacemaking activity. Yet, a potential downside of this technique is the deafferentation caused by the cutting process used to prepare the sample. Alternative techniques such as *in vivo* extracellular single-unit recordings could be used to study TH⁺ neurons (Farassat *et al.*, 2019); however, whole-cell recordings may be difficult to obtain *in vivo*, precluding the possibility to investigate intrinsic and synaptic properties of DA cells. Slice experiments therefore remain the gold-standard option for whole-cell recordings in DA neurons.

A great number of studies provide combinations of slice cutting and recording solutions that are specifically used for different brain regions (Bischofberger *et al.*, 2006) from young, adult, or aging mice (Ting *et al.*, 2014). Technical and manual precautions are obviously necessary in order to avoid, or at least minimize, various types of insults (mechanical, osmotic, metabolic, *etc.*) inflicted to the brain specimen during slice preparation. In particular, sucrose-based artificial cerebrospinal fluid (ACSF) has been used to prevent excessive intracellular influx of chloride and subsequent cell swelling and lysis (Aghajanian and Rasmussen, 1989). Here, we provide a sucrose-based cutting solution and slice preparation protocol tailored to SNc-containing brain slices. We describe all the necessary steps, including transcardiac perfusion, brain extraction, dissection, and patch-clamp recordings. We show how these methods can be used to study the pharmacological effects of acutely applied drugs as a tool to investigate potential novel targets for the treatment of neurodegenerative disorders such as PD (Regoni *et al.*, 2020).

Materials and Reagents

1. NaCl (Sigma-Aldrich, catalog number: 793566; store at room temperature (RT))
2. KCl (Sigma-Aldrich, catalog number: 409316; RT)
3. NaH₂PO₄ (Sigma-Aldrich, catalog number: S5011; RT)
4. CaCl₂ 1 M (Fluka, catalog number: 21114; store at 4°C)
5. NaHCO₃ (Sigma-Aldrich, catalog number: 792519; RT)
6. MgCl₂ (Sigma-Aldrich, catalog number: M8266; RT)
7. D-glucose (Sigma-Aldrich, catalog number: G5767; RT)
8. Sucrose (Sigma-Aldrich, catalog number: S9378; RT)
9. KH₂PO₄ (Sigma-Aldrich, catalog number: P9791; RT)
10. HEPES (Sigma-Aldrich, catalog number: H4034; RT)
11. EGTA (Sigma-Aldrich, catalog number: 03777; RT)
12. Na₂-ATP (Sigma-Aldrich, catalog number: A7699; store at -20°C)

13. Na-GTP (Sigma-Aldrich, catalog number: G8877; store at -20°C)
14. KOH (Fluka, catalog number: 319376; store at 4°C)
15. NaOH (Sigma-Aldrich, catalog number: S2770; store at 4°C)
16. Agarose (Fisher Scientific, catalog number: BP1356; RT)
17. Ketamine-HCl (Anesketin (100 mg/mL), Dechra; RT)
18. Xylazine (Rompun (20 mg/mL), Bayer; RT)
19. Ketamine/xylazine anaesthetic mixture (see Recipes)
20. Artificial cerebrospinal fluid (ACSF) 10× stock solution (w/o CaCl₂ and MgCl₂; see Recipes)
21. MgCl₂ 1 M stock solution (see Recipes)
22. Artificial cerebrospinal fluid (ACSF) 1× (see Recipes)
23. Cutting solution (see Recipes)
24. Internal solution (see Recipes)

Equipment

A. Equipment for brain slice preparation

1. VT1000S vibratome (Leica Microsystems, Wetzlar, Germany)
2. Osmometer 3320 (Advanced Instruments, Norwood, MA)
3. TW2 thermostatic water bath (Julabo, Seelbach, Germany)
4. Peristaltic pump with perfusion tubing line (Gilson Minipuls 3)
5. Paper filter disk (Millipore, catalog number: GSWPP04700)
6. Glass Petri dish (diameter: 10 cm; Merck, catalog number: BR455701)
7. Gas diffusing stone (Fisher Scientific, catalog number: 10686185)
8. 50-mL beaker
9. Stainless steel vibratome blades (Campden Instruments, catalog number: 752/1/SS)

B. Equipment for custom-made slice chamber

1. Plastic Petri dish (Thermo Fisher Scientific, catalog number: 150318)
2. Nylon mesh
3. Cyanoacrylate glue (*e.g.*, Super Attack; Loctite)
4. 100-mL beaker
5. Borosilicate glass capillaries (Sutter Instrument, catalog number: BF100-50-7.5 or equivalents)
6. Two plastic Pasteur pipettes
7. Assembly: The maintenance chamber is made up of a plastic Petri dish (diameter 3.5 cm), in which the bottom surface has been substituted with a soft nylon mesh (Figure 1A). The mesh is fixed to the dish rim with cyanoacrylate glue. The chamber is positioned inside a 100-mL beaker containing ACSF (70 mL) (Figure 1C). A glass capillary attached to a gas-impermeable tube is placed inside the chamber to supply oxygen (95% O₂ + 5% CO₂) (Figure 1D). The heads of two plastic Pasteur pipettes, one embedded into the other, are used to shim the chamber and hold the capillary inside the beaker (Figure 1B, C), to avoid bubble diffusion directly onto the slices. During preparation, individual slices are gently positioned on the mesh immediately after being cut away from the brain. After use, the maintenance chamber should be regularly disassembled for careful cleaning or replacement of its components.

C. Dissection tools

1. Surgical scissors, sharp blunt (*e.g.*, Fine Science Tools (FST), catalog number: 14001-14)
2. Fine scissors, sharp 11.5 cm (*e.g.*, FST, catalog number: 14060-11)
3. Fine scissors, sharp 10.5 cm (*e.g.*, FST, catalog number: 14060-10)

4. Dumont #5, fine forceps (*e.g.*, FST, catalog number: 11254-20)
5. Dumont #3c, forceps (*e.g.*, FST, catalog number: 11231-20)
6. Blunt forceps (Aven Forceps, Straight Serrated Tips, catalog number: 18433)
7. Vannas spring scissors (*e.g.*, FST, catalog number: 15018-10)
8. Disposable sterile scalpel blade No.21
9. Spoon (similar to VWR, catalog number: USBE3317)
10. Flat spatula (similar to VWR, catalog number: RSGA038.185)
11. Cyanoacrylate glue (“superglue,” *e.g.*, Super Attack, Loctite)

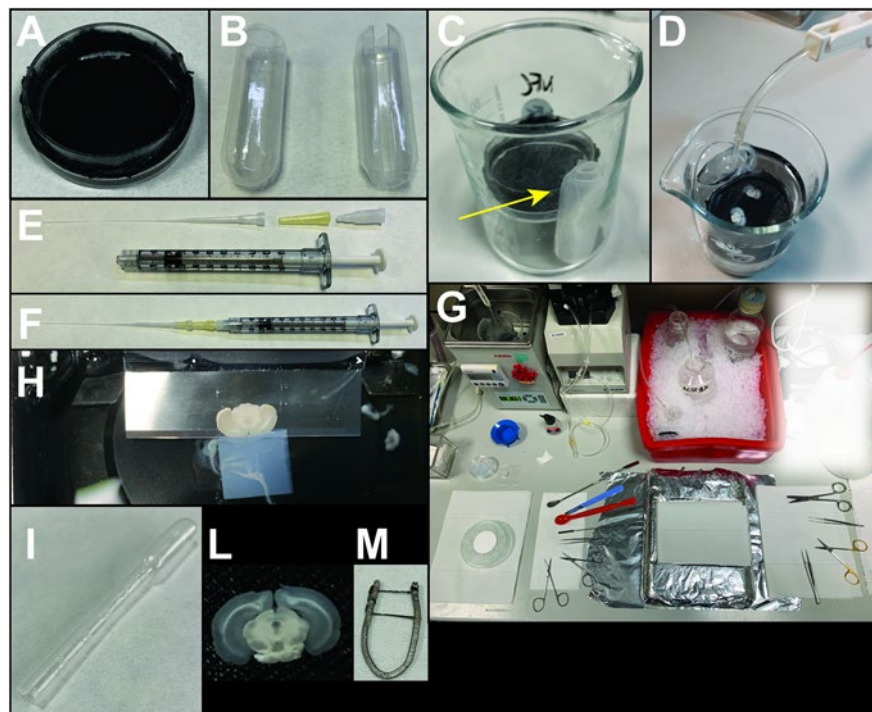


Figure 1. Representative images of the equipment required for SNC brain slice preparation.

(A) Maintenance chamber. (B) Heads of plastic Pasteur pipettes used to create the envelope for the glass capillary oxygenator (arrow in C). (C, D) Custom-made slice chamber. (E-F) Components and assembled syringe for back-filling the electrode (see Note 4). (G) Preparation of the perfusion/slicing desk. (H) Coronal slice cut by the vibratome blade. Note the agarose cube positioned behind the brain specimen. (I) Plastic Pasteur pipette used to handle the brain slices. (L) Example of an SNC-containing brain slice. (M) U-shaped custom-made anchor (see Note 3).

D. Equipment for electrophysiology experiments (Figure 2)

1. BX51WI upright microscope (Olympus, Japan) equipped with infrared-differential interference contrast optics (IR-DIC)
2. IsoStation anti-vibration table (Newport, Irvine, CA)
3. Charge-coupled device (CCD) camera (*e.g.*, Hamamatsu, QImaging, Sentech, Teledyne, *etc.*)
4. MultiClamp 700B operational amplifier (Molecular Devices, Sunnyvale, CA)
5. Digidata 1440A digitizer (Molecular Devices, Sunnyvale, CA)
6. Personal computer
7. Mini 25 micromanipulator unit (Luigs & Neumann)
8. SM-5 electronic control (Luigs & Neumann)
9. Badcontroller V temperature controller (Luigs & Neumann)

10. PC-10 electrode puller (Narishige, Japan)
11. 1-ml BD Luer-Lok™ insulin syringe without needle (BD, catalog number: 329651)
12. Microloader tips (Eppendorf, catalog number: 5242956003)
13. Syringe-driven filter unit (PVDF, 0.22 µm; SLGVR04NL Millex)
14. Home-made brain U-shaped anchor (see Note 3)
15. Borosilicate glass capillaries with filament (O.D.: 1.5 mm, I.D.:1.10 mm; 7.5 cm length) (Sutter Instrument, catalog number: BF150-110-7.5HP)



Figure 2. Patch-clamp setup

Software

1. pClamp 10 (Molecular Devices, <https://www.moleculardevices.com>)
2. GraphPad Prism (La Jolla, CA, <https://www.graphpad.com/scientific-software/prism/>)

Procedure

A. Prepare fresh ACSF 1× (see Recipe section below)

B. Setup instruments and solutions for brain slice preparation (see Note 2 and Figure 1G)

1. Fill the slice maintenance chamber with ACSF, deliver 95% O₂ + 5% CO₂ through a small glass capillary (same as those used to pull patch clamp pipettes, Figure 1D), and place the chamber in the thermostatically controlled water bath at 32°C.
2. Place a glass bottle containing ~20 ml ACSF in a tray filled with ice and oxygenate (95% O₂ + 5% CO₂) the solution using a gas-diffusing stone for at least 20 min (see Note 1).
3. Mount a perfusion tubing onto the peristaltic pump. Place the suction end into the oxygenated ice-cold ACSF and mount a 25 G needle at the opposite end.
4. Fill the vibratome tray with ice. Mount the vibratome buffer chamber (which will receive the specimen plate; see Section F).
5. Take 200 ml sucrose-containing cutting solution (kept at 4°C) and fill the vibratome buffer chamber. Oxygenate the cutting solution with 95% O₂ + 5% CO₂.
6. Prepare a 10-cm glass Petri dish filled with ice and capped with its own lid. Place a paper filter disk over the lid and wet the filter with 2-3 ml ice-cold cutting solution.
7. Prepare a 2% agarose cube (~1 cm³ in volume; see Note 6).

C. Animal anesthesia

1. Use a stock ketamine/xylazine mixture (see Recipes section below), adjusting the volume of injection according to the mouse weight (in our experiments, we injected ~300 µL in 25- to 30-day-old mice of both genders).
2. Perform an intraperitoneal injection of the anesthetic solution, then put the mouse back in the cage.
3. Carefully monitor the status of anesthesia before proceeding with transcardiac perfusion. Correctly anesthetized mice should be completely unresponsive to paw pinching. Do not proceed with cardiac perfusion until the animal is completely anesthetized.

D. Transcardiac perfusion

1. Set the speed of the peristaltic pump so that 1-2 drops per second of ice-cold ACSF flow through the 25 G needle (if using a Gilson minipuls 3, a speed of 4.5 is recommended). Before continuing, be sure that no bubbles are present in the perfusion tubing line.
2. Place the mouse (ventral side facing up) on a polystyrene tray covered with aluminum foil.
3. To facilitate the surgical procedure, fix the mouse limbs to the tray using syringe needles.
4. Pour a few ml 70% ethanol on the mouse abdomen to prevent fur dispersion.
5. Using forceps (*e.g.*, Dumont #3c), lift the skin of the mouse at the level of the liver and use fine scissors to perform a V-shaped cut through the abdominal wall, starting from beneath the rib cage to the collarbone to expose the liver and the diaphragm (Figure 3A).
6. Carefully separate the liver from the diaphragm using blunt forceps.
7. Using sharp scissors, make a small incision at the center of the diaphragm and cut from side to side to expose the pleural cavity.
8. While lifting the sternum, cut the sternopericardial ligament to separate the heart from the bone.
9. Holding the heart with blunt forceps, insert the perfusion needle into the left ventricle (Figure 3A).
10. Once the needle is in place, cut the right atrium of the heart with Vannas spring scissors (avoid touching the descending aorta).
11. Increase the speed of the peristaltic pump to 5 mL/min. The animal will be correctly perfused when the liver and limbs have turned pale white (taking approximately 20-30 s starting from the moment the

perfusion speed is raised).

E. Brain collection

1. Remove the head of the mouse using surgical scissors. Place the head onto the ice-filled glass Petri dish.
2. Expose the skull by cutting the mouse skin from the neck to the nose tip. Remove skin and muscle residues using fine forceps (Dumont #5) (Figure 3B).
3. Use fine scissors to cut the skull at the level of the lambda and remove the cerebellum and occipital bone (Figure 3B).
4. Use fine scissors to carefully cut along the lateral part of the skull starting from the most posterior part of the parietal bone to the eye socket. Subsequently, cut the nasal bone from side to side at the level of the anterior frontal bone suture (Figure 3B).
5. Using fine forceps, peel away the dorsal part of the skull. If performed correctly, minimal strength is sufficient to detach the skull and expose the brain.
6. Insert a small flat spatula at the level of the olfactory bulbs and separate the brain from the base of the skull in the rostro-caudal direction. Cut the cranial nerves in the most ventral part, and carefully detach the anterior part of the brain.
7. Trim any residual connection of the brain with the skull and delicately drop the brain into a 50-ml beaker filled with oxygenated, ice-cold ACSF.

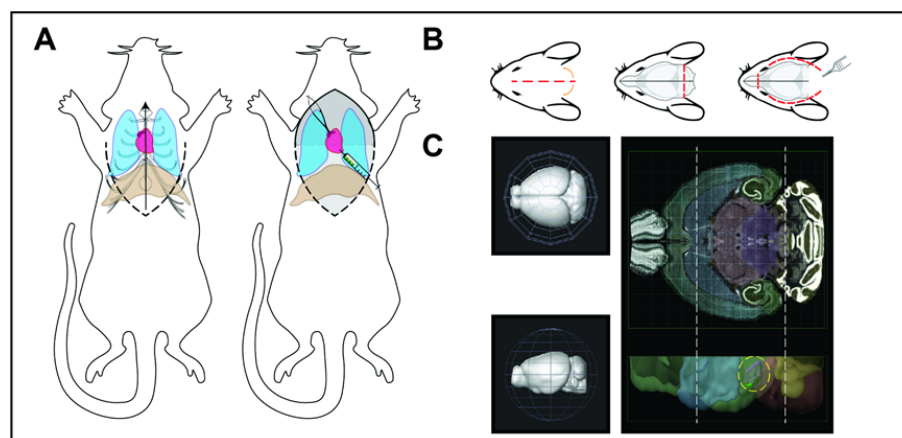


Figure 3. Representation of the essential steps for brain slice preparation.

(A) Schematic images of mouse transcardiac perfusion. Left, a V-shaped cut in the abdomen skin is represented by the dashed lines. Right, needle insertion into the left ventricle and subsequent cut in the right atrium with Vannas scissors. (B) Scheme of skull cuts prior to brain implant. Red dashed lines represent cutting trajectories as described in section E (brain collection). (C) 3D dorso-ventral and antero-posterior views of the mouse brain (Allen Institute; Brain Explorer 2). White dashed lines represent coronal cuts, both anterior (at the level of the striatum) and posterior (to remove the residual cerebellum). The yellow dashed circle highlights the SN.

F. Brain slice cutting (see Video 1)



Video 1. Brain slice cutting procedure.

Preparation of SNC coronal slices using a vibratome and slice collection in a maintenance chamber.

1. Pick up the brain from the ACSF solution using a spoon and lay it onto the ice-filled glass Petri dish (with the ventral part touching the filter paper disk).
2. Using a scalpel, perform a coronal cut at the level of the striatum and a second coronal incision to remove the residual cerebellum (Figure 3C). Be careful not to cut the midbrain region containing the SNC.
3. Pour 1-2 drops superglue at the center of the vibratome specimen plate and spread to form a thin layer. The layer surface should be large enough to host the brain block and the agarose cube.
4. Lift the brain with a spatula and carefully remove the residual ACSF using absorbent paper.
5. Lay the brain onto the glue on the vibratome specimen plate, with the posterior coronal plane facing up.
6. Glue the 2% agarose cube close to the cortices (*i.e.*, behind the brain block). This will help to keep the brain steady and firm throughout the cutting process (Figure 1H).
7. Insert and lock the specimen plate into the vibratome buffer chamber with the ventral side of the brain facing the blade (such that the SNC will be closer to the blade; Figure 1H).
8. Set the vibratome frequency at approximately 85 Hz, slice thickness at 250 µm, and advance speed at 0.15 mm/s. Start cutting the tissue.
9. Discard all slices that do not contain the SNC.
10. Approximately 4-5 slices containing the SNC will be obtained with these cutting settings (Figure 1L).

Note: We advise using Sylvius aqueduct and hippocampal formation as supplementary elements to clearly define the anteroposterior coronal plane (Figure 4).

11. Transfer the brain slices containing the SNC into the maintenance chamber at 32°C and allow them to recover for 30 min. Cover the chamber with a plastic lid. To handle the slices, use a plastic Pasteur pipette (Figure 1I) previously cut at 2/3 of its length or a fine brush (the use of a brush requires particular attention to avoid pinching the tissue with the bristles).

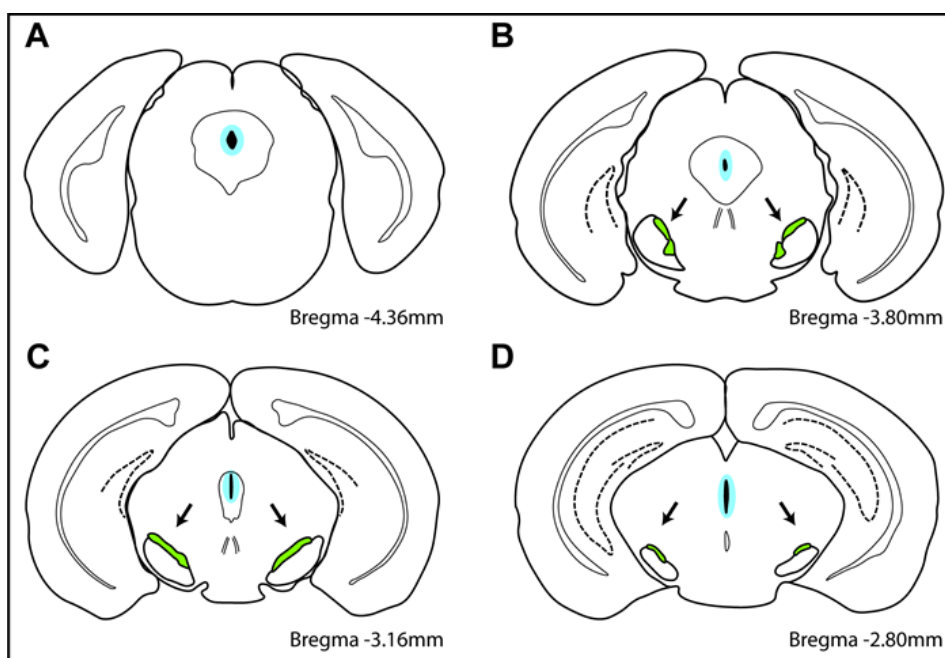


Figure 4. Schematic representation of coronal sections containing the SNc.

Arrows point to SNc areas (green) through different cutting planes. Light blue outlines the Sylvius aqueduct.

In this section, we will discuss the experimental setup used in a recent study published by our lab (Regoni *et al.*, 2020).

G. Cell-attached and whole-cell patch-clamp electrophysiology

1. Turn on the perfusion system of the electrophysiology setup so that oxygenated ACSF will continuously flow in the recording chamber at a rate of 2-3 mL/min. Turn on a suction system (vacuum- or peristaltic pump-driven) to maintain a constant level of liquid in the recording chamber.
2. Turn on the bath temperature controller and set it to 32°C. Wait until the ACSF temperature in the bath has reached the desired level.
3. If multiple drug concentrations are to be tested, prepare the proper volume of oxygenated ACSF supplemented with the different drug concentrations. In our custom-made perfusion setup, we used three 50-ml syringes connected to a Luer-lok 3-way manifold system that could be easily switched on/off according to the experimental protocol.
4. Carefully position an SNc-containing slice in the recording chamber and fix it to the chamber bottom using the U-shaped anchor (Figure 1M).
5. Visually identify the SNc using a 4× objective (Figure 5A). As previously mentioned, use the Sylvius aqueduct and hippocampal formation as supplementary elements to clearly define the antero-posterior coronal plane of the brain slice.
6. Switch to a larger objective (40×) to visually identify dopaminergic neurons. These cells are packed next to each other within a relatively narrow area at the edge of the SNr. As shown in Figure 5A, dopaminergic neurons display an ovoidal, elongated soma (longer axis of about 20 µm) and are easily recognizable.
7. Fill a patch-clamp pipette with the internal solution, remove any air bubbles, and load it on the electrode holder (see Note 4 and Figure 1E, F).
8. Apply slight positive pressure to the pipette tip before moving toward the brain slice.
9. Using the micromanipulator, gently move the pipette toward the cell, while continuously monitoring the pipette tip resistance. Upon touching the cell membrane, the pipette resistance progressively increases,

- and a small indentation of the membrane beneath the pipette tip becomes visible.
10. Quickly remove the positive pressure.
 11. Carefully apply slight and continuous negative pressure until the resistance increases to at least $1\text{ G}\Omega$ (giga-seal), reaching a cell-attached configuration.
 12. Dopaminergic cells of the SNc spontaneously fire action potentials in a pace-making fashion. Cell firing will be stable approximately 2 min after obtaining a cell-attached configuration. Under our conditions, the DA neuronal spontaneous firing pattern is mostly regular, with a mean firing frequency of $1.75 \pm 0.18\text{ Hz}$ in WT animals (Regoni *et al.*, 2020) (Figure 5C).
 13. Pharmacological studies on drugs able to modify the firing pattern of these cells can be performed by acutely switching the perfusion from control to drug-supplemented ACSF at different concentrations.
 14. Finally, move into whole-cell patch clamp configuration by quickly applying brief negative pressure to the pipette to open the cell membrane (“break-in”).
 15. At this stage, current-clamp experiments can be performed to univocally identify the firing pattern of DA neurons, as shown in Figure 5C (see also Figure 5D and Note 5). This step is necessary because different types of cells in the SNc are able to fire action potentials spontaneously. Cell recognition may be ambiguous in the cell-attached configuration; thus, whole-cell recordings are required to better detect membrane potential responses to hyperpolarizing current steps (namely, a prominent and fast I_{h} -mediated depolarizing sag that is typical of DA cells). Firing and electrical membrane parameters of SNc TH^+ neurons are summarized in Table 1.

Table 1. Firing and electrical membrane parameters of SNc TH^+ neurons

Input resistance ($\text{M}\Omega$)	Spontaneous firing frequency (Hz)	AP amplitude (mV)	AP threshold (mV)	AHP amplitude (mV)	AP halfwidth (ms)	Sag amplitude (mV)
120 ± 10	1.75 ± 0.18	60 ± 1.7	-37 ± 0.7	21 ± 1.2	1.73 ± 0.05	44 ± 5

Data are given as the mean \pm S.E.M. AP, action potential; AHP, afterhyperpolarization.

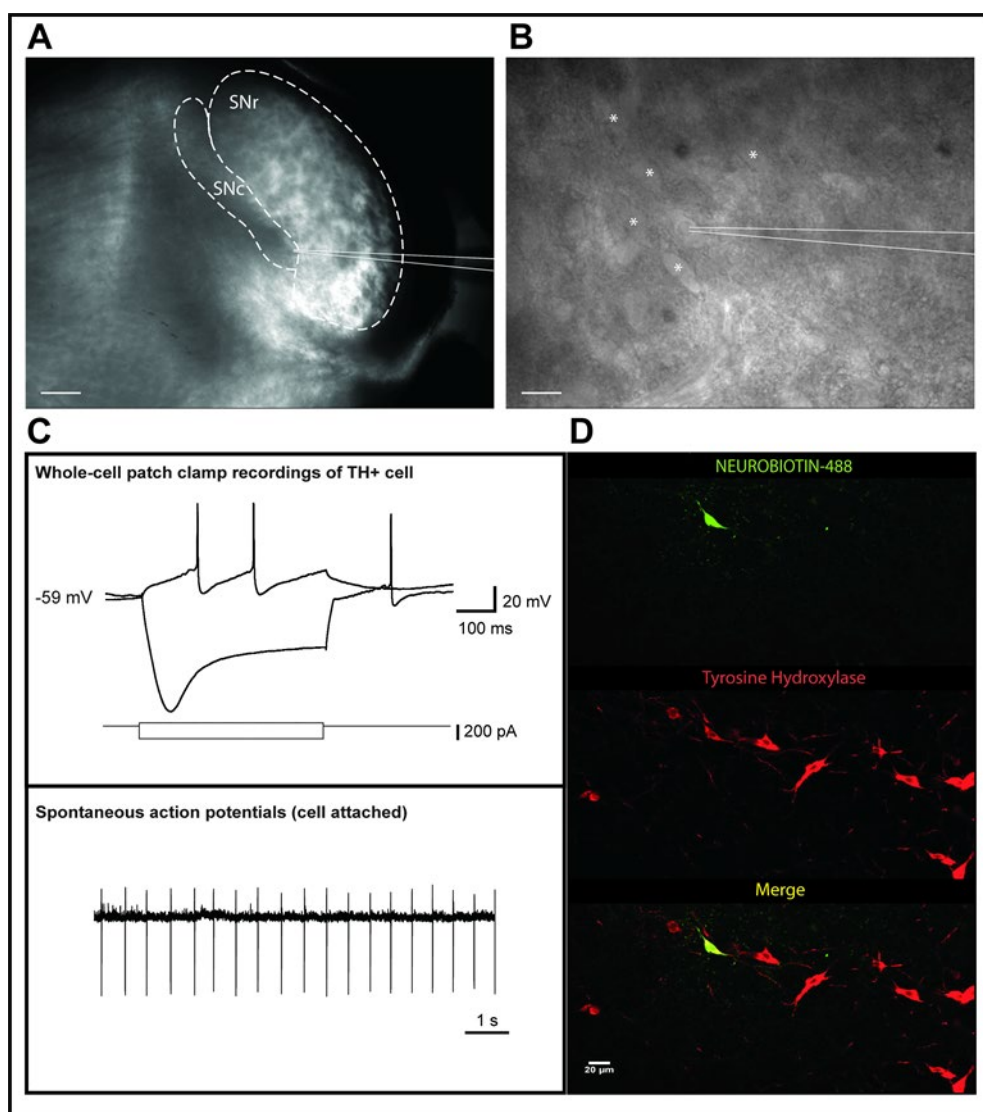


Figure 5. Electrophysiological recordings in dopaminergic neurons of the SNc. (A) Brightfield microphotograph showing an SNC-containing brain slice ($4\times$ objective; scale bar: 200 μm). (B) Example of a visually identified TH^+ cell approached by a patch-clamp pipette (outlined by white lines). Asterisks mark other putative dopaminergic neurons (note the ovoidal shape of cell bodies; scale bar: 20 μm). (C) Example of patch-clamp whole-cell recordings in current-clamp mode from an SNC DA neuron in an acute slice. The upper traces show membrane potential hyper- and depolarizing responses to intracellular injection of negative and positive current steps, respectively (-200/+50 pA, 500 ms). Traces in the lower panel show cell-attached recordings of spontaneous regular action potential firing in a different SNC DA neuron. (D) Confocal images showing one TH^+ neuron, previously filled with Neurobiotin-488 (green) during a whole-cell recording, surrounded by other TH^+ (red) neurons in the SNC.

Data analysis

Data analysis details can be found in the Materials and Methods section of Regoni *et al.* (2020). Under our conditions, the DA neuronal spontaneous firing pattern is regular and the signal-to-noise ratio of cell-attached recordings is high.

Thus, the firing frequency can be easily assessed by eye counting the number of action potentials within a given time interval (*e.g.*, 20 s).

Notes

1. To oxygenate physiological solutions, we use gas-diffusing stones or glass capillaries attached to gas-impermeable tubing connected to a source (*e.g.*, tank or pipe system) of 95% O₂ + 5% CO₂ gas mixture.
2. A key aspect for good brain slice preparation is to be as rapid and precise as possible. During transcardiac perfusion and brain collection, being fast will reduce the risk of hypoxia-induced cell death. Moreover, it is important to be manually accurate to avoid excessive mechanical stress on the brain sample during the dissection process.
3. The U-shaped anchor is made up of a flat platinum wire with 2-3 nylon threads crossing through the two arms of the U, as shown in Figure 1M. The nylon is fixed to the platinum wire with superglue.
4. To easily load the patch-clamp electrode with a clean intracellular solution, we use a custom-made syringe made up of the following components: a 1-mL BD Luer-Lok™ insulin syringe without a needle; a microloader tip; a syringe-driven filter unit; and a 200-μL micropipette tip.
5. To build the system: (1) attach one side of the filter unit to the Luer-Lok™ syringe; (2) cut the 200-μL tip at 2/3 of its length and insert it into the other side of the filter unit; and (3) insert the 200-μL tip into the microloader tip.
6. A further control step may be performed to univocally identify the patched cell. As shown in Figure 5D, the recording internal solution containing 1.5 mg/mL Neuobiotin-488 Tracer (Vector Laboratories, catalog number: SP-1125-2) was added. The dye diffused into the DA cell soma during the whole-cell recording. Subsequently, the brain slice was collected, fixed in 4% PFA, and cryopreserved. Sections of 14-μm thickness were obtained using a Leica cryostat (Leica CM1850), collected onto Superfrost slides, and air-dried overnight before storage at -80°C until staining. Immunostaining using a monoclonal antibody against tyrosine-hydroxylase (1:500; Mab318, Millipore) was performed to molecularly identify the patched neuron. Leica SP5 equipped with a 40× objective (Germany) was used to acquire the images.
7. To prepare a 2% agarose cube, add 1 g agarose to 50 ml water. Heat the solution in a microwave oven until the agarose is completely dissolved, then pour it into a 10-cm Petri dish. Once the agarose solution becomes solid, store at 4°C. Use a surgical knife to cut small cubes (approx. 1 cm³ in volume).

Recipes

Always use high-quality water with a resistivity of at least 18.2 MΩ·cm (*e.g.*, Millipore Milli-Q) for patch-clamp experiment solutions.

1. Ketamine/xylazine anesthetic mixture

500 μL ketamine-HCl
250 μL xylazine
5.25 mL 0.9% (w/v) NaCl

2. Artificial cerebrospinal fluid (ACSF)

125 mM NaCl
3.5 mM KCl
1.25 mM NaH₂PO₄
2 mM CaCl₂
25 mM NaHCO₃
1 mM MgCl₂
11 mM D-glucose

Saturated with 95% O₂ and 5% CO₂ (pH 7.3)

3. Cutting solution

50 mM sucrose
125 mM NaCl
2.5 mM KCl
1.25 mM NaH₂PO₄
0.1 mM CaCl₂
25 mM NaHCO₃
6.2 mM MgCl₂
2.5 mM D-glucose
Saturated with 95% O₂ and 5% CO₂

4. Internal solution

10 mM NaCl
124 mM KH₂PO₄
10 mM HEPES
0.5 mM EGTA
2 mM MgCl₂
2 mM Na₂-ATP
0.02 mM Na-GTP
Adjust pH to 7.2 with KOH

Preparation of stock and “ready-to-use” solutions:

- a. MgCl₂ 1 M stock solution (100 mL)
9.52 g MgCl₂
Filter and store at 4°C
- b. Artificial cerebrospinal fluid (ACSF) 10× stock solution (1 L; w/o CaCl₂ and MgCl₂)
73.05 g NaCl
21 g NaHCO₃
2.6 g KCl
1.72 g NaH₂PO₄
1.98 g glucose
Filter and store at 4°C
- c. ACSF 1× (1 L)
1 mL MgCl₂ 1 M
2 mL CaCl₂ 1 M
Add ~700 mL water
Add 100 mL 10× ACSF
Add water to adjust volume to 1 L
Check osmolarity. Correct value must be 300 ± 2.5 mOsm
- d. Cutting solution 1× (1 L)
7.305 g NaCl
2.1 g NaHCO₃
186 mg KCl
172 mg NaH₂PO₄
450 mg glucose
17.11 g sucrose
6.2 mL MgCl₂ 1 M
100 μL CaCl₂ 1 M
Filter and store at 4°C up to 1 week
- e. Internal solution (50 mL)

844 mg KH₂PO₄
29 mg NaCl
120 mg HEPES
9 mg EGTA
100 µL MgCl₂
55 mg Na₂-ATP
0.5 mg Na-GTP
Adjust pH to 7.2 with KOH
Check osmolarity. Correct value must be 290 ± 2.5 mOsm
Aliquot 1 mL in 50 capped tubes and store at -20°C

Acknowledgments

This work was supported by the Michael J. Fox Foundation for Parkinson's Research (Grant MJFF14110 to JS) and the Italian Ministry of Health (GR-2016-02361366 to JS). Procedures described in this protocol were used in the original research paper (Regoni *et al.*, 2020).

Competing interests

There are no conflicts of interest or competing interests.

Ethics

Mice were maintained and bred at the Animal Facility of the San Raffaele Scientific Institute in compliance with institutional guidelines and international laws (EU Directive 2010/63/EU EEC Council Directive 86/609, OJL 358, 1, December 12, 1987, NIH Guide for the Care and Use of Laboratory Animals, U.S. National Research Council, 1996). All experiments were conducted with the aim of minimizing the number of sacrificed animals.

References

- Aghajanian, G. K., and Rasmussen, K. (1989). [Intracellular studies in the facial nucleus illustrating a simple new method for obtaining viable motoneurons in adult rat brain slices](#). *Synapse* 3: 331-338.
- Bischofberger, J., Engel, D., Li, L., Geiger, J. R. P., and Jonas, P. (2006). [Patch-clamp recording from mossy fiber terminals in hippocampal slices](#). *Nat Protoc* 1: 2075-2081.
- Choi, W.-S., Kim, H.-W., and Xia, Z. (2013). [Preparation of primary cultured dopaminergic neurons from mouse brain](#). *Methods Mol Biol* 1018: 61-69.
- Farassat, N., Costa, K. M., Stojanovic, S., Albert, S., Kovacheva, L., Shin, J., Egger, R., Somayaji, M., Duvarci, S., Schneider, G. and Roepke, J. (2019). [In vivo functional diversity of midbrain dopamine neurons within identified axonal projections](#). *Elife* 8: e48408.
- Gerfen, C. R. and Bolam, J. P. (2010). [The Neuroanatomical Organization of the Basal Ganglia](#). In: *The Neuroanatomical Organization of the Basal Ganglia*. Steiner, H. and Tseng, K. Y. (Eds.). 20: 3-38.
- Gerfen, C. R., and Surmeier, D. J. (2011). [Modulation of Striatal Projection Systems by Dopamine](#). *Annu Rev Neurosci* 34: 441-466.
- Masuko, S., Nakajima, S., and Nakajima, Y. (1992). [Dissociated high-purity dopaminergic neuron cultures from the substantia nigra and the ventral tegmental area of the postnatal rat](#). *Neuroscience* 49: 347-364.

- Regoni, M., Cattaneo, S., Mercatelli, D., Novello, S., Passoni, A., Bagnati, R., et al. (2020). [Pharmacological antagonism of kainate receptor rescues dysfunction and loss of dopamine neurons in a mouse model of human parkin-induced toxicity](#). *Cell Death Dis* 11(11): 963.
- Surmeier, D. J., Obeso, J. A., and Halliday, G. M. (2017). [Selective neuronal vulnerability in Parkinson disease](#). *Nat Rev Neurosci* 18: 101-113.
- Ting, J. T., Daigle, T. L., Chen, Q., and Feng, G. (2014). [Acute brain slice methods for adult and aging animals: application of targeted patch clamp analysis and optogenetics](#). *Methods Mol Biol* 1183: 221-242.
- Zhai, S., Shen, W., Graves, S. M., and Surmeier, D. J. (2019). [Dopaminergic modulation of striatal function and Parkinson's disease](#). *J Neural Transm* 126: 411-422.

3D-printed Recoverable Microdrive and Base Plate System for Rodent Electrophysiology

Mihály Vöröslakos^{1,6}, Hiroyuki Miyawaki³, Sébastien Royer⁴, Kamran Diba⁵, Euisik Yoon^{6,7,8}, Peter C. Petersen¹, * and György Buzsáki^{1,2, *}

¹Neuroscience Institute, Langone Medical Center, New York University, New York, NY 10016, USA

²Department of Neurology, Langone Medical Center, New York University, New York, NY 10016, USA

³Department of Physiology, Osaka City University Graduate School of Medicine, Asahimachi 1-4-3, Abeno-ku, Osaka, 545-8585, Japan

⁴Center for Functional Connectomics, Korea Institute of Science and Technology, Seoul 02792, Republic of Korea;

⁵Department of Anesthesiology, University of Michigan, Ann Arbor, MI 48109, USA

⁶Department of Electrical Engineering and Computer Science, University of Michigan, Ann Arbor, MI, 48109, USA;

⁷Department of Biomedical Engineering, University of Michigan, Ann Arbor, MI, 48109, USA

⁸Center for Nanomedicine, Institute for Basic Science (IBS) and Graduate Program of Nano Biomedical Engineering (Nano BME), Yonsei University, Seoul, Korea

*For correspondence: petersen.peter@gmail.com; gyorgy.buzsaki@nyulangone.org

Abstract

Extracellular recordings in freely moving animals allow the monitoring of brain activity from populations of neurons at single-spike temporal resolution. While state-of-the-art electrophysiological recording devices have been developed in recent years (*e.g.*, μLED and Neuropixels silicon probes), implantation methods for silicon probes in rats and mice have not advanced substantially for a decade. The surgery is complex, takes time to master, and involves handling expensive devices and valuable animal subjects. In addition, chronic silicon neural probes are practically single implant devices due to the current low success rate of probe recovery. To successfully recover silicon probes, improve upon the quality of electrophysiological recording, and make silicon probe recordings more accessible, we have designed a miniature, low cost, and recoverable microdrive system. The addition of a novel 3D-printed skull baseplate makes the surgery less invasive, faster, and simpler for both rats and mice. We provide detailed procedural instructions and print designs, allowing researchers to adapt and flexibly customize our designs to their experimental usage.

Keywords: Electrophysiology, Silicon probe, Microdrive, 3D printing, Freely moving, Behavior, Mice, Rats

This protocol was validated in: eLife (2021); DOI: 10.7554/eLife.65859

Background

High-channel-count and high-density silicon probes can provide unique spatial and temporal information about brain activity (Jun *et al.*, 2017; Steinmetz *et al.*, 2021). Despite the advancement in probe technology, performing extracellular recording is complicated and expensive in freely moving animals using newly developed silicon probes (high-channel-count Neuropixels probe (Jun *et al.*, 2017), light-emitting μ LED probe (Wu *et al.*, 2015), or 128-channel active probe (Diagnostic Biochips, Glen Burnie, MD)). Effective probe recovery procedures are highly desirable due to the high cost of these devices (Chung J. E. *et al.*, 2017; Juavinett *et al.*, 2019). A 3D printed, recoverable microdrive system for mice (Chung J. *et al.*, 2017; Sariev *et al.*, 2017) and rats (github.com/Mizuseki-Lab/microdrive) allows researchers to reuse silicon probes with ease, decreasing the effective cost of probes. Despite the popularity of head-fixed preparation, there are scientific questions that can be better addressed using freely moving rodents. Therefore, we have designed a microdrive system that can be used for both mice and rats in freely moving experiments (Figure 1). This system allows the user to move the silicon probe inside the brain tissue and fine-tune the position of the recording sites. Although our main goal is to advance the recording device in the brain, other fixed/non-movable approaches are also gaining popularity, especially those combined with Neuropixels probes (Juavinett *et al.*, 2019; Luo *et al.*, 2020; Schoonover *et al.*, 2021). Furthermore, to reduce the complexity of the surgery (Vandecasteele *et al.*, 2012), we have designed a hybrid head cap system that consists of a 3D printed plastic base plate with a copper mesh attached to the skull using dental cement. The copper mesh provides structural protection and electrical shielding to the implanted hardware and electronics. The head cap system can be used in a wide range of applications because it is easy to mold the shape of the copper mesh before hardening it with dental cement. Improving the implantation method made our surgeries less invasive and significantly faster, leading to a speedier recovery of the animal. All 3D designs can be printed in the laboratory with a *Formlabs Form 2*, 3D resin printer, or a 3D printer with similar printing capabilities. We provide detailed procedural instructions and videos, allowing researchers to adapt the head cap and recoverable microdrive system. The baseplate was developed for Petersen and Buzsáki (2020) and Vöröslakos *et al.* (2021), and the microdrives were developed for Vöröslakos *et al.* (2021).

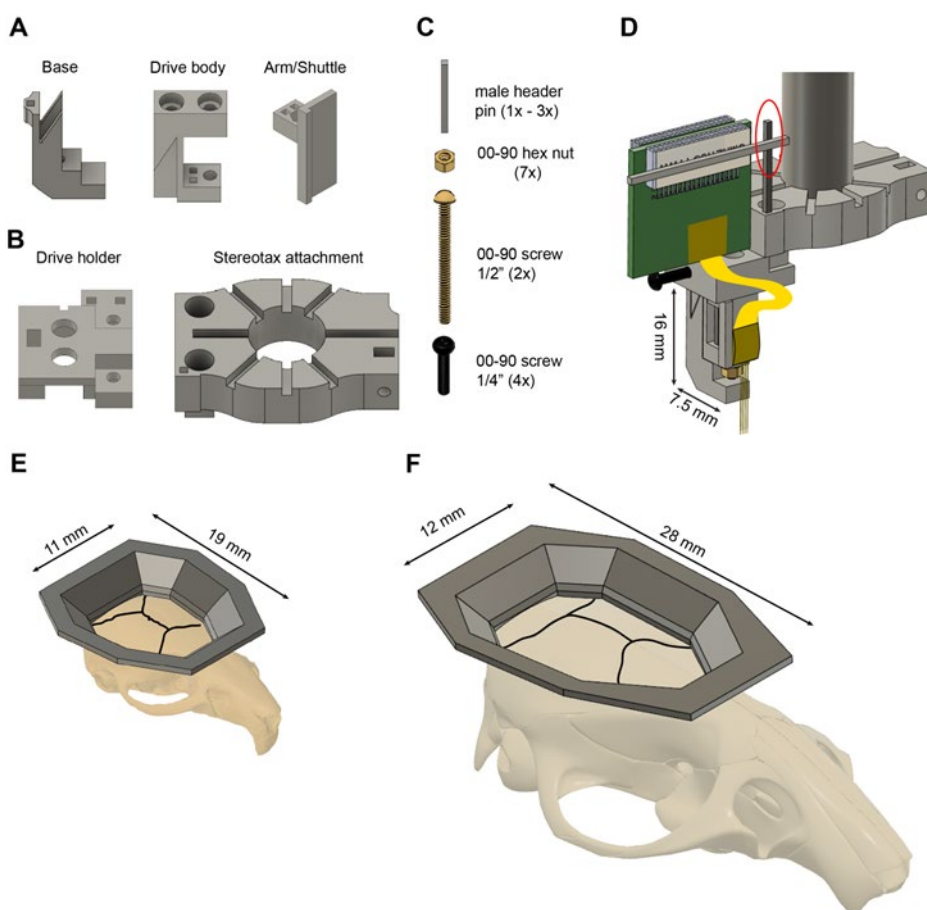


Figure 1. Reusable 3D printed plastic microdrive and base plates for mice and rats.

A. The three parts of the 3D printed plastic microdrive: a drive body, a movable arm/shuttle, and a removable base. B. 3D printed stereotaxic attachment and drive holder. All components are 3D printed using resin (Grey-v04, Formlabs Inc.). C. Additional necessary components are 00-90, 1/2" brass screw, a 00-90 brass hex nut, a 00-90, 1/4" stainless steel screw, and header metal bars. D. Stereotaxic attachment with the assembled microdrive and a probe attached, ready for implantation (the red circle indicates the temporary soldering joint for the Omnetics connector). E-F. 3D printed plastic base plate for mice (E) and rats (F) shown on their respective skulls. The black lines represent the sutures of the skull.

Materials and Reagents

Note: All 3D prints were printed and tested in Grey and Clear resins (version-04) using a Formlabs, Form2 3D printer with 50- μm resolution. All design files are available at github.com/buzsakilab/3d_print_designs, and specific links are provided below in the material lists.

A. Microdrive materials

1. 3D-printed microdrive components: body, arm, and base: github.com/buzsakilab/3d_print_designs/tree/master/Microdrives/Plastic_recoverable
2. 00-90 nut (3) (McMaster, catalog number: 92736A112)
3. 00-90 screws, 1/2" (2) (McMaster, catalog number: 92482A235)
4. Male header pin (DigiKey, catalog number: SAM1067-40-ND)

5. 00-90 tap (McMaster, catalog number: 2504A14)
6. Cyanoacrylate (Loctite, catalog number: 45208)
7. Playdough
8. 1.2 mm drill bit (McMaster, catalog number: 2958A29)

B. Microdrive holder materials and assembly tools

1. 3D-printed drive holder:
github.com/buzsakilab/3d_print_designs/tree/master/Microdrives/Plastic_recoverable (Figure 1B)
2. 00-90 nut (3) (McMaster, catalog number: 92736A112)
3. 00-90 screws, $\frac{1}{4}$ " (1) (McMaster, catalog number: 93701A005)
4. Male header pin (DigiKey, catalog number: SAM1067-40-ND)
5. Cyanoacrylate (Loctite, catalog number: 45208)
6. T2 screwdriver (McMaster, catalog number: 52995A31)
7. 1.2 mm drill bit (McMaster, catalog number: 2958A29)

C. Stereotax attachment materials and assembly tools

1. 3D-printed stereotax attachment:
github.com/buzsakilab/3d_print_designs/tree/master/Microdrives/Plastic_recoverable
2. 00-90 nut (1) (McMaster, catalog number: 92736A112)
3. 00-90 screws, $\frac{1}{4}$ " (3) (McMaster, catalog number: 93701A005)
4. Male header pin (DigiKey, catalog number: SAM1067-40-ND)
5. Cyanoacrylate (Loctite, catalog number: 45208)
6. T2 screwdriver (McMaster, catalog number: 52995A31)
7. 1.2 mm drill bit (McMaster, catalog number: 2958A29)

D. Hybrid base materials

1. 3D-printed mouse base: github.com/buzsakilab/3d_print_designs/tree/master/Mouse_hat_base
2. 3D-printed rat base: github.com/buzsakilab/3d_print_designs/tree/master/Rat_hat_base
3. Copper mesh (Dexmet, catalog number: 3CU6-050FA)
4. Dental acrylic (Pearson Dental, catalog number: G05-1224 and G05-1226)

E. Surgery materials

1. Kimwipes (Kimtech, catalog number: 34120)
2. Gelfoam (Fisher Scientific, catalog number: NC1861013)
3. H₂O₂ (Swan, catalog number: S12794v)
4. C&B Metabond Base 10 ml (Parkell, catalog number: P16-0116)
5. C&B Gold Catalyst (Parkell, catalog number: P16-0052)
6. C&B Metabond Clear Powder (Parkell, catalog number: P16-0121)
7. Ceramic mix dish for metabond (Parkell, catalog number: S387)
8. Measuring spoons for metabond (Parkell)
9. Brushes for metabond (Amazon, catalog number: B071F8WSW8)
10. Unifast Trad Powder Ivory (Pearson Dental, catalog number: G05-1224)
11. Unifast Trad Liquid (Pearson Dental, catalog number: G05-1226)
12. Unifast™ 1:2 Package A2 (Pearson Dental, catalog number: G05-0037)
13. Hair removal cream (Nair)
14. Povidone-Iodine (Amazon, catalog number: B07MWTH4MW)
15. Eye ointment (Puralube, catalog number: 0574-4025)

16. Fountain pen (AmazonBasics, catalog number: FC008A-1-M)
17. Isoflurane
18. Bupivacaine
19. Atropine
20. Steroids
21. Buprenex
22. Cyanoacrylate (Loctite, catalog number: 45208)
23. Distilled water
24. Ultrazyme Enzymatic Cleaner Tablets (Ultrazyme, catalog number: B000LM0ZYS)

Equipment

A. Silicon probes and equipment for attachment to microdrive

1. Silicon probe (Neuronexus, Cambridge Neurotech, Diagnostic Biochips)
2. 3D printed, assembled microdrive
3. 3D printed, assembled drive holder and stereotax attachment
4. Helping hand with alligator clip (Ridgerock Tools Inc., catalog number: 01902)

Note: Cover the alligator clip with electrical tape.

5. Blade (SPI Supplies, catalog number: 05025-MB)

B. Surgery

1. Stereotaxic apparatus (Kopf, catalog number: Model 962)
2. Heating pad (Physitemp, catalog number: TCAT-2LV)
3. Scalpel handle (Fine Science Tools, catalog number: 10003-12)
4. Scalpel blade (Fine Science Tools, catalog number: 10015-00)
5. Fine scissors (Fine Science Tools, catalog number: 14090-09)
6. Dumont fine forceps (Fine Science Tools, catalog number: 11254-20)
7. Scraper tool (Fine Science Tools)
8. Micro Curettes (Fine Science Tools, catalog number: 10080-05)
9. Dieffenbach Vessel Clips Straight (Harvard Apparatus, catalog number: ST2 72-8815)
10. Diethrich Mini Bulldog Clamp (Harvard Apparatus, catalog number: ST2 72-8817)
11. Cotton swabs (Fisher Scientific, catalog number: 19-062-616)
12. Screwdriver (Amazon, catalog number: B0058ECJIE)
13. 000-120 screw 1/16" (Antrin Miniature Specialties, catalog number: AMS120/1B-25)
14. Dental drill (NSK, catalog number: Ultimate XL)
15. Burrs for micro drill 0.7 mm (Fine Science Tools, catalog number: 19008-07)
16. Soldering iron (Stannol, catalog number: 574104)
17. Soldering station (Weller, catalog number: WD1)
18. Solder Flux (Worthington, catalog number: 331928)
19. Solder Paste (Quick Chip, catalog number: 23271700)
20. Hair clipper (Wahl, catalog number: 9990-1201)
21. Dental LED Light (Aphrodite, catalog number: AP-016B)
22. Ground/reference wire (Phoenix Wire Inc., catalog number: 36744MHW-PTFE)

Procedure

A. Microdrive assembly (Figure 2A-2M)

1. Apply a little cyanoacrylate glue (Loctite gel) on the outer surface of a 00-90 brass hex nut, and insert it into the arm.
2. Push the arm into the opening of the body and align the rectangular holes of the drive body with the rectangular holes of the arm.
3. Insert male header pins into the drive body through the rectangular holes of the arm.

Critical step: Cut the metal bars to the proper length and make sure they do not extrude from the bottom part of the drive body

4. Move down the arm with the male header pins. Apply cyanoacrylate glue on both ends of the male header pins and push back the male header pins into the drive body.

Critical step: Do not apply an excessive amount of superglue on the top of the male header pins as it can flow out and glue the arm to the male header pins. To further prevent this, keep a sufficient gap between the top part of the male header pins and the arm before applying superglue. Wait until the glue is completely cured (15-20 min). If the metal bars extrude at the bottom of the drive, file them and make sure this surface is completely flat and even.

5. Tap the plastic of the arm component through the brass nut using a 00-90 tap. The diameter of the hole of the arm is 1 mm (right, top part), but the outer diameter of the 00-90 screw is 1.2 mm (right, bottom part).
6. Insert a 00-90, 1/2" brass screw through the drive body and the arm nut.

Critical step: Make sure the head of the screw is pushed all the way inside the hole on top of the drive body.

7. Put a 00-90 brass hex nut on the screw.

Critical step: Tighten it completely and then release a quarter-turn (or less). If it is too tight, the arm cannot be moved: if it is too loose, the arm can wiggle and eventually introduce a lot of damage to the brain tissue.

8. Apply soldering flux and solder to the nut to join the screw and nut together.

Critical step: Try to minimize the amount of time of soldering because an excessive amount of heat will be transferred to the plastic through the metal components. Excessive heat can reduce the structural integrity of the plastic.

9. Apply superglue on the outer surface on a 00-90 brass nut and insert it into the base component.

Critical step: Make sure that the nut is oriented properly (right side) and inserted all the way. Once inserted, check alignment with the hole (look from the top).

10. Seal the nut with playdough.

Critical step: Cement needs to be prevented from flowing into this hole during surgery.

11. Insert assembled drive body into the base.
12. Insert a 00-90 1/2" brass screw into the drive body and secure the drive body to the base.

Critical step: Hold the base component still using a plier and try to move the arm while looking for any movement of the body relative to the base under a microscope. If the body moves, then 1) the bottom of the drive might not be flat, 2) the back screw might not tightened enough, or 3) the print did not come out with proper dimensions, and there is extra space somewhere between the base and drive body

The fully assembled microdrive weighs 0.67 g, and its dimensions are $3.2 \times 7.5 \times 16$ mm (width \times length \times height).

Additional features:

- a. The arm can be customized to any size. We share arm designs on our Github page for 64 and 32-ch silicon probes with 5 mm shank length.
- b. There is a rectangular hole in the back of the base component in which a male header pin can be ‘glued’ using dental cement. This male header pin can serve as a temporary soldering joint during multi-probe implants.

Critical step: Do not use super glue to attach this bar. The advantage of using dental cement is that the male header pin can be removed post-surgery by melting it with a soldering iron. Applying heat to the metal bar can release it from cement but not from superglue. Be careful with heat because an excessive amount of heat can deteriorate the base component..

- c. The drive holder has a hole to accommodate this male header pin during probe recovery, but it makes the alignment more difficult.

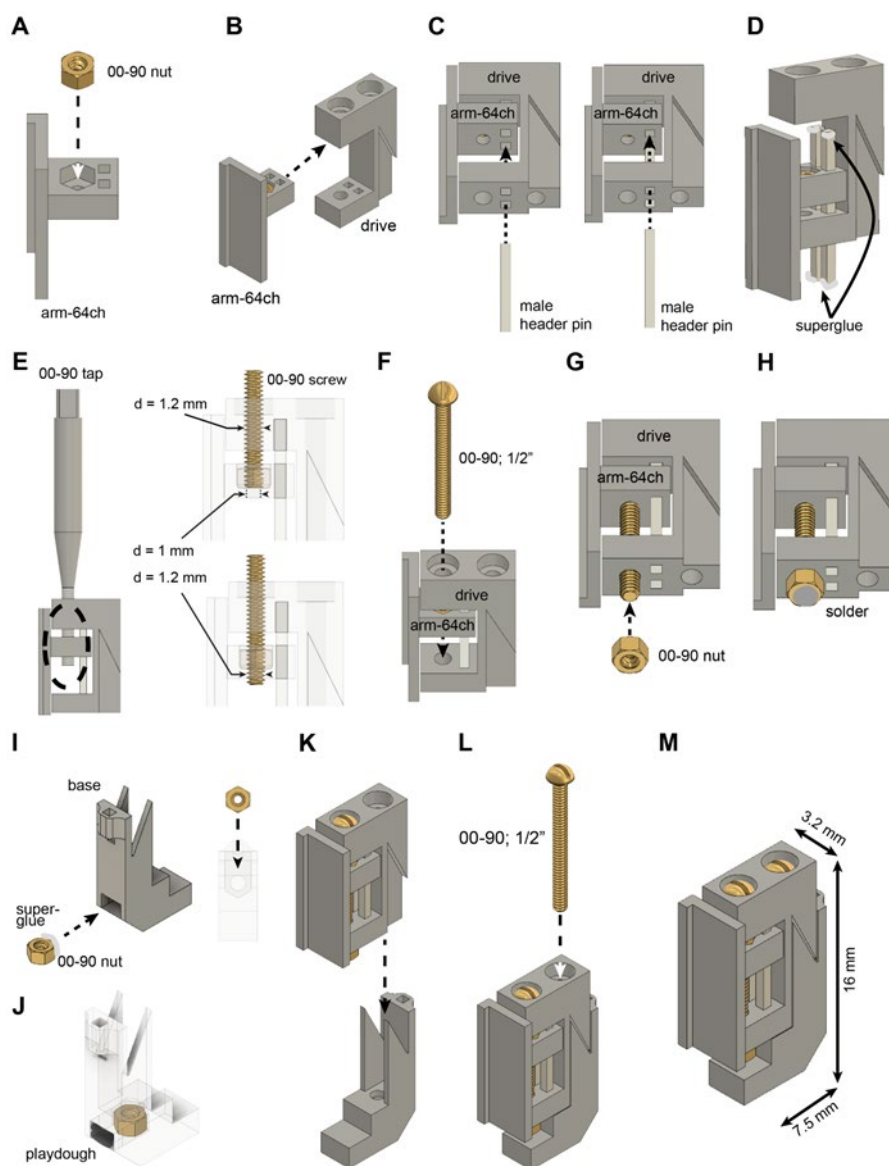


Figure 2. Assembly of recoverable microdrive.

See instructions in section A above.

B. Drive holder and stereotax attachment assembly (Video 1 and Figure 3)

1. Apply superglue on the outer surface on a 00-90 brass nut and insert it into the stereotax attachment component (Figure 3A).

Critical step: Make sure that the nut is oriented properly (similar orientation to base) and inserted all the way. Once inserted, check alignment with the hole (look from the side).

2. Apply super glue on one side of a male header pin and insert it into the stereotax attachment component (Figure 3A).

Critical step: Once the glue is cured completely, apply soldering flux and solder to the metal bar (around the height where you expect to solder your omnics connector).

3. Insert a 00-90 1/4" stainless steel screw (Figure 3B).

Critical step: When attached to the arm of the stereotax, never tighten this screw too much as it can break the plastic.

4. Apply superglue on the outer surface of a 00-90 brass nut and insert it into the bottom of the drive holder component (Figure 3C).
5. Apply superglue on the outer surface of a 00-90 brass nut and insert it into the drive holder component (Figure 3D).

Critical step: Make sure that the nut is oriented properly (similar orientation to base) and inserted all the way. Once inserted, check alignment with the hole (look from the side).

6. Attach stereotax attachment to drive holder using two 00-90 1/4" stainless steel screws (Figure 3E, step 1).
7. Insert a 00-90 1/4" stainless steel screw into the drive holder component (Figure 3E, step 2).

Additional features:

- a. There are two rectangular holes on the drive holder component that can be used for male header pins. These pins can serve as a temporary soldering joint for the Omnetics connector of the silicon probe.
- b. The drive holder can be redesigned in multiple ways, e.g., the securing screw can be moved from the side to the front.



Video 1. How to assemble drive holder, stereotax attachment, and recoverable microdrive

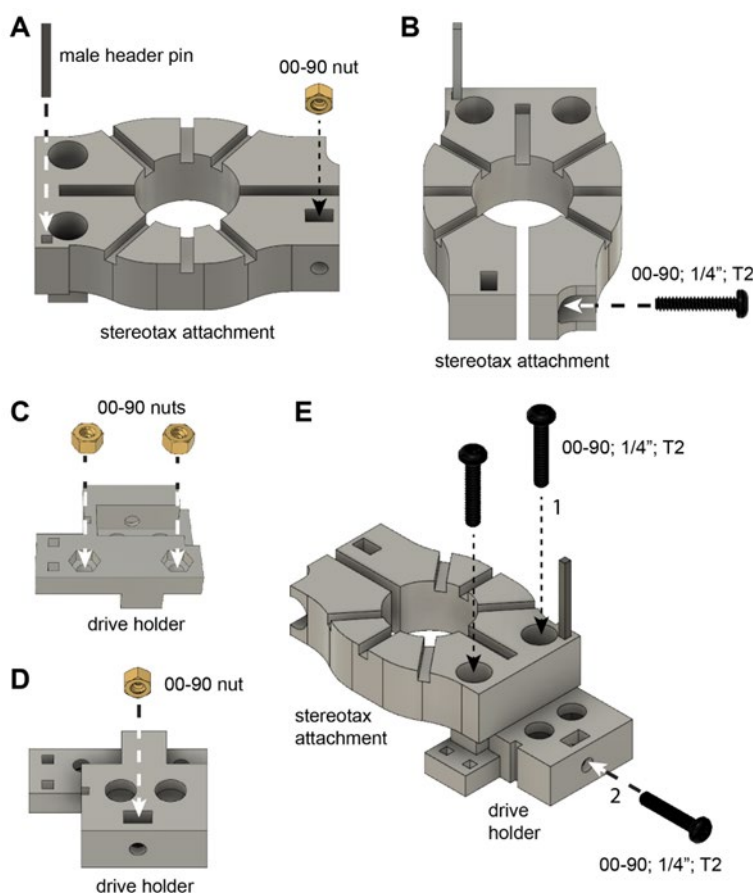


Figure 3. Assembly of stereotax attachment and drive holder.

See instructions in section B above.

C. Attaching the probe to the microdrive (Video 2 and Figure 4)

1. Scratch the surface of the Omnetics connector using a blade (Figure 4A).

Critical step: It is important to increase the surface of the plastic connector to ensure better adhesion between Omnetics and the male header pin.

2. Attach male header pin to the Omnetics connector using superglue or dental cement (Figure 4B).

Critical step: Wait until the glue is cured completely.

3. Cover the male header pin with dental cement (arrow in Figure 4C).

Critical step: Make sure to use relatively liquid cement to let it flow between the metal bar and the Omnetics. Pay attention not to let the cement flow into the Omnetics connector. In general, one male header pin is enough for 32-ch silicon probes, but two should be used for 64-ch probes.

4. Apply soldering flux and solder to both ends of the male header pin (arrow in Figure 4D).

Critical step: Excessive heat can melt the cement and/or Omnetics. Try to work as fast as possible.

5. Hold the drive with one helping hand and the probe with another one. Align the probe backend with the arm of the drive (Figure 4E).
6. Apply superglue or dental cement to the arm (Figure 4F).
7. Attach the backend of the probe to the arm. Fine-tune the position of the probe using a tweezer (Figure 4G).

Critical step: For 10-15 s, the backend of the probe can be moved, and alignment can be fine-tuned.

8. Holding the stereotax attachment with the hand, attach the drive holder to the drive and tighten the screw (Figure 4H).

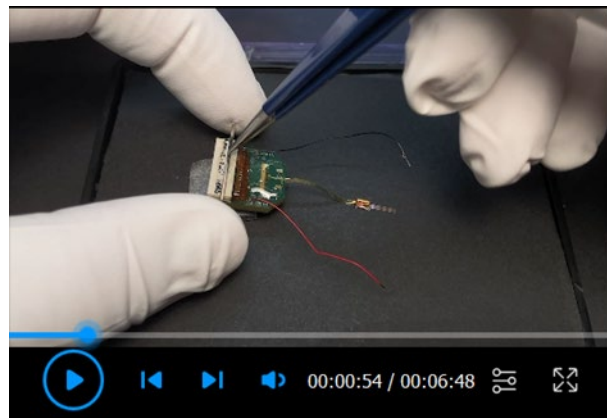
Critical step: Make sure it is tight enough but do not force it because the metal screw can break the plastic drive.

9. Solder the Omnetics connector to the male header pin (circle in Figure 4I).
10. Realign the drive inside the drive holder (if necessary). Hold the stereotax attachment with your hand and flip it upside down. Loose the screw of the drive holder and realign the drive (Figure 4J).
11. Tighten the screw again (Figure 4K).

Critical step: Make sure it is tight enough but do not force it because the metal screw can break the plastic drive.

12. Make sure there is no tension on the flexible cable of the silicon probe (Figure 4L).

Critical step: If there is tension on the cable, solder the Omnetics to a new position where the tension is released.



Video 2. How to attach a silicon probe to a recoverable microdrive

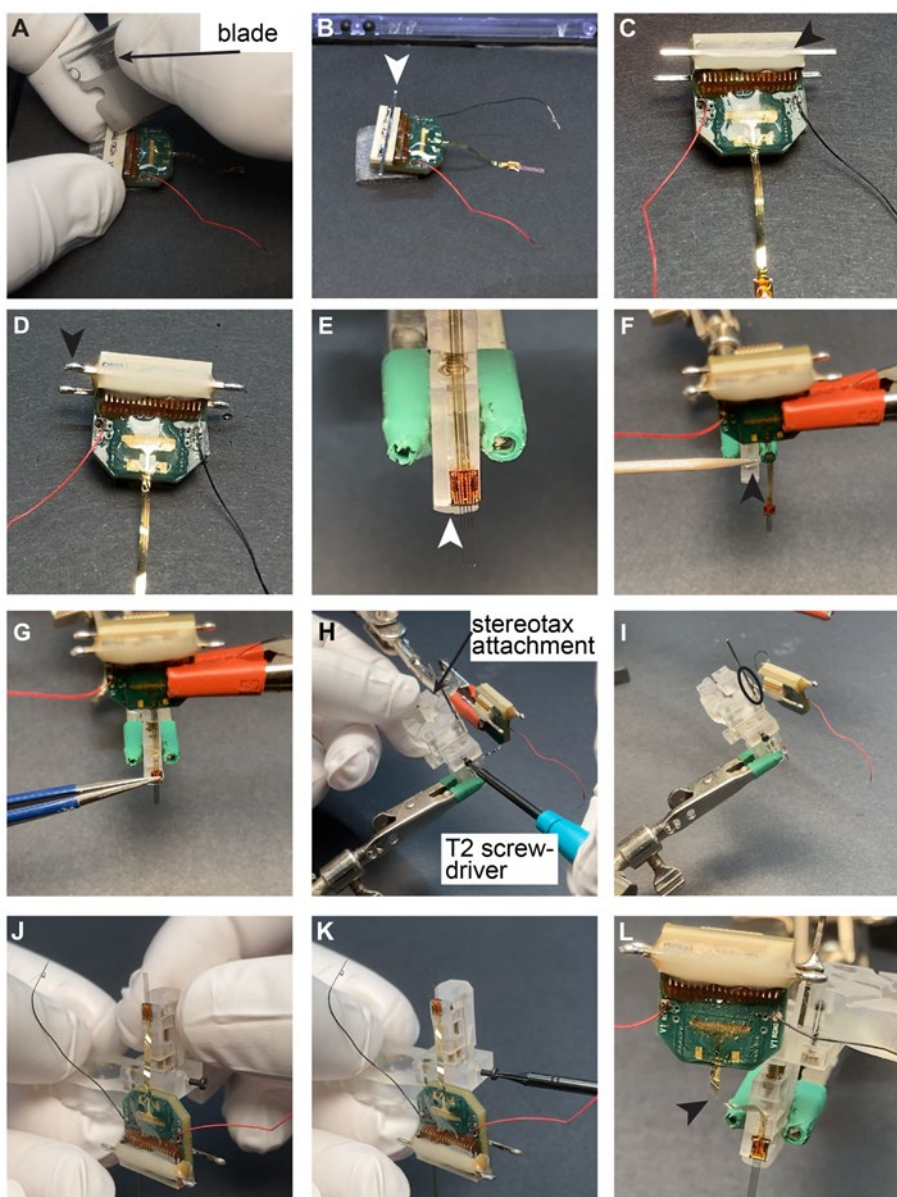


Figure 4. Attaching the silicon probe to the recoverable microdrive.
See instructions in section C above.

D. Attaching copper mesh to mouse base plate (Video 3)

1. Cut a 7 cm × 7 cm square of copper mesh (Figure 5A).
2. Mark the interior of the base plate at the center of the copper mesh with a pen and carefully cut out the interior with small scissors (Figure 5B and 5C).
3. Realign the copper mesh to the base plate and mold the mesh to the shape of the plastic base (Figure 5D).

Critical step: Make sure the copper mesh does not overhang at the bottom.

4. Attach the copper mesh to the base plate using very liquid dental cement (Figure 5E).

Critical step: The cement must be liquid enough to flow between the holes of the copper mesh to attain a strong bond to the plastic base.

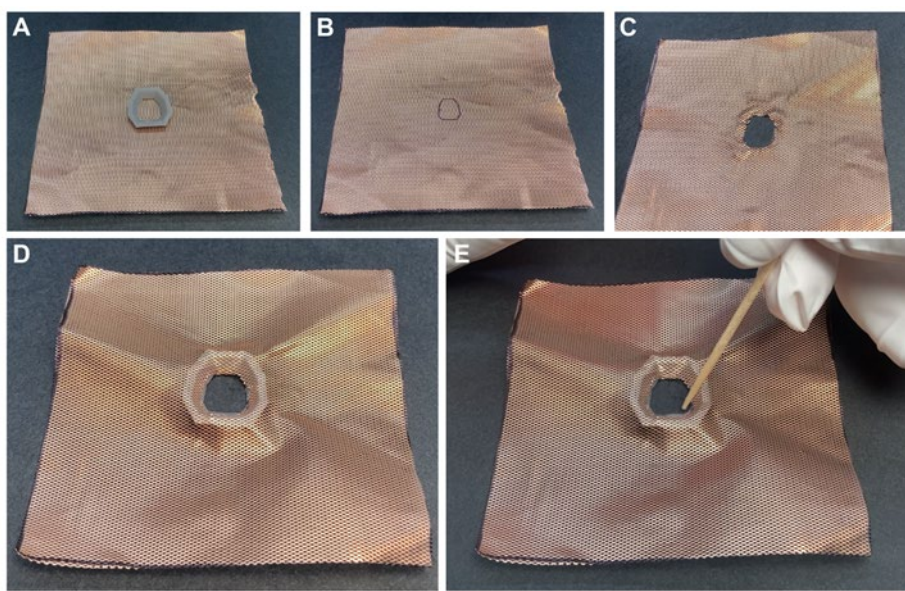


Figure 5. Preparing base plate for mice.

A. Copper mesh with the baseplate. B. Cutout of the interior of the base plate. C. Cutout at the center of the copper mesh. D. Realigned copper mesh to the base plate. E. Attachment of the copper mesh to the base plate with dental cement.

E. Attaching copper mesh to rat base plate (Figure 6)

1. Cut an 8 cm × 16 cm piece of copper mesh. Fold it in the middle to obtain an 8 × 8 cm double layer of copper mesh (Figure 6A).

Critical step: Apply soldering flux and solder in different points (Figure 6B).

2. Mark the interior of the base plate on the copper mesh (Figure 6C and 6D).
3. Cut out the copper mesh.
4. Attach the copper mesh to the base plate (Figure 6E).

Critical step: Make sure the copper mesh does not overhang at the bottom.

5. Attach copper mesh to the base plate using very liquid dental cement (Figure 6F).

Critical step: If the cement is not liquid enough, it cannot flow between the holes of the copper mesh, and it cannot attach the copper mesh to the plastic properly.

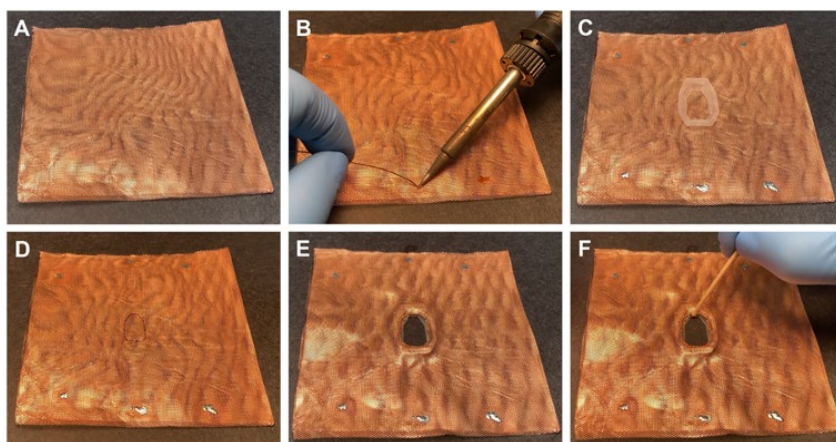


Figure 6. Preparing base plate for rats.

A. Copper mesh folded into a square. B. Applying solder to the copper mesh. This will prevent the opening of the folded, double-layer copper mesh during surgery. C. Copper mesh with baseplate. D. Cutout at the center of the copper mesh. E. Realigned copper mesh to the base plate. F. Attachment of the copper mesh to the base plate with dental cement.

F. Preparing ground and reference wire (Figure 7)

1. Cut the ground wire to the appropriate length and remove the insulation from both sides (Figure 7A).
2. Apply solder to the uninsulated part of the wire (Figure 7B).
3. Cut the end of the wire that will be soldered to the screw very short (it should not be longer than the head of the screw, see Figure 7C).
4. Hold a 000-120 1/16" pan head screw in a wise or helping hand and apply liquid soldering flux on the head of the screw (Figure 7D, arrow).
5. Apply a small amount of solder to the head of the screw (Figure 7E).

Critical step: Make sure not to fill up the hole for the screwdriver with solder.

6. Solder the ground wire to the head of the screw (Figure 7F).

Note: Store the ground wire in alcohol (at least 70%) until surgery.

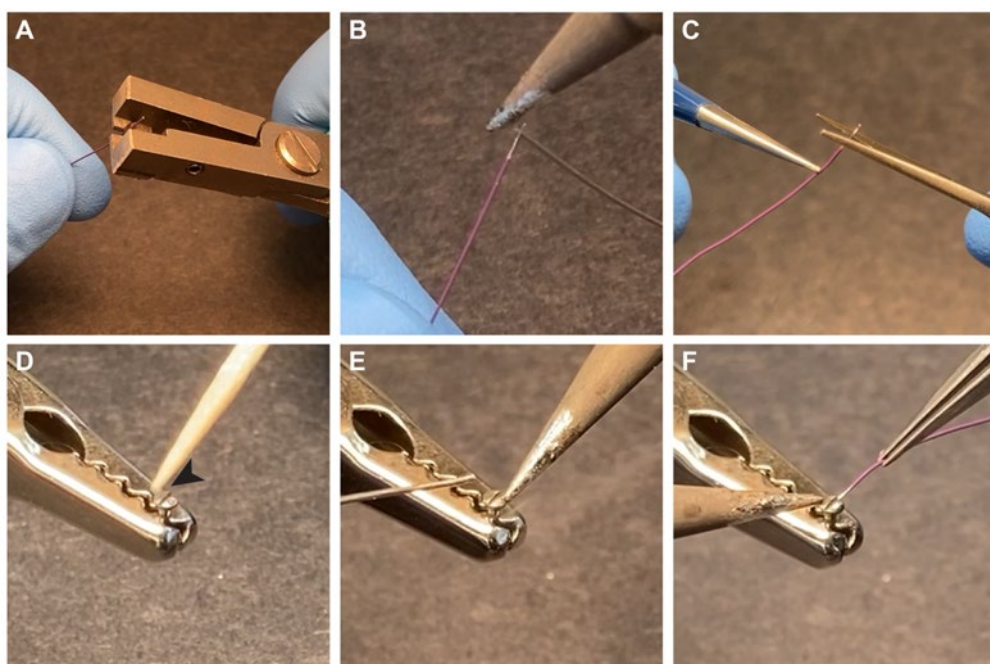


Figure 7. Preparing ground screw.

A. Wire isolation is stripped with a wire stripper. B. Solder is applied to the uninsulated part of the wire. C. Cut the stripped wire so that it is the same length as the head of the screw. D-F. Flux paste is applied (D) to the steel ground screw (000-120 1/16" screw), and a drop of solder is attached to the screw (E) before the ground wire is soldered to it (F).

G. Implanting procedure (Video 3)

Numbered steps are not shown in any of the pictures.

1. Prepare the stereotaxic apparatus and tools.
 - a. Place the heating pad under the position of the ear bars.
 - b. Sterilize surgical instruments.
 - c. Weigh the animal subject.
2. Anesthesia and pre-incision preparations.
 - a. The animal is anesthetized for 3 min (after it passes out) in an anesthesia-bucket with 2.5:1.5 (Anesthetic % to Airflow ratio).
 - b. Fixate animal with ear bars and closed ventilation nosepiece. Once the animal is in the stereotax, the level of anesthesia can be lowered (1.2-2%). Apply a local anesthetic to the tips of the ear bars before inserting them into the ears (LMX-4 Lidocaine 4% topical cream).
 - c. Remove the fur on the head of the animal around the surgery incision using either Nair-hair remover or a hair trimmer.
 - d. The hairless skin is cleaned with antiseptic solution (Povidone-Iodine – 10% topical solution). The skin is cleaned by three separate antiseptic cleanings, performed with Kimtech wipes by anterior to posterior swipes. The last swipe must be done in one stroke to minimize infections. Between each swipe, the skin is cleaned with 70% alcohol.
3. Incision and skull cleaning.
 - a. Inject bupivacaine (0.4-0.8 mL/kg of a 0.25% solution) as local anesthesia subcutaneously along the scalp midline. Make one injection site and distribute the anesthetics along the midline.
 - b. A median incision is made from the position of the eyes to the back of the skull (neck).
 - c. The skin is released from the skull, pulled aside, and fixated with four bulldogs. The bulldogs are attached to the second skin layer.

- d. Scrape the skull with a sharp object (forceps or scalpel) to remove any tissue along the top flat surface of the skull. This minimizes electric noise artifacts and affirms a strong bond of the 3D printed base.
 - e. Clean the skull with saline and vacuum suction.
 - f. Clean the skull with hydrogen peroxide and rinse with saline. The hydrogen peroxide is applied with cotton swabs (about 5 s) and rinsed quickly and thoroughly thereafter with saline.
 - g. Cauterize any bleedings along with the skull and exposed skin.
4. Attaching the base to the skull.
 - a. Mix four drops of base with one drop of catalyzer. Paint, using a brush, the whole surface of the cleaned and dried skull and let it dry (Figure 8A). Mix a new solution of Metabond with powder: four drops of base, one drop of catalyzer, and two scoops of powder and paint the skull surface with Metabond. Pay attention to paint along the edge of the skull surface.

Critical step: Prepare the Metabond on ice as it will extend the working time. We recommend using clear powder, which makes it possible to see through it (the sutures and skull landmarks remain visible).

- b. Paint the bottom surface of the 3D printed base with Unifast LC cement (arrow), align it above the skull, and attach it to the skull before it solidifies (Figure 8B).

Critical step: Paint only a small portion of the base at a location far from the region of interest. This step helps to quickly attach the base to the skull. This step can also be performed with metabond, but the curing takes longer.

- c. Cure the Unifast LC using blue light (10-20 s, Figure 8C).
- d. Paint along the inner contact line between the hat base and the skull with relatively liquid dental cement, creating a sealed area inside the hat (Figure 8D, black arrow – already sealed side, white arrow – not yet sealed).

Critical step: The cement should be liquid enough to be able to flow between the skull and base.

The finished result should look like Figures 12A-12C.

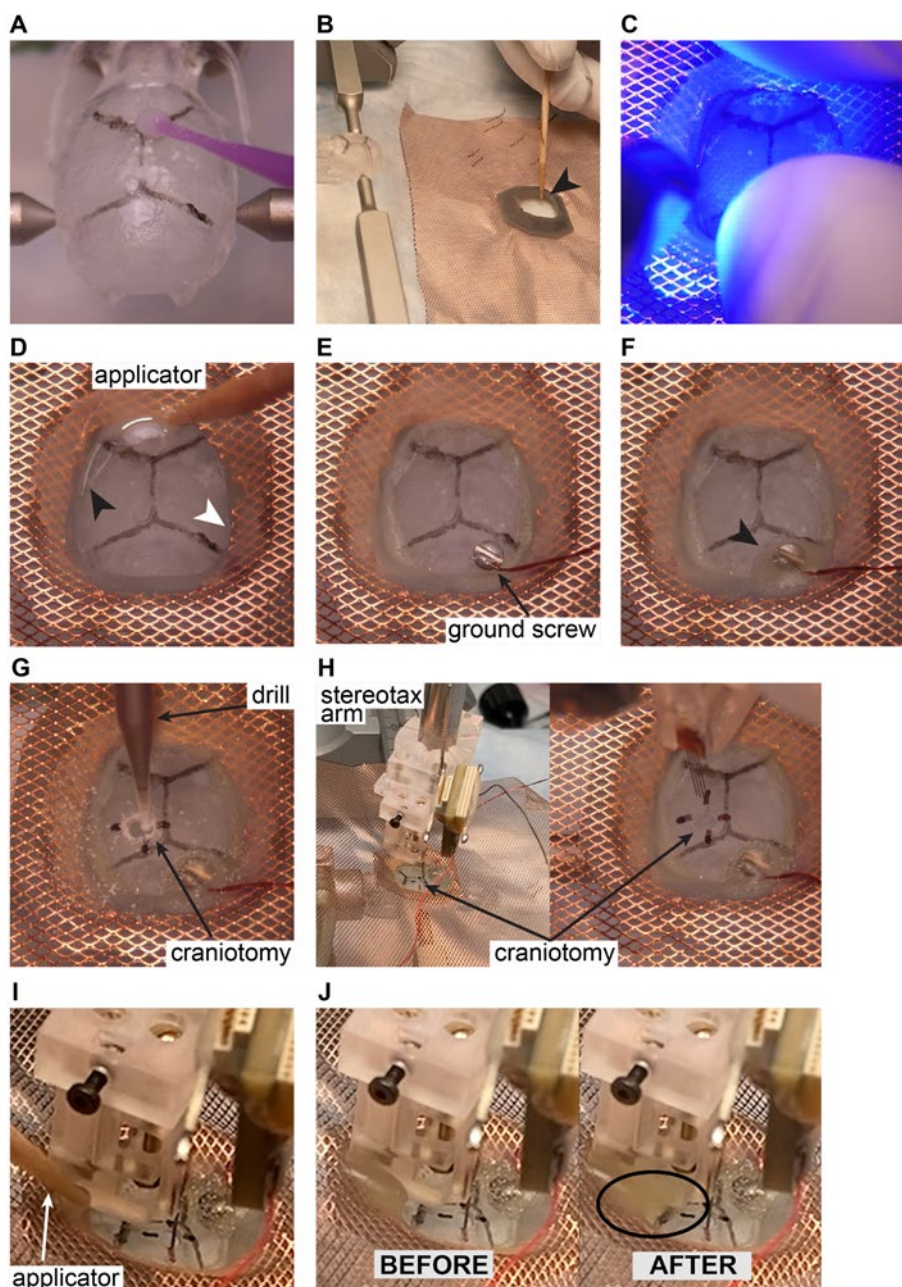


Figure 8. Silicone probe implantation in rodents.

The ‘surgery’ is performed on a 3D-printed mouse skull. Note that all these steps are identical for mice and rats.

5. Craniotomy marking and screw placement.
 - a. Align Bregma and Lambda in the same horizontal plane. Determine the position of Bregma using stereotactic coordinates with a fine syringe needle attached to the stereotactic arm.
 - b. Calculate the relative positions of the probe incision points.
 - c. Mark the positions of the craniotomies with scalpel and pen (fill the scalpel-drawn lines with the pen).
 - d. Mark the position of the reference and ground screws with the scalpel/pen.
 - e. Remove the stereotaxic arm.

- f. Drill holes for the ground screw over the cerebellum with the drill (0.7 mm). If bleeding occurs, rinse with saline and vacuum suction until bleeding stops. Screw the ground screw in (Figure 8E). Begin with a slight counterclockwise turn.

Critical step: For mice, allow a margin of about 0.5 mm (about the height of the forceps). In rats, screw the screws tight. Position the head of the screw in such a way that the ground cable is not in the way (facing outward).

Note: 125 µm steel wires can also be used for reference and ground instead of screws.

- g. Cover and completely seal the ground screw with dental cement (Figure 8F, arrow).

Note: We recommend using Unifast LC cement as it can be fully cured in 20 s.

6. Craniotomy.

- a. Using a 0.7-mm drill, prepare the craniotomy (Figure 8G). Rinse with saline and vacuum suction to ensure visibility while drilling.

Critical step: Clean around the craniotomy with the drill or the scraping/sharp scooping tool. Remove the dura with a hooked-shaped needle at the incision points of probes: Bend the tip of the 30G needle to form the hook shape to create a better grip-angle to pull the dura without damaging the cortex. You can lift the dura while pulling back with the needle tip and perform the cut with a scalpel. Avoid blood vessels. Apply saline and Gelfoam to the craniotomy to maintain a wet brain surface.

7. Probe implantation.

- a. Attach the implantation tool with a silicon probe to the stereotax arm and position the silicon probe according to specified surface coordinates (Figure 8H).

Critical step: Drive the silicon probe to the surface of the brain and mark the dorsoventral coordinate. Implant the probe to the desired target depth.

- b. Attach the base of the microdrive to the skull and hat-base with dental cement (Figure 8I).

Critical step: Use relatively liquid dental cement to let it flow between the skull and base component but be careful not to let it flow into the craniotomy. Do not ever touch the microdrive. If the gap is too big, start building up cement from the skull.

Note: We recommend using Unifast LC cement as it can be fully cured in 20 s. As this step can take multiple rounds of application of dental cement, fast curing can save significant time on the overall time of the surgery.

- c. Fill all gaps with dental cement between the base component and the skull surface (Figure 8J).
- d. Apply silicone to the craniotomy, letting the silicone run along the shanks, sealing the craniotomy completely. This protects the brain long term and limits bleedings and coagulation (Figure 9K).

Note: Alternatively, apply paraffin oil/wax to the craniotomies with narrow forceps and heat (using the soldering tip)

- e. Loosen the screw of the drive holder using a T2 screwdriver (Figure 9L).
- f. Detach the probe PCB from the stereotax attachment (Figure 9M, black circle).

Critical step: Lay down the probe PCB on the copper mesh, and make sure there is no tension on the flexible cable

-
-
-
-
-
-
-
- g. Move the stereotax arm upwards (Figure 9N, dashed arrow).
Critical step: Monitor shanks while moving upwards with the stereotax. If there is any movement of the shanks, stop immediately and check that everything is properly aligned.
8. Building a copper mesh cage for mice.
 - a. Attach a male header pin (Figure 9O, arrow) to the plastic base/skull. Hold the metal bar with a tweezer until the dental cement is cured with blue light.
Critical step: Bend the metal bar (making an L-shape with 100-120 degrees angle) and apply dental cement to this short, bent part of the metal bar; and attach it to the base. Make sure to cut the metal bar to the proper height before attaching it to the base.
 - b. Apply solder to the tip of the metal bar (Figure 9P, arrow).
Critical step: Do not apply an excessive amount of heat (long time of soldering) because the heat transferred by the metal can melt the dental cement causing structural deterioration of the copper mesh cage.
 - c. Attach the probe PCB to the male header pin installed in the previous step (Figure 9Q).
 - d. Attach three more male header pins in the three remaining corners (Figure 9R, arrows). Apply solder on the tip of all of them.
 - e. Attach a male header pin across one side. Repeat with the remaining open sides (Figure 9S).
Critical step: Cut the length of the metal bar to the proper length before soldering it to the cage.
 - f. Cut the copper mesh along the diagonals, all the way to the plastic base (Figure 9T).
 - g. Fold up the copper mesh and cut it to the appropriate height (Figure 9U, arrow).
 - h. Solder the copper mesh to the male header pins (Figure 9V).
 - i. Repeat the cutting, folding, and soldering on all sides (Figure 9W).
 - j. Attach ground wire from probe PCB and from ground screw to copper mesh using solder (Figure 9X).
-
-
-
-
-
-
-
-
- k. Using the handle of a tweezer (Figure 9Y, circle), smooth out the edges, if necessary. Secure the edges with solder if necessary.

Note: If using separate ground and reference wires, attach them accordingly.



Video 3. Preparation of mouse base plate and implantation of silicon probe

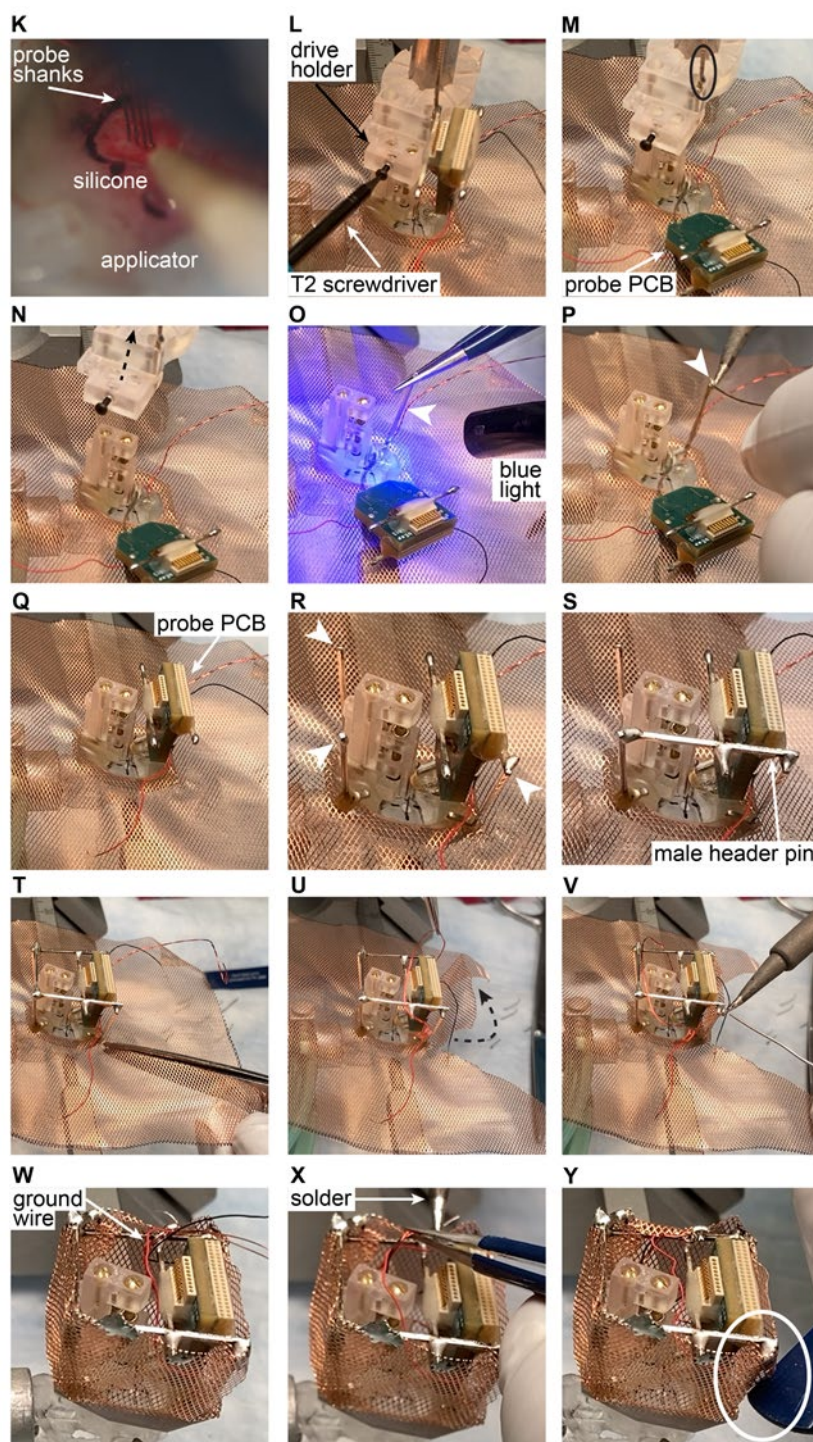


Figure 9. Silicone probe implantation in rodents (K-N) and cap building in mice (O-Y).

The ‘surgery’ is performed on a 3D-printed mouse skull. Note that steps K-O are identical for mice and rats.

9. Building a copper mesh cage for rats.
 - a. Cut the copper mesh along the diagonals, all the way to the plastic base (Figure 10O).
 - b. Repeat with the remaining three corners (Figure 10P).
 - c. Fold up the copper mesh and attach the pieces using solder (Figure 10Q).

- d. Using the handle of a tweezer, smooth out the edges, if necessary (Figure 10R).

Critical step: Make sure there is no sharp edge around the plastic base.

- e. Using scissors, cut the height of the copper mesh to the appropriate height all around (Figure 10S). Figure 10T shows the completed step.
- f. Paint the outer surface of the copper mesh with relatively liquid dental cement using a large surface spatula (Figure 10U).

Critical step: Make sure that dental cement is not dripping onto the fur or the face of the rat. Make sure that the plastic base – copper mesh connection is properly covered (if not covered completely, it can introduce a lot of muscle artifacts).

Note: We recommend using Unifast Trad cement.

- g. Cover the top of the copper mesh with dental cement (Figure 10V).

Note: Follow the instructions as shown in Figure 10U.

- h. Steps are not shown in the Figure: solder the male header pin of the probe PCB to the copper mesh. Solder probe ground and wire of ground screw to the copper mesh.
- i. Cover the top with Coban™ tape. Turn off the anesthesia and release the animal from the stereotaxis setup.

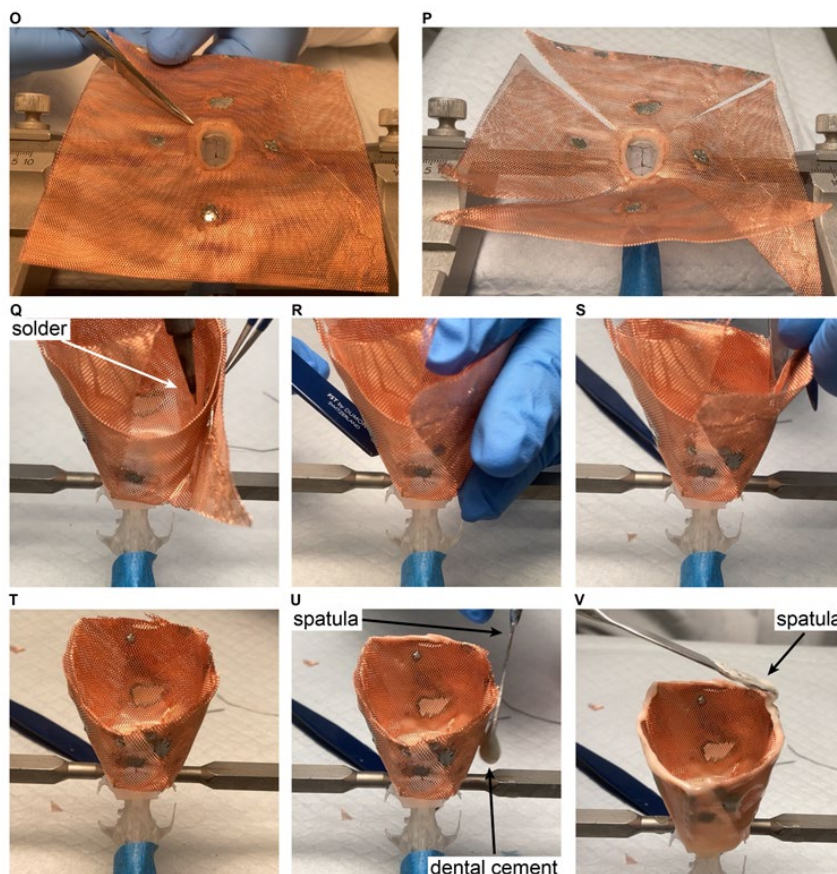


Figure 10. Cap building in rats.

The ‘surgery’ is performed on a 3D-printed rat skull.

10. Post anesthesia.
 - a. Weigh the animal again to determine the weight of the crown.
 - b. Put the animal in a home cage without bedding and place the cage on a heating pad the first night.
 - c. Inject Buprenex subcutaneously after 20 min (0.05-0.1 mg/kg).
11. General notes.
 - a. Apply mineral oil to the eyes of the animal at regular intervals.
 - b. To keep the animal hydrated for the first few days, provide an aqua-gel and a small container with water. Provide regular rodent pills.

H. Probe recovery procedure (Video 4 and Figure 11).

1. Align the drive holder with the drive using the stereotactic frame. Once the position is aligned in the x-y plane, move the drive holder down (Figure 11A, step 1). Next, secure the top of the drive with the screw located on the side of the drive holder (Figure 11A, step 2).

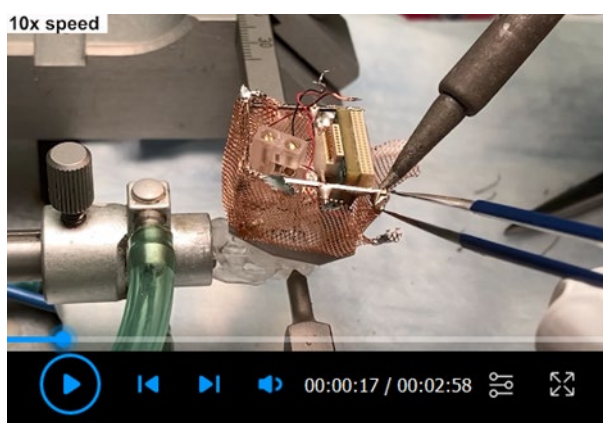
Critical step: Do not tighten the screw too strongly as the metal screw can break the plastic drive.

2. Loosen the back screw from the base (Figure 11B, step 1) and move the drive carefully upwards (Figure 11B, step 2).

Critical step: Monitor the shanks of the probe under the microscope during the entire recovery procedure and, if any unexpected movement of the probe is observed, return to the previous step to make sure that everything is secured properly.

3. Release the stereotax attachment from the stereotax arm and clean the probe. Store the probe attached to the stereotax attachment.

Note: The probe can be cleaned by initially rinsing it in distilled water, then contact lens solution (containing protease) and distilled water again; each washing step should last for at least 12 h. If extra tissue or debris is detected between the shanks, it can be removed by a fine needle under a microscope. Another way to clean the probe is by inserting it into 2-4% agarose gel a couple of times. This will push any debris away from the sites along the shanks.



Video 4. How to recover a silicon probe using a recoverable microdrive

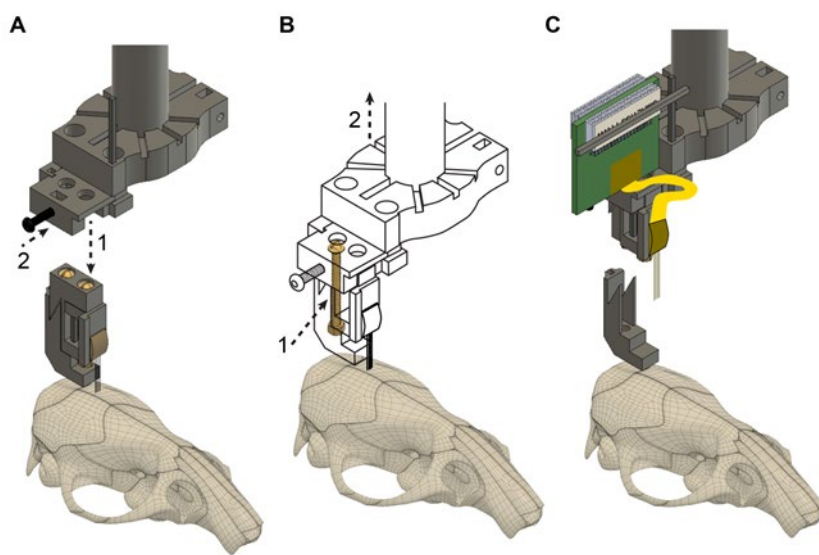


Figure 11. Probe recovery.

A. The implantation tool is attached to the microdrive (step 1) and is fixed with the black screw (step 2). The flexible cable and Omnetics connector are not shown. B. The back screw is loosened completely (step 1), detaching the microdrive from the base; then, the implantation tool is raised using the stereotax manipulator (step 2), explanting the probe. C. The fully recovered microdrive and silicon probe with flexible cable and Omnetics connector. The probe shanks can be cleaned, and a new microdrive base can be attached, making the whole device ready for reimplantation in a new animal subject.

Figure 12, panels D-G show the wide applicability of the hybrid base for silicon probe recordings with temperature manipulations and optic fiber stimulation.

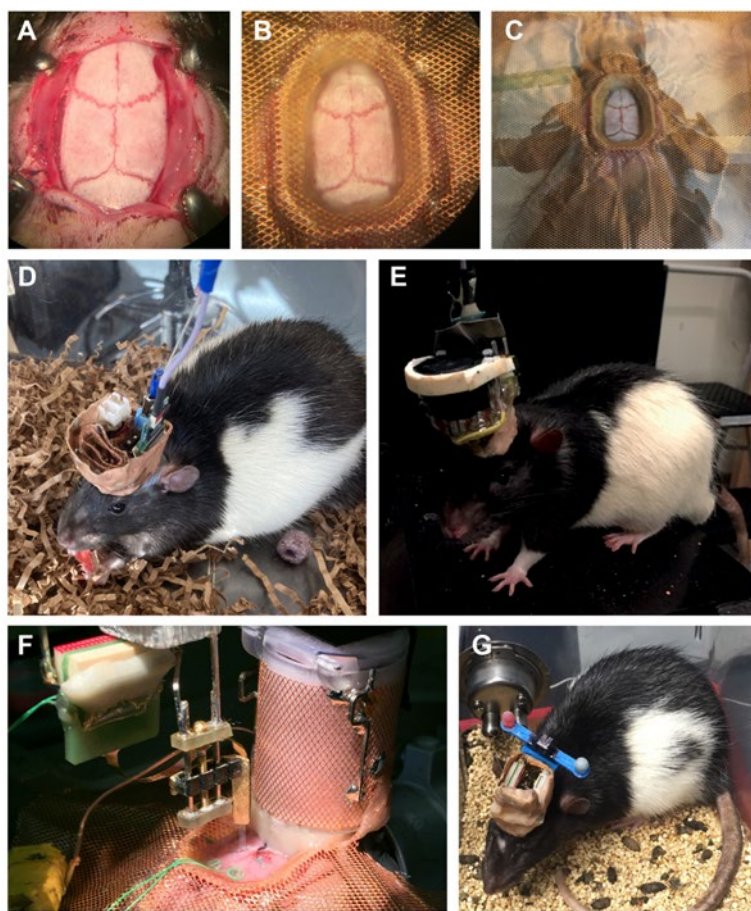


Figure 12. Applicability of the hybrid base.

A. Exposed skull before the base is attached. B-C. Close up (B) and wide view (C) of the attached hybrid cap system. D. Peltier cooling device with passive cooling, thermistor, and silicon probes implanted at two different insertion sites. E. Peltier cooling device with an active 20 mm electric fan for cooling, thermocouple, wires, and silicon probe implants. F. Bilateral CA1 probe implants (shown during implantation of the left hemisphere implantation) with dry ice cooling chamber already implanted. G. Virus injected animal for optogenetic experiments. Four 50- μ m diameter optic fibers were implanted with two diodes along with a silicon probe in CA1. Two diodes (blue bar) are attached for head position tracking via ceiling-mounted camera. Panels A-C and E-G from Petersen and Buzsáki (2020). Rat shown in panel D is from an ongoing unpublished study. All pictures are of Long Evans rats.

Notes

Members of our labs have performed invasive silicon probe implant surgeries on hundreds of rodents (mice and rats) just within the last year and have used variations of the base plate system for most of our probe implantations during the last few years. Based on individual estimates (of two rat and three mouse researchers), using the rat and mouse base system saves about 30-60 min during surgery. This time was originally spent on building the dental cement perimeter and the drilling craniotomies for anchoring skull screws and on attaching the copper mesh to this dental cement base (Vandecasteele *et al.*, 2012).

According to a recent internal survey based on about 25 silicon probes with the recoverable microdrive, on average, each probe was recovered two times and reimplanted successfully in new animal subjects. Out of 48 recovery attempts, only five failed. All users were able to recover silicon probes successfully if there was no surgery/time of

implant-related complications. Coagulated blood, dried bone wax, or debris attached to the shanks were the most frequent causes of complication resulting in failed probe recovery. Before attempting a probe recovery in these cases, we recommend soaking the implanted silicon probe for at least 10 min in saline and removing as much debris beforehand as possible. The recovery procedure takes 30 min on average compared to 1-2 h (Vandecasteele *et al.*, 2012).

Acknowledgments

We would like to thank our early adaptors in Royer, Diba, and Buzsaki Labs for testing the microdrive and the baseplate and for providing feedback. We also thank Dmitry Rinberg for advice and feedback on designs. This work was supported by U19 NS107616, U19 NS104590, R01 MH122391, NeuroNex MINT (NSF 1707316), and The Lundbeck Foundation. The baseplate was developed for Petersen and Buzsáki (2020) and Vöröslakos *et al.* (2020), and the microdrives were developed for Vöröslakos *et al.* (2020).

Competing interests

E.Y. is co-founder of NeuroLight Technologies, a for-profit manufacturer of neurotechnology. The remaining authors have no conflict of interest.

Ethics

All experiments were approved by the Institutional Animal Care and Use Committee at New York University Medical Center.

References

- Chung, J., Sharif, F., Jung, D., Kim, S. and Royer, S. (2017). [Micro-drive and headgear for chronic implant and recovery of optoelectronic probes](#). *Sci Rep* 7(1): 2773.
- Chung, J. E., Magland, J. F., Barnett, A. H., Tolosa, V. M., Tooker, A. C., Lee, K. Y., Shah, K. G., Felix, S. H., Frank, L. M. and Greengard, L. F. (2017). [A Fully Automated Approach to Spike Sorting](#). *Neuron* 95(6): 1381-1394 e1386.
- Juavinett, A. L., Bekheet, G. and Churchland, A. K. (2019). [Chronically implanted Neuropixels probes enable high-yield recordings in freely moving mice](#). *Elife* 8: e47188.
- Jun, J. J., Steinmetz, N. A., Siegle, J. H., Denman, D. J., Bauza, M., Barbarits, B., Lee, A. K., Anastassiou, C. A., Andrei, A., Aydin, C., Barbic, M., Blanche, T. J., Bonin, V., Couto, J., Dutta, B., Gratiy, S. L., Gutnisky, D. A., Hausser, M., Karsh, B., Ledochowitsch, P., Lopez, C. M., Mitelut, C., Musa, S., Okun, M., Pachitariu, M., Putzeys, J., Rich, P. D., Rossant, C., Sun, W. L., Svoboda, K., Carandini, M., Harris, K. D., Koch, C., O'Keefe, J. and Harris, T. D. (2017). [Fully integrated silicon probes for high-density recording of neural activity](#). *Nature* 551(7679): 232-236.
- Luo, T. Z., Bondy, A. G., Gupta, D., Elliott, V. A., Kopec, C. D. and Brody, C. D. (2020). [An approach for long-term, multi-probe Neuropixels recordings in unrestrained rats](#). *Elife* 9: e59716.
- Petersen, P. C. and Buzsáki, G. (2020). [Cooling of Medial Septum Reveals Theta Phase Lag Coordination of Hippocampal Cell Assemblies](#). *Neuron* 107(4): 731-744 e733.
- Sariev, A., Chung, J., Jung, D., Sharif, F., Lee, J. Y., Kim, S. and Royer, S. (2017). [Implantation of Chronic Silicon Probes and Recording of Hippocampal Place Cells in an Enriched Treadmill Apparatus](#). *J Vis Exp* (128): 56438.

- Schoonover, C. E., Ohashi, S. N., Axel, R. and Fink, A. J. P. (2021). [Representational drift in primary olfactory cortex](#). *Nature* 594(7864): 541-546.
- Steinmetz, N. A., Aydin, C., Lebedeva, A., Okun, M., Pachitariu, M., Bauza, M., Beau, M., Bhagat, J., Bohm, C., Broux, M., Chen, S., Colonell, J., Gardner, R. J., Karsh, B., Kloosterman, F., Kostadinov, D., Mora-Lopez, C., O'Callaghan, J., Park, J., Putzeys, J., Sauerbrei, B., van Daal, R. J. J., Volland, A. Z., Wang, S., Welkenhuysen, M., Ye, Z., Dudman, J. T., Dutta, B., Hantman, A. W., Harris, K. D., Lee, A. K., Moser, E. I., O'Keefe, J., Renart, A., Svoboda, K., Hausser, M., Haesler, S., Carandini, M. and Harris, T. D. (2021). [Neuropixels 2.0: A miniaturized high-density probe for stable, long-term brain recordings](#). *Science* 372(6539): eabf4588.
- Vandecasteele, M., M. S., Royer, S., Belluscio, M., Berenyi, A., Diba, K., Fujisawa, S., Grosmark, A., Mao, D., Mizuseki, K., Patel, J., Stark, E., Sullivan, D., Watson, B. and Buzsaki, G. (2012). [Large-scale recording of neurons by movable silicon probes in behaving rodents](#). *J Vis Exp* (61): e3568.
- Vöröslakos, M., Petersen, P. C., Vöröslakos, B. and Buzsaki, G. (2021). [Metal microdrive and head cap system for silicon probe recovery in freely moving rodent](#). *Elife* 10: e65859.
- Wu, F., Stark, E., Ku, P. C., Wise, K. D., Buzsaki, G. and Yoon, E. (2015). [Monolithically Integrated muLEDs on Silicon Neural Probes for High-Resolution Optogenetic Studies in Behaving Animals](#). *Neuron* 88(6): 1136-1148.

Cortical Laminar Recording of Multi-unit Response to Distal Forelimb Electrical Stimulation in Rats

Charles-Francois V. Latchoumane¹, Rameen Forghani¹ and Lohitash Karumbaiah^{1, 2, §, *}

¹Animal and Dairy Science, University of Georgia, Athens, GA, USA

²Regenerative Bioscience Center, University of Georgia, Athens, GA, USA

§Present address: 425 river road, ADS complex, University of Georgia, Athens, 30601, USA

*For correspondence: lohitash@uga.edu

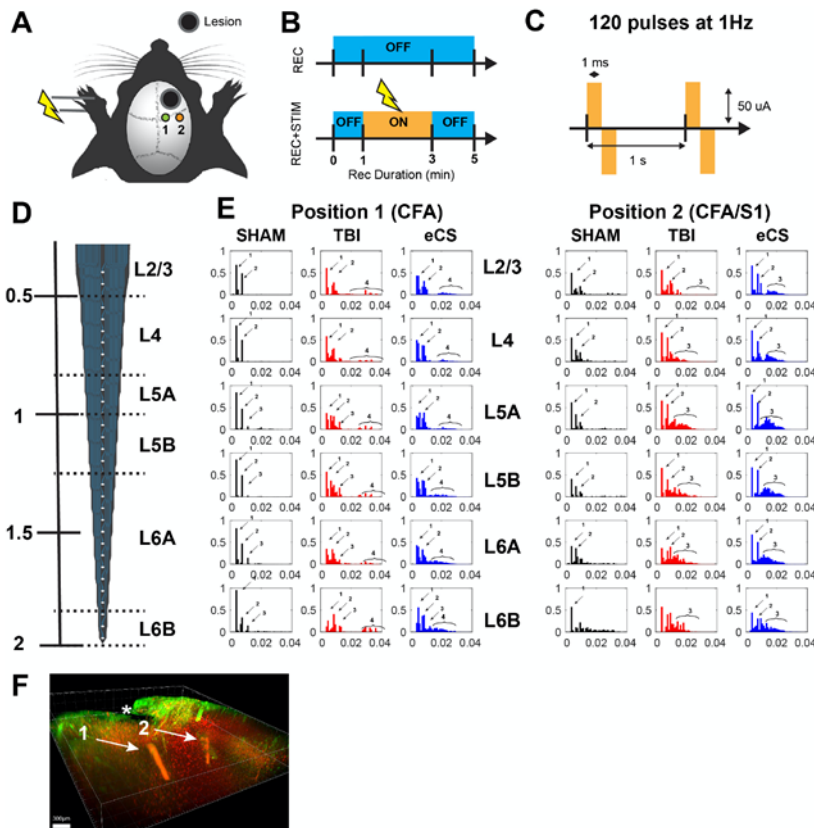
Abstract

Severe traumatic brain injury (sTBI) survivors experience permanent functional disabilities due to significant volume loss and the brain's poor capacity to regenerate. Chondroitin sulfate glycosaminoglycans (CS-GAGs) are key regulators of growth factor signaling and neural stem cell homeostasis in the brain. In this protocol, we describe how to perform recordings to quantify the neuroprotective and regenerative effect of implanted engineered CS-GAG hydrogel (eCS) on brain tissue. This experiment was performed in rats under three conditions: healthy without injury (Sham), controlled cortical impact (CCI) injury on the rostral forelimb area (RFA), and CCI-RFA with eCS implants. This protocol describes the procedure used to perform the craniotomy, the positioning of the cortical recording electrode, the positioning of the stimulation electrode (contralateral paw), and the recording procedure. In addition, a description of the exact electrical setup is provided. This protocol details the recordings in the brain of injured animals while preserving most of the uninjured tissue intact, with additional considerations for intralesional and laminar recordings of multi-unit response.

Keywords: Linear silicone probe, Caudal forelimb area, Paw stimulation, Laminar cortical recording, Multi-unit sensory response.

This protocol was validated in: Sci Adv (2021), DOI: 10.1126/sciadv.abe0207

Graphical Abstract:



Sensorimotor response to paw stimulation using cortical laminar recordings.

Background

Traumatic brain injury (TBI) is a common and increasingly prevalent problem that affects approximately 69 million people globally, without an effective treatment to date (Dewan *et al.*, 2018). Given the failure of secondary neuroprotective strategies, such as decompressive craniotomy, or tight blood pressure regulation, in ameliorating poor functional outcomes, increased attention has turned to re-establishing damaged neuronal circuitry in the brain through biomaterial implants, with or without concurrent cell transplantation (Tan *et al.*, 2020). Apart from providing the ability to inject any one of several natural or synthetic biomaterials into an injury lesion, it is unclear what functional effect these implants have on restoring native neuronal circuits and on higher-order cognitive and motor outcomes. In our manuscript (Latchoumane *et al.*, 2021, DOI: [10.1126/sciadv.abe0207](https://doi.org/10.1126/sciadv.abe0207)), we implanted rats with engineered chondroitin-sulfate glycosaminoglycans (eCS) as a potential treatment for the loss of tissue and consequent loss of motor function following TBI. To assess the physiological recovery promoted by eCS implants, we recorded the laminar cortical activity in response to electrical stimulation of the paw in anesthetized rats. Previous works in the field have used *ex vivo* planar multielectrode arrays on 300 μ m brain slices to evaluate field excitatory postsynaptic potentials (fEPSPs) post-biomaterial implant (Yang *et al.*, 2015; Hao *et al.*, 2017). Other labs have performed steady-state evoked potentials (SSEP) recordings with chronically implanted electrodes in the mouse brain to measure brain responses post-implant (Fernández-García *et al.*, 2016). We present a simple protocol that can be carried out in a single procedure, using a multichannel system recording and stimulation setup for the evaluation of the sensorimotor integration in animals implanted with eCS following TBI. Our protocol demonstrates

the feasibility and reproducibility of recording perilesionally to assess biomaterial integration, the impact of eCS on surrounding tissue, and the extent of live neuronal proliferation within and around the implant.

Materials and Reagents

1. Suture 4-0 Ethicon Absorbable plus antibacterial (Vicryl, catalog number: 109162)
2. Self tapping screws (18-8 Stainless Steel Slotted Flat Head Screws, M0.8 × 0.2 mm Thread, 2 mm Long; McMastercarr, catalog number: 91430A143)
3. Sterile cotton swabs, Cotton Tipped Applicators 6"/Sterile 100/box (Dynarex)
4. Stimulation needles, sterile stainless steel needle 24 gauge (BD, Microlance, catalog number: 1730738)
5. Animals: Sprague-Dawley Rats, male, age (7-10 weeks) (Charles River, catalog number: 400)
6. 32 channel linear probe (Neuronexus, A1x32-6mm-50-177-CM32, 15 µm thickness, Gen4, lot# P994)
7. Ketamine 100 mg/mL (Coventrus, catalog number: 056347361-4)
8. Xylazine cocktail, 100 mg/mL (Sigma-Aldrich, catalog number: 7361-61-7)
9. Isofluorane (Coventrus, catalog number: 029405)
10. Buprenorphine, 0.03 mg/mL (Coventrus, catalog number: 059122)
11. Marcaine, 0.5% (Coventrus, catalog number: 054893)
12. Povidone-Iodine, 10% topical solution (CVS, catalog number: 59779-085)
13. Etch-Gel, phosphoric acid 40% (DMG, catalog number: 61901)
14. Gel Foam® (Pfizer, catalog number: 115631)
15. SeaKem® agarose (Lonza, catalog number: 50004)
16. Triple antibiotics, 0.9 g Pouch (25 ct. Box) (Safetec, catalog number: 53205)
17. Ketamine/Xylazine Cocktail (see Recipes)

Ketamine/Xylazine Cocktail:

- For 1 ml solution: 0.9 mL of Ketamine (100 mg/mL) + 0.1 mL of Xylazine (100 mg/mL)
- KX rat cocktail 0.1 mL/100g rat wt. IP (Ketamine: 90 mg/kg, Xylazine: 9.0 mg/kg)

Equipment

1. Multichannel acquisition system (MCS, Wireless Recording, model: W2100)
2. Multichannel recording and stimulation headstage (MCS, headstage, model: HS32-EXT0.5mA)
3. Dell PC i7, RAM:8Go, SSD: 500 GoPremium Silicone
4. Kopf Stereotaxic frame for rodent with manipulating arm
5. Electronic breadboard (Half-size breadboard; 63; adafruit.com)
6. Electronic cables (Covered Male-Male Jumper Wires, 200 mm × 40; Adafruit.com, catalog number: 4482)
7. MCS coaxial TTL cable (C-BNC-Lemo1m; Multichannel system accessories)
8. Electric Shaver (Philips, Norelco oneblade QP2520/90)
9. Electric Drill and trephine bur (Micromotor shiyang, H102S)
10. CCI tip, 3 mm diameter (Custom made)
11. CCI impactor machine (UGA workshop custom made)

Software

1. Acquisition Software: MCS experimenter (Multichannel Systems, <https://www.multichannelsystems.com/>)
2. System configuration: MCS IPconfig (Multichannel Systems, <https://www.multichannelsystems.com/>)
3. Data analysis: Matlab + MCS toolbox (Multichannel Systems, <https://www.multichannelsystems.com/>)
4. Matlab R2019b (Mathworks Inc., [mathworks.com](https://www.mathworks.com))

Procedure

A. System setup

The system setup is described in detail in Figure 1.

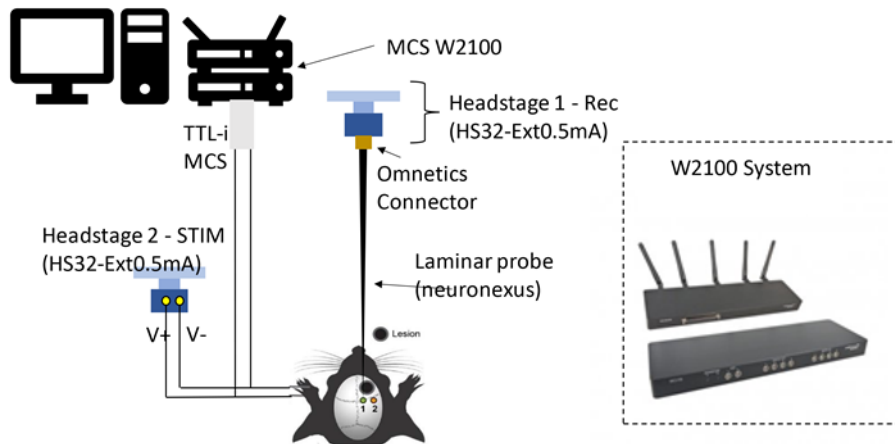


Figure 1. Setup for the recording of cortical activity with simultaneous electrical stimulation of the paw in the anesthetized rat.

We used two battery-powered HS32-Ext0.5 mA headstages synchronized through the W2100 from multichannel systems (MCS). This system allowed the use of separate grounds for recording and stimulation, limiting the eStim-induced artefacts (*i.e.*, electrical artifacts). The HS32 headstages can electrically stimulate in a bipolar setup while providing simultaneous recording through a 32-channel omnnetics connector. The recording headstage was connected to a 32-lead linear silicone probe (Neuronexus). To obtain the exact time of stimulation, the stimulation headstage was connected to the paw of the animal and returned the voltage to the MSC. This system allowed a precisely synchronized stimulation and recording of events with neural response. We recorded from 2 regions (sequentially) in order to assess the laminar response of the S1 region and S1/M1 regions in the rat following paw stimulation.

B. Controlled Cortical Injury (CCI) Surgical Procedure and eCS gel implant

1. Prior to CCI injury, anesthetize each animal with 5% isoflurane (switched to maintenance 2-3% as soon as the incision was performed – Step B4).
2. Inject buprenorphine (0.3 mg/mL, 0.05 mL/300g, Henry Schein) subcutaneously,
3. Place animals with their scalp shaved and sanitized (70% Ethanol and 3% povidone-iodine) on a stereotaxic frame attached to a temperature-controlled heating pad (37°C).
4. Perform a sagittal incision and clean the periosteum using Etch-gel (phosphoric acid etching, Henry Schein).
5. Perform a craniotomy using a 5-mm-diameter trephine bur fitted to an electric drill.
6. Fit a 3-mm CCI tip onto the pneumatic piston, position it in contact with the surface of the dura (fully extended position), and then retract it to adjust for an impact depth of 2 mm.
7. Launch the 3-mm CCI tip to create an impact. A severe CCI injury is induced by programming the piston speed to 2.25 m/s with a dwell time of 250 ms, resulting in an initial 3-mm-diameter injury with a depth of 2 mm.
8. Apply absorbable gelatin (Gel Foam®, Pfizer pharmaceutical) to the injury site, using sterile cotton swabs to remove excess blood.
9. Remove the gelatin and completely cover the injury site with a layer of 1% sterile agarose (SeaKem®).

- Lonza).
10. Suture skin flaps were together to close the wound. Apply triple antibiotic cream on the sutured skin.
 11. *Optional:* For the eCS group, the eCS gel was implanted 48 h post-CCI using a pre-photocrosslinked gel delivered through a 32 gauge Hamilton syringe (speed: 20 μ L/10min) in the center of the CCI lesion (1 mm depth).

C. Electrode placement surgical procedure (8 weeks post-CCI)

1. See Structure Denomination for brain region names.

Structure Denomination:

- M1: primary motor cortex
- RFA: rostral forelimb area, part of the M1 region for hand control
- CFA: caudal forelimb area, part of the M1 region for hand and leg control
- S1: primary sensory cortex
- AP/ML/DV: stereotaxic positioning relative to the bregma point (reference); AP: anterior-posterior, ML: middle-lateral, DV: dorsal-ventral

2. From 8 to 10 weeks post-CCI, anesthetize rats that received RFA-targeted lesions using a ketamine/xylazine cocktail (100 mg/Kg) and place them on a stereotaxic frame.
3. Following sagittal scalp incision, perform a craniotomy (Figure 2) caudally to the injury (AP: 0 mm, ML: 2 to 4mm, relatively to bregma). Using a dental drill with trephine bur (2 mm diameter), draw a square shape within the skull, from the half width of the injury site down to the bregma (AP: 0 mm), with a width of 3-4 mm, and covering the entire lateral side (from the midline to the temporal cranial muscles). Then, lift and carefully remove the bone flap with fine forceps.

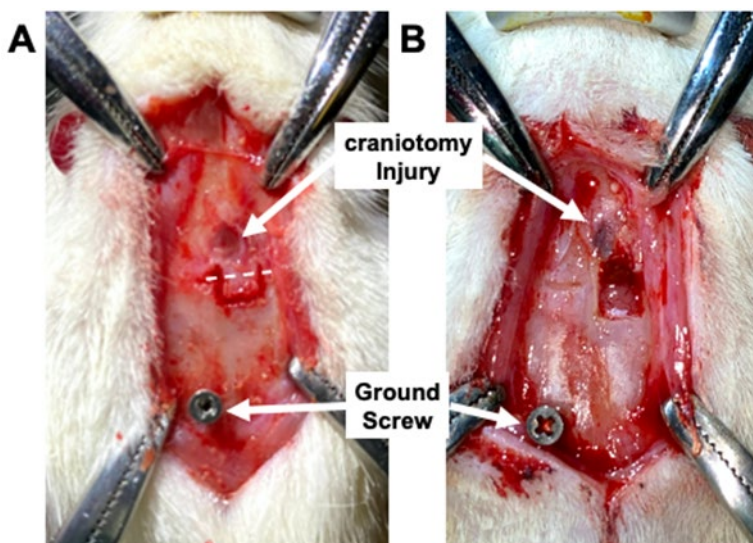


Figure 2. Position and description of the craniotomy post-lesion.

4. Perform a durotomy to allow for the insertion of a 32-channel silicone probe (Neuronexus). Using the tip of a 1 mL insulin needle bent at 90° penetrate the dura tangentially to the brain to avoid any damage to the grey matter. Move the needle across the length of the craniotomy to tear the dura, and flip its pieces outside of the craniotomy region.
5. Insert the silicone probe (Figure 3, Video 1) in the motor area adjacent to the RFA (position 1: CFA, AP: 0 mm, ML: 2.5 mm) or in the sensorimotor area (position 2: S1, AP: 0 mm, ML: 3.5 mm) at a depth of 2 mm from the surface of the brain. Important: since the CCI was performed on the RFA, the CFA region should remain intact. If necrosis is observed in the CFA region, chances are that the recording will yield

a low number of healthy unit spiking. Necrosis in the CFA/S1 region can be identified by the presence of liquified or brownish tissue with poor consistency, missing tissue volume, or dark tissue with a mix of coagulated and non-coagulated blood.

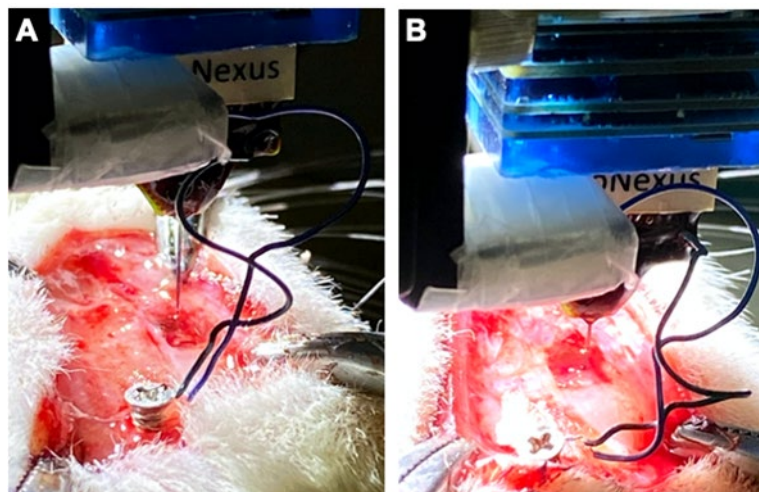


Figure 3. Poisitioning and setup of the recording electrode following craniotomy.



Video 1. General setup for the terminal recording of cortical activity following paw stimulation (somatosensory evoked response). (This video was made at the University of Georgia (UGA) according to guidelines from the IACUC of UGA under protocol # A2020-06-002.)

6. Use the probe reference (top ground electrode) as the main reference, and a screw positioned above the left cerebellum (posterior, contralateral hemisphere) as ground. The probe reference is described in the main manufacturer website: <https://www.neuronexus.com/files/technicalsupportdocuments/Chronic-Wiring-Configurations.pdf> (see chronic probe reference description for internal reference).

D. Paw electrode placement procedure

1. Use a bipolar configuration for the paw stimulation. Use close positioning of the sink and source electrode to produce a short distance electrical stimulation, which results in a very localized electrical field excitation of the tissue. The bipolar configuration is the opposite of a monopolar configuration,

where the sink and source are placed far apart, with the stimulation area becoming larger and less specific as a consequence.

2. Connect the anode and cathode of the stimulator to stainless steel needles.
3. Insert the two electrode tips at 2 mm from each other in the ventral section of the forelimb (palm of the paw). Then, place the paw and the entire forearm on the sterile pad.

E. Recording Procedure

1. Digitize and record neural data at 20 kHz (unit gain) using a multichannel system (MCS) W2100 acquisition module and a wireless headstage (HS32-EXT-0.5 mA, 16 bit; Figure 4A).
2. For spike analysis, filter the broadband electrophysiological through a real-time bandpass (300-5,000 Hz) and use a baseline pre-calculated threshold as trigger to save spike waveforms and spike event timestamps (threshold: 5 standard deviations). Do not sort for single-unit data; rather use multiunit spikes as a measure of population activity (Figure 4B, Video 2).
3. Perform all recordings for 5 min after stabilization for 10 min.

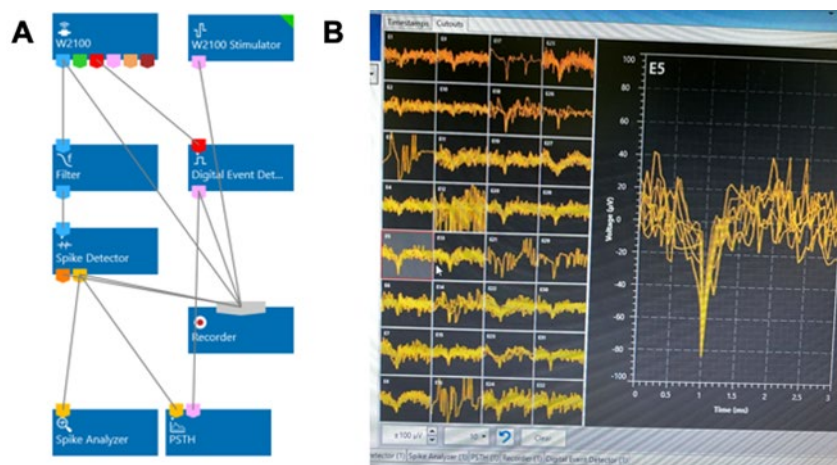
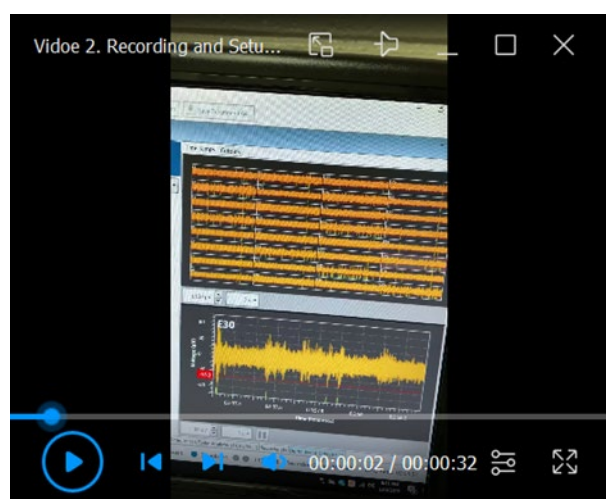


Figure 4. Recording setup using multichannel system software.



Video 2. Example of recording during ketamine anesthesia with laminar electrode.

F. Stimulation Protocols

1. Perform all paw stimulations using a single pulse (biphasic, on phase 1 ms) with a 1 s inter-pulse interval (1 Hz). Deliver the stimulation for a total of 120 pulses (2 min). Record continuously for 5 min and set the stimulation to start after 1 min of baseline and stop 2 min before the end of the recording, to obtain a return to baseline period.
2. Choose a stimulation intensity of 50 μ A, as this induced a visible S1 response without the presence of artifacts due to electrical stimulation. Use two separate, battery-powered headstages to perform the stimulation on the paw and the recording of the electrode, allowing for independent grounding and low cross-electrical artifact formation.
3. Co-register each stimulation triggering to the recording system to match the real delivery of stimulation, rather than the estimated onset of the stimulation.

Data analysis

1. Analyze all data using custom-made Matlab[®] codes (Mathworks Inc.) and the provided Multichannel systems matlab toolbox. Upon reasonable request, the script used for analysis can be shared via email.
2. Record data from a 32-channel linear electrode, and group recorded channels according to the laminar organization as described in Figure S11D (abe0207 manuscript) or the graphical abstract. Use the same channel grouping for all recordings, considering that the depth (2mm from the dura) and ground position (electrode ref/ground placed in layer 1) were placed similarly (Layer 1: none; Layer 2/3: ch1-3; Layer 4: ch4-10; Layer 5A: ch11-14; Layer 5B: ch15-19; Layer 6A: ch20-29; Layer6B: ch30-32). Data analysis included:
 - a. Stim-triggered histograms: use bin histograms to estimate the number of spikes elicited following the stimulation (Figure 5E; Figure S11E in Latchoumane *et al.*, 2021).
 - b. From the average multiunit waveform (Figure 6A), estimate the spike wave width and peak-to-trough values to obtain the distribution of cell type (*i.e.*, regular spiking units showing wider widths and lower amplitudes; fast spiking units showing shorter widths and larger amplitude).
 - c. Using the 5 min recording time separated into pre (1 min), STIM (2 min), and post (last 3 min), estimate the mean firing rate across channels in each layer. Compute the z-score using the mean and standard deviation of the firing rate during baseline (either a preceding recording without STIM or the pre-STIM period). This estimation can be obtained for each group (Sham, TBI, eCS) and each location (CFA and CFA/S1) (Figure 6B).

Results

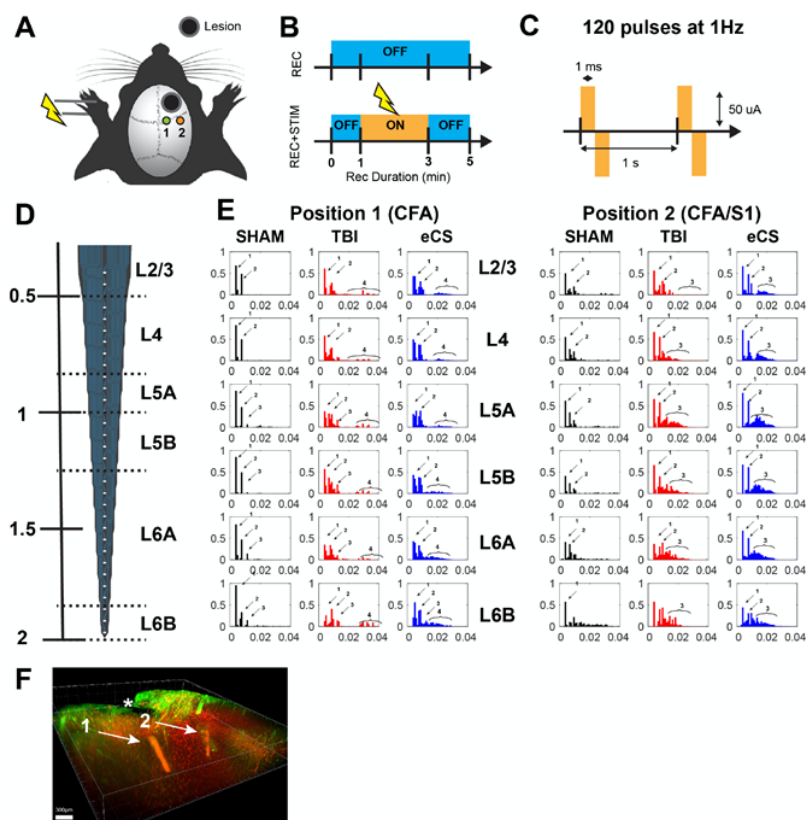


Figure 5. eCS matrix implants promote sensorimotor connectivity 10 weeks post-TBI.

A. Experimental schedule for recording session in ketamine anesthetized rats. To avoid disruption to the injury or eCS implant, use two positions for recording perilesionally for each rat. Position 1: CFA; Position 2: CFA/S1. B. Perform the recording for each position only after the probe insertion has been stabilized (top), followed by a stimulation session (2 min) with pre and post stimulation baseline recording of 1 and 2 min, respectively. Deliver 120 stimulation pulses for each position and each rat. C. The stimulation protocol used a bipolar pulse of 1 ms width (phase 1) at 1 Hz with an amplitude fixed at 50 μ A for all rats. The stimulation amplitude was determined to minimize stimulation artifacts on recording while still eliciting sensorimotor response. Note: Perform stimulations and recordings using two separate wireless headstages (Multichannel Systems, W2100 HS32-Ext0.5mA) to guarantee ground and stimulation isolation from recording electrodes. Record each rat without (5 min) and with stimulation (5 min, out of which 2 min where stimulated) for the two positions CSA and CSA/S1. D. Use a 32 channel linear silicone electrode (iridium-iridium oxide, recording sites: 50 μ m spacing) with a total span of approximately 1.6 mm. Perform implantation up to a depth of 2 mm from the surface of the pia. The layer position was based on the depth of the electrode and previously characterized layer distribution in the sensorimotor cortex. E. For the two recording positions, a treatment- and layer-dependent stimulation-locked response was observed. Following stimulation, a multimodal distribution typically revealed two major sharp peaks of neuronal activity (mono/di-synaptic; arrow indicating peaks 1 and 2) and later a response that revealed multi-synaptic activation of the area post-paw stimulation (arrow indicating peaks 3 and 4). Arrows indicate detected peaks of activity response, numbered in order of delay from stimulation start. F. Representative localization of the electrode positioning in a TBI rat brain, post-recording/stimulation. The arrow indicates the position of recording for position 1 and 2 shown in A. * indicates the position of the lesion. Scale bar: 300 μ m.

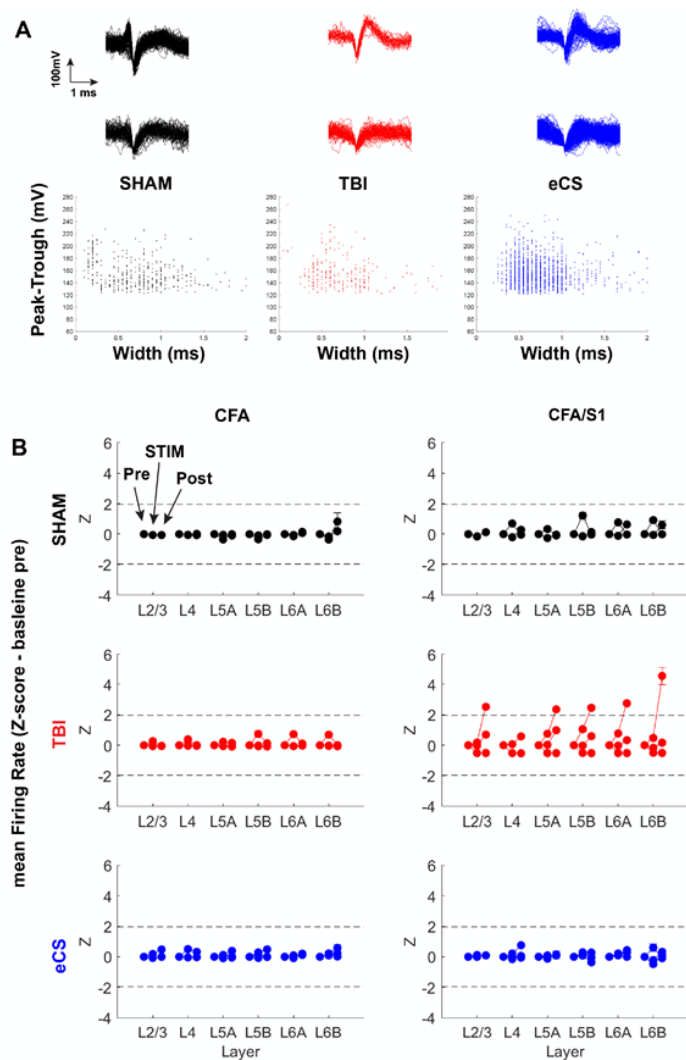


Figure 6. Characterization of multi-unit activity in all treatment groups using linear probe recording under ketamine anesthesia.

A. Extract a multi-unit spike wave form during the resting period for each treatment group and for all recording sites. The top panel shows two representative waveforms for each treatment group, and the bottom panel shows the width vs. peak-trough length scatter plot for all detected multi-units. B. Derive a Z-score from the average population firing frequency normalized to the pre-stimulation period (1 min) for each treatment and the two recording positions CFA and CFA/S1/CFA. Note: the TBI group showed maladaptive sustained firing post stimulation for two rats out of three. Graphs show mean \pm S.E.M.

Notes

Important consideration for reproducibility:

1. Grounding issue: consider the use of battery-based separate recording and stimulation systems to reduce the chance of recording noise, electrical stimulation-induced artifacts, and other electrical interactions that might affect the recording quality.
2. If using multi-shank silicone probes (not described in this protocol): Using probes that can span across the space and would be inserted once for the entire recording could be advantageous for this kind of recording. It

- would help reduce the total recording time, as well as provide simultaneous response for all layers and neighboring cortical regions involved in sensorimotor processing.
3. Positioning of the stimulation probes: As for every silicone probe recording, use a slow speed during the insertion of the electrode to avoid sheering damages.
 4. Anesthetic depth: Perform recordings within the first 40-60 min of the ketamine-induced anesthesia to obtain the most stable data. Following a ketamine boost, the level of anesthesia might get more variable, leading to lower reproducibility. The recordings provided by the electrode are essentially local field potentials (LFP) with single neuron action potentials, which can be filtered out using 0-300Hz and 500-3000Hz bandpass filters. In particular, monitor the level of anesthesia using the LFP response of the cortical region, and include some of the delta-theta waves (0-4Hz brain waves) usually observed during the stable unconscious stage. Regularly monitor the animal response to tail and paw pinching to ensure the animal does not return to consciousness. This procedure should be performed during the recording, using the same setup as multi-unit recording.

Acknowledgments

This work was supported by an NIH (RO1NS099596) award to LK, and partially supported by a Georgia Partners in Regenerative Medicine seed grant from the Regenerative Engineering and Medicine (REM) research center to LK, and an Alliance for Regenerative Rehabilitation Research and Training (AR3T) technology development grant to LK and C-FL. Original work (Latchoumane *et al.*, 2021), DOI: [10.1126/sciadv.abe0207](https://doi.org/10.1126/sciadv.abe0207).

Competing interests

There are no conflicts of interest or competing interests.

Ethics

All procedures on animals were approved by the Institutional Animal Care and Use Committee (IACUC). Protocols were performed in accordance with the Guide for the Care and Use of Laboratory Animals published by the National Institution of Health (NIH), protocol number A2020-06-002 (period 2020-2023).

References

- Dewan, M. C., Rattani, A., Gupta, S., Baticulon, R. E., Hung, Y. C., Punchak, M., Agrawal, A., Adeleye, A. O., Shrime, M. G., Rubiano, A. M., *et al.* (2018). [Estimating the global incidence of traumatic brain injury](#). *J Neurosurg*: 1-18.
- Fernández-García, L., Marí-Buyé, N., Barrios, J. A., Madurga, R., Elices, M., Pérez-Rigueiro, J., Ramos, M., Guinea, G. V. and González-Nieto, D. (2016). [Safety and tolerability of silk fibroin hydrogels implanted into the mouse brain](#). *Acta Biomater* 45: 262-275.
- Hao, P., Duan, H., Hao, F., Chen, L., Sun, M., Fan, K. S., Sun, Y. E., Williams, D., Yang, Z. and Li, X. (2017). [Neural repair by NT3-chitosan via enhancement of endogenous neurogenesis after adult focal aspiration brain injury](#). *Biomaterials* 140: 88-102.
- Latchoumane, C. V., Betancur, M. I., Simchick, G. A., Sun, M. K., Forghani, R., Lenear, C. E., Ahmed, A., Mohankumar, R., Balaji, N., Mason, H. D., *et al.* (2021). [Engineered glycomaterial implants orchestrate large-scale functional repair of brain tissue chronically after severe traumatic brain injury](#). *Sci Adv* 7(10): eabe0207.
- Tan, H. X., Borgo, M. P. D., Aguilar, M. I., Forsythe, J. S., Taylor, J. M. and Crack, P. J. (2020). [The use of bioactive matrices in regenerative therapies for traumatic brain injury](#). *Acta Biomater* 102: 1-12.

Yang, Z., Zhang, A., Duan, H., Zhang, S., Hao, P., Ye, K., Sun, Y. E. and Li, X. (2015). [NT3-chitosan elicits robust endogenous neurogenesis to enable functional recovery after spinal cord injury.](#) *Proc Natl Acad Sci U S A* 112(43): 13354-13359.

Macroscopic Structural and Connectome Mapping of the Mouse Brain Using Diffusion Magnetic Resonance Imaging

Tanzil Mahmud Arefin¹, Choong Heon Lee¹, Jordon D. White², Jiangyang Zhang¹ and Arie Kaffman², *

¹Bernard Irene Schwartz Center for Biomedical Imaging, Department of Radiology, New York University Grossman School of Medicine, New York, USA

²Department of Psychiatry, Yale University School of Medicine, New Haven, Connecticut, USA

*For correspondence: arie.kaffman@yale.edu

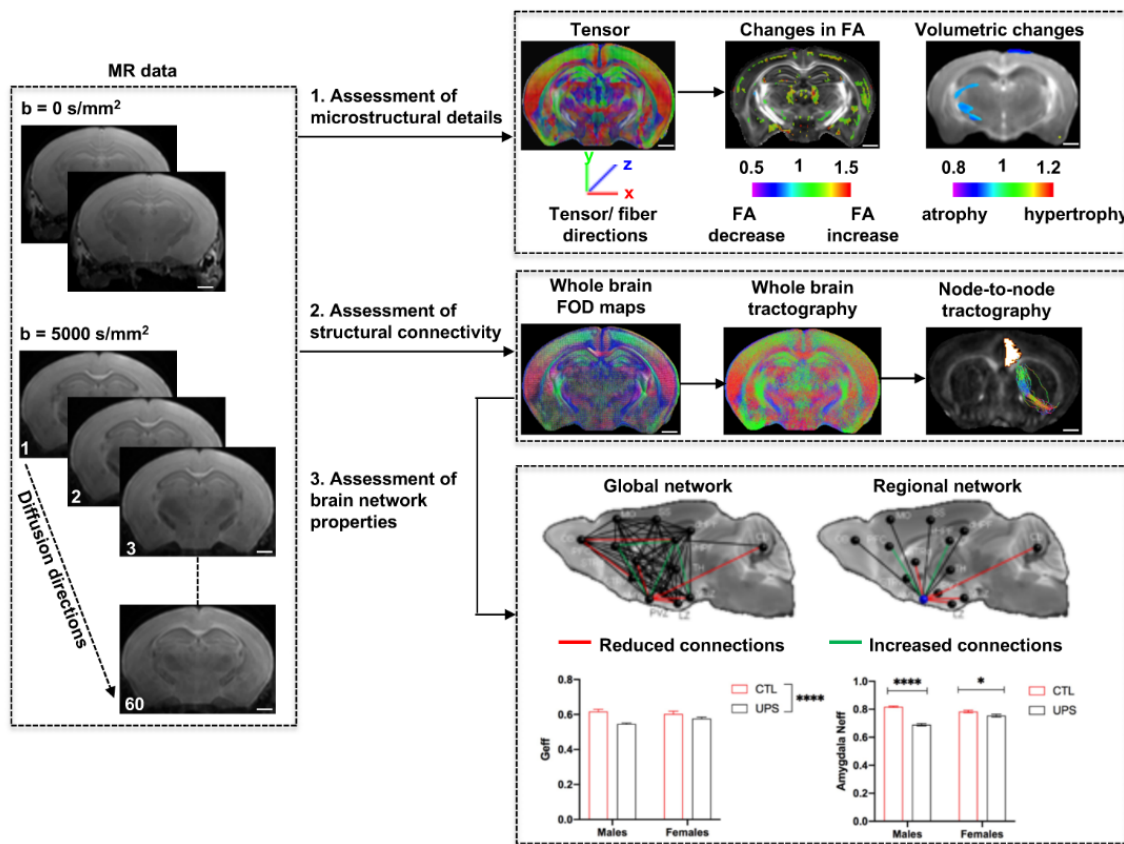
Abstract

Translational work in rodents elucidates basic mechanisms that drive complex behaviors relevant to psychiatric and neurological conditions. Nonetheless, numerous promising studies in rodents later fail in clinical trials, highlighting the need for improving the translational utility of preclinical studies in rodents. Imaging of small rodents provides an important strategy to address this challenge, as it enables a whole-brain unbiased search for structural and dynamic changes that can be directly compared to human imaging. The functional significance of structural changes identified using imaging can then be further investigated using molecular and genetic tools available for the mouse. Here, we describe a pipeline for unbiased search and characterization of structural changes and network properties, based on diffusion MRI data covering the entire mouse brain at an isotropic resolution of 100 µm. We first used unbiased whole-brain voxel-based analyses to identify volumetric and microstructural alterations in the brain of adult mice exposed to unpredictable postnatal stress (UPS), which is a mouse model of complex early life stress (ELS). Brain regions showing structural abnormalities were used as nodes to generate a grid for assessing structural connectivity and network properties based on graph theory. The technique described here can be broadly applied to understand brain connectivity in other mouse models of human disorders, as well as in genetically modified mouse strains.

Keywords: Diffusion MRI, Fiber tractography, Structural connectivity, Brain network properties, Mouse brain.

This protocol was validated in: eLife (2020), DOI: 10.7554/eLife.58301

Graphical Abstract:



Pipeline for characterizing structural connectome in the mouse brain using diffusion magnetic resonance imaging. Scale bar = 1 mm.

Background

Diffusion magnetic resonance imaging (dMRI) is an imaging technique that uses the random diffusion of water molecules to probe tissue microstructure (Le Bihan, 2003; Mori and Zhang, 2006; Novikov, 2021). Recent advances in imaging and computational processing allowed dMRI images with 100 μm resolution or higher to be obtained from rodents (Aggarwal *et al.*, 2010; Calabrese *et al.*, 2015). These can then be used to assess local volumetric changes through microstructural alterations in dMRI parameters, such as fractional anisotropy (FA), and to determine structural connectivity between different brain regions (Wu *et al.*, 2013; Lerch *et al.*, 2017; Feo and Giove, 2019; Badea *et al.*, 2019; White *et al.*, 2020; Pallast *et al.*, 2020).

High resolution dMRI studies in small rodents provide a novel and promising frontier for improving the translational utility of preclinical studies (Kaffman *et al.*, 2019; Muller *et al.*, 2020). This is primarily because of the direct comparison that can be drawn with parallel studies in humans. In addition, unbiased voxel-based screening can identify specific brain regions that show structural changes. In turn, these can be used as nodes to construct a network and to characterize structural connectivity between specific nodes, identify critical hubs, and quantify network properties, such as global efficiency and small-worldness (Feo and Giove, 2019; Pallast *et al.*, 2020; White *et al.*, 2020). This unbiased agnostic approach is conceptually different from the more traditional region of interest (ROI) approach, in which structural changes in specific brain regions or connectomes are examined (Helmstaedter *et al.*, 2013; Takemura *et al.*, 2013; Saleeba *et al.*, 2019). Nonetheless, dMRI studies are highly complementary with traditional neuroscience approaches, as structural changes identified by dMRI can be further examined using

microscopy and genomic/proteomic approaches, and their contribution to complex behavior can be rigorously tested using chemogenetic and optogenetic tools (Kaffman *et al.*, 2019; Muller *et al.*, 2020).

dMRI provides multi-level information about structural changes in the intact tissue, including volumetric changes, dMRI parameters related to microstructure, and structural connectivity. The last fifteen years have witnessed rapid development in dMRI-based tract reconstruction, or tractography (Tuch *et al.*, 2002; Mori and van Zijl, 2002; Tournier *et al.*, 2007; Wedeen *et al.*, 2008), which serves as an important component of the Human Connectome Project (Toga *et al.*, 2012; Van Essen *et al.*, 2013). With the development of high-resolution dMRI acquisition and tractography methods, dMRI tractography can now quickly survey macroscopic structural connectivity in the entire brain without sectioning, which is time consuming and prone to distortions and tissue damage (Moldrich *et al.*, 2010; Wu *et al.*, 2013; Calabrese *et al.*, 2015; Xiong *et al.*, 2018). It also permits simultaneous examination of multiple white matter connections in the same specimen, further reducing the time and cost. With the latest tools for brain connectivity analysis, tractography results can be used to examine changes at both individual pathways and entire connectome levels (Edwards *et al.*, 2020).

dMRI also has several drawbacks, including lower resolution in gray matter regions compared to T1/T2-weighted MRI (Dorr *et al.*, 2008; White *et al.*, 2020) and limited spatial resolution and specificity compared to light microscopy findings with chemical or viral tracers (Wu and Zhang, 2016; Edwards *et al.*, 2020). The need to rigorously correct for multiple comparisons when conducting whole-brain voxel analysis further hinders the detection of subtle changes and is particularly challenging when looking for interaction between two variables, such as early life stress (ELS) and sex (White *et al.*, 2020). High resolution dMRI usually requires perfusing the animal, which prevents longitudinal rescanning of the same animals. Although techniques for *in vivo* high resolution dMRI of rodent brains have emerged (Wu *et al.*, 2013; Wu *et al.*, 2014), the exposure to anesthesia during MRI (2-3 h per session) may introduce additional confounding factors. Therefore, portraying a standardized procedure for reliable and reproducible estimation of microstructural changes in the mouse brain is crucial.

The protocol described here covers image acquisition, whole brain voxel analyses for volumetric and FA changes, tractography, and analysis. Compared to similar methods described before (Calabrese *et al.*, 2015; Edwards *et al.*, 2020), this protocol is based on the structural labels in the Allen Mouse Brain Atlas, which makes it relatively straightforward to compare tractography results with viral tracer results in the Allen Mouse Brain Connectivity Atlas (Oh *et al.*, 2014; White *et al.*, 2020). Unbiased whole-brain voxel analyses were used to identify brain regions that show changes in volume and dMRI parameters (*e.g.*, FA) induced by ELS, and to compare them with those reported in humans exposed to early adversity. Fourteen brain regions that showed structural changes were used as nodes to generate a 14×14 matrix in each hemisphere. The network properties of this grid were then characterized using graph theory and compared with findings in humans exposed to early adversity (White *et al.*, 2020). Our protocol relies on precise image registration to transfer structural labels from the atlas to subject images and will not work when there are large tissue deformations, such as those caused by brain tumors or severe necrosis. The protocol also has a node-to-node analysis step for small connections (*e.g.*, in the amygdala network) that may be obscured in a whole brain analysis. Altogether, the protocol is useful for characterizing whole brain structural connectivity in mouse models of diseases.

Materials and Reagents

1. 5 mL syringe (Sigma-Aldrich, catalog number: Z683582-100EA)
2. Vacutainer safety-lock blood collection set (25 G \times 3/4" \times 12", 0.5 \times 19 \times 305 mm, Becton Dickinson, catalog number: 367283)
3. Nylon Zip ties (4" and 8" in length, LECO plastics, part# L-4-18, L-8-50)
4. 50 mL conical tubes (Corning, catalog number: 352070)
5. BALB/cByJ mice (Jackson Laboratories, catalog number: 001026, 8-10 weeks old, males and females)
6. Chloral hydrate (Sigma, catalog number: 102425)
7. Heparin (Sigma, catalog number: H3393-50KU)
8. PBS (Corning, catalog number: 21-031)
9. Gadodiamide (Omniscan, CAS# 131410-48-5)
10. 10% Formalin solution (PolyScience, catalog number: 08279-20)

11. Perfluoropolyether (Fomblin®, PerkinElmer LLC, CAS# 69991067-9, Sigma-Aldrich, catalog number: 317926)

Equipment

1. Tools for routine transcardiac perfusion in mice (peristaltic pump and tubing, sharp small scissors, blunt tweezers, 21 G infusion butterfly (Becton Dickinson, catalog number: 367281), large container for blood collection, top of an insulated foam box to pin the mouse, and 23 G needles).
2. Horizontal 7 Tesla (T) Magnetic Resonance (MR) system (Bruker Biospin, Billerica, MA, USA) or other high-field (7T or greater) MRI system
3. 4-channel receive only cryogenic probe (Bruker Biospin, Billerica, MA, USA)
4. 72 mm inner diameter volume transmit coil (Bruker Biospin, Billerica, MA, USA)
5. Animal holder for the cryogenic probe (Bruker Biospin, Billerica, MA, USA)
6. Vacuum and vacuum chamber (*e.g.*, 1-gal)

Software

1. Paravision (PV 6.0.1 or later)
2. Matlab R2019b or later (www.mathworks.com)
3. DTIStudio (www.mristudio.org)
4. AMIRA (thermofisher.com, version 5.0 or later)
5. DiffeoMap (www.mristudio.org) or ANTs (<http://stnava.github.io/ANTs/>)
6. Mrtrix (www.mrtrix.org)
7. Graph theoretical network analysis toolbox (GRETNA) (www.nitrc.org/projects/gretna)
8. GraphPad Prism (Version 8.4.3 for Windows, GraphPad Software, La Jolla California USA) (www.graphpad.com)

Procedure

A. *Ex-vivo* brain sample preparation

1. Anesthetize the mouse with chloral hydrate (intraperitoneal injection 100 mg/kg in sterile PBS).
2. Transcardially perfuse the mouse with 35 mL of cold PBS/heparin (50 units/mL) solution followed by 35 mL of 10% formalin. The perfusion rate is approximately 12 mL/min for PBS and formalin, with good perfusion assessed by the liver changing color from dark red to brownish/grey and the animal carcass becoming stiff.
3. Decapitate the mouse at the mid-cervical line (around C3-C4), making sure not to damage the spinal cord, and place the head in 50 mL 10% Formalin solution at 4°C for 24 h in a 50 mL conical tube.
4. After 24 h post-fixation, replace the formalin with PBS. Samples can be stored at 4°C at this point until ready to be scanned.
5. Replace the PBS solution with 50 mL of 2 mM gadodiamide solution in PBS.
6. Store the sample at 4°C for one week for the gadodiamide to diffuse into the tissue.
7. Trim the skin and muscle tissues but keep the skull and eyeballs intact (Figure 1A). Remove the mandible bone and the tongue.
8. Place one brain in the barrel of a 5 mL syringe, with the nose facing the hub of the syringe, then place 2-3 small pieces of bent zip-tie at the bottom and back of the brain to properly fix the specimen within the syringe barrel (Figure 1A).

9. Replacing the cap of the syringe with a loosely tied vacutainer, fill the syringe with perfluoropolyether (Fomblin®), insert the plunger, flip the syringe so that the hub points upward, and remove the cap.
10. Place the syringe with its hub pointing upward in a vacuum chamber for 30 min to remove air bubbles (Figure 1B).
11. Remove the syringe from the vacuum chamber, push out the remaining air and PBS in the barrel, and seal the cap of the syringe by tightening the vacutainer (Figure 1C).

B. MR data acquisition

1. Place the syringe horizontally in the animal holder for the cryogenic probe and adjust the sample position so that the dorsal part of the brain is as close to the cryogenic coil as possible to maximize sensitivity. Use tape to fix the syringe to the animal holder (Figure 1D).
2. Insert the animal holder into the magnet under the cryogenic probe (Figure 1E).
3. Acquire a pilot scan using the Bruker Localizer protocol. For any MRI studies, Localizer is the very first scan that acquires reference images of the subject in three orthogonal planes. The images of the resulting scan appear in the ‘geometry editor,’ where the first three viewports show the reference brain slices in axial, sagittal, and coronal orientations. Therefore, the Localizer provides a quick view of the specimen in the magnet (Figure 1F). Check whether the sample is in the most sensitive region of the cryogenic probe with no apparent tilt toward the left or right sides. Adjust the position of the subject and re-run the Localizer protocol prior to proceeding to the next step.
4. Adjust the tuning and match of the cryogenic probe and acquire a map of the main magnetic field (B0 field) over the entire sample.
5. Use the Bruker MapShim procedure to adjust shimming currents to achieve a relatively homogeneous B0 field. In brief, select the specific scan to calculate the shim. Then choose Map shim from the setup tab and define the target volume of interest in cubic, cylinder, or ellipsoid shapes. Shift, resize or rotate the target volume in the geometry editor such that the volume covers the entire specimen. Run the scan to compute the optimum shim values in the target volume based on the B0 map measured in the previous step.
6. Acquire high angular resolution diffusion weighted imaging (HARDI) of the whole mouse brain using a modified 3D gradient and spin echo (GRASE) sequence (Wu *et al.*, 2013) (an alternative is the 3D multi-shot diffusion weighted echo planar imaging (EPI) sequence provided by Bruker) and with the following imaging parameters:
 - a Echo time (TE)/repetition time (TR): 33/400 min.
 - b Number of non-diffusion weighted images (b_0 s): 2.
 - c Number of diffusion weighted images (DWIs): 60, auto-generated by the sequence.
 - d b-value: 5,000 s/mm².
 - e Resolution: 100 μm isotropic.

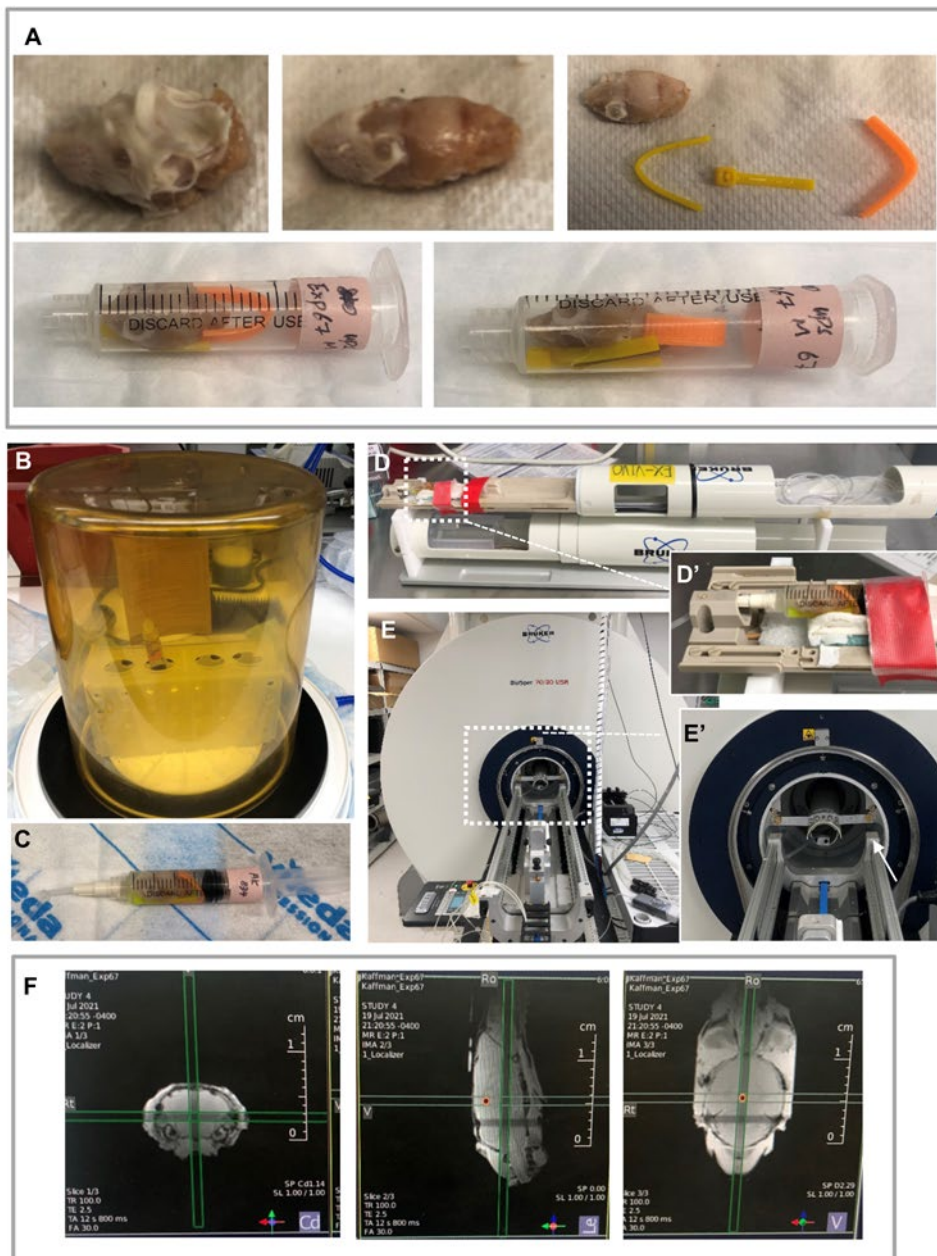


Figure 1. Preparation for MRI.

A. Sample preparation: Remove the tissues outside of the skull carefully without damaging the eyeballs (top panel). Place the brain in a 5 mL syringe with small pieces of zip-ties to fix its position (bottom panel). B-C. Remove air from the syringe: Connect the syringe to a loosely tied vacutainer filled with Fomblin® (shown in C) and place in the vacuum chamber (shown in B). Remove the vacutainer and turn on the vacuum for 30 min to remove air bubbles. Push out the remaining air after vacuum and seal the top by tightening the vacutainer. D. Place the sample in a manufacturer-made sample holder designed for the cryogenic probe. D'. A zoom-in view of the sample. E. Insert the sample holder into the magnet bore of the magnet. E'. A zoom-in view of the holder (indicated by the white arrow). F. Three orthogonal plane images acquired using the Localizer protocol on a 7 Tesla Bruker preclinical MRI system.

Data analysis

A. Data pre-processing:

For each dataset, perform the following steps accordingly:

3. Motion correction: Using DTIStudio (Jiang *et al.*, 2006), align all DWIs to the average of b0s to remove small sample displacements due to vibrations and B0 field drift during the long scan (Figure 2A).
4. Skull-stripping: Use AMIRA segmentation editor to remove non-brain tissues and define the subject specific whole brain mask (Figure 2B).
5. Estimation of diffusion tensor: From the raw data, compute the tensor model (Mori and Zhang, 2006) within the respective brain mask using weighted linear least squares estimations as implemented in MRtrix (command: dwi2tensor) (Figure 2C) (Tournier *et al.*, 2012).
6. Computation of average DWIs and fractional anisotropy (FA): Compute the average DWI (aDWI) from 60 DWIs using Matlab, and calculate the FA map from the tensor using MRtrix (command: tensor2metric) (Basser *et al.*, 1994; Tournier *et al.*, 2012).
7. Image registration and transfer of atlas labels into subject's native space: Using DiffeoMap, normalize the aDWI and FA maps to an MRI-based atlas (Chuang *et al.*, 2011; Arefin *et al.*, 2019) via multi-channel (aDWI + FA) large deformation diffeomorphic metric mapping (LDDMM) (Ceritoglu *et al.*, 2009) (Figure 3A). Next, transfer the structural labels (*i.e.*, brain regions or nodes) to the subject's-native space using the inverse mapping from LDDMM (Figure 3B, also see Note 1). If DiffeoMap is not available, ANTs (<http://stnava.github.io/ANTs/>) can be used instead (Figure 2D).

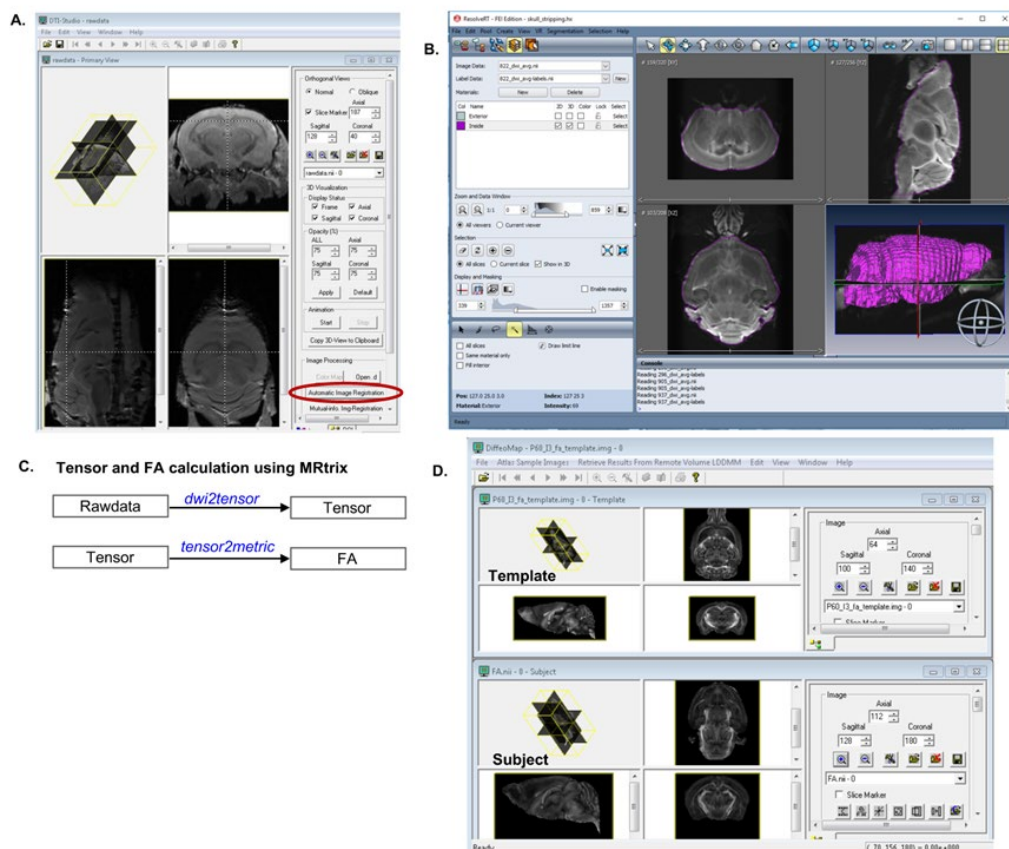


Figure 2. Illustration of the data pre-processing steps.

A. Motion correction using DTIStudio. Run Automatic Image Registration (circled) to align all diffusion weighted images (DWIs) to the non-diffusion-weighted image (b0). B. Use the AMIRA segmentation editor to generate a binary mask (purple) for the brain. C. Schematic diagram of the steps to compute the tensor and FA from the rawdata using Mrtrix. D. Use DiffeoMap for image registration and transformation of atlas labels into subject's native image space.

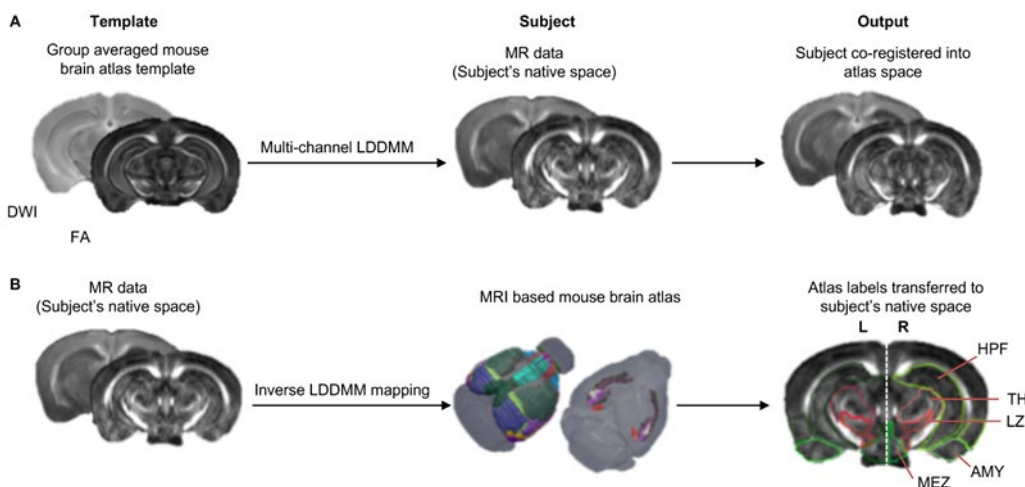


Figure 3. Image registration pipeline.

A. Co-registration of the MR data (subject) into group averaged mouse brain atlas template using multi-channel LDDMM. B. Transformation of structural labels from MRI-based atlas to subject's native space.

B. Data post-processing

Assessment of brain microstructural changes

At first, compute the Jacobian determinant value for each voxel from the mapping between atlas and subject images generated by LDDMM, and conduct whole-brain voxel-based morphometric analysis in Matlab to identify local volumetric changes affected by rearing, sex, and their interaction (2×2 ANOVA, FDR corrected, $\alpha = 0.1$, $P < 0.0105$, cluster size > 25 voxels). See the Matlab codes (source data 1) used to conduct 2×2 ANOVA (White *et al.*, 2020). Then, similarly perform 2×2 ANOVA (FDR corrected, $\alpha = 0.1$, $P < 0.007$, cluster size > 25 voxels) to examine the voxel-wise changes in FA (White *et al.*, 2020). These analyses will provide unbiased overviews of morphometric changes due to rearing, sex, and rearing by sex interaction.

Selection of brain regions (nodes) for structural connectivity assessment

Identify nodes that show rearing-mediated volumetric and FA changes to investigate structural connectivity alterations between nodes, as well as modifications in the brain global and regional network properties (also see Note 2). These nodes will be identical for both left and right hemispheres.

Assessment of brain structural connectivity using fiber tractography

Upon pre-processing the data and selection of potential brain nodes, execute the following steps accordingly for each individual subject to map axonal projections between nodes using probabilistic fiber tractography in Mrtrix:

Step 1: From the pre-processed raw data, estimate the response function for spherical deconvolution (command: dwi2response) (Tournier *et al.*, 2012, Tournier *et al.*, 2013). Specify the algorithm name ‘tournier’ (other options: dhollander, manual, fa, msmt_5tt, tax), gradient table, brain mask, and the maximum harmonic degree ($l_{max} = 6$).

Step 2: Estimate the whole brain fiber orientation distribution (FOD) map from the pre-processed raw data and respective response function (command: dwi2fod) (Tournier *et al.*, 2007). Define the algorithm name ‘CSD,’ gradient table, and brain mask.

Step 3. Generate the whole brain fiber tractogram from the FOD map (command: tckgen) (Tournier *et al.*, 2009). Use the whole brain mask as the ‘seed region’ to enable tracking fibers throughout the brain for whole brain tractography (whole brain tractogram) (Figure 4A). Set the tractography method to probabilistic, the FOD amplitude cut-off to 0.05, the minimum length of the fiber to 3 mm, and the target number of the streamLines to be counted to 5 million.

Step 4: For node-to-node tractography, the whole brain tractography in step 3 may not generate enough streamLines for small nodes (*e.g.*, amygdala). Further increasing the total number of streamLines (> 5 million) may not resolve this issue but requires significant computational resources. In this case, extract the regions of interest (ROIs) from the atlas co-registered into the subject’s native space using Matlab. Next, define a specific node as ‘seed region’ to initiate the fiber tracking from and another node as ‘target’ to define the fiber termination point. Then use these two nodes to extract the streamLines connecting two nodes (seed and target) using the tckedit command (Figure 4B). Consider two nodes as ‘connected’ if there is at least one streamLine terminating at the target node; otherwise, they are ‘not connected.’

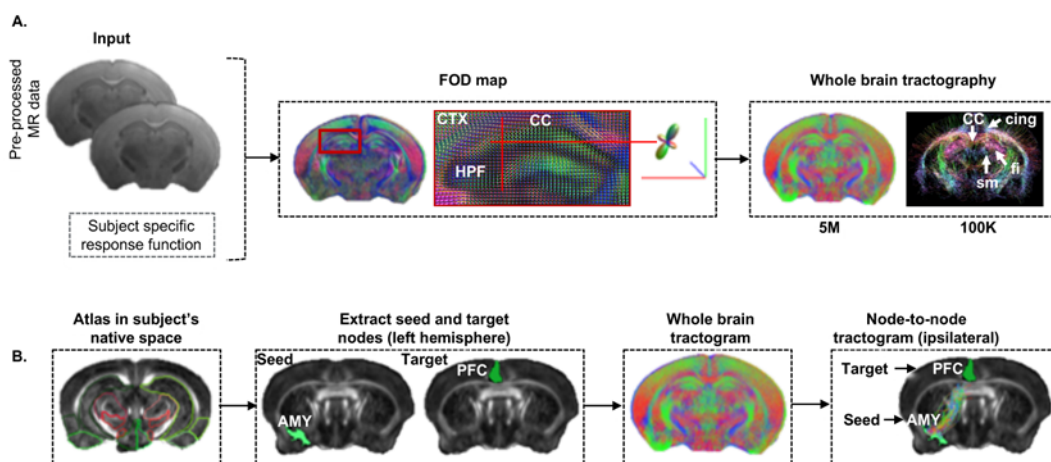


Figure 4. Fiber tractography pipeline.

A. Estimation of mouse whole brain fiber tractogram from the fiber orientation distribution (FOD) map. Red, green, and blue colors represent the fiber projections in x, y, and z-axis, respectively. Five million fibers were generated from each subject; 100 K streamLines were extracted for better visualization of the brain structures. B. Extraction of fibers connecting two specific nodes (seed = amygdala and target = PFC).

Generating brain structural connectome matrix

Repeat step 4 to estimate the structural connections between all possible pairs of nodes (ignore intra-regional connectivity) for both hemispheres (Figure 5A). For example, for 14 nodes in one hemisphere, the total number of tractograms would be the number of nodes $N = 14$ multiplied by $N-1$, or $14 \times 13 = 182$. Finally, for M number of seed regions and N number of target regions, generate an $M \times N$ matrix individually for the left and the right hemispheres. Assign the seed and target regions in horizontal and vertical axis, respectively, so that each cell represents the number of streamLines connecting the corresponding seed and target nodes (Figure 5B). Consider the number of streamLines between nodes as a measure of the connection strength. Generate the connectome matrix for all subjects and name them according to the subject IDs.

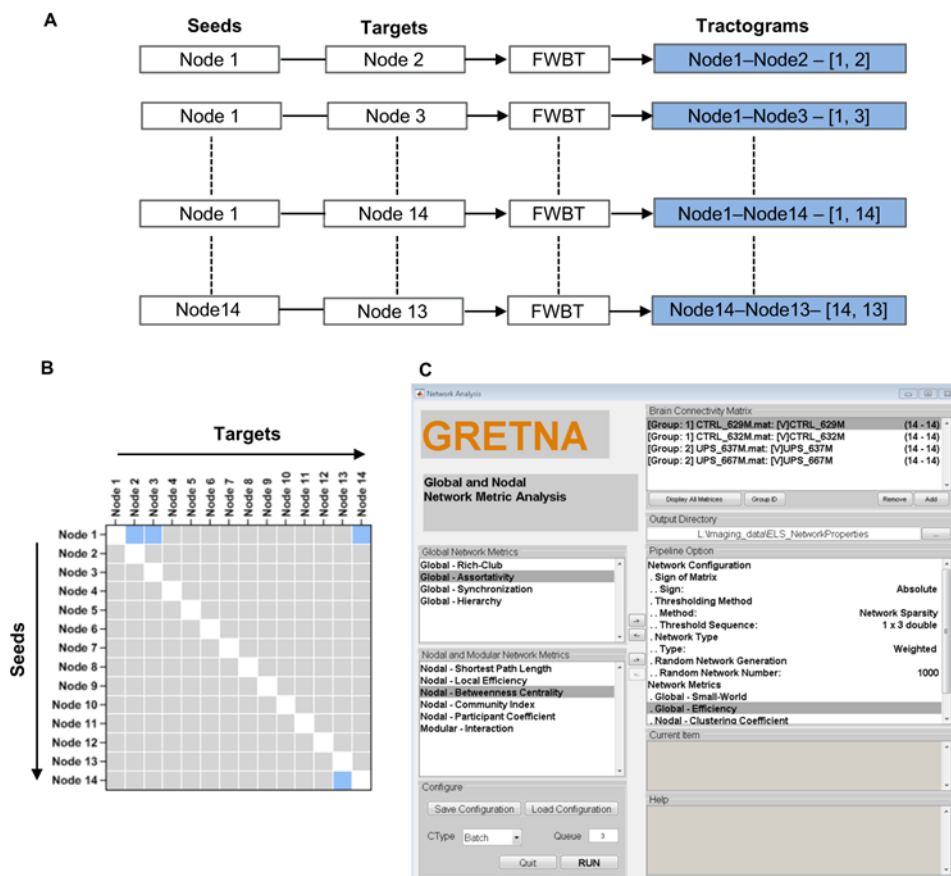


Figure 5. Generation of the mouse brain structural connectome.

A. Extraction of fibers connecting seed and target nodes. B. Generation of structural connectome from the tractograms estimated from selected seed and target nodes. Blue cells correspond to the tractograms shown in A, and white cells indicate intra-regional connectivity (not counted). C. Use the GRETNA software to compute global and regional brain network properties. Panels on the left list all possible properties available for computation. Select the properties based on the study design and transfer them to the pipeline option on the right panel using the respective arrows. Load the connectome matrix for all subjects belonging to one group with specific group ID and then load for the next group with different ID. Specify the output folder to store the results and define the network configuration. Finally, hit the ‘Run’ button to start computation.

Brain network properties analysis

Use the Matlab based Graph theoretical network analysis toolbox (GRETNA) to compute the brain global and regional network properties (Wang *et al.*, 2015). Perform the following steps accordingly for brain network-based analysis (Figure 5C):

1. Create an individual data folder containing two sub-folders for left and right hemispheres for each group.
2. Save the connectome matrices as ‘.mat’ files in the respective folders.
3. Open GRETNA in Matlab and select ‘Network Analysis’ (GRETNA >> Network Analysis).
4. In the ‘Brain Connectivity Matrix’ tab, load all connectivity matrices of one hemisphere from one group and assign the group ID. Do the same for the other group.
5. Locate a directory for saving the results in the ‘output directory’ tab.
6. Next, select network properties to be computed from the Global Network Metrics and Nodal and Modular Network Metrics tabs.
7. For global brain network analysis, select ‘Global – Small-World (SW)’ and ‘Global – Efficiency (Geff).’ For regional network properties, select ‘Nodal – Clustering Coefficient (NCp),’ ‘Nodal – Efficiency (Neff),’

and ‘*Nodal – Degree Centrality (Dcent)*.’ Other properties can be selected as per the study design or requirements.

8. Configure the brain network in the ‘Network Analysis’ tab as follows:

Parameters	Value
Sign of matrix	Absolute
Thresholding method	Network sparsity
Threshold sequence	0.05, 0.1, 0.15 (or as per the study design)
Network type	Weighted
Random network number	1,000

9. Recheck the loaded data and the network configuration. Hit the ‘Run’ button if everything looks alright. Computation time depends on the number of subjects, size of the connectome matrices, random network number, and the threshold sequence.
10. Once the computation is done, results can be retrieved from the output directory. For further assistance, please refer to the following manual from Neuroimaging Tools and Resources Collaboratory (NITRC): https://www.nitrc.org/docman/view.php/668/2262/manual_v2.0.0.pdf.

Statistical analysis of the estimated structural connectivity and brain network properties

To investigate the effect of rearing and sex on brain structural connectivity and brain network properties, perform a two-way ANOVA with rearing condition (CTL or UPS) and sex as fixed factors, followed by post-hoc comparisons using Tukey’s HSD or Sidak’s test using GraphPad Prism.

Notes

1. It is very important to check whether structural labels were correctly transferred and show good agreement with the corresponding structures. We recommend refining the segmentation manually, slice by slice, along the axial orientation, forfeiting attention to the other two orientations as well as to the slices preceding and following if necessary.
2. Selection of nodes for brain network analysis is crucial. Using unbiased voxel-based analyses, identify only those nodes which show UPS-mediated volumetric and FA alterations and are highly connected based on the Allen Mouse Brain Connectivity Atlas (Oh *et al.*, 2014). Furthermore, selected nodes should be non-overlapping, having a unique set of connections to other nodes, and well delineated using a standard parcellation scheme that is comparable across species (Kaiser, 2011).

Acknowledgments

This work was supported by NIMH R01MH119164 (AK and JZ), NIMH R01MH118332 (AK and JZ), and R01NS102904 (JZ). For the original research paper where this protocol has been used, see White *et al.* (2020)

Competing interests

The authors declare no conflict of interest.

Ethics

Animal experimentation: All studies were approved by the Institutional Animal Care and Use Committee (IACUC) at Yale University, protocol #2020-10981, and were conducted in accordance with the recommendations of the NIH Guide for the Care and the Use of Laboratory Animals.

References

- Aggarwal, M., Mori, S., Shimogori, T., Blackshaw, S. and Zhang, J. (2010). [Three-dimensional diffusion tensor microimaging for anatomical characterization of the mouse brain](#). *Magn Reson Med* 64(1): 249-261.
- Dorr, A. E., Lerch, J. P., Spring, S., Kabani, N. and Henkelman, R. M. (2008). [High resolution three-dimensional brain atlas using an average magnetic resonance image of 40 adult C57Bl/6J mice](#). *Neuroimage* 42(1):60-9.
- Badea, A., Ng, K. L., Anderson, R. J., Zhang, J., Miller, M. I. and O'Brien, R. J. (2019). [Magnetic resonance imaging of mouse brain networks plasticity following motor learning](#). *PLoS One* 14(5): e0216596.
- Basser, P. J., Mattiello, J. and LeBihan, D. (1994). [MR diffusion tensor spectroscopy and imaging](#). *Biophys J* 66(1): 259-267.
- Calabrese, E., Badea, A., Cofer, G., Qi, Y. and Johnson, G. A. (2015). [A Diffusion MRI Tractography Connectome of the Mouse Brain and Comparison with Neuronal Tracer Data](#). *Cereb Cortex* 25(11): 4628-4637.
- Ceritoglu, C., Oishi, K., Li, X., Chou, M. C., Younes, L., Albert, M., Lyketsos, C., van Zijl, P. C., Miller, M. I. and Mori, S. (2009). [Multi-contrast large deformation diffeomorphic metric mapping for diffusion tensor imaging](#). *Neuroimage* 47(2): 618-627.
- Chuang, N., Mori, S., Yamamoto, A., Jiang, H., Ye, X., Xu, X., Richards, L. J., Nathans, J., Miller, M. I., Toga, A. W., Sidman, R. L. and Zhang, J. (2011). [An MRI-based atlas and database of the developing mouse brain](#). *Neuroimage* 54(1): 80-89.
- Edwards, T. J., Fenlon, L. R., Dean, R. J., Bunt, J., Consortium, I. R. C., Sherr, E. H. and Richards, L. J. (2020). [Altered structural connectivity networks in a mouse model of complete and partial dysgenesis of the corpus callosum](#). *Neuroimage* 217: 116868.
- Feo, R. and Giove, F. (2019). [Towards an efficient segmentation of small rodents brain: A short critical review](#). *J Neurosci Methods* 323: 82-89.
- Helmstaedter, M., Briggman, K. L., Turaga, S. C., Jain, V., Seung, H. S. and Denk, W. (2013). [Connectomic reconstruction of the inner plexiform layer in the mouse retina](#). *Nature* 500(7461): 168-174.
- Jiang, H., van Zijl, P. C., Kim, J., Pearlson, G. D. and Mori, S. (2006). [DtiStudio: resource program for diffusion tensor computation and fiber bundle tracking](#). *Comput Methods Programs Biomed* 81(2): 106-116.
- Kaffman, A., White, J. D., Wei, L., Johnson, F. K. and Krystal, J. H. (2019). [Enhancing the Utility of Preclinical Research in Neuropsychiatry Drug Development](#). *Methods Mol Biol* 2011: 3-22.
- Kaiser, M. (2011). [A tutorial in connectome analysis: topological and spatial features of brain networks](#). *Neuroimage* 57(3): 892-907.
- Le Bihan, D. (2003). [Looking into the functional architecture of the brain with diffusion MRI](#). *Nat Rev Neurosci* 4(6): 469-80.
- Lerch, J. P., van der Kouwe, A. J., Raznahan, A., Paus, T., Johansen-Berg, H., Miller, K. L., Smith, S. M., Fischl, B. and Sotiroopoulos, S. N. (2017). [Studying neuroanatomy using MRI](#). *Nat Neurosci*. 20(3): 314-326.
- Moldrich, R. X., Pannek, K., Hoch, R., Rubenstein, J. L., Kurniawan, N. D. and Richards, L. J. (2010). [Comparative mouse brain tractography of diffusion magnetic resonance imaging](#). *Neuroimage* 51(3): 1027-1036.
- Mori, S. and van Zijl, P. C. (2002). [Fiber tracking: principles and strategies - a technical review](#). *NMR Biomed* 15(7-8): 468-480.
- Mori, S. and Zhang, J. (2006). [Principles of diffusion tensor imaging and its applications to basic neuroscience research](#). *Neuron* 51(5): 527-539.
- Muller, H. P., Roselli, F., Rasche, V. and Kassubek, J. (2020). [Diffusion Tensor Imaging-Based Studies at the Group-Level Applied to Animal Models of Neurodegenerative Diseases](#). *Front Neurosci* 14: 734.

- Novikov, D. S. (2021). [The present and the future of microstructure MRI: From a paradigm shift to normal science](#). *J Neurosci Methods* 351: 108947.
- Oh, S. W., Harris, J. A., Ng, L., Winslow, B., Cain, N., Mihalas, S., Wang, Q., Lau, C., Kuan, L., Henry, A. M., et al. (2014). [A mesoscale connectome of the mouse brain](#). *Nature* 508(7495): 207-214.
- Pallast, N., Wieters, F., Nill, M., Fink, G. R. and Aswendt, M. (2020). [Graph theoretical quantification of white matter reorganization after cortical stroke in mice](#). *Neuroimage* 217: 116873.
- Saleeba, C., Dempsey, B., Le, S., Goodchild, A. and McMullan, S. (2019). [A Student's Guide to Neural Circuit Tracing](#). *Front Neurosci* 13: 897.
- Takemura, S. Y., Bharioke, A., Lu, Z., Nern, A., Vitaladevuni, S., Rivlin, P. K., Katz, W. T., Olbris, D. J., Plaza, S. M., Winston, P., et al. (2013). [A visual motion detection circuit suggested by Drosophila connectomics](#). *Nature* 500(7461): 175-181.
- Toga, A. W., Clark, K. A., Thompson, P. M., Shattuck, D. W. and Van Horn, J. D. (2012). [Mapping the human connectome](#). *Neurosurgery* 71(1): 1-5.
- Tournier, J. D., Calamante, F. and Connelly, A. (2009). [Improved probabilistic streamLines tractography by 2nd order integration over fibre orientation distributions](#). *Proc Intl Soc Mag Reson Med* 18: 1670.
- Tournier, J. D., Calamante, F. and Connelly, A. (2012). [MRtrix: Diffusion tractography in crossing fiber regions](#). *Int J Imaging Syst Technol* 22(1): 53-66.
- Tournier, J. D., Calamante, F. and Connelly, A. (2007a). [Robust determination of the fibre orientation distribution in diffusion MRI: non-negativity constrained super-resolved spherical deconvolution](#). *Neuroimage* 35(4): 1459-1472.
- Tournier, J. D., Calamante, F. and Connelly, A. (2007b). [Robust determination of the fibre orientation distribution in diffusion MRI: non-negativity constrained super-resolved spherical deconvolution](#). *Neuroimage* 35(4): 1459-1472.
- Tournier, J. D., Calamante, F. and Connelly, A. (2013). [Determination of the appropriate b value and number of gradient directions for high-angular-resolution diffusion-weighted imaging](#). *NMR Biomed* 26(12): 1775-1786.
- Tuch, D. S., Reese, T. G., Wiegell, M. R., Makris, N., Belliveau, J. W. and Wedeen, V. J. (2002). [High angular resolution diffusion imaging reveals intravoxel white matter fiber heterogeneity](#). *Magn Reson Med* 48(4): 577-582.
- Van Essen, D. C., Smith, S. M., Barch, D. M., Behrens, T. E., Yacoub, E., Ugurbil, K. and Consortium, W. U.-M. H. (2013). [The WU-Minn Human Connectome Project: an overview](#). *Neuroimage* 80: 62-79.
- Wang, J., Wang, X., Xia, M., Liao, X., Evans, A. and He, Y. (2015). [GRETNA: a graph theoretical network analysis toolbox for imaging connectomics](#). *Front Hum Neurosci* 9: 386.
- Wedeen, V. J., Wang, R. P., Schmahmann, J. D., Benner, T., Tseng, W. Y., Dai, G., Pandya, D. N., Hagmann, P., D'Arceuil, H. and de Crespigny, A. J. (2008). [Diffusion spectrum magnetic resonance imaging \(DSI\) tractography of crossing fibers](#). *Neuroimage* 41(4): 1267-1277.
- White, J. D., Arefin, T. M., Pugliese, A., Lee, C. H., Gassen, J., Zhang, J. and Kaffman, A. (2020). [Early life stress causes sex-specific changes in adult fronto-limbic connectivity that differentially drive learning](#). *Elife* 9: e58301.
- Wu, D., Reisinger, D., Xu, J., Fatemi, S. A., van Zijl, P. C., Mori, S. and Zhang, J. (2014). [Localized diffusion magnetic resonance micro-imaging of the live mouse brain](#). *Neuroimage* 91: 12-20.
- Wu, D., Xu, J., McMahon, M. T., van Zijl, P. C., Mori, S., Northington, F. J. and Zhang, J. (2013). [In vivo high-resolution diffusion tensor imaging of the mouse brain](#). *Neuroimage* 83: 18-26.
- Wu, D. and Zhang, J. (2016). [In vivo mapping of macroscopic neuronal projections in the mouse hippocampus using high-resolution diffusion MRI](#). *Neuroimage* 125: 84-93.
- Xiong, J., Ren, J., Luo, L. and Horowitz, M. (2018). [Mapping Histological Slice Sequences to the Allen Mouse Brain Atlas Without 3D Reconstruction](#). *Front Neuroinform* 12: 93.

Pericyte Mapping in Cerebral Slices with the Far-red Fluorophore TO-PRO-3

Sandra P. Mai-Morente¹, Juan P. Irigoyen¹, Victoria M. Carriquiry¹, Virginia M. Marset¹, Mariana Di Doménico², Eugenia Isasi³ and Verónica Abudara^{1,*}

¹Departamento de Fisiología, Facultad de Medicina, Universidad de la República, General Flores 2125, Montevideo, CP 11 800, Uruguay

²Departamento de Biofísica, Facultad de Medicina, Universidad de la República, General Flores 2125, Montevideo, CP 11 800, Uruguay

³Departamento de Histología y Embriología, Facultad de Medicina, Universidad de la República, General Flores 2125, Montevideo, CP 11 800, Uruguay

*For correspondence: abudara@fmed.edu.uy

Abstract

This protocol describes a method for high-resolution confocal imaging of pericytes with the far-red fluorophore TO-PRO™-3 Iodide 642/661 in cerebral slices of murine. Identification of pericytes with TO-PRO-3 is a short time-consuming, high cost-effective and robust technique to label pericytes with no need for immunostaining or generation of reporter mice. Since the TO-PRO-3 stain resists immunofluorescence, and lacks spectral overlap, the probe is well suited for multiple labelling. Our procedures also combine TO-PRO-3-staining of pericytes with fluorescent markers for astrocytes and vessels in brain slices. These approaches should enable the assessment of pericyte biology in gliovascular unit.

Keywords: Pericyte imaging, TO-PRO-3, Fluorescence confocal microscopy, Brain slices, Astrocytes, vessels

This protocol was validated in: J Neurochem (2021), DOI: 10.1111/jnc.15193

Background

Fluorescence imaging at the cellular level offers an exceptional tool to track pericytes under confocal or bi-photonic microscopy. Tagging specific pericyte surface antigens, such as chondroitin sulphate proteoglycan neuron-glial 2 (NG2) and platelet-derived growth factor receptor beta (PDGFR β), proved to be an excellent approach to identify pericytes in the cerebral microvasculature. Antigen labelling is achieved via immunofluorescence with specific antibodies or through fluorescent protein expression under the control of specific promoters for NG2 and PDGFR β (Ozerdem *et al.*, 2001; Mishra *et al.*, 2014; Hartmann *et al.*, 2015a and 2015b; Jung *et al.*, 2018; Smyth *et al.*, 2018). Notwithstanding, immune techniques involve several steps that take place over hours or days, whereas generation of reporter mice is costly and laborious, mainly in studies employing transgenic mouse models. Herein, we describe a simple, robust and rapid (*e.g.*, min) fluorescent labelling assay to image pericytes in murine brain slices with the far-red fluorophore TO-PRO™-3 Iodide 642/661. This carbocyanine monomer probe has recently been recognized as a pericyte biomarker in both *ex vivo* (Mai-Morente *et al.*, 2021) and *in vivo* (Tong *et al.*, 2021) conditions. TO-PRO-3 stains nucleus in fixed tissue (Van Hooijdonk *et al.*, 1994; de Mazière *et al.*, 1996; Suzuki *et al.*, 1997), but is selectively incorporated by living pericytes *ex vivo* when applied into the physiological saline or *in vivo* after topical administration (Lacar *et al.*, 2012; Mai-Morente *et al.*, 2021; Tong *et al.*, 2021). Identification of murine brain pericytes by TO-PRO-3 is unambiguous in the tested age range (P06-P90) and, as reported (Mai-Morente *et al.*, 2021), TO-PRO-3-stained pericytes express the classical pericyte immunomarkers NG2 and PDGFR β and incorporate the pericyte dye NeuroTrace 500/525 (Damisah *et al.*, 2017). Only a subset of TO-PRO-3 pericytes expresses the contractile protein alpha-smooth muscle actin (α -SMA) (Mai-Morente *et al.*, 2021). The far-red emitting TO-PRO-3 dye exhibits negligible autofluorescence and phototoxicity (Suseela *et al.*, 2018), which favours its use in live imaging; additionally, TO-PRO-3-loaded slices can be fixed and processed for immunolabelling (Lacar *et al.*, 2012; Mai-Morente *et al.*, 2021). Since TO-PRO-3 resists immunostaining and fluoresces far from the green and red fluorophores in the light spectrum, it is appropriate for multiple labelling with fluorescent-conjugated probes and antibodies or green fluorescent protein (GFP) reporters. The protocols described here include procedures to identify vessels and astroglia intimately associated with TO-PRO-3-labelled pericytes. Given the ease and reliability of the technique, mapping pericytes with TO-PRO-3 should facilitate future research on pericyte structure and function in cerebral slices.

Materials and Reagents

Biological Materials

1. 96-well plate
2. 6-well plate
3. 12/24-well plate
4. Ice plastic tray with silicone bottom for domestic use
5. Nylon mesh of a tea plastic strainer
6. Plastic transfer pipettes (Biologix, catalog number: 30-0138)
7. Sartorius mLINE® mechanical Biohit pipettors 2, 20, 200 and 1,000 μ L
8. Six-well, twenty-four-well and ninety-six-well multidishes (DeltaLab, catalog numbers: 657160, 662160 and 655180, respectively)
9. Custom-made strainer
10. Perfusion chamber
11. Transparent (glass or polypropylene) cylindrical test tubes with rounded bottom
12. Conventional 21 gauge (21 G) syringe needles
13. BD Intramedic™ Polyethylene Tubing, 100 ft \times 0.034" \times 0.050" (Becton Dickinson, catalog number: 427421)
14. Microscope glass slides (Deltalab, catalog number: D 100001)

15. Microscope glass coverslips (Deltalab, catalog number: D 102440) and N1.5 (Knittel Glass, catalog number: VM52440Y1A0.1)
16. Aluminium foil
17. Absorbent tissue
18. Adhesive tape
19. Permanent marker pen
20. Fine-tipped paintbrushes
21. Nail varnish
22. Hippocampal and cortical slices (300-400 μm thick) from P06-P90 male and female mice [*Mus musculus* on a C57BL/6 background (Jackson Laboratory, RRID: IMSR_JAX: 000664)] and *Rattus norvegicus* [Sprague-Dawley (Charles River Laboratories, Strain code 400)]
23. MilliQ-water or double-distilled water (ddH₂O)
24. Quinolinium, 4-[3-(3-methyl-2(3H)-benzothiazolylidene)-1-propenyl]-1-[3-(trimethylammonio) propyl]-, diiodide/157199-63-8 or TO-PROTM-3 Iodide 642/661 (Life Thermo Fisher Scientific, catalog number: T3605)
25. Neurotrace™ 500/525 Green Fluorescent Nissl (Life Thermo Fisher Scientific, catalog number: N21480)
26. Poly-L-Lysine (Sigma-Aldrich, catalog number: P4832)
27. Lycopersicon Esculentum (Tomato) Lectin DyLight 488 (LEL-DyLight 488) (Life Thermo Fisher Scientific, catalog number: L32470)
28. Isolectin B4 conjugated to fluorescein isothiocyanate (FITC-ISOB4) (Sigma-Aldrich, catalog number: L2895)
29. Rabbit anti-GFAP-Cy3™ (Sigma-Aldrich, catalog number: C9205)
30. 2-[4-(Aminooiminomethyl) phenyl]-1H-Indole-6-carboximidamide hydrochloride (DAPI) (Sigma-Aldrich, catalog number: D09542)
31. Hoechst 33342 (Sigma Aldrich, catalog number: 23491-45-4)
32. Bovine serum albumin (BSA) (Sigma-Aldrich, catalog number: 048-46-8)
33. Glycine (Sigma-Aldrich, catalog number: 56-40-6)
34. Glycerol or Fluoromont-G™ Mounting Medium (Life Thermo Fisher Scientific, catalog number: 00-4958-02)
35. NaCl (Sigma-Aldrich, catalog number: 7647-14-5)
36. KCl (Sigma-Aldrich, catalog number: 7447-40-7)
37. NaHCO₃ (Sigma-Aldrich, catalog number: S5761)
38. NaH₂PO₄·H₂O (Sigma-Aldrich, catalog number: 10049-21-5)
39. Na₂HPO₄·H₂O (Sigma-Aldrich, catalog number: S9763)
40. KH₂PO₄ (Sigma-Aldrich, catalog number: P0662)
41. Glucose (Sigma-Aldrich, catalog number: G5767)
42. MgSO₄ (Sigma-Aldrich, catalog number: M7506)
43. CaCl₂·2H₂O (Sigma-Aldrich, catalog number: C3881)
44. Paraformaldehyde powder (PFA) (Sigma-Aldrich, catalog number: 158127)
45. NaOH and HCl
46. Artificial cerebrospinal fluid solution (ACSF) (see Recipes)
47. Blocking/permeabilizing solution (see Recipes)
48. Diluting solution for antibodies (see Recipes)
49. Fixing solution (see Recipes)
50. Phosphate buffered saline (PBS) (see Recipes)
51. PBST (see Recipes)

Equipment

1. Gas tank 5% CO₂, 95% O₂
2. Digital pHmeter (ORION, model: 410A)
3. Digital Analytical Balance (RadWag, AS82/220.R2)
4. Thermolyne Type 16700 Mixer Maxi-Mix1 vortex mixer
5. TS-2000A VDRL Shaker

6. Fume hood 1300 Series A2 Class II, Type A2 Bio Safety Cabinets
7. Thermo Scientific™ Cimarec™ Basic Stirring Hotplates SP13132033 (ThermoFisher Scientific)
8. Confocal Laser Scanning Microscope (Leica TCS SP5 TANDEM SCANNER) equipped with:
 - a. A 40× oil immersion objective Leica N.A 1,3 with UV correction.
 - b. 405 nm diode laser, argon gas laser emission at 488 nm and HeNe lasers for 543 nm and 633 nm emission.
9. Coverslip Clamp Chamber (ALA Scientific Instruments Inc.)
10. HCT-10 Temperature Controller (ALA Scientific Instruments Inc.)
11. Peristaltic Pump (Scientific Industries Inc., Model 203)
12. Refrigerator and freezer
13. Thermostatic water bath

Software

1. Image acquisition and storage system (LAS AF Lite Software)
2. Image analysis software (Fiji, ImageJ version 1.53c)
3. Photo editing software (Adobe Photoshop CS6 13.0 × 64 and Adobe Illustrator CS6 16.0.0)

Procedure

Before getting started, obtain acute cortical and hippocampal slices (300 µm thick) from mice and allow them to stabilize for 45 min in a storage chamber resting on a nylon mesh submerged in ACSF equilibrated with 95% O₂ and 5% CO₂, at room temperature (RT: 22°C-25°C). Detailed protocols for preparing acute cerebral and hippocampal slices from rodents can be found elsewhere (Lein *et al.*, 2011; Pannasch *et al.*, 2012; Mishra *et al.*, 2014; Papouin and Haydon, 2018).

Note: To obtain good quality slices, heed the following recommendations: (1) rapidly remove the brain after confirming the animal's death, (2) use chilled materials (chambers, dishes, instruments) and keep the tissue immersed in ice-cold ACSF carbogenated with 95% O₂ and 5% CO₂ throughout dissection and slicing procedures, and (3) employ one fresh razor blade per brain to prevent tissue deformation.

A. Vessel and pericyte labelling with lectins in brain slices

For simultaneous identification of lectin-labelled vessels and TO-PRO-3-marked pericytes, follow Procedures A and B. If not interested in visualizing vessels, proceed to Procedure B.

1. In our experiments, we succeeded in visualizing vessel walls and pericyte contours using any of these two probes, (a) Lycopersicon Esculentum (Tomato) Lectin conjugated to DyLight 488 (LEL-DyLight 488) or (b) IsolectinB4 conjugated to FITC (FITC-ISOB₄). Prepare the dye solution by dissolving (a) LEL-DyLight 488 in carbogenated ACSF to yield a 10 µg/ml final concentration or (b) FITC-ISOB₄ in carbogenated ACSF to yield a 5-10 µg/ml final concentration. Pre-warm (35°C-37°C) the dye solution in a thermostatic water bath protected from light.

Notes:

- a. Lectins bind to glycoconjugate residues in basement membranes of endothelium and pericytes (Peters and Goldstein, 1979; Laitinen, 1987; Mishra *et al.*, 2014).
- b. Vortex stock solutions prior to use.
- c. Use freshly prepared dye solutions.

2. Transfer acute slices with a plastic pipette (Figure 1A) from the storage chamber to an empty cylindrical transparent tube provided with fine-tipped tubing for gas delivery (95% O₂ and 5% CO₂) (Figure 1B).

With a 1,000 μ L pipettor, pull the ACSF out of the tube. Keep slices on the bottom and immediately add 1 mL minimum of the pre-warmed dye solution into the tube (Video 1).

Notes:

- a Use the fine-tipped plastic pipette to transport hippocampal slices and a modified transfer pipette (without tip) for cortical slices (see Figure 1A).
- b In one tube accommodate, at least 6-10 hippocampal slices or 3-4 cortical slices.
- c The described procedure decreases the chances of diluting a small volume of dye solution.

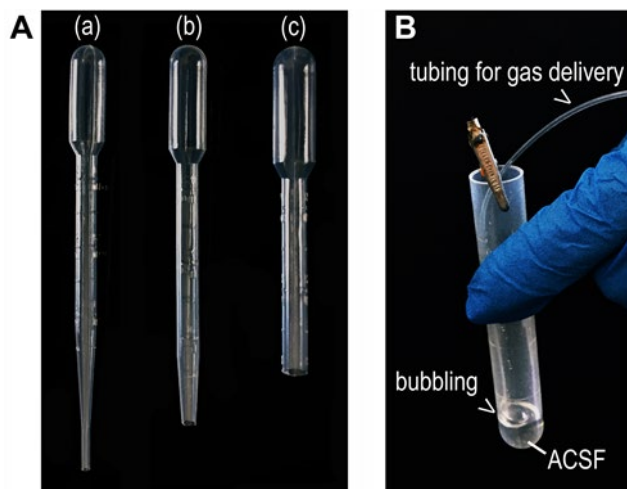


Figure 1. Transfer pipettes and dye-loading tube.

A. Plastic pipettes (3 mL) used to transfer hippocampal (a) or cortical (b and c) acute slices. The length of the pipette in (a) is 16 cms. In (b) and (c), the fine tip of the plastic pipette has been cut and removed to prevent damage to the cortical slices during their passage through it. B. Rounded bottom dye-loading tube with fine tubing for gas delivery.



Video 1. Slice transfer procedure

3. After transferring the slices, place the dye loading tube with the slices into the thermostatic water bath (35°C-37°C). Keep slices incubated in the dye solution carbogenated with 95% O₂ and 5% CO₂ for 30 min in the dark.

Note: Maintain the fine-tip of the gas tubing as distant as possible from the bottom of the loading tube to prevent bubbling from disturbing the slices (see Video 1).

- After 30 min, remove the dye solution from the tube with a 1,000 μL pipettor while keeping slices at the bottom. Rapidly, add a minimum of 1 mL of normal ACSF into the tube to rinse slices for 15 min.

Notes:

- a Rinsing slices will stop labelling and reduce background.
- b During and following the rinsing period, protect slices from light

B. Pericyte identification with TO-PRO-3 in brain slices

- Prepare dye-loading and rinsing chambers. To do so, fill two chambers with 10 mL of ACSF and bubble the solution with 95% O₂ and 5% CO₂ for at least 20 min before submerging the slices. Add 10 μL of the stock solution of TO-PRO-3 into the dye-loading chamber to yield a 1 μM final concentration. Protect solutions from light with aluminium foil. Place a little strainer into a contiguous chamber (Figures 2a-2b).

Notes:

- a Wells of a 6-well plate can be used as adequate dye loading and rinsing chambers, as shown in Figure 2.
- b A little homemade strainer with adequate size to fit into the well allows simultaneous transport of all slices and exchange of both slice surfaces with carbogenated ACSF during the whole procedure (Figure 2). To build the strainer, follow the procedure described in Figure 3.
- c Place recording and rinsing chambers side by side to facilitate the rapid transfer of slices between chambers (Figure 2).
- d Wear latex or nitrile gloves to protect yourself when manipulating TO-PRO-3.
- e Vortex the stock vial of TO-PRO-3 before use.
- f Use freshly and daily prepared dye solution.
- g Agitate the dye-loading chamber to dissolve the dye into the ACSF until the dilution becomes homogenous.
- h If slices from numerous animals are going to be loaded, it is convenient to prepare an additional loading chamber. In our hands, it is possible to use the same dye solution twice (up to 20 hippocampal slices each)

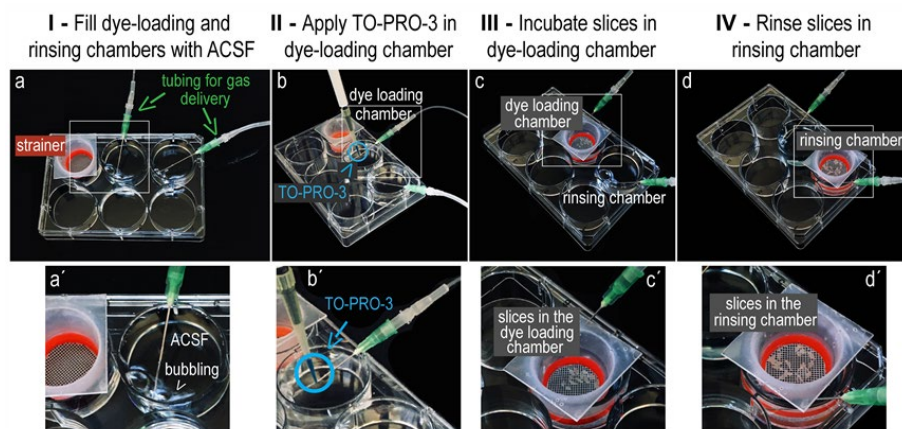


Figure 2. Step-by-step procedure employed to load pericytes with TO-PRO-3 in acute hippocampal slices.

(a, a') Fill two wells of a six-well plate (12×8 cms) with 10 mL of ACSF each and bubble the solution with 95% O₂ and 5% CO₂ through a fine tubing. Place a little strainer into an empty well. (b, b') Apply a volume (10 μ L) of the TO-PRO-3 stock solution into the dye-loading chamber and agitate to facilitate dye dissolution. (c, c') Pick up brain slices with a transfer pipette and pour them on the top of the strainer (the ACSF contained in the transfer pipette will drop into the empty chamber while the mesh will retain the slices). Rapidly incubate the strainer carrying the slices into the dye-loading chamber. (d, d') After a dye-loading period of 20 min, transfer the strainer with the TO-PRO-3-loaded slices into the rinsing chamber for 15 min. During the whole procedure, maintain slices and solutions protected from light with aluminium foil. The fields within the white rectangles in pictures (a-d) have been zoomed (2.4 \times) and are shown below (a', b', c' and d'). Hereinafter, acute slices with TO-PRO-3 loaded pericytes can be either fixed or used in living experiments (e.g., electrophysiological recordings or calcium dynamics analysis).

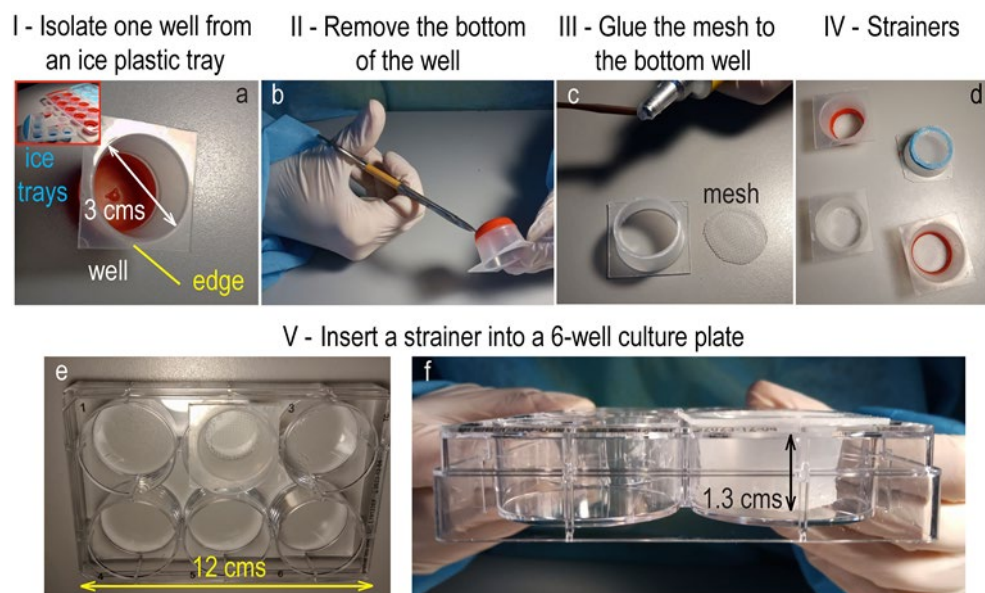


Figure 3. Construction of a custom-built strainer to hold and transfer acute brain slices.

(a) Isolate one well from a plastic ice tray and preserve an edge around the well. (b) Remove the bottom well. Be aware that the final height of the strainer measures more than 1,3 cms (shown in f). (c) Cut a round piece of nylon mesh, ensuring that the mesh diameter fits the well diameter. Glue the borders of the mesh to the outside borders of the well hole with a silicone sealer. (d) Allow the strainer to dry for 24 h and rinse with ddH₂O before use. (e and f) Introduce the strainer into the 6-well plate and check that the mesh allows ACSF to pass through it with ease.

2. Pick up the acute slices from the tube or from a storage chamber with a plastic pipette (Figure 1), and place them over the nylon mesh of the little strainer, allowing the ACSF to drop into the empty well. Rapidly introduce the strainer carrying the slices into the loading chamber for 20 min at RT in the dark (Figure 2c).

Notes:

- Transferring the slices with a strainer instead of using a plastic pipette will prevent diluting the dye solution in the loading chamber.*
 - Protect slices and solutions from light with aluminium foil during dye loading and post-loading periods.*
3. Following the incubation period with TO-PRO-3, transfer the strainer carrying the slices from the loading chamber to the rinsing chamber for 15 min (Figure 2d).

Notes:

- a. Rinsing slices will stop dye incorporation into cells, reduce background labelling and prevent unspecific uptake.
 - b. Since the TO-PRO-3 probe shows a high affinity for DNA (Suzuki et al., 1997), once bound to the nucleic acids, the dye is expected not to leak through the membrane and stay intracellular.
4. Following the rinsing period, counterstain with Hoechst 33342 (0.5 µM in ACSF) for 10 min at RT, if TO-PRO-3-loaded slices are to be used in living experiments (e.g., electrophysiological recordings or calcium dynamics analysis).
 5. To use fixed slices, submerge the TO-PRO-3-loaded slices in fixing solution for 40 min at RT under mild shaking. Rinse fixed slices in PBS twice, for 5-10 min each rinse.

Note: Do not use materials (chambers, tubes, pipettes, tubing, and instruments) in contact with fixed tissue to manipulate living tissue.

6. Counterstain with DAPI (1-5 µM in PBST) or Hoechst 33342 (0.5 µM in PBST) for 10 min at RT under gentle shaking. Rinse fixed slices in PBS, 1-2 times for 5-10 min each.

Notes:

- a. Use DAPI or Hoechst 33342 to label DNA in fixed slices and Hoechst 33342 to counterstain nucleus in acute slices; Hoechst 33342 is relatively nontoxic and nonmutagenic to living cells (Durand and Olive, 1982).
 - b. Counterstaining with DAPI or Hoechst 33342 favours referencing of the slice structure in the hippocampus.
 - c. For steps B5 and B6, it is convenient to employ a 12/24-well plate.
 - d. Fixed slices can be stored in PBS at 4°C, protected from light for 24-48 h before being mounted.
7. To mount fixed slices, pick up the sections from the well with a fine-tipped paintbrush and place them on a microscope slide. Remove the excess PBS with an absorbent tissue or dry it by incubating slides at 37°C for 5 min. Add a drop of mounting solution (glycerol or Fluoromont-GTM Mounting Medium) to cover the slices. Gently apply a coverslip over the mounting media, avoiding the generation of bubbles, and seal the coverslip by applying nail varnish at its borders. Store slides at 4°C in the dark for at least 24 h before analysis with a confocal laser-scanning microscope.
- Figures 4 and 5 illustrate representative examples of TO-PRO-3-labelled pericytes from rodents in fixed hippocampal slices. Figure 5 shows TO-PRO-3-stained pericytes in adjacency to lectin-stained vessels.

Notes:

- a. Waiting overnight before taking photos decreases photobleaching.
- b. In our hands, mounted sections stored in the dark at 4°C preserve the bright TO-PRO-3 stain in pericytes for at least 1-1.5 months (Mai-Morente et al., 2021).

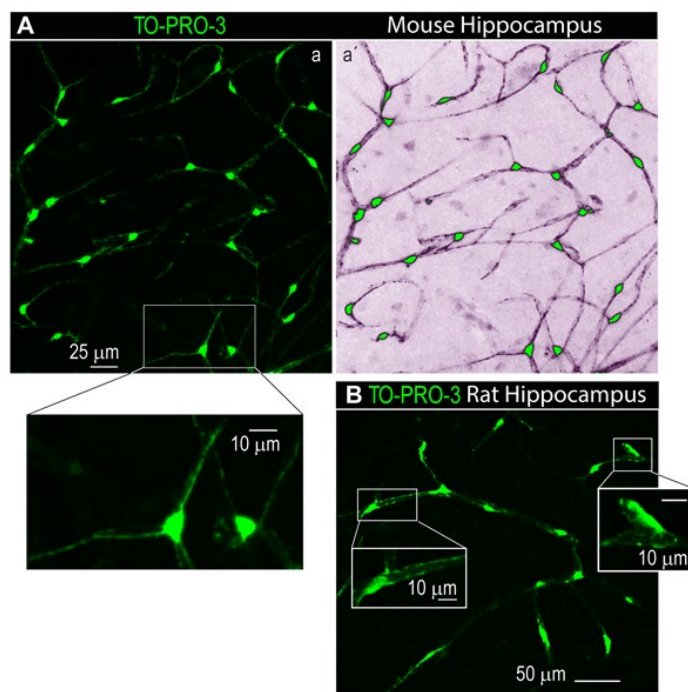


Figure 4. TO-PRO-3-labelled pericytes in fixed slices of the murine hippocampus.

A. Confocal images of mouse hippocampus illustrate a fluorescent field of the stratum radiatum with TO-PRO-3-stained pericytes (a) and the inverted fluorescent version of the same field (a'). The area within the white rectangle in (a) has been zoomed and is shown below. Note the bright spindle-shaped TOPRO-3 somas giving origin to longitudinal processes. The inverted image in (a') evidences pericyte prolongations marked with the fluorophore. Each image is representative of the hippocampi of 40 mice. B. The fluorescent image illustrates pericytes labelled with TO-PRO-3 in the rat hippocampus. The pericytes within the white rectangles have been zoomed to facilitate the visualization of prolongations stained with TO-PRO-3. Each image is representative of the hippocampi of 10 rats. In all images, the TO-PRO-3 fluorescence is pseudo-coloured in green.

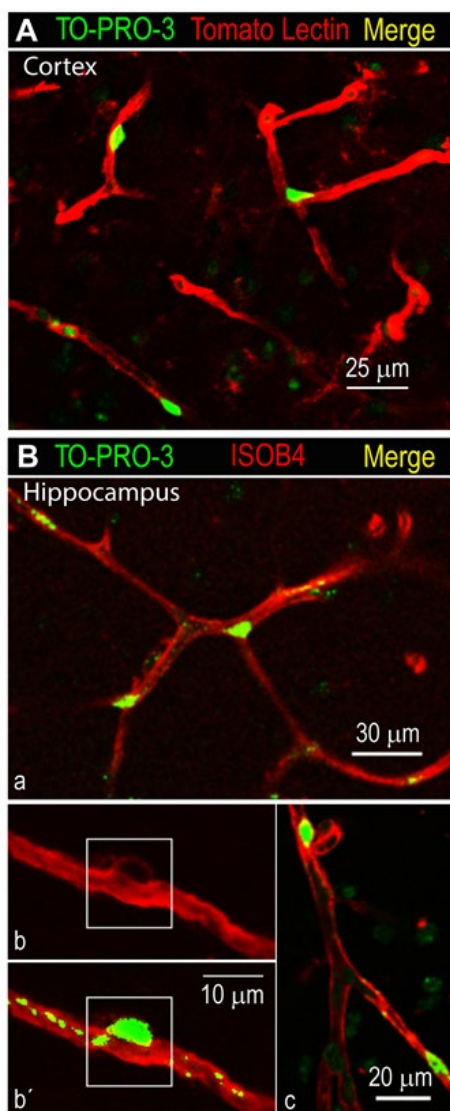


Figure 5. TO-PRO-3-pericyte somas outline the cerebral microvasculature.

A. The fluorescent micrograph illustrates TO-PRO-3-labelled pericytes in the mouse cerebral cortex associated with Tomato Lectin-marked vasculature. The image is representative of five mice. B. Different fluorescent views of mouse hippocampus (a; b, b'; c) illustrate TO-PRO-3-labelled pericytes and Isolectin B4 (FITC-ISOB4)-marked pericytes and vessels. The picture in (b') represents the same field as (b) in which the TO-PRO-3 view has been merged. The FITC-ISOB4 probe stains basement membranes of endothelium and pericytes. Note the ISOB₄ mark shaping the contour of the TO-PRO-3-labelled soma in (b) and the TO-PRO-3 prolongations delineating the vessel wall in (b'). Each image is representative of 10 mice. In all images, the TO-PRO-3 fluorescence is pseudo-coloured in green, and the fluorescence of Tomato Lectin and ISOB₄ is pseudo-coloured in red.

C. Identification of astrocytes and pericytes in brain slices

For simultaneous identification of pericytes and astrocytes, follow Procedures B and C. To include vessel identification, follow Procedures A, B and C.

1. Immerse fixed slices pre-loaded with TO-PRO-3 in a blocking/permeabilizing solution for 2 h in agitation at RT in the dark.

Notes:

- a. *To do this step, it is possible to use a 12/24-well plate.*
- b. *Blocking/permeabilizing solution and antibody and fixing solutions are freshly prepared. In our experience, these solutions can be stored at 4°C for one week.*
- c. *The blocking/permeabilizing solution blocks unspecific sites and permeabilizes cell membranes prior to antibody application.*

2. Wash slices three times in PBST for 5-10 min each under gentle shaking. Protect the slices from light with aluminium foil.
3. Incubate slices in diluting solution for antibodies with primary antibody anti-GFAP conjugated with Cy3 (1:400) for 2 h at RT under gentle agitation and protected from light.

Notes:

- a. *Incubate hippocampal slices in antibody solution using a 96-well plate to save antibody. The volume of the antibody solution should be sufficient to cover the slices (200 µl minimum).*
- b. *Use a fine-tip paintbrush to transfer slices into the well or to remove them from it.*

4. Rinse slices three times in PBST for 10 min each under agitation and protected from light.
5. Treat slices for 10 min with DAPI (1-5 µM in PBST) or Hoechst 33342 (0.5 µM in PBST) at RT under mild agitation and rinse them again with PBST.

Note: In steps C4 and C5, it is possible to use a 12/24-well plate.

6. To mount slices, follow the guidelines detailed in Step B7. Store slides at 4°C in the dark for at least 24 h before analysis with a confocal laser-scanning microscope.

Figure 6 illustrates different fields of the mouse hippocampus with TO-PRO-3-stained pericytes and GFAP-labelled astrocytes. The intimate rapport between pericyte somata and astrocyte end feet is evidenced. Triple labelling of TO-PRO-3-stained pericytes, GFAP-positive astrocytes and IsoB4-labelled vessels is also shown (Figure 6D).

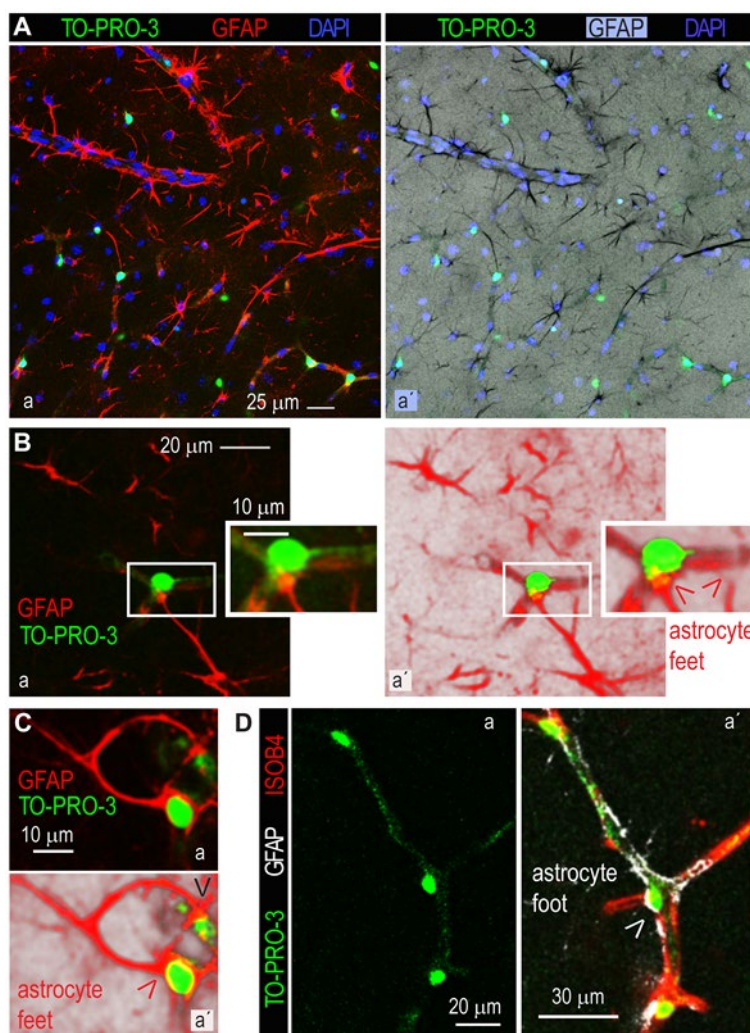


Figure 6. TO-PRO-3-stained pericytes are components of the gliovascular unit.

(A) (a, a') A fluorescent view of a mouse hippocampus field (stratum radiatum) illustrates TO-PRO-3-labelled pericytes and GFAP-labelled astrocytes (a). The inverted fluorescent version of this field is shown in (a'). Nuclei stained with DAPI have been superimposed. (B) and (C) (a, a') Photos of mouse hippocampus illustrate the intimate relationship between GFAP-stained astrocyte foot processes and TO-PRO-3-labelled pericyte somas. The inverted fluorescent version of the field shown in (a) is revealed in (a'). The area within the white box in (B) has been zoomed to evidence the rapport between the pericyte and the astrocyte foot process. Images are representative of the hippocampi of six mice. (D) (Same field a, a') Fluorescent images illustrate TO-PRO-3-labelled pericyte somas lining a vessel in the hippocampus and GFAP-stained astrocyte prolongations reaching the vasculature and the pericyte somas. The basal lamina of the vessel endothelium has been stained with ISOB4. Images are representative of hippocampi of 10 mice. In all images, the TO-PRO-3 fluorescence is pseudo-coloured in green, and the fluorescence of ISOB4 is pseudo-coloured in red.

Notes:

- a. If required, additional immunostaining is possible (e.g., microglial or neuronal markers) in TO-PRO-3 slices (Mai-Morente et al., 2021).
- b. Waiting overnight before taking photos decreases photobleaching.
- c. Alternatively, slices derived from transgenic hGFAP-eGFP mice (Nolte et al., 2001) that allow easy identification of astrocytes can be subjected to procedures described in Item B for the simultaneous staining of astrocytes and pericytes in either acute or fixed slices.

D. Pericyte identification with TO-PRO-3 and NeuroTrace 500/525 in acute slices

1. Repeat procedures described in Steps B1 to B3 but in addition to TO-PRO-3, apply NeuroTrace 500/525 (NeuroTr) (1:50 to 1:500 dilution of the stock solution) into the loading chamber for double labelling of pericytes (NeuroTr/TO-PRO-3). For exclusive staining with NeuroTr just dilute this probe into the loading chamber.

Notes:

- a. Adjust the optimal dilution of NeuroTr to your preparation.
- b. As for TO-PRO-3, vortex the stock solution of NeuroTr prior to use, prepare fresh dye solutions and protect solutions and slices from light during loading and post-loading periods.
- c. For simultaneous identification of pericyte somas with NeuroTr and vessels with lectins, use commercially available lectins conjugated to fluorophores other than FITC, Alexa 488 or DyLight 488 to prevent spectral overlap between these fluorophores and NeuroTr.
- d. NeuroTrace 500/525 has been recently identified as a pericyte marker in vivo (Damisah et al., 2017) and ex vivo (Mai-Morente et al., 2021).

2. If desired, counterstain the nucleus by incubating acute slices in carbogenated (95% O₂ and 5% CO₂) ASCF containing Hoechst 33342 (0.5 μM final concentration) at RT for 15 min. Wash once in carbogenated ASCF for 10 min at RT. After the rinsing period, the dye-loaded living slices are ready to use in living experiments.

Figure 7 illustrates live pericytes co-stained with NeuroTr and TO-PRO-3 adjoining a vessel in a mouse hippocampal acute slice.

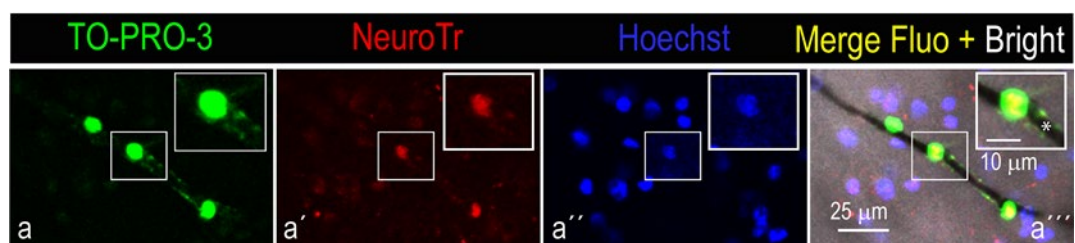


Figure 7. TO-PRO-3 labels live pericytes in acute slices of mouse hippocampus.

(a-a'') The same field of the mouse hippocampus illustrates live pericytes identified with TO-PRO-3 (a) and NeuroTrace 500/525 (a'); co-localization of both dyes plus Hoechst 33342 is shown in (a'') where the brightfield view has been merged to fluorescent images. The pericyte within the white box has been zoomed. In (a''), pericytes lie down adjacent to a microvessel; the asterisk within the zoomed box indicates blood accumulation. Note TO-PRO-3-stained prolongations surrounding the vessel wall. Images are representative of hippocampi of 15 mice. The TO-PRO-3 fluorescence is pseudo-coloured in green, whereas the fluorescence of NeuroTr is pseudo-coloured in red.

Notes:

- a. Counterstaining with Hoechst 33342 enables referencing the slice structure in the hippocampus.
- b. In addition to NeuroTr-labelled pericytes, living astrocytes might be imaged with the fluorescent dye sulforhodamine 101 (SR101; Exc. 586/Em. 605), which enables staining of glial cells *in vivo* and *ex vivo* (Nimmerjahn et al., 2004; Nimmerjahn and Helmchen, 2012; Kafitz et al., 2008). Alternatively, for concurrent labelling of pericytes and astrocytes in living sections, slices derived from transgenic hGFAP-eGFP mice that allow detailed visualization of the astrocyte morphology (Nolte et al., 2001) can be loaded with TO-PRO-3. Notice that the same laser allows visualization of NeuroTr 500/525-loaded pericytes and hGFAP-eGFP astrocytes; therefore, NeuroTr is not appropriate to identify pericytes in acute slices derived from transgenic eGFP-mice.

E. Image acquisition

1. For fixed preparations, mount microscope slides with TO-PRO-3-loaded hippocampal sections onto the stage of a confocal microscope (Leica SP5 TANDEM SCANNER). Labelled cells are visualized with a 40 \times oil immersion objective. Capture images and z-stacks with a digital camera connected to the imaging LAS AF Lite Software in data acquisition mode “xyz”, acquisition speed of 400 Hz (*i.e.*, 400 lines/s), image resolution of 1,024 \times 1,024 pixels and value of “line average” equal to 2 to reduce noise. Under UV, select the field of interest and focus the area under study. Then, switch to the He-Ne 633 nm filter and tune “gain and offset” parameters in the detection system to optimize the signal intensity/noise ratio of TO-PRO-3, avoiding oversaturation so that bright fluorescent pericytes can easily be discriminated from the background and other cells. Switch to channels 488 nm and 543 nm to visualize lectin-stained vessels and GFAP-labelled astrocytes, respectively, and set up microscope parameter values. Determine the z-stack size and set the “start” and “end” values of the z-stack step. Take images at distances $> 15\text{--}20 \mu\text{m}$ from the slice surface, as in surface areas reside damaged cells and reactive astrocytes due to membrane injury during slicing (Takano et al., 2014). These are shown in Figure 8.

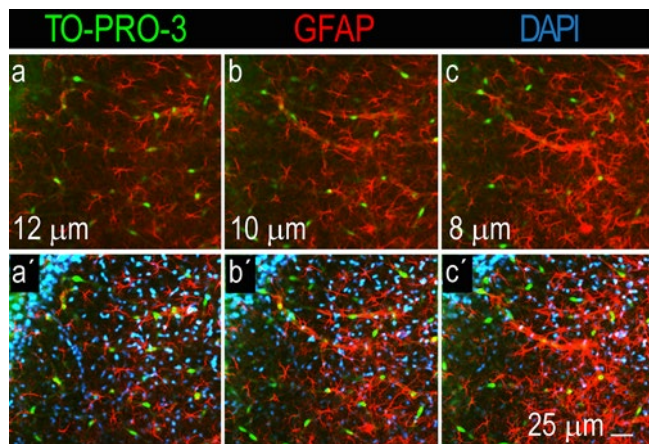


Figure 8. Reactivity gradient of astroglia at different distances from the slice surface.

Fluorescent photos of mouse hippocampus acquired at 12 μm (a, a'), 10 μm (b, b') and 8 μm (c, c') from the slice surface are shown; note the GFAP up-regulation in the outermost areas of the slice indicative of reactive astrogliosis. Fields (a, b and c) are the same as those (a', b' and c' respectively) in which the DAPI fluorescence has been merged. Images are representative of the hippocampi of seven mice. In all images, the TO-PRO-3 fluorescence is pseudo-coloured in green.

2. For acute slices, after setting the perfusion system, transfer one or two slices to the bottom of the recording chamber. Mount the perfusion chamber onto the stage of a confocal microscope and perfuse with ACSF equilibrated with 95% O₂ and 5% CO₂ at 1 mL/min. Keep the flow rate steady and set the temperature of

the ACSF at 34–37°C by using a heating system. Figure 9 displays the setup employed to image brain pericytes from acute slices stained with TO-PRO-3 and NeuroTr. Under UV, select the working area; thereafter switch to 488 nm and 633 nm lasers to image stained pericytes with NeuroTr and TO-PRO-3. To decrease fading, during time-lapse experiments, acquire images at 512 × 512 pixels resolution and 800 Hz. When zooming, laser gains and exposure times should be optimized to decrease fading.

Notes:

- a. *In the hippocampus, the anatomical segregation of DAPI/Hoechst 33342-stained nucleus facilitates the recognition of different areas (CA1, CA2 and CA3 layers, stratum oriens, stratum radiatum, and dentate gyrus).*
- b. *Minimize the exposure of living slices to UV to preclude phototoxicity (Suseela et al., 2018).*
- c. *As reported by our group, in healthy slices, TO-PRO-3 labelling of pericytes exhibits an excellent signal-to-noise ratio; incorporation of TO-PRO-3 by living pericytes is mediated by an actively operated transport mechanism that concentrates the dye into pericytes, resulting in bright labelling of somas and prolongations (Mai-Morente et al., 2021). Therefore, staining with TO-PRO-3 facilitates the identification of pericyte morphology and location during fluorescence imaging. According to our experience, pericytes from unhealthy slices fail to concentrate the dye.*
- d. *The bottom of the perfusion chamber is made of a poly-L-lysine-coated coverslip (Nr 1.5), which helps to immobilize the slices.*
- e. *In our hands, the bright fluorescence of the TO-PRO-3-stain in pericytes is very stable in PFA-fixed slices and lasts up to 1.5 months for sections mounted on slides and stored at 4°C in the dark. Under time-lapse acquisition of living slices, TO-PRO-3 fluorescence is more labile than in fixed slices (Mai-Morente et al., 2021). Indeed, NeuroTr fluorescence is more resistant to photobleaching than TO-PRO-3 fluorescence during image acquisition in acute brain slices.*
- f. *Work in the same range distance (e.g., from 20 to 50 µm from the slice surface) for conditions whose data will be compared since responses might depend along a spatial gradient propagation through the slice depth (Tian et al., 2010; Hall et al., 2014; Mishra et al., 2014).*

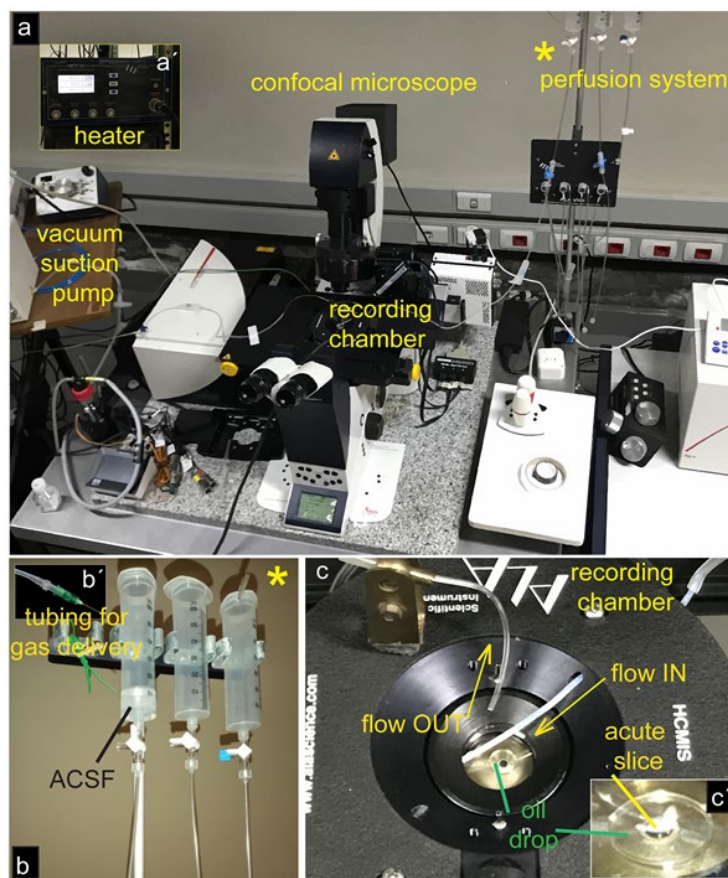


Figure 9. Setup for high-resolution imaging of TO-PRO-3-labelled and NeuroTrace-labelled pericytes in acute brain slices.

(a) General overview of the setup employed for recording TO-PRO-3-labelled pericytes in living hippocampal slices. The inset in (a') illustrates the system heater employed to regulate the temperature of the recording chamber. (b) (*) Detail of recipients containing ACSF. The solution is equilibrated by a mixture of 95% O₂ and 5% CO₂ delivered by the tubing shown in (b') (the tubing should be introduced into the ACSF). (c and c') Zoomed views of the recording chamber without (c) and with (c') a hippocampal slice. The oil drop between the 40× oil objective and the bottom of the chamber is visible. The bottom of the chamber is made of a poly-L-lysine-coated coverslip to secure the slice. The tubing for flow perfusion of ACSF (flow IN/flow OUT) has been represented.

Recipes

Note: Use freshly prepared solutions.

1. Artificial cerebrospinal fluid (ACSF)

In 1 L of MilliQ-water or ddH₂O dissolve:

7.824 g NaCl
0.21 g KCl
2.476 g NaHCO₃
0.155 g NaH₂PO₄
2.23 g glucose
0.36 g MgSO₄

Bubble with 95% O₂ and 5% CO₂ for 20 min.
Add 0.368 g CaCl₂ and adjust the pH to 7.4.
Test osmolarity (300-310 mOsm).
Store at 4°C.

2. Phosphate-buffered saline (PBS)

In 1 L of MilliQ-water or ddH₂O, dilute:
8 g NaCl
0.2 g KCl
1.44 g Na₂HPO₄
0.24 g KH₂PO₄
Adjust pH to 7.4.
Store at 4°C.

3. Phosphate-buffered saline (PBS)

In 1 L of MilliQ-water or ddH₂O, dilute:
Adjust pH to 7.4.
Store at 4°C.

4. Phosphate-buffered saline with 0.5% Triton X-100 (PBST)

To obtain 100 mL of PBST, add 500 µL of Triton X-100 to 99.5 mL of PBS.
Store at 4°C.

5. Blocking/permeabilizing solution

Dilute 2% bovine serum albumin (BSA) and 0.2 M glycine in PBST.
Store at 4°C.

6. Diluting solution for antibodies

Dilute 2% bovine serum albumin (BSA) in PBST.
Store at 4°C.

7. Fixing solution 4% PFA in PBS

Note: Toxicity/Safety. PFA is a toxic, corrosive, irritant, and carcinogenic compound. To avoid skin contact and inhalation, wear protective clothing (e.g., gloves, mask, and robe) and work under a gas extraction cabinet while manipulating PFA.

Dilute 4 g PFA in 100 mL of PBS, stir the solution at 80°C, adjust pH to 7.4 using NaOH, and filter the solution.
Store at 4°C.

Acknowledgments

This work was funded by Proyecto de Investigación y Desarrollo CSIC I+D 2014, ID 48 (Comisión Sectorial de Investigación Científica – Universidad de la República Oriental del Uruguay (CSIC-UDELAR) and Proyecto de Investigación Fundamental Fondo Clemente Estable FCE_1_2017_1_136103 (Agencia Nacional de Investigación e Innovación del Ministerio de Educación y Cultura del Uruguay (ANII-MEC) to VA. Master Fellowship to VM was funded by ANII-MEC; Doctoral Fellowship to SMM and Master Fellowships to JI and VC were supported by UDELAR.

The protocols describing labelling of cerebral pericytes, astrocytes and vessels were adapted from Mai-Morente *et al.* (2021). The authors thank Luis Vitureira (Departamento de Fisiología), Unidad de Reactivos para Biomodelos de Experimentación (URBE), FUNDACIBA and Unidad de Microscopía Confocal, from Facultad de Medicina - Universidad de la República Oriental del Uruguay, for technical assistance.

Competing interests

The authors declare no competing interests.

Ethics

Experimental procedures were processed following the National Institutes of Health guidelines for the care and use of laboratory animals (NIH Publications No. 8023, revised 1978) and the local regulation (CDC Exp. 4332/99, Diario Oficial No. 25467, Feb. 21/00, Universidad de la República, Uruguay).

References

- Damisah, E. C., Hill, R. A., Tong, L., Murray, K. N. and Grutzendler, J. (2017). [A fluoro-Nissl dye identifies pericytes as distinct vascular mural cells during in vivo brain imaging](#). *Nat Neurosci* 20(7): 1023-1032.
- de Mazière, A. M., Hage, W. J. and Ubbels, G. A. (1996). [A method for staining of cell nuclei in Xenopus laevis embryos with cyanine dyes for whole-mount confocal laser scanning microscopy](#). *J Histochem Cytochem* 44(4): 399-402.
- Durand, R. E. and Olive, P. L. (1982). [Cytotoxicity, Mutagenicity and DNA damage by Hoechst 33342](#). *J Histochem Cytochem* 30(2):111-6.
- Hall, C. N., Reynell, C., Gesslein, B., Hamilton, N. B., Mishra, A., Sutherland, B. A., O'Farrell, F. M., Buchan, A. M., Lauritzen, M. and Attwell, D. (2014). [Capillary pericytes regulate cerebral blood flow in health and disease](#). *Nature* 508(7494): 55-60.
- Hartmann, D. A., Underly, R. G., Grant, R. I., Watson, A. N., Lindner, V. and Shih, A. Y. (2015a). [Pericyte structure and distribution in the cerebral cortex revealed by high-resolution imaging of transgenic mice](#). *Neurophotonics* 2(4): 041402.
- Hartmann, D. A., Underly, R. G., Watson, A. N. and Shih, A. Y. (2015b). [A murine toolbox for imaging the neurovascular unit](#). *Microcirculation* 22(3): 168-182.
- Jung, B., Arnold, T. D., Raschperger, E., Gaengel, K. and Betsholtz, C. (2018). [Visualization of vascular mural cells in developing brain using genetically labeled transgenic reporter mice](#). *J Cereb Blood Flow Metab* 38(3): 456-468.
- Kafitz, K. W., Meier, S. D., Stephan, J. and Rose, C. R. (2008). [Developmental profile and properties of sulforhodamine 101--Labeled glial cells in acute brain slices of rat hippocampus](#). *J Neurosci Methods* 169(1): 84-92.
- Lacar, B., Herman, P., Platel, J. C., Kubera, C., Hyder, F. and Bordey, A. (2012). [Neural progenitor cells regulate capillary blood flow in the postnatal subventricular zone](#). *J Neurosci* 32(46): 16435-16448.
- Laitinen, L. (1987). [Griffonia simplicifolia lectins bind specifically to endothelial cells and some epithelial cells in mouse tissues](#). *Histochem J* 19(4): 225-234.
- Lein, P. J., Barnhart, C. D. and Pessah, I. N. (2011). [Acute hippocampal slice preparation and hippocampal slice cultures](#). *Methods Mol Biol* 758: 115-134.
- Mai-Morente, S. P., Marset, V. M., Blanco, F., Isasi, E. E. and Abudara, V. (2021). [A nuclear fluorescent dye identifies pericytes at the neurovascular unit](#). *J Neurochem* 157(4): 1377-1391.
- Mishra, A., O'Farrell, F. M., Reynell, C., Hamilton, N. B., Hall, C. N. and Attwell, D. (2014). [Imaging pericytes and capillary diameter in brain slices and isolated retinae](#). *Nat Protoc* 9(2): 323-336.

- Nimmerjahn, A. and Helmchen, F. (2012). [In vivo labeling of cortical astrocytes with sulforhodamine 101 \(SR101\)](#). *Cold Spring Harb Protoc* 2012(3): 326-334.
- Nimmerjahn, A., Kirchhoff, F., Kerr, J. N. and Helmchen, F. (2004). [Sulforhodamine 101 as a specific marker of astroglia in the neocortex in vivo](#). *Nat Methods* 1(1): 31-37.
- Nolte, C., Matyash, M., Pivneva, T., Schipke, C. G., Ohlemeyer, C., Hanisch, U. K., Kirchhoff, F. and Kettenmann, H. (2001). [GFAP promoter-controlled EGFP-expressing transgenic mice: a tool to visualize astrocytes and astrogliosis in living brain tissue](#). *Glia* 33(1): 72-86.
- Ozerdem, U., Grako, K. A., Dahlin-Huppe, K., Monosov, E. and Stallcup, W. B. (2001). [NG2 proteoglycan is expressed exclusively by mural cells during vascular morphogenesis](#). *Dev Dyn* 222(2): 218-227.
- Pannasch, U., Sibille, J. and Rouach, N. (2012). [Dual electrophysiological recordings of synaptically-evoked astrogial and neuronal responses in acute hippocampal slices](#). *J Vis Exp*(69): e4418.
- Papouin, T. and Haydon, P. G. (2018). [Obtaining Acute Brain Slices](#). *Bio-protocol* 8(2): e2699.
- Peters, B. P. and Goldstein, I. J. (1979). [The use of fluorescein-conjugated Bandeiraea simplicifolia B4-isolectin as a histochemical reagent for the detection of alpha-D-galactopyranosyl groups. Their occurrence in basement membranes](#). *Exp Cell Res* 120(2): 321-334.
- Smyth, L. C. D., Rustenhoven, J., Scotter, E. L., Schweder, P., Faull, R. L. M., Park, T. I. H. and Dragunow, M. (2018). [Markers for human brain pericytes and smooth muscle cells](#). *J Chem Neuroanat* 92: 48-60.
- Suseela, Y. V., Narayanaswamy, N., Pratihar, S. and Govindaraju, T. (2018). [Far-red fluorescent probes for canonical and non-canonical nucleic acid structures: current progress and future implications](#). *Chem Soc Rev* 47(3): 1098-1131.
- Suzuki, T., Fujikura, K., Higashiyama, T. and Takata, K. (1997). [DNA staining for fluorescence and laser confocal microscopy](#). *J Histochem Cytochem* 45(1): 49-53.
- Takano, T., He, W., Han, X., Wang, F., Xu, Q., Wang, X., Oberheim Bush, N. A., Cruz, N., Dienel, G. A. and Nedergaard, M. (2014). [Rapid manifestation of reactive astrogliosis in acute hippocampal brain slices](#). *Glia* 62(1): 78-95.
- Tian, P., Teng, I. C., May, L. D., Kurz, R., Lu, K., Scadeng, M., Hillman, E. M., De Crespigny, A. J., D'Arceuil, H. E., Mandeville, J. B., et al. (2010). [Cortical depth-specific microvascular dilation underlies laminar differences in blood oxygenation level-dependent functional MRI signal](#). *Proc Natl Acad Sci U S A* 107(34): 15246-15251.
- Tong, L., Hill, R. A., Damisah, E. C., Murray, K. N., Yuan, P., Bordey, A. and Grutzendler, J. (2021). [Imaging and optogenetic modulation of vascular mural cells in the live brain](#). *Nat Protoc* 16(1): 472-496.
- Van Hooijdonk, C. A., Glade, C. P. and Van Erp, P. E. (1994). [TO-PRO-3 iodide: a novel HeNe laser-excitable DNA stain as an alternative for propidium iodide in multiparameter flow cytometry](#). *Cytometry* 17(2): 185-189.

Visual-stimuli Four-arm Maze test to Assess Cognition and Vision in Mice

Jean-Philippe Vit¹, Dieu-Trang Fuchs¹, Ariel Angel², Aharon Levy², Itschak Lamensdorf², Keith L. Black¹, Yosef Koronyo¹ and Maya Koronyo-Hamaoui^{1,3,*}

¹Department of Neurosurgery, Maxine Dunitz Neurosurgical Research Institute, Cedars-Sinai Medical Center, Los Angeles, CA, 90048, USA

²Pharmaseed Ltd., Ness Ziona 74047, Israel

³Department of Biomedical Sciences, Division of Applied Cell Biology and Physiology, Cedars-Sinai Medical Center, Los Angeles, CA, USA

*For correspondence: maya.koronyo@csmc.edu

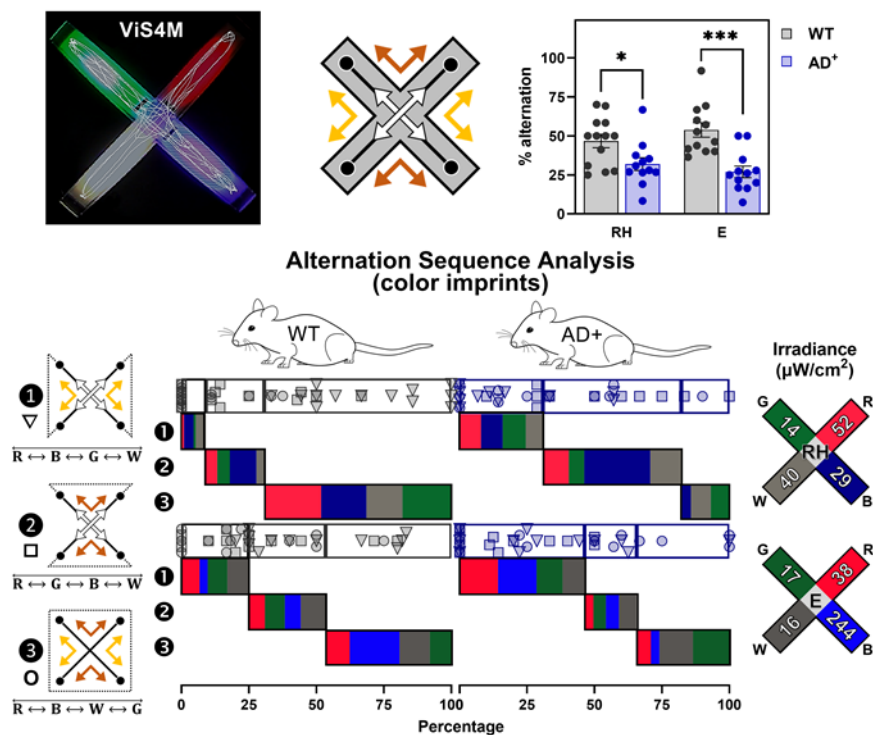
Abstract

Visual impairments, notably loss of contrast sensitivity and color vision, were documented in Alzheimer's disease (AD) patients yet are critically understudied. This protocol describes a novel visual-stimuli four-arm maze (ViS4M; also called visual x-maze), which is a versatile x-shaped maze equipped with spectrum- and intensity-controlled light-emitting diode (LED) sources and dynamic grayscale objects. The ViS4M is designed to allow the assessment of color and contrast vision along with locomotor and cognitive functions in mice. In the color testing mode, the spectral distributions of the LED lights create four homogenous spaces that differ in chromaticity and luminance, corresponding to the mouse visual system. In the contrast sensitivity test, the four grayscale objects are placed in the middle of each arm, contrasting against the black walls and the white floors of the maze. Upon entering the maze, healthy wild-type (WT) mice tend to spontaneously alternate between arms, even under equiluminant conditions of illumination, suggesting that cognitively and visually intact mice use both color and brightness as cues to navigate the maze. Evaluation of the double-transgenic APPSWE/PS1ΔE9 mouse model of AD (AD⁺ mice) reveals substantial deficits to alternate in both color and contrast modes at an early age, when hippocampal-based memory and learning is still intact. Profiling of timespan, entries, and transition patterns between the different arms uncovers variable aging and AD-associated impairments in color discrimination and contrast sensitivity. The analysis of arm sequences of alternation reveals different pathways of exploration in young WT, old WT, and AD⁺ mice, which can be used as color and contrast imprints of functionally intact versus impaired mice. Overall, we describe the utility of a novel visual x-maze test to identify behavioral changes in mice related to cognition, as well as color and contrast vision, with high precision and reproducibility.

Keywords: Rodent maze, Cognition, Visual impairments, Behavioral changes, Neurodegenerative disease, Aging, Apparatus, Retinal pathology

This protocol was validated in: Sci Rep (2021), DOI: 10.1038/s41598-021-80988-0.

Graphical Abstract:



Exploratory behavior of AD⁺ mice versus age- and sex-matched WT mice is tracked (top left: trajectory from a 5-min video file) in a novel visual-stimuli four-arm maze (ViS4M; also named visual x-maze) equipped with spectrum- and intensity-controlled LED sources or grayscale objects.

Consecutive arm entries reveal that APPswe/PS1 Δ E9 (AD⁺) mice alternate less between arms, as opposed to WT mice. Sequence analysis, according to the three alternation pathways (depicted by white, yellow, and brown arrows) under different conditions of illumination, uncovers specific deficits linked to color vision in AD⁺ mice, evidenced by a color imprint chart.

Background

Mounting evidence indicates that the pathology of Alzheimer's Disease (AD) is not restricted to the brain but also extends to the retina. Multiple studies have shown that the retina of mild cognitively impaired (MCI) and AD patients exhibit the neuropathological hallmarks of AD – amyloid β -protein (A β) plaques and hyperphosphorylated tau – along with gliosis, vascular dysfunctions, and neuronal degeneration (Blanks *et al.*, 1996a and 1996b; Koronyo-Hamaoui *et al.*, 2011; La Morgia *et al.*, 2016; Koronyo *et al.*, 2017; Dumitrascu *et al.*, 2020; Lee *et al.*, 2020; Lemmens *et al.*, 2020; Shi *et al.*, 2020b; Dumitrascu *et al.*, 2021; Shi *et al.*, 2021; Ngolab *et al.*, 2021; Tadokoro *et al.*, 2021). Moreover, retinal pathology appears to mirror the disease in the brain (Koronyo-Hamaoui *et al.*, 2011; La Morgia *et al.*, 2016; Koronyo *et al.*, 2017; Doustar *et al.*, 2020; Dumitrascu *et al.*, 2020; Shi *et al.*, 2020a and 2020b; Risacher *et al.*, 2020). Clinically, both color and contrast sensitivity were significantly impaired in AD patients when compared with healthy individuals (Chang *et al.*, 2014; Polo *et al.*, 2017). Indeed, visual impairments are among the earliest symptoms documented in these patients, especially loss of contrast sensitivity (Crow *et al.*, 2003; Risacher *et al.*, 2013; Javaid *et al.*, 2016; Salobrar-García *et al.*, 2019) and altered color vision reminiscent of tritanomaly, an abnormality of blue-sensitive retinal cones (Cronin-Golomb *et al.*, 1993; Wijk *et al.*, 1999; Salobrar-García *et al.*, 2019).

Sporadic and transgenic animal models of AD recapitulate AD pathology in the retina and present A β deposits and tauopathy that are linked with inflammation, vasculopathy, and neurodegeneration (Perez *et al.*, 2009; Koronyo-Hamaoui *et al.*, 2011; Koronyo *et al.*, 2012; Hart *et al.*, 2016; Doustar *et al.*, 2017; Grimaldi *et al.*, 2018; Hampel *et al.*, 2018; Georgevsky *et al.*, 2019; Chibhabha *et al.*, 2020; Doustar *et al.*, 2020; Habiba *et al.*, 2020; Shi *et al.*, 2020a; Shi *et al.*, 2021). Transgenic mouse models of AD also show disturbances in the visual system, reduced function of ganglion cells and photoreceptors, as well as reduction of inner retinal thickness and atrophy of the visual cortex (Criscuolo *et al.*, 2018; Chiquita *et al.*, 2019). However, the specific visual changes in color and contrast vision have not been previously examined in transgenic mouse models of AD.

Behavioral assessment of color vision and contrast sensitivity in C57BL/6 mice has been previously conducted by optomotor response (Sinex *et al.*, 1979; Prusky *et al.*, 2004), optokinetic reflex (van Alphen *et al.*, 2009), and forced-choice procedures. The latter includes the visual water task (Jacobs *et al.*, 2004; Prusky and Douglas, 2004), psychometric curves in freely moving mice (Busse *et al.*, 2011), and the visual-stimulation environment (Denman *et al.*, 2018). Forced-choice paradigms require days of training and thousands of trials, which are less suitable for aged mice, especially for sensitive, high-attribution rate AD-model mice.

We created the behavioral visual-stimuli four-arm maze (ViS4M or visual x-maze), a novel, controlled, and user-friendly behavioral apparatus specialized for the detection of vision changes in mice (Vit *et al.*, 2021). Unlike previous behavioral tests, the ViS4M is highly sensitive and reproducible, allowing mice to move freely without introducing stress. Importantly, the test relies entirely on innate exploratory behavior and does not require a pre-training phase nor rewards. Moreover, this test can simultaneously assess locomotor, cognitive, and visual functions. We investigated color and contrast sensitivity in the double-transgenic APP_{SWE}/PS1_{ΔE9} (AD $^+$) mice. These AD-model mice and wild-type (WT) mice were tested at three different ages, during six sessions (5 min each) of testing, in five color modes (five conditions of illumination), and one contrast mode. Using the novel ViS4M, we identified early and progressive impairments in color vision and contrast sensitivity in AD-model mice.

In the present manuscript, we provide a detailed description and step-by-step configuration of the ViS4M and accessories, with numerous notes and tips in the equipment and procedure sections. In the data analysis section, we review all the parameters analyzed in the original study (total entries, timespan, alternation, and transitions) with their calculations and supported by relevant examples. We also present an additional analysis of alternation arm sequences and make freely available our own ViS4M Toolbox V1, which includes two Excel spreadsheets to automatically calculate all the aforementioned parameters upon inputting a sequence of arm entries in color and contrast modes. The comprehensive analysis of alternation sequences, as well as unidirectional and bidirectional transitions in combination with linear regressions and visualization tools, allow a better understanding of the locomotor, cognitive, and visual functions of mice measured in the ViS4M.

Materials and Reagents

Animals

1. Double transgenic B6.Cg-Tg(APP_{SWE}/PSEN1_{ΔE9})85Dbo/Mmjax hemizygous (AD $^+$) mouse strain [RRID:MMRRC_034832-JAX], initially purchased from the Mutant Mouse Resource and Research Center (MMRRC) at the Jackson Laboratory, then bred and maintained at Cedars-Sinai Medical Center.
2. Non-transgenic wild-type (WT) littermates (Jackson Laboratory, catalog number: 000664)
The mouse colony is housed in a humidity- and temperature-controlled (21–22°C) vivarium on a 12:12-h light/dark cycle (lights on at 8:00 am; lights off at 8:00 pm) with free access to food and water.
Three different cohorts of mice are tested, each representing a different age: 8.5-month-old WT (n=13; 9 males and 4 females) and AD $^+$ (n=12; 9 males and 3 females), 13-month-old WT (n=11; 6 males and 5 females) and AD $^+$ (n=11; 4 males and 7 females), and 18-month-old WT (n=19; 11 males and 8 females) and AD $^+$ (n=9; 5 males and 4 females).

Note: The double-transgenic APP_{SWE}/PS1_{ΔE9} is a well-established mouse strain, with early-onset pathology of AD in the hippocampus and cortex (β -amyloid plaques, severe astrogliosis, and microgliosis, as well as brain

plasticity deficits and synaptic loss). We and others also reported AD manifestation in the retina of these mice (Ning et al., 2008; Koronyo et al., 2012; Mirzaei et al., 2019; Doustar et al., 2020, Shi et al., 2020a and 2020b). Importantly, cognitive deficits in these mice have been well documented and reproducible. We developed the ViS4M to further characterize visual function, especially color vision and contrast sensitivity. AD pathology in the retina of other mouse strains has been confirmed, such as the aggressive-phenotype 5xFAD or the triple-transgenic 3xTg mice (Criscuolo et al., 2018; Grimaldi et al., 2018; Habiba et al., 2020). This protocol could be implemented on different AD mouse strains, normal aging, and other neurodegenerative models to evaluate visual function.

Equipment

A. Visual-stimuli four-arm maze (ViS4M) apparatus

Note: The visual-stimuli four-arm maze (ViS4M or Visual X-maze) that we describe below was conceived and developed in-house by our team. The prototype used to collect the present data shares the same specifications (including the color LED lights) with the now commercially available ViS4M manufactured by Maze Engineers (<https://conductscience.com/maze/portfolio/visual-x-maze-vis4m/>).

1. Backbone of apparatus
2. Custom-made x-shaped enclosure built with 15 cm-high black plexiglass walls attached to a glass base
 - Each arm is perpendicular to the two adjacent arms and is 45 cm long and 10 cm wide (Figure 1A-1B).
 - b. Removable transparent floor plates that can be installed at two different levels (6 cm or 11 cm above the glass base) in each arm and in the center of the ViS4M (Figure 1C).
 - c. White translucent acrylic plates that can be inserted below each floor level by sliding within small track brackets made of plexiglass (Figure 1C-1D).

Note: Behavioral testing is carried out either on the upper level (color mode) or the lower level (contrast mode) but not simultaneously on both levels.

- d. The center of the apparatus is a neutral area with no white translucent plate and no light source directly below it (Figure 1A-1C).
- e. Plastic transparent covers with perforated holes to help with breathing.

Note: Color vision and contrast sensitivity are different aspects of vision that involve different photoreceptors. While the contrast mode involves the function of rods (lower mesopic range), the color mode requires functional cones (transition between mesopic and photopic range). These two modalities of testing are complementary to appreciate the functionality of rod and cone photoreceptors.

3. Light-emitting diode (LED) lights (for color mode)

Each LED strip source consists of an array of surface-mounted device (SMD) 3528 LED chips evenly spaced in four rows (27 LED chips per row) and is individually inserted in each arm of the ViS4M, directly onto the glass base (Figure 1D). Spectra of the light sources were determined using an Ocean Optics USB2000 spectrometer and further validated with a Sekonic C700-U spectrometer (Figure 1E).

- a. Red monochromatic light: wavelength (λ) = 628 nm, full width at half maximum (FWHM) = 17 nm
- b. Green monochromatic light: λ = 517 nm, FWHM = 31 nm
- c. Blue monochromatic light: λ = 452 nm, FWHM = 22 nm
- d. White light: λ_1 = 441 nm, FWHM = 19 nm and λ_2 = 533 nm, FWHM = 104 nm

Note: The criterion for choosing the LED colors is as follows: the red light as a dark-space control arm with low- to no-color stimulus; the green light to stimulate the mouse retinal M-opsin in M-cones, without stimulating S-opsin; and the blue light to stimulate the mouse retinal S-opsin in S- and M-cones, in addition to the M-opsin.

The white LED is made of a blue-emitting diode that also excites a yellow-emitting phosphor [cerium doped yttrium aluminum garnet (Ce:YAG-Y₃Al₅O₁₂) crystals] embedded in the epoxy dome.

The following components control the brightness of the light stimuli.

- e. LED single color dimmers using pulse width modulation (PWM) technology
- f. Individual remote devices to control the dimmers

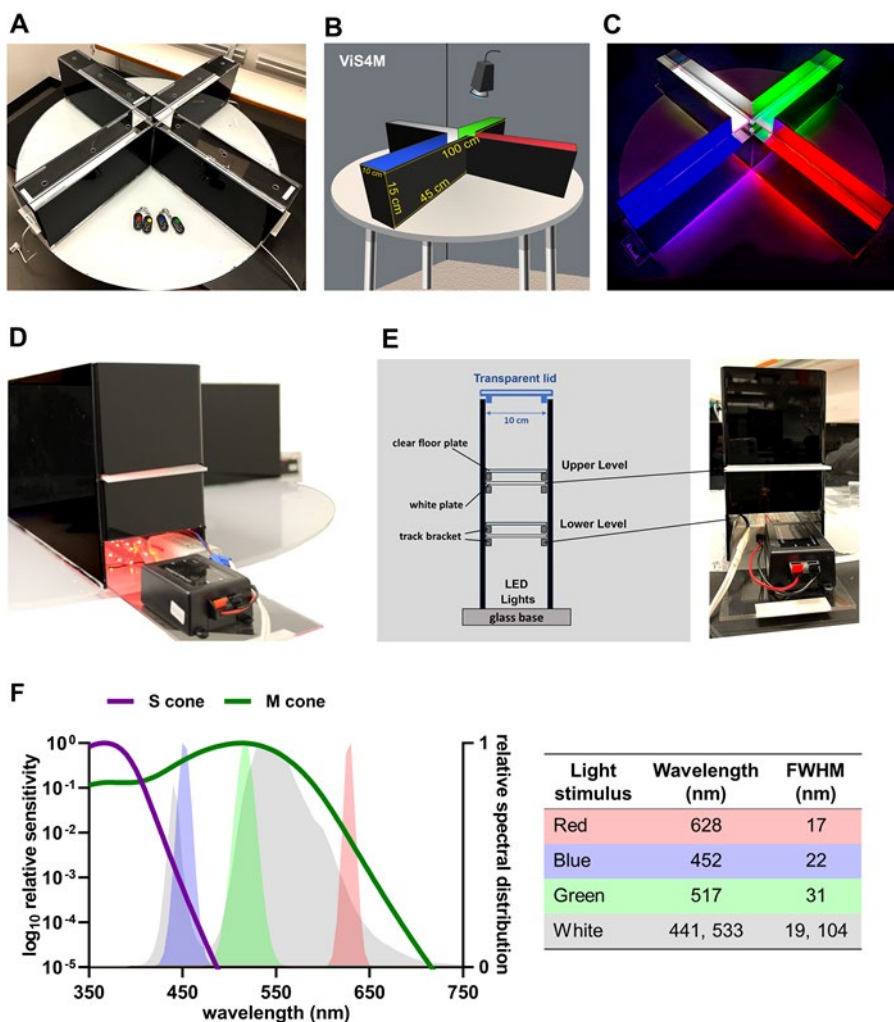


Figure 1. Characteristics of the ViS4M in color mode.

(A) Photograph and (B) illustration of the x-shaped ViS4M in color mode with apparatus measurements. (C) Photograph of the ViS4M in color mode, E condition, showing the illuminated arms. (D) Photograph of an arm with the opening for the red lights and with the white translucent plate inserted at the upper level. (E) Illustration of the positioning of the clear floor and white translucent diffuser plates within the arms of the maze, paired with a photograph of the outside front-view of an arm. (F) Spectral distribution of the LED sources according to mouse M- and S-opsins sensitivity with table showing the characteristics of the light stimuli (wavelength, FWHM).

4. Grayscale objects (for contrast mode)

Four objects have the following characteristics (Figure 2A)

- a. Identical shape of a right-angled triangular prism
 - b. Dimensions: base (adjacent side) = 5 cm; height (opposite side) = 1 cm
 - c. Different shades (black, gray, white, and clear) that create different contrasts with the black walls and white floors of the maze (Figure 2B)
- The luminance ratios of the objects against the black walls and/or white floors as measured with a light meter are indicated below
- d. Black object against the black walls = 1.06 (minimal to no contrast)
 - e. Gray object against the black walls = 6.00
 - f. White object against the black walls = 9.69 (high contrast against the black walls but minimal contrast with the white floor)
 - g. Clear object against the black walls = 6.56
 - h. Flexible positioning and location for the placement of the grayscale objects to accommodate investigator's goals

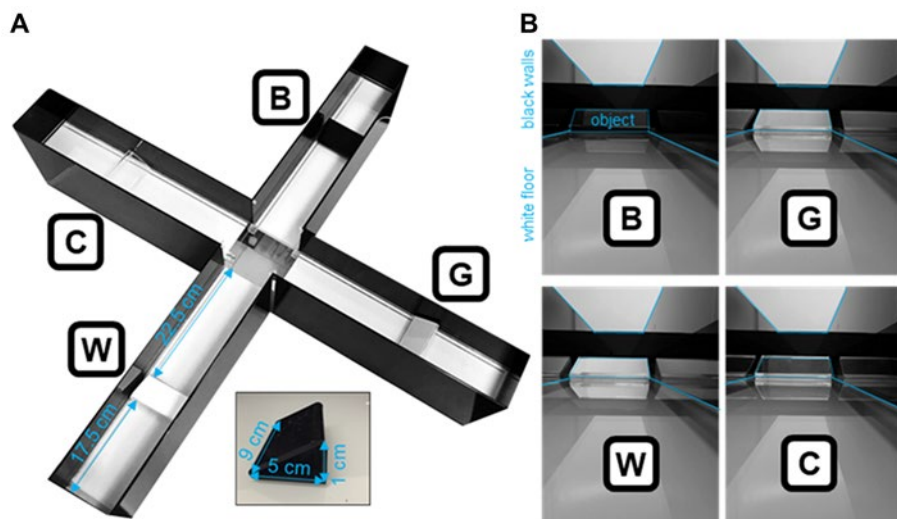


Figure 2. Characteristics of the ViS4M in contrast mode.

(A) Photograph of the ViS4M in contrast mode with measurements for positioning of the grayscale objects. (B) Photographs of the objects within each arm as seen from the center of the ViS4M. Objects, black walls, and white floors are delineated to better assess contrasts. (A-B) B, Black; C, Clear; G, Gray; W, White.

B. Other accessories

1. Sekonic Flashmate L-308S light meter (Sekonic, catalog number: 401-309)
2. Timer
3. Digital USB camera

Note: A color camera is preferable to identify the colored arms. However, a black and white camera can be used, provided the position of each arm on the screen is recorded. A short clip of the apparatus positioning can be made prior to each testing session with the lights of the room turned on and the arms identified by name.

4. USB camera varifocal lens with 2.8-12 mm focal length

Software

1. Rodent Toolbox V1 (freely available at <https://www.ndcn.ox.ac.uk/team/stuart-peirson>)
2. ANY-maze behavior tracking software 6.3 (www.stoeltingco.com/anymaze/video-tracking/software.html) or other video tracking software, such as EthoVision XT (www.noldus.com/ethovision-xt)
3. ViS4M Toolbox V1 (Supplementary file: [ViS4M Toolbox V1](#))
4. GraphPad Prism 9.0
5. ParallelSets V2 (freely available at [Parallel Sets \(eagereyes.org\)](http://Parallel Sets (eagereyes.org)))
6. Circos online (freely available at mkweb.bcgsc.ca/tableviewer/)

Procedure

A. Configuration of the ViS4M

1. Place the transparent floor inside the arms at the chosen level and insert the center zone transparent floor at the same level (color mode: upper level; contrast mode: lower level) (Figure 1C).
2. Position the clear plastic covers on top of the arms.
3. Slide the translucent white plates within the brackets below the floors (Figure 1D).
4. Set up the visual stimuli.
5. Color mode only: Install the LED light sources directly on top of the glass base in their respective arm (Figure 1D).

Note: The arrangement of the LED chips in combination with the white translucent plates and the clear covers is optimized to allow the light to diffuse equally in all directions and create a spatially homogenous stimulus. No individual LED spots are discernable.

6. Contrast mode only: position the grayscale objects individually, in the middle of their respective arm, on their base, with their opposite side facing at $\frac{1}{2}$ -length (22.5 cm) of the entrance of the arm (Figure 2A-2B)

B. Configuration of the light intensities according to the illumination conditions

1. Plug the light sources into a power outlet.
2. Turn on the lights using the individual remote controls, then turn off the ambient light of the room.
The following steps pertain to the use of a Sekonic Flashmate L-308S light meter to measure incident illuminance (page 19 of operating manual).
3. Attach the Lumidisc accessory to the light meter.
4. Set EV (Exposure Value) mode and ISO 100 on the device.
5. Position the flat surface of the light meter sensor facing and about 2 cm above the floor (mouse eye level) at a locus situated in the middle of the arm.

Note: The positioning of the sensor and locus of measurement were chosen for consistency and practicability, assuming the light coming from each LED source diffused in all directions equally into its respective arm.

6. Take the measurement.
7. Adjust the brightness of the light stimulus using the remote control and take a new measurement, if necessary.
8. Record the EV and proceed to the other three arms following steps 5 through 7.
9. Convert the recorded EV to illuminance units (lux) and luminance units (cd/m^2) using the relationships lux

$= 2.5 \times 2\text{EV}$ and $\text{cd}/\text{m}^2 = 2(\text{EV}-3)$, respectively.

Note: Illuminance and luminance are photometric measures of perceived brightness of a light source as it relates to the human eye according to the spectral sensitivity function. Although they provide informative characteristics of the light source to the human experimenter, they are irrelevant to the mouse visual system. Radiometric measures of irradiance should be used and can be estimated using the Rodent Toolbox V1 (freely available at <https://www.ndcn.ox.ac.uk/team/stuart-peirson>).

10. In the Rodent Toolbox V1 (under Toolbox tab), select the type of light source.
11. Enter the details (λ , FWHM) and illuminance (lux) of the light stimulus.
12. Record the estimated irradiance ($\mu\text{W}/\text{cm}^2$).

Note: In our original Scientific Reports manuscript (Vit et al., 2021), we describe five different conditions of illumination. For the purpose of this protocol, we provide data analysis from two out of these five configurations: Red High (RH) and Equal (E) conditions. Photometric and radiometric characteristics of these two conditions are shown in Table 1.

Table 1. Photometric and radiometric measures and estimations of the light stimuli

Red High				Equal				
	R	B	G	W	R	B	G	W
EV	5.4	1.9	4.7	6.0	4.9	4.9	4.9	4.7
Illuminance (lux)	103	9	66	164	76	75	73	67
Luminance (cd/m^2)	4.4	0.4	3.2	8.1	3.7	3.6	3.7	3.3
Irradiance ($\mu\text{W}/\text{cm}^2$)	52	29	14	40	38	244	17	16

From the measurements of EV (using the Sekonic L-308S light meter) to the calculation of estimated photometric (illuminance, luminance) and radiometric characteristics (irradiance) of the four light sources under RH and E conditions of illumination

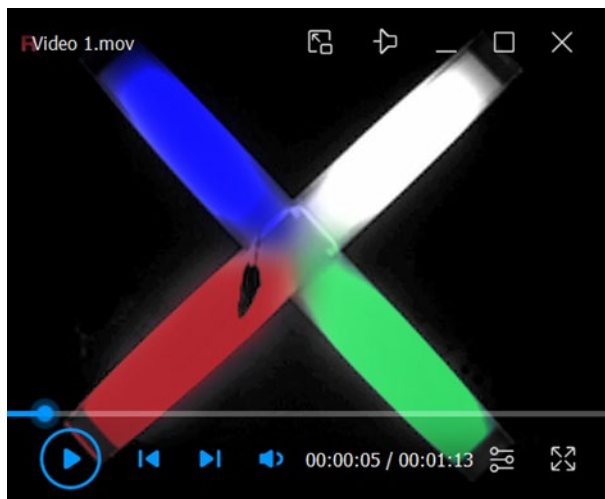
C. Configure the camera for video recording

1. Position the camera with the varifocal lens above the ViS4M.
2. Connect the camera to a laptop via USB port and open ANY-maze behavior tracking software.

Note: We do not track animal trajectory in real time. However, we use ANY-maze behavior tracking software to record and save video files of all testing sessions for later analysis. A free version of the software can be used for this purpose.

3. Use the varifocal lens so the entire apparatus fits the image.
4. Adjust the exposure to obtain acceptable contrast of the mouse over the background for tracking
5. Re-adjust the exposure in between each condition of illumination.

Note: A small portion at the end of the arms is significantly darker upon illumination as compared to the middle of the arms. To set the exposure, we use small black objects (remote controls) across the arms to verify contrast is sufficient in the entire apparatus.



Video 1. A video of a mouse exploring the ViS4M in the color mode.

The sequence of colored arm entries and alternations are indicated (speed $\times 2$).

D. Behavioral testing (Video 1)

1. Turn off the ambient light of the room.
2. (Contrast mode only) Turn on dim red-light illumination (mesopic, $\sim 0.1 \text{ cd/m}^2$).

Note: All testing takes place in the dark during the last third of the light cycle (between 4:00 pm and 8:00 pm). The sole light source is provided by the illuminated arms of the ViS4M. Mice are only tested once a day. Different conditions of testing (in color and contrast mode) are carried out on consecutive days.

3. Bring the mice to the testing room.
4. Leave the animals undisturbed for a short 30-min period of time to habituate to the dark room.

Note: We recommend tail-marking mice the day prior to testing for easy and fast identification. Since the lights of the testing room are turned off, a flashlight can be used if necessary.

5. At the end of the acclimation period, proceed with the testing of the first mouse.
6. Start the video recording and present the mouse ID to the camera.
7. Identify the mouse in its home cage and place it in the center of the maze through the opened top.
8. Cover the opened center of the apparatus with a clear plastic or Plexiglass plate and start the timer.
9. Leave the mouse to freely explore the maze for 5 min.

Note: We recommend counting the number of entries during testing. A minimum of eight entries is required to assure an appropriate number of four-arm alternations (see Data analysis for definition of parameters). In contrast mode, the presence of the objects does not prevent the mice from fully exploring the arms of the ViS4M. Most of the mice show no hesitation to jump over the objects to reach the distal part of the arms.

10. After 5 min, return the mouse to its home cage and pause the video recording.

11. Wipe the floors and walls with a solution of 70% isopropyl alcohol, then thoroughly wipe any excess of alcohol with a dry cloth.

Note: By the time the next mouse is placed in the apparatus following this procedure (~3 min, steps 6-7), any residual trace of alcohol will have evaporated.

12. Proceed with the next mouse following steps 6 through 10.

Data analysis

The data generated from behavioral testing in the ViS4M cover several behavioral domains. A list of parameters, behaviors, and analysis tools is shown in Table 2.

Table 2. List of analyzed parameters

Parameter	Behavior	Analysis tool
Distance traveled	Locomotion, general activity	ANY-maze
Average speed	Locomotion, general activity	ANY-maze
Total number of entries	Locomotion, general activity	ViS4M Toolbox V1
% spontaneous alternation	Cognition, color/contrast discrimination	ViS4M Toolbox V1
% time in each colored arm	Color/contrast preference	ANY-maze
% entries in each colored arm	Color/contrast preference	ViS4M Toolbox V1
% unidirectional transitions	Color/contrast discrimination	ViS4M Toolbox V1
% bidirectional transitions	Color/contrast discrimination	ViS4M Toolbox V1

We created the ViS4M Toolbox V1, two Excel spreadsheets made available freely with this protocol. Upon entering the sequence of arm entries recorded from video files (see Video 1), the ViS4M Toolbox V1 calculates the total number of entries, the percentage of spontaneous alternation, the percentage of entries in each colored arm, as well as the percentages of unidirectional and bidirectional transitions between arms.

All the cells in the spreadsheet that pertain to the identification of the study, the mice, and the condition of testing (columns A through F) are unlocked and can be filled according to the user's experiment.

The text sequence of arm entries is entered in column G in lower case. The keys differ in the two spreadsheets: 'r' for 'red,' 'b' for 'blue,' 'g' for 'green,' 'w' for 'white' in the color toolbox, and 'c' for 'clear,' 'b' for 'black,' 'g' for 'gray,' 'w' for 'white' in the contrast toolbox. All the cells with calculated parameters are locked to prevent the inclusion of errors.

Additional information specific to these parameters and their calculation in the ViS4M Toolbox V1 is detailed below as well as in Table 3.

Note: Alternatively, the user can choose to calculate these parameters directly in a video tracking software. However, the use of definitions other than those described below will lead to discrepancies with the data generated in the ViS4M Toolbox V1.

Table 3. Description of parameters and calculations

Parameters	wrbwgrrgrwbgrwbgrgbwbr characters (x)	n	Calculation
entries (e)	_eeeeeeeeeeeeeeeeeee	$e = x - 1$	20
4-arm sequences (s)	---ssssssssssssssss	$s = e - 2$	18

-rbwg --bwgr -----wrbg -----bgrw -----grwb -----rwbg -----wbgr -----rgwb -----gwbr			
alternation (a)	9	$\% a = (a \times 100) \div (e - 2)$	50%
red entries (r)	7	$\% r = (r \times 100) \div e$	35%
blue entries (b)	4	$\% b = (b \times 100) \div e$	20%
green entries (g)	5	$\% g = (g \times 100) \div e$	25%
white entries (w)	4	$\% w = (w \times 100) \div e$	20%
2-arm transitions (t)	-ttttttttttttttttttttttt	$t = e$	20
red-to-blue ($r \rightarrow b$)	-rb-----rb-----	2	$\% r \rightarrow b = (r \rightarrow b \times 100) \div t$
blue-to-red ($b \rightarrow r$)	-----br-----	1	$\% b \rightarrow r = (b \rightarrow r \times 100) \div t$
bidirectional ($r \leftrightarrow b$)		3	$\% r \leftrightarrow b = \% r \rightarrow b + \% b \rightarrow r$
red-to-green ($r \rightarrow g$)	-----rg-----rg---	2	$\% r \rightarrow g = (r \rightarrow g \times 100) \div t$
green-to-red ($g \rightarrow r$)	-----grgr---gr---gr---	4	$\% g \rightarrow r = (g \rightarrow r \times 100) \div t$
bidirectional ($r \leftrightarrow g$)		6	$\% r \leftrightarrow g = \% r \rightarrow g + \% g \rightarrow r$
red-to-white ($r \rightarrow w$)	-----rw---rw-----	2	$\% r \rightarrow w = (r \rightarrow w \times 100) \div t$
white-to-red ($w \rightarrow r$)	wr-----wr-----	2	$\% w \rightarrow r = (w \rightarrow r \times 100) \div t$
bidirectional ($r \leftrightarrow w$)		4	$\% r \leftrightarrow w = \% r \rightarrow w + \% w \rightarrow r$
blue-to-green ($b \rightarrow g$)	-----bg--bg-----	2	$\% b \rightarrow g = (b \rightarrow g \times 100) \div t$
green-to-blue ($g \rightarrow b$)	-----	0	$\% g \rightarrow b = (g \rightarrow b \times 100) \div t$
bidirectional ($b \leftrightarrow g$)		2	$\% b \leftrightarrow g = \% b \rightarrow g + \% g \rightarrow b$
blue-to-white ($b \rightarrow w$)	--bw-----	1	$\% b \rightarrow w = (b \rightarrow w \times 100) \div t$
white-to-blue ($w \rightarrow b$)	-----wb---wb-	2	$\% w \rightarrow b = (w \rightarrow b \times 100) \div t$
bidirectional ($b \leftrightarrow w$)		3	$\% b \leftrightarrow w = \% b \rightarrow w + \% w \rightarrow b$
green-to-white ($g \rightarrow w$)	-----gw--	1	$\% g \rightarrow w = (g \rightarrow w \times 100) \div t$
white-to-green ($w \rightarrow g$)	---wg-----	1	$\% w \rightarrow g = (w \rightarrow g \times 100) \div t$
bidirectional ($g \leftrightarrow w$)		2	$\% g \leftrightarrow w = \% g \rightarrow w + \% w \rightarrow g$

From a text sequence to entries, alternation, and transitions: example entered in the ViS4M Toolbox V1.

E. Total entries

Instrumental to obtaining an accurate arm sequence is the definition of arm entry. We implement the following rules when recording arm entries:

1. In general, while exploring the maze, mice enter an arm, then walk within the arm until they reach the other end (dead-end), turn around, exit the arm, and visit another arm (see Video 1). In this case, this is straightforward, and we count an entry as the entire body of the mouse (tail not included) crossing the virtual border between the squared center and the open end of the arm.

2. There are occurrences when mice enter the arm as described above but do not reach the end of the arm (see Video 1). Whether these events should be counted as entries is difficult to generalize to the entire population or a specific group of mice. We include these entries or not after careful review of video files. For consistency, we do not make our choice at the entry level; thus, for a particular mouse, we either count all or do not count any of this type of entry.
3. Two or more consecutive entries in the same arm are counted as one entry. (Alternatively: account re-entries as multiple entries but ensure consistency within the same experiment.)

Note: There are several reasons why we counted consecutive entries in the same arm as a single entry. First, they are infrequent events (5%). Second, to our knowledge, it is customary to analyze revisiting the same arm as a single entry with similar mazes, such as the Y-maze. Third, it would not alter the sequence of exploration in terms of color or contrast cues. Lastly, accounting for them considerably complicates the combinations for successful and unsuccessful alternations, requires analyzing 5-arm sequences (for example, the sequences 'brgw' and 'brrgw' are both successful alternations between the 4 colors), and consequently increases the possibility of calculation errors.

4. The first entry of the sequence is not counted. Indeed, when the mouse is released in the center of the maze at the beginning of the test, it often runs inside the arm it is facing, and this is not considered a deliberate choice.

Note: Although the first arm in the sequence is not counted as an entry, it is taken into consideration for the first alternation and first transition.

The total number of entries can be used as an indicator of locomotor activity since it predicts with high fidelity the distance traveled ($R^2 = 0.8275, P < 0.0001$) and the average speed ($R^2 = 0.8317, P < 0.0001$) of the animal estimated with the tracking software ANY-maze (Figure 3A). The coefficient factor of 1.1 between entries and distance corresponds to twice the sum of the lengths of an arm and the center of the maze [$((0.45 \text{ m} + 0.10 \text{ m}) \times 2) = 1.1 \text{ m}$].

Note: The distance traveled and the average speed are two basic features of most tracking software; consequently, their estimation using ANY-maze is not described in the present protocol.

F. Alternation

Perhaps the main feature of the ViS4M is its capability to assess both cognition and visual function. Spontaneous alternation is defined as the consecutive visits of the four different arms without returning to an arm already visited in a four-arm sequence (see Video 1). In standard three-arm models such as the Y-maze or the T-maze, the percentage of spontaneous alternation (number of alternations out of total number of three-arm sequences during the testing session) represents spatial navigation and working memory (Kraeuter *et al.*, 2019).

The following are characteristics of four-arm sequences and alternations in the four-arm ViS4M (see also Table 3).

1. The first four-arm sequence is counted at the third arm entry, and each subsequent entry adds a new four-arm sequence.
2. From a specific starting arm, there are 6 alternation sequences out of 27 four-arm sequence possibilities (total in the entire apparatus: 24 alternations out of 108 possible sequences). Thus, the chance to perform an alternation in a four-arm sequence is 2/9 or about 22%.

When introduced to a uniformly configured ViS4M (NS, no stimulus), WT mice alternate about 10% above chance (Figure 3B). However, when the four arms are set with predefined light modalities or grayscale objects, the percentage of alternation is significantly increased to about 50% as compared to NS (Stimulus, $F(2.599, 38.98) = 5.007, P = 0.0069$) in these same mice (Figure 3B). This result suggests that cognitively and visually intact mice use the visual stimuli of the ViS4M as cues to navigate the maze, and are consequently able to discriminate between some or all of the arms, based on differences in chromaticity, brightness, and/or contrast.

AD^+ mice are largely inept to alternate as early as 8.5 months up to 18 months of age when compared to WT littermates (Figure 3C) in color mode, under RH (Genotype, $F_{(1,69)} = 35.31, P < 0.0001$) and E conditions (Genotype, $F_{(1,67)} = 38.14, P < 0.0001$), and in contrast mode (Genotype, $F_{(1,71)} = 57.90, P < 0.0001$), suggesting visual and/or cognitive deficits (see discussion in Vit *et al.*, 2021). There is no significant difference in alternations between males and females within each genotype at any age in RH, E, and CT conditions (Figure 3D). However, in color mode, while the impairment appears earlier in male (8.5 months) than in female (13–18 months) AD^+ mice compared to gender-matched WT mice (Figure 3D), the progression with age is more noticeable in female AD^+ mice, with a dramatic decline in alternation between 8.5 and 18 months, especially under E condition (Age, $F_{(2,26)} = 4.312, P = 0.0241$). In contrast mode, early deficits appear in both male and female AD^+ mice (Figure 3D). Between 8.5 and 18.5 months, decline in contrast sensitivity is most apparent in WT mice (Genotype \times Age, $F_{(2,71)} = 3.869, P = 0.0254$), independently of gender (Figure 3C–3D).

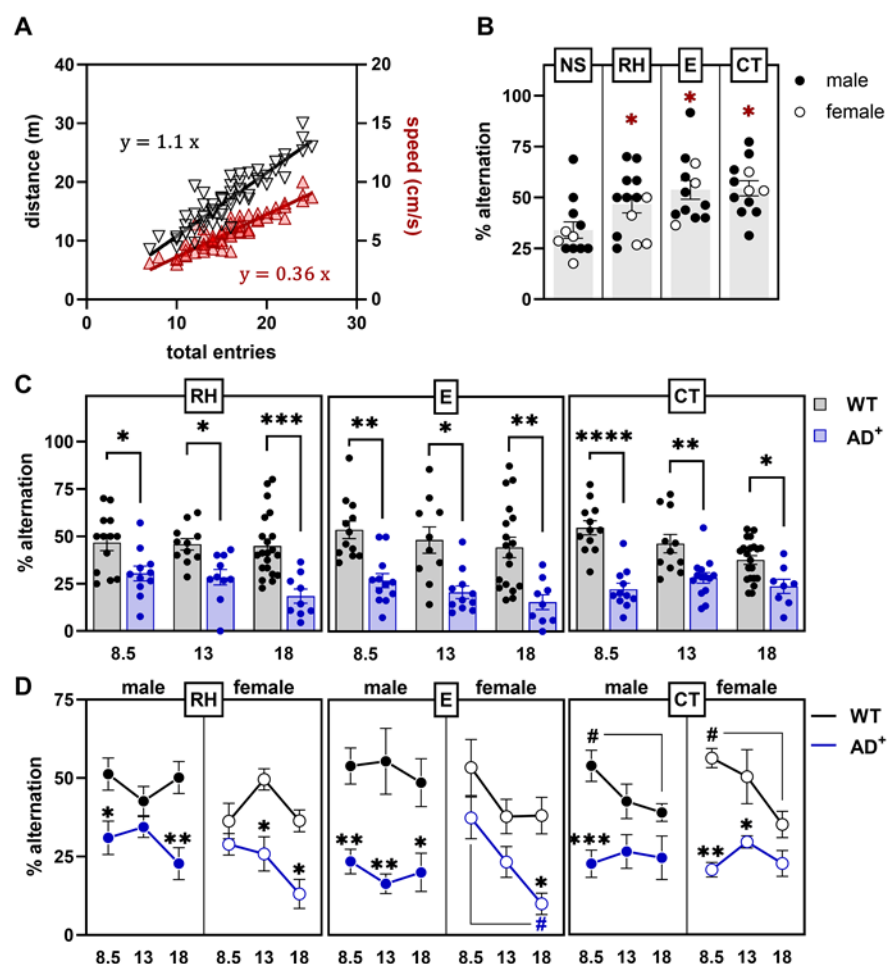


Figure 3. Spontaneous alternation with and without color illumination.

Linear regression of the total number of arm entries during a 5-min testing session, with the distance traveled in the ViS4M and the average speed of mice. (B) Percentages of alternation in the ViS4M without stimuli (NS, no stimulus), with color illumination (RH, red high; E, equal), or with grey-scale objects (CT, contrast) of young adult (8.5 months) WT mice. * $P < 0.05$, NS versus RH, E, CT modes. (C) Percentages of alternation in 8.5-, 13-, and 18-month-old WT and AD^+ mice under RH, E, and CT conditions. * $P < 0.05$, ** $P < 0.01$, *** $P < 0.001$, **** $P < 0.0001$, WT versus AD^+ mice. (D) Percentages of alternation in 8.5-, 13-, and 18-month-old male and female WT and AD^+ mice

under RH, E, and CT condition. * $P < 0.05$, ** $P < 0.01$, gender-matched WT versus AD⁺ mice; # (WT) or # (AD+) $P < 0.05$, 8.5 versus 18 months.

Additional characteristics of alternation are listed below.

3. The sequences of alternations can be categorized into three pathways as shown in Table 4 and as illustrated in Figure 4A-4B.
4. In each pathway, alternation sequences can start at each of the four arms and in two directions, leading to eight combinations (Figure 4C). The lack or the abundance of an alternation sequence starting at a specific arm can indicate the position of discontinuities within a pathway of alternation.
5. In the ViS4M, the paths are: ① ($\overleftarrow{R} \leftrightarrow B \leftrightarrow G \leftrightarrow W$), ② ($\overleftarrow{R} \leftrightarrow G \leftrightarrow B \leftrightarrow W$), and ③ ($\overleftarrow{R} \leftrightarrow B \leftrightarrow W \leftrightarrow G$) (Table 4 and Figure 4B).

Table 4. Classification of pathways of alternation and four-arm sequences

Parameters	wrbwggrgrwbgrwbgrgwbr _eeeeeeeeeeeeeeeeeee	n	Calculation	
entries (e)				20
4-arm sequences (s)	---ssssssssssssssssss	$s = e - 2$		18
4-arm alternation (a_4)	-rbwg --bwgr -----wrbg -----bgrw -----grwb -----rwbg -----wbgr -----rgwb -----gwbr	9	% $a_4 = (a_4 \times 100) \div (e - 2)$	50%
path① $\overleftarrow{r} \leftrightarrow b \leftrightarrow g \leftrightarrow w$	-----wrbg	1	% ① = (① $\times 100) \div a_4$	12%
path② $\overleftarrow{r} \leftrightarrow g \leftrightarrow b \leftrightarrow w$	-----bgrw -----grwb -----rwbg -----wbgr	4	% ② = (② $\times 100) \div a_4$	44%
path③ $\overleftarrow{r} \leftrightarrow b \leftrightarrow w \leftrightarrow g$	-rbwg --bwgr -----rgwb -----gwbr	4	% ③ = (③ $\times 100) \div a_4$	44%
3-arm alternation (a_3)	wrbw -----rbgr	2	% $a_3 = (a_3 \times 100) \div (e - 2)$	11%
2/3-arm alternation ($a_{2/3}$)	---wgrg ----rgrw -----grwr -----rwrb -----bgrg -----grgw	6	% $a_{2/3} = (a_{2/3} \times 100) \div (e - 2)$	33%
2-arm alternation (a_2)	----grgr	1	% $a_2 = (a_2 \times 100) \div (e - 2)$	6%

Categories (4-arm, 3-arm, 2/3-arm, and 2-arm alternations) and subcategories (pathways **1**, **2**, and **3** of alternation): same example as in Table 3.

The detailed analysis of alternation sequences of 8.5-month-old WT and AD⁺ mice under the RH condition is presented in Figures 4B and 4C. The stacked bar graph with individual data points [Path **1** (○), Path **2** (□), Path **3** (▽)] in Figure 4B shows that WT mice more frequently alternate in path **3**, as opposed to paths **1** and **2**, while AD⁺ mice alternate mostly in paths **1** and **2** (Genotype × Path, $F_{(2,44)} = 14.50, P < 0.0001$). Within path **3**, AD⁺ mice are not or rarely capable of completing an alternation when starting from the red or the blue arm as opposed to WT mice (Genotype, $F_{(1,22)} = 30.34, P < 0.0001$).

We use parallel sets charts to visualize sequences of alternation. Figure 4C illustrates the alternation pathway **3** of WT and AD⁺ mice under RH condition. WT mice (green ribbons) show eight ribbons of equal proportion, corresponding to the eight possible alternations in this pathway. AD⁺ mice (purple ribbons) only exhibit limited sequences of alternations, suggesting deficient discrimination between colored arms. Overall, these data point out an incapacity of AD⁺ mice to visit the green, white, and blue arms successively, suggesting difficulties in discriminating between these three arms.

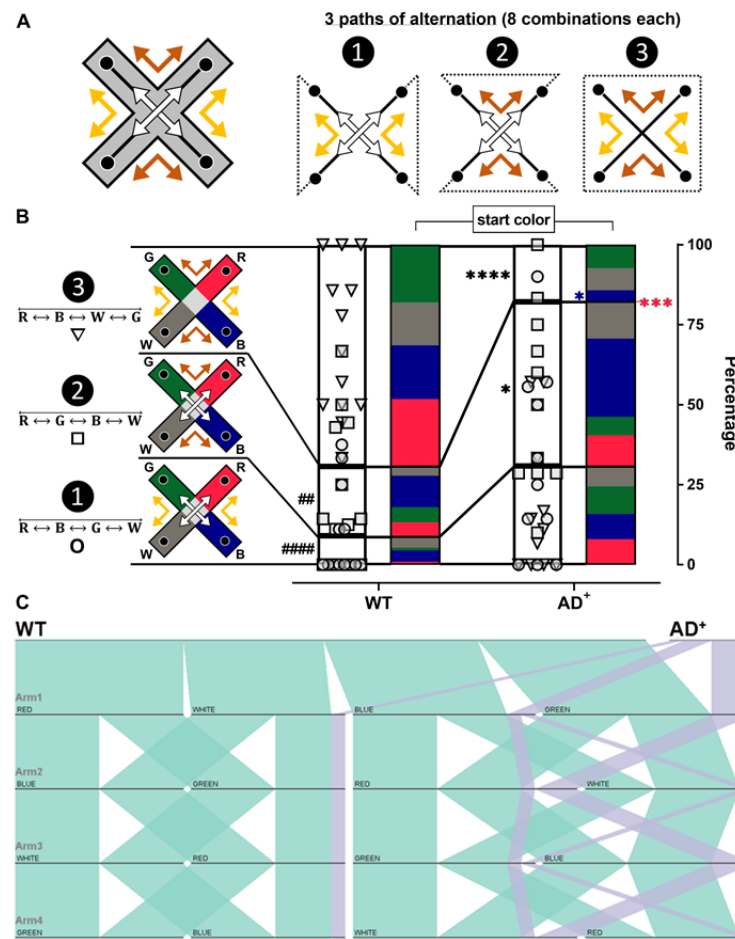


Figure 4. Arm sequence analysis of alternations in the color mode test.

(A) Illustration of the 3 pathways of alternation in the ViS4M. (B) Proportions of the three pathways and their starting arm in 8.5-month-old WT and AD⁺ mice under RH condition. Alternation sequence pathways are shown as stacked bars with individual data points. Path **1** (○), Path **2** (□), Path **3** (▽).

(∇). ## $P < 0.01$, ##### $P < 0.0001$, WT mice, Paths ① and ② versus Path ③; * $P < 0.05$, *** ** $P < 0.0001$, Paths ② and ③, WT versus AD⁺ mice; ** * $P < 0.001$, Path ③, red arm start, WT versus AD⁺ mice; * $P < 0.05$, Path ③, blue arm start, WT versus AD⁺ mice. (C) Visualization of alternation sequences in 8.5-month-old WT (green ribbons) and AD⁺ mice (purple ribbons) under RH condition (Path ③ ($R \leftrightarrow B \leftrightarrow W \leftrightarrow G$) using parallel sets chart.

Since alternations only account for approximately 50% and 20% of all four-arm sequences in WT and AD⁺ mice, respectively, we further analyze 4-arm sequences. In addition to the 4-arm alternations, we categorize aborted alternations as follows (see Table 4):

1. 3-arm alternations correspond to the consecutive exploration of 3 different arms, followed by the re-entry in the first arm of the sequence, such as $\overleftarrow{A} \leftrightarrow B \leftrightarrow C \leftrightarrow \overrightarrow{A}$
2. 2/3-arm alternations correspond to the visits of 3 different arms but not in a consecutive manner, such as $\overleftarrow{A} \leftrightarrow B \leftrightarrow A \leftrightarrow \overrightarrow{C}$
3. 2-arm alternations are the exploration of only 2 arms in a 4-arm sequence, such as $\overleftarrow{A} \leftrightarrow B \leftrightarrow A \leftrightarrow \overrightarrow{B}$
In contrast mode, 8.5-month-old AD⁺ mice show a significant decrease of 4-arm alternations and concomitant increase of 2/3-arm and 2-arm alternations (Figure 5A) when compared to age-matched WT mice (Genotype \times Sequence, $F_{(3, 69)} = 14.38$, $P < 0.0001$). We further classify aborted alternations (3-arm and 2/3-arm alternations) into pathways of alternations (Figure 4A) as we do for full 4-arm alternations. 3-arm alternations contain sequences from two pathways and correspond to a change of path during exploration.
4. 2/3-arm alternations represent changes of direction within a path.
While AD⁺ mice show a general decrease of all three pathways for 4-arm alternations and increase for 2/3-arm alternations, the change in 3-arm alternations is specific to path ③ (Genotype \times Path, $F_{(8, 184)} = 2.770$, $P = 0.0065$). Parallel sets charts show the detailed sequences in path ③ of 4-arm and 2/3-arm alternations under contrast mode for 8.5-month-old WT and AD⁺ mice (Figure 5B).

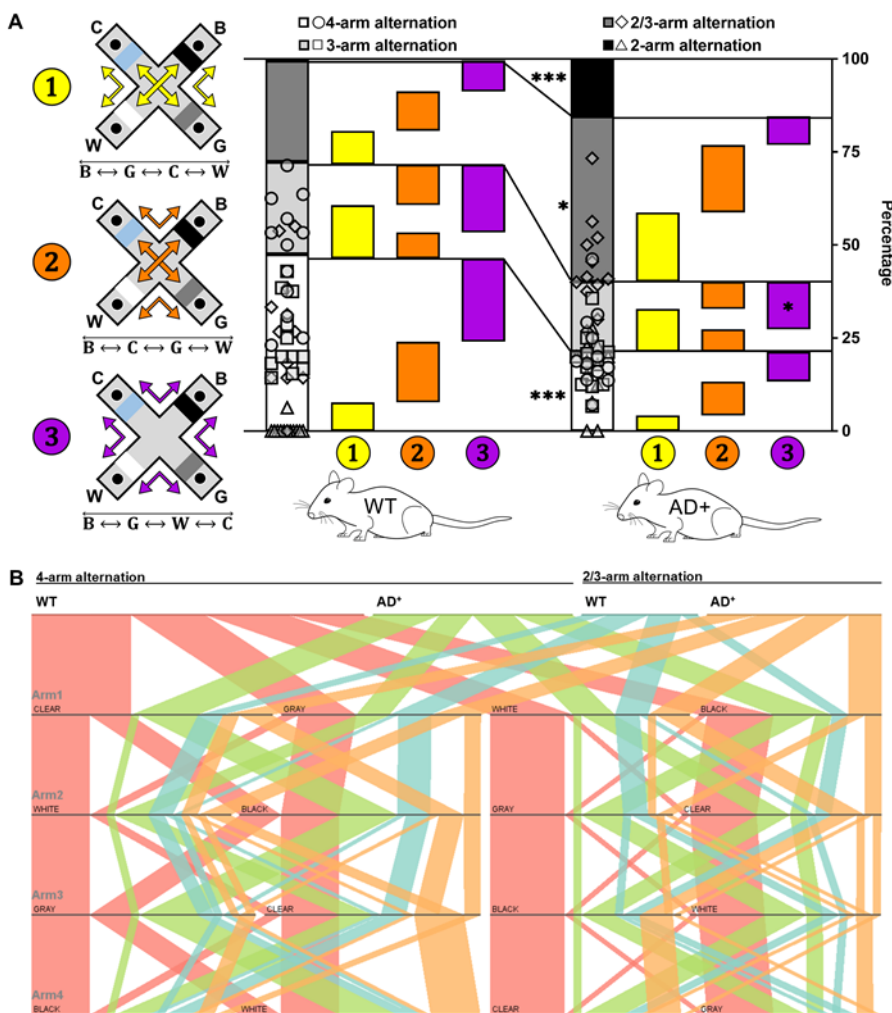


Figure 5. Four-arm sequence analysis in the contrast mode test.

(A) Proportions of the four types of 4-arm sequences and distributions of the three pathways for 8.5-month-old WT and AD⁺ mice in the contrast mode. 4-arm alternations (○), 3-arm alternations (□), 2/3-arm alternations (◇), 2-arm alternations (△). * $P < 0.05$, *** $P < 0.001$, WT versus AD⁺ mice. (B) Visualization of 4-arm (WT: red ribbons; AD⁺: green ribbons) and 2/3-arm alternations (WT: blue ribbons; AD⁺: orange ribbons) in 8.5-month-old WT and AD⁺ mice in the contrast mode (Path ❸ $\overleftarrow{B} \leftrightarrow G \leftrightarrow W \leftrightarrow C$) using parallel sets charts.

G. Percentages of time and entries in colored arms

Arm preferences are measured as percentages of time and entries in the differently configured arms. As shown in Figure 6A-6C, between RH and E conditions with different irradiance levels, the proportion of arm visits differ in WT mice. Overall, the red arm, seen as a dark area, is preferred across all conditions of illumination (Figure 6B-6C and see Vit *et al.*, 2021). The difference between conditions occurs essentially in the exploration of the blue, green, and white arms (Figure 6B-6C). While under RH condition these three arms are visited equally, under E condition, when the intensity of the blue source is dramatically increased, the blue becomes the least visited (Time: Condition × Color, $F(1.876, 20.63) = 6.069, P = 0.0094$; Entries: Condition × Color, $F(1.730, 52.49) = 6.826, P = 0.0035$). These results further validate that the mice use the lights as cues to navigate the ViS4M.

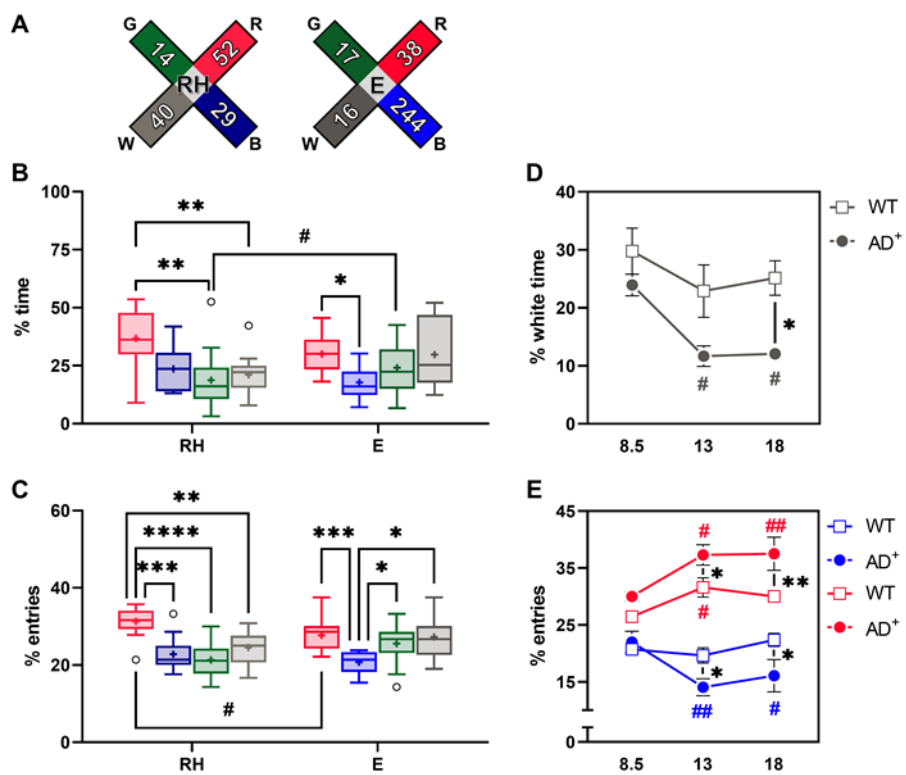


Figure 6. Time and entries in colored arms.

(A) Illustration of the RH and E conditions with measured irradiances in $\mu\text{W}/\text{cm}^2$. (B) Percentages of time spent in each colored arm of young adult (8.5 months) WT mice under RH and E conditions. (C) Percentages of entries in each colored arm of young adult (8.5 months) WT mice under RH and E conditions. (B-C) * $P < 0.05$, ** $P < 0.01$, *** $P < 0.001$, **** $P < 0.0001$, Red versus Blue versus Green versus White arms; # $P < 0.05$, RH versus E conditions. (D) Percentages of time spent in the white arm of 8.5-, 13- and 18-month-old WT and AD⁺ mice under E condition. (E) Percentages of entries in the red and blue arms of 8.5-, 13- and 18-month-old WT and AD⁺ mice under E condition. (D-E) * $P < 0.05$, WT versus AD⁺ mice; # $P < 0.05$, ## $P < 0.01$, 8.5 versus 13 and 18 months.

The ViS4M allows the detection of avoidance of both the white and the blue arms by AD⁺ mice under E condition, as shown by the percentage of time spent in the white arm (Genotype, $F_{(1, 67)} = 13.28, P = 0.0005$; Age, $F_{(2, 67)} = 5.004, P = 0.0094$) and the percentage of entries in the blue arm (Genotype \times Age, $F_{(2, 57)} = 3.541, P = 0.0355$) when compared to WT mice (Figure 6D-6E). These results could indicate an age-dependent hypersensitivity of AD⁺ mice to light that is related to its wavelength rather than its absolute irradiance. In humans, AD is associated with both the degeneration of intrinsically photosensitive melanopsin-containing retinal ganglion cells (ipRGCs) and a loss of the pupillary light reflex (PLR), which may give rise to higher light sensitivity.

H. Transitions between arms

Since WT mice tend to alternate between the four arms of the ViS4M in presence of light stimuli, we speculate that transitions between arms could potentially indicate their discrimination between color, light intensity, and/or contrast.

Below are definitions of unidirectional and bidirectional transitions (see example and calculations in Table 3).

1. Unidirectional transitions are defined as the movements from an arm to the following arm in a sequence.
2. From each arm, there are 3 possible destinations, which gives a total of 12 unidirectional transitions.

As presumed from the alternation sequence analysis, the comprehensive study of overall unidirectional transitions highlights visual deficits of AD⁺ mice in discrimination of the white, blue and green light stimuli (Genotype \times Transition, $F_{(3, 89)} = 9.469, P < 0.0001$) under RH condition (Figure 7). AD⁺ mice are less likely to transition between the blue and white arms in both directions, and between the green and white arms, especially from green to white when compared to WT mice (Figure 7A). However, they favor straight-line transitions between the blue and green arms (Figure 7A), likely reflecting repetitive/impulsive behavior. These results support the preferential use of the path ③ of alternation in WT mice and paths ① and ② in AD⁺ mice (Figure 4B-4C).

We use chord diagrams to visualize unidirectional transitions between colored arms. The diagrams are created using the freely available Circos online software. The following rules describe our chord diagrams for unidirectional transitions (Figure 7B):

- The segments correspond to and are colored as the four arms of the ViS4M.
- The ribbons between segments represent unidirectional transitions and are colored as the originating arm.
- Ribbon caps are added at the start to better appreciate their destination.
- The most frequent (fourth quartile) and the least frequent (first quartile) transitions are presented on separate diagrams to prevent an overload of ribbons.

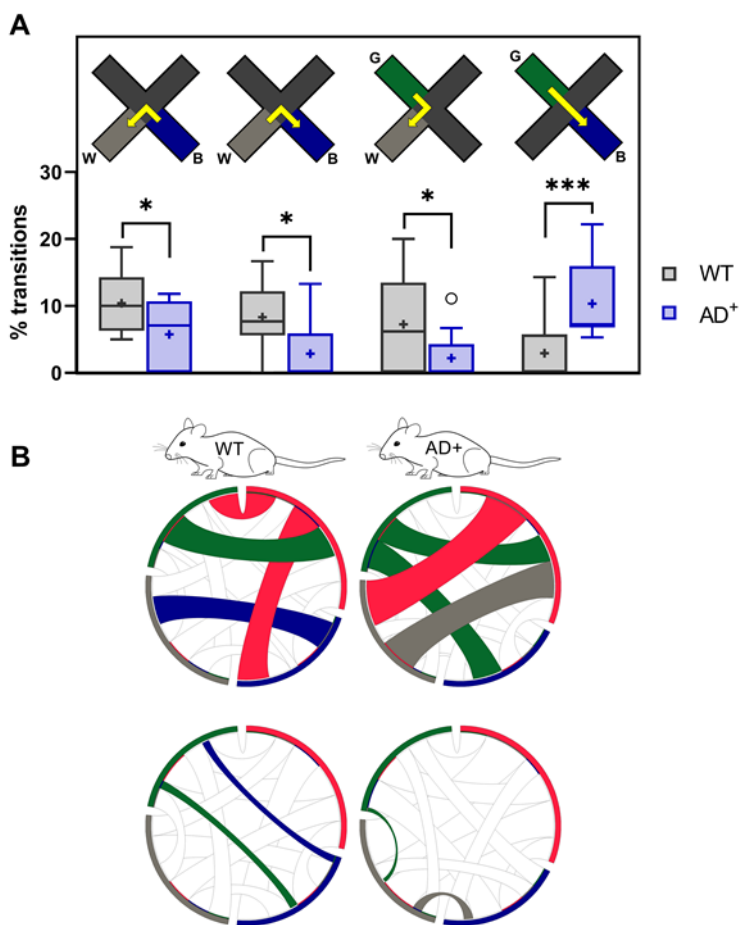


Figure 7. Unidirectional transitions in 8.5-month-old WT and AD⁺ mice under RH condition.

(A) Percentages of B→W, W→B, G→W, and G→B transitions. * $P < 0.05$, *** $P < 0.001$, WT versus AD⁺ mice. (B) Chord diagrams of the most frequent (top) and least frequent (bottom) unidirectional transitions.

The following pertains to the description of bidirectional transitions.

3. Bidirectional transitions are the transitions between two arms in both directions.
 4. The transitions between two arms in both directions do not need to be consecutive to be counted as bidirectional (see red-green transitions in Table 3).
 5. There are a total of 6 bidirectional transitions.
 6. Bidirectional transitions do not take into account preferences to transition in one particular direction.
 7. They are less likely to represent choices based on differences in absolute irradiance.
- For bidirectional transitions, all ribbons are color-coded to correspond to the heat-map chart (Figure 8A-8B) as follows:
- a. Black = first quartile (least frequent)
 - b. Grey = second quartile
 - c. White = third quartile
 - d. Orange = fourth quartile (most frequent)

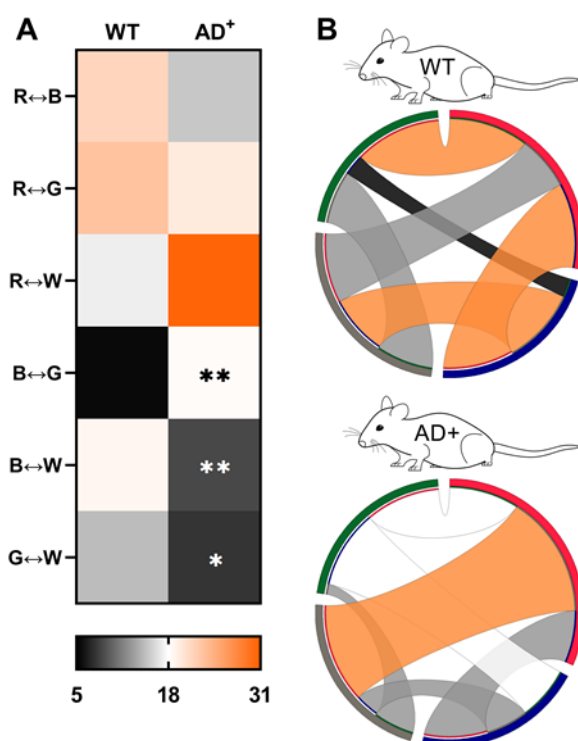


Figure 8. Bidirectional transitions in 8.5-month-old WT and AD⁺ mice under RH condition.

(A) Heat map of R↔B, R↔G, R↔W, B↔G, B↔W, and G↔W transitions. * $P < 0.05$, ** $P < 0.01$, WT versus AD⁺ mice. (B) Heat map-coded chord diagrams from the most frequent (orange) to the least frequent (black) bidirectional transitions.

Bidirectional transitions confirm results from alternation sequences and unidirectional transitions analysis. The low percentage of transitions between the blue and green arms in WT mice is expected due to the small difference in irradiance between these two arms (Table 2). It would also mean that WT mice cannot distinguish between the blue and green arms based on chromaticity, which suggests that under the RH condition, the blue light stimulus intensity is below the threshold of activation of the “true” S-cones required for color opponency in mice. However, WT mice are fully able to transition between the blue and white, and green and white arms, with the white arm only slightly brighter than the blue and green arms (the difference of absolute irradiance between the blue and white is even smaller than between the blue and green arms), suggesting that

discrimination is likely based on chromaticity, and indicating that the intensity of the white light stimulus is sufficient to activate “true” S-cones as opposed to blue light.

I. Correlations

We use linear regression to determine how closely related alternations and transitions are, which could indicate the contributions of cognition and visual function to the behavior seen in the ViS4M.

As previously shown (Vit *et al.*, 2021), under the RH condition, alternations and green-white transitions are tightly correlated in both 8.5 month-old WT and AD⁺ mice (Figure 9A). In addition, in WT but not AD⁺ mice alternations are inversely proportional to red-white transitions (Figure 9B). This is consistent with the preference of path ③ in WT mice and path ① in AD⁺ mice. Here, we demonstrate this by the direct positive relationship of green-white transitions to the paths ① and ③ of alternation in AD⁺ and WT mice, respectively (Figure 9C). Moreover, as expected, green-white transition increase correlates with a decrease in path ② in both groups of mice (Figure 9D), indicating the importance of this type of transition, at least under the RH condition of illumination. Interestingly, blue-white transitions did not have any sort of relationship with alternation in AD⁺ mice, showing their limiting effect on color discrimination under RH condition. This is further demonstrated with the parallel sets chart of path ① in 8.5-month-old WT and AD⁺ mice under RH condition (Figure 9E).

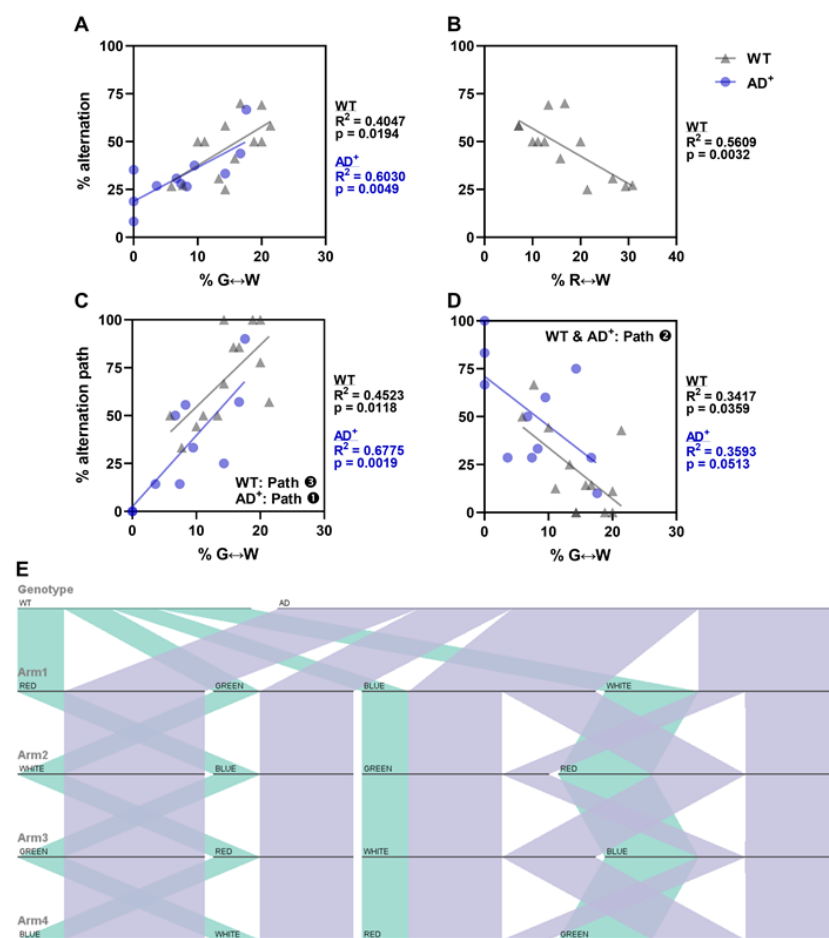


Figure 9. Correlations of alternation performance in 8.5-month-old WT and AD⁺ mice under RH condition.

(A-B) Linear regressions of spontaneous alternation with bidirectional transitions between the green and white arms (A) or between the red and white arms (B). (C-D) Linear regressions of alternation pathways ① and ③ (C), or alternation pathway ② (D) with bidirectional transitions between the green and white arms. (E) Visualization of alternation sequences in 8.5-month-old WT and AD⁺ mice under RH condition (Path ① R↔B↔G↔W) using parallel sets chart.

Notes

In the present manuscript, we sought to provide a detailed but non-exhaustive analysis of our data and share tools that we found helpful to uncover vision deficiencies in AD⁺ mice. We highlight the multi-functionality of the ViS4M. Indeed, we showed that the visual x-maze can be used to measure:

1. Cognitive ability and working memory directly linked to visual function: spontaneous alternation under different conditions of illumination. The ViS4M could offer a great advantage over other cognitive tests that also rely on visual cues and for which locomotor activity can be a bias, such as the Barnes maze. Indeed, in the ViS4M, spontaneous alternation is less likely to be affected by general activity of the animals. In addition, the total number of entries provides an internal control for activity; thus, adding another behavioral test for locomotor activity, such as the open field test, is not necessary.
2. Color and contrast discrimination: arm transitions, alternation sequence analysis. The light stimuli that we chose in our study do not allow us to separate the contribution of S-opsins versus M-opsins. We decided not to use UV lights in our study for obvious safety concerns for the experimenter and the mice. However, future studies may take advantage of the modulatory features of ViS4M and replace blue with UV LEDs, to confirm behavior directly related to S-cone activation and color discrimination. Even though brightness is a confounding factor, our findings support that color (wavelength) discrimination has a key role in mouse visual behavior and in AD⁺ mice deficiency. Although our conditions of illumination can provide a helpful starting point for the design of experiments, the use of the ViS4M is not limited to these settings. We encourage investigators to configure the intensities of the light according to their research goal.
3. Photosensitivity: percentages of time spent/entries in the different arms. We provide evidence that the ViS4M is able to detect simple innate responses to dark (overall preference for the red arm) and bright lights (avoidance of the blue arm). The ViS4M could provide an alternative to the light-dark box test in models of photophobia and anxiety with the possibility to control the brightness of each stimulus.
4. Even though not tested in our study, the ViS4M offers the possibility to pair a light stimulus to an aversive footshock. Thus paradigms of conditioned learning and passive/active avoidance could be imagined using this apparatus.

Overall, the visual-stimuli four-arm maze test, coupled with the analytical tools described here, offers the flexibility to explore multiple behavioral domains in rodents that could be beneficial for the investigation of a wide range of neurological, psychiatric, and ocular conditions.

Acknowledgments

We thank Samuel Fuchs for his original illustration of Figure 1A, Sarah Fuchs for video editing of Supplementary Video 1, and Mia Oviatt for editing the manuscript. The authors dedicate the manuscript to the memories of Dr. Salomon Moni Hamaoui and Lillian Jones Black, who died of Alzheimer's disease.

This manuscript is supported by the National Institute on Aging of the National Institutes of Health under Awards R01 AG055865 and R01 AG056478 (M.K.H.), and The Haim Saban and The Tom Gordon Foundations (M.K.H.). We acknowledge the original research paper where this protocol is derived from: Vit JP, Fuchs DT, Angel A, Levy A, Lamensdorf I, Black KL, Koronyo Y, Koronyo-Hamaoui M. Color and contrast vision in mouse models of aging and Alzheimer's disease using a novel visual-stimuli four-arm maze. Sci Rep. 2021 Jan 13;11(1):1255. doi: 10.1038/s41598-021-80988-0. PMID: 33441984; PMCID: PMC7806734 (Vit *et al.*, 2021).

Competing interests

MKH, YK and KLB are co-founders and stockholders of NeuroVision Imaging, Inc., 1395 Garden Highway, Suite 250, Sacramento, CA 95833, USA. MKH, YK and KLB are co-inventors on a patent "Visual stimuli maze test for detecting visual abnormalities in prodromal alzheimer's disease and in alzheimer's disease" application number US16/301,585, filing date 6/2/2017, licensed to Maze Engineers, 5250 Old Orchard Rd., Skokie, Illinois. Ariel Angel, Aharon Levy and Itschak Lamensdorf are former or current employees of Pharmaseed Ltd., Ness Ziona 74047, Israel. Jean-Philippe Vit and Dieu-Trang Fuchs have no competing interests.

Ethics

All experiments followed the NIH Guidelines for the Care and Use of Laboratory Animals and were approved by Cedars-Sinai Medical Center Institutional Animal Care and Use Committee (IACUC protocols 6617 and 8475, valid from February 2016 to February 2022). The study was carried out in compliance with the ARRIVE guidelines.

References

- Blanks, J. C., Schmidt, S. Y., Torigoe, Y., Porrello, K. V., Hinton, D. R. and Blanks, R. H. (1996a). [Retinal pathology in Alzheimer's disease. II. Regional neuron loss and glial changes in GCL](#). *Neurobiol Aging* 17(3): 385-395.
- Blanks, J. C., Torigoe, Y., Hinton, D. R. and Blanks, R. H. (1996b). [Retinal pathology in Alzheimer's disease. I. Ganglion cell loss in foveal/parafoveal retina](#). *Neurobiol Aging* 17(3): 377-384.
- Busse, L., Ayaz, A., Dhruv, N. T., Katzner, S., Saleem, A. B., Scholvinck, M. L., Zaharia, A. D. and Carandini, M. (2011). [The detection of visual contrast in the behaving mouse](#). *J Neurosci* 31(31): 11351-11361.
- Chang, L. Y., Lowe, J., Ardiles, A., Lim, J., Grey, A. C., Robertson, K., Acosta, M. L. (2014). [Alzheimer's disease in the human eye. Clinical tests that identify ocular and visual information processing deficit as biomarkers](#). *Alzheimers Dement* 10(2): 251-261.
- Chibhabha, F., Yang, Y., Ying, K., Jia, F., Zhang, Q., Ullah, S., Liang, Z., Xie, M. and Li, F. (2020). [Non-invasive optical imaging of retinal Abeta plaques using curcumin loaded polymeric micelles in APPswe/PS1DeltaE9 transgenic mice for the diagnosis of Alzheimer's disease](#). *J Mater Chem B* 8(33): 7438-7452.
- Chiquita, S., Campos, E. J., Castelhano, J., Ribeiro, M., Sereno, J., Moreira, P. I., Castelo-Branco, M. and Ambrosio, A. F. (2019). [Retinal thinning of inner sub-layers is associated with cortical atrophy in a mouse model of Alzheimer's disease: a longitudinal multimodal in vivo study](#). *Alzheimers Res Ther* 11(1): 90.
- Criscuolo, C., Cerri, E., Fabiani, C., Capsoni, S., Cattaneo, A., and Domenici, L. (2018). [The retina as a window to early dysfunctions of Alzheimer's disease following studies with a 5xFAD mouse model](#). *Neurobiol Aging* 67: 181-188.
- Cronin-Golomb, A., Sugiura, R., Corkin, S. and Growdon, J. H. (1993). [Incomplete achromatopsia in Alzheimer's disease](#). *Neurobiol Aging* 14(5): 471-477.
- Crow, R. W., Levin, L. B., LaBree, L., Rubin, R. and Feldon, S. E. (2003). [Sweep visual evoked potential evaluation of contrast sensitivity in Alzheimer's dementia](#). *Invest Ophthalmol Vis Sci* 44(2): 875-878.
- Denman, D. J., Luviano, J. A., Ollerenshaw, D. R., Cross, S., Williams, D., Buice, M. A., Olsen, S. R. and Reid, R. C. (2018). [Mouse color and wavelength-specific luminance contrast sensitivity are non-uniform across visual space](#). *Elife* 7: e31209.
- Doustar, J., Rentsendorj, A., Torbati, T., Regis, G. C., Fuchs, D. T., Sheyn, J., Koronyo-Hamaoui, M. (2020). [Parallels between retinal and brain pathology and response to immunotherapy in old, late-stage Alzheimer's disease mouse models](#). *Aging Cell* 19(11): e13246.
- Doustar, J., Torbati, T., Black, K. L., Koronyo, Y. and Koronyo-Hamaoui, M. (2017). [Optical Coherence Tomography in Alzheimer's Disease and Other Neurodegenerative Diseases](#). *Front Neurol* 8: 701.

- Dumitrascu, O. M., Lyden, P. D., Torbati, T., Sheyn, J., Sherzai, A., Sherzai, D., Sherman, D. S., Rosenberry, R., Cheng, S., Johnson, K. O., et al. (2020). [Sectoral segmentation of retinal amyloid imaging in subjects with cognitive decline](#). *Alzheimers Dement (Amst)* 12(1): e12109.
- Dumitrascu, O. M., Rosenberry, R., Sherman, D. S., Khansari, M. M., Sheyn, J., Torbati, T., Sherzai, A., Sherzai, D., Johnson, K. O., Czeszynski, A. D., et al. (2021). [Retinal venular tortuosity jointly with retinal amyloid burden correlates with verbal memory loss: a pilot study](#). *Cells* 10 (11): 2926.
- Georgevsky, D., Retsas, S., Raoufi, N., Shimoni, O. and Golzan, S. M. (2019). [A longitudinal assessment of retinal function and structure in the APP/PS1 transgenic mouse model of Alzheimer's disease](#). *Transl Neurodegener* 8: 30.
- Grimaldi, A., Brighi, C., Peruzzi, G., Ragazzino, D., Bonanni, V., Limatola, C., Ruocco, G. and Di Angelantonio, S. (2018). [Inflammation, neurodegeneration and protein aggregation in the retina as ocular biomarkers for Alzheimer's disease in the 3xTg-AD mouse model](#). *Cell Death Dis* 9(6): 685.
- Habiba, U., Merlin, S., Lim, J. K. H., Wong, V. H. Y., Nguyen, C. T. O., Morley, J. W., Bui, B. V. and Tayebi, M. (2020). [Age-Specific Retinal and Cerebral Immunodetection of Amyloid-beta Plaques and Oligomers in a Rodent Model of Alzheimer's Disease](#). *J Alzheimers Dis* 76(3): 1135-1150.
- Hampel, H., Toschi, N., Babiloni, C., Baldacci, F., Black, K. L., Bokde, A. L. W., Bun, R. S., Cacciola, F., Cavedo, E., Chiesa, P. A., et al. (2018). [Revolution of Alzheimer Precision Neurology. Passageway of Systems Biology and Neurophysiology](#). *J Alzheimers Dis* 64(s1): S47-S105.
- Hart, N. J., Koronyo, Y., Black, K. L. and Koronyo-Hamaoui, M. (2016). [Ocular indicators of Alzheimer's: exploring disease in the retina](#). *Acta Neuropathol* 132(6): 767-787.
- Jacobs, G. H., Williams, G. A. and Fenwick, J. A. (2004). [Influence of cone pigment coexpression on spectral sensitivity and color vision in the mouse](#). *Vision Res* 44(14): 1615-1622.
- Javaid, F. Z., Brenton, J., Guo, L. and Cordeiro, M. F. (2016). [Visual and Ocular Manifestations of Alzheimer's Disease and Their Use as Biomarkers for Diagnosis and Progression](#). *Front Neurol* 7: 55.
- Koronyo, Y., Biggs, D., Barron, E., Boyer, D. S., Pearlman, J. A., Au, W. J., Kile, S. J., Blanco, A., Fuchs, D. T., Ashfaq, A., et al. (2017). [Retinal amyloid pathology and proof-of-concept imaging trial in Alzheimer's disease](#). *JCI Insight* 2(16): e93621.
- Koronyo, Y., Salumbides, B. C., Black, K. L. and Koronyo-Hamaoui, M. (2012). [Alzheimer's disease in the retina: imaging retinal abeta plaques for early diagnosis and therapy assessment](#). *Neurodegener Dis* 10(1-4): 285-293.
- Koronyo-Hamaoui, M., Koronyo, Y., Ljubimov, A. V., Miller, C. A., Ko, M. K., Black, K. L., Schwartz, M. and Farkas, D. L. (2011). [Identification of amyloid plaques in retinas from Alzheimer's patients and noninvasive in vivo optical imaging of retinal plaques in a mouse model](#). *Neuroimage* 54 Suppl 1: S204-217.
- Kraeuter, A. K., Guest, P. C. and Sarnyai, Z. (2019). [The Y-Maze for Assessment of Spatial Working and Reference Memory in Mice](#). *Methods Mol Biol* 1916: 105-111.
- La Morgia, C., Ross-Cisneros, F. N., Koronyo, Y., Hannibal, J., Gallassi, R., Cantalupo, G., Sambati, L., Pan, B. X., Tozer, K. R., Barboni, P., et al. (2016). [Melanopsin retinal ganglion cell loss in Alzheimer disease](#). *Ann Neurol* 79(1): 90-109.
- Lee, S., Jiang, K., McIlmoyle, B., To, E., Xu, Q. A., Hirsch-Reinshagen, V., Mackenzie, I. R., Hsiung, G. R., Eadie, B. D., Sarunic, M. V., Beg, M. F., Cui, J. Z. and Matsubara, J. A. (2020). [Amyloid Beta Immunoreactivity in the Retinal Ganglion Cell Layer of the Alzheimer's Eye](#). *Front Neurosci* 14: 758.
- Lemmens, S., Van Craenendonck, T., Van Eijgen, J., De Groef, L., Bruffaerts, R., de Jesus, D. A., Charle, W., Jayapala, M., Sunaric-Megevand, G., Standaert, A., et al. (2020). [Combination of snapshot hyperspectral retinal imaging and optical coherence tomography to identify Alzheimer's disease patients](#). *Alzheimers Res Ther* 12(1): 144.
- Mirzaei, M., Pushpitha, K., Deng, L., Chitranshi, N., Gupta, V., Rajput, R., Mangani, A. B., Dheer, Y., Godinez, A., McKay, M. J., et al. (2019). [Upregulation of Proteolytic Pathways and Altered Protein Biosynthesis Underlie Retinal Pathology in a Mouse Model of Alzheimer's Disease](#). *Mol Neurobiol* 56(9): 6017-6034.
- Ngolab, J., Donohue, M., Belsh, A., Salazar, J., Cohen, P., Jaiswal, S., Tan, V., Gesser, D., Korouri, S., Aggarwal, N. T., et al. (2021). [Feasibility study for detection of retinal amyloid in clinical trials: the anti-amyloid treatment in asymptomatic Alzheimer's disease \(A4\) trial](#). *Alzheimers Dement (Amst)* 13 (1): e12199.
- Ning, A., Cui, J., To, E., Ashe, K. H. and Matsubara, J. (2008). [Amyloid-beta deposits lead to retinal degeneration in a mouse model of Alzheimer disease](#). *Invest Ophthalmol Vis Sci* 49(11): 5136-5143.

- Perez, S. E., Lumayag, S., Kovacs, B., Mufson, E. J. and Xu, S. (2009). [Beta-amyloid deposition and functional impairment in the retina of the APPswe/PS1DeltaE9 transgenic mouse model of Alzheimer's disease](#). *Invest Ophthalmol Vis Sci* 50(2): 793-800.
- Polo, V., Rodrigo, M. J., Garcia-Martin, E., Otin, S., Larrosa, J. M., Fuertes, M. I., Bambo, M. P., Pablo, L. E. and Satue, M. (2017). [Visual dysfunction and its correlation with retinal changes in patients with Alzheimer's disease](#). *Eye (Lond)* 31(7): 1034-1041.
- Prusky, G. T. and Douglas, R. M. (2004). [Characterization of mouse cortical spatial vision](#). *Vision Res* 44(28): 3411-3418.
- Prusky, G. T., Alam, N. M., Beekman, S. and Douglas, R. M. (2004). [Rapid quantification of adult and developing mouse spatial vision using a virtual optomotor system](#). *Invest Ophthalmol Vis Sci* 45(12): 4611-4616.
- Risacher, S. L., Wudunn, D., Pepin, S. M., MaGee, T. R., McDonald, B. C., Flashman, L. A., Wishart, H. A., Pixley, H. S., Rabin, L. A., Pare, N., et al. (2013). [Visual contrast sensitivity in Alzheimer's disease, mild cognitive impairment, and older adults with cognitive complaints](#). *Neurobiol Aging* 34(4): 1133-1144.
- Risacher, S., WuDunn, D., Tallman, E. F., West, J. D., Gao, S., Farlow, M. R., Brosh, J. R., Apostolova, L. G., Saykin, A. J. (2020). [Visual contrast sensitivity is associated with the presence of cerebral amyloid and tau deposition](#). *Brain Commun* 2(1): fcaa019.
- Salobrar-García, E., de Hoz, R., Ramirez, A. I., Lopez-Cuenca, I., Rojas, P., Vazirani, R., Amarante, C., Yubero, R., Gil, P., Pinazo-Duran, M. D., et al. (2019). [Changes in visual function and retinal structure in the progression of Alzheimer's disease](#). *PLoS One* 14(8): e0220535.
- Shi, H., Koronyo, Y., Fuchs, D. T., Sheyn, J., Wawrowsky, K., Lahiri, S., Black, K. L. and Koronyo-Hamaoui, M. (2020a). [Retinal capillary degeneration and blood-retinal barrier disruption in murine models of Alzheimer's disease](#). *Acta Neuropathol Commun* 8(1): 202.
- Shi, H., Koronyo, Y., Rentsendorj, A., Fuchs, D. T., Sheyn, J., Black, K. L., Mirzaei, N. and Koronyo-Hamaoui, M. (2021). [Retinal vasculopathy in Alzheimer's disease](#). *Front Neurosci*. 15: 731614.
- Shi, H., Koronyo, Y., Rentsendorj, A., Regis, G. C., Sheyn, J., Fuchs, D. T., Kramerov, A. A., Ljubimov, A. V., Dumitrascu, O. M., Rodriguez, A. R., et al. (2020b). [Identification of early pericyte loss and vascular amyloidosis in Alzheimer's disease retina](#). *Acta Neuropathol* 139(5): 813-836.
- Sinex, D. G., Burdette, L. J. and Pearlman, A. L. (1979). [A psychophysical investigation of spatial vision in the normal and reeler mutant mouse](#). *Vision Res* 19(8): 853-857.
- Tadokoro, K., Yamashita, T., Kimura, S., Nomura, E., Ohta, Y., Omote, Y., Takemoto, M., Hishikawa, N., Moribara, R., Morizane, Y. et al. (2021). [Retinal amyloid imaging for screening Alzheimer's disease](#). *J Alzheimers Dis* 83 (2): 927-934.
- van Alphen, B., Winkelmann, B. H. and Frens, M. A. (2009). [Age- and sex-related differences in contrast sensitivity in C57BL/6 mice](#). *Invest Ophthalmol Vis Sci* 50(5): 2451-2458.
- Vit, J. P., Fuchs, D. T., Angel, A., Levy, A., Lamensdorf, I., Black, K. L., Koronyo, Y. and Koronyo-Hamaoui, M. (2021). [Color and contrast vision in mouse models of aging and Alzheimer's disease using a novel visual-stimuli four-arm maze](#). *Sci Rep* 11(1): 1255.
- Wijk, H., Berg, S., Sivik, L. and Steen, B. (1999). [Colour discrimination, colour naming and colour preferences among individuals with Alzheimer's disease](#). *Int J Geriatr Psychiatry* 14(12): 1000-1005.